Universitat de Girona

MORPHOMETRIC SEAGRASS THRESHOLDS FOR HYDRODYNAMICS AND SEDIMENT CAPTURE

Aina Barcelona Arbat

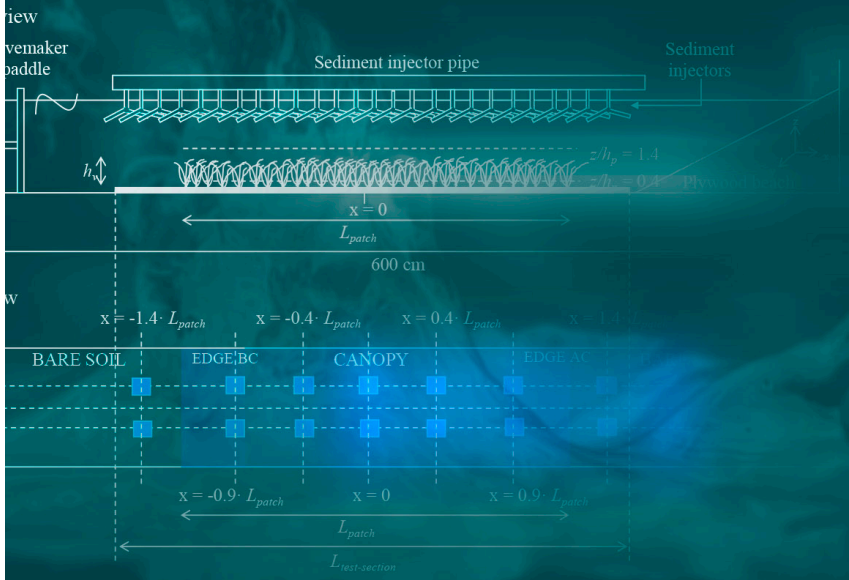

DOCTORAL THESIS

Morphometric seagrass thresholds for hydrodynamics and sediment capture.

Aina Barcelona Arbat 2023

DOCTORAL THESIS

Morphometric seagrass thresholds for hydrodynamics and sediment capture

Aina Barcelona Arbat 2023

Universitat de Girona

Universitat de Girona

DOCTORAL THESIS

MORPHOMETRIC SEAGRASS THRESHOLDS FOR HYDRODYNAMICS AND SEDIMENT CAPTURE

Aina Barcelona Arbat

2023

Universitat de Girona

DOCTORAL THESIS

MORPHOMETRIC SEAGRASS THRESHOLDS FOR HYDRODYNAMICS AND SEDIMENT CAPTURE

Presented to obtain the degree of PhD at the University of Girona

Doctorate Programme in the Environment

Aina Barcelona Arbat

2023

Supervised by:

Dr Jordi Colomer Feliu

Supervised by:

Dra Teresa Serra Putellas

Barcelona, A (2023). Morphometric seagrass thresholds for hydrodynamics and sediment capture. PhD thesis. Universitat de Girona.

Cover design: Carles Arbat

A l'avi Quimet i la iaia Maria

Per ensenyar-me a sempre mirar endavant

i a no rendir-me

La filosofia del Sol

Agraïments

Des de la vora del penya segat d'acabar l'etapa d'estudiant de doctorat, puc mirar enrere i veure amb orgull el camí pel qual he anat pujant per arribar fins aquí. Però aquest camí no l'he fet sola, he tingut la sort de comptar amb l'ajuda i el suport de moltes persones que m'han donat una empenta quan l'he necessitat, que m'han donat la mà i que m'han ajudat a aixecar en els moments més difícils.

En primer lloc, voldria agrair als meus directors de tesi, el Dr. Jordi Colomer i la Dra. Teresa Serra del grup de recerca de Física Ambiental, que hagin confiat amb mi. Crec que puc dir amb encert que una de les millors decisions que he pres va ser venir a fer el treball de final de grau amb vosaltres. Durant aquell any em vau ensenyar la passió per la recerca i em vau obrir un món nou. Allà, alguna cosa dins meu va canviar i vaig posar la mira a un nou objectiu: "vull dedicar-me a la recerca". Així que només puc agrair-vos la confiança i les oportunitats que m'he donat per poder arribar on sóc ara. Així com totes les hores que heu dedicat a ajudar-me ja sigui amb correccions, quadrant dades o tornant a explicar-me com fer un model adimensional. Gràcies un cop més, m'heu ajudat a créixer tant professional com personalment.

Tampoc puc oblidar-me de la Dra. Marianna Soler, sempre m'has donat el teu suport i m'has ensenyat a ser millor persona. També, vull agrair la col·laboració dels co-autors, al Dr. Nuno Gracias per l'ajuda amb la construcció del mosaics, la Dra. Carolyn Oldham, thank you for the deep discussions to enhance the manuscripts quality; i finalment, agrair al Dr. Jordi Garcia-Orellana per la discussió que va ajudar a enriquir la publicació i ensenyar-me a vendre'm, la frase "*porqué yo lo valgo*" em va quedar gravada per tota la vida.

Me gustaría agradecer también al Dr. Eduardo Infantes del Kristineberg Research Marine Center de Suécia por su amabilidad en recibirme y permitir que formase parte de su equipo durante las dos estancias. Gracias por la confianza. I also want to express my gratitude to Kristineberg staff and all researchers and students that share that time with me and made it easy and fun. Especially, I have to mention Carrie Chen and Damboia Cossa, you know that you are my Seagrass Ladies, thank you to accept me from the first day. One of the best things from the time I spent on Sweden is your friendship.

També, vull donar les gràcies a la meva família, en Pedro i amics, vosaltres m'heu vist i acompanyat durant els moments de frustració quan no em quadraven les dades o rebia un *reject* i durant també els moments d'eufòria quan finalment m'acceptaven un article. Quantes vegades m'heu escoltat parlar dels estudis que he anat fet, tots aquells experiments fets amb aigua bruta com dius tu Núria, quantes videotrucades a l'hora de sopar quan era fora.

Finalment, agrair a en Carles Arbat el disseny de les portades i coberta que formen part d'aquesta tesi doctoral.

Gràcies a tots vosaltres per acompanyar-me en aquesta etapa tan bonica.

Universitat de Girona

Dr Nuno Gracias, as co-author of the following articles:

Aina Barcelona, Jordi Colomer, Marianna Soler, Nuno Gracias, Teresa Serra (2021). Meadow fragmentation influences *Posidonia oceanica* density at the edge of nearby gaps. Estuarine, Coastal and Shelf Science 249, 107106. doi: 10.1016/j.ecss.2020.107106.

Accepts that Ms Aina Barcelona presents the cited articles as the principal author and as part of her doctoral thesis and that said articles cannot, therefore, form part of any other doctoral thesis.

And for all intents and purposes, hereby signs this document.

THE UNIVERSITY OF WESTERN AUSTRALIA

School of Engineering
Dept Civil, Environmental and Mining Engineering
The University of Western Australia
M019
35 Stirling Highway
Perth, Western Australia 6009
AUSTRALIA

Professor Carolyn Oldham
+61 8 6488 3531
carolyn.oldham@uwa.edu.au

5 July 2023

To:

University of Girona

I, Professor Carolyn Oldham, as co-author of the following articles:

> *Aina Barcelona, Carolyn Oldham, Jordi Colomer, Jordi Garcia-Orellana, Teresa Serra (2021). Particle capture by seagrass canopies under an oscillatory flow. Coastal Engineering 169, 103972. doi: 10.1016/j.coastaleng.2021.103972.*
>
> *Aina Barcelona, Carolyn Oldham, Jordi Colomer, Teresa Serra (2021). Functional dynamics of vegetated model patches: the minimum patch size effect for canopy restoration. Science of the Total Environment 795, 148854. doi: 10.1016/j.scitotenv.2021.148854.*

Hereby authorise Ms Aina Barcelona to present the above articles as the principal author and as part of her doctoral thesis, and that the above articles cannot, therefore, form part of any other doctoral thesis.

And for all intents and purposes, hereby signs this document.

Perth, Western Australia

July 5th 2023

Universitat de Girona

Dr Eduardo Infantes, as co-author of the following articles:

Aina Barcelona, Jordi Colomer, Teresa Serra, Damboia Cossa, Eduardo Infantes (2023). The role of epiphytes on particle capture by seagrass canopies.

Accepts that Ms Aina Barcelona presents the cited articles as the principal author and as part of her doctoral thesis and that said articles cannot, therefore, form part of any other doctoral thesis.

And for all intents and purposes, hereby signs this document.

Universitat de Girona

Ms Damboia Cossa, as co-author of the following articles:

Aina Barcelona, Jordi Colomer, Teresa Serra, Damboia Cossa, Eduardo Infantes (2023). The role of epiphytes on particle capture by seagrass canopies.

Accepts that Ms Aina Barcelona presents the cited articles as the principal author and as part of her doctoral thesis and that said articles cannot, therefore, form part of any other doctoral thesis.

And for all intents and purposes, hereby signs this document.

This PhD thesis is presented as a compendium of publications. It includes six publications, five of them already published and the other one is under review.

List of manuscripts of the thesis, organized by chapters, with indication of journal impact factor (IF), quartile (Q) and publication stage.

CHAPTER 2: **Aina Barcelona**[1], Jordi Colomer[1], Marianna Soler[1], Nuno Gracias[2], Teresa Serra[1] (2021). Meadow fragmentation influences *Posidonia oceanica* density at the edge of nearby gaps. Estuarine, Coastal and Shelf Science 249, 107106. doi: 10.1016/j.ecss.2020.107106. JCR/JIF (2021): 3.2, Q: Q1, Stage: Published.

CHAPTER 3: **Aina Barcelona**[1], Carolyn Oldham[3], Jordi Colomer[1], Jordi Garcia-Orellana[4], Teresa Serra[1] (2021). Particle capture by seagrass canopies under an oscillatory flow. Coastal Engineering 169, 103972. doi: 10.1016/j.coastaleng.2021.103972. JCR/JIF (2021): 5.4, Q: Q1, Stage: Published.

CHAPTER 4: **Aina Barcelona**[1], Carolyn Oldham[3], Jordi Colomer[1], Teresa Serra[1] (2021). Functional dynamics of vegetated model patches: the minimum patch size effect for canopy restoration. Science of the Total Environment 795, 148854. doi: 10.1016/j.scitotenv.2021.148854. JCR/JIF (2021): 10.8, Q: Q1, Stage: Published.

CHAPTER 5: **Aina Barcelona**[1], Jordi Colomer[1], Teresa Serra[1] (2023). Spatial sedimentation and plant captured sediment within seagrass patches. Marine Environmental Research 188, 105997. doi: 10.1016/j.marenvres.2023.105997. JCR/JIF (2022): 3.3, Q: Q1, Stage: Published.

CHAPTER 6: **Aina Barcelona**[1], Jordi Colomer[1], Teresa Serra[1] (2023). Stem stiffness functionality in a submerged canopy patch under oscillatory flow. Scientific Reports 13: 1904. doi: 10.1038/s41598-023-28077-2. JCR/JIF (2022): 4.6, Q: Q2, Stage: Published.

CHAPTER 7: **Aina Barcelona**[1], Jordi Colomer[1], Teresa Serra[1], Damboia Cossa[5,6], Eduardo Infantes[7] (2023). The role epiphytes play in particle capture of seagrass canopies. Marine Environmental Research, 192, 106238. doi: 10.1016/j.marenvres.2023.106238 JCR/JIF (2022): 3.3, Q: Q1, Stage: Published.

Authors affiliations:

[1] Department of Physics, University of Girona, 17071 Girona, Spain

[2] Computer Vision and Robotics Institute, University of Girona, 17071 Girona, Spain

[3] School of Engineering, The University of Western Australia, Perth, WA, 6009, Australia

[4] Department of Física, Univesitat Autònoma de Barcelona (UAB), Campus UAB, 08193, Bellaterra, Barcelona, Spain

[5] Eduardo Mondlane University, Department of Biological Sciences, Maputo, Mozambique

[6] Department of Marine Sciences, Kristineberg, University of Gothenburg, 45178, Sweden

[7] Department of Biological and Environmental Sciences, Kristineberg, University of Gothenburg, 45178, Sweden

Financial Support

I have had financial support by the pre-doctoral grant 3-year fellowship 2020FI SDUR 00043 from the “Generalitat de Catalunya” and the travel fellowship MOB2021 financed by the University of Girona. The research conducted on this thesis has been supported by the “Ministerio de Economía, Industria y Competitividad” of the Spanish Government through the grant CGL 2017-86515-P, by the “Ministerio de Ciencia e Innovacion” the Spanish Government through the grant PID 2021-123860O3-100. Chapter 2 was also contributed to the ICTA ‘Unit of Excellence’ (MinECo, MDM2015-0552) and the “Generalitat de Catalunya” research program (2017 SGR-1588). Finally, Chapter 6 was also funded by the Swedish Research Council (FORMAS) Dnr:2019-01192.

CONTENTS

LIST OF FIGURES

Chapter 1

Chapter 2

Chapter 3

Chapter 4

Chapter 5

Chapter 6

Chapter 7

LIST OF TABLES

Chapter 2

Chapter 3

Chapter 5

Chapter 6

Chapter 7

LIST OF ABBREVIATIONS

Variable	units	definition
A	cm	wave amplitude (Chapter 3) / the total epiphyted area of the canopy (Chapter 7)
a	cm^2	frontal area
ad	non-dimensional	fractional volume occupied by plants
A_{gap}	m^2	gap area
A_{inj}	m^2	injection area
aL	non-dimensional	frontal area per canopy lenght
A_p	m^2	plant epiphyted area
A_w	cm	wave excursion length
A_w/S_b	non-dimensional	ratio of wave excursion to plant-to-plant distance between blades
A_z	m^2	area at each z
B_o	$m^2 \cdot s^{-3}$	buoyancy flux
c	%	particle concentration
c_0	$\mu L \cdot L^{-1}$	initial sediment concentration
C_D	non-dimensional	drag of the form of the obstacle along the fluid patch
$C_{D\text{-}patch}$	non-dimensional	drag generated by the patch
c_p	$\mu L \cdot L^{-1}$	concentration of sediment attached to blades
c_s	$\mu L \cdot L^{-1}$	suspended sediment concentration at steady state
c_t	$\mu L \cdot L^{-1}$	suspended sediment concentration with time
d	cm	blade diameter
D	m	injector ID
d	cm	stem diameter
D50	µm	representative particle diameter
DBL	-	diffusive boundary layer
d_p	µm	particle diameter
e	non-dimensional	ratio between the shoot desnity and the mean shoot density for the highest densities

f	Hz	wave frequency
g	$m \cdot s^{-2}$	gravitational acceleration
h	cm	water height
h_p	m	plant height
h_v	m	effective plant height
ID	cm	inner diameter
I_{frag}	%	percentage of fragmentation
k	$radians \cdot cm^{-1}$	spatial frequency
L	cm	canopy length
L/S	non-dimensional	ratio between the characteristic lenght of the gap and the plant to plant distance
LCL	-	lower canopy layer
$L_{longshore}$	m	longshore distance
L_M	cm	length scale
$L_{onshore}$	m	onshore distance
L_{patch}	cm	patch lenght
lt	cm	characteristic eddy lenght-scale
M_b	kg	mass of sediment deposited to the bottom
M_{ep}	kg	mass of sediment trapped by epiphyted plant leaves
M_{nep}	kg	mass of sediment trapped by non-epiphyted plant leaves
M_o	$m^4 \cdot s^{-2}$	volume flux
M_s	kg	mass of suspended sediment
n	$stems \cdot m^{-2}$	canopy density
n_b	blades	number of blades
N_{ep}	Shoots	number of epiphyted plants
n_{inj}	injectors	number of injectors
N_{nep}	Shoots	number of non-epiphyted plants
P_C	%	partition coefficient of V_{SP} and V_{SC}
P_{edge}	non-dimensional	porosity at the edge of the gap
Q	$m^3 \cdot s^{-1}$	injection flow
Q_o	$m^4 \cdot s^{-3}$	momentum flux
S_b	cm	blade-to-blade distance
S_B	µL	sediment settled to the bed

S_C	µL	suspended sediment within the canopy (z/h_v=0.4)
SD	shoots·m^{-2}	shoot density
SD_{max}	shoots·m^{-2}	mean shoot density for the highest densities
SP	µL	sediment attached to plants
SPF	%	solid plant fraction
SW	µL	suspended sediment within the canopy (z/h_v=1.4)
t	min	time
TKE	cm^2·s^{-2}	turbulent kinetic energy
TM_i	kg	mass of sediment accumulated
T_s	min	time of the steady state
u	cm·s^{-1}	Eulerian velocity in the x direction
u'	cm·s^{-1}	turbulent velocity
U_c	cm·s^{-1}	steady velocity associated with the current
UCL	-	upper canopy layer
U_i	cm·s^{-1}	instantaneous velocity
$U_i(\varphi)$	cm·s^{-1}	instantaneous velocity according to the phase
U_w	cm·s^{-1}	wave velocity
U_w^{rms}	cm·s^{-1}	orbital velocity
v	cm·s^{-1}	Eulerian velocity in the y direction
V_{IN}	%	total volume of particles injected into the flume
V_{SB}	%	volume of sediment settled to the bed
V_{SC}	%	volume of suspended sediment inside the canopy (z/h_v=0.4)
V_{SP}	%	volume of sediment captured by the plants
V_{SW}	%	volume of suspended sediment above the canopy (z/h_v=1.4)
w	radians·s^{-1}	angular frequency
w	cm·s^{-1}	Eulerian velocity in the z direction
w_o	cm·s	injection velocity
x	cm	longitudinal direction
x=0	cm	position of the wave paddle
x_0	cm	initial position of the canopy
y	cm	lateral direction
z	cm	vertical direction
z/h_v	non-dimensional	measurement position

α_w	non-dimensional	ratio of U_w
β'	non-dimensional	vertical TKE attenuation
β_{LCL}	non-dimensional	TKE attenuation at the lowe canopy layer
β_{UCL}	non-dimensional	TKE attenuation at the upper canopy layer
β_w	non-dimensional	ratio of TKE
βw	non-dimensional	TKE attenuation
$\delta 50$	non-dimensional	porosity level of 50%
Δb_o	$m \cdot s^{-2}$	buoyancy of the resting plume fluid
λ	m	wave length
ρ_s	$kg \cdot m^{-3}$	water density
ρ_w	$kg \cdot m^{-3}$	sediment density
φ	radians	wave phase
Φ	%	solid volume fraction

ABSTRACT

Seagrass meadows are globally extensive nearshore ecosystems known as coastal engineers that provide key ecological services in coastal areas such as attenuating wave and turbulence and promoting sediment deposition. However, seagrass meadows have been threatened by natural and anthropogenic pressures, which result in physical damage to the meadow, resulting in plant loss and habitat fragmentation. Seagrass fragmentation may compromise the ecosystem services provided by the meadows, due to the transition from continuous canopies to a network of vegetated patches. Although the overall sediment input from external sources has decreased, extreme events have increased due to the climate change. That is the frequency and intensity of the heavy rains have lead to increased episodic river and runoff outflow, as well as sediment plumes generated by subglacial transported meltwater, meltwater runoff or iceberg melting. Most of the studies carried out on seagrass meadows are focused on the sediment deposition and resuspension of the internal sediment on the meadow itself. Therefore, this thesis aims to understand how the morphometric parameters (plant density, patch length, plant stiffness, plant height and epiphyte colonization) influence the hydrodynamics and sediment distribution within seagrass meadows. Also, it is aimed at establishing morphometric thresholds for both hydrodynamics and sediment capture for fragmented seagrass meadows to maintain the same ecosystem services than continuous meadows do.

This thesis can be structured on the effect of the morphometric parameters of the canopy on the hydrodynamics (wave velocity and turbulent kinetic energy) and the effect of both on the sediment

distribution within the canopy. Firstly, the effect of the level of fragmentation on the plant density has been studied in Chapter 2. The increase in the fragmentation level has been demonstrated to impact at both local and meadow-scale effects by decreasing the plant density of the vegetation surrounding the gaps (non-vegetated areas). The effect of the structural parameters on the modification on the hydrodynamics has been determined on Chapters 3, 4 and 6. Chapter 3 points the effect on the plant density. Chapter 4 is focused on the effect of the patch length and Chapter 6 determines the morphological thresholds (in terms of patch length, plant stiffness and plant density) that hold the interaction between hydrodynamics and the structure of the canopy. The modification on the sediment distribution by both structural canopy parameters and hydrodynamics has been demonstrated in Chapters 3, 5 and 7. Chapter 3 determines the effect of the plant density on the sediment capture distribution (the amount of sediment captured on the plant leaves, settled to the seabed and remained in suspension within the vegetation) from an external source. Chapter 5 demonstrates the effect of the patch length on the sediment distribution and Chapter 7 states that the distribution of sediment is directly related to the amount of epiphytes on the seagrass leaves.

The experiments from Chapter 3 to Chapter 7 were carried out in laboratory flumes at the University of Girona (Chapters 3, 4, 5 and 6) and the Kristineberg Research Station, at the University of Gothenburg (Chapter 7). The experiments were performed under oscillatory flows with different wave conditions, and different seagrass models, i.e., artificial flexible plants (mimicking *Posidonia oceanica* plants), artificial rigid plants, and real *Zostera marina* plants characterized by different plant densities and patch lengths. Chapter 8 contains the general

discussion and Chapter 9 presents the conclusions for each Chapter and the overall conclusions of the thesis.

In agreement with the regulations of the University of Girona, Chapters 2, 3, 4, 5 and 6 are a transcription of published articles in the following journals: *Estuarine Coastal and Shelf Science*, *Coastal Engineering*, *Science of the Total Environment*, *Marine Environmental Research* (two of them) and *Scientific Reports*. A copy of these articles can be also found at the end of this thesis.

RESUM

Els prats de fanerògames marines són extensos ecosistemes costaners distribuïts globalment coneguts com a enginyers costaners. Aquests proporcionen serveis ecosistèmics claus en zones costaneres com estabilització de l'atenuació de les ones i la turbulència, així com promoure la deposició de sediment. Malgrat això, els prats de fanerògames marines es troben amenaçats per pressions naturals i antropogèniques, les quals resulten en danys físics sobre el prat provocant pèrdua de plantes i fragmentació de l'hàbitat. La fragmentació en fanerògames marines pot comprometre els serveis ecosistèmics que proporcionen, a causa de la transició de prats continus cap a una xarxa de clapes de plantes. Tot i que l'aport de sediment extern ha disminuït, el canvi climàtic ha provocat l'increment d'episodis extrems. Tal com, l'increment en la freqüència i intensitat de pluges fortes, les quals han suposat un increment en les descàrregues episòdiques de rius i escorrentia. De la mateixa manera que en els plomalls de sediment generats pel desglaç subglacial, escorrentia del desglaç o el desglaç d'icebergs. La majoria dels estudis realitzats en prats de fanerògames marines estan centrats en la deposició de sediment i resuspensió del propi sediment del mateix prat. En conseqüència, aquesta tesi té com a objectiu entendre com els paràmetres morfomètrics (densitat de plantes, llargada de la clapa de vegetació, rigidesa de la planta, alçada de la planta i la colonització d'epífits) influencien a la hidrodinàmica i la distribució de sediment en els prats de fanerògames marines. També té com a objectiu establir llindars morfomètrics per la hidrodinàmica i la distribució de sediment per tal de que els prats de fanerògames marines mantinguin els serveis ecosistèmics.

Aquesta tesi es pot estructurar en l'efecte dels paràmetres morfomètrics del prat sobre la hidrodinàmica (velocitat de l'ona i l'energia cinètica turbulenta) i l'efecte d'ambdós en la distribució de sediment dins el prat de fanerògames. En primer lloc l'efecte del nivell de fragmentació sobre la densitat de plantes s'ha estudiat en el Capítol 2. S'ha demostrat com l'increment de fragmentació impacte tant a escala local com a escala de prat, disminuint la densitat de plantes al voltant dels blancs de vegetació (zones sense vegetació). L'efecte dels paràmetres estructurals sobre la modificació de la hidrodinàmica s'ha demostrat en els Capítols 3, 4 i 6. El capítol 3 prova l'efecte de la densitat de plantes. El Capítol 4 se centra en l'efecte de la longitud de la clapa de vegetació i el capítol 6 determina llindars morfològics (en termes de longitud de la clapa de vegetació, rigidesa de la planta i densitat de plantes) que suporta la interacció entre la hidrodinàmica i l'estructura del prat. La modificació de la distribució de sediment per ambdós els paràmetres estructurals del prat i la hidrodinàmica ha estat demostrada en els Capítols 3, 5 i 7. El Capítol 3 determina l'efecte de la densitat de plantes sobre la distribució de la captura de sediment (la quantitat de sediment capturada sobre les fulles, depositada al fons marí i la restant en suspensió dins el prat) d'una font externa. El Capítol 5 demostra l'efecte de la llargada de la clapa de vegetació sobre la distribució de sediment i el Capítol 7 prova que la distribució de sediment està directament relacionada amb la quantitat d'epífits que es troben sobra les fulles.

Els experiments des del Capítol 3 fins el Capítol 7 es van dur a terme en canals de laboratori a la Universitat de Girona (Capítols 3, 4, 5 i 6) i al Kristineberg Research Center de la Universitat de Gothenburg (Capítol 7). Els experiments es van realitzar en condicions de corrents oscil·latoris amb diferents condicions d'onatge, i diferents models de

fanerògames marines, és a dir, plantes flexibles artificials (mimetitzant plantes de *Posidonia oceanica*), plantes rígides artificials, i plantes reals de *Zostera marina* caracteritzades per diferents densitats de plantes i llargades de clapes vegetades. El Capítol 8 conte la discussió general i el Capítol 9 presenta les conclusions per cada capítol i les conclusions generals de la tesi.

D'acord ambles regulacions de la Universitat de Girona, els Capítols 2, 3, 4, 5, i 6 són transcripcions dels articles publicats en les següents revistes: *Estuarine Coastal and Shelf Science*, *Coastal Engineering*, *Science of the Total Environment*, *Marine Environmental Research* (dos d'ells) and *Scientific Reports*. Una còpia d'aquests articles es pot trobar al final de la tesi.

RESUMEN

Las praderas de fanerógamas marinas son extensos ecosistemas costeros distribuidos globalmente conocidos como los ingenieros costeros. Éstos proporcionan servicios ecosistémicos claves en zonas costeras como estabilización de la atenuación de las olas y la turbulencia, así como promover la deposición del sedimento. Aun así, las praderas de fanerógamas marinas se encuentran amenazados por presiones naturales y antropogénicas, las cuales resultan en daños físicos sobre la pradera provocando pérdidas de plantas y fragmentación del hábitat. La fragmentación en fanerógamas marinas puede comprometer los servicios ecosistémicos que proporcionan, a causa de la transición de praderas continuas hacia una red de zonas vegetadas. No obstante el aporte de sedimento externo ha disminuido, el cambio climático ha provocado el augmento de los eventos extremos. Tal como el incremento en la frecuencia e intensidad de lluvias fuertes, las cuales han supuesto un incremento en las descargas episódicas de ríos y escorrentía. Del mismo modo que en las plumas de sedimento generados por el deshielo subglacial, escorrentía del deshielo o el deshielo de icebergs. La mayoría de los estudios realizados en praderas de fanerógamas marinas están centrados en la deposición del sedimento y resuspensión del propio sedimento de la misma pradera. En consecuencia, esta tesis tiene como objetivo entender como los parámetros morfométricos (densidad de plantas, largo de la zona de vegetación, rigidez de la planta, altura de la planta y la colonización de epífitos) influyen en la hidrodinámica y la distribución del sedimento en las praderas de fanerógamas marinas. También tiene como objetivo establecer límites morfométricos para la

hidrodinámica y la distribución de sedimento para que las praderas de fanerógamas marinas mantengan los servicios ecosistémicos.

Esta tesis se puede estructurar en el efecto de los parámetros morfométricos de la pradera sobre la hidrodinámica (velocidad de la ola y la energía cinética turbulenta) y el efecto de ambos en la distribución de sedimento dentro de la pradera de fanerógamas. En primer lugar, el efecto del nivel de fragmentación sobre la densidad de plantas se ha estudiado en el Capítulo 2. Se ha demostrado como el incremento de fragmentación impacta tanto a escala local como a escala de pradería, disminuyendo la densidad de plantas alrededor de blancos de vegetación (zonas sin vegetación). El efecto de los parámetros estructurales sobre la modificación de la hidrodinámica se ha demostrado en los Capítulos 3, 4 y 6. El Capítulo 3 prueba el efecto de la densidad de plantas. El Capítulo 4 se centra en el efecto de la longitud de la zona de vegetación y el capítulo 6 determina límites morfológicos (en términos de longitud de zona de vegetación, rigidez de la planta y densidad de plantas) que soporta la interacción entre la hidrodinámica y la estructura de la pradera. La modificación de la distribución de sedimento por ambos los parámetros estructurales de la pradera y la hidrodinámica se ha demostrado en los Capítulos 3, 5 y 7. El Capítulo 3 determina el efecto de la densidad de plantas sobre la distribución de la captura de sedimento (la cantidad de sedimento capturado sobre las hojas, depositada en el fondo del mar y la restante en suspensión dentro de la pradera) de una fuente externa. El Capítulo 5 demuestra el efecto de la longitud de zonavegetación sobre la distribución de sedimento y el Capítulo 7 prueba que la distribución de sedimento está directamente relacionada con la cantidad de epífitos que se encuentran encima de las hojas.

Los experimentos desde el Capítulo 3 hasta el Capítulo 7 se realizaron en canales de laboratorio en la Universitat de Girona (Capítulos 3, 4, 5 y 6) y en el Kristineberg Research Center de la Universidad de Gothenburg (Capítulo 7). Los experimentos se realizaron en condiciones de corrientes oscilatorias con diferentes condiciones de oleaje, y diferentes modelos de fanerógamas marinas, es decir, plantas flexibles artificiales (mimetizando plantas de *Posidonia oceánica*), plantas rígidas artificiales, y plantas reales de *Zostera marina* caracterizadas por diferentes densidades de plantas y longitudes de zonas vegetadas. El Capítulo 8 contiene la discusión general y el Capítulo 9 presenta las conclusiones para cada capítulo y las conclusiones generales de la tesis.

De acuerdo con las regulaciones de la Universidad de Girona, los Capítulos 2, 3, 4, 5 y 6 son transcripciones de los artículos publicados en las siguientes revistas: *Estuarine Coastal and Shelf Science*, *Coastal Engineering*, *Science of the Total Environment*, *Marine Environmental Research* (dos de ellos) y *Scientific Reports*. Una copia de estos artículos se puede encontrar al final de la tesis.

CHAPTER 1

General introduction and objectives.

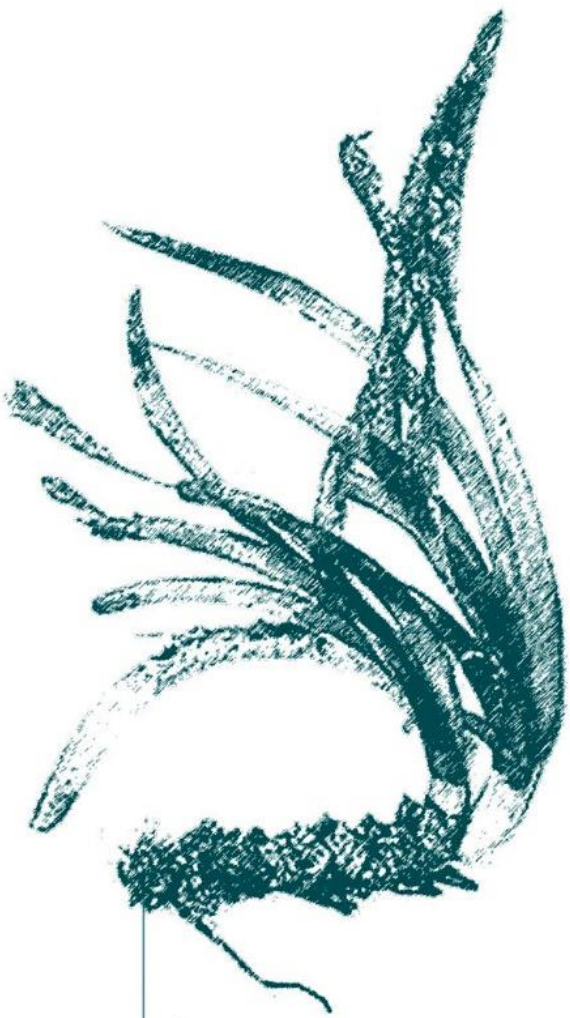

Cover design: Carles Arbat

1.1 SEAGRASS MEADOWS

Seagrasses are marine monocotyledon angiosperms with a polyphyletic origin (Les et al. 1997) divided into four families: Cymodoceacea, Hydrocharitacae, Posidoniaceae and Zosteraceae (Apostoloumi et al. 2021). Seagrasses are globally extended in most shallow coastal areas around the world except for the Antarctic regions (Waycott et al. 2009, Unsworth et al. 2019) due to the wide tolerance range of salinity in most of the species (Duarte et al. 2008). Seagrass mainly grow on sandy to muddy substrates but some species can also grow on rocky areas (Hemminga & Duarte 2000, Spalding et al. 2003), forming meadows from patches to mosaics typically monospecific (Spalding et al. 2003). Most of the seagrass species inhabit at depths lower than 10-20 m, but some species have been reported to resist even down to 90 m (Spalding et al. 2003). The depth limit of seagrass is the result of both the compensation of the irradiance form growth required to provide sufficient carbon gains to compensate the carbon losses (Hemminga & Duarte 2000) and the resistance to the hydrodynamics that depends on the seagrass species.

The coastal areas where seagrasses develop are dominated by waves and currents (Figure 1). Infantes et al. (2009) determined that there is a clear dependence of *Posidonia oceanica* cover with wave energy. They determined that *P. oceanica* can persist long-term under orbital velocities between 38 to 42 cm s^{-1}. However, Fonseca et al. (1983) determined that continuous *Zostera marina* meadows can resist unidirectional velocities up to 120-150 cm s^{-1}, while in fragmented *Z. marina* meadows the unidirectional flow resistance decrease to 53 cm s^{-1}. However, experimental transplantation of *Z. marina* plants in a coastal area proved that plants could not survive wave velocities above 63 cm s^{-1}. Fonseca and

Bell (1998) found that mixed meadows of *Zostera marina* and *Halodule weightii* may resist current velocities up to 25 cm s^{-1}.

Among the biotic parameters that define seagrass, there is a common agreement that plant height, plant stiffness, and plant density are the main characteristic parameters of the system. In addition, the level of epiphytes on leaves is also a key parameter defining the leaves morphometry. Among the abiotic parameters, seagrass meadows are characterized by their dimensions, which might span from the scales of meters to kilometres (Kendrick et al., 1999; Virnstein and Hall, 2009). *P. oceanica* meadows can present a canopy density between 100 to 800 shoots m^{-2} (Di Maida et al., 2013; Guidetti, 2000; Mabrouk et al., 2013) with plant height between 0.3 m and 1 m (Borg et al., 2005; Mabrouk et al., 2013). In contrast, the canopy density for *Z. marina* varies between 200 and 1000 shoots m^{-2} and the plant length between 0.3 m to 1 m as well *P. oceanica* (Lee et al., 2006). Colomer et al. (2017) found that the *P. oceanica* morphometrics, including plant density, and plant height vary with time, with significant differences across time, but smaller across several stations. The canopy density in Cala Montgó (North-East of Spain) was found to vary between 230 and 310 shoots m^{-2}, which are considered intermediate plant densities. Seagrasses are characterized by higher flexibility than other aquatic coastal vegetation, for instance, shoots of *Zostera noltii* are much flexible than those of *Spartina anglica* (Bouma et al., 2005).

Seagrass meadows are considered key ecosystems, providing numeral ecosystem services (Duarte, 2002; Montefalcone, 2009).They serve as nursery habitats acting as a refuge from the predators for numerous commercial fisheries (Metz et al., 2020) and ecologically important species of fishes, birds and invertebrate species (Hughes et al., 2009). They

also provide food to grazer organisms such as manatees (Lefebvre et al., 2017) and green turtles (Piovano et al., 2020). Seagrasses are also known as coastal engineers (Schotanus et al., 2020) for their capacity to change environmental conditions, attenuating wave and current energy, stabilizing sediments (Koch, 2001; Pujol et al., 2013a), mitigating storm surges and marine heat waves (Verdura et al., 2021; Zhu et al., 2020), and influencing nutrient cycling (Hughes et al., 2009). They also play a crucial role in blue carbon burial (Trevathan-Tackett et al., 2015). Specifically between 48 and 112 $TgCyr^{-1}$ is estimated that is accumulated by seagrass meadows (Greiner et al., 2016) at first in their organic debris, roots, rhizomes, and leaves then progressively buried forming the 'matte' (Mateo et al., 1997). For all these key ecosystem services, seagrasses are used as biological indicators of water quality and health (Güreşen et al., 2020; Malea et al., 2019) by the Water Framework Directive (WFD, 2000/60/EC) (Montefalcone, 2009).

However, the shallow distribution of the seagrass meadows makes them prone to be potentially vulnerable to human pressures, which may cause direct physical damage to the meadow, resulting in plant loss and in consequence habitat fragmentation (Abadie et al., 2016). The increase in seagrass fragmentation caused by anthropogenic pressures can be due to direct damages such as anchoring, trawling, dredging and urban or port infrastructure development. Seagrass fragmentation is presented by the transition from a continuous landscape of vegetation into meadows with interspersed gaps (i.e., areas of bare soil interspersed within the meadow) and to a network of vegetated patches, which will be losing the interconnection between them as more endangered the seagrass canopy will be (Sleeman et al., 2005). The increase in the fragmentation may compromise the ecosystem services, as vegetated patches are

characterized to have lower plant densities, shorter leaves and lower nutrient storage (Colomer et al., 2017; Gera et al., 2013; Tanner, 2005). Since 1980, 29% of the world's seagrass has been lost (Waycott et al., 2009), resulting in exposed areas of bare sediment, which will be more vulnerable to erosion and remineralisation of the carbon stored. Fragmented seagrass meadows can present up to 3 times lower percentage of mud and 1.5 times lower sedimentary organic carbon stocks compared with continuous meadows (Casal-Porras et al., 2022). Fourqurean et al. (2012) found that in fragmented meadows the sea soil remineralisation and carbon stock release rise up to 299 $TgCyr^{-1}$.

Therefore, the ecosystems services provided by seagrass meadows will depend on the structural parameters of the seagrasses, such as, plant height, plant stiffness, plant density, patch length and gap size. The interaction between these structural parameters with the hydrodynamics (i.e., current velocity and wave velocity) will directly affect the hydrodynamic attenuation and sediment dynamics within the meadow.

1.1.1 Seagrass meadow responses to hydrodynamic forcings

The local hydrodynamics in coastal areas are highly related to the vegetation of such areas, canopy structural characteristics and flow conditions (Fonseca and Bell, 1998). Seagrasses are known to play a crucial role in reducing the local waves and currents (Pujol et al., 2013a). In order to describe the role of submerged vegetation several authors performed studies under both unidirectional and oscillatory flow using rigid and flexible vegetation in both laboratory flumes and field experiments (Folkard, 2005; Hansen and Reidenbach, 2012; Nepf, 1999;

Nepf and Vivoni, 2000; Zhang et al., 2018). Previous studies carried out in oscillatory flows described a reduction in the mean velocity and wave velocity within and after a submerged flexible vegetation (Folkard, 2005; Pujol et al., 2013a). Continuous fragmentation implies a reduction on the structural complexity and prevalence of the habitat edges (Colomer and Serra, 2021). In addition, field studies demonstrated that seagrass reduces the near-bottom mean velocities by 70 to 90% and wave velocities within the seagrass canopy may be reduced up to 20% in eelgrass (*Zostera marina*) canopies (Hansen and Reidenbach, 2012). Gacia et al. (1999) also found a reduction on the wave velocity within *Posidonia oceanica* canopies. The attenuation of these velocities is produced by the conversion of the wave energy to stem-wake turbulence (Pujol et al., 2013a), which is generated by the production of a shear vortex created behind the stiff part of the plant (Nepf, 1999). The level of wave velocity attenuation by submerged flexible vegetation is a function of the canopy structural characteristics, such as the canopy density, plant stiffness or plant height, canopy fragmentation. Pujol et al. (2013b) found that both plant density and plant height modify the wave velocity within the canopy, resulting in a higher U_w reduction for denser and higher canopies.

For the effect of submerged vegetation on the turbulence, some studies found a reduction in the turbulent kinetic energy (TKE) within the submerged flexible canopy meaning that all the energy in the mean flow may be dissipated without turbulence production (Pujol et al., 2013a; Ros et al., 2014). Ros et al. (2014) found that higher canopy densities enhance the reduction in the TKE compared to the non-vegetated cases. However, Zhang et al. (2018) found an increase in the TKE within submerged flexible canopies. Therefore, there is a need to parametrize the flow conditions and canopy structure in order to be able to compare them in

terms of turbulence. Lowe et al. (2005) described that the Kaulegean Karpenter number A_w/S (where A_w is the orbital length scale and S is the plant-to-plant distance for rigid plants or S_b for flexible, see the methodology for their complete definition) is the most relevant parameter to explain the attenuation of the flow within the canopy.

Zhang et al. (2018) used the parameter A_w/S_b, and found an increase in the TKE within the vegetation for $A_w/S_b > 1$, while for $A_w/S_b < 1$, the TKE remained constant. This aligns with Pujol et al., (2013b) and Ros et al., (2014) as their studies were conducted under conditions of $A_w/S_b < 1$. Therefore, submerged flexible vegetation generates TKE under $A_w/S_b > 1$ conditions, whereas for $A_w/S_b < 1$ the TKE generated by the bed is attenuated.

Therefore, the capacity of canopies to attenuate both the wave velocity (U_w), and the turbulent kinetic energy, TKE, may be compromised in fragmented canopies (Serra et al., 2018) as a result of the increase in the vegetation edges (Granata et al., 2001). In order to understand the effect of the fragmentation on the hydrodynamics and sediment pattern most of the studies were carried out under unidirectional flows. They revealed that once again the structural parameters of the canopy modify the hydrodynamical and sedimentary patterns. Folkard (2005) found that the distance between the vegetated patches modifies the hydrodynamics, increasing the TKE between the patches when the distance between patches was larger. However, the density of the vegetated patch also influences the hydrodynamics of the downstream flow, as denser patches presented lower wave velocities behind the patch compared with sparse patches (Li et al., 2019). Some authors also studied fragmented canopies under oscillatory flows, demonstrating that higher fragmented canopies

(i.e., with larger amounts of gaps) reduce the sheltering offered by the vegetation due to the increase in the TKE within the larger gaps (El Allaoui et al., 2016). This agrees with the results of the field experiments of Serra et al. (2020), who found higher wave velocities and TKE for larger gaps, and Colomer et al. (2017), who demonstrated also the effect of the leaf height on the wave attenuation.

Another parameter that modifies the seagrass capacity to dissipate the hydrodynamic forces is the stiffness of the plants. Bouma et al. (2005) determined that canopies with stiffer plants have up to three times higher dissipation capacity than flexible canopies. Flexible plants move back and forth with the flow reducing in this way the wave dissipation capacity by the vegetation (Bradley and Houser, 2009). Thus, the drag exerted by the flow will limit the on-shore distribution of the more rigid species. In contrast, in more exposed areas under high flow energy environments flexible species will prevail, producing a transition between the extension of both types of ecological engineers (Bouma et al., 2005).

1.1.2 Seagrass meadows distributing external sediment sources

Due to the wave velocity attenuation, seagrass meadows stabilize the sediment within the canopy. By reducing the sediment resuspension (Ros et al., 2014) and settling the suspended sediment to the seabed (Gacia and Duarte, 2001). Structural canopy parameters such as plant density, plant heigh and the bending of the leaves were found to determine the sediment retention in flexible submerged vegetation (Gacia et al., 1999; Ros et al., 2014). Hendriks et al. (2008) found that the sediment particle trapping on the seagrass meadows is caused also by the particle collisions on the plants' surface enhancing the vertical particle transport and settling the particles to the seabed. Some authors performed laboratory flume experiments in

order to determine the effect of the seagrass canopies on the sediment resuspension, Flume experiments determined that sediment resuspension is lower in denser canopies with higher wave frequencies compared to bare sand (Ros et al., 2014; Zhang and Nepf, 2019), agreeing with Gacia and Duarte (2001), who also found a reduction in the resuspension in natural seagrass meadows. Furthermore, the sedimentation within the seagrass meadows increases for denser canopies compared to the bare sand (Gacia et al., 1999; Gacia and Duarte, 2001). The reduction in the sediment resuspension and the increase in the sediment deposition to the seabed result in clear waters, which enhance the ecological feedback of the seagrass meadows (Lopez-y-Royo et al., 2011).

The meadow seascape (i.e., pattens of fragmentation) may modify the sediment distribution. Ganthy et al. (2015) found higher sediment deposition on *Zostera noltii* patches than in base sand and denser the patches higher the sediment deposition. In addition, sparse vegetated patches show heterogeneous distributions of sediment, while fine sediment particles accumulates within the patch, and coarse particles accumulates in its exterior. In contrast, dense vegetated patches present a homogeneous sediment distribution (van Katwijk et al., 2010). Therefore, as a result seagrass fragmentation level influence on the carbon sequestration. Larger patches and more highly connected meadows (low distance between patches) store higher carbon rates (Johannessen, 2022).

Another parameter that can alter the sediment distribution on the seagrass meadows is the amount of epiphytes, as seagrass leaves are naturally colonized by them. The term epiphyte can be defined as the invertebrates and macroalgae organisms growing on the leaves of seagrass leaves and forming assemblages (Trautman and Borowitzka, 1999). The abundance

of epiphytes depends on the seagrass leaf area available for them to grow. The presence of epiphytes on seagrass meadows suggests the quality status of the ecosystem, as they act as ecological indicators, implying that more complex ecosystems present higher ecosystem quality (Cambridge et al., 2007). However, the abundance of epiphytes can impact negatively on the growth of the seagrass plants as the light available and the gas exchange will be diminished compared with the seagrass plants without epiphytes (Brodersen and Kühl, 2022). Thus, there is a need in determininf the effect of the epiphytes on the sediment capture as they will increase the seagrass surface available to trap sediment and they may also affect the stiffness of the plant.

1.1.3 External sediment sources that can impact on seagrass meadows

Most of the sediment distribution studies performed in seagrass meadows were focused on the sediment resuspension from the meadow itself (Gacia et al., 1999; Gacia and Duarte, 2001; Ros et al., 2014). However, climate change has been proven to increase the frequency and intensity of the heavy rains, which has increased episodic river and runoff outflow that may reach seagrass meadows (Vautard et al., 2014). Other external sediment sources that can reach seagrass meadows as sediment plumes can be originated by subglacial transported meltwater, which collected glacially eroded fine-grained sediment (Hallet et al., 1996) meltwater runoff (Chu et al., 2009), iceberg submarine melting (Fried et al., 2015) and iceberg calving (Koppes et al., 2010). Also, Asplund et al. (2021) found higher carbon burial in seagrass meadows near to deforested mangroves, which suggests that mangrove material can be washed into seagrass meadows. Moreover, anthropogenic activities can also produce sediment outputs that can reach seagrass meadow as sediment plumes,

such as, urban and industrial runoff, aquaculture and agriculture runoff (Abadie et al., 2016; Grech et al., 2012; Montefalcone, 2009).

Therefore, there is a need to understand the fate of an external sediment source that reach seagrass meadows. That is, there is a need to understand how sediment reaching a seagrass meadow, is distributed vertically, as a function of structural parameters such as plant height, plant stiffness, plant density, patch length and gap size. Also, there is a need to understand the impact of external sediment sources on the ecological status of the meadows, and the feedbacks between the sediment and the meadow characteristics.

1.2 OBJECTIVES

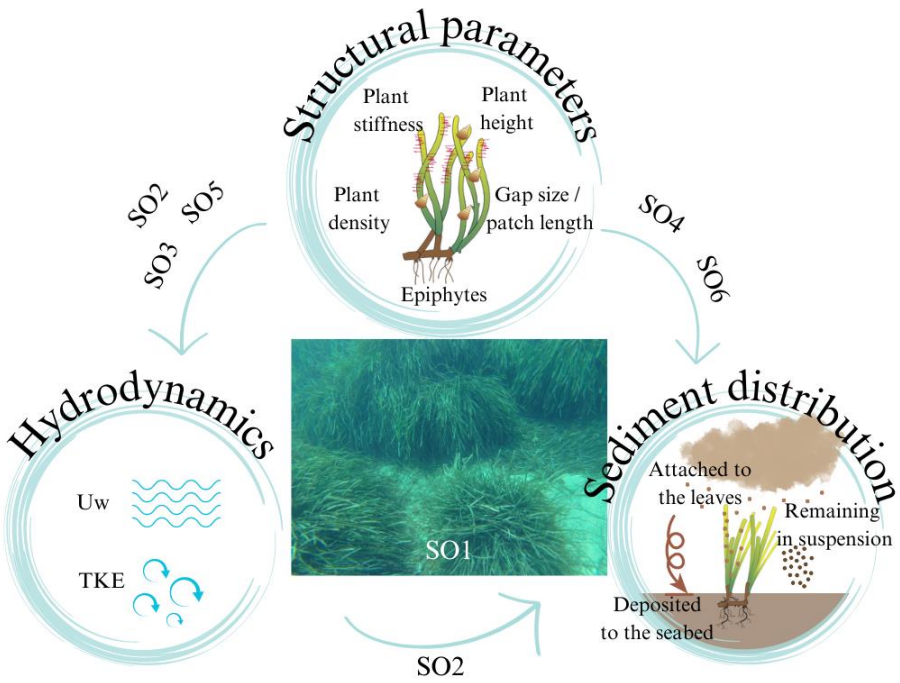

Figure 1.1 Conceptual diagram of the structural parameters, hydrodynamics and sediment distribution that characterize the seagrass seascape (Graphical Abstract of the Thesis). The structural parameters of a patch or a meadow of seagrass are the plan stiffness, the plant height, the gap size, the patch length and the plant density. A meadow might present a wide range of these structural parameters along with patches of vegetation interspersed by zones (gaps) without vegetation. Leaves can present a certain level of epiphytes. The hydrodynamics is characterized by the wave velocity (U_w) and the turbulent kinetic energy (TKE). The interaction between the seagrass canopy and external sediment sources may be identified by the amount of sediment in suspension, and the amount of sediment attached to the leaves or deposited to the seabed.

Most of the studies relating hydrodynamics to sediment dynamics in seagrass meadows are focused on the sediment resuspension. However, other types of sediment and seagrass interactions are still not addressed. For example, the role of the seagrass meadows in retaining sediment from outsider sources, such as river runoff in coastal areas. Also, seagrass loss generates modifications in the structural parameters of the meadow (i.e., plant density, patch length, plant height, etc). Therefore, there is a need of understanding the morphometric parameters of the meadow that are expected to modify both the hydrodynamics and the sediment dynamics. Also, it is crucial to determine the thresholds that will maintain the best ecological services of seagrass meadows.

This thesis raises two main objectives. First, to understand how the morphometric parameters (plant density, patch length, plant stiffness, plant height and epiphyte colonization) influence the hydrodynamics and sediment distribution within seagrass meadows. The second aim is to establish morphometric thresholds for hydrodynamics and sediment capture for seagrass meadows to maintain ecosystem services.

In order to fulfil the two main objectives, this thesis is structured in 6 Specific objectives associated to the different Chapters:

Specific Objective 1 (SO1): The effects that meadow fragmentation has on the plant density at the edge of gaps of vegetation (areas with no vegetation) within the seagrass meadow in two levels is investigated (**Chapter 2**). First, at meadow-scale, i.e., the effect of the total fragmentation (i.e., percentage of gap areas) on the plant density at the edge of the gap. And second, at local-scale, i.e., the effect of the gap size on the plant density at the edge of the gap. In addition, in this chapter, the effect the seagrass fragmentation has on plant density is determined. From

this study, it can be observed that different morphometries can be found in coastal seagrasses. With different canopy densities, patch lengths and plant heights (i.e., different plant flexibilities). The following objectives will be inspired in this first part of the thesis, that will be the initial aim (see Figure 1.1).

Specific Objective 2 (SO2): Determine the effect of plant density on both hydrodynamics and sediment capture. First, the effect on the hydrodynamics, the modification on both wave velocity and turbulent kinetic energy due to plant density will be studied (**Chapter 3**). Second, the sediment capture distribution, the amount of sediment captured on the plant leaves, settled to the seabed and remained in suspension within the vegetation will be quantified. This chapter will provide plant density thresholds for hydrodynamics and sediment capture to both optimal wave attenuation and sediment capture for the ecological feedback of seagrass meadows (Figure 1.1).

Specific Objective 3 (SO3): The effect of the patch length on coastal hydrodynamics (wave velocity and turbulent kinetic energy) is evaluated (**Chapter 4**). This chapter will provide the threshold of the minimum patch size, depending on both the local hydrodynamics and the plant density of the patch with the same behaviour than a continuous canopy (Figure 1.1).

Specific Objective 4 (SO4): The effect of the patch length on the sediment capture will be quantified (**Chapter 5**) (see Figure 1.1). Following the design of Chapter 3, the amount of sediment captured on the plant leaves, settled to the seabed and remained in suspension within the vegetation will be quantified. This chapter will provide patch length thresholds to ensure the optimal sediment capture distribution to obtain a positive seagrass feedback.

Specific Objective 5 (SO5): The interaction between hydrodynamics and canopy structure (in terms of patch length, plant stiffness and plant density) is determined (**Chapter 6**) (Figure 1.1). A non-dimensional model based on the hydrodynamics under morphometric structures of the canopy is given.

Specific Objective 6 (SO6): The effect of the epiphyte morphology on the sediment capture and distribution is determined (**Chapter 7**). Following the experimental design described in Chapters 3 and 5, the amount of sediment settled to the seabed, remained in suspension, and captured by the plant leaves will be quantified (Figure 1.1). However, in this chapter the amount of sediment captured on the plant leaves will correspond to the amount of sediment captured on the surface of the epiphytic leaves.

This thesis combines field work (**Chapter 2**) and laboratory experiments, conducted on hydraulic flumes (**Chapters 3**, **4**, **5**, **6** and **7**). The different specific objectives for each chapter are summarised in Figure 1, in which the interaction between the structural parameters, the hydrodynamics and the external sediment sources is presented.

CHAPTER 2

Meadow fragmentation influences posidonia oceanica density at the edge of nearby gaps

Aina Barcelona, Jordi Colomer, Marianna Soler, Nuno Gracias, Teresa Serra (2021). Meadow fragmentation influences *Posidonia oceanica* density at the edge of nearby gaps. Estuarine, Coastal and Shelf Science 249, 107106. doi: 10.1016/j.ecss.2020.107106.

Cover design: Carles Arbat

Abstract

Seagrass meadows are globally threatened by anthropogenic and natural pressures that cause habitat fragmentation and ecosystem degradation. Seagrass fragmentation is manifested by the loss of vegetation in gaps within a meadow. Depending on the degree of fragmentation, the ecological services provided by the seagrass meadows may be compromised. This study aims to understand the effect meadow fragmentation has on the shoot density of the canopy (large-scale or meadow-scale effect), as well as the effect the local gap size has on the shoot density at the edge of the gap (local-scale or gap-scale effect). In other words, determine whether the effects on the large scale can impact the local scales of the gap. This study demonstrates that the greater the gap area is, the lower the shoot density of the vegetation surrounding the gap. Moreover, the effect of fragmentation at the meadow-scale has been proved: the higher the fragmentation degree of the meadow is, the lower the shoot density is in the surrounding vegetation near the gap. Hence, the differences in shoot density at the edges of a gap are proven to be produced by both meadow fragmentation and gap characteristics.

Keywords: *seagrass meadows, Posidonia oceanica, fragmentation, canopy density, gap-scale, meadow-scale.*

2.1 INTRODUCTION

Seagrass meadows are globally-extensive nearshore ecosystems (Smith et al., 2010; Unsworth et al., 2019; Waycott et al., 2009) and provide significant ecosystem services such as the stabilization of habitats for fish feeding and predation (Unsworth et al., 2019), wave and turbulence attenuation (Gacia et al., 1999; Pujol et al., 2013b; Pujol and Nepf, 2012), and sediment deposition (Zong and Nepf, 2011), which creates new substrates, that will enhance the canopy growth (Folkard, 2019). Seagrass meadows provide an immensely rich fauna diversity and high water quality and ensure carbon storage and sequestration (Duarte et al., 2013; Grech et al., 2012; Ricart et al., 2015). Organic carbon can be accumulated, buried and preserved for millennia by seagrass meadows (Mateo et al., 1997), thus contributing to mitigating the effects of climate change (Mazarrasa et al., 2017)-

Seagrass meadows are threatened by natural and anthropogenic pressures, which result in meadows with differing degrees of habitat fragmentation. The principal causes for the increase in seagrass fragmentation are coastal development and overexploitation, both of which have a major impact on the seafloor where the meadows grow. Destructive fishing activities, anchoring and boat moorings have also resulted in the direct loss of seagrass meadow biomass; as has the ever-increasing nutrient and sediment pollution in the coastal waters (Colomer et al., 2017; Unsworth et al., 2017). These practices have been reported to decrease the number of herbivores that predate over the fouling algae in seagrass leaves, resulting in diminishing the quality of the seagrass meadows (Waycott et al., 2009). Furthermore, trawling and aquaculture have led to the introduction and dispersion of non-native species like *Caulerpa taxifolia* (M.Vahl) C.Agardh, *Caulerpa cylindracea* Sonder,

Codium fragile subsp. fragile (Suringar) Hariot, among others (Williams, 2007). Global change has also triggered an increase in the salinity and temperature of the water which, in turn, generates a regression of the coastal seagrass meadows (Boudouresque et al., 2009; Espel et al., 2019; Grech et al., 2012; Unsworth et al., 2019). All these pressures are accompanied by the rapid degradation of the coastal seafloor and by the continuous increase in seagrass meadow fragmentation worldwide (Abadie et al., 2015; Montefalcone et al., 2010). Patchy seagrass meadows are the result of the loss of both their stability and their shoot density (Colomer et al., 2017; Smith et al., 2010). In the Mediterranean *Posidonia oceanica* (Linnaeus) Delile seagrass meadows, Montefalcone et al. (2019) found that the extent of the regressed upper limits ranges between 18% to 99%. Therefore, continuous meadows shift to fragmented meadows where gaps of vegetation (where the seabed remains exposed to the hydrodynamics) are interspersed within the meadow (where the vegetation shelters the seabed). The resulting habitat patchiness, where large areas of habitat are removed or damaged, influences the ecosystem's integrity to the point that its ecological functions are compromised. Reversing vegetation loss is difficult because of complicated feed-back mechanisms that either reinforce vegetation dominance or threaten its resilience. For example, in the absence of seagrass vegetation, a drift to macroalgae proliferation can occur (Valdemarsen et al., 2010). Also, the reduction in sheltering (caused by the decrease in the density of vegetation) can lead to a decrease in seabed protection. A decrease in the seabed sheltering will lead to a high sediment resuspension which, in turn, might result in a further decrease in the vegetation density (Valdez et al., 2020).

Seagrass habitat fragmentation increases the number of gaps and edges in meadows, which then influence the physical and biological patterns of the meadow's structure(Ricart et al., 2015). El Allaoui et al. (2016)found lower wave and turbulent kinetic energy attenuation in fragmented canopy areas with large vegetation gaps than in canopies with small gaps albeit with the same degree of fragmentation. They also found that the overall turbulence in a canopy will increase with the degree of fragmentation in the canopy, thus highlighting the roles vegetation and gaps play at the meadow-scale. Likewise, an increase in the turbulent diffusion in the fragmented canopies of *Zostera noltei* Hornemann, indicated that fragmented habitats are more susceptible to dissolving pollutants (Lara et al., 2012). The physical modifications resulting from the gaps in fragmented canopies have been found to alter the carbon sequestering abilities of the seagrass. For instance, Ricart et al. (2015) found lower carbon storage in sediments within fragmented *Zostera muelleri* Irmisch ex Ascherson meadows. Edges can also have a negative effect on a seagrass meadow by increasing the risk of predation and/or encouraging invasions by exotic species. Habitat fragmentation can also endanger species that require interior habitats (Tanner, 2005), thus reducing their abundance at the edges and within the meadow itself (Smith et al., 2010).

How canopy fragmentation affects seagrass meadow morphology and functionality is still unclear. In particular, the impact that global fragmentation (meadow-scale fragmentation) or the local presence of a nearby gap (gap-scale characteristics) affect the shoot density of the edges of the canopy or the canopy density itself, are still to be fully determined. Therefore, using extensive field measurements from three *Posidonia oceanica* meadows on the northeast coast of Spain monitored

over two consecutive years, this manuscript aims to determine how both gap-scale characteristics and meadow-scale fragmentation impact canopy density. Two hypotheses are tested in this study: i) an increase in gap size is expected to affect shoot density at the edges of the gap (the surrounding vegetation of the gaps) and ii) an increase in the degree of meadow fragmentation is expected to reduce shoot density at both the edge of the gaps and within the fully-vegetated zone.

2.2 METHODOLOGY

Three *Posidonia oceanica* seagrass meadows on the NE coast of Spain (NW Mediterranean Sea) were studied over two consecutive years. The meadows were located 7 m deep off the bay of Cala Aiguablava and 10 m deep off the Cala Montgó and Cala Vigatà bays (Figure 2.1). Cala Aiguablava and Cala Montgó are semi-closed bays exposed to incoming winds and waves from the east i.e., the onshore is the exposed direction and the longshore the sheltered direction. On the contrary, Cala Vigatà is an open bay exposed to southerly and easterly winds and waves, i.e., both the onshore and the longshore are exposed to waves and currents. The three sites were surveyed in October 2018 and then again in October 2019.

The three *Posidonia oceanica* seagrass meadows were mapped over a prefixed area of analysis through video transects recorded by a scuba diver with a GoPro action camera and swimming 2 m above the meadows. The diver swam back and forth in both onshore and longshore directions to obtain the seascape view (photomosaic) of each meadow. The diver's trajectories were such that each sequential path (back and forth) ensured a 30% overlap between the recorded images in order to

minimize the presence of holes in the photomosaics. The photomosaics were obtained by joining the images from the videos using the technique described in (Elibol et al., 2011; Gleason et al., 2007). The regions mapped presented outlined rectangular or quadratic shapes, consistent with the specific positions of the meadows (Figure 2.1). Georeferencing was added during the photomosaic optimization process by using the fixed GPS coordinates of a set of easily identifiable seafloor features and manually annotated to create additional information in the analysis of the video images (Lirman et al., 2010), mainly by distinguishing the vegetated areas from the non-vegetated gaps. Three seascape photomosaics were created covering an area of 2247, 2622 and 2442 m^2 for Cala Aiguablava, Cala Montgó and Cala Vigatà, respectively (Figure 2.1).

Gaps were classified in three classes (i.e., GAP1, GAP2, and GAP3), according to the ratio between their maximum lengths and the *Posidonia oceanica* leaf length. Since the mean leaf length of the plant (h_v) was 0.53 m, GAP1 includes gaps with a maximum size of $2h_v$, i.e., <1.06 m; GAP2 are gaps with between $3h_v$ and $2h_v$, i.e., 1.06< size <1.59 m and GAP3 greater than $3h_v$, i.e., >1.59 m. Since the gaps in the field were not exactly circular, but often elliptical, their final classification was made based on their area. The area (in m^2) of each gap was calculated by considering an ellipse-shaped area around the two axes $L_{onshore}$ and $L_{longshore}$, and using the equation (2.1):

$$A_{gap} = \pi \cdot \frac{L_{onshore}}{2} \cdot \frac{L_{longshore}}{2} \quad (2.1)$$

Therefore, GAP1 has a gap area $A_{gap} < 0.9$ m^2, GAP2 in the range of 0.9 $m^2 < A_{gap} < 2$ m^2, and GAP3 in the range of 2 $m^2 < A_{gap} < 3.5$ m^2, whilst gaps > 3.5 m^2 were discarded. A total of twenty-one gaps were

categorised, ten gaps in the GAP1 class, seven in GAP2, and four in GAP3 (Table 2.1). In correspondence with each gap, four transects in the vegetation surrounding the gap were established: two in the longshore and two in the onshore directions (see scheme in Figure 2.2). Considering the starting point of each transect at the edge of the gap (corresponding to x_1 = 0 m), the subsequent longshore and onshore positions identified in the adjacent vegetation surrounding the gap were x_2 = 0.5 m, x_3= 1 m and x_4= 2 m, where the shoot density of the vegetation was measured. Therefore, for each gap, a total of sixteen positions in the vegetation were established and studied; four at the very edge of the gap and twelve in the vegetation adjacent to the gap, totalling 336 measurement points in the three meadows investigated. All the gaps in the analysis were chosen by considering that the inter-gap distances, (i.e., the distance between gap edges), were greater than 4 m to ensure that the furthest position of analysis (2 m from the edge) in each gap, did not overlap with the adjacent gap. From the total number of gaps observed in the three meadows over both years, 25% of them would be included in the study (Table 2.1).

The ratio between the area of the gaps and the whole area of the studied meadow (in %), corresponded to the degree of fragmentation (I_{Frag}) of the meadow in each bay. In their study, Sleeman et al. (2005) used five categories (from highly fragmented to continuous seagrass seascapes) to classify meadow fragmentation: many/small patches for seagrass cover less than 7%, medium patches for 16% to 37% of seagrass cover, few/large patches for 32 to 45% of seagrass cover, perforated continuous meadows to 45% to 86% and continuous meadows for seagrass cover greater than 93%. For each gap and at each measurement point, the shoot density (SD, hereafter) was measured and considered to be the key

parameter with which to characterise the structural condition of the vegetation surrounding the gap. SD was measured following Colomer et al. (2017), by counting shoots within a 40 cm x 40 cm square subdivided into four 20 cm x 20 cm sub-quadrates, and placed on the top of the canopy. SD data at each gap edge distance for the two longshore and the two onshore directions were averaged in each gap and then averaged in all the gaps in Cala Aiguablava and Cala Montgó. In contrast, in Cala Vigatà, all SD data were averaged independent of the direction of the transect (i.e., longshore or onshore) because, due to the particular orientation of the bay, the gaps in Cala Vigatà were equally exposed to the incoming winds and waves from the south and the east (see Figure 1). For this reason, all transects in Cala Vigatà have been considered to have the same characteristics and have been averaged all together and named “onshore”.

Table 2.1 Classes and characteristics of the gaps measured in the three meadows investigated in the two survey periods (2018, 2019). A_{gap} is the area of the gap, $L_{onshore}$ and $L_{longshore}$ are the two axes in the ellipse-shaped area of the gap.

Meadow	Year	GAP class	A_{gap} (m^2)	$L_{onshore}$ (m)	$L_{longshore}$ (m)
Aiguablava	2019	1	0.55	0.70	1.00
		1	0.50	0.40	1.60
		2	1.80	1.00	2.30
	2018	1	0.69	0.80	1.10
		1	0.94	0.75	1.60
		2	2.04	1.00	2.60
Montgó	2019	1	0.35	0.40	1.10
		1	0.94	1.50	0.80
		2	1.63	2.60	0.80
	2018	1	0.82	1.10	0.95
		2	1.84	1.18	1.30
		3	2.76	2.70	1.30
		1	0.71	0.70	1.30
		2	1.48	0.90	2.10
		3	2.76	1.30	2.70
Vigatà	2019	1	0.75	1.20	0.80
		2	1.56	0.90	2.20
		3	2.83	1.50	2.40
	2018	1	0.85	1.05	1.03
		2	1.51	1.60	1.20
		3	2.68	3.10	1.10

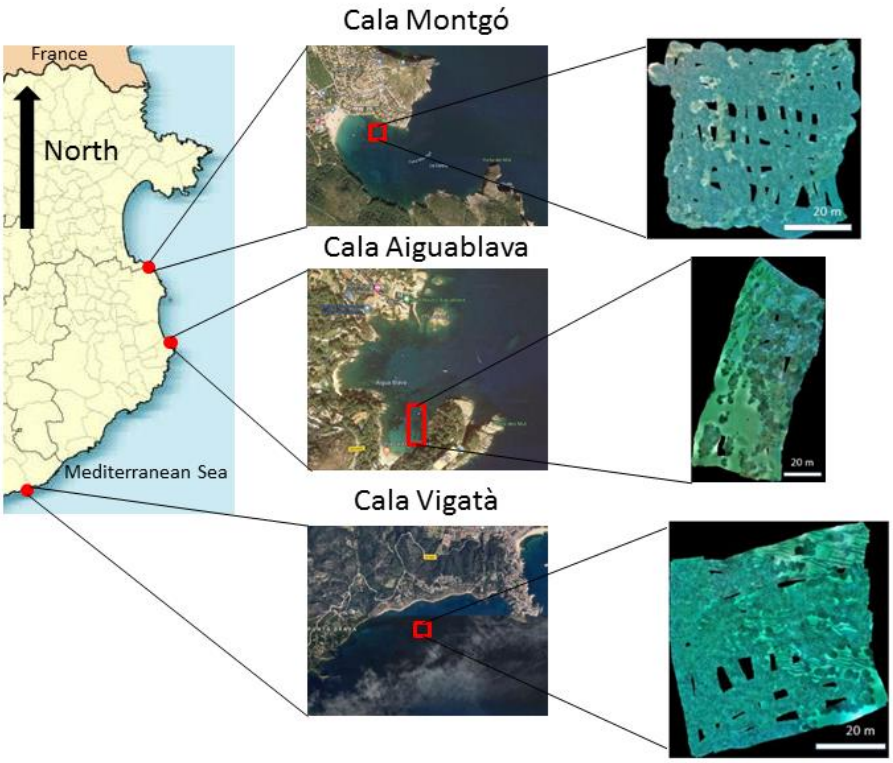

Figure 2.1 Study sites located in Cala Montgó (42º6.305'N, 3º10.308''E), Cala Aiguablava (41º56.118´N, 3º13.034´E) and Cala Vigatà (41º46.389´N, 3º1.554´E), on the NE coast of Spain (NW Mediterranean Sea). Figures on the right represent reconstructed images (photomosaics) of the studied seagrass meadows. Dark zones correspond to missing data due to no overlapping data images being captured during the video trajectories.

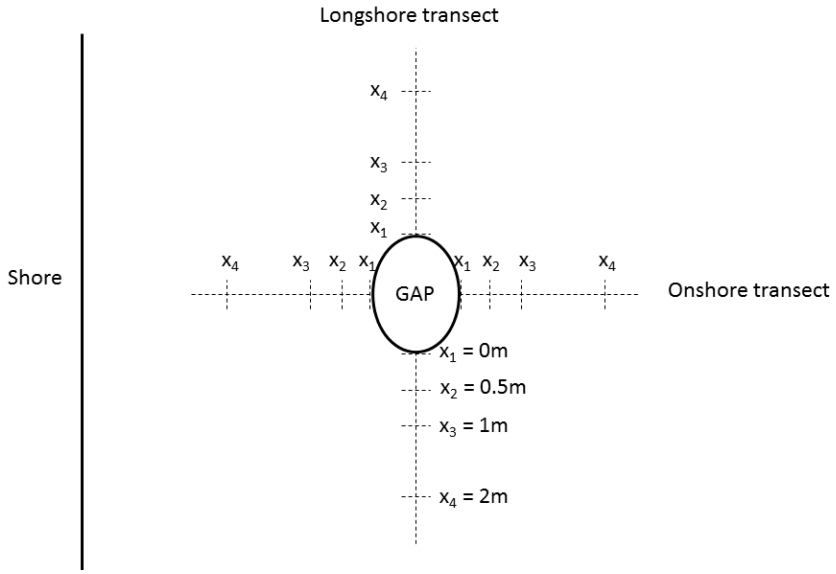

Figure 2.2 Schematic representation of the measurement positions (x1 to x4) on both longshore and onshore transects.

For a suitable comparison of shoot density data among the three meadows, the non-dimensional parameter, ε, was calculated using the equation (2.2):

$$\varepsilon = \frac{SD}{SD_{max}} \tag{2.2}$$

where SD is the shoot density averaged for longshore or onshore positions in each transect of each gap, and SD_{max} is the mean value of the four highest shoot densities measured at the position x = 2 m of longshore or onshore directions for each gap. ε represents the local density of the meadow compared to the maximum density of the canopy. ε < 1 indicates that the vegetation at the local scale has a density lower than the mean shoot density of the inner canopy areas for the study site.

Maximum shoot density for each year in each meadow (Year SD_{max}) was calculated by averaging SD_{max} in each meadow during each survey period.

The porosity of the vegetation at the edge of the gap (P), measured in the position $x_1 = 0$ m (see Figure 2.2), was calculated according to equation (2.3):

$$P_{\substack{edge \\ x_1=0}} = 1 - \varepsilon_{edge} \tag{2.3}$$

The porosity at the edge of the gap (at $x_1 = 0$ m) represents the part of the edge adjacent to the seafloor region without plants. Porosity was also related to the parameter L/S, where L is the characteristic length of the gap in both longshore ($L_{Longshore}$) and onshore ($L_{Onshore}$) directions and S is the plant-to-plant distance at the gap edge. The parameter δ50, which is the $L_{Onshore}/S$ value corresponding to a distance with porosity of 0.5 (50%), has been computed in each meadow.

2.3 RESULTS

The degree of I_{Frag} was 63.4%, 22.1% and 13.6%, for Cala Aiguablava, Cala Vigatà and Cala Montgó meadows, respectively. The lowest fragmented meadows were at Cala Montgó and Cala Vigatà which corresponded to the category "perforated continuous meadow", while the highest fragmented meadow was found at Cala Aiguablava corresponded to the "medium patches" category. Year SD_{max} did not change consistently with I_{Frag} (Table 2.2).

Table 2.2 Meadow characteristics: mean values (± standard deviations) of the maximum shoot density (Year SD_{max}) for each year in each meadow, depth where the measurements were taken and degree of meadow fragmentation (I_{Frag}).

Year	Meadow	Year SD_{max} (shoots·m^{-2})	Depth (m)	I_{Frag} (%)
2018	Aiguablava	449 ± 36	7.1 ± 0.6	63.36
2018	Vigatà	353 ± 89	10.4 ± 0.2	22.06
2018	Montgó	332 ± 50	9.5 ± 0.2	13.60
2019	Aiguablava	105 ± 7	4.9 ± 0.4	63.36
2019	Vigatà	119 ± 6	5.2 ± 0.3	22.06
2019	Montgó	122 ± 3	4.9 ± 0.9	13.60

2.3.1 Structural analysis of vegetation adjacent to the gaps at the gap scale

With distance from the edge of the gap towards the fully vegetated canopy, ε increased until reaching a plateau ($\varepsilon \approx 1$) at a distance x between 1 and 2 m from the gap edge in all cases (Figure 2.3a). Two regions can be differentiated: the edge of the vegetation (where $\varepsilon < 1$) and within the canopy (where $\varepsilon \approx 1$). The decrease in ε values with distance from within the meadow to the edge of the vegetation was more accentuated for large gaps than for small ones. Furthermore, ε decreased with the area of the gap, ranging from 0.92 for GAP1 to 0.38 for GAP3 (Figure 2.3a). Cala Montgó, which is the least fragmented meadow, exhibited higher ε at the edge of the gaps (at $x_1 = 0$ m) than the most

fragmented meadow at Cala Aiguablava. In Cala Montgó ε was higher than in Cala Aiguablava (Figure 2.3b).

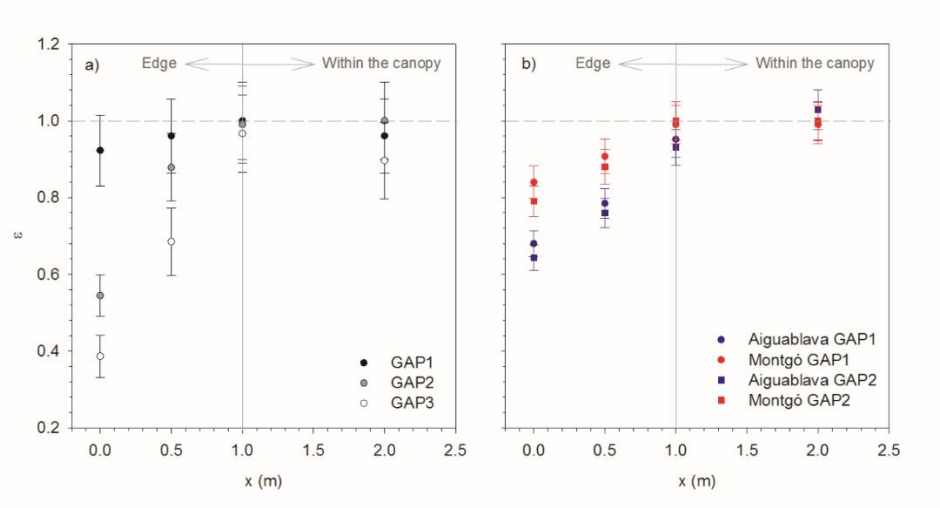

Figure 2.3 a) Mean ε values for Cala Montgó in the 2019 survey along the onshore transect. Black filled circles correspond to GAP1 measurements, grey filled circles to GAP2 measurements and unfilled circles to GAP3 measurements. Error bars represent the standard deviation of the two transects with the same directions in each gap. b) Mean ε values for all surveys in Cala Montgó and Cala Aiguablava for each gap size along the onshore transects. Blue symbols correspond to Cala Aiguablava and red to Cala Montgó. Circles correspond to measurements from GAP1 and squares from GAP2. The dashed horizontal line symbolizes the maximum ε value (ε ≈1), whilst the continuous vertical lines the distance (x) at which the gap edge reaches the maximum ε value.

The porosity (P) at edge of the meadow showed a linear relation with $L_{Onshore}/S$ in all three meadows (Figure 2.4a). In contrast, for Cala Aiguablava and Cala Montgó, P did not show any dependence with $L_{Longshore}/S$ (Figure 2.4b). Cala Aiguablava showed the highest

relationship with P, increasing with $L_{Onshore}/S$, followed by Cala Vigatà, and then Cala Montgó showing the smoothest increase (Figure 2.4a).

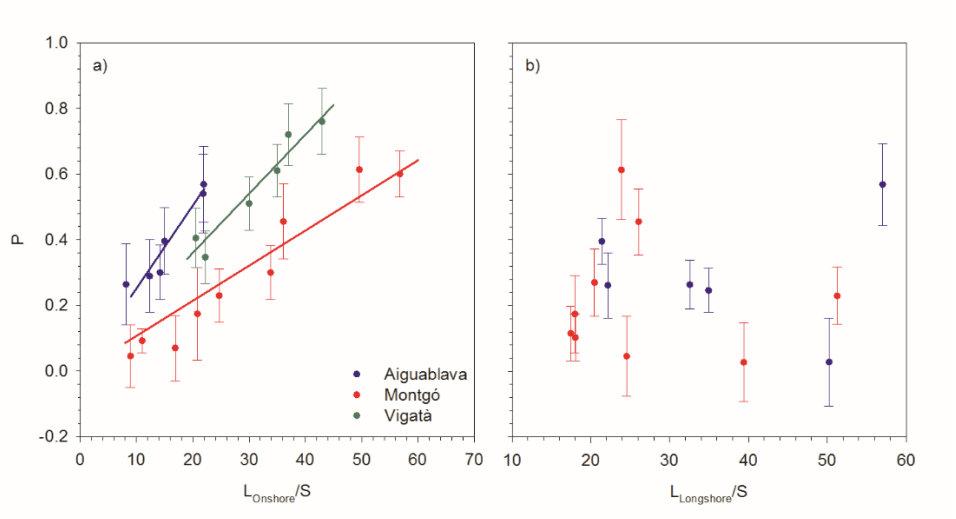

Figure 2.4: a) Relationships between the porosity (P) at the edge of the gaps and the ratio between $L_{Onshore}$ and plant-to-plant distance (S), for Cala Aiguablava (blue filled circles), Cala Montgó (red filled circles) and Cala Vigatà (green filled circles). The equations of the linear tendencies are: $P = 0.03(L_{Onshore}/S)$ with $R^2=0.911$ (for Cala Aiguablava), *p-value*=0.01 ($L_{Onshore}/S$) with $R^2=0.912$ (for Cala Montgó); *p-value*=0.02 ($L_{Onshore}/S$) with $R^2=0.939$ (for Cala Vigatà). b) Relationships between the porosity (P) at the edge of the gaps and the ratio between $L_{Longshore}$ and plant-to-plant distance (S), for Cala Aiguablava (blue filled circles) and Cala Montgó (red filled circles). Note that for Cala Vigatà, the longshore and onshore values of P were averaged since the Cala Vigatà meadow is situated in an open bay with both directions exposed to waves and currents.

2.3.2 Structural analysis of vegetation near gaps at the canopy scale

I_{Frag} presented an inverse relationship with δ50 (Figure 2.5). For a porosity level of 50%, the gap dimension ($L_{Onshore}$/S) expressed as δ50 was higher as the fragmentation was lower; as observed in Cala Montgó (Figures 2.5a, 2.5b). Cala Aiguablava showed the highest I_{Frag} (63.4 %, Figure 2.5a) and the lowest δ50 (19.8, Figure 2.5b). In Cala Montgó, displaying the lowest fragmentation (13.60 %, Figure 2.5a), fragmentation was inversely correlated with δ50.

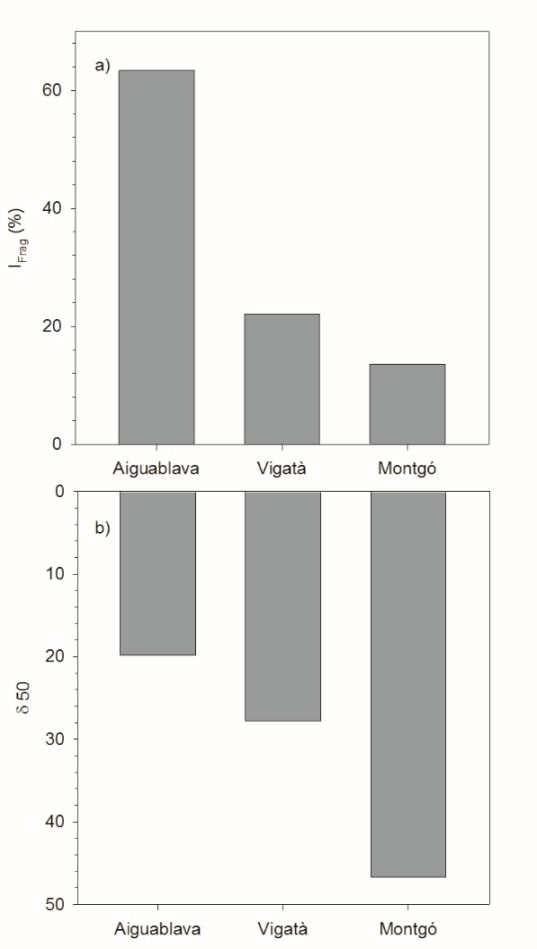

Figure 2.5 a) Degree of meadow fragmentation, IFrag, for Cala Aiguablava, Cala Montgó and Cala Vigatà. b) LOnshore/S value corresponding to a distance with porosity of 50%, δ 50 for the meadows of Cala Aiguablava, Cala Montgó and Cala Vigatà.

2.4 DISCUSSION

Meadow shoot density increased from the edge of a gap towards the fully-vegetated area to reach the highest canopy densities, whereby plant density stabilized. For all gap sizes and for all three meadows investigated, the highest canopy density was reached within 1 to 2 m from the edge of the gap. These results agree with Tanner (2005) who found that at the distance of 1 m from the *Zostera muelleri* and *Zostera muelleri* subsp. *macronuta* (Hartog) S.W.L. Jacobs meadows edges, the biomass of both seagrass species stabilized to the highest value of biomass (i.e., the biomass characteristic of the meadows). Colomer et al. (2017) found that the reduction in wave velocity and turbulent kinetic energy increased up to 1 m away from the edge of a vegetated patch, indicating that within a meadow at distances greater than 1 m from a meadow edge, the hydrodynamic parameters are attenuated. Unsworth et al. (2017) also found an increase in cover and canopy height for *Zostera marina* Linnaeus with increasing distance away from vegetation gaps. The present study proves that differences in vegetation gap sizes influence meadow density at the edge of a gap. On a local scale (i.e. gap-scale), larger gaps showed lower shoot density at the edge, while smaller gaps presented higher values of shoot density, which agrees with Colomer et al. (2017) where lower values of vegetation covers were found near larger gaps. A reduction in the canopy density is expected to lead to an increase in sediment resuspension (Gacia et al., 1999). Therefore, patchy meadows will have higher wave velocities and turbulence (El Allaoui et al., 2015), with higher sediment resuspension and erosion (El Allaoui et al., 2015) depending on the shoot density at the edges (Serra et al., 2018). These differences in canopy densities according to gap sizes could compromise meadow resistance due to an

increase in seabed erosion, thus enhancing the generation of further gaps and the change from continuous to patchy meadows (Abadie et al., 2018).

At the meadow scale, the degree of fragmentation of each zone has also been demonstrated to influence canopy density at the edge of gaps. This result agrees with the model by El Allaoui et al. (2016), who found that highly fragmented meadows have greater turbulent kinetic energy in the overall canopy, consequently reducing the shelter offered by the vegetation. Therefore, for the same gap size, the higher the overall meadow fragmentation is, the lower the meadow density at the edge. This result indicates that, given the same gap size, the gap remains more protected by the vegetated canopy in a continuous meadow than in a more fragmented meadow. These results confirm - in the field - the model created by El Allaoui et al. (2016), which hypothesised that fragmented canopies with smaller gaps produced higher shelter than fragmented canopies with larger gaps but with the same total fragmentation.

The degree of meadow fragmentation only affected the vegetation found in the onshore side of the gaps. In Cala Aiguablava and Cala Montgó, only the edges of the gaps perpendicular to the coast are exposed to incoming winds and waves from the east, with the canopy responding at a gap scale through changes in canopy density in the onshore direction. Meanwhile, north-south gap edges did not present any relationship with canopy density. In contrast, in Cala Vigatà, which is exposed to easterly and southerly winds and waves, all the vegetation surrounding the gaps presented canopy densities that depend on the size of the gaps. Likewise, Tanner (2003) found that the abundance of animal groups was distributed

depending on the orientation of vegetation patches to currents. For instance, greater numbers of adult and juvenile fishes were found in vegetated patches oriented parallel to the current; probably because they received a greater flux of feeding material. In contrast, larval forms, which are easily dispersed by higher currents, found refuge in patches perpendicular to the flow, i.e., in patches that provide a large extension of vegetation and hence higher protection.

The function of protection provided by seagrass is clearly conditioned by the local degree of fragmentation of each meadow. Thus, highly fragmented meadows like Cala Aiguablava, which corresponded to medium patch vegetation, will present vegetation gaps with lower surrounding canopy densities than zones that present lower fragmentation such as the Cala Vigatà or Cala Montgó meadows, both of which correspond to perforated meadows (Sleeman et al., 2005). Differences in canopy densities at the gap edges may imply changes in the vulnerability of the meadow to external pressures. For instance, Paquier et al. (2019) found that patchy meadows are not able to attenuate small and short waves. Higher canopy densities, however, are capable of attenuating not only wave velocity but also turbulent kinetic energy, thus providing greater protection (Granata et al., 2001; Hansen and Reidenbach, 2012; Hendriks et al., 2008). Colomer et al. (2017) found that vegetation gaps with greater surrounding plant cover present higher wave attenuation than gaps with lower surrounding plant cover. Lara et al. (2012) found an increase in turbulent diffusion in fragmented habitats of *Z. noltei*. Hence, higher fragmented seagrass meadows may present gap edges with low canopy density which might be more exposed to hydrodynamic processes and, in turn, make them more vulnerable. In contrast, gaps in less fragmented meadows may be more easily

recolonized than gaps in higher fragmented meadows because of the greater shelter provided by the greater density at the gap edges. However, in mixed-species communities, the increase in the resuspended sediments due to the decrease in the shoot density could imply a shift in the associated community composition, with an increase in turbidity tolerant species when the pressure persists over time (Ros et al., 2014; Sagerman et al., 2020). While some authors (Smith et al., 2010) have hypothesised that vegetated patch sizes can influence the magnitude and patterns of the edge effects, this study has proved that gap size modifies the structural vegetation characteristics found at the edges of gaps. In fact, the results of the present study have also proved that the fragmentation of meadows at the meadow-scale produced differential effects at the local scale; in particular, high fragmentation negatively impacted the vegetation around the gaps, especially in the directions where the canopy edge was more exposed to currents and waves. In contrast, because they were sheltered, non-exposed canopy edges remained the same.

Acknowledgments

This research was funded by the "Ministerio de Economía, Industria y Competitividad" of the Spanish Government through the grant CGL2017-86515-P.

CHAPTER 3

Particle capture by seagrass canopies under an oscillatory flow.

Aina Barcelona, Carolyn Oldham, Jordi Colomer, Jordi Garcia-Orellana, Teresa Serra (2021). Particle capture by seagrass canopies under an oscillatory flow. Coastal Engineering 169, 103972. doi: 10.1016/j.coastaleng.2021.103972.

Cover design: Carles Arbat

Abstract

Although seagrass canopies are known to enhance particle sedimentation, there is still limited knowledge about how seagrasses modify the vertical distribution of sediment particles; especially when particles come from allochthonous sources. This study determined the volume of particles trapped by the seagrass leaves, the amount that remains in suspension both within and above the canopy, and the amount deposited onto the seabed. A set of laboratory experiments were conducted in which hydrodynamic conditions and canopy densities were varied to mimic real field conditions. This study demonstrated and quantified previously recorded observations concerning the fate of sediment in seagrass meadows. Seagrass meadows decreased the amount of suspended sediment by capturing the sediment on the blades of the seagrass and by enhancing particle sedimentation on the seabed. However, particles trapped by the blades of seagrass in the whole canopy increased with canopy density and reduced the number of particles in suspension within the canopy. The ecological implications were significant, since a seabed covered by vegetation, when compared to a bare seabed, produced a reduction in the suspended sediment particles within the canopy, improving water clarity. Furthermore, canopies (compared to bare substrates) enhanced seabed sedimentation and the denser the canopy was, the greater the amount of sediment deposited on the seabed.

Keywords*: Seagrass, sediment transport, oscillatory flow, turbulent kinetic energy, sediment capture, sedimentation.*

3.1 INTRODUCTION

Seagrass canopies formed by *Posidonia oceanica* (Linnaeus) Delile or *Cymodocea nodosa* (Ucria) Ascherson are recognized in the EU Water Framework Directive (Todo and Sato, 2002) as water quality indicators as they provide many ecosystem functions and services and maintain the complex structure of habitats (Brodersen et al., 2018; Zucchetta et al., 2016). Species diversity in seagrasses increases with the structural complexity of the seagrass canopies (González-Ortiz et al., 2016). Seagrass meadows also play a role in 'blue carbon' sequestration because suspended particulate organic carbon can be trapped and buried by canopy action, thus mitigating the effect of the ongoing increase in CO_2 (Armitage and Fourqurean, 2016; Ricart et al., 2017). Furthermore, because damage to or the destruction of seagrass meadows can cause a release of carbon to the environment (Fourqurean et al., 2012), in developing 'blue carbon' strategies, management authorities and stakeholders could restore carbon sequestration capacities through coastal restoration projects (Duarte et al., 2015, 2013).

Allochthonous sediment particles transported by currents can impact coastal seagrass meadows negatively and consequently reduce the services they provide (Fraser et al., 2017). Some natural origins of the allochthonous sediment input can be coastal runoff, river plumes or natural resuspension (Pineda et al., 2017). Climate change has led to an increase in the frequency and intensity of heavy precipitation episodes which, in turn, has increased episodic river and runoff outflow (Vautard et al., 2014). Coastal development is also responsible for moving large amounts of sediment that can impact seagrass meadows (Wu et al., 2018). Suspended sediment input increases turbidity in the water column (Pineda et al., 2017;

Roy et al., 2013; Wu et al., 2018), leading to a decrease in light intensity that then limits phytoplankton and seagrass growth, and buries benthic communities (Fraser et al., 2017; Longstaff and Dennison, 1999; Vanderploeg et al., 2007).

Seagrass beds are one of the most valuable habitats in coastal zones because they promote the reduction of suspended particles within the seagrass meadows. Seagrasses affect particle sediment fluxes by reducing flow velocity, increasing sediment deposition and, via the plant leaves themselves within the seagrass canopy capturing particles (Granata et al., 2001; Hendriks et al., 2008), decreasing sediment resuspension (Gacia et al., 1999; Zong and Nepf, 2011). Hence, the allochthonous suspended sediment that is advected over a canopy can remain in suspension in the water column inside the canopy, or settle to the seabed and possibly be resuspended, or be captured by the seagrass. That said, little information is available about the physical role the canopy densities play in trapping particles and thus improving carbon sequestration in coastal waters (Greiner et al., 2016; Marbà et al., 2015). Until now, the effect seagrasses have on the fate of particles from allochthonous sources in coastal areas has been studied observationally. For instance, Lawson et al. (2012) found an increase in the sediment suspended from the seabed in low densities of *Agarophyton vermiculophylla* (Ohmi) Gurgel, although J.N Norris & Fredericq compared this with higher densities. Through field observations, Gacia et al. (1999)determined that, when compared to bare substrates, seagrass meadows promote sediment accretion. Other authors have studied sediment resuspension in laboratory experiments (Ros et al., 2014; Zhang et al., 2018; Zhang and Nepf, 2019). Ros et al. (2014), for example, found that the presence of vegetation produced a decrease in resuspension and an increase in sediment deposition compared to bare seabeds. Sediment

resuspension is reduced in dense model canopies because of the attenuation of the turbulent kinetic energy (TKE) (Bos et al., 2007; Gacia et al., 1999; Ros et al., 2014; Zhang et al., 2018). However, none of these studies quantifies the amount of sediment particles captured by plant leaves or how particles settling onto the seabed is enhanced by the presence of vegetation.

Hendricks et al. (2008) did, however, find that there was a reduction in resuspended sediments within a seagrass canopy compared to bare or eroded grasslands, not only because of reduced hydrodynamic energy, but also because of reduced particle transport due to the energy loss caused by collisions with seagrass leaves. Different rates of reduction in the suspended sediment were also found for different types of *Caulerpa* sp. and seagrass canopies (Hendriks et al., 2010), indicating the role the distinct architectures found within the canopy has in the behaviour of suspended particles. Furthermore, the particle retention by a single cylindrical collector was also quantified and found to increase as the diameter of the collector increased (Palmer et al., 2004). Short and Short (1984) also found a smaller overall turbidity in seagrasses with higher leaf surface area, indicating the potential role the leaves have in reducing water turbidity. In their study, however, no quantification of the sediment deposited on the leaves was carried out. Terrados and Duarte (2000) conducted experiments with leaf detritus samples situated within a seagrass bed and on an unvegetated bed and demonstrated that seagrasses reduce particle resuspension compared to bare sandy beds. Lovelock et al. (2014) found that, because of a higher sediment input in saltmarshes compared to areas of mangroves, a greater accumulation of carbon occurred in the saltmarshes. Howe et al. (2009) also found a higher carbon sequestration in undisturbed saltmarshes compared to disturbed

saltmarshes, with the increase in the carbon sequestration in undisturbed saltmarshes being driven by greater rates of vertical accretion. Finally, Agawin and Duarte (2002) studied the capture of particles by seagrass leaves in the field and observed that some of the suspended particles were phagocyted by the seagrass epiphytes found on the leaves of the plants. However, in their study they did not explore the role hydrodynamics play in capturing particles.

Despite the availability of all these studies concerning particle dynamics within a seagrass meadow, there are still no studies that address and quantify the effect of the canopy density and the trapping (capturing) of particles by seagrass leaves from allochthonous sources under different hydrodynamic conditions. Therefore, and considering that the fate of allochthonous particle sedimentation in seagrass canopies is not yet fully understood, or that most current findings have been obtained from field observations, the aim of this study was to identify and quantify the role seagrasses have in capturing sediments. To understand the ecological implications, laboratory experiments were carried out to: i) study how sediment particles of different sizes are trapped by plant leaves under different hydrodynamic conditions, ii) examine the suspended sediment concentration within and above the canopy and iii) determine the sedimentation on the seabed of different sized particles. Special attention was paid to the behaviour of the particle sizes for both particle trapping by plant blades, and sedimentation onto the seabed.

3.2 METHODOLOGY

3.2.1 The flume

The study was carried out in a methacrylate flume (600 x 50 x 50 cm; Figure 1) with a mean water depth of h=30 cm (Table 3.1). A vertical flap-type wavemaker was driven by a variable-speed motor at two frequencies (0.7, 1.2 Hz) and four strokes (12, 14, 16, and 18 cm). The wave lengths (λ) were calculated using the dispersion equation by Le Méhauté (1976), as $\lambda = 2.43$ m for f = 0.7 Hz and $\lambda = 1.03$ m for f = 1.2 Hz. These wave conditions, $\lambda/20 < h < \lambda/2$, corresponded to transitional water waves like those typically found in coastal regions (Serra et al., 2018) with the presence of seagrasses. The waves produced had amplitudes in the range A=2-4 cm. Therefore, $2A/\lambda = 0.08$, which is below the threshold of 0.14 and corresponds to breaking waves. However, while these waves fell far from the linear Stokes waves, they did correspond to third order Stokes waves, i.e., closer to the breaking limit than linear waves (Le Méhauté, 1976). Third order Stokes waves have been found to produce instabilities at the water surface (in the form of spilling) for $2A/\lambda = 0.10$, thus producing turbulence that is transported downwards in the water column (Iafrati, 2011). The waves used here had $2A/\lambda = 0.08$; close to the threshold found by Iafrati (2011). Therefore, although spilling was not observed through visual inspection, some TKE production at the surface could hold. The presence of seagrasses has been found from 1 m to nearly 18 m depths depending on the light attenuation (Duarte, 1991). From these above-mentioned considerations, the scaling of the vegetation in the flume could represent the behaviour of seagrasses in coastal areas. The combination of frequencies and strokes yielded eight wave amplitudes (A = 1.5, 2.0, 2.2, 3.0, 5.0, 5.6 cm). A plywood beach with a slope of 1:3 and

covered with a 7 cm thick layer of foam rubber was positioned at the end of the flume to eliminate wave reflection (Pujol et al., 2019, 2013b). The wavemaker was situated at x = 0 cm in the longitudinal direction, the centre of the tank at y = 0 cm in the lateral direction, and the flume bed at z = 0 cm in the vertical direction.

To mimic the injection of sediment particles from an allochthonous source, a methacrylate pipe (Internal diameter, ID = 3 cm, length = 300 cm) with 43 evenly distributed injectors (ID = 0.5 cm, length = 8.6 cm, 7 cm apart) was used to inject sediment-laden water (see Section 3.2.3) into the flume. The end of each injector was covered with a 1 mm mesh to slow down injection rates. The injection pipe was situated outside the water column so that the injectors protruded 5 cm into the water surface as the injection was carried out.

Throughout this study, an allochthonous sediment source is considered as the sediment input from outside the meadow. In the discussion, the results obtained will be compared to other studies carried out on the resuspension of sediment already deposited on the seabed, i.e., not coming from outside the meadow and therefore considered as autochthonous sediment.

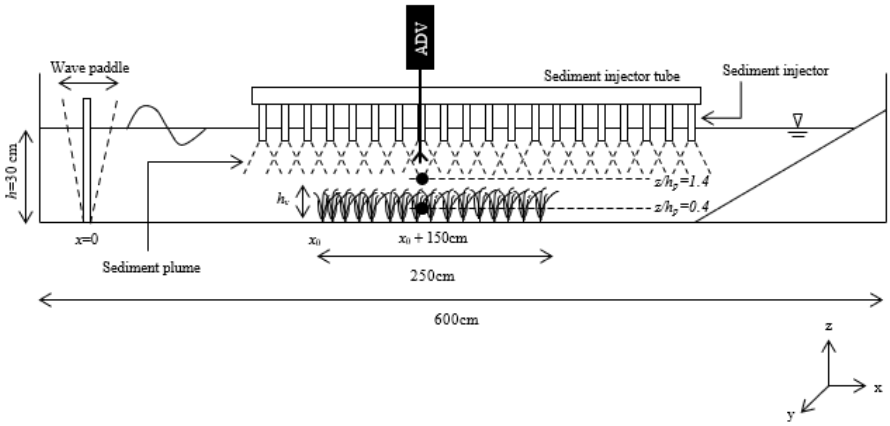

Figure 3.1 A lateral view of the experimental setup. Experiments were conducted in a 600x50x50 cm long flume, with a mean water depth of 30 cm. The model canopy was 250 cm long and canopy height was h_p = 14 cm. Filled circles show where both hydrodynamics and sediment measurements were taken. The triangle at the water-air interface represents the water level in the flume.

3.2.2 The canopy

Each plant in the canopy was made up of eight 0.075 mm-thick polyethylene canopy leaf blades attached to PVC dowels that had been randomly inserted into a perforated baseboard (L = 250 cm, Pujol et al., 2013a). The rigid dowel extended 1 cm above the bed (Zhang et al., 2018) and the canopy leaf blades were geometrically and dynamically similar to those of *Posidonia oceanica* (Folkard, 2005; Ghisalberti, 2002; Pujol et al., 2013a). The canopy height was h_p = 14 cm, however, the effective height when the leaf blades were bent by the waves was h_v = 13 ± 1 cm. The initial position of the vegetation (x_0) was situated 100 cm from the

wavemaker (Figure 3.1). The canopy density was quantified using the solid plant fraction (SPF) defined as:

$$\text{SPF}\ (\%)=100n\pi\left(\frac{d}{2}\right)^2 \qquad (3.1)$$

where n is the number of stems per unit area and d is the stem diameter (1 cm). Five SPFs were used (0%, 1%, 2.5%, 5% and 7.5%), which corresponded to canopy densities n= 0, 127, 318, 637 and 955 stems·m^{-2} (Figure 3.2) which fall within the range 78 to 1000 stems·m^{-2} found in the field (Folkard, 2005; Ghisalberti, 2002; Goring and Nikora, 2002; Hendriks et al., 2008; Zhang and Nepf, 2008). SPF=0% corresponded to unvegetated beds. Two frequencies and eight wave amplitudes varied across the five SPFs resulted in a total of 40 experiments (Table 3.2), each 90 minutes in duration.

The fractional volume occupied by the plants (ad) for each canopy density was calculated as the frontal area of the plant per unit volume, a, multiplied by the stem diameter, d (Zhang and Nepf, 2008). Greyscale photographs taken from the top of the canopy were analysed to calculate canopy cover in the absence of wave motion (Serra et al., 2018). The five canopy densities corresponded to a canopy cover of 0, 37.4, 52.1, 70.6 and 80.9% (Figure 3.2) and the photographs determining the cover were taken in the absence of wave motion. Canopy cover followed a non-linear trend with the fractional volume (Figure 3.2e) cover = 207*ad$^{0.4}$, indicating that full cover (100%) occurred at ad = 0.16, corresponding to an SPF of 12.5% and a canopy density of 1592 stems·m^{-2}.

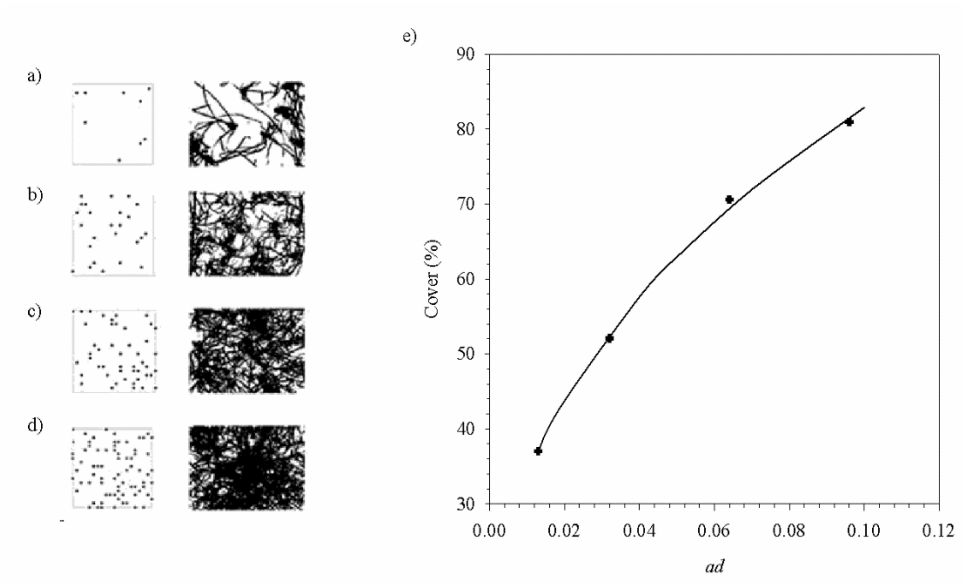

Figure 3.2 Plant distribution for the different SPFs a) 1%, b) 2.5%, c) 5%, and d) 7.5% on the PVC bases (left panels) and black and white digitized photography (right panels). e) is the relationship between the canopy cover (%) and the volume plant fraction (ad).

Table 3.1 Summary of the wave and vegetation parameters for each experiment.

Run	Canopy model	SPF (%)	n (stems·m^{-2})	Coverage (%)	ad	S_b (cm)	F (Hz)	λ (m)	A (cm)	A_w (cm)
WP1	Without vegetation	0	0	0	0		0.7	2.43	2.0	0.91
WP2									2.2	1.43
WP3									2.0	2.02
WP4									1.5	2.16
WP5							1.2	1.03	3.0	1.82
WP6									3.2	1.63
WP7									5.0	1.96
WP8									5.6	2.55
SFV9	Submerged flexible vegetation model	1	127	37	0.013	3.14	0.7	2.43	2.0	0.98
SFV10									2.2	0.65
SFV11									2.0	2.70
SFV12									1.5	2.18
SFV13							1.2	1.03	3.0	2.70
SFV14									3.2	1.24
SFV15									5.0	1.21
SFV16									5.6	1.11
SFV17		2.5	318	52	0.032	1.98	0.7	2.43	2.0	1.43
SFV18									2.2	0.80
SFV19									2.0	2.82
SFV20									1.5	2.83
SFV21							1.2	1.03	3.0	1.52
SFV22									3.2	1.39
SFV23									5.0	1.66
SFV24									5.6	1.77
SFV25		5	637	71	0.064	1.40	0.7	2.43	2.0	0.45
SFV26									2.2	1.18
SFV27									2.0	1.54
SFV28									1.5	1.51

Run		SPF (%)	n (stems·m^{-2})	Coverage (%)	ad	S_b (cm)	F (Hz)	λ (m)	A (cm)	A_w (cm)
SFV29							1.2	1.03	3.0	1.39
SFV30									3.2	1.61
SFV31									5.0	1.55
SFV32									5.6	1.96
SFV33		7.5	955	81	0.096	1.14	0.7	2.43	2.0	1.09
SFV34									2.2	0.61
SFV35									2.0	0.75
SFV36									1.5	1.56
SFV37							1.2	1.03	3.0	1.67
SFV38									3.2	1.82
SFV39									5.0	1.69
SFV40									5.6	1.72

3.2.3 Measuring velocities

The Eulerian velocity field was defined as (u, v, w) in the (x, y, z) directions, respectively. The three components of velocity were recorded (at a frequency of 50 Hz over 10 min) with a downwards-looking Acoustic Doppler Velocimeter (16-MHz MicroADV, Sontek). The ADV measures at a distance of 5 cm from the probe tip, and with a sampling volume of 0.09 cm^3. Beam correlations less than 80% were discarded and spikes were removed (Goring and Nikora, 2002; Pujol et al., 2013a). The number of spikes increased slightly with the presence of the plants and the canopy density compared with the unvegetated case. The percentage of spikes was from 0.33% for the unvegetated case to 0.77% for the most densely vegetated case.

To eliminate the lower order spatially periodic variation in wave and velocity amplitude associated with wave reflection (Luhar et al., 2010;

Pujol et al., 2013a), the longitudinal velocity was measured at an antinode. The model canopy was then shifted longitudinally along the flume to ensure measurements were taken 150 cm from the canopy edge. For the densest canopy experiments, some plants were removed and re-inserted into nearby holes to avoid blocking the ADV beams (Colomer et al., 2017; Pujol et al., 2010; Zhang et al., 2018; Zhang and Nepf, 2019).

3.2.4 Velocity and turbulent kinetic energy analysis

For oscillatory flows, the instantaneous velocity, $U_i(t)$, can be decomposed as:

$$U_i(t)=U_c+ U_w+ u' \tag{3.2}$$

where U_c is the steady velocity associated with the current, U_w is the unsteady wave motion which represents spatial variations in the phase-averaged velocity field, and u' is the turbulent velocity, that is, the instantaneous velocity fluctuation in the x-direction. U_c is the phase-averaged velocity:

$$U_c= \frac{1}{2\pi}\int_0^{2\pi} U_i(\varphi)\partial\varphi \tag{3.3}$$

where $U_i(\varphi)$ is the instantaneous velocity according to the phase (Lowe et al. 2005, Luhar et al. (2010). Wave velocity, U_w, was obtained by using a phase averaging technique. The Hilbert transform was used to average oscillatory flow velocities with a common phase (Pujol et al., 2013a; Ros et al., 2014). The root mean square (rms) of $U_i(\varphi)$ was considered as the characteristic value of the orbital velocity U_w^{rms} (U_w hereafter) at each depth, and was calculated according to:

$$U_w^{rms} = \sqrt{\frac{1}{2\pi}\int_0^{2\pi}(U_i(\varphi)-U_c)^2 \partial\varphi} \qquad (3.4)$$

For cases WP5 and SFV37, vertical profiles of the velocity were taken from which the wave velocity and turbulent kinetic energy profiles were calculated (Figure 3.3). The wave velocity decreased from the layer above the canopy to the bed. From the vertical profile of the wave velocity, two vertical regions were differentiated: the above-canopy layer and the within-canopy layer (Figure 3.3a). In the above-canopy layer, the wave velocity was the highest with similar results compared to the without-plants case. In the within-canopy layer, the velocity decreased gradually with depth until z = 5 cm (z/h_v=0.4) where the wave velocity remained nearly constant down to the bottom. In this layer, the velocity in the presence of plants was lower than that in the without-plants case.

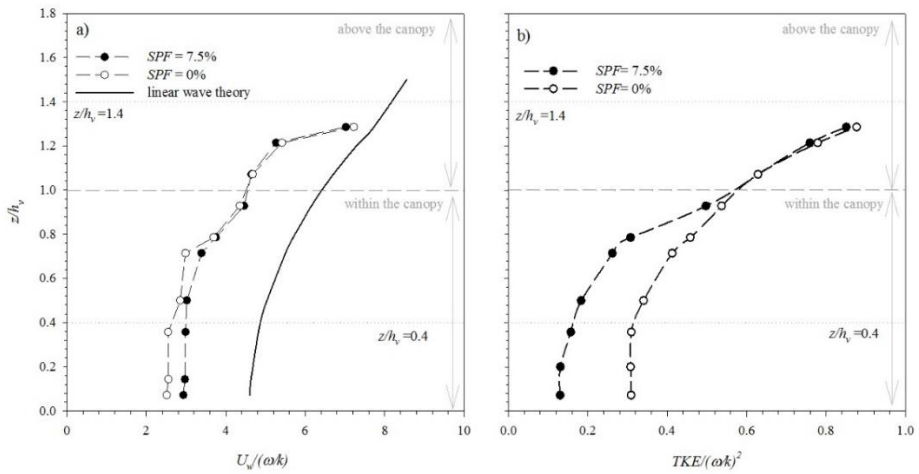

Figure 3.3 Vertical profiles of both the wave velocity $U_w/(\omega/k)$, where $\omega=2\pi f$ and $k=2\pi/\lambda$ (a) and the turbulent kinetic energy $TKE/(\omega/k)^2$ (b) for SPF = 0% (unfilled circles), SPF = 7.5% (filled circles) and the linear wave theory (solid line). The dashed line shows the top of the plant blades and the dotted lines show

the level where the measurements were taken. The vertical axis represents the non-dimensional depth z/h_v.

The turbulent velocity was obtained by:

$$u' = U_i - U_c - U_w \tag{3.6}$$

where U_c and U_w were calculated by Eqs. (3.3) and (3.4). The same methodology was used to calculate the other two turbulent velocity components (v' and w').

The turbulent kinetic energy (TKE) was calculated following Ros et al. (2014) as:

$$TKE = \frac{1}{2}\left(\langle u'^2\rangle + \langle v'^2\rangle + \langle w'^2\rangle\right) \tag{3.7}$$

where < > denotes the time average.

Like U_w, the TKE decreased with depth (Figure 3.3b) and the same two vertical layers (above-canopy and within-canopy) can be distinguished. The above-canopy layer presented similar TKE for both the with and without-plants experiments. Within the canopy, the TKE decreased compared to the without-plants experiments. From the results of the vertical profiles of both U_w and TKE, the depth of z = 5 cm was considered representative of the hydrodynamics of the within-canopy layer, and the depth of z = 20 cm representative of the hydrodynamics of the above-canopy layer. Therefore, for the rest of the experiments carried out, the current velocity was measured at these two vertical positions: z = 20 cm (z/h_v= 1.4, above the canopy) and z = 5 cm (z/h_v=0.4, within the canopy). Within the canopy layer (at z/h_v=0.4), the mean flow velocity was U_c=-0.04 cm s^{-1} and -0.10 cm s^{-1} for non-vegetated experiments and for the wave frequencies of f=0.7 Hz and f=1.2 Hz, respectively. For experiments

with vegetation, and at the same depth, the mean flow velocity among all the experiments as U_c=-0.22 cm s^{-1} for f=0.7 Hz and -0.25 cm s^{-1} for wave frequencies f=1.2 Hz. These flow velocities were negative in all the cases, indicating that they were directed towards the wave maker. They have lower values than those found in the experiments of Luhar et al. (2010), where they used a paddle type wave maker with frequencies of 0.5 Hz and U_c at this depth was directed towards the beach. In this present study, a flap-type wave maker was used, and higher wave frequencies were considered. This study gives similar results and directions for U_c as those found by (Pujol et al., 2013a) for the same type of wave maker and frequencies of 1 Hz and 1.4 Hz.

3.2.5 Sediment-laden injection

A synthetic dust powder (ISO 12103-1. A4 Coarse, Powder Technology Inc. Burnsville) was used as the sediment in the experiments. The volumetric concentrations of suspended sediment (in $\mu L \cdot L^{-1}$) were analysed using the LISST-100X (Laser In-Situ Scattering and Transmissometry, Sequoia Scientific, Inc, Bellevue, WA) particle size analyser. The LISST-100X consists of a laser beam and an array of detector rings of progressive diameters which allow the light received at the scattering angles of the beam to be analyzed. The device measures particle volume concentrations for 32 size-classes, (logarithmically distributed in the size range of 2.5-500.0 μm), using a procedure based on the diffraction theory of light. The LISST-100X has been found to perform well when determining particle size distribution and concentration for both organic (Serra et al., 2018) and inorganic particles (Serra et al., 2002b, 2002a)suspended in water. This instrument can be used in situ in the field, where it can be submerged in the water, or it can be employed in the

laboratory to measure small samples by using a measuring chamber. For laboratory use, the water sample has to have a volume between a minimum of 80 ml (to ensure the detector is completely covered) and a maximum of 100 ml (the maximum volume of the measuring chamber). The particle size distribution of the sediment used was bimodal, with fine particles, 2.5 - 6.0 µm in diameter, corresponding to strongly cohesive clay and very fine silts with a median D50 = 3.78 µm and making up 30% of the sediment, and coarse particles, 6.0 - 122 µm in diameter, corresponding to weakly cohesive fine to coarse silts and small sand particles with a median of D50 = 27.6 µm making up 70% of the sediment (Figure 3.4). The concentration of the particles in each size-class was calculated by the sum of the volume concentrations of the particles ranging between 2.5 – 6.0 µm for the fine particles and between 6.0 – 122.0 µm for coarse particles (Figure 4). The particle concentration will be expressed in volume concentrations in the whole manuscript to mitigate for the quantity of fine particles in every sediment mixture being higher than the coarse particles.

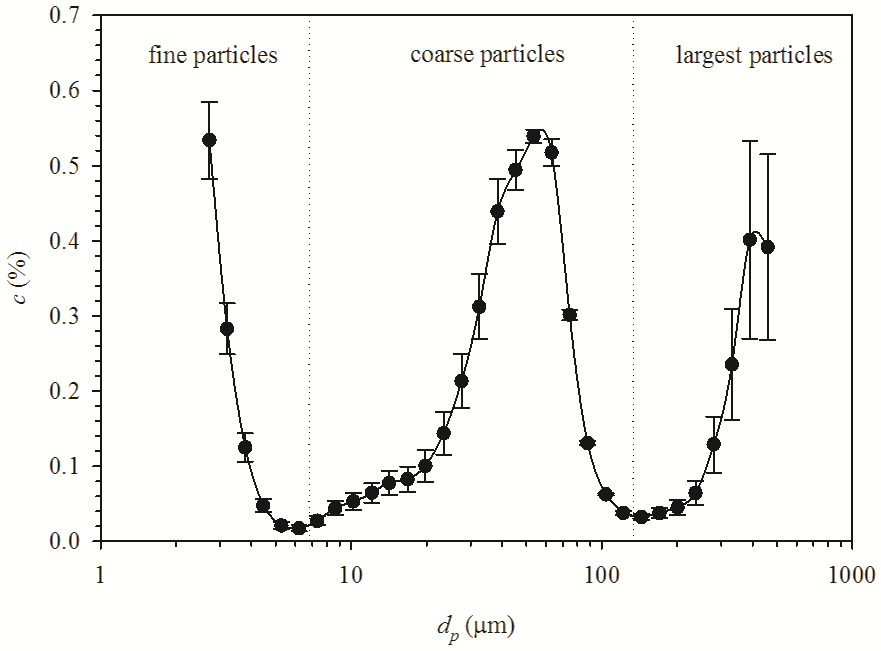

Figure 3.4: Sediment particle distribution in %. Three different particle sizes are shown: fine particles below 6 µm, coarse particles between 6 to 122 µm, and the largest size particles over 122.0 µm.

Before the injection, the wavemaker was started and left to run for 60 minutes to allow the system to reach equilibrium. After this time had elapsed, the particle-laden flow to be used in the injection was prepared with an initial volume (2 L) of sediment suspension (with a concentration of 40 $g \cdot L^{-1}$) introduced into one end of the sediment-injection pipe. The injection pipe was situated at y = 0 along the axis of the flume (Figure 3.1). While introducing the sediment into the pipe, the injectors faced upwards to avoid any uncontrolled spillage. Once the pipes had been filled with the sediment suspension, they were closed and then turned to face downwards with their ends protruding 5 cm below the water surface, thus producing an even release of suspended sediment along the flume. After 18 s, individual injector plumes started to merge. The injection of sediment

lasted less than 1.5 min. The sediment mass from the injection produced a total suspended sediment concentration (c_s) in the flume within the range 5-14 $\mu L \cdot L^{-1,}$, which coincides with the typical sediment concentration discharges, 4-400 $\mu L \cdot L^{-1}$, of river plumes in coastal waters (Mulder and Syvitski, 1995). A river plume in the Bay of Bengal was found to discharge concentrations in the range of 0.4 $\mu L \cdot L^{-1}$ to 20.7 $\mu L \cdot L^{-1}$ (Sridhar et al., 2008), also in a range similar to that in the present study.

The length scale, L_M (Colomer et al., 1999), was used to calculate the 'plume' or 'jet' nature of the injection. L_M indicates the distance up to where the injected fluid behaves as a jet and was calculated as:

$$L_M = \frac{M_O^{3/4}}{Q_O^{1/2}} \tag{3.9}$$

where M_o was the volume flux and Q_o was the momentum flux. Mo was calculated as:

$$M_O = \frac{\pi D^2 w_o^2}{4} \tag{3.10}$$

where D is the inner diameter of the injectors and w_o is the injection velocity, calculated as:

$$w_o = \frac{Q}{n_{inj} A_{inj}} \tag{3.11}$$

where Q is the injection flow, n_{inj} is the number of injectors and A_{inj} is the injector area.

Q_o was calculated as:

$$Q_o = \frac{\pi D^2 B_o}{4} \tag{3.12}$$

where Bo is the buoyancy flux per unit area, calculated as:

$$B_o = \Delta b_o w_o \quad (3.13)$$

where Δb_o is the buoyancy of the resulting plume fluid, calculated as:

$$\Delta b_o = \frac{(\rho_s - \rho_w)g}{\rho_w} \quad (3.14)$$

where ρ_s=2500 kg m^{-3} is the sediment density, ρ_w=1000 kg m^{-3} is the water density and g=9.8 m s^{-2} is the gravitational acceleration.

Merging equations (3.9), (3.10), (3.11), (3.12), (3.13) and (3.14) resulted in L_M= 0.025 cm. Therefore, the injection behaved like a jet for distances up to 0.025 cm from the injector and then plume-like once it got further away than that. As the water depth was 30 cm and the plants extended up 14 cm, the possibility the injectors being a source of turbulence within the canopy was discarded and the plume character of the injector was demonstrated. In addition, a test for the effect the injection has on the TKE measurements was carried out. That is, the TKE was measured with and without the injection. The TKE with the injection increased by 5.5%, which is within the standard deviation measured for the TKE. In addition, the injection time was less than 1.5 mins, representing 1.2% of the total running period of the sediment study. Therefore, any effect the injection might have had on the measuring point was disregarded.

3.2.6 Sediment measurements

In the first test, two transversal points (situated 25 cm apart) and two longitudinal (1 m apart) were considered for the particle concentration measurements and confirmed that, after 1.5 minutes of injection, the suspended sediment was not only homogeneously mixed in both the longitudinal and transversal directions of the flume with maximum

differences of 0.06 μL L^{-1} but was also below the standard deviation obtained for the measurements of the concentration at one single point (of 0.20 μL L^{-1}). Therefore, the samples of sediment were taken at y=0 and at the same x-position where the hydrodynamics were measured (x=150 cm from the edge of the canopy). The concentration of suspended sediment c_t ($\mu L \cdot L^{-1}$), was measured at the same water depths (z/h_v = 0.4 and at z/h_v = 1.4) considered representative for the hydrodynamics in both the above-canopy and the within-canopy layers (Figure 3a and b). Water samples, 20 mL in volume, were collected with a pipette from these two depths at different time steps t = 1, 5, 15, 30, 45, 60 and 90 minutes, and analysed for suspended sediment concentration. As the samples were not returned to the flume, this represented a total volume decrease of 280 mL (a 0.03% decrease in the total volume of the water volume) during the running time of the experiment. This change in the water volume produced a negligible change in the water height (<0.05 cm). The time evolution for the sediment concentration, c_t, decreased and reached the steady state (c_s) at t = 60 min (T_s, Figure 3.5). At the end of the experiment (t =90 min), ten model plants were gently removed from different evenly separated positions within the meadow and introduced into a beaker with a volume of 80 mL of water. The plants were then stirred in the fluid to remove the sediment trapped by the surface of the blades, after which particle concentration (c_p) was analysed with the particle size analyser (LISST-100X).

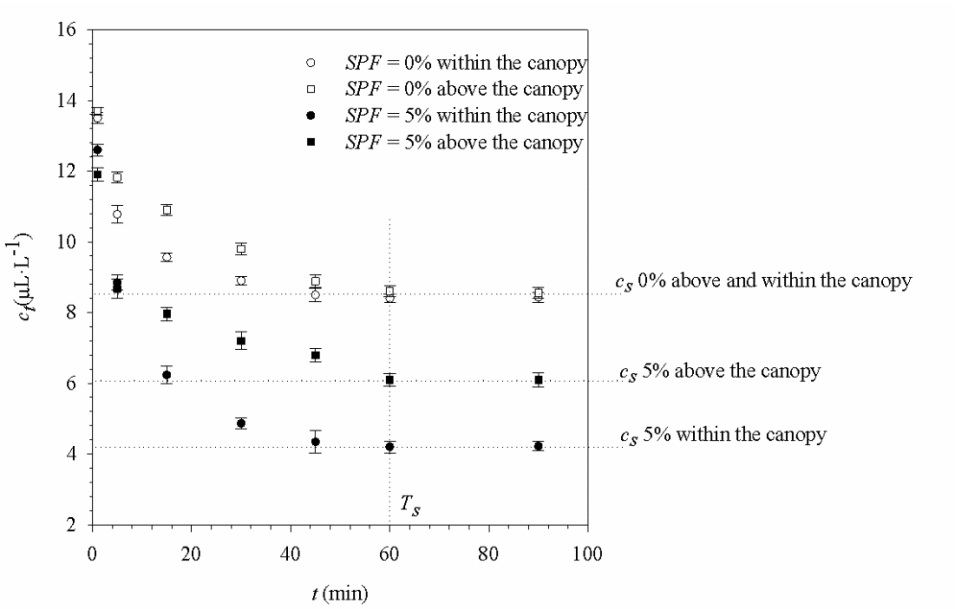

Figure 3.5 Decline in suspended sediment concentration, ct, with time, comparing experiments with canopy (SPF 5%) and at the equivalent heights in experiments without canopy (SPF 0%). Sediment concentrations were measured above the canopy (z/h_p = 1.4) and inside the canopy (z/h_p = 0.4). The vertical dashed line indicates the time (T_S) to reach steady state conditions, while the horizontal dashed lines indicate steady state sediment concentrations (c_s).

3.2.7 Sediment mass balance

A conceptual model was developed for the canopy system with four sediment compartments based on the hydrodynamics (Figure 3.3): sediment suspended within the canopy (S_C), sediment suspended in the water above the canopy (S_W), sediment attached to the leaf blades (S_P), and sediment settled at the bottom of the tank (S_B). For suspended sediments, the concentrations measured within each compartment were mutiplied by the volume of the compartment to estimate the volume (in

μL) of the suspended sediments in that compartment. To determine the total volume of sediment attached to the plant blades (μL), measured particle concentrations were normalised per plant and then multiplied by the total number of plants in the canopy (which varied with SPF). The volume of particles settled to the bottom was not directly measured, instead it was calculated as the difference between the total volume injected and the sum of the suspended particle volume and the volume attached to plants.

V_{IN} is the total volume injected, distributed in the region occupied by the canopy, calculated by multiplying the injected sediment mass by the volume of the canopy and divided by the total volume of the flume. Finally, the injected mass was converted to volume units using the sediment density (2500 $kg \cdot m^{-3}$). The injected volume was fractionated into fine and coarse particles using the previously-determined particle size distribution.

A volume balance was then determined as:

$$V_{IN}^{F} = V_{SC}^{F} + V_{SW}^{F} + V_{SP}^{F} + V_{SB}^{F} \quad (3.15)$$

where V_{IN}^{F} is the volume of fine particles injected above the canopy, V_{SC}^{F} is the volume of suspended fine sediment inside the canopy, determined at z/h_v=0.4, the volume inside the canopy corresponded to the water volume, which is inside the area and height of the vegetation, V_{SW}^{F} is the volume of suspended fine sediment in the water above the canopy, determined at z/h_v=1.4, V_{SP}^{F} is the volume of sediment captured by the plants, and V_{SB}^{F} is the volume of fine sediment settled to the bottom. An equivalent volume balance was made for coarse sediments:

$$V_{IN}^{C} = V_{SC}^{C} + V_{SW}^{C} + V_{SP}^{C} + V_{SB}^{C} \quad (3.16)$$

3.3 RESULTS

Differences in the turbulent kinetic energies were found between the bare substance and sparse and dense canopies. The results of the turbulent kinetic energy averaged over all the experiments carried out with different wave amplitudes and the same frequency and SPF are referred to as the mean turbulent kinetic energy (<TKE>). The <TKE> decreased gradually with the canopy cover for both wave frequencies. Considering the error margin, no differences in the TKE were obtained between the two frequencies studied (0.7 and 1.2 Hz) (Figure 3.6). The reduction in the <TKE> for sparse canopies and dense canopies ranged from 14%-35% to that of the <TKE> of the bare substrate.

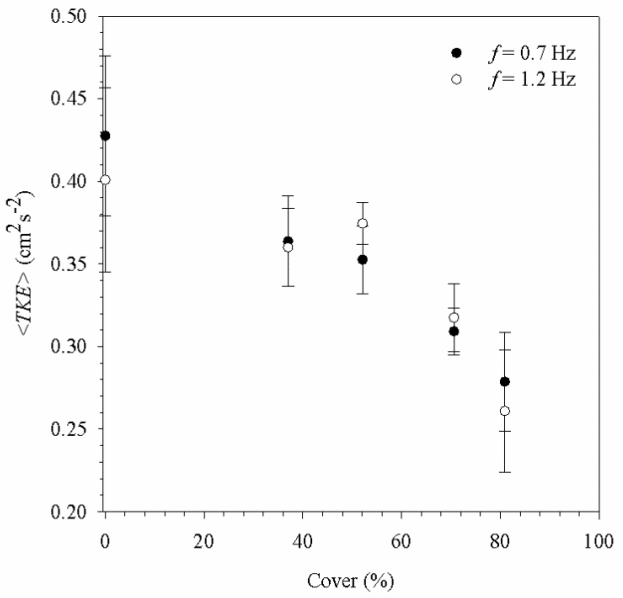

Figure 3.6 TKE values within the canopy averaged over the experiments, <TKE> with the same canopy density (SPF) versus the canopy cover for both the high frequency (1.2 Hz, unfilled circles) and the low frequency (0.7 Hz, filled circles) experiments.

The suspended sediment concentrations at steady state, c_s, for both fine and coarse particles, were linearly dependent on TKE (Figure 3.7a). Since the TKE depended on the cover, the average of the steady state concentrations ($<c_s>$) over the same cover experiments for both fine and coarse particles decreased as canopy cover increased (Figure 3.7b). The sediment trapped by the surface of the blades of each plant, c_p, was also analysed, (as described in Methods), and quantified as the concentration of sediment in the wash-off liquid. The coarse particles captured by each plant showed similar linear relationships with TKE as those observed for the steady state suspended sediment concentrations (Figure 3.7c) In contrast, the concentration of fine particles trapped by the blades of the plants was independent of the TKE (Figure 3.7c). The average of the particle concentration trapped by the plants in the whole canopy ($<c_p>$)

was calculated for each canopy cover and increased as the canopy cover increased (Figure 3.7d).

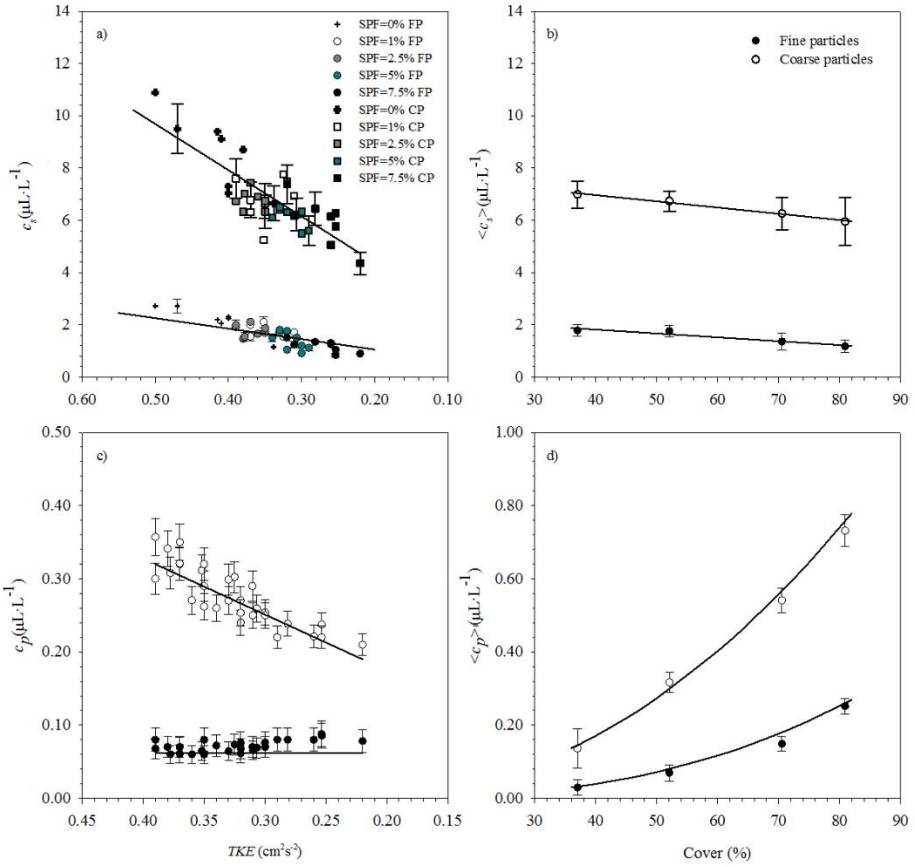

Figure 3.7 a) Steady state suspended sediment concentration, c_s, versus TKE, with variable SPF. Circles correspond to fine particles (F_P) and squares to coarse particles (C_P). Fine and coarse particles follow a linear trend with the expressions: c_s =17.69*TKE+0.84 (with a R^2 = 0.681 and 99% of confidence) and c_s =6.69*TKE-0.74 (with a R^2 = 0.742 and 99% of confidence), respectively; b) Steady state suspended sediment concentration averaged over the experiments with the same canopy cover versus canopy cover for fine particles (filled circles) and coarse particles (unfilled circles). The linear trends for fine and coarse particles are: $<c_s>$=-0.01*Cover+2.41 (with a R^2=0.919 and 95% of confidence) and $<c_s>$=-0.02*Cover+7.91 (with a R^2=0.988 and 99% of confidence),

respectively; c) Sediment captured by each plant c_p, for fine and coarse particles versus TKE. Coarse particles follow the linear trend expression: c_p=1.23*TKE–0.13 (with R^2=0.673 and 99% of confidence); d) Mean sediment concentration captured by all the plants in the canopy averaged over all the experiments with the same canopy cover versus canopy cover for fine and coarse particles. The potential trend expression followed by coarse particles is: $<c_p>=7*10^{-5}*Cover^{2.11}$ (with R^2=0.994 and 99% of confidence) and fine particles follow the expression: $<c_p>=2*10^{-6}*Cover^{2.68}$ (with R^2=0.994 and 99% of confidence). Vertical error bars represent the standard deviation in the concentration obtained by different measurements of the concentration for the same experiments. In Figure 3.7a, only some error bars have been shown to provide a clear plot of the data.

For all the experiments, the volume of fine and coarse sediment particles was calculated as outlined in the methodology. For example, the volume of particles suspended within the canopy was calculated by multiplying the concentration of suspended particles at z=0.4 h_p by the volume of the region occupied by the canopy. For the non-vegetated case, the volumes of the fine, $\mathbf{V_{SC}^F}$ (Figure 3.8a) and coarse, $\mathbf{V_{SC}^C}$ (Figure 3.8b) particles that remained in suspension in the bottom portion of the water where the canopy was present for the vegetated cases, were greater than those of the vegetated cases. Also, in both cases the volumes of the fine $\mathbf{V_{SP}^F}$ (Figure 3.8a) and coarse $\mathbf{V_{SP}^C}$ (Figure 3.8b) particles trapped by plant blades increased as the cover increased. The increase in the particles trapped by plant blades in the whole canopy, $\mathbf{V_{SP}}$, coincided with a decrease in $\mathbf{V_{SC}}$. The volume of suspended sediment above the canopy for both the fine and coarse particles ($\mathbf{V_{SW}^F}$ and $\mathbf{V_{SW}^C}$) decreased with the increase in canopy cover. Finally, the sedimentation (V_{SB}) to the bottom increased as the canopy density increased and ranged from 75% to 80% for fine particles

over the total volume of fine particles and from 57% to 60% for coarse particles over the total volume of coarse particles (following equations 15 and 16). For the non-vegetated cases, the sedimentation to the bottom was lower than that for vegetated cases, around 70% for fine particles and around 46% for coarse particles (Figures 3.8a, b). In each case, the percentage is given over the total amount per each particle range.

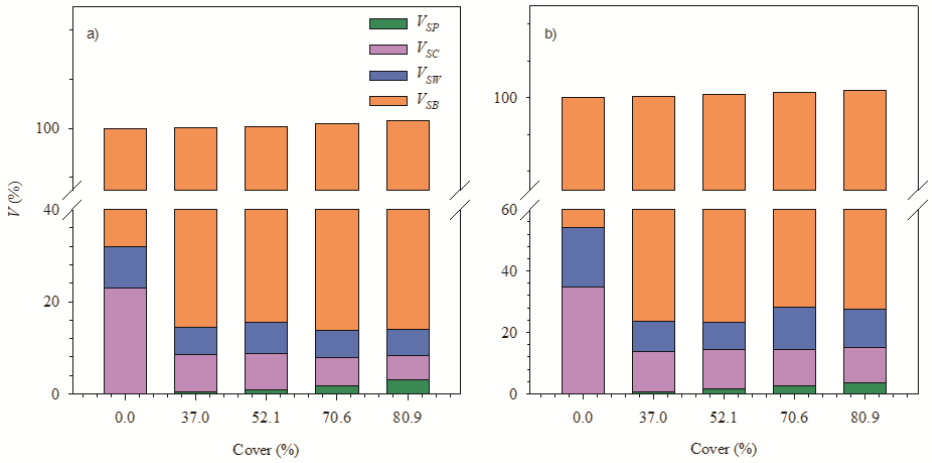

Figure 3.8 Sediment volume balance (V) of the volume trapped by the blades (V_{SP}), volume inside the canopy (at $z/h_p = 0.4$) (V_{SC}), volume above the canopy (at $z/h_p = 1.4$) (V_{SW}) for different covers for fine particles (a) and for coarse particles (b), and volume deposited to the bottom (V_{SB})

The partition coefficient (P_C) between the sediment trapped by the plant blades and the suspended sediment inside the canopy (V_{SC}) was calculated as:

$$P_C = \frac{V_{SP}}{V_{SC}} * 100 \qquad (3.17)$$

P_C decreased linearly with <TKE> for both fine and coarse particles (Figure 3.9a). For <TKE> above 0.36 cm^2s^{-2}, corresponding to cover

percentages <52%, the P_C for fine and coarse particles did not present any differences. For high canopy covers, the partition coefficient was greater for fine particles (Figure 3.9b) than for coarse particles. For the highest cover, P_C was 50% for fine particles, i.e., $V_{SP}^{F} = 0.5V_{SC}^{F}$, which indicates that the volume of particles captured by the leaf blades is half that remaining in suspension inside the canopy. P_C was 30% for coarse particles, i.e., $V_{SP}^{C} = 0.3V_{SC}^{C}$ (Figure 3.9b).

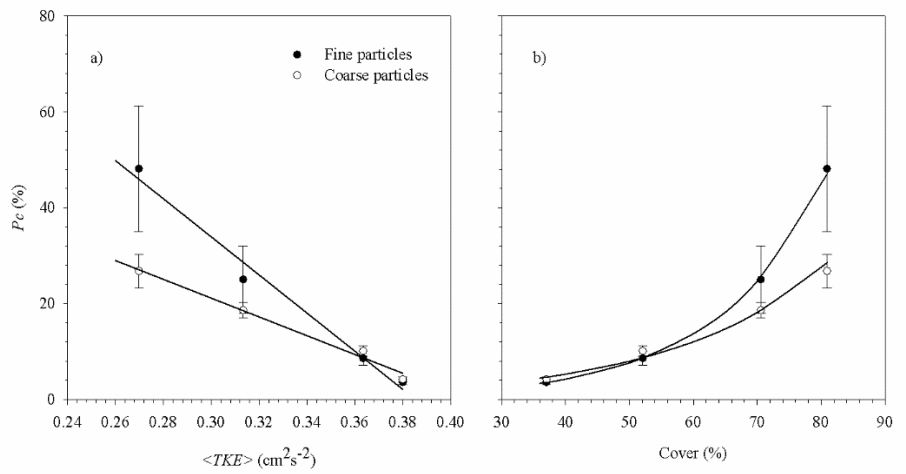

Figure 3.9 a) Partition coefficient of the sediment trapped by the blades versus the <TKE> for fine particles (filled circles) and for coarse particles (unfilled circles). <TKE> is the mean value of the TKE averaged over the experiments with the same cover. Fine and coarse particles follow a linear trend with the expressions: Pc=-397.8*<TKE>+153.3 (R^2=0.981 and 99% of confidence) and Pc=-196.2*<TKE>+80.0 (R^2=0.995 and 99% of confidence), respectively; b) Partition coefficient for the sediment trapped by blades for the two particle size ranges versus the cover. The relationship between Pc and the cover showed an exponential tendency ($Pc=0.4e^{0.06cover}$, R^2=0.994 and $Pc=e^{0.04cover}$, R^2=0.987 for fine and coarse particles, respectively). Error bars represent the standard deviation between the different experiments carried out at the same <TKE> (Figure 3.9a) and for the same cover (Figure 3.9b).

3.4 DISCUSSION

Experiments performed in the laboratory flume showed that allochthonous sediment encountering seagrass canopies can undergo different fates, namely be: i) maintained in suspension above the canopy, ii) maintained in suspension within the canopy, iii) captured by plant blades or iv) settle to the seabed. However, results show that submerged seagrass canopies under oscillatory conditions affect the hydrodynamics and the distribution and transport of sediments mainly by reducing the wave velocity and the turbulent kinetic energy that depends on both canopy density and wave frequency.

3.4.1 Submerged model vegetation hydrodynamics by oscillatory flow

Submerged canopies were found to attenuate both wave velocity and TKE within the canopy, in agreement with Pujol et al. (2013a) in their laboratory study and the results observed by Gacia et al. (1999) and by Hendriks et al. (2008) in their field studies. The TKE attenuation of between 14 – 35% found in this laboratory study, agrees with the 25% reduction in turbulence between bare substrate and *P. oceanica* bed found by Granata et al. (2001) in their field study. The fact that the TKE decreased with the canopy cover indicates that dense canopies shelter the seabed. This reduction in the TKE produces different distributions of sediment depending on the density of the cover. The decrease in the TKE with depth was also found by Zhang et al. (2018), but in their case, the TKE in the upper without-plant water layer was lower than in the present study. In laboratory conditions the plant height was h_v=14 cm, wave amplitudes were A = 1.5 cm and 5.6 cm and the periods were T = 1.43 s

and 0.83 s. Considering the flume height H = 30 cm and shallow field depth cases with H = 100 cm a scale factor of 3.3 would apply by using Froude scaling (Islam et al., 2016). Using the Froude scaling, the laboratory studied conditions would represent field waves with amplitudes of A = 4.95 and 18.48 cm and periods of T = 2.59 s and 1.51 s. Such field conditions might be found in river or lake environments and closed basin estuaries in marine systems (Pascolo et al., 2019; Smith et al., 2010), where particle laden river plumes may have a significant impact (Howley et al., 2018; Oey and Mellor, 1993).

3.4.2 Effect of the canopy on the suspended sediment from the allochthonous plume

The concentration of suspended sediment in the water column follows a linear relationship with the TKE. High TKE corresponds to the sparsest canopies, whereas low TKE corresponds to the densest. Therefore, the decrease in the suspended sediment concentration corresponded to the densest canopies. This result is in agreement with the reduction of turbidity found by Short and Short (1984) for a vegetated bed. Consequently, the presence of a seagrass canopy protects seagrass meadows in coastal regions by enhancing the sedimentation. This result has been observed in the field, where a greater sediment deposition was found on the seabeds sheltered by *P. oceanica* in the NE Spanish Mediterranean (Gacia et al., 1999; Grabowski et al., 2011).

3.4.3 Allochthonous sediment trapped by the blades of an individual plant

This study demonstrated that plant blades trap sediment particles. Sediment trapped by blades in sparse canopies was quantified and compared to that in dense canopies. The sediment concentration trapped by the blades of each plant, (c_p), was higher for coarse particles than it was for fine ones. The concentration of fine particles trapped on the leaf blades of each plant remained constant with the TKE and with the canopy density, which may be due to the leaves of the plants easily trapping fine particles until the surfaces become saturated. In contrast, the concentration of coarse particles trapped on the leaf blades of each plant increased with the TKE, i.e., decreased with cover. Therefore, for coarse particles the greatest concentration of particles trapped by plant leaves corresponded to the lowest canopy density. Two possible reasons could explain this result. A first hypothesis is that in sparse canopies there is a reduction in the interaction between leaf blades, whereas in dense canopies the contact between blades can wash off the sediment deposited on the blades of neighbouring plants, thus resulting in cleaner blades. As reported by Gacia et al. (1999) and Hendricks et al. (2008), an increase in the canopy density generates an increase in plant blade friction. The second hypothesis is that sparser canopies have higher TKE, thus favouring the contact between particles and blades and resulting in a greater amount of sediment being trapped on the surface of the plant blades. Short and Short (1984) also observed that seabeds covered by plants with blades of leaves with large surface areas produced a greater reduction in the turbidity of the water column compared to seabeds covered by plants with blades that have a small surface area.

3.4.4 Allochthonous sediment trapped by the overall canopy

Therefore, the decrease in the within-canopy suspended sediment could be attributed to two factors: the capture of suspended particles by plant blades or the particles settling onto the bed. This is consistent with the fact that the presence of plants increases the available surface where particles can settle and so an increase in plant density implies an increase in the available surface.

Agawin and Duarte (2002) observed that particles with diameters around 15 µm were trapped faster by canopy blades than those particles around 1-3 µm. The trapping rates were 0.24 d^{-1} and 0.50 d^{-1} for 15 µm and 3 µm, respectively. At first glance, it would seem that their results do not agree with the results obtained in this study, where a greater sediment volume was found for the coarse particles, however, in converting the volume of particles to the number of particles for a canopy cover of 80.9%, the volume trapped by plants corresponds to a number of particles of 9.44×10^{9} and 8.13×10^{6} for fine and coarse particles, respectively. Therefore, a larger number of fine particles (as opposed to coarse particles) are trapped by the leaf blades, which is consistent with Agawin and Duarte (2002). This may be caused by the greater cohesiveness of fine particles compared to coarse particles (Grabowski et al., 2011).

In terms of mass balance, the total volume of particles settled to the bed in one hour ranged from 5000 µlL to 6000 µlL, i.e., a mass of sediment from 12.5 g to 15 g, when considering a sediment density of 2500 g $\cdot L^{-1}$. This mass settled in the area under study equalling 2.5 m of in length per 0.5 m in width. This results in a range in the sedimentation rate of 240-288 $g\cdot m^{-2}\cdot day^{-1}$. This sedimentation rate within seagrass beds is greater than that found by some authors (Granata et al., 2001; Serra et al., 2020). However,

sedimentation rates in seagrass beds varies through the year in the range of 1.5-500 g m^{-2}·day^{-1} (Gacia and Duarte, 2001). These sedimentation rate values align with those in the present study. However, note that high sedimentation rates might cause plant burial that can negatively affect the growth of plants, thus compromising their survival (Cabaço et al., 2008; Manzanera et al., 1998). Manzanera et al. (1998) found that an increase in sediment deposition producing a 15 cm change in sediment height produced total mortality of the seagrass after 200-300 days. In the present study, considering a volume of 5000 μL of sediment deposited after 1 h, it would require 37500 h (i.e., 10.4 days) to reach such a change (i.e.15 cm) in the height of the sediment.

Particle sedimentation onto the seabed was affected by the presence of canopies and had a greater impact on coarse, rather than fine, particles, between 5.7 - 10.9% and 11.0 - 14.4% higher in the presence of vegetation, respectively. The annual cycle of the seagrasses could imply different regimes of sedimentation due to the continuous loss and renewal of leaves. *Posidonia oceanica* leaves grow progressively from winter to summer, when they obtain their maximum extension (Gruber and Kemp, 2010). In contrast, from late summer to autumn they shed their leaves, causing an accumulation of leaf litter on the seabed until the energy flow is able to transport them away (Paladini de Mendoza et al., 2018). This indicates that, at the end of the plant cycle, a portion of the dead leaves is likely to ultimately be transported to the bottom. Therefore, this study states that the presence of the canopy enhances the flux of allochthonous particles down to the bed in two different ways: it increases the direct sedimentation to the bed (through a reduction in the TKE) and it captures particles on its blades that may eventually end up on the seabed when the blades die.

This study demonstrated that under oscillatory flow for both fine and coarse sediment particles, shoot density also increased the sediment deposited to the seabed and reduced the suspended sediment particles. This aligns with the results found by Wilkie et al. (2012), who claimed that under a unidirectional flow, sediment deposition increased with seagrass density.

3.4.5 Sediment balance between sediment trapped by plant blades and by the canopy.

A partition coefficient higher than 18.5% for fine particles and 25.0% for coarse particles was found for low values of TKE, and which correspond to the highest canopy cover. This result indicates that a larger volume of suspended sediment was trapped on the surface of the plant leaves compared to the volume of suspended sediment that remained in suspension inside the canopy in denser canopies. This demonstrates the fact that, while denser canopies have fewer particles per blade, the higher density of the canopies balances this result, producing the greater overall particle trapping observed on blades in the denser canopies. These results show that, as has been pointed out by other authors (Ackerman, 2002; Hendriks et al., 2008; Short and Short, 1984), a significant portion of the suspended particles transported inside the seagrass canopies collides with the leaves. For canopy covers over 52.1%, the trapping of fine particles on plant blades was greater than that for coarse particles, while with lower covers, the blades had the same ability to trap both fine and coarse particles. So, a threshold of TKE = 0.36 $cm^2 \cdot s^{-2}$ indicates that for TKE below this value, leaf blades are able to trap the different sized suspended sediment particles. In addition to canopy density, plant height might also

impact the canopy cover because longer leaves can bend more and produce a greater cover under certain hydrodynamic conditions. This increase in the cover by larger plants can have an impact on the TKE. An increase in plant height has been found to increase wave attenuation (Koftis and Prinos, 2011; Pujol et al., 2013a). Furthermore, during the leaf growth, leaves might shift from a more rigid to a more flexible structure which can also impact the canopy cover. Rigid canopy structures can reduce the energy of the flow by three times that of flexible canopies (Bouma et al., 2005). Therefore, more work should be done to assess the effect both plant height and flexibility have on the hydrodynamics and the ability to capture particles on the leaves.

3.4.6 Ecological implications

Through the flume laboratory experiments carried out in this study, results contribute to confirming those obtained in field surveys where the importance of preserving seagrass meadows has been clearly demonstrated. The laboratory results allow us to demonstrate that the presence of seagrass in coastal areas does in fact have direct ecological implications on marine ecosystems since it favours the preservation of marine coastal seabeds and, therefore, the accumulation of sediments that contribute to storing and preserving carbon from autochthonous and allochthonous sources within the context of climate change.

Seagrass canopies play a crucial role in determining the characteristics of the seabed. van Katwijk et al. (2010)found, on the one hand, muddification (an increase in fine sediment on the seabed), in high density canopies and, on the other hand, sandification in sparse canopies which tended to have a

greater concentration of large sized particles. These results agree with the increase in the ratio between the mass of fine to coarse particles attached to blades from sparse (with $\frac{V_{SP}^{F}}{V_{SP}^{C}} = 0.5\%$ for SPF=1%) to dense canopies ($\frac{V_{SP}^{F}}{V_{SP}^{C}} = 0.8\%$ for SPF = 7.5%). A high level of attachment of fine particles to blades results from the increase in the available surface where particles can be deposited.

Brodersen et al. (2017) found that the silt/clay sediment attached to leaves of *Zostera muelleri* Irmisch ex Ascherson, has negative effects on the activity and efficiency of photosynthesis and on the night-time O_2 exchange between the leaf tissue and the surrounding water. According to our study, seagrass meadows with high canopy cover values will reduce the sediment trapped by each plant, thus favouring photosynthetic activity and O_2 exchange, while the sediment trapped by the whole canopy will be greater, thus reducing turbidity. Therefore, the overall effect of dense canopies will be twofold, less suspended sediment and cleaner leaves, which result in water of a better quality with greater clarity that can fulfil the photosynthetic requirements of the vegetation. This result may explain the existence of a potential threshold for the status of the water quality due to the effect canopies have. From Lopez-y-Royo et al. (2011), the threshold for moderate to good status water quality in seagrasses was for a shoot density of 210 shoots m^{-2}. From the present study, such a shoot density corresponds to a canopy cover of 46.3%; which coincides with the threshold where the Pc became differential for fine and coarse particles, i.e., to the greater cover of 50%. Therefore, the fact that plant blades trap a smaller portion of coarse than fine particles, may be related to water quality. Since fine particles trapped by each plant remain constant, the effect on plant fitness is as a result of the coarse particles trapped by plants.

We hypothesize that those lower values of coarse particles attached to the leaf blades of the plants will result in a thinner layer of sediment on the blades, thus allowing for a better gas exchange. Hence, photosynthetic activity is improved and so too the meadow's fitness. In addition, the reduction of suspended sediment within the canopy in the case of dense canopies, will improve the water quality of the ecosystem, producing positive feedback to the canopy.

Another important aspect of sediment deposition on seagrass meadows is the storage and preservation of carbon in the seabed which, by managing these ecosystems, would be a potential mechanism for mitigating CO_2 emissions. Ricart et al. (2015) found a higher content of organic carbon inside the seagrass canopies than at the edges of the canopy. The results presented here substantiate the argument for the seagrass restoration programmes conducted world-wide since the mid-20th century to mitigate climate change (Paling et al., 2009), help rebuild the lost carbon sink and conserve the remaining stores due to the ability of seagrass canopies to capture particles in an oscillatory flow.

Acknowledgments

This research was funded by the University of Girona, through the grant MPCUdG2016-006 and by the Ministerio de Economía, Industria y Competitividad of the Spanish Government through the grant CGL2017-86515-P. This work contributes to the ICTA 'Unit of Excellence' (MinECo, MDM2015-0552) and the Generalitat de Catalunya research program (2017 SGR-1588). Aina Barcelona was funded by the pre-doctoral grant 2020 FI SDUR 00043 by the "Generalitat de Catalunya".

CHAPTER 4

Functional dynamics of vegetated model patches: the minimum patch size efect for cannopy restoration

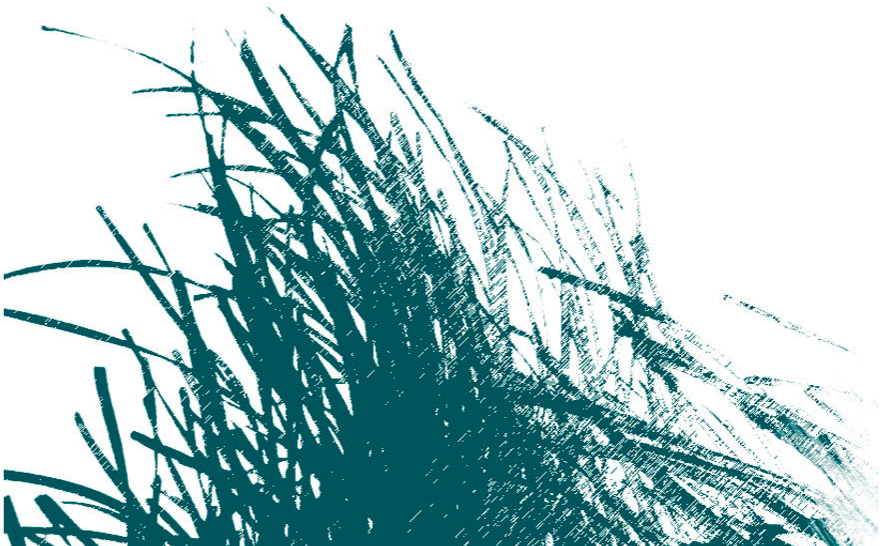

Aina Barcelona, Carolyn Oldham, Jordi Colomer, Teresa Serra (2021). Functional dynamics of vegetated model patches: the minimum patch size effect for canopy restoration. Science of the Total Environment 795, 148854. doi: 10.1016/j.scitotenv.2021.148854.

Cover design: Carles Arbat

Abstract

For the past two centuries coastal zones have been suffering seagrass loss resulting in a network of vegetated patches which are barely interconnected and which may compromise the ecological services provided by the canopy. To optimize management efforts for successful restoration strategies, questions need to be addressed about what appropriate canopy architectural considerations are required under certain hydrodynamic conditions. In this study, a set of laboratory experiments were conducted in which hydrodynamic conditions, plant densities and vegetated patch lengths were varied to determine minimum patch lengths for successful management strategies. Based on the TKE production, this study finds two possible canopy behaviours of seagrasses under oscillating flows: one where plants do not interact with the flow and the other where they interact with waves and produce TKE. A threshold from the first to second behaviour occurs for $\left[C_{D-Patch}\frac{nd^2}{2(1-\phi)}\right]^{\frac{1}{3}}U_w = 2$, where C_D is the drag of the vegetated patch, n is the number of stems per m^2, d is the stem diameter and ϕ is the solid plant fraction. Therefore, high canopy densities, large patches of vegetation or moderate wave velocities will produce plant-wave interaction, whereas low canopy densities, small vegetation patches or slow wave velocities will produce a behaviour akin to the non-vegetated cases.

Keywords*: seagrass patch length, turbulent kinetic energy, wave velocity, canopy density.*

4.1 INTRODUCTION

Seagrass meadows are seascape ecosystems providing key ecological services in coastal areas such as providing habitats for thousands of fish, bird and invertebrate species (Hughes et al., 2009), supporting commercial fisheries (Metz et al. 2020), regulating nutrient cycling (Montefalcone, 2009), stabilizing seabed sediments (Bouma et al., 2007; Waycott et al., 2009) and mitigating climate change through both carbon storage and sequestration (Fourqurean et al., 2012; Unsworth et al., 2019).

Seagrasses are found in shallow coastal waters (most less than 10 m deep), making them vulnerable to human pressure which can cause direct physical damage to the meadow itself through anchoring, trawling, dredging or urban/port infrastructure development, or indirect damage through nutrient over-enriched waters and/or high sediment loads coming from urban/industrial runoff, aquaculture, and agricultural runoff (Abadie et al., 2016; Grech et al., 2012; Montefalcone, 2009). Consequently, almost 15% of seagrass species worldwide are threatened (Hughes et al., 2009). Waycott et al. (2009) reported that since 1879, 29% of the world's seagrasses have been lost. Furthermore, since 1980 seagrass meadows have disappeared at a rate of 110 km^2 yr^{-1} which, in turn, results in sea soil remineralization and consequently a stock carbon release of up to 299 Tg C yr^{-1} (Fourqurean et al., 2012). Some of the less affected seagrass canopies end with gaps within vegetation patches, contributing to the meadow heterogeneity, while the most endangered seagrass canopies end up as a group of interconnected patches (Sleeman et al., 2005).

Seagrass loss is presented either by an increase in habitat fragmentation that transforms a continuous tract of vegetation into canopies with interspersed gaps (i.e., areas of bare soil interspersed within the meadow) or by a network of vegetated patches in which interconnections are compromised (Robbins and Bell, 1994; Tanner, 2003). Compared with continuous canopies and given their difficulties in coping with hydrodynamical stressors, vegetation patches are usually described as having lower plant densities, shorter leaves and lower nutrient storage (Gera et al., 2013). The functional dynamics of seagrass canopies depend on attenuating the wave velocity (Newell and Koch, 2004) and the turbulent kinetic energy (TKE) (Pujol et al., 2013a) which both hinge on plant density and flexibility and the submergence ratio and distance from the meadow edge. As such, the ecological services of fragmented seagrass canopies are expected to be compromised (Paul and Amos, 2011; Serra et al., 2018) because fragmented seagrasses are not fully able to reduce the energy of the flow and therefore the sheltering effect of vegetation is reduced (El Allaoui et al., 2016). Not only this, as the increase in seagrass fragmentation will result in an increase in edges over the canopy areas then the attenuation of the hydrodynamics is also reduced (Granata et al., 2001). Edges are transitional areas between the bare soil and the canopy and represent transition zones for local hydrodynamics. They are mainly a region of the canopy with low wave velocity and TKE attenuation compared to a bare bed and where both wave velocity and TKE decrease gradually towards the inner canopy region (Serra et al., 2018).

Most studies have focused on the patch size effect on unidirectional flows to discern the structural characteristic of patches and their role in optimising the ecological services provided. For instance, Licci et al.

(2019) evaluated the effects of patches of *Callitriche platycarpa* Kütz in lotic ecosystems and found that small patches induced little to no modification to physical parameters. Patches, however, as noted by Folkard (2005), can significantly modify hydrodynamic patterns depending on the distance between them. Likewise, Li et al. (2019) found that vegetated patches greatly impacted the downstream flow: the greater the plant density was, the lower the depth-averaged velocity adjacent to the patch. Concurrent with these results but under oscillatory wave conditions, El Allaoui et al. (2016) found that at the edges of vegetation the sheltering provided was reduced compared to within the canopy, although denser fragmented canopies produced greater sheltering than sparser ones did. The structural characteristics, such as plant density and leaf length, of *Posidonia oceanica* (Linnaeus) Delile meadows determine flow attenuation, with vegetation sheltering nearby gaps (depending on the length of the gaps) in such a way that larger gaps were less protected by the nearby canopy (Colomer et al., 2017). Therefore, fragmented seagrasses that undergo patchiness result in more vulnerable meadows that are then exposed to higher levels of energy which may amplify sediment resuspension and turbidity and produce negative feedback on the canopies (Carr et al., 2010; Zhang et al., 2018).

All of these results have strong implications for seagrass ecosystem restoration strategies which are designed to recover seascapes, their ecosystem biodiversity and the services they provide (Gilby et al., 2020; van Katwijk et al., 2016). Although the first trials for seagrass restoration started during the first half of the twentieth century, it was not until 1970 that interest in restoring seagrass ecosystems increased (van Katwijk et al., 2016). Furthermore, the increased effect that anthropogenic emissions and activities have on the fate of fragmented canopies has

meant there is an urgent need to restore world's seascapes, among which include seagrass canopies. Some studies have also modelled seagrass restoration efficiency using chemical and physical abiotic variables such as light, temperature and salinity (Stankovic et al., 2019). For successful restorations, strategies such as improving water quality, removing exotic species, and ensuring the minimum number of shoots planted is within the range of 1000-10000 shoots/seeds have been implemented (Kupsky and Dornbush, 2019). Many attempts to transplant plants into fragmented canopies have resulted in limited survival rates varying from 9 % to 40 % according to Paling et al., (2003), while van Katwijk et al. (2016) found that the survival rate was estimated at 37 % for the majority of the seagrass restoration trials. Such results indicate the importance of establishing functional dynamic criteria for the patch length scales required if plants are to be successfully replanted in the canopies. Infantes et al. (2009) indicated that high wave velocities produce a loss in the *Posidonia oceanica*' cover. Therefore, despite all the studies carried out, none of them focus on the functional dynamics of the patch, which is dependent on the patch scale; therefore there is a need to include hydrodynamics in the parametrization for future projects of plant restoration.

This study, then, is focused on determining whether there is (or not) an optimal patch length in which the hydrodynamics of the patch mimics those of a canopy without fragmentation. The objective of this study is to determine whether (or not) a single patch behaves dynamically as a canopy. As such, the minimum patch size was defined as the critical length over which a single patch was dynamically mimicking a continuous canopy under a certain oscillatory flow regime. It is expected that a patch with functional dynamics akin to those of a canopy might be

optimal for successful replantation. Thus, different patches with different lengths and vegetation densities were combined to obtain the structural scale that can guarantee successful seagrass canopy restoration.

4.2 METHODOLOGY

4.2.1 The flume

The study was carried out in a laboratory methacrylate flume (600 cm long, 50 cm wide and 60 cm deep, Figure 4.1) with a mean water height of h = 30 cm (Table 1). The flume was equipped with a vertical paddle-type wavemaker at the entrance. The wavemaker was driven by a variable-speed motor at two frequencies (f = 0.50, 1.12 Hz). A plywood beach (slope = 1:2) covered with foam rubber to eliminate wave reflection was placed at the end of the flume (Pujol et al., 2013; Serra et al., 2018). At the measurement depth, the percentage of U_c reduction was 39% and 59% for the wave frequencies of 1.12 Hz and 0.5 Hz, respectively. There was also a reduction of 3.0% and 2.9% for the wave velocity for frequencies of 1.12 Hz and 0.5 Hz, respectively. In the longitudinal direction, x = 0 cm was situated at the wavemaker, in the lateral direction, y = 0 cm was at the centre of the tank, and in the vertical direction, z = 0 cm was situated at the flume bed.

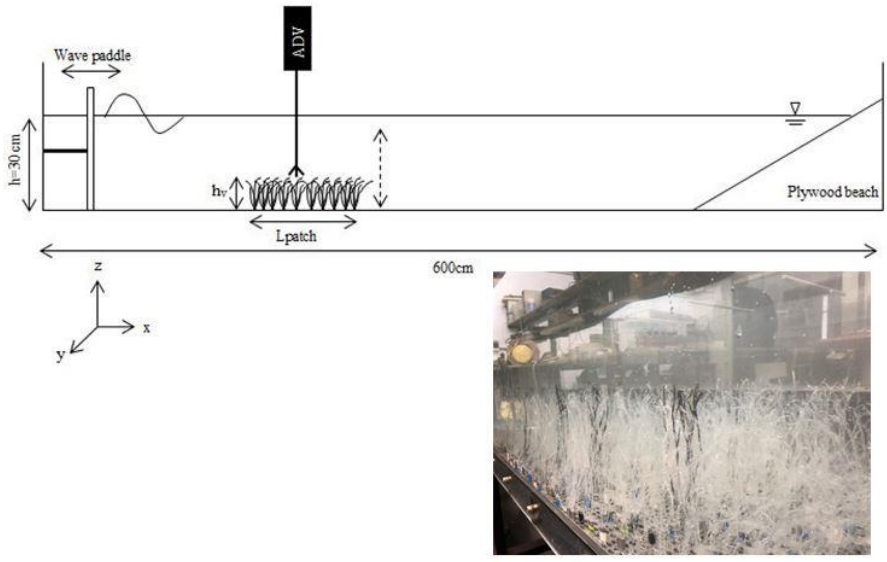

Figure 4.0.1 A lateral view of the experimental setup (top), with the wave paddle on the left to provide waves from left to right. Experiments were conducted in a 600x50x50 cm long flume, with a mean water depth of 30 cm. The model patch had patch lengths that ranged from 2.8 cm to 42 cm. The triangle at the water-air interface represents the water level in the flume. An ADV was vertically mounted to measure the instantaneous velocities at selected vertical heights. A photograph of the experimental setup (bottom), with the simulated vegetation.

4.2.2 Patches of flexible vegetation

The system of laboratory model vegetation consisted of a series of flexible plants made from eight 0.075 mm thick polyethylene canopy blades attached to PVC dowels that had been randomly inserted into a perforated baseboard ($L_{base\text{-board}}$ = 250 cm, Pujol et al., 2013a), with a rigid dowel extending 1 cm above the bed (Zhang et al., 2018). The model plants were geometrically and dynamically similar to *Posidonia*

oceanica plants (Ghisalberti, 2002; Pujol et al., 2013a). The leaf length was 14 cm, and the effective height when the leaves were bent by the waves was h_v = 8.5 cm for f = 1.12 Hz and h_v = 10.5 cm for *f* = 0.5 Hz. The effective heights were calculated by the mean between both the maximum and the minimum bending heights of the plants for 25 oscillations The initial position of the vegetation (x_0) was situated 100 cm from the wavemaker (Figure 4.1). The vegetation density of patches was quantified using the solid plant fraction (SPF) defined as:

$$\text{SPF}\ (\%)=100n\pi\left(\frac{d}{2}\right)^2 \tag{4.1}$$

where n is the number of stems per unit area and *d* is the stem diameter (1 cm). Six SPFs were used (0%, 2.5%, 3.5%, 5%, 7.5% and 10%), which corresponded to vegetation densities of *n*= 0, 318, 446, 637, 955 and 1273 stems·m^{-2} (Figure 4.2) and similar to the canopy densities between 78 to 1000 stems·m^{-2} found in coastal areas (Bacci et al., 2017; Colomer et al., 2017; Gera et al., 2013; van Katwijk et al., 2010); SPF=0% corresponded to the case with no vegetation. For each SPF, different patch sizes, L_{patch}, ranging from 32 to 240 cm were considered (Table 4.2). In this study, the longest patch L_{patch}=240 cm. A total of 67 experiments were performed for the different SPFs, patch lengths and wave frequencies (Table 4.2). In the experiments, the patch edge was considered as the interface from the vegetated region and the non-vegetated region (Schoelynck et al., 2018). For all patch lengths, flow velocity profiles were measured at the centre of the patch. The length of the patch increased from this centre point outwards (i.e., to the wave maker and to the beach, see Figure 4.1) so that the measuring point was always the same for all patches.

Table 4.1 Summary of the experiment characteristics.

Run	f (Hz)	SPF (%)	n (stems·m^{-2})	L_{patch} (cm)	aL	A_w/S_b
WP1	0.5	0	0		0	
WP2	1.12	0	0		0	
SFV3	0.5	1	127	42	0.53	0.94
SFV4				70	0.89	0.92
SFV5				112	1.42	0.92
SFV6				196	2.49	0.94
SFV7		7.5	955	42	4.01	2.84
SFV8				70	6.69	2.75
SFV9				112	10.7	2.77
SFV10				196	18.72	2.67
SFV11		10	1273	42	5.35	3.11
SFV12				70	8.91	3.08
SFV13				84	10.69	2.97
SFV14				98	12.48	2.96
SFV15				112	14.26	2.92
SFV16				133	16.93	2.98
SFV17				140	17.82	2.84
SFV18				154	19.6	2.97
SFV19				182	23.17	3.04
SFV20				224	28.52	2.89
SFV21				240	30.3	2.86
SFV22	1.12	2.5	318	42	1.34	0.59
SFV23				70	2.23	0.6
SFV24				84	2.67	0.59
SFV25				98	3.12	0.59
SFV26				112	3.56	0.58
SFV27				126	4.01	0.59
SFV28				140	4.45	0.59
SFV29				154	4.9	0.59
SFV30				168	5.34	0.59
SFV31				182	5.79	0.59
SFV32				196	6.23	0.59
SFV33				240	7.57	0.59

Run	f (Hz)	SPF (%)	n (stems· m^{-2})	L_{patch} (cm)	aL	A_w/S_b
SFV34	1.12	3.5	446	70	3.12	0.7
SFV35				112	5	0.69
SFV36				126	5.62	0.69
SFV37				140	6.24	0.7
SFV38				154	6.87	0.68
SFV39				168	7.49	0.68
SFV40				196	8.74	0.68
SFV41				240	10.61	0.67
SFV42		5	637	42	2.68	0.83
SFV43				70	4.46	0.83
SFV44				98	6.24	0.83
SFV45				126	8.03	0.82
SFV46				168	12.49	0.8
SFV47				196	10.7	0.81
SFV48				210	13.38	0.8
SFV49				240	15.16	0.8
SFV50		7.5	955	42	4.01	1.03
SFV51				70	6.69	1.04
SFV52				84	8.02	1.01
SFV53				98	9.36	1.01
SFV54				112	10.7	0.99
SFV55				133	12.03	0.98
SFV56				154	14.71	0.99
SFV57				196	18.72	0.96
SFV58				240	22.73	0.97
SFV59		10	1273	42	5.35	1.18
SFV60				70	8.91	1.18
SFV61				84	10.69	1.15
SFV62				98	12.48	1.15
SFV63				112	16.04	1.13
SFV64				133	24.95	1.1
SFV65				168	19.6	1.12
SFV66				196	21.39	1.12
SFV67				240	30.3	1.11

4.2.3 Measuring velocities

The Eulerian velocity field was defined as (u, v, w) in the (x, y, z) directions, respectively. The three components of velocity were recorded (50 Hz over 5 min) with a downwards looking Acoustic Doppler Velocimeter (16-MHz MicroADV, Sontek). The ADV measured at a distance of 5 cm from the probe tip and with a sampling volume of 0.09 cm^3. Beam correlations less than 70% were discarded and spikes were removed (Goring and Nikora, 2002; Pujol et al., 2013a). The longitudinal velocity was measured at an antinode to eliminate the lower order spatially periodic variation in wave and velocity amplitude associated with wave reflection (Luhar et al., 2010; Pujol et al., 2013a). The ADV was mounted on a movable vertical frame (at y = 0 cm, Figure 4.1) and manually adjusted to measure a vertical profile. Some plants were removed to avoid blocking the ADV beams (Ros et al., 2014; Zhang et al., 2018), and were re-inserted into nearby holes.

4.2.4 Hydrodynamic analysis

For oscillatory flows, the instantaneous velocity in the x direction, $U_i(t)$, can be decomposed as:

$$U_i(t)=U_c+ U_w+ u' \quad (4.2)$$

where U_c is the steady velocity associated with the wave, U_w is the unsteady wave motion in the x direction which represents spatial variations in the phase-averaged velocity field, and u’ is the turbulent velocity, that is, the instantaneous velocity fluctuation in the x-direction. U_c is the phase-averaged velocity:

$$U_c = \frac{1}{2\pi}\int_0^{2\pi} U_i(\varphi)\partial\varphi \quad (4.3)$$

where $U_i(\varphi)$ is the instantaneous velocity according to the phase (Lowe et al., 2005; Luhar et al., 2010). Wave velocity, U_w, was obtained by using a phase averaging technique. The Hilbert transform was used to average oscillatory flow velocities with a common phase (Pujol et al., 2013b; Ros et al., 2014). The root mean square (rms) of $U_i(\varphi)$ was considered as the characteristic value of the orbital velocity U_w^{rms} (U_w hereafter) at each depth and was calculated according to:

$$U_w^{rms} = \sqrt{\frac{1}{2\pi}\int_0^{2\pi}(U_i(\varphi)-U_c)^2\partial\varphi} \quad (4.4)$$

The ratio α_w of the wave velocity (U_w) was calculated following Lowe et al., (2005):

$$\alpha_w = \frac{U_{w,}}{U_{w,\,WP}} \quad (4.5)$$

where U_w is the wave velocity within the patch at z = 4 cm for vegetated cases and $U_{w,WP}$ is the wave velocity at z = 4 cm for non-vegetated cases. The measurements within the vegetation at z = 4 cm corresponded to z/h_v = 0.47 for f = 1.12 Hz and z/h_v = 0.38 for f = 0.5 Hz. This depth was chosen from the wave velocity profile, shown later on in the results section so that it was situated out of the shear region situated at the top of the vegetation and also far from the bed of the flume. Therefore, α_w provided a measure of the wave velocity attenuation within the patch for vegetated cases compared to non-vegetated cases. Consequently, values of $\alpha_w \approx 1$ indicated a weak or negligible attenuation of the wave velocity by the vegetation, whereas low values of $\alpha_w < 1$ indicated high wave velocity attenuation.

The turbulent velocity was obtained by:

$$u' = U_i - U_c - U_w \tag{4.6}$$

where U_c and U_w were calculated by Eqs. 4.3 and 4.4. The turbulent velocity was calculated for all directions (u', v' and w') for z= 4 cm.

Turbulent kinetic energy (TKE) was calculated following Ros et al. (2014) as:

$$TKE = \frac{1}{2}\left(\langle u'^2\rangle + \langle v'^2\rangle + \langle w'^2\rangle\right) \tag{4.7}$$

where < > denotes the time average.

The ratio, β_w, was calculated following Colomer et al. (2017):

$$\beta_w = \frac{TKE}{TKE_{WP}} \tag{4.8}$$

where TKE was the turbulent kinetic energy within the patch at z = 4 cm for vegetated cases and TKE_{WP} was the TKE measured at z = 4 cm for the non-vegetated case. Therefore, values of $\beta_w \approx 1$ indicated a weak or negligible attenuation of the TKE, whereas low values of $\beta_w < 1$ indicated a high TKE attenuation compared to the non-vegetated case.

In order to gain knowledge of the vertical distribution of TKE within the patch, a non-dimensional model was set following Zhang et al. (2018). For a full canopy, Zhang et al. (2018) found that the relationship between the TKE, U_w and the main canopy parameters followed:

$$\frac{\sqrt{TKE}}{U_w} = \delta\left[C_D \frac{l_t}{d}\frac{nd}{2(1-\phi)}\right]^{\frac{1}{3}} \tag{4.9}$$

where δ is the scale constant, ϕ is the solid volume fraction, $\phi = n\frac{\pi}{4}d^2$, l_t is characteristic eddy length-scale, and C_D is the drag of the form of the

obstacle along the fluid patch, with C_D = 1.4 being used in both studies. In Equation (4.9), the characteristic length scale, L_{patch} / L_{canopy}, for each frequency, is introduced to account for the volume of the patch in relation to the maximum canopy volume in the form of $\frac{V_{Patch}^{1/3}}{V_{Canopy}^{1/3}} = \left(\frac{aL_{patch}}{aL_{canopy}}\right)^{\frac{1}{3}} = \left(\frac{L_{patch}}{L_{canopy}}\right)^{\frac{1}{3}}$, therefore Equation (4.9) is expressed following:

$$\frac{\sqrt{TKE}}{U_w} = \delta\left[C_D\left(\frac{L_{patch}}{L_{canopy}}\right)^{\frac{1}{3}}\frac{l_t}{d}\frac{nd^2}{2(1-\phi)}\right]^{\frac{1}{3}} \quad (4.10)$$

Zhang et al. (2018) considered l_t = d for S > 2d whereas l_t = S for S < 2d. In the present study, since S > 2d, l_t = d, therefore:

$$\frac{\sqrt{TKE}}{U_w} = \delta\left[C_D\left(\frac{L_{patch}}{L_{canopy}}\right)^{\frac{1}{3}}\frac{nd^2}{2(1-\phi)}\right]^{\frac{1}{3}} \quad (4.11)$$

Defining $C_{D\text{-}Patch}=C_D(L_{patch}/L_{canopy})^{1/3}$ as the drag generated by the patch, equation (4.11) results:

$$\frac{\sqrt{TKE}}{U_w} = \delta\left[C_{D-Patch}\frac{nd^2}{2(1-\phi)}\right]^{\frac{1}{3}} \quad (4.12)$$

4.3 RESULTS

For the longest patch considered (L_{patch}=240 cm), the wave velocity U_w decreased with depth for all the experiments i.e., with and without plants (Figure 4.2). Three vertical layers could be differentiated based on the vertical profile of U_w. A first layer above the patch ($z/h_v>1$), where U_w for the vegetated case was similar to that of the without-plants case. A second layer within the patch ($0.7<z/h_v<1$), where U_w for the case with plants was lower than that for the non-vegetated case and decreased gradually with depth. A third layer within the patch, the inner vegetation layer ($z/h_v<0.7$), where U_w was nearly constant with depth down to the bed. The vertical decrease of U_w for the higher frequency case (1.12 Hz) was stronger than for the low frequency (0.5 Hz) (Figures 4.2a and 2b). For the higher frequency, a decrease in the U_w from the lowest to greatest depth was found for all the vegetated and non-vegetated cases (Figure 4.2a), while for the lower frequency, U_w presented the slowest vertical reduction, especially for the non-vegetated cases (Figure 4.2b). For the non-vegetated cases and for the high frequency, TKE decreased with depth down to $z/h_v = 0.7$. Below $z/h_v = 0.7$, the TKE remained constant down to the bed (Figure 4.2c). In contrast, for the low frequency in non-vegetated cases, TKE was constant with depth (Figure 4.2d). Unlike what had been obtained for U_w, the TKE was higher for vegetated than for non-vegetated cases, except for SPF=3.5% at the higher frequency (Figures 4.2c and 4.2d). For the higher frequency and the vegetated and non-vegetated cases, the TKE decreased with depth. However, for the vegetated cases, the TKE slightly increased with depth from $z/h_v = 0.7$ down to the bed (Figure 4.2c).

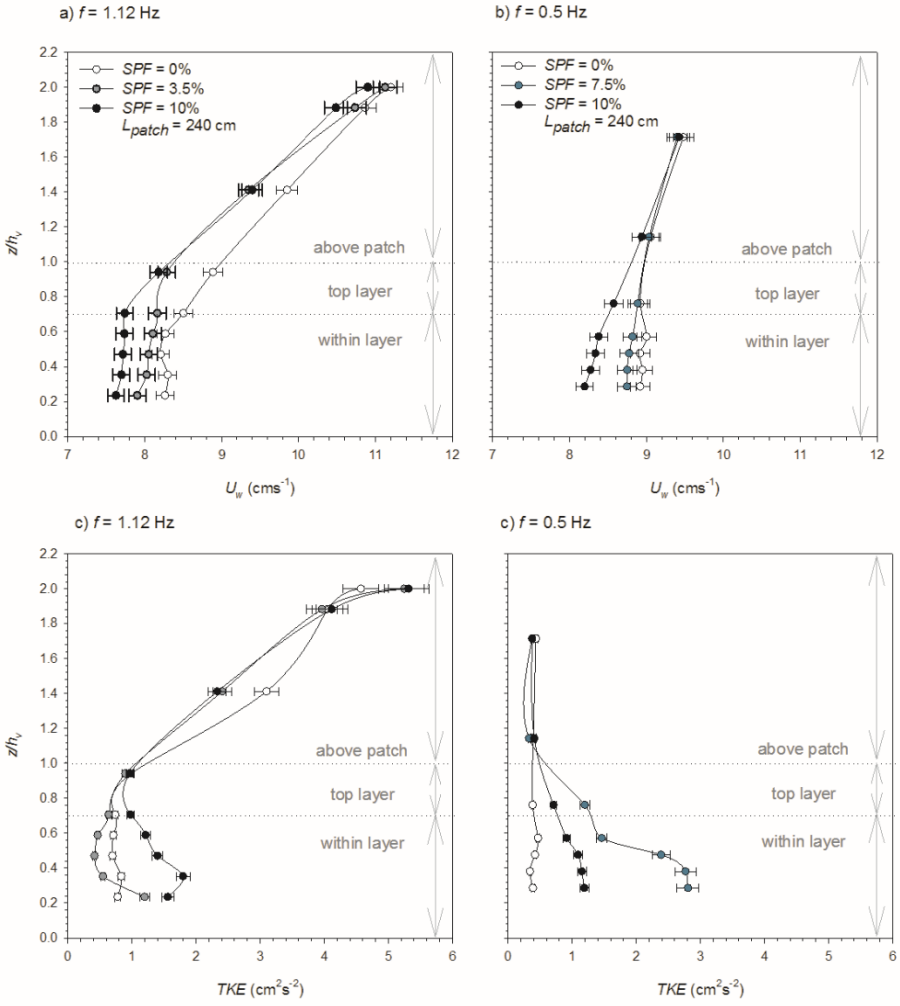

Figure 4.2 Wave velocity (U_w) vertical profiles for a) f = 1.12 Hz, b) f = 0.5 Hz and TKE vertical profiles for c) f = 1.12 Hz and d) f = 0.5 Hz. Unfilled circles correspond to the cases of SPF = 0%, whereas black, blue and grey filled symbols correspond to SPF = 10%, 7.5%, and 3.5% respectively. The experiments presented here correspond to the L_{patch} = 240 cm patch length case.

Both wave attenuation (α_w) and TKE attenuation (β_w) were calculated for the different non-dimensional patch length scales (L_{patch}/h_v) and for the different SPFs studied (Figure 4.3). For both frequencies, the greater the

SPF was, the lower α_w was (Figures 4.3a and 4.3b). For the high frequency studied (f=1.2Hz) and for SPF =2.5%, α_w remained constant with L_{patch}/h_v (Figure 4.3a). For the other SPF studied (>2.5%), α_w was constant for low L_{patch}/h_v decreasing afterward as L_{patch}/h_v increased. Therefore, for the low frequency and all SPFs considered, the decrease in α_w started from a threshold in the patch length characterised by $L_{patch}/h_v = 4$ (Figure 4.3b). For the low frequency studied, and for all SPFs considered, α_w decreased with an increase in L_{patch}/h_v (Figure 4.3b), without any threshold in L_{patch}/h_v. For the high frequency, f = 1.12 Hz, α_w remained constant for $L_{patch}/h_v > 20$, whereas for f=0.5Hz, α_w remained constant for $L_{patch}/h_v > 10$. The value of α_w reached decreased as SPFs increased (Figure 4.3a, b).

In contrast to U_w, β_w remained constant with L_{patch}/h_v for both frequencies (1.12 Hz and 0.5 Hz) and for all SPFs studied (Figures 4.3c and 4.3d). However, for the high frequency studied, the low vegetation densities SPF = 2.5%, 3.5% and 5% showed values of $\beta_w < 1$, while β_w was above 1 for SPF = 7.5 and 10%, with β_w increasing with SPF (Figure 4.3c). Contrary to this, for the low frequency studied, $\beta_w > 1$ except for the case of SPF = 1%, for which $\beta_w = 1$ (Figure 4.3d). For this frequency, β_w for SPF=10% was lower than that for SPF=7.5%, contrary to what had been found for the high frequency.

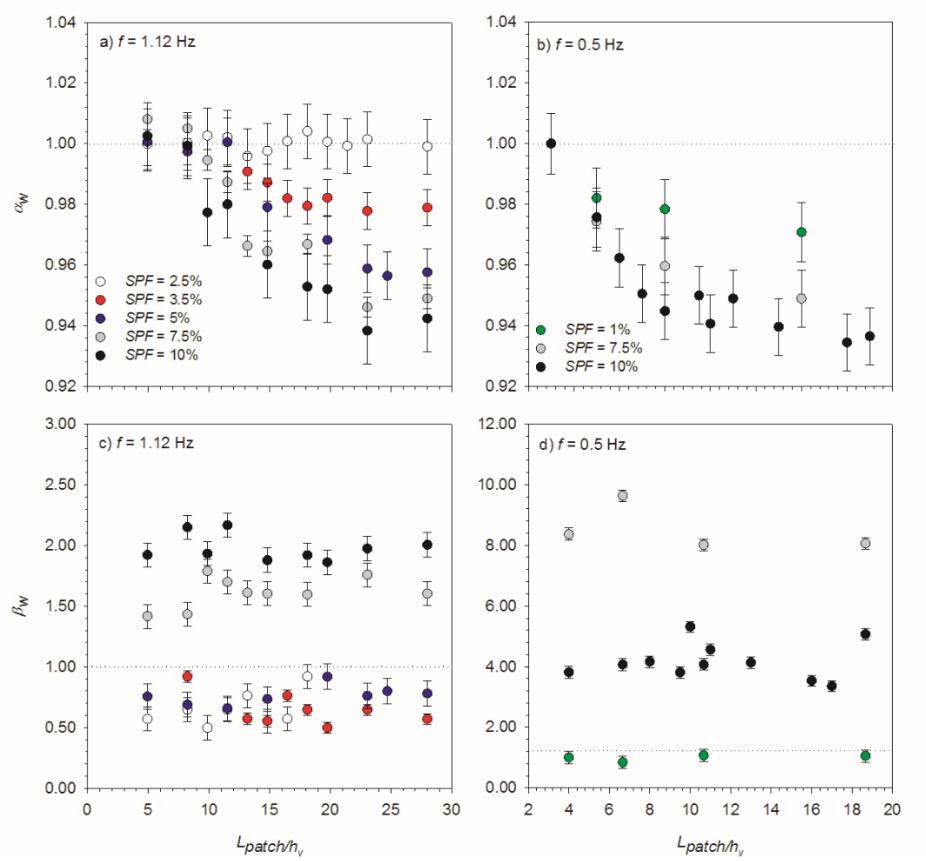

Figure 4.3 Wave attenuation (α_w) versus L_{patch}/h_v for a) f = 1.12 Hz and b) f = 0.5 Hz, and TKE attenuation (β_w) for c) f = 1.12 Hz and d) f = 0.5 Hz at z = 4 cm, for different SPFs ranging from 1 to 10%.

Following Eq (4.11), two behaviours could be distinguished when considering $TKE^{1/2}$ versus $\left[C_{D-Patch}\frac{nd^2}{2(1-\phi)}\right]^{\frac{1}{3}} U_w$, and deduced by applying the non-dimensional analysis, which is shown in Figure 4.4. For $\left[C_{D-Patch}\frac{nd^2}{2(1-\phi)}\right]^{\frac{1}{3}} U_w < 2$, $TKE^{1/2}$ remained constant with $\left[C_{D-Patch}\frac{nd^2}{2(1-\phi)}\right]^{\frac{1}{3}} U_w$ at a value of $TKE^{1/2}=0.56$, while for

$\left[C_{D-Patch}\frac{nd^2}{2(1-\phi)}\right]^{\frac{1}{3}} U_w$> 2, $TKE^{1/2}$ presented a linear trend versus $\left[C_{D-Patch}\frac{nd^2}{2(1-\phi)}\right]^{\frac{1}{3}} U_w$ with a slope of 0.56 (Figure 4.4). The first regime (on the left in Figure 4.4) corresponded to the cases where the dynamics were governed by either single stems of vegetation or the cases without vegetation. The second regime (on the right in Figure 4) corresponded to the case where the dynamics were governed by the patch scale.

The transition of both regimes determines the minimum patch length $L_{patch,min}$, for which for L_{patch}< $L_{patch,\ min}$ the $TKE^{1/2}$ was independent of $\left[C_{D-Patch}\frac{nd^2}{2(1-\phi)}\right]^{\frac{1}{3}} U_w$. In this region $TKE^{1/2}$ was equal to that found for non-vegetated cases, indicating that the vegetation did not contribute to increasing the $TKE^{1/2}$. In contrast, for L_{patch}>$L_{patch,min}$ a linear trend between $TKE^{1/2}$ and $\left[C_{D-Patch}\frac{nd^2}{2(1-\phi)}\right]^{\frac{1}{3}} U_w$ was obtained. This result indicated that the experimental cases with high L_{patch}> $L_{patch,\ min}$ produced an increase in the $TKE^{1/2}$, therefore in this regime dominated by the patch scale the minimum patch length was calculated following Eq. 4.12, observing a dependence of the minimum patch length on L_{canopy}, canopy density and U_w, and calculated as follows:

$$L_{patch} = L_{canopy}\left[\frac{2(1-\phi)}{C_D nd^2}\left(\frac{2}{U_w}\right)^3\right]^3 \quad (4.12)$$

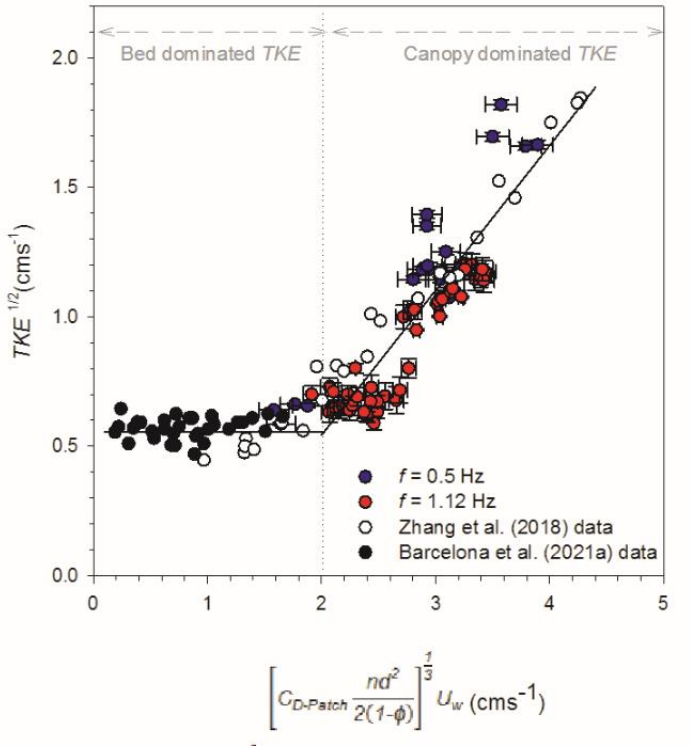

Figure 4.4 Non-dimensional model for $TKE^{1/2}$ for high frequencies (red filled circles), low frequencies (blue filled circles), and Zhang et al. (2018) data (unfilled circles). H. Nepf (personal communication provided the original data from Zhang et al.'s (2018) and Barcelona et al. (2021b) data (black filled circles). The vertical dashed line represents the minimum value of $\left[\mathbf{C_{D-Patch}}\frac{\mathbf{nd^2}}{\mathbf{2(1-\phi)}}\right]^{\frac{1}{3}}\mathbf{U_w}$ that separates the different trends observed for $TKE^{1/2}$. The horizontal solid line at $TKE^{1/2}$ = 0.0056 represents that for $\left[\mathbf{C_{D-Patch}}\frac{\mathbf{nd^2}}{\mathbf{2(1-\phi)}}\right]^{\frac{1}{3}}\mathbf{U_w} <$ 2, where $TKE^{1/2}$ remained constant. For $\left[\mathbf{C_{D-Patch}}\frac{\mathbf{nd^2}}{\mathbf{2(1-\phi)}}\right]^{\frac{1}{3}}\mathbf{U_w} >$ 2 a linear tendency was found: $TKE^{1/2} = \mathbf{0.47} * \left[\mathbf{C_{D-Patch}}\frac{\mathbf{nd^2}}{\mathbf{2(1-\phi)}}\right]^{\frac{1}{3}}\mathbf{U_w} - \mathbf{0.47}$, with R^2 = 0.73 and 99% of confidence.

4.4 DISCUSSION

In this study, the capacity of submerged patches of flexible plants to attenuate waves, in terms of their velocity and TKE, has been found to depend on the wave penetration within the patch and the volume occupied by the vegetation. The wave penetration was a function of the orbital excursion length scale and the plant-to-plant distance, while the volume of the vegetation patch was a function of its length and density. All of this information provides clues for determining the structural analysis of functional patches of seagrass that facilitate hydrodynamical services comparable to those of continuous seagrass meadows.

4.4.1 Effect of the canopy density of the patch

Here, the dynamics of functional patches that were observed to mimic the properties of a continuous vegetated canopy were characterized by the attenuation of the wave velocity with a magnitude that depended on the shoot density within the patch. This aligns with the results found previously by other authors (Gacia et al., 1999; Paul and Amos, 2011; Pujol et al., 2013a). According to the results from Ros et al. (2014) and Zhang et al. (2018), a continuous canopy also attenuates the turbulent kinetic energy generated by the bed when the wave can enter within the vegetation (i.e., $A_w/S_b<1$, where A_w was the wave excursion length, S_b was the plant-to-plant distance between leaves, calculated as $S_b = (n_b)^{-1/2}$ (Zhang et al., 2018). In these cases, the denser the canopy, the greater the sheltering provided. In contrast, when $A_w/S_b>1$, the turbulent kinetic energy increases with A_w/S_b due to the interaction of the flow with the vegetation and the wakes generated by plant stems. Therefore, high canopy densities (i.e., small S_b and high A_w/S_b) result in higher TKE due

to the production of stem wake turbulence. A range of A_w/S_b from 0.58 to 3.04 was considered in this study, covering cases with $A_w/S_b<1$ where the TKE generated by the bed is attenuated and cases with $A_w/S_b>1$ where TKE is generated by plant stems. In the case studied here, wave velocities at the vegetated patch ranged from 7 cm s^{-1} to 10 cm s^{-1}, resulting in stem Reynolds numbers between Re_s= 700 and 1000, respectively. Stem Reynolds numbers above 200 have been found to produce vortex shedding (Nepf et al., 1997) which is a source of turbulence in the system. The increase in the canopy density is expected to also produce an increase in the number of wakes generated and, in turn, an increase in the turbulent kinetic energy in the system. This aligns with the increase in the turbulent kinetic energy for the high patch densities observed in the present study.

However, this study demonstrates the contrary in that β_w remains constant with the patch size for both different SPFs and frequencies. Nevertheless, the results also show how patches, instead of reducing TKE, are capable of enhancing this energy for higher density patches (SPF $\leq$ 7.5%) for both frequencies (f = 0.5 and 1.12 Hz), while sparser patches attenuate the TKE in a range between β_w 0 to 0.5. These results agree with Zhang et al. (2018), who found that for $A_w/S_b>1$ TKE was generated within the canopy. This coincides with the present study where, for both frequencies, the A_w/S_b was found to be greater than 1. These results are attributed to the increase in the number of wakes generated by the plant stems as the patch density increases which, in turn, is related to the reduction of the wave velocity (Tang et al., 2019). Folkard (2005) also found an increase of the Reynolds stress downstream of a single patch of flexible vegetation under unidirectional flow increasing with the flow velocity. Likewise, under the unidirectional

flow, Tinoco and Coco (2014) also found higher TKE in denser canopies, thus agreeing with the results of this study even though they used emergent rigid stems.

4.4.2 Effect of wave velocity and frequency

Moreover, wave frequency plays a relevant and important role in wave attenuation within vegetated patches. Intermediate patch densities under oscillating flows provide greater wave attenuation for low frequencies than for high frequencies. This result is in accordance with Hansen and Reidenbach (2012) who found that lower frequencies produced a higher wave attenuation compared to higher frequencies. However, high patch densities of *SPF*=10% produced equal wave attenuations for the two frequencies studied. These results agree with Paquier et al. (2019) who found that the attenuating capability of waves of the patchy meadows is related to wave heights and frequencies. They also found that in the case of *Zostera noltei* Hornemann, patchy meadows are only capable of attenuating high frequency waves. These results are also in accordance with the concept that under low wave frequencies, a higher wave attenuation is produced than under high wave frequencies. Furthermore, for the low frequency case, the change from SPF=7.5% to SPF=10% did not produce a notable reduction in the U_w. This result might be because in high patch densities wakes are produced by stem overlap and occupy the entire region between plant stems. Therefore, a further increase in vegetation might not produce a subsequent increase in the turbulent kinetic energy locally. This result is in accordance with the definition of a patch of vegetation as described by Schoelynck et al. (2018).

4.4.3 Effect of the patch length scale

This study also demonstrates that the patch size plays a crucial role in determining the hydrodynamics within the vegetated patches. For low wave frequencies, the wave attenuation at the centre of the patch depended on its shoot density. These results may be related to the studies from Zong and Nepf (2011) and Devi and Kumar (2016), who found a lower linear velocity attenuation through sparse patches than through dense patches. In contrast, for high wave frequencies, small patches with $L_{patch}<6h_v$, do not provide any reduction in the wave velocity compared with the without-plants case, whereas patches of $L_{patch}>6h_v$ reduce the wave velocity as the canopy density increases. These results align with those from Licci et al. (2019), who found that the effect of small patches ($L_{patch}/h_v > 9$) of *Callitriche platycarpa*, Kütz in the attenuation of the linear velocity was little or negligible, while larger patches induced significant modifications in the linear velocity.

4.4.4 Patch length-scale thresholds

The non-dimensional model for the $TKE^{1/2}$ indicated that $TKE^{1/2}$ remains nearly constant for $\left[C_{D-Patch}\frac{nd^2}{2(1-\phi)}\right]^{\frac{1}{3}} U_w < 2$. Low values of $\left[C_{D-Patch}\frac{nd^2}{2(1-\phi)}\right]^{\frac{1}{3}} U_w$ can hold for both, low wave frequencies, sparse patches, or small patches. Therefore, a low volume of vegetation produces a constant value of $TKE^{1/2}=0.56$, which is the same value obtained for the non-vegetated cases, hence the TKE source is generated by the bed friction. This threshold means that the minimum patch size required for a certain patch density and under certain hydrodynamical

conditions to be dynamically functional as a continuous canopy can be determined. Conversely, it also means that the minimum density required for a certain patch length to play a role as a patch (instead of a non-vegetated case) can be determined, increasing the TKE by the interaction between the wave and the plants. That said, the results presented here not only show this, but also that the behaviour of a patch also depends on the hydrodynamics i.e., wave frequency and velocity. For cases of $\left[C_{D-Patch}\frac{nd^2}{2(1-\phi)}\right]^{\frac{1}{3}} U_w$>2, the $TKE^{1/2}$ increased with $\left[C_{D-Patch}\frac{nd^2}{2(1-\phi)}\right]^{\frac{1}{3}} U_w$. It is interesting to notice that a certain patch with a certain canopy density might not generate TKE for low U_w i.e., $\left[C_{D-Patch}\frac{nd^2}{2(1-\phi)}\right]^{\frac{1}{3}} U_w < 2$, but after an increase in U_w it can interact with the wave field, producing TKE i.e., $\left[C_{D-Patch}\frac{nd^2}{2(1-\phi)}\right]^{\frac{1}{3}} U_w > 2$.

4.4.5 Management strategies

From a hydrodynamical point of view, a minimum patch size is required for the patch to interact with the wave flow and move from of a regime dominated by either the single stem scale or the non-vegetated case towards a regime dominated by the canopy. From this point of view, this study provides management strategies for potential successful seagrass meadow restoration. West et al. (1990) studied the survival of *Zostera muelleri* subsp, *capricorni* (Ascherson) S.W.L. Jacobs, and *Posidonia australis*, J.D. Hooker, transplants. For *P. australis* canopies, single shoots, or clumps of 2-3 shoots were transplanted, while for *Z. mulleri* subsp. *capricorni* about 20-30 shoots were used as transplanted units.

The transplants were monitored and only very few survived under high energetic events, indicating that the parametrization of the transplanted shoots may have been incomplete. In addition, Infantes et al. (2009) reported that $U_w > 38 – 42$ cm·s^{-1} caused a decrease in the cover of the *Posidonia oceanica* meadows meaning that, for these velocities, the generation of TKE within the patch will become extremely high and will produce a sufficient level of seabed erosion to potentially cause irreversible plant loss. Therefore, hydrodynamics needs to be included in the parameterization for future seagrass restoration projects.

Furthermore, Stipek et al. (2020) demonstrated that the mortality rate of seagrass patches depended on the size of the patch, with small patches (<50 m^2, $L_{patch} < 7.07$ m) undergoing a high annual mortality rate (of 57%) compared to the lower mortality rate (< 5%) found for larger patches. If a mean leaf length of 0.8 m is considered (Gruber and Kemp, 2010), assuming that leaf would bend the same percentage like that in the current study for a typical frequency of 0.5 Hz (h_v=10.5 cm for a leaf length of 14 cm, 75% of the leaf length), h_v in the field would be 0.6 m. Then their small patches would correspond to lengths equal to or smaller than $L_{patch} = 7.07$ m= 11.78 h_v. This finding aligns with the transition observed in this study, where for $L_{patch} > 10h_v$ and for typical ocean waves of f = 0.5 Hz, α_w remains constant, indicating that the patch behaves like a continuous canopy. In contrast, for $L_{patch} < 10h_v$, α_w increases towards the value for the non-vegetated case as L_{patch} decreases.

By applying the model found in the current study, the behaviour of patches found in natural seagrass meadows under different hydrodynamic conditions can be determined. In fact, two behaviours

have been observed: one where plants do not interact with the wave field and another where they do, thus generating TKE. Considering the findings of the present study, the results found by Barcelona et al. (2021a) for Cala Aiguablava and Cala Vigatà - two fragmented meadows found on the northeast Spanish coast - have been analyzed. The meadow in Cala Aiguablava presents 66% fragmentation, with the smallest patch lengths being 0.64 m and the largest 8.06 m. The plant density oscillated between 449 to 105 plants·m^{-2} between the two years studied. Meanwhile, the meadow in Cala Vigatà presents 22% fragmentation, with the smallest patches being 5.23 m long and the largest 24.82 m. The plant density in Cala Vigatà oscillated between 353 and 119 plants·m^{-2} (Barcelona et al., 2021a). These meadows are categorized as a medium patch vegetation and a perforated meadow, respectively, following the classification by Sleeman et al. (((2005, see Barcelona et al., 2021a). Using the model proposed in this study, the minimum patch size required for the vegetation to produce *TKE* for these bays has been determined by considering the typical wave frequency of the Mediterranean Sea (0.5 Hz) and a range of wave velocities between 0.5 to 30 cm·s^{-1}. For h_v = 0.6 m, $L_{canopy} = 10h_v$ would be L_{canopy} = 6 m For the high canopy densities and for U_w < 5 cm·s^{-1}, the minimum patch size required to produce TKE was L_{patch}>225 m for Cala Aiguablava and L_{patch}>963 m for Cala Vigatà, indicating unfavourable conditions for small patches under these wave velocities. In contrast, for U_w > 5 cm·s^{-1}, the minimum patch size required decreased to very low values in both bays (<0.06 m in Cala Aiguablava and <0.25 m in Cala Vigatà). In contrast, for low canopy densities and U_w> 5 cm·s^{-1} the minimum patch size was L_{patch} = 36 m for Cala Aiguablava and 24 m for Cala Vigatà, due to the different canopy densities in both meadows. Therefore, patches smaller than this threshold

would be threatened. In the low-density canopy cases and $U_w < 5$ cm·s^{-1}, the minimum patch size required would be 194,606 m for Cala Aiguablava and 125,720 m for Cala Vigatà. Under such conditions all patches would be threatened. These results align with those found by Pujol et al. (2019) for oxygen transport through the diffusive boundary layer (DBL). They found that by increasing the flow velocity, the DBL becomes thinner and the gas exchange by the plant is enhanced. They also found that for $U_w < 6$ cm·s^{-1}, the gas exchange through the DBL is reduced. This result is close to the velocity limit found for the two bays analyzed in the present study, where $U_w > 5$ cm·s^{-1} produce plant-wave interactions, generating TKE and enhancing the particle mixing.

Acknowledgements

This research was funded by the "Ministerio de Economía, Industria y Competitividad" of the Spanish Government through the grant CGL2017-86515-P. Aina Barcelona was funded by the pre-doctoral grant 2020 FI SDUR 00043 by the "Generalitat de Catalunya".

CHAPTER 5

Spatial sedimentation and plant captured sediment within seagrass patches

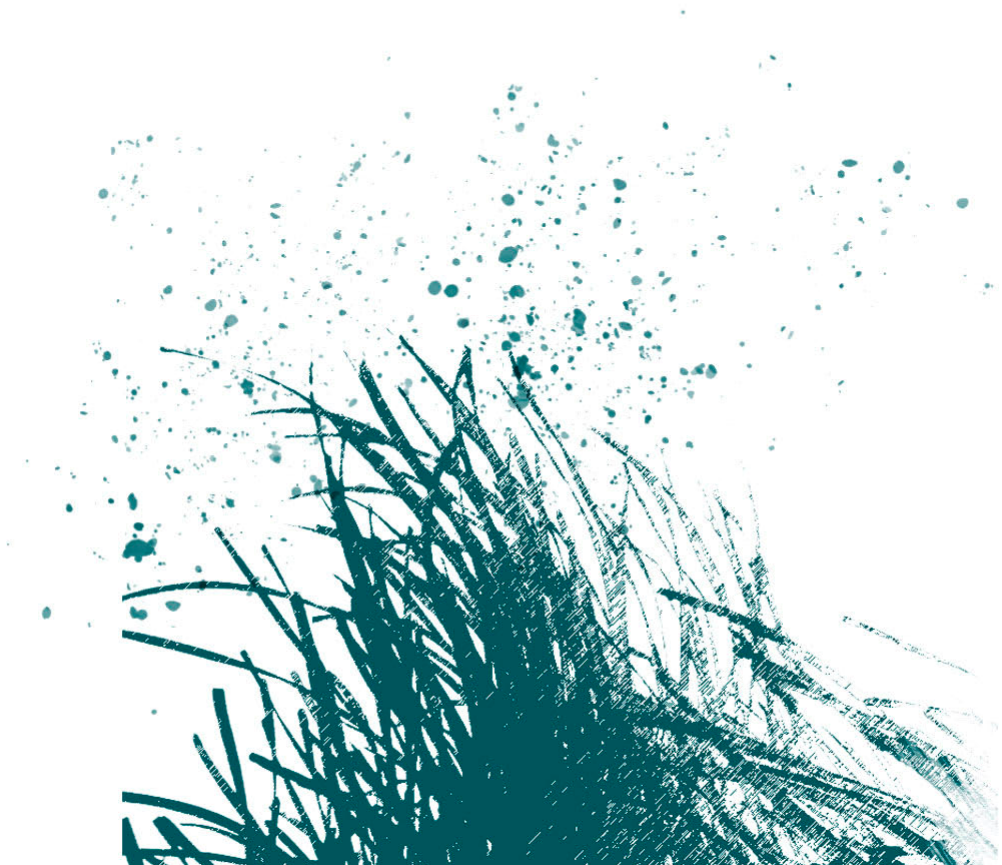

Aina Barcelona, Jordi Colomer, Teresa Serra (2023). Spatial sedimentation and plant captured sediment within seagrass patches. Marine Environmental Research 188, 105997. doi: 10.1016/j.marenvres.2023.105997.

Cover design: Carles Arbat

Abstract

Habitat degradation in coastal ecosystems has resulted in the fragmentation of coastal aquatic vegetation and compromised their role in supplying essential ecological services such as trapping sediment or sequestering carbon. Fragmentation has changed seagrass architecture by decreasing the density of the canopy or engendering small patches of vegetated areas. This study aims to quantify the role different patch sizes of vegetation with different canopy densities have in the spatial distribution of sediment within a patch. To this aim, two canopy densities, four different patch lengths, and two wave frequencies were considered. The amounts of sediment deposited onto the bed, captured by plant leaves, remaining in suspension within the canopy, and remaining in suspension above the canopy were used to understand the impact hydrodynamics has on sediment distribution patterns within seagrass patches. In all the cases studied, patches reduced the suspended sediment concentrations, increased the capture of particles in the leaves, and increased the sedimentation rates to the bed. For the lowest wave frequency studied (0.5 Hz), the sediment deposited to the bottom was enhanced at canopy edges, resulting in spatial heterogeneous sedimentation patterns. Therefore, restoration and preservation of coastal aquatic vegetation landscapes can help face future climate change scenarios where an increase in sedimentation can help mitigate predicted sea level rise in coastal areas.

Keywords: *seagrass, sedimentation, leaves capture, suspension, seagrass patch, fragmentation*

5.1 INTRODUCTION

The maritime coastal seascape has suffered from both short and long-term structural changes because of increased anthropogenic impacts, population growth in coastal areas, habitat degradation, and the increasing impact of climate change (Barsanti et al., 2007; Cacabelos et al., 2022; Leriche et al., 2006; Montefalcone et al., 2019; Valero et al., 2009; van de Koppel et al., 2012). Coastal seagrass meadows have been losing coverage over time, resulting in an increasingly fragmented landscape configuration (Barcelona et al., 2021a; Montefalcone et al., 2010). Therefore, coastal seagrasses can form large continuous meadows or more heterogeneous structures with different sized patches of vegetated areas mixed with assorted unvegetated sand or rocky beds. When a continuous seagrass meadow loses some of its vegetated area, it transforms into patchier areas with unvegetated bare soil and exhibits increasing gaps within the vegetation itself. The ability of coastal canopies to deal with both natural and anthropogenic disturbances has become a challenge for coastal marine ecosystem management and conservation as coastal canopies display patchiness that can persist over extended time scales (Bell et al., 2001; Colomer and Serra, 2021; Montefalcone et al., 2010). Consequently, individual patches of vegetation are now a typical sight in seascapes (Barcelona et al., 2021c; Borfecchia et al., 2021; Hovel et al., 2021; Pastor et al., 2022). High meadow fragmentation levels result in low shoot density in the surrounding area near gaps (Barcelona et al., 2021a), indicating the degrading effect fragmentation has.

Continuous coastal canopies are known to supply numerous ecological services such as reducing storm surges and marine heat waves, preventing the erosion of coastal beds (Madsen et al., 2001; Verdura et

al., 2021), promoting sediment accretion (Granata et al., 2001) and heterogeneous litter decomposition, impacting carbon sequestration rates (Ettinger et al., 2017), influencing estuarine geomorphology (Lera et al., 2019) as well as providing refuge and nursery grounds for the local biota (Bell et al., 2001). However, when coastal seagrasses are fragmented, their role in supplying ecological services has been reported to be increasingly compromised. The ensuing levels of deterioration depend on the degree of local patchiness and the abiotic impacts (Colomer et al., 2017). The rise in sea levels predicted by future climate change scenarios, coupled with the low input of sediments from rivers, are expected to drown deltas (Dunn et al., 2019). Restauration of aquatic vegetation landscapes is a sedimentation enhancing strategy that can be used to compensate rising sea levels (Cox et al., 2022). More rigid submerged structures like coral reefs are also known to enhance sediment accretion and offset the erosive effects of rising sea levels (Tuck et al., 2021). Therefore, to cope with future climate change scenarios, preserving aquatic vegetation among other coastal landscapes is of special relevance.

Within canopies habitat complexity generally increases not only from patch edges to patch interiors (Moore and Hovel, 2010), patch-to-patch interactions (Abadie et al., 2017; Cornacchia et al., 2019) and fragmented to full canopies (Colomer and Serra, 2021) , but also in sparse to dense vegetation (Barcelona et al., 2021c) and in the differing leaf configurations of submerged and emergent plants (Barcelona et al., 2021a; Colomer et al., 2017; Montefalcone et al., 2006). Coastal canopies provide high flow resistance, and flow and waves are diverted and intensified above and/or next to the canopy, thus increasing water velocity and turbulence along the boundaries of the patch (Chen et al.,

2013; Sand-Jensen and Mebus, 1996; Sand-Jensen and Pedersen, 2008). The balance between flow inertia, canopy drag, and canopy patch dimension determines, for example, particle deposition, which is laterally uniform (Zhu et al., 2021; Zong and Nepf, 2011) and decreases inside the canopy patch (Zhu et al., 2021), indicating that within a patch sedimentation increases.

Gacia and Duarte (Gacia and Duarte, 2001) reported that *Posidonia oceanica* meadows significantly buffer sediment resuspension. For instance, within the patch, sediment resuspension is three-fold lower than an area of bare sand. In their study, Serra et al. (2020) observed that constant sedimentation rates were found across gaps (zones without vegetation) of different sizes within a *Posidonia oceanica* meadow. They also found that sedimentation rates in the gaps within the meadow were close to those inside the canopy. In salt marshes, patches of vegetation have been found to participate in the sequestration and longstanding accumulation of sediments before they are then transported to the ocean (Pinheiro et al., 2022). Deposition of particle fluxes in patches of the seagrass *Zostera noltii* have been found higher within the patch than on bare sediments, i.e., the greater the vegetation density is, the higher the deposition rates are (Ganthy et al., 2015). Likewise, dense *Zostera marina* patches promoted the accumulation of fine sediments and organic content, therefore producing muddification in the interior of the patch. van Katwijk (2010) found that dense vegetated patches presented homogeneous sedimentation distribution, whereas although sparse vegetated patches presented a heterogeneous distribution of sediment, there was a decrease in fine particles compared to coarse particles. However, turbidity currents travelling through dense vegetated patches presented heterogeneous distributions of sediment, with fine sediment

particles accumulating in the interior of a patch and coarse particles in its exterior (Soler et al., 2021). Barcelona et al. (2021b) reported that seagrass meadows may also capture sediment on the blades and thus enhance particle sedimentation on the seabed. The number of particles trapped by the blades of seagrass plants, and subsequently deposited on the seabed, increased with canopy density which, in turn, reduced the concentration of sediments in suspension within the canopy, thus improving the water clarity within the canopy. The impact meadows have on particle deposition and resuspension depends on the degree of current and wave attenuation, indicating that patches of vegetation can reduce particle resuspension from the bottom seabed, and enhance particle deposition and carbon burial (Gacia and Duarte, 2001; Oreska et al., 2017; Paladini de Mendoza et al., 2018). Deforestation of mangrove forests has also been shown to reduce blue carbon sequestration, showing the role that large continuous vegetation landscapes can play in facing future climate change scenarios (Chatting et al., 2022).

Nevertheless, both small and sparse vegetated patch behaviour has been found to deviate from large, dense seagrass patches. Pastor et al. (2022) pointed out that once seagrass degradation reaches a tipping point, functionality is lost and patches transition to a bare soil steady state, thus compromising potential restoration. Furthermore, Sweatman et al. (2017) suggested that fragmented seagrass beds shift their nutrient loads, which subsequently impacts their ecosystem functions in many ways by, for instance, reducing the availability of suitable habitats for animals or altering the available resources. Seagrass habitat fragmentation has also been found to threaten carbon sequestration (Mazarrasa et al., 2018). Continuous meadows are expected to be more efficient sequestering carbon than fragmented meadows. Previous

experiments on the hydrodynamics of vegetated patches under oscillatory flows demonstrate that a minimum patch size is required to reduce the flow velocity through the turbulent kinetic energy being produced by plant stems (Barcelona et al., 2021c). A patch that is too small is unable to reduce waves and presents scouring at the meadow's edges (Marin-Diaz et al., 2020). However, there is still a lack of knowledge concerning the capacity seagrass patches have to capture sediment from allochthon sources. Therefore, this current study attempts to acquire knowledge as to the effect patch length and canopy density can have on the capture of sediment from allochthon sources under different hydrodynamic conditions. The sediment captured by leaves, the sediment deposited at the bottom and the sediment remaining in suspension will be studied for small (five times the leaf length) to large (14 times the leaf length) vegetated patch lengths, for two canopy densities (dense and sparse) and two different wave frequencies. The study was performed in a laboratory flume under conditions mimicking real field scenarios.

5.2 METHODOLOGY

5.2.1 The flume

The study was carried out in a methacrylate laboratory flume 600 cm long, 50 cm wide and 60 cm deep (Figure 5.1) with a mean water height of h = 30 cm. The flume was equipped with a vertical piston-type wavemaker at the entrance. The wavemaker was driven by a variable-speed motor at two frequencies (f = 0.5, and 1.12 Hz). To eliminate wave reflection, a plywood beach (slope = 1:2) covered with foam rubber was placed at the end of the flume (Barcelona et al., 2021c; Serra et al., 2018).

5.2.2 Patches of flexible vegetation

The vegetation model consisted of a series of flexible plants made from eight 0.075 mm-thick polyethylene canopy blades attached to PVC dowels that had been randomly inserted into a 250-cm long perforated baseboard (Pujol et al., 2013a). PVC rigid dowels extended 1 cm above the bed (Zhang et al., 2018). The model plants were geometrically and dynamically close to *Posidonia oceanica* plants (Ghisalberti, 2002). Leaf length, h_p, was 14 cm, and the effective height when the leaves were bent by the waves was h_v = 8.4 cm for f = 1.12 Hz and h_v = 10.5 cm for f = 0.5 Hz (Barcelona et al., 2021c). The vegetation density of patches was quantified using the solid plant fraction (SPF) defined as:

$$\mathrm{SPF}\ (\%) = 100 n \pi \left(\frac{d}{2}\right)^2 \tag{5.1}$$

where n is the number of shoots per unit area and d is the stem diameter (1 cm). Three SPFs were used (0%, 3.5% and 10%), which corresponded to vegetation densities of n = 0, 446 and 1273 stems·m^{-2}, according to the range of canopy densities (78 to 1000 stems·m^{-2}) found in coastal areas (Bacci et al., 2017; Boström et al., 2014; Colomer et al., 2017; Gera et al., 2013). SPF = 0% corresponded to the non-vegetated set-up. For each SPF, four patch sizes, L_{patch}, ranging from 70 to 196 cm in length were considered. A total of 18 experiments were performed for the different SPFs, L_{patch} and f (Table 1).

Table 5.1 Summary of the experimental conditions considered: each experimental run number (with the seagrass flexible vegetation as SFV), wave frequency (f, in Hz), solid plant fraction (SPF, in %), canopy density (n, in shoots m^{-2}), length of the vegetated patch (L_{patch}, in times the leaf length h_p), U_w (in cm s^{-1}) at z/h_v=0.4 and the ratio between the orbital excursion length (A_w), and plant-to-plant distance (S).

Run	f (Hz)	SPF (%)	n (stems· m^{-2})	L_{patch}/h_p	U_w at z/h_v=0.4 (cm s^{-1})	A_w/S
SFV 1	0.5	0	0		8.95	
SFV 2		3.5	446	0.36	9.40	0.63
SFV 3				0.64	9.37	0.63
SFV 4				0.86	8.93	0.60
SFV 5				1.00	9.22	0.62
SFV 6		10	1273	0.36	9.42	1.07
SFV 7				0.64	9.16	1.04
SFV 8				0.86	9.26	1.04
SFV 9				1.00	9.07	1.03
SFV 10	1.12	0	0		8.21	
SFV 11		3.5	446	0.36	8.33	0.25
SFV 12				0.64	7.99	0.24
SFV 13				0.86	8.02	0.24
SFV 14				1.00	8.01	0.24
SFV 15		10	1273	0.36	8.29	0.42
SFV 16				0.64	7.88	0.40
SFV 17				0.86	7.80	0.40
SFV 18				1.00	7.70	0.39

5.2.3 Sediment injection

The sediment used in the experiments was a synthetic dust powder (ISO 12103-1. A4 Coarse, Powder Technology Inc. Burnsville) with a median of 41.7 μm (Figure 5.2) and a density of 2,650 kg m^{-3}. The mean settling velocity for these sediment particles ($w_{settling}$= 1.57×10^{-3} m s^{-1}) was estimated by the Francalaci et al. (2021) formula assuming that sediment particles were nearly spherical (i.e., with a Corey shape factor equal to 1). Since the suspended sediment concentration in all the experiments was below 17.46 g L^{-1}, the sediment concentration was not expected to have any effect on the settling velocity (Colomer et al., 1998). The volumetric concentrations of suspended sediment (in $\mu L \cdot L^{-1}$) were analysed using a LISST-100X (Laser In-Situ Scattering and Transmissometry, Sequoia Scientific, Inc, Bellevue, WA) particle size analyser. The LISST-100X consists of a laser beam and an array of detector rings of progressive diameters which allow the light received at the scattering angles of the beam to be analysed. The device measures particle volume concentrations for 32 size classes (logarithmically distributed in the size range of 2.5-500.0 μm), using the procedure based on the diffraction theory of light. This instrument has been widely used for organic (Serra et al., 2001) and inorganic particles (Serra et al., 2002a). The particle size distribution of the sediment used was bimodal, with fine particles being 2.5-6.0 μm in diameter, i.e., corresponding to strongly cohesive clay and very fine silts, and coarse particles were 6.0-122.0 μm in diameter, i.e., corresponding to weakly cohesive fine to coarse silts and small sand particles (Figure 5.2). In this case, d_{50}=41.7 μm, is of the order of the grain size of river plumes in coastal areas (40-65 μm, Pitarch et al., 2019). Pitarch et al. (2019) found that the largest

non-cohesive particles settled at the mouth of the river and the finest sediment fractions were transported offshore.

The wavemaker was switched on and left to run for 15 minutes to allow the system to reach equilibrium before sediment injection. The particle-laden flow used in the injection was prepared using an initial volume (2L) of sediment suspension (with a concentration of 80 $g \cdot L^{-1}$) and introduced into one end of the sediment-injector pipe. The injector pipe was situated at y = 0 cm along the axis of the flume (Figure 5.1) While introducing the sediment into the pipe, the injectors faced upwards to avoid any uncontrolled spillage. Once the pipe had been filled with the sediment suspension, it was then closed and turned down so that injectors face downwards, protruding 5 cm below the water surface and therefore remaining at the very top of the water column and above the vegetated patch.

The sediment injector pipe consisted of a large 2.5 m-long pipe, with 42 sediment injectors evenly distributed 7 cm apart from each other. The Y-shape design of the sediment injectors was 26 cm long and each arm pipe was 22.5 cm long (see Figure 5.1a). Each arm of the pipe had 12 holes, from where the sediment injected was released into the flume, thus resulting in a homogeneous injection along both the x-axis and the y-axis.

5.2.4 Sediment measurements

To obtain the sediment particle distribution along the canopy, three different types of sediment measurements were collected: sediment settled on the bed, suspended sediment, and sediment attached to plant

leaves. To obtain the amount of sediment settled on the bed, fourteen sediment traps were distributed in two rows along the main axis of the flume and situated at y = ±16.7 cm (Figure 5.1b). The traps' positions along the x-axis of the flume for each run were related to the patch length, x = ± 0, 0.4, 0.9 and $1.4 \cdot L_{patch}$ (Figure 5.1b). Sediment traps were distributed into three subgroups: canopy, corresponding to the traps at x = ± 0 and $0.4 \cdot L_{patch}$; edge, corresponding to the traps at x = ± $0.9 \cdot L_{patch}$; and bare soil, corresponding to the traps outside the vegetated patch at x = ± $1.4 \cdot L_{patch}$. The sediment samples from the sediment traps were collected at t = 60 min from the injection time. In order to obtain information on the suspended sediment, 80 mL of suspended sediment samples were pipetted at the same x position where the sediment traps were positioned for each run, at y = 0 cm, and at two water depths (at $z/h_v = 0.4$ and at $z/h_v = 1.4$). These samples were chosen as representative samples for within and above the canopy, respectively. In this case, samples were collected at different times (t = 2, 30 and 60 min) from the injection time, and analysed for suspended sediment concentration. To obtain information about the amount of sediment deposited on the plant leaves, at the end of each experiment (t=60 min) five plants were gently removed at the same x positions within the vegetated patch as the sediment traps had been placed. They were then introduced into a beaker with 80 ml of water and the plants were stirred in the fluid to remove the sediment trapped by the surface of the leaves, after which particle concentration was analysed with the particle analyser LISST-100X.

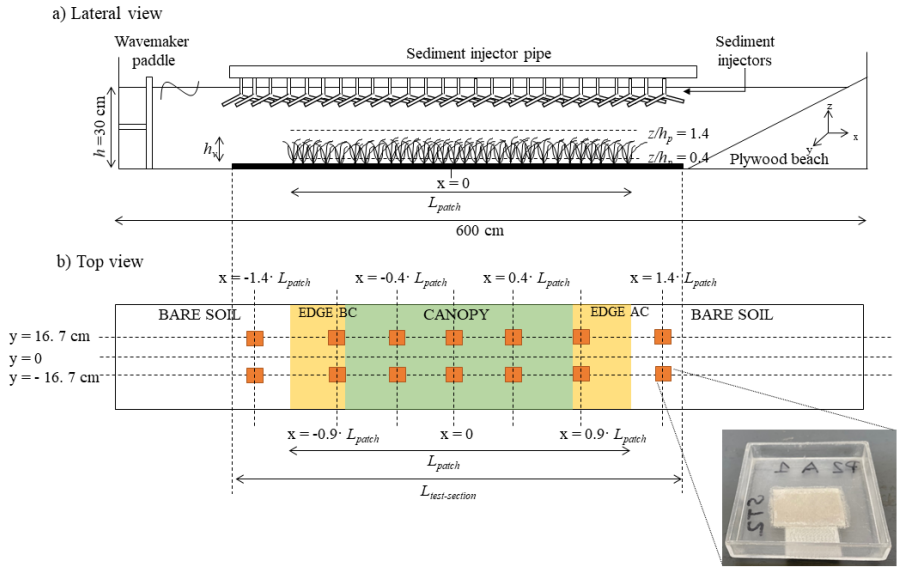

Figure 5.1 Scheme of the experimental set-up a) Lateral view of the flume with the patch of flexible vegetation. The patch lengths ranged from L_{Patch}= 70 to 196 cm. b) Top view of the set-up. The region coloured in orange and green correspond to the patch. The green coloured area corresponds to the inner canopy region and the orange-coloured area corresponds to the edge region of the canopy. The Edge BC corresponds to the edge closest to the wavemaker and the Edge AC corresponds to the edge furthest from the wavemaker. Orange squares represent the sediment traps distributed along the flume bed.

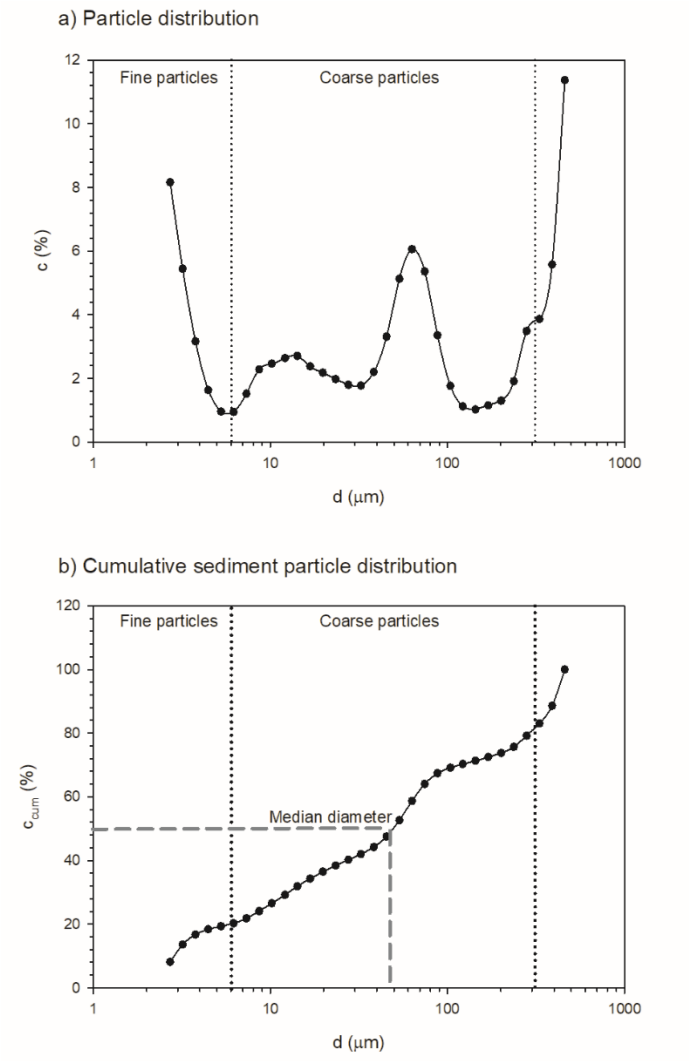

Figure 5.2: a) Volumetric sediment particle size distribution (c, in %). b) Cumulative sediment particle size distribution (c_{cum}, in %). Dashed lines show the median diameter (i.e., the diameter where 50% of the cumulative distribution holds, d_{50}=41.7 µm). In both figures, two different particle sizes are shown: fine particles below 6 µm, and coarse particles between 6 µm and 122 µm.

5.2.5 Sediment capture distribution analysis

To calculate the amount of sediment collected in the different compartments of the system, a test section of $14h_p$ was considered. In other words, it coincided with the longest patch studied (see Figure 5.1). The test section had different configurations depending on the presence or absence of vegetation. In the cases with vegetation, patch length and canopy density determined the amount of vegetation in the system. The test section had a vegetated vertical region within the canopy and an unvegetated vertical region above the canopy. In the non-vegetated experiments, the same two vertical layers were considered for the purpose of comparison.

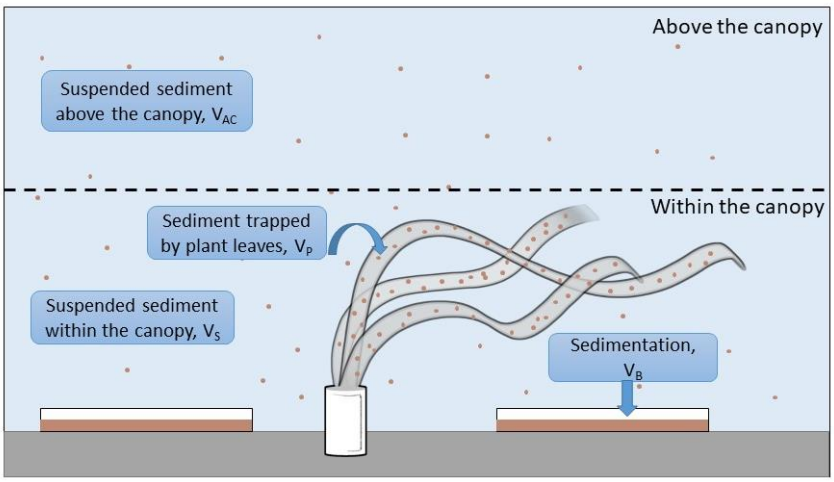

Figure 5.3 Distribution of sediment in the four different compartments: on the plants (V_P), on the bed (V_B), in suspension within the canopy (V_S) and in suspension above the canopy (V_{AC}).

The sediment trapped by the leaves, V_P (Figure 5.3), corresponded to the sediment attached to the surface of the plant leaves. The concentration of sediment measured with the LISST -100x was divided by the number of plants collected for sampling and the volumetric concentration of sediment collected per plant was obtained. The concentration obtained was afterwards multiplied by the volume of the water used to rinse the plants (80 mL) and the total volume of sediment deposited was obtained (V_P, in μL).

The amount of sediment in suspension within the canopy (V_S, Figure 5.3) was calculated from the samples collected in suspension at a 5 cm depth above the bottom of the flume. The same depth was considered for the non-vegetated cases. For experiments carried out with vegetation, the test section had a vegetated part and a bare soil part. The volume of particles in suspension (V_S, in μL) was calculated by multiplying the concentration within the canopy by the volume of the patch ($L_p \times h_v \times W$, where W is the width of the flume) plus the concentration in suspension in the bare soil multiplied by the volume of sediment collected in the bare soil ($(L_{test\text{-}section}-L_p)\times h_v \times W$). In the case without vegetation, the volume of sediment in suspension was calculated by multiplying the concentration of sediment in suspension by the volume of the test section ($L_{test\text{-}section} \times h_v \times W$). The same calculation was carried out for the suspended sediment concentration above the canopy (at 20 cm above the bottom, V_{AC}, in μL). However, the vertical extension in this case was ($h-h_v$) instead of h_v used for the within canopy section.

The amount of sediment deposited at the bottom of the flume (V_B, in μL, Figure 5.3) was calculated from the samples collected with the sediment traps. The concentration of sediment collected by the sediment traps was

measured by the LISST-100X. The volume of sediment was obtained by multiplying the concentration obtained by the volume of the sample. Since the volume of sediment obtained corresponded to the area of the sediment trap (5 cm × 5 cm), the total volume of sediment deposited in the region where the trap was positioned was obtained by multiplying by the ratio of the total area of the region where the trap was situated (edge, bare soil, or vegetation) divided by the area of the test section. The total volume of sediment (V_B) at the bottom of the test section was calculated as the sum of the volume of sediment collected at the bottom of the bare soil plus the sediment collected at the edge and the sediment collected at the canopy regions.

The total volume of sediment was obtained by adding the volume of particles for each compartment in the test section ($V_{TOTAL}=V_P+V_{AC}+V_S+V_B$). From the total volume, the percentage of sediment particles in each compartment was calculated.

5.2.6 Measuring velocities

The Eulerian velocity field was defined as (u, v, w) in the (x, y, z) directions of the flume, respectively. The three components of velocity were recorded with a downwards looking Acoustic Doppler Velocimeter (16-MHz MicroADV, Sontek) at a frequency of 50 Hz over 10 min (obtaining a set of 30000 data for each sampling point). Flow velocity profiles were measured at the centre of the patch and at z= 17 cm, 16 cm, 12 cm, 8 cm, 6 cm, 5 cm, 4 cm, 3 cm, and 2 cm from the bed of the flume. The ADV measures 5 cm from the probe tip with a sampling volume of 0.09 cm^3. Beam correlations less than 80% were discarded and spikes

were removed (Goring and Nikora, 2002; Pujol et al., 2013a). For oscillatory flows, the instantaneous velocity, $U_i(t)$, can be decomposed as:

$$U_i(t)=U_c+ U_w+ u' \quad (5.2)$$

where U_c is the steady velocity associated with the current, U_w is the unsteady wave motion which represents spatial variations in the phase-averaged velocity field, and u' is the turbulent velocity, that is, the instantaneous velocity fluctuation in the x-direction. U_c is the phase-averaged velocity:

$$U_c= \frac{1}{2\pi}\int_0^{2\pi} U_i(\varphi)\partial\varphi \quad (5.3)$$

where $U_i(\varphi)$ is the instantaneous velocity according to the phase (Lowe et al. 2005, Luhar et al.(2010). In the current study U_c at z/h_v=0.4 above the bed (i.e. within the canopy layer) was always smaller than U_w, with mean values of 0.44 cm s^{-1} and -0.05 cm s^{-1} for the wave frequencies of 1.12 Hz and 0.5 Hz, respectively.

Wave velocity, U_w, was obtained by using a phase averaging technique. The Hilbert transform was used to average oscillatory flow velocities with a common phase (Pujol et al., 2013a; Ros et al., 2014). The root mean square (rms) of $U_i(\varphi)$ was considered as the characteristic value of the orbital velocity U_w^{rms} (U_w hereafter) at each depth, and was calculated according to:

$$U_w^{rms} = \sqrt{\frac{1}{2\pi}\int_0^{2\pi} (U_i(\varphi)-U_c)^2\partial\varphi} \quad (5.4)$$

5.2.7 Theory

A non-dimensional model was constructed based on the Pi-Buckingham theorem. Four main variables and two dimensions were considered in this current study. The variables are the wave excursion length ($A_w=U_w/(2\pi f)$), the plant-to-plant distance ($S=n^{-1/2}$), the patch length (L_p) and the effective vegetation height (h_v). The effective vegetation height is the height of bent plants when they swing with the flow and will depend on the wave frequency (Barcelona et al., 2023a, 2021b). The two dimensions are metres and seconds. Therefore, two governing non-dimensional parameters can be constructed to describe the results. First, A_w/S, i.e., the ratio between the wave excursion length and the plant-to-plant distance, accounts for the penetration of the wave within the vegetated patch. And second, L_p/h_v, which is the ratio between the length of the patch, L_p and the effective vegetation height h_v. Based on the above governing parameters, it is possible to expect that the percentage of sediment trapped by the leaves, the sediment in suspension and the sediment settled at the bottom of the tank, is a function of the dimensionless parameters, A_w/S and L_p/h_v (Zong & Nepf 2011).

5.3 RESULTS

After 60 min (from injection) had lapsed, the concentration levels of the sediment in suspension reached a steady state. In this steady state, the injected sediment was distributed into the four regions considered

(Figure 5.3): attached to the plant leaves, deposited at the bottom of the flume, or in suspension either above or within the canopy.

For each wave frequency considered, the concentration of particles trapped by individual plant leaves did not differ between the different regions (canopy and edges) (Figure 5.4a and b). However, the behaviour of the sediment concentration with L_p/h_v was different depending on wave frequency. For the lower frequency (f = 0.5 Hz), the longer the patch length, the greater the amount of sediment trapped on the leaves (Figure 5.4a). In contrast, for the highest frequency (f = 1.12 Hz), the longer the patch length, the lower the amount of sediment trapped by plant leaves (Figure 5.4b).

The sediment concentration deposited at the bottom behaved differently depending on wave frequency. For the lowest wave frequency (f = 0.5 Hz), an increase in the patch length resulted in an increase in the sediment deposited at the bottom. Likewise, lower sediment concentrations were found within the canopy instead of at the edges (Figure 5.4c). Meanwhile, for the highest frequency (f = 1.12 Hz), the sediment deposited at the bottom remained constant for all the patch lengths studied (Figure 5.4d). In addition, for this wave frequency, there were no differences in sediment concentration levels between the edges and the canopy (Figure 5.4d).

The suspended sediment concentration levels presented the same behaviour for the two wave frequencies studied: f = 0.5 and 1.12 Hz. The greater the patch length, the lower the sediment concentration that remained in suspension. In this case, there were no differences in

suspended sediment concentration levels between the edge and the canopy (Figure 5.4e and f).

Furthermore, it must be noted that, although both the sediment deposited on the leaves and the sediment remaining in suspension had the same range for the two wave frequencies studied (Figure 5.4a, b, e and f), the range of the amount of sediment deposited at the bottom for f = 0.5 Hz was ten times that for f = 1.12 Hz (Figure 5.4c and d).

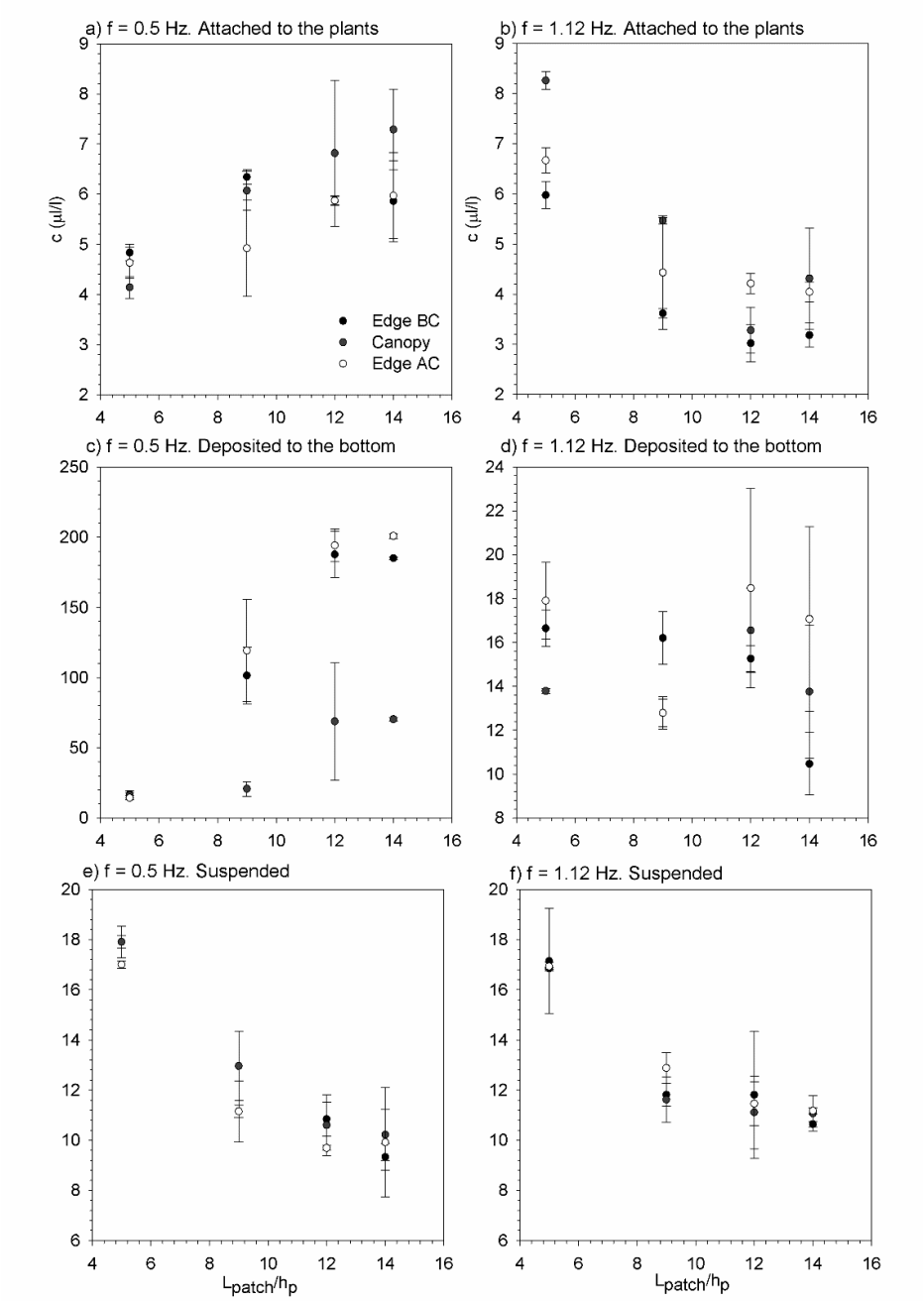

Figure 5.4 Sediment concentration, c, trapped by the plant leaves vs. the ratio between patch length and plant height, L_{patch}/h_p for experiments carried out at SPF=3.5%. Blue circles correspond to measurements taken at the edge BC (Figure 5.1); red circles to the measurements taken in the inner canopy area;

and unfilled circles to the measurements taken at the edge AC (Figure 5.1). For a) f = 0.5 Hz and for d) f = 1.12 Hz. Sediment concentration, c, deposited at the bottom of the flume vs. L_{patch}/h_p, for b) f = 0.5 Hz and for e) f = 1.12 Hz. Suspended sediment concentration, c, remained in suspension within the canopy at $z/h_p = 0.4$, for c) f = 0.5 Hz and for f) f = 1.12 Hz.

The dependence of the percentage of the volume of sediment particles trapped by the leaves, $V_{P,}$ with the non-dimensional parameter $(A_w/S)/(L_p/h_v)$ presented two regimes (Figure 5). For $(A_w/S)/(L_p/h_v) < 8$, a first regime where V_P remained constant with $(A_w/S)/(L_p/h_v)$ with V_P = 4.7 %. However, for $(A_w/S)/(L_p/h_v) > 8$, V_P increased linearly with $(A_w/S)/(L_p/h_v)$ (Figure 5.5). The first regime (left part of Figure 5.5) mainly corresponded to cases with the highest frequency (f = 1.12 Hz). In contrast, the second regime (right part of Figure 5.5) corresponded mainly to the experiments carried out with the lowest frequency (f = 0.5 Hz), independent of the canopy density.

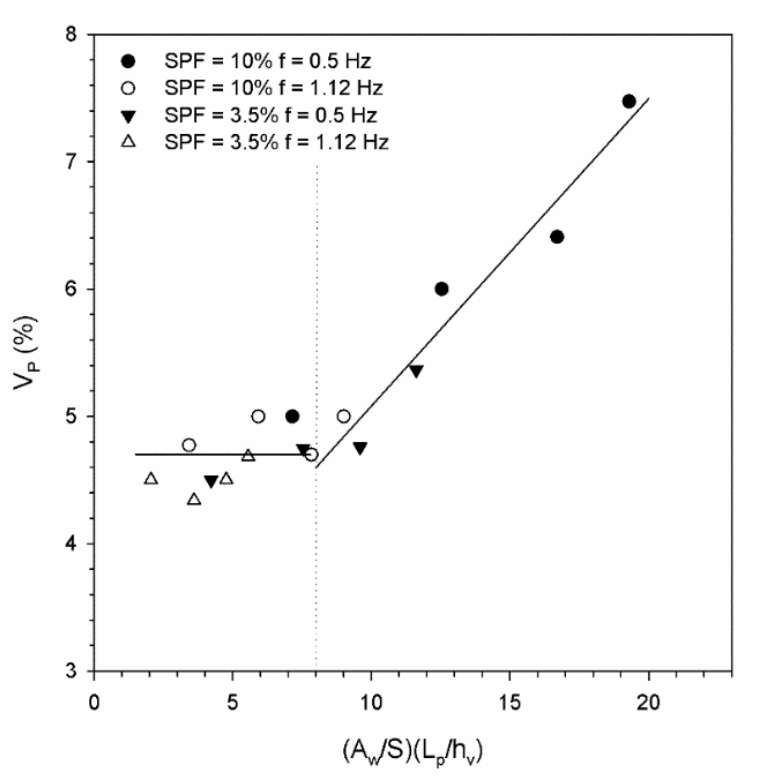

Figure 5.5 Relationship between the volume of sediment trapped by the leaves, V_P, and $(A_w/S)/(L_p/h_v)$ for all the experiments carried out. The vertical dashed line represents the minimum value of $(A_w/S)/(L_p/h_v)$ that separated the different behaviours observed. The horizontal solid line at V_P = 4.7 % represents the mean value of V_P for $(A_w/S)/(L_p/h_v) < 8$, where the V_P remained constant. For $(A_w/S)/(L_p/h_v) > 8$ a linear tendency was found with $V_P = 0.17 * (A_w/S)/(L_p/h_v) + 3.31$, with $R^2 = 0.80$ and 95% of confidence.

The volume of particles remaining in suspension (in %) within the canopy was found to decrease linearly with $(A_w/S)/(L_p/h_v)$ (Figure 5.6).

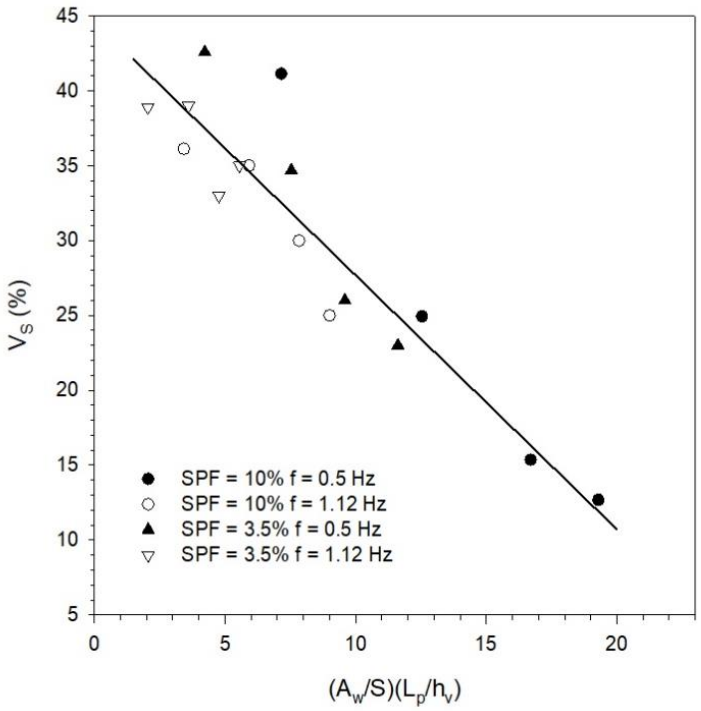

Figure 5.6 Relationship between the sediment that remained in suspension, Vs, for all the experiments carried out. The solid line represents the linear tendency that was found Vs = -1.76 * $(A_w/S)/(L_p/h_v)$ + 44.60, with R^2 = 0.88 and 99% of confidence.

The volume of the sediment deposited at the bottom (V_B, in %) versus $(A_w/S)/(L_p/h_v)$ presented two regimes (Figure 5.7). A first regime for $(A_w/S)/(L_p/h_v) < 8$, where V_B remained constant with $(A_w/S)/(L_p/h_v)$ with V_p = 22.6 %. A second regime for $(A_w/S)/(L_p/h_v) > 8$, where V_P increased linearly with $(A_w/S)/(L_p/h_v)$ (Figure 5.7). As with V_P, the first regime (left part of Figure 5.7) mainly corresponded to the cases carried out with the highest frequency (f = 1.12 Hz) and the second regime (right part of Figure 5.7) to the experiments carried out with the lowest frequency (f =0.5 Hz).

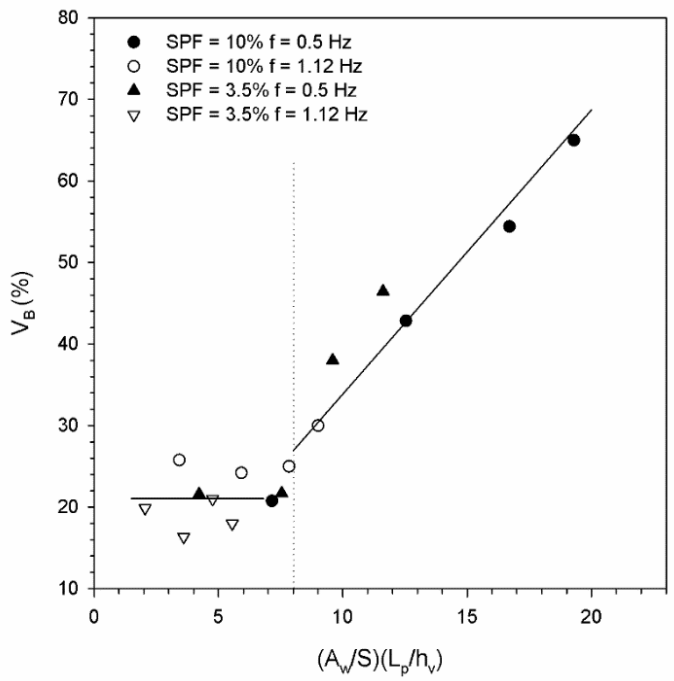

Figure 5.7 Relationship between the volume of sediment deposited at the bottom, V_B, for all the experiments carried out. The vertical dashed line represents the minimum value of $(A_w/S)/(L_p/h_v)$ that separated the different trends observed for the V_B. The horizontal solid line at $V_B = 22.58\%$ represents that for $(A_w/S)/(L_p/h_v) < 8$, where the V_B remained constant. For $(A_w/S)/(L_p/h_v) > 8$, a linear tendency was found $V_B = 3.15^* (A_w/S)/(L_p/h_v) + 3.92$, with $R^2 = 0.95$ and 99% of confidence.

5.4 DISCUSSION

The current study demonstrates that both the architectural structure of a seagrass patch and the hydrodynamics impact sediment distribution. That is, the amount of sediment deposited on the bed and plant leaves, and the suspended sediment presents different percentages depending on

the structural characteristics: patch length and plant density, and on the hydrodynamics, here the through-the-wave frequency.

Plant leaves captured sediment with a concentration that did not differ between whether the plants were situated within the canopy or at the edges of the canopy. However, it is interesting to notice that the sediment concentration captured by plant leaves increased with the patch size for the wave frequency of 0.5 Hz and decreased with the patch size for 1.12 Hz. This difference might be because plants in large seagrass patches and low frequency wave environments have a large swing movement with a greater stroke, which would increase the chance of sediment particles being captured by single plants. On the other hand, the fast movement of the plant leaves in large seagrass patches and under a wave frequency of 1.12 Hz may increase the friction between leaves and cause the ejection of particles, thus reducing the chance of particles being potentially captured by plant leaves (Barcelona et al., 2021b).

Sediment particles deposited on the bottom also presented different behaviours depending on the wave frequency. In wave frequency environments of 0.5 Hz, plants in large seagrass patches played a synergistic role, consequently increasing by nearly ten times, the amount of sediment deposited onto the bottom from the smaller patch of $5h_p$ up to the largest patch of $14h_p$. In this case, sedimentation was maximized at the edges of large patches. This result agrees with those of Navarrete-Fernández et al. (2022) who found that microparticles presented the maximum sedimentation rates at the edges of the canopy, while decreasing towards the inner canopy. Zong and Nepf (2011) also found a heterogeneous distribution of sediment deposition in a patch of

vegetation in a unidirectional flow. In their case, high deposition rates were observed at the edge of dense patches of vegetation, while also decreasing towards the patch interior. The sedimentation within the vegetation obtained for the case of wave frequencies of 1.12 Hz, was also lower than that for wave frequencies of 0.5 Hz. This can be attributed to the different movements of waves of different frequencies. In the case of 0.5 Hz, plants moved back and forth. In contrast, in the case of 1.12 Hz, plants were bent and oscillated asymmetrically to one side (see videos in the Supplementary Material). The different movements could cause different boundary layers for the different wave frequencies. Measurements of the suspended particle concentration levels above the canopy reveal that for the frequency of 0.5 Hz the suspended concentration levels was 25% lower than for 1.12 Hz. Therefore, the low sedimentation associated to 1.12 Hz could be because more particles accumulate above the canopy than in the case of 0.5 Hz. The different behaviour of the vegetation under different wave frequencies results in different boundary conditions being produced by the plants which can also explain why 0.5 Hz presents heterogeneous horizontal patterns compared 1.12 Hz, where a horizontal homogeneous sedimentation pattern holds. Likewise, note that the sediment concentration obtained in the non-vegetated experiment was 15.0 μL/L, i.e., close to that obtained for the small patch of $5h_p$. This indicates that the effect of the small patch of $5h_p$ on sedimentation does not deviate much from the non-vegetated case. This result is in accordance with the findings by Colomer et al. (2017), who found that $6.6h_p$ patches of *Posidonia Oceanica* produce low sheltering of the bed, i.e., close to bare soil conditions.

Under a wave frequency of 1.12 Hz, the concentration of sediment deposited onto the bottom for all the patches studied was close to that

obtained for the smallest patch with the lower wave frequency, and to the sedimentation for the non-vegetated case for that same wave frequency (11.0 μL/L). Contrary to the wave frequency of 0.5 Hz, under the wave frequency of 1.12 Hz, the concentration of sediment deposited at the bottom of the patch did not depend on patch length. In this case, the sediment concentration was distributed homogeneously throughout the patch without any differences between canopy edges and the inner region. Therefore, the impact of a seagrass patch on the sedimentation rates also depends on the hydrodynamics of the flow, with heterogeneous distribution in wave frequencies of 0.5 Hz, and homogeneous distribution in wave frequencies of 1.12 Hz.

Contrary to what has been observed for the flux of sediment to the bottom and the capture of sediment by plant leaves, suspended sediment presents the same behaviour under both wave frequencies, 0.5 Hz and 1.12 Hz. In both cases, an increase in the patch length caused a decrease in the concentration levels of suspended sediment within the canopy. In addition, the suspended sediment concentration levels for the 1.12 Hz wave frequency was close to that obtained for 0.5 Hz. Therefore, the water quality within the patch, through a reduction in particle concentration, improves as the length of the patch increases. It must also be noted that under both frequencies no differences in suspended sediment concentration levels were observed between canopy edges and patch interiors. The suspended sediment concentration ranged between 10 μL L^{-1} to 18 μL L^{-1}. The density of the sediment used in the current study was 2,650 Kg m^{-3}, which resulted in a suspended sediment concentration of 45 mg L^{-1}. This concentration is within the

concentration range of river sediment plumes in natural environments (Liu et al., 2022; Tassan, 1997; Warrick et al., 2004).

The percentage of particles captured by plant leaves was nearly constant 4.7% versus the non-dimensional parameter $(A_w/S)(L_p/h_v)$ up to a threshold of $(A_w/S)(L_p/h_v)=8$. For $(A_w/S)(L_p/h_v)>8$, the percentage of particles captured by plant leaves increased linearly with $(A_w/S)(L_p/h_v)$. This second region indicates that more sediment particles are captured by plant leaves when A_w/S or L_p/h_v increase. The volume of sediment deposited on the bed presents the same threshold at $(A_w/S)(L_p/h_v)=8$, from where the percentage of sedimentation increases with $(A_w/S)(L_p/h_v)$ for $(A_w/S)(L_p/h_v)>8$. In contrast, for $(A_w/S)(L_p/h_v)<8$ the percentage of deposited particles on the bed remains constant at its lowest value of 22.6%, indicating that the vegetated patch does not produce any effect on the sedimentation.

For $A_w/S>0.35$, seagrass patches dissipate wave velocity by generating turbulent kinetic energy (Barcelona et al., 2023). In this regime seagrass patches behave like canopies, in contrast, for $A_w/S<0.35$ seagrass patches present a single stem-like behaviour and do not generate turbulent kinetic energy. In the current study, all cases with $A_w/S>0.35$ correspond to $(A_w/S)(L_p/h_v)>8$, where the seagrass patch has the role of both increasing sediment capture by plant leaves and sedimentation at the bottom. Therefore, from the results of the current study, seagrass patches behave as canopies when $(A_w/S)(L_p/h_v)>8$. This case is expected to hold for both high A_w/S or L_p/h_v. High values of A_w/S indicate that waves interact with the canopy dissipating the mean energy of the flow, and it also means that the orbital excursion length of the wave is greater than the plant to

plant distance. Therefore, the canopy protects the bed from the oscillatory flow. L_p/h_v represents the longitudinal extension of the vegetated patch. The larger the patch, the greater its effect on the bed will be. This result agrees with Zhu et al. (2021) who observed that seagrass meadows trapped sediment due to the reduction of the mean energy of the flow (waves and currents). They observed this result when seagrass meadow density was high. *Posidonia oceanica* seagrasses have been found to increase the deposition of sediment particles compared to bare soil (Gacia and Duarte, 2001). In their work, waves of frequencies between 0.33 s^{-1} and 0.07 s^{-1} lead to bed orbital velocities of 2-10 cm s^{-1}, and mean shoot densities of 200 shoots m^{-2}, resulting in $A_w/S=0.672>0.35$. Therefore, this case corresponds to the case of a canopy that reduces the mean energy of the flow through the production of turbulent kinetic energy and, in turn, enhances the deposition of sediment to the bed.

Therefore, the current study demonstrates that the threshold for when a seagrass patch of length L_p preserves canopy characteristics depends on the hydrodynamics (through A_w), the seagrass density (through S) and the effective plant height h_v, which, in turn, depends on the hydrodynamics and the plant flexibility. From the current study, small patches of vegetation produce a low deposition of sediment on the bottom and on their leaves, thus presenting a high suspended sediment concentration. These patches of vegetation are expected to be more vulnerable under adverse conditions. These results might also explain how an increase in patchiness leads to small fragmented *Zostera marina* seagrass patches of 5.6-10 m long disappearing due to anthropogenic pressures (García-Redondo et al., 2019a). Olesen and Sand-Jensen

(1994) observed high rates of *Zostera marina* mortality for small and sparse seagrass patches. Moreover, López-y-Royo et al. (2011) used ecological indicators to categorize the water quality in the evolution of *Posidonia oceanica*. In their study, low water quality was associated with *Posidonia oceanica* densities below 200 shoots m^{-2}. The current study demonstrates that for a sparse canopy to provide the required ecological services compared to a dense canopy, it must have a large patch. Therefore, the current study highlights the fact that canopy density is not the only crucial parameter indicating meadow quality, as so too does the length of the seagrass patch. Long and continuous seagrass meadows are expected to provide seabed sediment stabilization and boost sediment trapping, thus providing a sediment enhancing strategy to cope with future sea level rises or improve carbon sequestration levels.

Acknowledgments

This project has been funded by the Ministerio de Ciencia e Innovación of the Spanish Government through the grant PID2021-123860O3-100. Aina Barcelona was founded by the pre-doctoral grant 2020 FI SDUR 00043 by the “Generalitat de Catalunya”.

CHAPTER 6

Stem stiffness functionality in a submerged canopy patch under oscilation flow.

Aina Barcelona, Jordi Colomer, Teresa Serra (2023). Stem stiffness functionality in a submerged canopy patch under oscillatory flow. Scientific Reports 13: 1904. doi: 10.1038/s41598-023-28077-2.

Cover design: Carles Arbat

Abstract

Seagrass canopies are coastal ecosystems that are able to modify the abiotic environment through their architectural structure. They have different structural parameters, such as plant stem stiffness, patch length and canopy density, all of which determine their overall functionality in modifying the seafloor hydrodynamics within coastal areas. To determine the interaction between hydrodynamics and the canopy structure, a set of laboratory experiments were carried out with both rigid and flexible stems for different canopy densities, patch lengths and wave frequencies. In the upper part of the canopy, flexible plants move with the flow without generating drag or producing turbulent kinetic energy, while rigid plants generate drag and produce turbulent kinetic energy. In the inner canopy layer, both types of plants behave like rigid stems and produce turbulent kinetic energy. A non-dimensional model based on the turbulent kinetic energy, the wave velocity and the plant characteristics is presented to describe the behaviour of flexible and rigid plants under an oscillating flow. Flexible plants behave in a stiffer manner under high wave frequencies than under low wave frequencies, thus making their behaviour closer to that of rigid plant stems. This difference between both canopy structures can explain their distribution in the environment, with rigid canopies being more extended in more sheltered regions while flexible plants are characteristic of more exposed regions with high flow energy.

Keywords: *waves, coastal seagrasses, rigid vegetation, flexible vegetation, seagrass fragmentation.*

6.1 INTRODUCTION

Seagrasses are valuable coastal ecosystems that protect the seabed from waves and currents (Gacia et al., 1999; Pujol et al., 2013a). They also provide habitats for aquatic life, improve water quality, sequester carbon, and stabilize sediment (Ricart et al., 2015; Unsworth et al., 2019; Zong and Nepf, 2011). However, they are situated in regions where anthropogenic activities like anchoring, dredging, trawling, or sewage outflow cause their decline (Colomer et al., 2017; Unsworth et al., 2017). Human pressure has produced a 30%-60% decline in seagrasses (Evans et al., 2018). In some places, seagrasses have completely disappeared, while in others seagrass landscapes have changed from large continuous meadows to fragmented canopies (Sleeman et al., 2005), where a patchy distribution of plants dominates the seascape.

There is a lack of data concerning the hydrodynamics for all types of canopies, patch characteristics and the degree of landscape fragmentation (Folkard, 2019).While the hydrodynamics in continuous meadows is expected to be spatially homogeneous, in fragmented meadows (El Allaoui et al., 2016) it is likely to be spatially heterogeneous. In addition, the increase in the degree of meadow's fragmentation also increases the overall turbulent kinetic energy, thus enhancing mixing for a greater sediment resuspension (El Allaoui et al., 2016). Therefore, it is expected that canopy fragmentation increases meadow vulnerability under external pressures (Gera et al., 2013).

Considering that fragmented landscape seagrasses are made up of patches of different sizes (Robbins and Bell, 1994), patch length, then, is expected to determine the hydrodynamics in fragmented meadows. Interspersed within vegetation of fragmented meadows are gaps (i.e.,

zones without vegetation). The larger the gap, the greater the turbulent kinetic energy and wave velocity within that gap is (Serra et al., 2020). However, for a certain gap size, the degree of meadow fragmentation has not been found to impact the hydrodynamics (Serra et al., 2020). In contrast, the degree of fragmentation does impact canopy density at canopy interfaces near a gap (Barcelona et al., 2021a). These results reveal the need for more studies into the effect fragmentation has on the hydrodynamics within a fragmented meadow.

Vegetation produces a flow resistance that can differ depending on the plants' distinct structural characteristics, i.e., stem diameter, height, thickness, whether plants are submerged or emergent, their flexibility and horizontal distribution (density, staggered or random). Laboratory studies using models of rigid stems under oscillatory flows have shown that the wave velocity attenuation is greater for emergent stems than submerged ones (Pujol et al., 2013b). Many of the studies into the hydrodynamics in rigid meadows under oscillatory and unidirectional flows have been conducted in laboratory flumes (Chen et al., 2020; Pujol et al., 2013a; Tinoco and Coco, 2014) in order to understand the role seagrasses play in sheltering the seabed. In addition, studies of the hydrodynamics in flexible meadows have also been carried out in the laboratory to better mimic seagrasses and understand the effect of flexibility. A flexible plant exhibits different configurations compared to rigid plant stems as they can remain erect, sway or be prone (Nepf and Vivoni, 2000). The turbulent kinetic energy within a meadow of submerged flexible plants has been found to depend on A_w/S, i.e., the ratio between the orbital wave excursion A_w and the plant-to-plant distance S (Zhang et al., 2018). For $A_w/S>1$ the turbulent kinetic energy (TKE) increases with A_w/S whereas it remains constant for $A_w/S<1$

(Zhang et al., 2018). It must be pointed out that, despite the different structure of rigid and flexible stems, for low flow velocities the behaviour of flexible plant stems can be close to that of rigid plant stems due to the small amount of bending involved. However, the behaviour of patches of vegetation with different sizes of flexible and rigid plants has yet to be studied.

Understanding the relationship between all of the above-mentioned structural characteristics of the vegetation, along with the hydrodynamics might, offer clues as to what the optimal patch length scales, meadow densities or plant distributions are that could explain the resilience exhibited by some meadows. Some studies reveal that there are positive ecological interactions that favour the success of seagrass restoration (Valdez et al., 2020). The authors of these studies note that canopy density might play a positive dependence role, thus improving the survival of a seagrass population. Other structural parameters might likewise play critical roles in facilitating restoration projects, for instance, the minimum patch size that a patch of vegetation has to have or the arrangements of the stems in the patch. Hydrodynamics and plant characteristics have been found to determine sediment scouring that in turn can compromise seagrass restoration strategies (Bouma et al., 2009). High turbulent flows can lead to sediment scouring around plant stems.

Bouma et al. (2005) compared the role of *Spartina alternifora* plants to that of *Zostera noltii*. (*Spartina alternifora* shoots are much stiffer than *Zostera noltii* shoots) in terms of their capacity to dissipate hydrodynamic forces) and found that dissipation was three times higher in vegetation with stiffer leaves than in vegetation with flexible leaves. They hypothesized that the drag exerted by the flow limits how far off

the coast *Spartina* can grow. In more exposed areas, where the hydrodynamics are strong, other drag-minimizing species like *Zostera noltii* will grow, generating a sharp interface or transition between the extension of both types of ecological engineers. Therefore, seagrasses need to withstand hydrodynamic forces so that the costs (through drag) and benefits (their ability to modify the habitat conditions) are advantageous for their survival (Bouma et al., 2005). In addition, seagrasses have been found to have the capacity to adapt to certain environmental conditions by acclimation of their flexibility (Bouma et al., 2005). Paul and de los Santos (2019) found that *Zostera marina* leaves were more rigid in summer than in winter and in deep sheltered zones than in shallow exposed zones where they presented more flexible leaves.

Hydrodynamics being modified by different types of plants (flexible or rigid) and patch lengths is still of concern and the role patch length plays for different plants' stiffness needs to be investigated. In the present study, the behaviour of single patches of different sizes formed by a random distribution of rigid or flexible plants under oscillatory conditions has been investigated. To this purpose, laboratory experiments were carried out in a flume using models of both rigid and flexible plants. To determine the behaviour of plants (rigid and flexible) under different hydrodynamic conditions two wave frequencies were considered. In addition, previous results obtained by other authors for a fixed patch length have been included in the study to provide a wider range of flow conditions and to compare between rigid and flexible plants. The modification of the hydrodynamics on the vertical axis by each type of plant and for each wave field was studied through the behaviour of the turbulent kinetic energy (TKE). The TKE can then be

an indicator of the sediment resuspension in each set-up and provide clues on the possible resilience of seagrasses under different hydrodynamic conditions.

6.2 METHODOLOGY

6.2.1 The flume

The study was carried out in a laboratory methacrylate flume (600 cm long, 50 cm wide, and 60 cm deep, Figure 6.1) with a mean water height of h = 30 cm (Table 6.1). The flume was equipped with a vertical paddle-type wavemaker at the entrance. The wavemaker was driven by a variable-speed motor at two frequencies (f = 0.5 Hz, 1.12 Hz). Wave heights measured by a wave gauge indicated that wave amplitudes were 6 cm and 3 cm for wave frequencies of 1.12 Hz and 0.5 Hz, respectively. A plywood beach (slope = 1:2) was placed at the end of the flume and covered with foam rubber to eliminate wave reflection (Pujol et al., 2013a; Serra et al., 2018). In the longitudinal direction, x = 0 cm was situated at the wavemaker, in the lateral direction, y = 0 cm was in the centre of the tank, and in the vertical direction, z = 0 cm was situated at the flume bed.

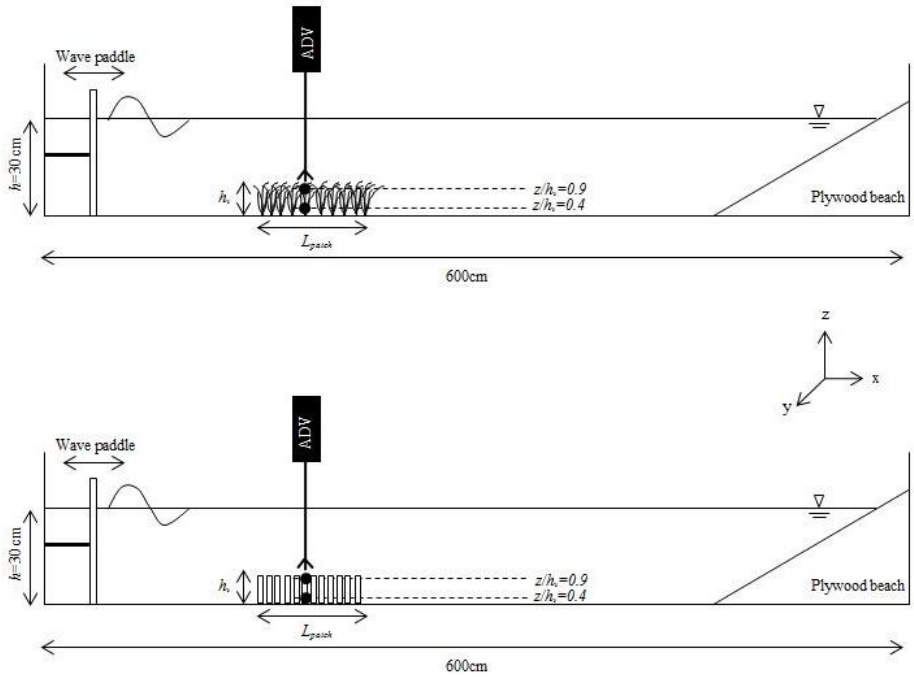

Figure 6.1 Lateral view of the experimental setup, with the wave paddle on the left. Experiments were conducted in a 600x50x50 cm long flume, with a mean water depth of 30 cm. The model patch had lengths that ranged from 2.8 cm to 42 cm and a patch height of effective height h_v. The triangle at the water-air interface represents the water level in the flume. An ADV was vertically mounted to measure the instantaneous velocities at selected vertical heights. The upper panel corresponds to the case of flexible plants and the bottom panel to rigid plants.

6.2.2 Patches of flexible vegetation

Two types of submerged vegetation models, rigid and flexible, were used (Figure 6.1). The rigid vegetation (SRV) consisted of a series of 1 cm thick 14 cm high PVC dowels. The flexible vegetation (SFV) consisted of a series of flexible plants of eight 0.075 mm thick polyethylene canopy blades attached to PVC dowels 1 cm in diameter and 2 cm high that had

been randomly inserted into a perforated baseboard (Pujol et al., 2013a) (250 cm in length), with the rigid dowel extending 1 cm above the bed (Zhang et al., 2018). The plants in the flexible model were geometrically and dynamically similar to *Posidonia oceanica* plants (Pujol et al., 2019, 2013a). The plant leaves in the flexible vegetation model were of 14 cm long. However, the effective height for the flexible vegetation when the leaves were bent by the waves was h_v = 8.5 cm for the wave frequency f = 1.12 Hz and h_v = 10.5 cm for the wave frequency f = 0.5 Hz. In contrast, the effective height for the rigid plants was the length of the PVC dowel, h_p=14 cm. The effective heights were calculated as the mean between both the maximum and minimum bending heights of the plants for 25 oscillations. From the observations, the effective plant height increased as the wave frequency decreased. A linear fit between these two data points was made (h_v=-3.23f+12.11). For the other studies considered here, the effective plant height was not always available, but it was estimated by the linear fit above between h_v and f.

The density of the vegetated patches was quantified using the solid plant fraction (SPF) defined as:

$$\text{SPF}\ (\%)=100n\pi\left(\frac{d}{2}\right)^2 \tag{6.1}$$

where n is the number of stems per unit area and d is the stem diameter (1 cm). Therefore, SPF represents the percentage of vegetation covering the base to the flume. For the rigid vegetation three SPFs were used (0%, 3.5% and 10%) and for the flexible vegetation six SPFs were used (0%, 2.5%, 3.5%, 5%, 7.5% and 10%). These SPFs corresponded to vegetation densities of n= 0, 318, 446, 637, 955 and 1273 stems·m^{-2} that are in the range of canopy densities found in coastal areas (78-1000

stems·m^{-2}) (Bacci et al., 2017; Colomer et al., 2017; Gera et al., 2013; van Katwijk et al., 2010). SPF=0% corresponded to the case with no vegetation. For each SPF different patch sizes, L_{patch}, were considered, with L_{patch} ranging from 42 to 245 cm, corresponding to 2 to 17 time the leaf length (Table 6.2). To determine L_{patch} in the experiments, the patch edge was considered as the interface between the vegetated and the non-vegetated regions. Thus, for the different SPFs, L_{patch}, and the two wave frequencies, a total of 87 experiments were performed (Table 6.2).

6.2.3 Measuring velocities

The Eulerian velocity field was defined as (u, v, w) in the (x, y, z) directions, respectively. The three components of velocity were recorded for 5 min at a measuring frequency of 50 Hz with a downwards looking Acoustic Doppler Velocimeter (16-MHz MicroADV, Sontek). The ADV was mounted on a movable vertical frame (at y = 0 cm, Figure 6.1) and manually adjusted to measure a vertical profile. Some plants were removed (and re-inserted into nearby holes) to avoid blocking the ADV beams (Ros et al., 2014; Zhang et al., 2018). The ADV measured at a 5 cm distance from the probe tip, and with a sampling volume of 0.09 cm^3. The longitudinal velocity was measured at an antinode to eliminate the lower order spatially periodic variation in wave and velocity amplitude associated with wave reflection (Luhar et al., 2010; Pujol et al., 2013a). Beam correlations less than 70% were discarded and spikes were removed (Goring and Nikora, 2002; Pujol et al., 2013a).

6.2.4 Hydrodynamic analysis

For oscillatory flows, the instantaneous velocity in the x direction, $U_i(t)$, can be decomposed as:

$$U_i(t)=U_c+ U_w+ u' \tag{6.2}$$

where U_c is the steady velocity associated with the wave, U_w is the unsteady wave motion in the x direction which represents spatial variations in the phase-averaged velocity field, and u' is the turbulent velocity, that is, the instantaneous velocity fluctuation in the x-direction. U_c is the phase-averaged velocity:

$$U_c= \frac{1}{2\pi}\int_0^{2\pi} U_i(\varphi)\partial\varphi \tag{6.3}$$

where $U_i(\varphi)$ is the instantaneous velocity according to the phase (Ros et al., 2014). Wave velocity, U_w, was obtained by using a phase averaging technique. The Hilbert transform was used to average oscillatory flow velocities with a common phase (Pujol et al., 2013a; Ros et al., 2014). The root mean square (rms) of $U_i(\varphi)$ was considered as the characteristic value of the orbital velocity U_w^{rms} (U_w hereafter) at each depth, and was calculated according to:

$$U_w^{rms} = \sqrt{\frac{1}{2\pi}\int_0^{2\pi} (U_i(\varphi)-U_c)^2\partial\varphi} \tag{6.4}$$

The turbulent velocity was obtained by:

$$u' = U_i - U_c - U_w \tag{6.5}$$

where U_c and U_w were calculated by Eqs. 6.3 and 6.4. The turbulent velocity was calculated for all directions (u', v', and w') for z= 4 cm.

Following Ros et al. (2014), turbulent kinetic energy (TKE) was calculated as:

$$TKE = \frac{1}{2}\left(\langle u'^2\rangle + \langle v'^2\rangle + \langle w'^2\rangle\right) \quad (6.6)$$

where < > denotes the average over the wave phase.

The ratio, β, was calculated following Colomer et al. (2017) for both, the UCL and the LCL:

$$\beta_{UCL} = \frac{TKE_{UCL}}{TKE_{WP,UCL}} \quad \text{and} \quad \beta_{LCL} = \frac{TKE_{LCL}}{TKE_{WP,LCL}} \quad (6.7)$$

where TKE_{UCL} TKE_{LCL}were the turbulent kinetic energy values in the UCL and LCL, respectively. For the TKE_{UCL}, TKE at z = 12 cm was the characteristic TKE considered, whereas for the TKE_{LCL}, TKE at z=4 cm was considered. For the non-vegetated cases and TKE_{WP},the TKE considered was also that measured at z = 12 cm and z=4 cm, respectively. Therefore, the values of $\beta_{UCL} \approx 1$ and $\beta_{UCL} \approx 1$ indicated a weak or negligible attenuation of the TKE, whereas low values of $\beta_{UCL} < 1$ and $\beta_{UCL} < 1$ indicated a high TKE attenuation compared to the non-vegetated case.

The vertical TKE attenuation was calculated as β':

$$\beta' = \frac{TKE_{LCL}}{TKE_{LCL}} \quad (6.8)$$

where TKE_{LCL} and TKE_{UCL} were the turbulent kinetic energies in the LCL and UCL, respectively. For TKE_{UCL} , the TKE at z = 4 cm was considered the characteristic TKE of this layer, whereas the TKE measured at z = 12 cm was the characteristic TKE for the UCL. Therefore, values of $\beta' \approx 1$ indicated a weak or negligible vertical

attenuation of the TKE, whereas low values of $\beta' < 1$ indicated a high TKE vertical attenuation, meaning greater TKE at z = 4 cm comparted to z = 12 cm.

To gain knowledge about the vertical distribution of TKE within the patch, a model was set up following Zhang et al. (2018). For a full canopy, Zhang et al. (2018) found that the relationship between the TKE, U_w, and the main canopy parameters followed:

$$\frac{TKE}{{U_w}^2} = \delta \left[C_D \frac{l_t}{d} \frac{nd^2}{2(1-\phi)} \right]^{\frac{2}{3}} \quad (6.9)$$

where δ is the scale constant, ϕ is the solid volume fraction, $\phi = n\frac{\pi}{4}d^2$, l_t is characteristic eddy length-scale, and C_D is the drag of the form of the obstacle along with the fluid patch, with C_D = 1.4 being considered in the study. In Equation (6.9), the characteristic length scale, L_{patch} / L_{canopy} is introduced to account for the volume of the patch in relation to the maximum canopy volume in the form of $\left(\frac{L_{patch}}{L_{canopy}}\right)^{\frac{1}{3}}$. L_{canopy} was considered as the length of the vegetation patch from where the wave velocity did not change with a further increase in its length. Barcelona et al. (2021c) found that L_{canopy} depended on the wave frequency, f, with $L_{canopy}=20h_v$ for f=1.12 Hz and $L_{canopy}=10h_v$ for f=0.5 Hz. Therefore Equation (6.9) is expressed following:

$$\frac{TKE}{{U_w}^2} = \delta \left[C_D \left(\frac{L_{patch}}{L_{canopy}}\right)^{\frac{1}{3}} \frac{l_t}{d} \frac{nd^2}{2(1-\phi)} \right]^{\frac{2}{3}} \quad (6.10)$$

Zhang et al. (2018) considered $l_t = d$ for $S > 2d$ whereas $l_t = S$ for $S < 2d$. In the present study, $S > 2d$, $l_t = d$. Therefore,

$$\frac{TKE}{{U_w}^2} = \delta \left[C_D \left(\frac{L_{patch}}{L_{canopy}} \right)^{\frac{1}{3}} \frac{nd^2}{2(1-\phi)} \right]^{\frac{2}{3}} \quad (6.11)$$

The parameter ϕ has been substituted by its definition to obtain two differentiated parameters (one related to patch length and the other to shoot density), as:

$$\frac{TKE}{{U_w}^2} = \delta \left[\left(\frac{L_{patch}}{L_{canopy}} \right)^{\frac{1}{3}} \frac{2C_D nd^2}{4-\pi nd^2} \right]^{\frac{2}{3}} \quad (6.12)$$

To obtain a more complete model the experiments from Zhang et al. (2018), Barcelona et al. (2021c) and Pujol et al. (2013b)were added to the comparison (Table 6.3).

Table 6.1 Summary of the experimental conditions tested. Where SFV correspond to Submerged Flexible Vegetation and SRV to Submerged Rigid Vegetation. LCL denotes the lower canopy layer and UCL the upper canopy layer.

Run	f (Hz)	SPF (%)	n (stems· m^{-2})	L_{patch} (cm)	A_w/S LCL	A_w/S UTL
WP1	0.5	0	0			
WP2	1.12	0	0			
SFV3	0.5	1	127	42	0.33	0.35
SFV4				70	0.33	0.35
SFV5				112	0.33	0.34
SFV6				196	0.33	0.33
SFV7		7.5	955	42	1.01	
SFV8				70	0.97	0.99
SFV9				112	0.98	0.96
SFV10				196	0.94	0.94
SFV11		10	1273	42	0.83	1.11
SFV12				70	0.83	1.06
SFV13				84	0.79	1.13
SFV14				98	0.79	1.09
SFV15				112	0.78	1.25
SFV16				133	0.8	1.14
SFV17				140	0.76	1.13
SFV18				154	0.8	1.1
SFV19				182	0.81	1.13
SFV20				224	0.77	1.09
SFV21				238	0.77	1.08
SFV22	1.12	2.5	318	42	0.21	0.25
SFV23				70	0.21	0.25
SFV24				84	0.21	0.25
SFV25				98	0.21	0.25
SFV26				112	0.21	0.24
SFV27				126	0.21	0.24
SFV28				140	0.21	0.24
SFV29				154	0.21	0.24
SFV30				168	0.21	0.24

Run	f (Hz)	SPF (%)	n (stems·	L_{patch} (cm)	A_w/S LCL	A_w/S UTL
SFV31	1.12	2.5	318	182	0.21	0.24
SFV32				196	0.21	0.24
SFV33				238	0.21	0.24
SFV34		3.5	446	70	0.25	0.29
SFV35				112	0.24	0.28
SFV36				126	0.24	0.28
SFV37				140	0.24	0.28
SFV38				154	0.24	0.28
SFV39				168	0.24	0.29
SFV40				196	0.24	0.28
SFV41				238	0.24	0.28
SFV42		5	637	42	0.29	0.36
SFV43				70	0.29	0.37
SFV44				98	0.29	0.36
SFV45				126	0.29	0.36
SFV46				168	0.28	0.36
SFV47				196	0.28	0.35
SFV48				210	0.28	
SFV49				238	0.28	0.35
SFV50		7.5	955	42	0.36	0.44
SFV51				70	0.37	0.45
SFV52				84	0.36	0.45
SFV53				98	0.36	0.44
SFV54				112	0.35	0.44
SFV55				126	0.35	0.45
SFV56				154	0.35	0.44
SFV57				196	0.34	0.44
SFV58				238	0.34	0.42
SFV59		10	1273	42	0.41	0.49
SFV60				70	0.41	0.52
SFV61				84	0.4	0.52
SFV62				98	0.39	0.52
SFV63				126	0.38	0.5
SFV64				154	0.39	0.5

Run	f (Hz)	SPF (%)	n (stems·	L_{patch} (cm)	A_w/S LCL	A_w/S UTL
SFV65		10	1273	168	0.39	0.52
SFV66				196	0.4	0.51
SFV67				238	0.37	0.47
SRV68	0.5	3.5	446	42	0.53	0.54
SRV69				70	0.51	0.55
SRV70				126	0.57	0.57
SRV71				182	0.52	0.55
SRV72				238	0.49	0.5
SRV73		10	1237	42	0.92	1.02
SRV74				70	0.95	1.04
SRV75				126	0.92	1.03
SRV76				182	0.91	1.01
SRV77				238	0.85	0.96
SRV78	1.12	3.5	446	42	0.23	0.3
SRV79				70	0.23	0.3
SRV80				126	0.27	0.32
SRV81				182	0.23	0.29
SRV82				238	0.26	0.32
SRV83		10	1273	42	0.32	0.38
SRV84				70	0.43	0.5
SRV85				126	0.38	0.47
SRV86				182	0.39	0.45
SRV87				238	0.35	0.4

Table 6.2 Summary of the experimental conditions tested by Zhang et al. (2018), Barcelona et al.(2021c) and Pujol et al. (2013b).

	Run	f (Hz)	SPF (%)	n (stems· m^{-2})	L_{patch} (n^o h_v)	A_w/S ICL	A_w/S CTL
Ros et al. (2014)	R. SFV 1	0.6	real	128	17.5	0.04	
	R. SFV 2		1	128	17.5	0.03	
	R. SFV 3		5	640	17.5	0.06	
	R. SFV 4		10	1280	17.5	0.18	
	R. SFV 5	0.8	real	128	17.5	0.06	
	R. SFV 6		1	128	17.5	0.06	
	R. SFV 7		5	640	17.5	0.34	
	R. SFV 8		10	1280	17.5	0.31	
	R. SFV 9	1	real	128	17.5	0.06	
	R. SFV 10		1	128	17.5	0.06	
	R. SFV 11		5	640	17.5	0.24	
	R. SFV 12		10	1280	17.5	0.34	
	R. SFV 13	1.2	real	128	17.5	0.06	
	R. SFV 14		1	128	17.5	0.06	
	R. SFV 15		5	640	17.5	0.21	
	R. SFV 16		10	1280	17.5	0.32	
	R. SFV 17	1.4	real	128	17.5	0.05	
	R. SFV 18		1	128	17.5	0.05	
	R. SFV 19		5	640	17.5	0.13	
	R. SFV 20		10	1280	17.5	0.26	
	R. SFV 21	1.6	real	128	17.5	0.03	
	R. SFV 22		1	128	17.5	0.03	
	R. SFV 23		5	640	17.5	0.08	
	R. SFV 24		10	1280	17.5	0.16	
	R. SRV 25	0.6	1	128	17.5	0.03	
	R. SRV 26		5	640	17.5	0.06	
	R. SRV 27		7.5	960	17.5	0.18	
	R. SRV 28		10	1280	17.5	0.14	
	R. SRV 29	0.8	1	128	17.5	0.06	
	R. SRV 30		5	640	17.5	0.11	
	R. SRV 31		7.5	960	17.5	0.14	

	Run	f (Hz)	SPF (%)	n (stems· m^{-2})	L_{patch} (n^o h_v)	A_w/S ICL	A_w/S CTL
	R. SRV 32	0.8	10	1280	17.5	0.2	
	R. SRV 33	1	1	128	17.5	0.05	
	R. SRV 34		5	640	17.5	0.16	
	R. SRV 35		7.5	960	17.5	0.2	
	R. SRV 36		10	1280	17.5	0.24	
	R. SRV 37	1.2	1	128	17.5	0.07	
	R. SRV 38		5	640	17.5	0.18	
	R. SRV 39		7.5	960	17.5	0.23	
	R. SRV 40		10	1280	17.5	0.31	
	R. SRV 41	1.4	1	128	17.5	0.05	
	R. SRV 42		5	640	17.5	0.12	
	R. SRV 43		7.5	960	17.5	0.16	
	R. SRV 44		10	1280	17.5	0.24	
	R. SRV 45	1.6	1	128	17.5	0.03	
	R. SRV 46		5	640	17.5	0.08	
	R. SRV 47		7.5	960	17.5	0.1	
	R. SRV 48		10	1280	17.5	0.14	
	Z. SFV 1	1	1.1	280	14.3	1.21	
Zhang et al. (2018)	Z. SFV 2				14.3	0.94	
	Z. SFV 3				14.3	0.74	
	Z. SFV 4				14.3	0.54	
	Z. SFV 5				14.3	0.42	
	Z. SFV 6				14.3	0.29	
	Z. SFV 7		2.3	600	14.3	2.01	
	Z. SFV 8				14.3	1.52	
	Z. SFV 9				14.3	1.21	
	Z. SFV 10				14.3	0.88	
	Z. SFV 11				14.3	0.68	
	Z. SFV 12				14.3	0.46	
	Z. SFV 13		3.2	820	14.3	2.01	
	Z. SFV 14				14.3	1.66	
	Z. SFV 15				14.3	1.4	
	Z. SFV 16				14.3	1.06	
	Z. SFV 17				14.3	0.8	

	Run	f (Hz)	SPF (%)	n (stems·m^{-2})	L_{patch} (n^o h_v)	A_w/S ICL	A_w/S CTL
	Z. SFV 18	1	3.2	820	14.3	0.49	
	Z. SFV 19		5.3	1370	14.3	2.22	
	Z. SFV 20				14.3	1.9	
	Z. SFV 21				14.3	1.57	
	Z. SFV 22				14.3	1.19	
	Z. SFV 23				14.3	0.91	
	Z. SFV 24				14.3	0.55	
	B. SFV 1	0.7	1	127	17.5	0.03	
Barcelona et al. (2021c)	B. SFV 2				17.5	0.04	
	B. SFV 3				17.5	0.11	
	B. SFV 4				17.5	0.09	
	B. SFV 5		2.5	318	17.5	0.07	
	B. SFV 6				17.5	0.03	
	B. SFV 7				17.5	0.15	
	B. SFV 8				17.5	0.17	
	B. SFV 9		5	637	17.5	0.04	
	B. SFV 10				17.5	0.07	
	B. SFV 11				17.5	0.12	
	B. SFV 12				17.5	0.12	
	B. SFV 13		7.5	955	17.5	0.11	
	B. SFV 14				17.5	0.06	
	B. SFV 15				17.5	0.07	
	B. SFV 16				17.5	0.14	
	B. SFV 17	1.2	1	127	17.5	0.07	
	B. SFV 18				17.5	0.04	
	B. SFV 19				17.5	0.05	
	B. SFV 20				17.5	0.04	
	B. SFV 21		2.5	318	17.5	0.06	
	B. SFV 22				17.5	0.07	
	B. SFV 23				17.5	0.08	
	B. SFV 24				17.5	0.08	
	B. SFV 25		5	637	17.5	0.08	
	B. SFV 26				17.5	0.1	
	B. SFV 27				17.5	0.15	
	B. SFV 28				17.5	0.12	

	Run	f (Hz)	SPF (%)	n (stems· m^{-2})	L_{patch} (n^o h_v)	A_w/S ICL	A_w/S CTL
	B. SFV 29		7.5	955	17.5	0.13	
	B. SFV 30				17.5	0.14	
	B. SFV 31				17.5	0.15	
	B. SFV 32				17.5	0.15	
	P.SRV 1	0.8	1	127	17.5	0.07	0.06
Pujol et al. (2013b)	P.SRV 2		5	637	17.5	0.18	0.15
	P.SRV 3		10	1280	17.5	0.25	0.18
	P.SRV 4	1	1	127	17.5	0.05	0.07
	P.SRV 5		5	637	17.5	0.13	0.14
	P.SRV 6		10	1280	17.5	0.16	0.22
	P.SRV 7	1.4	1	127	17.5	0.04	0.06
	P.SRV 8		5	637	17.5	0.08	0.14
	P.SRV 9		10	1280	17.5	0.11	0.17
	P.SFV 1	0.8	1	127	17.5	0.06	0.06
	P.SFV 2		5	637	17.5	0.14	0.15
	P.SFV 3		10	1280	17.5	0.15	0.19
	P.SFV 4	1	1	127	17.5	0.06	0.08
	P.SFV 5		5	637	17.5	0.12	0.17
	P.SFV 6		10	1280	17.5	0.26	0.21
	P.SFV 7	1.4	1	127	17.5	0.04	0.06
	P.SFV 8		5	637	17.5	0.1	0.14
	P.SFV 9		10	1280	17.5	0.13	0.19

6.3 RESULTS

The vertical profiles of TKE/U_w^2 presented different patterns depending on the wave frequency (Figure 6.2a). For the non-vegetated set ups, and for the wave frequency of 1.12 Hz, TKE/U_w^2 presented a constant value at the top of the water column. Below this layer, a gradual decrease of TKE/U_w^2 was noted until a constant value situated at the bottom layer was observed. In contrast, for the wave frequency of 0.5 Hz, TKE/U_w^2 presented a constant value with z (Figure 6.2a). From the vertical profiles of the normalized turbulent kinetic energy (TKE/U_w^2) in the vegetated set-ups, three layers could be distinguished. The above-canopy layer (ACL) corresponded to the layer above the maximum canopy height (h_p, determined as the leaf length for flexible plants and the stem length for the rigid canopy). In this layer TKE/U_w^2 presented three behaviours depending on the wave frequency. In the ACL, for the wave frequency of 1.12 Hz, TKE/U_w^2 tended to decrease (rigid, Figure 2b) or remain constant (flexible, Figure 6.2c) moving upwards from the canopy. In contrast, for the wave frequency of 0.5 Hz, TKE/U_w^2 increased with z/h_p for both rigid and flexible vegetation. From the TKE/U_w^2 profiles, a second interface could be observed. For the rigid canopy model, an interface between the upper-canopy layer (Figure 6.2b), and which was situated at the same depth (z/h_p=0.44) for both wave frequencies, was observed. In the lower-canopy layer (LCL), TKE/U_w^2 presented a smaller decrease with z/h_p in the case of the wave frequency of 1.12 Hz compared with the upper-canopy layer (UCL). In contrast, for the wave frequency of 0.5 Hz and for the LCL, TKE/Uw^2 decreased with z/h_p contrary to its behaviour in the UCL. For the flexible vegetation, the interface between the UCL and the LCL depended on the wave frequency (Figure 6.2c), and the interface was situated at the depth of the effective plant height h_v (i.e., the height of the plant bent by the wave).

In the LCL, for flexible vegetation and for a both wave frequencies, TKE/Uw^2 increased downwards as z/h_p decreased (Figure 6.2c).

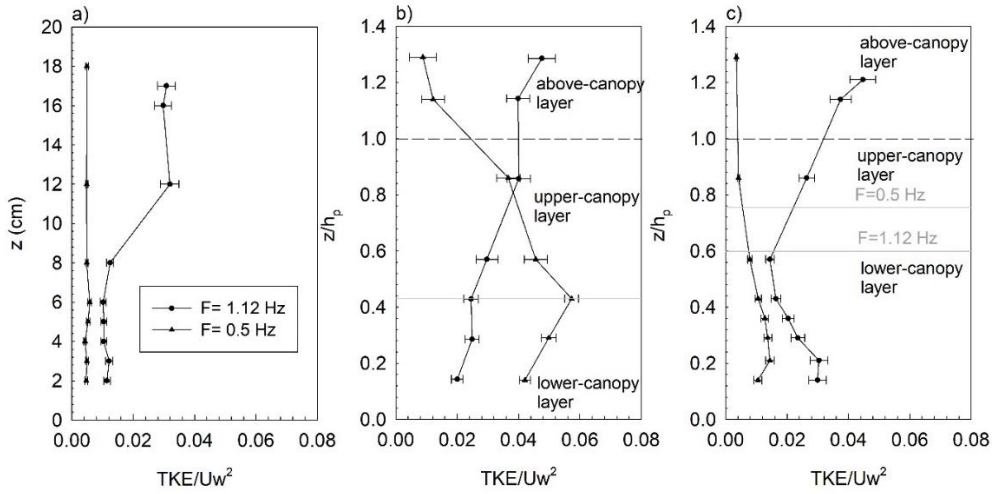

Figure 6.2 TKE/Uw^2 vertical profiles a) versus z for non-vegetated set ups, and versus z/h_p for b) rigid vegetation and c) flexible vegetation for the two wave frequencies studied f = 1.12 Hz (circles) and b) f = 0.5 Hz (triangles). The horizontal dashed lines in Figures 1b and 1c represent the height of the plant leaf for flexible plants (h_p) or the height of the plant stem for rigid plants. The vegetated experiments presented here correspond to cases with a patch length of 238 cm and SPF=10%. The horizontal grey lines represent the interface between the upper-canopy layer and the lower-canopy layer for both types of vegetation.

The TKE attenuations comparing vegetated with non-vegetated cases for both the UCL and LCL(β_{UCL} and β_{LCL}), were considered for all the rigid and flexible vegetation set-ups. For the flexible vegetation, β_{UCL} was found to be nearly 1 for all A_w/S (where $A_w=U_w/2\pi f$, U_w is the wave velocity and S is the plant to plant distance, see the Methods section for more information) and both frequencies (Figure 6.3a). However, for the rigid vegetation, β_{UCL} increased

with A_w/S, from the threschold of $A_w/S>0.35$ and followed a linear trend ($\beta_{UCL}=9.08A_w/S-1.38$, $R^2=0.837$, $p<0.05$) (Figure 6.2b).

At the LCL for flexible vegetation, the same threshold at $A_w/S = 0.35$ was found for β_{LCL} (Figure 6.3c). For $A_w/S < 0.35$ the values of β_{LCL} were close to 1, while for $A_w/S > 0.35$, β_{LCL} was higher than 1 (Figure 6.3c). In this latter case, β_{LCL} increased with A_w/S following a linear trend. Otherwise, for the rigid vegetation $\beta_{LCL} > 1$ was found for all A_w/S. In this case, β_{LCL} increased with A_w/S following a linear trend with a greater slople than for the flexible vegetaion case (Figure 6.3d).

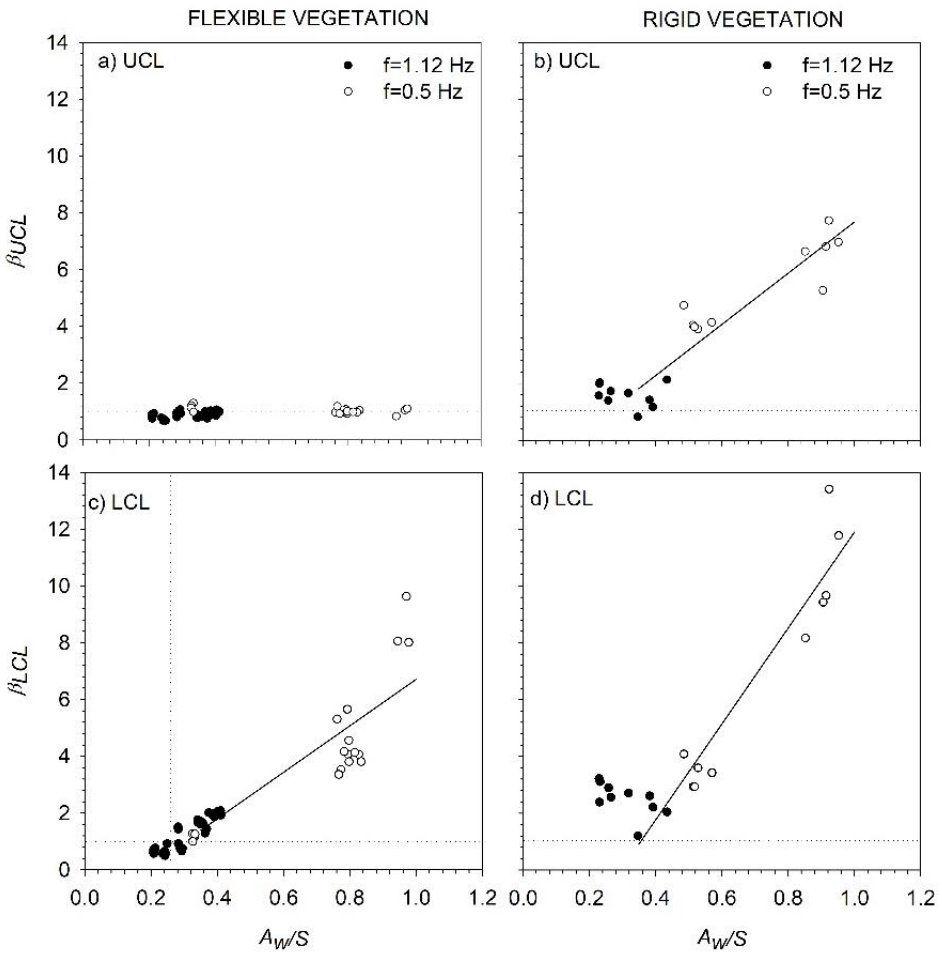

Figure 6.3 TKE attenuation in relation to the non-vegetated cases at the UCL (β_{UCL}) for a) flexible vegetation a) and for b) rigid vegetation b). TKE attenuation in relation to the non-vegetated cases at the LCL (β_{LCL}) for c) flexible vegetation and for d) rigid vegetation. Unfilled circles correspond to f = 0.5 Hz, and solid black circles to f = 1.12 Hz. Lines correspond to the linear best fit for the cases $A_w/S>0.35$ when β increased linearly with A_w/S, independent of the wave frequency. In the UCL for rigid vegetation, $\beta=9.02\times A_w/S-1.34$ ($R^2=0.8625$, p-value<0.01). In the LCL for rigid vegetation, $\beta=16.90\times A_w/S-5.00$ ($R^2=0.9224$, p-value<0.01), and for the flexible vegetation $\beta=8.19\times A_w/S-1.48$ ($R^2=0.7819$, p-value<0.01). Vertical dashed lines

represent the x-axis position where $A_w/S=0.35$, and horizontal dashed lines correspond to the y-axis position where $\beta=1$.

For the flexible vegetation, the vertical attenuation of the TKE (β', see the Methods for its definition) was lower than 1 for f = 1.12 Hz, while for f = 0.5 Hz two different behaviours were found: for $A_w/S < 0.35$ $\beta' \approx 1$ whereas for $A_w/S > 0.35$ $\beta' > 1$ (Figure 6.4a). For the rigid vegetation two behaviours were also found: for $A_w/S < 0.8$ $\beta' < 1$, which included all the cases with f = 1.12 Hz and some cases of f = 0.5 Hz; meanwhile for $A_w/S > 0.8$ $\beta' > 1$, which included the rest of the cases of f = 0.5 Hz (Figure 6.4b).

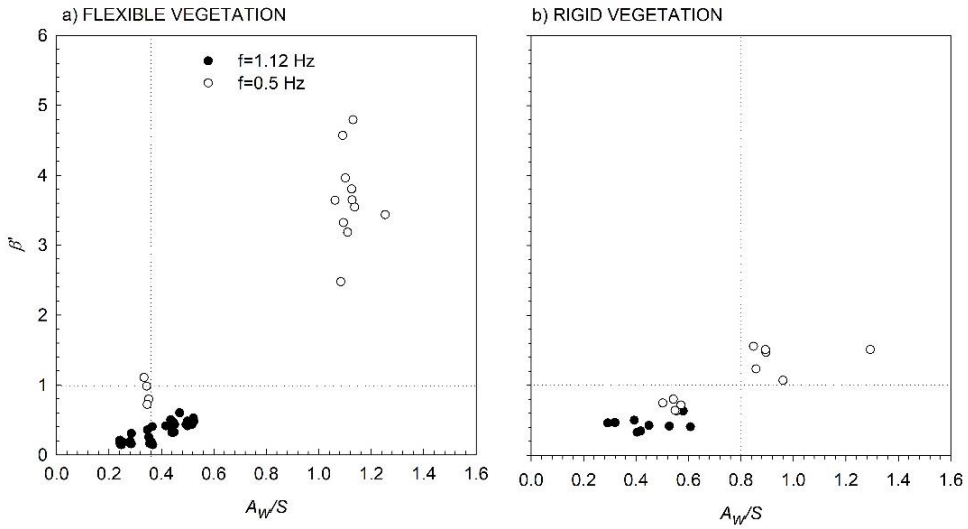

Figure 6.4 Vertical TKE attenuation, β', for the a) flexible vegetation model and b) rigid vegetation model. Unfilled circles correspond to f = 0.5 Hz, and solid black circles correspond to f = 1.12 Hz. The vertical dashed lines indicate the threshold of A_w/S for each type of plant, and the horizontal dashed line represents the y-axis value of $\beta'=1$.

The model from Eq. (6.12), was used to represent the TKE versus $\left[C_{D-Patch}\frac{nd^2}{2(1-\emptyset)}\right]^{\frac{2}{3}}U_w{}^2$ (where n is the canopy density, d the stem diameter and the solid plant fraction is $\phi = n\frac{\pi}{4}d^2$) for all experiments carried out with both the rigid and flexible models, where $C_{D-Patch} = C_D\left(\frac{L_{Patch}}{L_{Canopy}}\right)^{\frac{1}{3}}$, (see the Methods section for a complete description of the model). For both the flexible and rigid vegetation models, two regions could be differentiated (Figure 6.5a and b). For the flexible vegetation model (Figure 6.5a), and for those cases with $\left[C_{D-Patch}\frac{nd^2}{2(1-\emptyset)}\right]^{\frac{2}{3}}U_w{}^2 < 4$, TKE was constant, at TKE = 0.33 cm^2s^{-2}. In contrast, for $\left[C_{D-Patch}\frac{nd^2}{2(1-\emptyset)}\right]^{\frac{2}{3}}U_w{}^2 > 4$ two different behaviours were found. For the UCL, TKE for flexible vegetation was constant, with TKE = 0.41 cm^2s^{-2} for f= 0.5 Hz and TKE = 3.10 cm^2s^{-2} for f = 1.12 Hz, corresponding to the TKE measured without plants (SPF=0%) for each frequency. For the LCL, the TKE increased linearly (TKE = $0.20\left[C_{D-Patch}\frac{nd^2}{2(1-\emptyset)}\right]^{\frac{2}{3}}U_w{}^2 - 0.6$, R^2=0.832, p<0.05) (Figure 5a). For the rigid vegetation model (Figure 6.5b), the threshold where TKE changed from being constant to increasing linearly from $\left[C_{D-Patch}\frac{nd^2}{2(1-\emptyset)}\right]^{\frac{2}{3}}U_w{}^2 = 2$. Therefore, for $\left[C_{D-Patch}\frac{nd^2}{2(1-\emptyset)}\right]^{\frac{2}{3}}U_w{}^2 > 2$, TKE followed a linear trend (TKE = $0.27\left[C_{D-Patch}\frac{nd^2}{2(1-\emptyset)}\right]^{\frac{2}{3}}U_w{}^2 - 0.5$, R^2=0.512, p<0.05), while for $\left[C_{D-Patch}\frac{nd^2}{2(1-\emptyset)}\right]^{\frac{2}{3}}U_w{}^2 < 2$, TKE remained constant with TKE = 0.37 (Figure 6.5b).

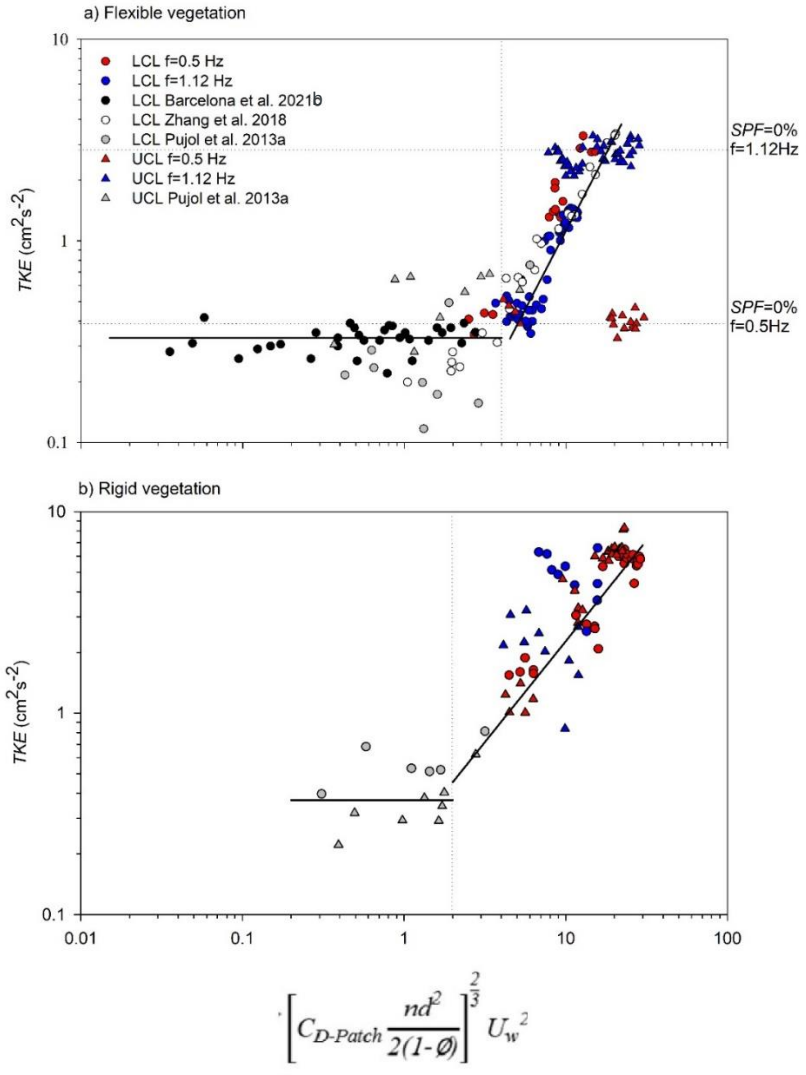

Figure 6.5 TKE versus $\left[\mathbf{C_{D-Patch}}\frac{\mathbf{nd^2}}{\mathbf{2(1-\emptyset)}}\right]^{\frac{\mathbf{2}}{\mathbf{3}}}\mathbf{U_w}^{\mathbf{2}}$ for a) flexible and b) rigid vegetation. Data from Barcelona et al. (2021b), and Zhang et al. (2018) for flexible vegetation have been included and data from Pujol et al.(2013b) for flexible vegetation and rigid vegetation have been included as well. The vertical dashed line indicates the threshold that separated the two behaviours. The solid line corresponds to the best fit line of the

data points to the model for $\left[C_{D-Patch}\frac{nd^2}{2(1-\emptyset)}\right]^{\frac{2}{3}}U_w{}^2 > 2$ or $\left[C_{D-Patch}\frac{nd^2}{2(1-\emptyset)}\right]^{\frac{2}{3}}U_w{}^2 > 4$, for both flexible and rigid plants. Horizontal dashed lines in Figure 5a) correspond to the TKE for cases without plants and for both wave frequencies.

6.4 DISCUSSION

In coastal zones, the structural characteristics of aquatic vegetation: stiffness, canopy density, height and patch length, play a crucial role in determining their functionality as ecological engineers. Rigid canopy patches provide greater drag than flexible canopy patches do under the same hydrodynamic conditions. This result might pose some limitations for rigid canopies if they are to sustain high energy flows.

Over bare soil, (i.e., without the presence of plants), the TKE declines with depth for all the wave frequencies studied. These results are in accordance with previous findings by Pujol et al.(2013b) and Zhang et al. (2018)who found that TKE decreases with depth in non-vegetated beds. However, depending on the interaction between waves and plant stems, plants can reduce the TKE or in contrast, they can increase it due to the drag exerted by plant stems. In this case, the flexibility of the plant also determines the attenuation of the TKE. Rigid plants can produce drag along the entire plant stem, whereas flexible plants behave like a blade at the top, i.e. they move back and forth with the flow, thus reducing the relative motion between the flow and the blade (Schaefer and Nepf, 2022). However, they behave like a stem at the bottom, i.e., remain stiff with an increase in their relative motion.

In this study, the vertical attenuation of the TKE was studied by using two attenuation parameters: vertical attenuation (β') and attenuation by comparing the TKE with plants to the TKE without plants (β). For the rigid vegetation,

the vertical attenuation β' is always below 1, indicating that the TKE in the LCL is lower than that at the UCL due to the drag produced by rigid stems in these two layers. However, for the flexible vegetation, β' is lower than 1 for those cases with $A_w/S<0.35$, accounting for all the experiments carried out for f=1.12 Hz and some at 0.5 Hz. In contrast, β'>1 for all the experiments with $A_w/S>0.35$, corresponding to some experiments carried out at f=0.5 Hz. This result can be attributed to the fact that at high frequencies when $A_w/S>0.35$, waves interact with the canopy of flexible plants producing TKE along the entire plant blade (due to the wakes generated) and so the plants remain stiff (i.e., behaving more like rigid plant stems). In contrast, low wave frequencies with $A_w/S<0.35$ do not interact with the canopy, presenting a greater oscillatory excursion length at the top of the plant that at the bottom of it without producing wakes around the blades. In this case, flexible plants bend with the flow following a back and forth movement. These results align with the findings by van Veelen et al. (2020) who studied wave damping by vegetation with differing flexibilities. In their study they found that flexible plants swayed with the flow and did not dampen wave velocities. In contrast, rigid plants produced a greater resistance, thus damping wave velocities. Wave damping is expected to be related to the production of TKE, thus coinciding with the results of the current study.

The attenuation of the TKE in both the UCL and LCL when compared to the without-plants experiments indicated that for the experiments carried out with rigid plants, and for all the wave frequencies studied $\beta_{UCL} >1$ and $\beta_{UCL}>1$ for both the UCL and LCL layers, also indicating that rigid plants produced TKE due to the greater relative motion between the waves and the rigid stems. These results align with the conclusions of Pujol et al. (2013a), who described the production of *TKE* by rigid canopies in the UCL due to the generation of

stem-wake turbulence associated to a large reduction in wave velocity. For the case of a canopy of flexible plants, β_{UCL} was nearly 1 for the UCL since, at this depth, there is no plant-generated TKE because flexible plants swing with the flow and do not add any additional drag resistance to the movement; this behaviour could be described as a blade-like behaviour (Zhang et al., 2018). In this case, flexible plants reduce the drag to withstand the energy of the flow. This aligns with Paul and de los Santos (2019) who found that the more rigid *Zostera marina* plants acclimatise in shallower regions far from energetic flow conditions while the more flexible *Zostera marina* plants extend far out from the coast.

This behaviour observed in the UCL changed in the LCL. For the case of a canopy of flexible plants and in the LCL, $\beta_{LCL} > 1$ for cases when $A_w/S > 0.35$, whereas $\beta_{LCL} < 1$ for cases when $A_w/S < 0.35$. This threshold obtained for $A_w/S = 0.35$ is equal to $A_w/S_b = 1$ (where S_b is the spacing considering that stems have eight blades, (i.e., $S_b = 1/(8N)^{1/2}$ and N is the stem density). This transition was also found by Zhang et al. (2018) for the inner canopy layer of flexible plants. The experiments carried out by Pujol et al. (2013b) for flexible plants all corresponded to the cases $A_w/S < 0.35$. In such conditions, single stems do not contribute to TKE generation, instead, stems dampen the near-bed generated TKE relative to the non-vegetated cases. In contrast, for flexible meadows with $A_w/S > 0.35$, the TKE will be enhanced within the vegetated region relative to the non-vegetated cases. This TKE production determines that flexible vegetation in the LCL for $A_w/S > 0.35$ presents stem-like behaviour similar to rigid stems. A decrease in the TKE within a meadow of *Posidonia oceanica* was also found by Serra et al. (2020) when compared to nearby gaps (areas without vegetation). In such cases, the canopy density was $N = 400$ stems m^{-2}, $T = 3.64$ s and $U_w = 0.01$ m s^{-1}, resulting in $A_w/S = 0.12 < 1$.

Granata et al. (2001) also found a vertical attenuation of TKE in a meadow of *Posidonia oceanica*. They compared the TKE above the canopy with the TKE within the canopy. In this case, the meadow sheltered the bed, i.e., stabilizing the sediment. Barcelona et al. (2021b) studied the capture of sediment particles via a model canopy of flexible plants in a flume and found that a meadow of flexible plants enhances sedimentation compared to non-vegetated conditions.

The present study demonstrates that TKE production by vegetation depends on wave velocity, canopy density, the plant flexibility and patch length for both rigid and flexible vegetation models. The thresholds $\left[C_{D-Patch}\frac{nd^2}{2(1-\emptyset)}\right]^{\frac{2}{3}}U_w{}^2 > 4$ (for flexible plants, also observed by Barcelona et al.(2021c)) and $\left[C_{D-Patch}\frac{nd^2}{2(1-\emptyset)}\right]^{\frac{2}{3}}U_w{}^2 > 2$ (for rigid plants, observed in the current study) is required for the canopy to produce TKE. It is important to notice that the production of TKE holds at a lower threshold for rigid than for flexible plants, because flexible plants move with the flow. van Veelen et al. (2020) also found that for low submergence ratios of the vegetation, like that in the current study ($h_p/H=0.47$), the drag produced by the canopy varies depending on the type of plants (rigid or flexible). In their study, they found that the drag for flexible vegetation and for this submergence ratio was $C_D=0.39$ compared to rigid plants, with $C_D=1$. Considering this C_D for flexible plants, the threshold of $\left[C_{D-Patch}\frac{nd^2}{2(1-\emptyset)}\right]^{\frac{2}{3}}U_w{}^2=2$ would increase to $\left[C_{D-Patch}\frac{nd^2}{2(1-\emptyset)}\right]^{\frac{2}{3}}U_w{}^2=3.8$, being closer, therefore, to that obtained for rigid plants $\left[C_{D-Patch}\frac{nd^2}{2(1-\emptyset)}\right]^{\frac{2}{3}}U_w{}^2 = 4$.

As Pujol et al. (2013b) pointed out, TKE production the correct diffusion of oxygen at the leaves' boundary layer. The current study demonstrates that the behaviour the seagrass not only depends on the hydrodynamics, but also on the structural characteristics of the canopy, i.e., canopy density, patch length, and plant stiffness. Below the threshold of $\left[C_{D-Patch}\frac{nd^2}{2(1-\emptyset)}\right]^{\frac{2}{3}}U_w{}^2$, the behaviour of the canopy changes and its role is to reduce the seabed generated TKE. The current study also demonstrates that on the vertical axis, two regions can be differentiated for the flexible vegetation in terms of TKE behaviour. For the flexible vegetation and for $\left[C_{D-Patch}\frac{nd^2}{2(1-\emptyset)}\right]^{\frac{2}{3}}U_w{}^2 > 4$, the TKE in the UCL remains constant and is close to that for the non-vegetated cases. In this case, in the UCL the plants behave like blades, moving with the flow but not producing any additional TKE than that already present for the non-vegetated set-ups. In contrast, in the LCL, the TKE increases with $\left[C_{D-Patch}\frac{nd^2}{2(1-\emptyset)}\right]^{\frac{2}{3}}U_w{}^2$. In this case, plants in the LCL behave like stems, with small swaying movements, thus creating drag in the flow and producing TKE.

This result also aligns with that found by Bouma et al. (2005) when comparing the dissipation of wave height by *Spartina alternifora* to that of *Zostera noltii*. In their case, greater wave height dissipation was obtained for the more rigid *Spartina alternifora* vegetation. This is in accordance with Zhang et al. (2018) who divided the vertical structure of a flexible plant into two parts. The upper part was named the blade-like region and the lower part the stem-like region. In the stem-like region, they found a greater production of TKE compared with the blade-like region due to the greater relative motion between the flow velocity and the plant.

Contrary to flexible stems, rigid plants for $\left[C_{D-Patch}\frac{nd^2}{2(1-\emptyset)}\right]^{\frac{2}{3}}U_w{}^2 > 2$ present stem-like behaviour along the entire stem. In this case, TKE production is due to the greater relative motion between the flow and the rigid stem compared to the flexible blades. Contrary to flexible stems, in the UCL of rigid stems, TKE increases with $\left[C_{D-Patch}\frac{nd^2}{2(1-\emptyset)}\right]^{\frac{2}{3}}U_w{}^2$.From the results of the vertical attenuation of the TKE and the TKE attenuation compared to the non-vegetated cases, rigid plants exhibit a similar behaviour to flexible plants for high wave frequencies (f=1.12 Hz). In contrast, under low wave frequencies, when flexible plants have a large sway movement, the hydrodynamics are far from those obtained by rigid plants.

Considering the thresholds for both rigid and flexible vegetation, the required canopy density to begin to produce TKE could be determined in terms of either the length of the patch or the canopy density. The ratio TKE/Uw^2 was considered to range from 0.004 to 0.04 as was found in the laboratory tests. Four ratios L_{patch}/L_{canopy} (see the Methods section for the definition of L_{patch} and L_{canopy}) will be considered, from 0.01 to 0.08. Considering these range of variation, flexible plants would require a canopy density ranging from 136 shoots m^{-2} to 6140 shoots m^{-2} (Figure 6.6a). In contrast, a patch of rigid plants would require a density ranging from 69 shoots m^{-2} to 4046 shoots m^{-2} (Figure 6.6b). Therefore, a patch of rigid plants would be capable of producing TKE in sparser canopy densities than a patch of flexible plants. This result might also have important implications for the sediment bed characteristics, with more provability of resuspension and scouring in regions covered with rigid canopies than in regions with flexible canopies when subject to high energetic conditions. This would align with the results of Bouma et al. (2005)who found that for hydrodynamic exposed areas, the flexible shoots of *Zostera* caused far

less scouring than the stiff shoots of *Puccinellia*. In addition, a small patch of flexible plants would require a denser vegetation to produce the same normalized TKE/U_w^2 than a larger patch but with sparser vegetation. Therefore, the parameter $\left[C_{D-Patch}\frac{nd^2}{2(1-\emptyset)}\right]^{\frac{2}{3}}$ is related to the total effect of the vegetation patch in terms of drag, length and density.

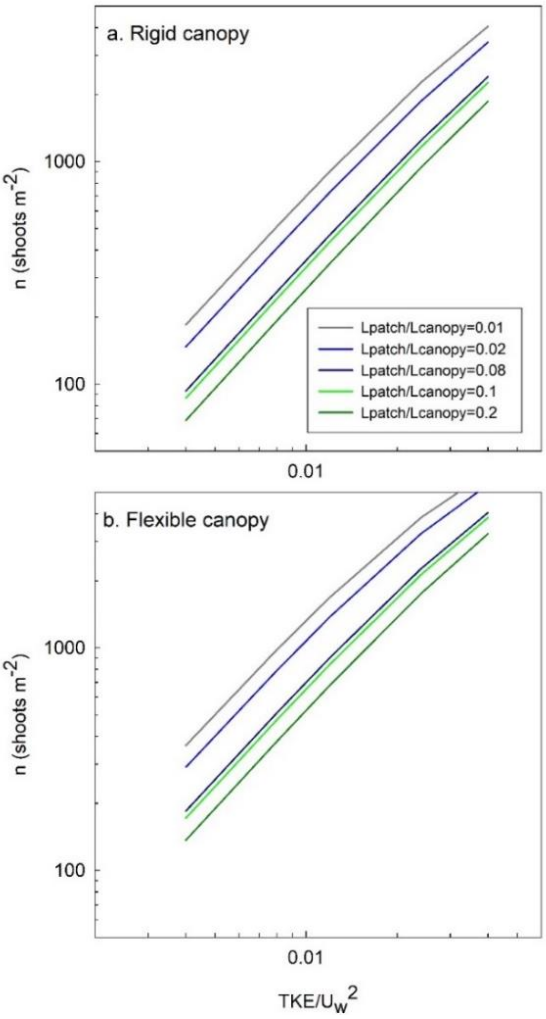

Figure 6.6 Number of shoots per m^2 (n) required to begin producing TKE versus TKE/U_w^2 for different patch lengths and for a) rigid and b) flexible plant structures.

Acknowledgments

This work was supported by the “Ministerio de Economía y Competitividad” of the Spanish Government through the grant PID2021-123860OB-I00. Aina Barcelona was funded by the pre-doctoral grant 2020 FI SDUR 00043 from the “Generalitat de Catalunya”.

CHAPTER 7

The role epiphytes play in particle capture of seagrass canopies.

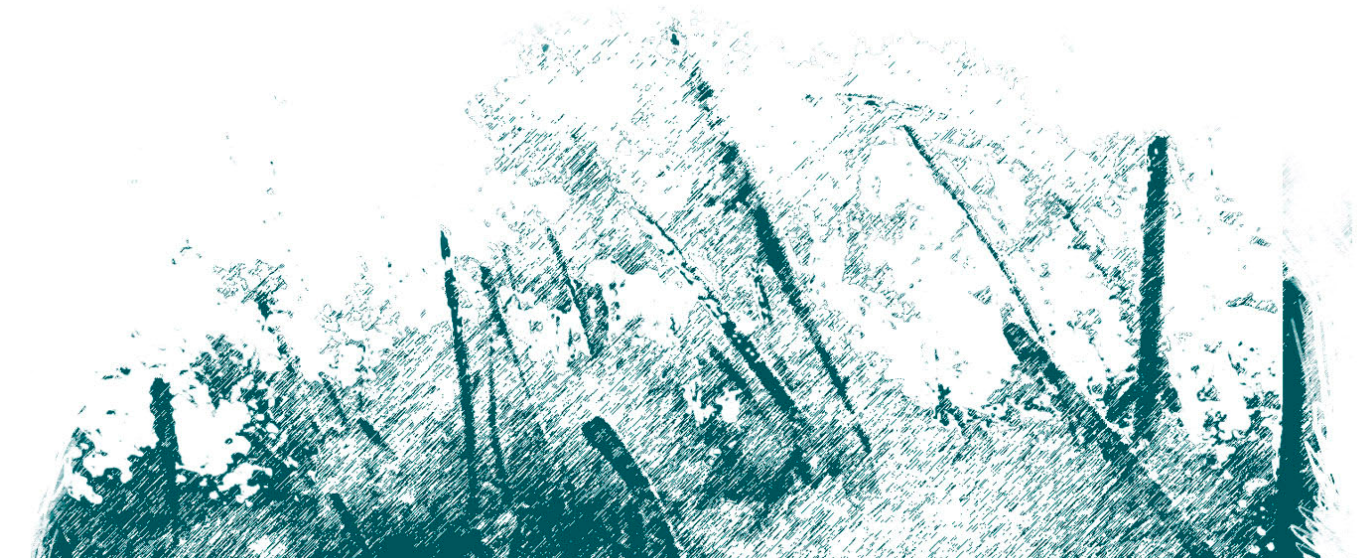

Aina Barcelona, Jordi Colomer, Teresa Serra, Damboia Cossa, Eduardo Infantes (2023). The role epiphytes play in particle capture of seagrass canopies. Marine Environmental Research, 192, 106238. doi: 10.1016/j.marenvres.2023.106238

Cover design: Carles Arbat

Abstract

Seagrass epiphytic communities act as ecological indicators of the quality status of vegetated coastal environments. This study aims to determine the effect leaf epiphytes has on the sediment capture and distribution from outside sources. Thirteen laboratory experiments were conducted under a wave frequency of 0.5 Hz. Three epiphyte models were attached to a *Zostera marina* canopy of 100 plants/m^2 density. The sediment deposited to the seabed, captured by the epiphytic leaf surface, and remaining in suspension within the canopy were quantified. This study demonstrated that the amount of epiphytes impacts on the sediment stocks. *Zostera marina* canopies with high epiphytic areas and long effective leaf heights may increase the sediment captured on the epiphyte surfaces. Also, reducing suspended sediment and increasing the deposition to the seabed, therefore enhancing the clarity of the water column. For largest epiphytic areas, a 34.5% increase of captured sediment mass is observed. The sediment trapped on the leaves can be 10 times greater for canopies with the highest epiphytic areas than those without epiphytes. Therefore, both the effective leaf length and the level of epiphytic colonization are found to determine the seagrass canopy ability at distributing sediment.

Keywords: *seagrass, eelgrass, epiphyte, sedimentation, leaves capture, suspension, leaf length, epiphytic area.*

7.1 INTRODUCTION

Coastal ecosystems are colonized by seagrass meadows that provide significant ecological and physical ecosystem services. For example, they act as refuge and nursery habitats for fish and macroinvertebrates (Unsworth et al., 2017), attenuate waves and turbulence (Gacia et al., 1999; Infantes et al., 2012; Pujol et al., 2013b), reduce erosion with the roots (Infantes et al., 2022), stabilize the bottom through decreasing sediment resuspension (Ros et al. 2014) and enhance sediment trapping (Barcelona et al., 2023b, 2021b). Seagrass plants have a complex structure, with invertebrates and macroalgae growing on the leaves and rhizomes forming assemblages named epiphytes (Trautman and Borowitzka, 1999). The abundance of epiphytes depends on the available leaf area of the seagrass and can impact the growth of the seagrass itself by decreasing the light reaching the canopy and reducing water fluxes (Cambridge et al., 2007).

The presence of epiphytes on seagrass leaves suggests ecological indications and signals the quality status of vegetated coastal environments (Mutlu et al., 2022). Overall, the quantity and quality of epiphytes serve as indicators of the level of intensity and the spatial distribution of ecological and anthropogenic processes such as eutrophication, productivity, herbivory, acidification, seasonality, turbidity, pollution, sedimentation, hydrodynamics, among others (Baggett et al., 2010; Balata et al., 2008; Ben Brahim et al., 2020; Mutlu et al., 2022). Likewise, leaf growth is regulated to maintain a proportion of uncolonized leaf surface, and epiphyte coverage plays a role in its regulation. In *Zostera marina,* the rate of leaf emergence positively correlates with epiphyte load (Ruesink, 2016). Additionally, epiphyte biomass increases exponentially with leaf age during the first days of colonization, whereas for older leaves epiphytes do not change in biomass (Borum, 1987). Among the

key processes, the patterns of the spatial variability of macro-epiphyte assemblages on *Posidonia oceanica* leaves differ in relation to anthropogenic interference in the Gulf of Gabes, with both biomass and mean percentage cover decreasing near a sewage outlet point compared to control locations (Ben Brahim et al., 2010). In *Cymodocea nodosa* and the invasive species *Halophila stipulucea*, shoot density and epiphytic biomass cover decreased when exposed to high levels of hydrodynamic activity (Ben Brahim et al., 2020). Seagrass epiphytes have been shown to progressively enrich seawater with minerals and nutrients (Brodersen and Kühl, 2022). However, high epiphytic colonization decreases light availability for seagrass leaves, thus increasing the diffusion distance between the leaf and the surrounding water, which may result in basification, warming and/or hypoxia for the seagrass (Brodersen and Kühl, 2022).

Seagrass meadows are highly productive habitats that can act as "blue carbon sinks" in coastal ecosystems by facilitating sedimentation and trapping particles (Jankowska et al., 2016; Röhr et al., 2018). Most of the variation in carbon stocks has been explained by sediment mud content, dry carbon density and degree of sorting, salinity, and water depth, along with plant attributes such as biomass and shoot density (Röhr et al., 2018). Settling particles within an artificial seagrass canopy can be trapped by the plant leaves or settle to the bottom, increasing with the canopy coverage (Barcelona et al., 2023b) and decreasing with the wave frequency (Barcelona et al., 2021b). However, the amount of sediment trapped by each single plant leaf was lower for high canopy densities compared to low canopy densities. Both processes can act synergistically to reduce the exchange of light and gases that could harm seagrass canopy development. Moreover, the total amount of sediment trapped on the seagrass leaves increased linearly with patch length (Barcelona et al.,

2023b), demonstrating the importance of canopy fragmentation in the trapping of sediment particles.

Epiphyte distribution on plant leaves can also modify the structure of the plants, impacting their flexural stiffness by modifying the cross-sectional area of the leaf (Fonseca and Koehl, 2006). In this case, the behaviour of a canopy can approach that of a rigid canopy and produce more turbulent kinetic energy or can approach a flexible canopy, i.e., moving with the flow and without producing turbulent kinetic energy (Barcelona et al., 2023a). Since hydrodynamics drive the capacity of seagrass to capture sediment particles (Barcelona et al., 2021b), it is worth determining how large amounts of sediment not only from coastal runoff, river plumes, natural resuspension, and heavy rains (Pineda et al., 2017; Vautard et al., 2014) but also from anthropogenic sources such as coastal development (Wu et al., 2018) reach seagrass meadows and are finally redistributed through the meadows. Therefore, it is expected that the distribution of epiphytes growing on plant leaves modifies sediment trapping capacity, thus regulating the sedimentation stocks in each canopy compartment. Indeed, suspended particles may be phagocyted by some seagrass epiphytes found on the leaves (Agawin and Duarte, 2002). Additionally, settling microplastics have been found to be trapped by seagrass (de los Santos et al., 2021), or adhere to eelgrass leaves and form biofilms, i.e., a sink of microplastics (Zhao et al., 2022).

The aim of the present study is to understand the role epiphytes on seagrass leaves have in the capture of sediment particles. The hypothesis of this study is formulated as follows: the area of the epiphytes colonizing a coastal canopy has the potential to modify the distribution and balance of sediment, including sediment suspended within the canopy, trapped by leaves and found on the canopy bed.

7.2 METHODOLOGY

7.2.1 Flume set-up

This study was conducted in the hydraulic flume at the Kristineberg Marine Research Station, Sweden (Figure 1). The flume was 800 cm long, 50 cm wide, 50 cm deep and equipped with an electronic piston that generated waves at a frequency of f = 0.5 Hz. To prevent wave reflection at the end of the flume, a PVC beach with a 20º slope covered by synthetic fibre was placed at the end of the flume (Marin-Diaz et al., 2020; Serra et al., 2018). To simulate the natural conditions of the seagrass in the field, the flume was filled with seawater, directly from Gullmarn Fjord with a salinity of S=27.65º/$_{oo}$ and the water temperature was T=15 ºC (+/- 1ºC). The mean water working height in the flume was h = 23 cm, and the test section was 200 cm long (Figure 1), starting 300 cm from the wave generator. The bottom of the test section was filled with sandy sediment with a diameter of d_{50}= 0.8-2 mm. To minimise additional turbidity from the sandy sediment bottom, the flume was filled with water and immediately discarded to remove the resuspended small particle content from the bed. This process was carried out three times before starting the experiment. Finally, prior to each experiment run, the flume was filled with water and left under the action of the waves for five minutes.

7.2.2 Vegetation

Eelgrass (*Zostera marina*) shoots were collected from the Gullmarn Fjord, located on the west coast of Sweden near the Kristineberg Marine Research Centre (58.25ºN, 11.45º W). The seagrass meadows from the Gullmarn Fjord have been reported to be composed of *Z. marina* and *Zostera noltii* individuals, although, the eelgrass *Z. marina* is the most abundant one. Only *Z. marina* individuals were collected and used in the experiments. Since both *Zostera*

noltii and *Z. marina* present the same morphology above ground, they are expected to behave similarly. Collection was carried out between June and August 2022 at a depth of 1-2 m. The eelgrass plants had an average of 3 ± 1 leaves·shoot^{-1}, with a shoot length of h_p = 20 ± 2 cm, a shoot width of 0.4 ± 0.1 cm, and a thickness of 0.045 ± 0.005 cm. The plants were kept in laboratory tanks with flow-through seawater from the fjord. To prevent any scouring and uprooting of the plants in the flume, the rhizome and roots were separated, and each shoot was fixed to a wooden stick (3 cm long and 0.5 cm in diameter) with a cable tie. The stick and cable tie were then buried into the sediment. The vegetated area in the flume was 1.5 m long (Figure 1a), with a plant density of n = 100 shoots·m^{-2} which falls within the range of shallow eelgrass densities found the west coast of Sweden (Boström et al., 2014).

7.2.3 Epiphyte distribution and treatments.

To simulate the effect of the epiphyte cover, three macroalgae species, namely: *Fucus vesiculosus*, *Fucus serratus* and *Furcellaria lumbricalis* were used to represent three levels of epiphytic structure. *F. serratus* presents the simplest structure with laminar leaves, *F. vesiculosus* presents a greater complexity with laminar leaves but with aerocysts. In contrast, *F. lumbricalis* presents the most complex structure with a filamentous shape and with the greatest 3D morphology. These macroalgae species were chosen to represent various epiphyte morphology structures that can potentially be found attached to eelgrass leaves (García-Redondo et al., 2019b). While these species may not commonly exist as epiphytes in eelgrass canopies, they were chosen due to their diverse morphologies which can be observed in actual epiphytes attached to eelgrass leaves. This selection allows for the simulation of different types of epiphytes that may occur naturally. Likewise, the constructed epiphyted covered the 35% of the plant leaf length according to the

percentages of epiphytes found in the field (Somma et al., 2023). This tries to mimic that in nature, epiphytes are more abundant in the apic part of the leaf than in the lower leaf sections (Reyes et al., 1998; Somma et al., 2023). The laboratory simulated epiphytic plants of epiphytic leaves with dimensions of 7 cm long x 0.5 cm wide piece of *F. serratus* or *F. vesiculosus* previously scraped with a scalpel to eliminate the epiphytic part on the algae, gently dried with a paper towel, and then glued to the eelgrass leaf with Loctite super glue. Therefore, each plant presented three epiphytic fragments; one for each leaf. In the case of *F. lumbricalis*, several 0.6 ± 0.1 cm fragments of *F. lumbricalis* were glued along the top 7-cm-long surface of the *Z. marina* leaves (Figure 2). The simulated epiphytes covered the upper part of the leaves, which is considered the flexible portion of each plant (Barcelona et al., 2023a). From now on, the plants epiphyted with *F. vesiculosus*, *F. serratus* and *F. lumbricalis* will be referred to as E1, E2 and E3, respectively, because these algae species were used to model a natural epiphyte. Four epiphyted canopy distributions were used for each epiphyte type, E1, E2 and E3: 0 %, 25 %, 50 %, 75 % and 100% of the total number of plants of the canopy were epiphyted, resulting in 13 treatments (Table 1). Then, a total of 13 set ups were considered, one for each treatment.

Table 7.1 Summary of the conducted experiments.

Run	Epiphyted plants (%)	Epiphyte type
1	0%	non-epiphyted
2	25%	E1
3	50%	E1
4	75%	E1
5	100%	E1
6	25%	E2
7	50%	E2
8	75%	E2
9	100%	E2
10	25%	E3
11	50%	E3
12	75%	E3
13	100%	E3

The effective height of the eelgrass without epiphytes, which refers to the bending of leaves caused by the waves, was determined by calculating the mean of the maximum and minimum bending heights observed during 25 oscillations. This measurement was repeated three times. The effective heights measured for each epiphyted plant (E1, E2 and E3) were h_v = 16.00 ± 0.47, 17.13 ± 0.92, and 17.67 ± 1.05 respectively, and for the non-epiphyte plant experiment it was 17.96 ± 0.51 cm.

7.2.4 Sediment injection

The wavemaker was activated and allowed to operate for 15 minutes to establish equilibrium in the system before sediment injection. Synthetic dust powder (ISO 12103-1, A4 Coarse, Powder Technology Inc., Burnsville) was used as sediment in the experiment. The sediment A4 was composed by particles from 5 mm to 120 mm with a d50 = 41.7 µm (Barcelona et al., 2023b; Mancini et al., 2023). Therefore, it was composed from fine silts to fine sand particles. This is in accordance with the size of sediment particles composing river plumes (Grifoll et al., 2014).

The particle-laden flow for injection was prepared by taking an initial volume of sediment suspension (2 L), with a concentration of 120 $g \cdot L^{-1}$, which was then introduced into one end of the sediment-injector pipe. The injector pipe was positioned at y = 0 cm along the flume axis (Figure 1a). During the sediment injection process, the injectors were oriented upwards to prevent any unintended spillage. Once the pipe was filled with the sediment suspension, it was closed and turned downward so that the injectors extended 5 cm below the water surface facing down. The injectors remained positioned at the top of the water column, above the vegetated patch, at a depth of 5 cm from the surface. Since the suspended sediment concentration in all the trials remained below 17.46 g L^{-1}, the sediment concentration was not expected to have any effect on the settling velocity of particles (Colomer et al., 1998).

The sediment injector pipe was a large 2.5 m-long pipe equipped with 42 sediment injectors evenly distributed 7 cm apart from each other. The design of the sediment injectors resembled a Y-shape, with a total length of 26 cm. Each arm of the injector pipe was 22.5 cm long (Figure 1a). To ensure a uniform distribution of sediment, each arm of the pipe had 12 holes from which the sediment was released into the flume. This setup allowed for a

homogeneous injection of sediment along both the x-axis and the y-axis of the flume.

7.2.5 Sediment measurements

To obtain the sediment concentration and distribution along the canopy, three types of sediment measurements were conducted: 1) sediment deposited on the bed, 2) suspended sediment, and 3) sediment attached to plant leaves with epiphytes.

Sediment deposition. To measure the sediment deposited on the bed, eight sediment traps were distributed in two rows along the main axis of the flume at y = ± 10 cm and x = 0 ± 40 cm, ± 80 cm (Figure 1b). Sediment samples from traps were collected at t = 60 min after the injection.

Suspended sediment. To measure suspended sediment, 50 mL water samples were pipetted at the same x position where the sediment traps were located for each run, at y = 0 cm, and at two water depths, at z/h_p = 0.3 (within the canopy) and at z/h_p =0.8 (above the canopy). These sampling locations were chosen to provide representative measurements within and above the canopy. Water samples were collected at various time points (t = 2, 30 and 60 min) after the sediment injection, and were later analysed to determine the concentration levels of the suspended sediment.

Sediment trapping. To measure the influence of epiphytes on sediment trapping, five percentages of epiphyted seagrass leaves were considered in order to mimic natural occurrence observed in the field (Borowitzka et al., 2005). The following percentages of epiphyted leaves were examined: 0%, 25%, 50%, 75% and 100% of the plant leaves covered with epiphytes. For all the cases of 0% and 100%, three sets of five plants were collected for the

analysis. For the cases of 25%, 50% and 75%, three sets of five epiphyted plants were collected, along with three sets of three epiphyted plants and two non-epiphyted for further analysis. In all cases, the plants were gently removed from the same x positions within the vegetated patch where the sediment traps had been placed at t = 60 min after the sediment injection. Afterwards, the plants were placed in a glass beaker with 100 mL of filtered seawater and stirred to remove the sediment trapped on the leaf surfaces or by the epiphytes.

To ensure the independency of the measurements a protocol was established. First, the suspended sediment samples were taken. Secondly, the sediment traps were covered with a lid. Thirdly, the fifteen plants were gently removed to measure the sediment trapped by the leaves and finally, the sediment traps were collected from the bottom of the flume and their content analysed.

The mass (in grams) of sediment in each sample was obtained by filtering them with glass microfiber filters (GF/F). The sediment traps and suspended sediment samples were filtered using filters with diameters of 50 mm and 25 mm, respectively. Firstly, the empty filters were weighted to obtain a zero weight. Then, the samples were filtered, dried at 60 ºC over 24 h and then weighed again (Brouwer et al., 2023).

7.2.6 Measuring velocities

The Eulerian velocity field was defined as (u, v, w) in the (x, y, z) directions, respectively. The three components of the velocity were recorded with a downwards-facing Acoustic Doppler Velocimeter (ADV, Nortek, Vectrino) at a frequency of 25 Hz for 10 min, resulting in 15,000 measurements. Beam correlations less than 90% were discarded and spikes were removed (Goring and Nikora, 2002). The ADV was mounted on a movable vertical frame (at x = 0, Figure 1b) and manually adjusted to measure at z = 5 cm, 6 cm, and 12

cm. Some plants were temporarily removed to prevent obstruction of the ADV beams (Zhang et al., 2018), and were re-inserted into the nearby area when measurements were completed.

For oscillatory flows, the instantaneous velocity, $U_i(t)$, can be decomposed as:

$$U_i(t) = U_c + Uw + u' \tag{7.1}$$

where, U_c is the mean current velocity associated to the wave, U_w is the unsteady wave motion which represents spatial variations in the phase-averaged velocity field, and u' is the turbulent velocity; that is, the instantaneous velocity fluctuation in the x-direction. U_c is the phase-averaged velocity:

$$U_c = \frac{1}{2\pi}\int_0^{2\pi} U_c(\varphi)\delta\varphi \tag{7.2}$$

where, $U_c(\varphi)$ is the instantaneous velocity according to the phase (Lowe et al., 2005; Luhar et al., 2010). In the current study, U_c at z/h_v= 0.3 above the bed (i.e., within the canopy layer) was always smaller than U_w, with mean values of -0.8 cm s^{-1}.

The wave velocity, U_w, was determined using a phase averaging technique. The Hilbert transform was used to average the oscillatory flow velocities with a common phase (Pujol et al., 2013b; Ros et al., 2014). The root mean square (rms) of U_w was considered as the characteristic value of the orbital velocity U_w^{rms} (U_w hereafter) at each depth, and was calculated according to:

$$U_w^{rms} = \sqrt{\frac{1}{2\pi}\int_0^{2\pi}(U_i(\varphi) - Uc)^{\ 2}\delta\varphi} \tag{7.3}$$

7.2.7 Theory

The sediment injected in the flume was distributed into four different compartments: captured by the epiphyted surface, deposited to the bottom, and remaining in suspension (above and within the canopy). A non-dimensional model was constructed based on the Pi-Buckingham theorem. Four variables and two dimensions were considered. The variables were the mass of sediment accumulated in each compartment (TM_i, where i=*b*, *s*, *p*, *ab*, where *b* represents sediment deposited at the bottom, *s* represents the sediment in suspension within the canopy, *p* represents the sediment deposited on the epiphyted surface of the plants and *ab* represents the sediment in suspension above the canopy), the sediment density (ρ), the total epiphyted area of the canopy (A) and the effective height (h_v). The dimensions were grams and metres. Therefore, two governing non-dimensional parameters can be constructed to describe the results. First, $TM_i/(A\rho h_v)$, representing the total mass of sediment captured by each compartment (TM_i) per total mass of the epiphyted canopy area, and second A/h_v^2, defined as the normalized area of the epiphyted meadow. This last parameter is a function of the normalized epiphyte length scale ($(L_{ep}/h_v)^2$), where L_{ep} is the epiphyte's length, which corresponded to the square root of A. A/h_v^2 indicates the increase in the frontal area between a non-epiphyted canopy and the different levels of epiphyted canopies. TM_p is the total mass of sediment collected by all plants in the canopy, obtained multiplying the mass of sediment collected by each single plant (M_p) by the number of plants in the canopy. TM_s is the total mass of sediment in suspension that was calculated by multiplying the mass of suspended sediment in the sample (M_s) by the ratio between the total volume within the canopy and the volume of the sample (100 mL). TM_b is the total mass of sediment deposited to the bottom that was calculated by multiplying

the mass of sediment in the trap (M_b) by the ratio between the total area of the vegetated bottom and the area of a single trap (of 0.05 x 0.02 m^2).

Therefore, a non-dimensional model should consider the relationship between the above governing non-dimensional parameters. It is possible to expect:

$$\frac{TM_i}{A\rho hv} = f\left(\frac{A}{h_v^2}\right) = a\left(\frac{A}{h_v^2}\right)^c \quad (7.4)$$

where f is function of the dimensionless parameter A/h_v^2, and *a* and *c* are constants of the relationship.

The epiphyted area of each plant A_p was considered the effective area of the flow trapped inside the area of the epiphyte (Figure 2). To obtain A_p, photographs of plants with epiphytes were converted to grayscale and later to black and white using MATLAB (MathWorks, Inc.). The threshold considered for the conversion to black and white corresponded to that representing the area of the region inside the epiphyte (Figure 2a and 2b). The plant epiphyted area A_p was calculated as the vertical sum along the plant leaf of the area at each z (A_z) for each case (Figure 2c). Therefore, the total epiphyted area of the canopy (A) was obtained multiplying A_p by the total number of epiphytes for each experiment.

7.2.8 Data analysis

TM_i was regressed against the percentage of epiphyted plant. The differences between the percentage of epiphyted plants and the epiphyted areas (A_p) were determined using ANOVA one-factor. The Shapiro-Wilk, and Levene's tests were performed to ensure normality and homogeneity.

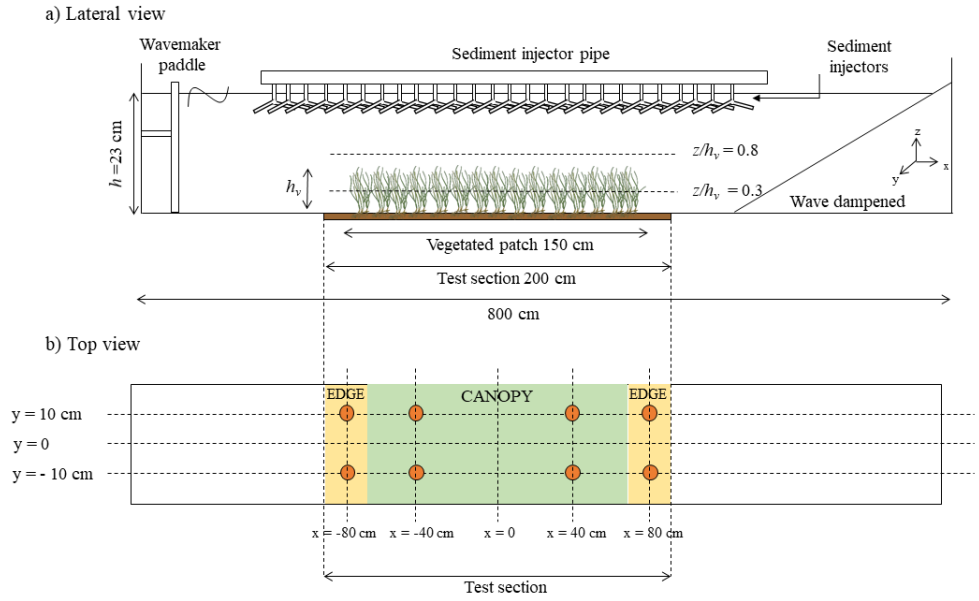

Figure 7.1 Experimental setup and canopy regions with sediment trap locations, a) Lateral view of the experimental setup in the flume, with the wave paddle generator located on the left. Waves propagate from left to right. b) Top view of the setup illustrates two regions: the inner canopy region (in green) and the edge region of the canopy (in yellow). Additionally, orange circles indicate the position of sediment traps distributed along the flume bed in both the canopy and edge regions.

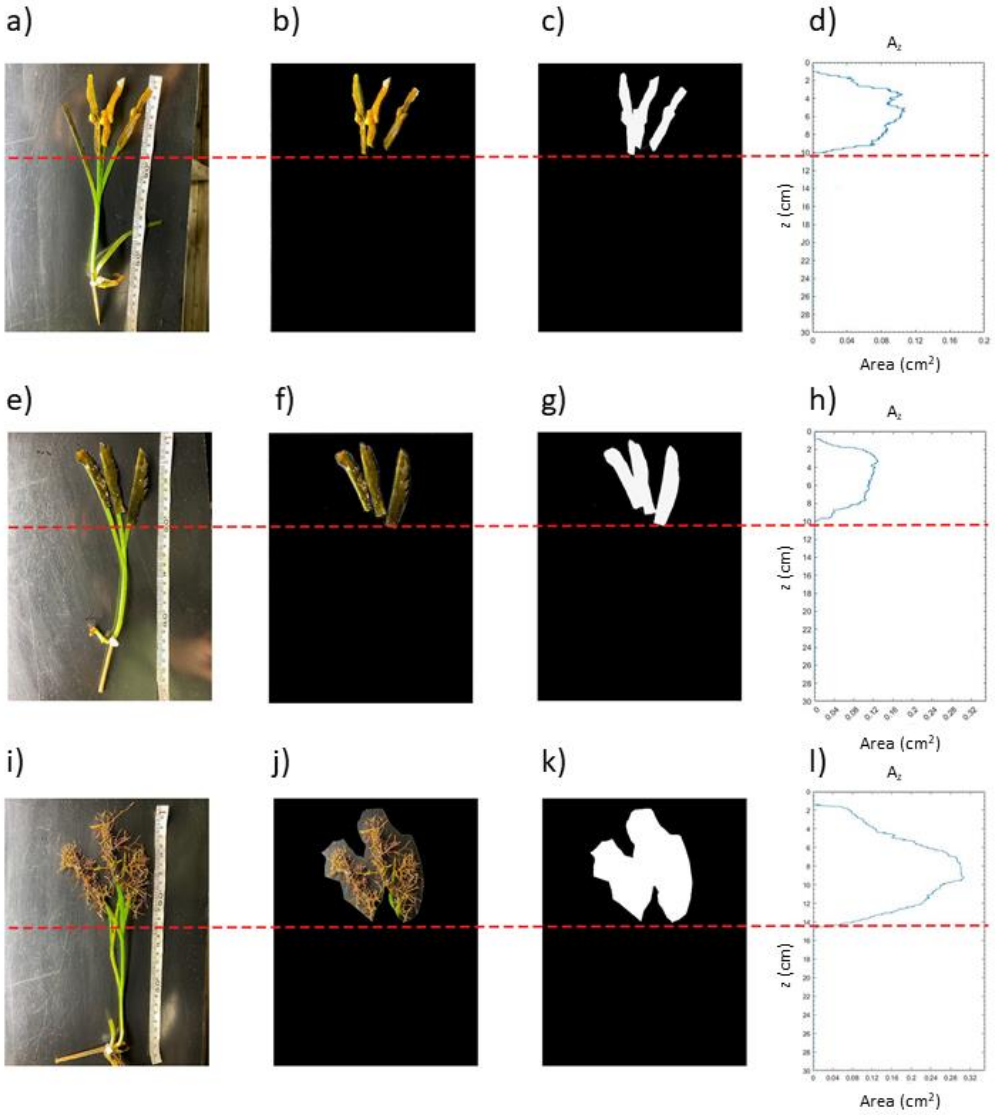

Figure 7.2 Eelgrass shoots with epiphyted areas and vertical distribution of epiphyte coverage. Photograph of eelgrass shoots displaying the epiphytic area of a single plant located at the top of the leaves for the three epiphytes considered: *Fucus vesiculosus* (E1), *Fucus serratus* (E2, and *Furcellaria lumbricalis* (E3) (a, e, and i, respectively) (left panels). Furthermore, photographs of the epiphyte area for each type of species (central panels), and a plot illustrating the vertical distribution of the epiphyte area A_z with height for each type of epiphyte (d, h and l in the right panels) was generated.

7.3 RESULTS

7.3.1 Distribution of sediment mass in the different compartments

The sediment was distributed into four compartments: sediment trapped by the seagrass leaves (Figure 7.3a), sediment deposited on the bottom of the flume (Figure 7.3b), sediment remaining in suspension within the canopy (Figure 7.3c) and sediment remaining in suspension above the canopy (not considered). For the trials conducted with epiphytes E2 and E3, the mass of sediment, TM_p, trapped by all plant leaves increased linearly with the percentage of epiphyted plants (0%-100% epiphyted plants), following the tendencies for each epiphyte: $TM_p = 0.02$ (% epiphyted plants) + 0.75 for the E3 ($A_p = 94.51$ cm^2) and $TM_p = 0.01$ (% epiphyted plants) + 1.09 for the E2 ($A_p = 38.15$ cm^2) (Figure 3a). However, for the lowest epiphyted area studied, corresponding to experiments with E1 ($A_p = 31.56$ cm^2), the mass of sediment trapped by plant leaves remained constant regardless of the percentage of epiphyted plants. In contrast, the mass of sediment deposited on the bottom did not show significant differences (p-value > 0.05) between epiphyte types E1, E2 and E3, but did present a decreasing trend linearly correlated with the percentage of epiphyte plants, with a p-value < 0.05 (Figure 7.3b). In contrast, the sediment remaining in suspension did not show significant differences in relation to either the epiphyted area or the percentage of epiphyted plants (p-value > 0.05, obtained by performing a one-way ANOVA) (Figure 7.3c).

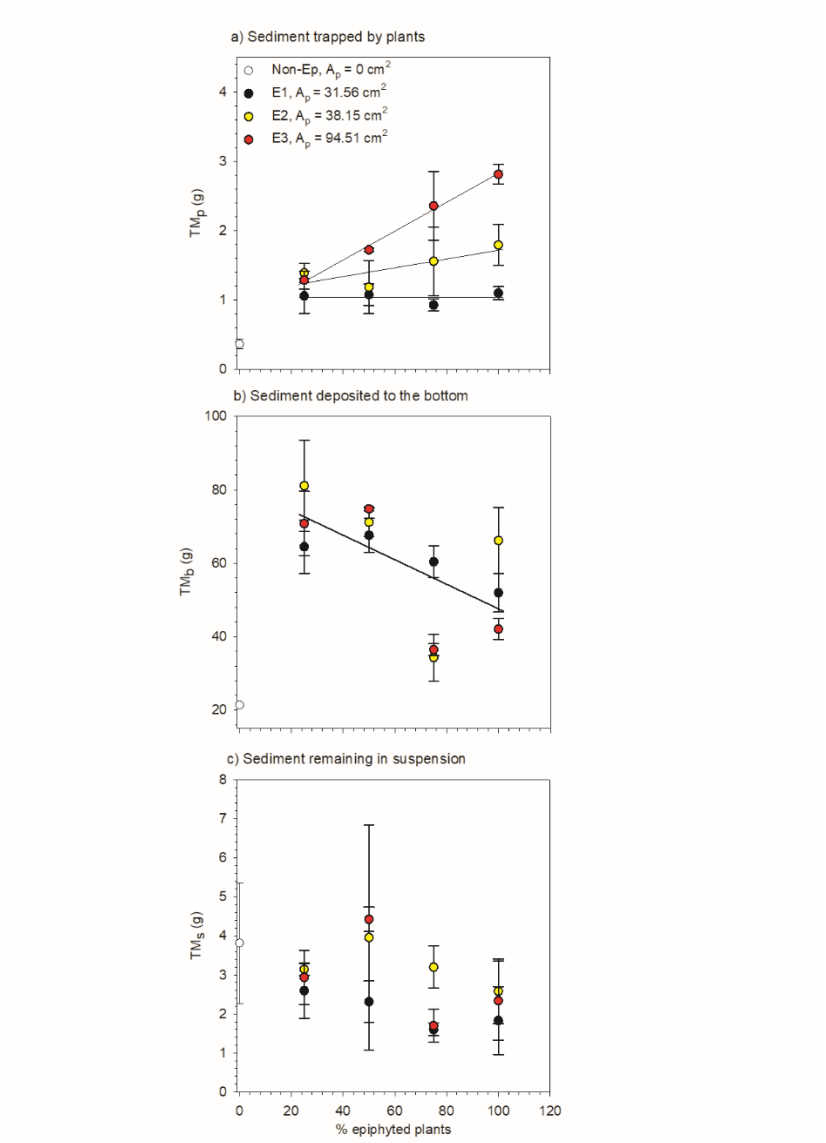

Figure 7.3 Sediment distribution patterns associated with epiphyted plants. Mass of sediment a) trapped by plant leaves. The linear expressions for E2 and E3 found are: $TM_p = 0.02$ (% epiphyted plants) + 0.75 and $TM_p = 0.01$ (% epiphyted plants) + 1.09 respectively, p-value < 0.05 in both cases, b) deposited to the bottom. The linear expression found is: $TM_b = -0.33$ (% epiphyted plants) + 81.00, p- value < 0.05 and c) remaining in suspension for the number epiphyted plants in the canopy (in percentage).

7.3.2 Non-dimensional model for sediment capture in each compartment

To quantify the sediment captured by the seagrass canopy, three non-dimensional models were developed to represent each compartment: sediment trapped by the plant leaves (Figure 7.4), sediment deposited on the bottom (Figure 7.5) and sediment remaining in suspension within the canopy (Figure 7.6). These models were derived using Equation 7.4, as described in the Materials and Methods section.

For the sediment trapped by the plant leaves, a negative power trend was found and is shown in Figure 4. The expression has been solved for TM_p, following:

$$TM_p = 7 \cdot 10^{-5} \rho A^{0.27} h_v^{2.46}, \text{ with a } R^2 = 0.90 \qquad (7.5)$$

and showing that the sediment trapped by the leaves increased with both the total epiphyted area A and the effective leaf length h_v (Figure 7.4).

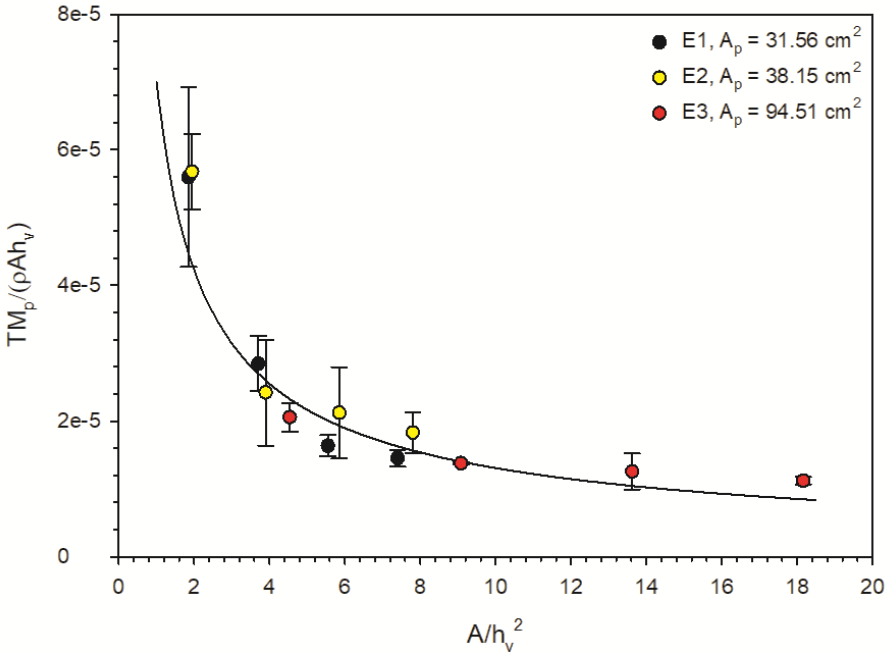

Figure 7.4 Non-dimensional model for the mass sediment trapped by plant leaves, $TM_p/(\rho Ah_v)$ for the different A/h_v^2 tested. E1, A_p = 31.56 cm^2 (black filled circles), E2, A_p = 38.15 cm^2 (blue filled circles) and E3, A_p = 94.51 cm^2 (red filled circles). The power tendency found follows the expression: $TM_p/(\rho Ah_v) = 7 \cdot 10^{-5} (A/h_v^2)^{-0.73}$, with an $R^2 = 0.90$, p-value < 0.05.

The non-dimensional mass deposited at the bottom in the complete area covered by vegetation, $TM_b/\rho Ah_v$, also presented a negative power trend with A/h_v^2 (Figure 5). The dependence of the mass deposited at the bottom was obtained as a function of A and hv, according to the following equation:

$$TM_b = 8.6 \cdot 10\text{-}3\rho A\text{-}0.34hv3.68, \text{ with a } R^2 = 0.94 \quad (7.6)$$

Therefore, the sediment deposited to the bottom depended negatively on the total epiphyted area (A) and positively on the effective height (h_v), as shown in Figure 5. Equation 6 implies that the greater the epiphyted area, the lower the amount of sediment deposited to the bottom. However, the greater the

effective height, the greater the amount of sediment deposited to the bottom (Figure 7.5).

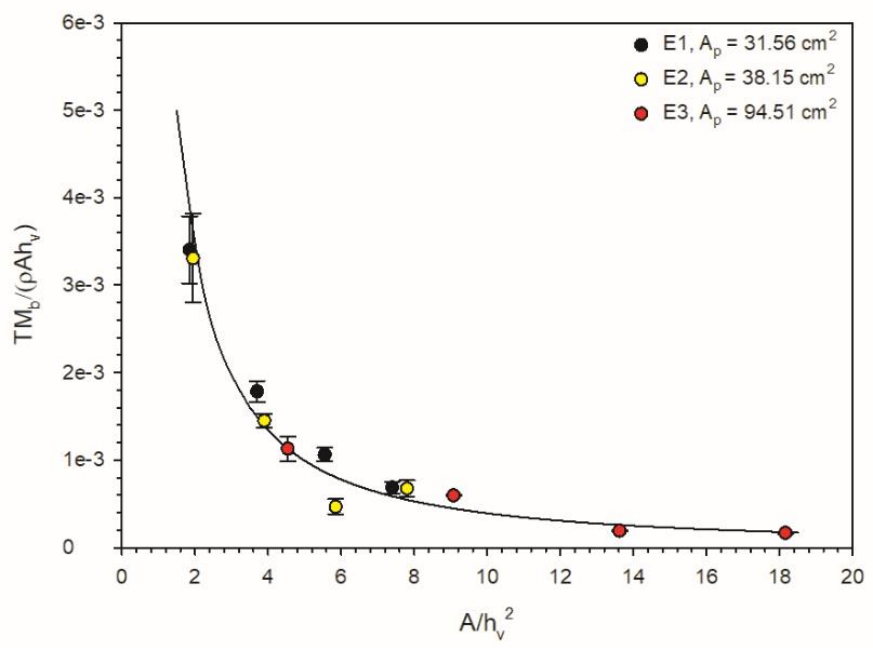

Figure 7.5 Non-dimensional model for the mass sediment deposited to the bottom, $TM_b/(\rho Ah_v)$ for the different A/h_v^2 tested, E1, A_p = 31.56 cm^2 (black filled circles), E2, A_p = 38.15 cm^2 (blue filled circles) and E3, A_p = 94.51 cm^2 (red filled circles). The power tendency found follows the expression: $TM_p/(\rho Ah_v) = 8.6 \cdot 10^{-3} (A/h_v^2)^{-1.34}$, with an $R^2 = 0.94$, p-value < 0.05.

The sediment remaining in suspension within the total canopy region (TM_s), followed a negative power relationship (Figure 7.6). The expression (as for the other compartments) was also solved by TM_s. TM_s decreased with the total epiphyted area (A) and increased with the effective height (h_v) with the following expression:

$$TM_s = 3 \cdot 10^{-4} \rho A^{-0.22} h_v^{3.43}, \text{ with a } R^2 = 0.92 \qquad (7.7)$$

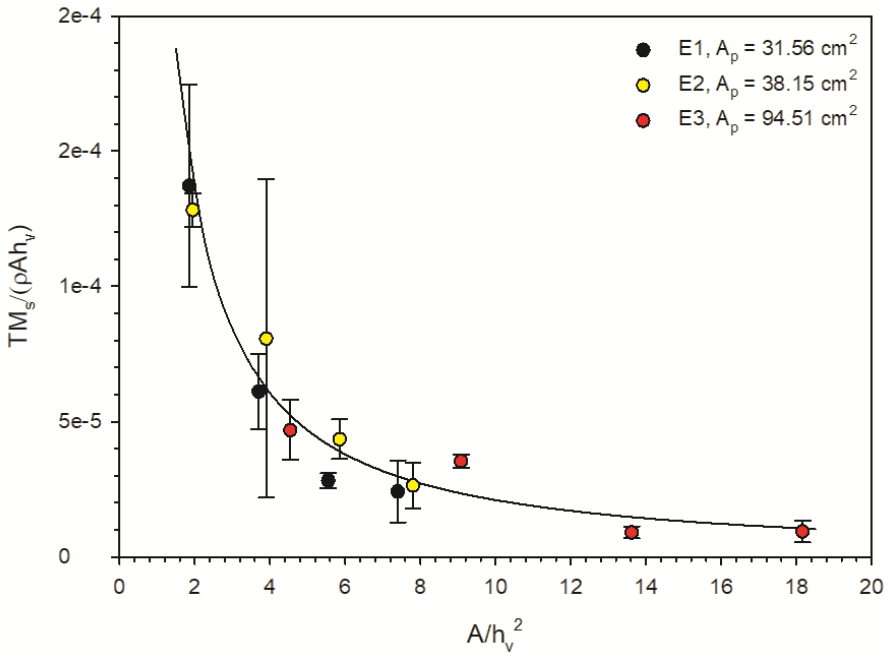

Figure 7.6 Non-dimensional model for the mass sediment remained in suspension, $TM_s/(\rho A h_v)$ for the different A/h_v^2 tested, E1, A_p = 31.56 cm^2 (black filled circles), E2, A_p = 38.15 cm^2 (blue filled circles) and E3, A_p = 94.51 cm^2 (red filled circles). The power tendency found follows the expression: $TM_s/(\rho A h_v) = 3 \cdot 10^{-4} (A/h_v^2)^{-1.22}$, with an $R^2 = 0.92$, p-value < 0.05.

For the experiments conducted with 50% and 100% of epiphyted plants and for the different types of epiphytes, the total volume of sediment captured in each compartment (suspended, plant leaves, and bottom) was calculated. For the sediment trapped by the plant leaves, the total volume of sediment trapped was obtained as follows:

$$V_p = (M_{nep}\, N_{nep} + M_{ep}\, N_{ep}) / \rho \qquad (7.8)$$

where N_{nep} and N_{ep} are the number of non-epiphyted and epiphyted plants, respectively. M_{nep} and M_{ep} are the mass of sediment captured by single both non-epiphyted and epiphyted plants, respectively.

For the sediment in suspension, the total volume of sediment within the canopy, V_s, was calculated as follows:

$$V_s = M_s L_p h_v / \rho \quad (7.9)$$

where L_p is the canopy length.

For the sediment deposited on the bottom, the total volume of sediment V_b was calculated as follows:

$$V_b = M_b L_p W \quad (7.10)$$

where W is the width of the flume.

The volume of particles deposited to the bottom (V_b) presented the largest percentage compared to the other two compartments (V_s and V_p). For the non-epiphytic case to the 100% of epiphyted plants (Figure 7.7), the volume of sediment trapped by the plant leaves (V_p) increased with the total epiphyted area. The non-epiphytic case presented the lowest V_p= 0.6%, for the 50% of total epiphyted plants V_p increased from 1.5 to 2.1% with the total epiphyted area, and from 2.5 to 6.0% for the 100% of epiphyted plants (Figure 7.7). In contrast, the volume of sediment deposited on the bottom (V_b) decreased with the total epiphyted area; being 93.5 for the non-epiphytic case, from 95% to 92.4% for the 50% epiphyted plants and from 93.8 to 90% for the 100% epiphyted plants (Figure 7.7). V_s decreases with the presence of epiphytes, reaching a value of 5.9% for the non-epiphytic. However, V_s decreased as the total epiphytic area increased, from 3.3% to 5.1% for 50% of epiphyted plants and from 3.7% to 5.0% for experiments with 100% of epiphyted plants (Figure 7.7).

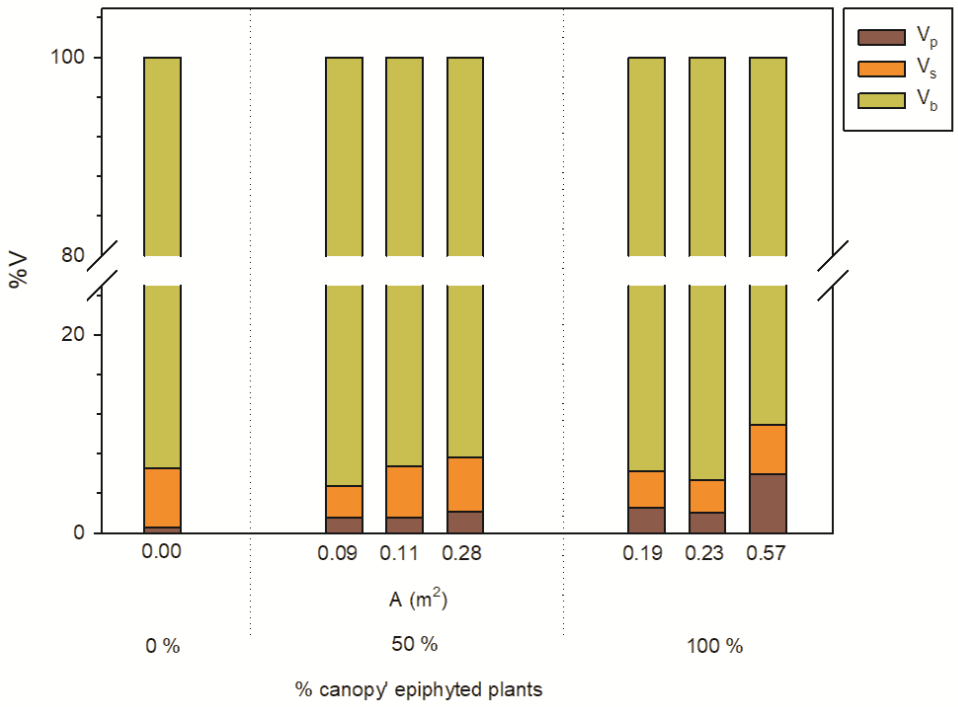

Figure 7.7 Distribution of total sediment volume. Total sediment volume (V, in %) distributed in the different compartments: total volume of sediment trapped by the plant leaves (V_p), total volume of sediment, remaining in suspension within the canopy (V_s), and total volume of sediment deposited to the bottom (V_b) versus the total epiphytic area (A) for the cases 0%, 50% and 100% of epiphyted plants of the canopy. A (total epiphytic area), corresponds to each epiphyte used: E1 = 0.09; E2 = 0.11 and E3 = 0.28 m^2 for 50% of epiphyted plants and E1 = 0.19; E2 = 0.23 and E3 = 0.57 m^2 for 100% of epiphyted plants.

7.4 DISCUSSION

Seagrass habitats present a range of structural characteristics that affect the ecological services they provide (Ward et al., 2022). Factors such as plant stiffness, presence of bare sediment areas within seagrass canopies, leaf height, canopy density, stem diameter, patch length and presence of epiphytic

communities, impact the functioning of seagrasses. This study demonstrates that sedimentation patterns at the bottom of epiphyted canopies and sediment capture by epiphyted leaves depend on both the effective height (h_v) of the plant and the total epiphyted area (A). Three types of epiphytic structures on eelgrass canopies were used to model three levels of epiphytic areas and compared to the non-epiphyted case.

The sediment trapped by the plant leaves was found to follow $TM_p=A^{0.27}h_v^{2.46}$. Therefore, the total mass of sediment attached to plant leaves increased with both the total epiphytic area and plant height. Increasing the effective plant height by 3.2% (when comparing E2 and E3) and 10.4% (when comparing E1 and E3) resulted in an increase in the total mass of sediment captured on the plant leaves of 7.9% to 27.7%, respectively. Similarly, increasing the total epiphytic area by 2.5 and 3 (comparing E2 and E3, and E1 and E3, respectively) led to an increase in the total mass of sediment attached to the leaves of 27.7% and 34.5%, respectively. As the accumulation of sediment on plant leaves increases with the epiphytic area, it might produce a negative feedback on seagrasses, reducing their gas exchange capabilities (Pujol et al., 2019) and their ability to meet light requirements (Brodersen and Kühl, 2022), due to the presence of epiphytes leading to a build-up on the diffusive boundary layer which may impeded oxygen transfer between the seagrass leaf and the surrounding water (Noisette et al., 2020). However, this negative effect might be counteracted in dense canopies, which capture less sediment per plant leaf but a higher overall amount when considering the sediment captured by the entire canopy (Barcelona et al., 2021b). Furthermore, the mass of sediment in suspension slightly decreases with the epiphytic area following $TM_s=A^{-0.33}h_v^{3.43}$. That is, the presence of epiphytes on the surface of the plant leaves reduces the mass of suspended sediment, resulting in a clearer water column. This result partially counteracts the negative effects of epiphyte

presence, which otherwise would reduce the light availability and compromise the light requirements for plant leaves (Brodersen and Kühl, 2022).

The mass of sediment deposited at the bottom was found to depend on A and h_v following the relationship $TM_b=A^{-0.34}h_v^{3.68}$. This indicates that larger epiphytic areas increase the capture of sediment by plant leaves, resulting in a reduction of the sediment reaching the bottom. Additionally, the mass of sediment settling at the bottom increased with the effective plant height, indicating that higher plant leaves provide a greater surface area for particle capture (Borum, 1987; Ruesink, 2016). Stiffer plants, associated with higher effective plant heights, are expected to enhance the chances of particles settling to the bottom, increasing the overall sediment mass deposited in the bed.

In the absence of epiphytes, the majority of sediment particles, particularly those in the silt and clay ranges, reached the seagrass bottom (93.5%), while only a small portion was trapped by the plant leaves (0.6%). When the entire canopy was epiphyted (100% of plants in the canopy were epiphyted), the sedimentation at the seagrass bottom diminished to 90.0%, while the particles captured by the epiphyted leaves increased to 6.0%. Notably, the epiphyte with the greater surface area (E3), captured 10 times more sediment on the leaves when compared to the non-epiphyted canopy. In all cases with epiphytes, the volume of suspended sediment was lower than in cases without epiphytes. Therefore, colonization of epiphytes on eelgrass leaves may regulate the sedimentation stocks in each canopy compartment and reduce the amount of suspended sediment within the canopy, enhancing the role of the seagrass in clearing the water column.

However, in cases with a high epiphytic area, the presence of epiphytes on seagrass leaves, along with an increase in the sediment captured by leaves

might lead to a reduction in available light, which is essential for plant requirements (Brodersen and Kühl, 2022). While moderate epiphytic cases may modulate light harvesting, high percentages of epiphytes can have a negative effect on seagrasses, compromising the survival of the canopy (Brodersen and Kühl, 2022). Generally, there is higher leaf growth and productivity at the centre of a seagrass meadow than at the edges (Turner, 2007). However, in dense seagrass beds, light competition can result in greater productivity at the edges compared to the centre (Nakaoka and Aioi, 1999). Also, a high epiphytic community growing on long seagrass leaves in the centre of a meadow might also compromise the seagrass, which experiences less light stress at the edges compared to the centre.

The percentage of epiphytic area was found to have no effect on eelgrass growth up to 60% (Ruesink, 2016). However, other studies have found a reduction in seagrass productivity with an increase in epiphyte mass (Reynolds et al., 2014; Whalen et al., 2013). Therefore, differences in seagrass responses to epiphytic areas might arise when resources are below saturating levels (Sand-Jensen, 1977), which could explain variations found between studies.

The variation in canopy epiphytic area may also impact the flexural capacity of plants, resulting in more rigid or more flexible structures which can modify plant behaviour under different hydrodynamic conditions. Rigid plants can produce more turbulent kinetic energy than flexible plants can (Barcelona et al., 2023a), which subsequently reduces the thickness of the diffuse boundary layer through increased flow velocity (Pujol et al., 2019) and potentially alters nutrient uptake (Cornelisen and Thomas, 2004).

Eelgrass, being an annual species, undergoes variations in leaf length during the year (Birgit Olesen and Sand-Jensen, 1994), resulting in seasonal changes in the available leaf area for epiphytes (Brodersen and Kühl, 2022). The non-

dimensional model proposed indicates that the ecological function of the seagrass leaves in capturing sediment is going to vary following an annual cycle. Therefore, these seasonal variations in epiphytes may play a significant role in the sediment retention in coastal areas. This ecological service provided by eelgrass is of relevance considering the observed increase in heavy rainfall events that produce particle sediment-laden plumes in Europe in recent years (Vautard et al., 2014). Epiphytes also contribute to reducing the impact of the sediment output from the dredging activities related to coastal development (Wu et al., 2018).

Therefore, the structural characteristics of plant and canopies, in addition to hydrodynamic conditions, time of the year, and imposed natural or anthropogenic disturbances, are crucial factors for the development of seagrass habitats (Barcelona et al., 2023b, 2023a, 2021c, 2021a, 2021b; Duarte et al., 2013, 2005; Eckardt et al., 2023; Granata et al., 2001; Hendriks et al., 2008). As shown in this study, epiphyte presence on plant leaves is also a key component to consider when determining the overall behavior of the canopy and its role in the capture of sediment from sediment output sources.

The hypothesis raised in the introduction has been confirmed. That is, the morphology and quantity of the epiphytes colonizing a *Z. marina* meadow have been found to be enhance the capture of particles by seagrass leaves, with epiphytes possessing larger effective areas capable of trapping more particles compared to those with smaller epiphytic areas. This behavior impacts on the other compartments. Then, the epiphytic community has been also found to modify both the deposition of sediment on the bed and the suspended sediment, with a decrease of the sediment deposited and the sediment suspended as the epiphytic area increased. These laboratory results a first step

to understand the role of real epiphytic communities in the field in trapping suspended particles.

Acknowledgments

We would like to thank FORMAS grant Dnr. 2019-01192. We would also like to thank Michael

Gitzen, Tristan Dickinson, and Kirsten Wohak for the field and laboratory assistance. This work was supported by the Ministerio de Economía y Competitividad of the Spanish Government through Grant PID2021-123860OB-100. Aina Barcelona was funded by the pre-doctoral grant 2020 FI SDUR 00043 from the “Generalitat de Catalunya”.

CHAPTER 8

General discussion

Cover design: Carles Arbat

This PhD thesis has been prepared as a collection of papers (most of them published, with a total impact factor of 30.6), from Chapter 2 to 7, each of it comprises of its own discussion. In order to not transcribe the discussions again, this chapter aims to describe a global discussion, connecting the results from Chapters 2 to 7 and comparing and contextualizing the results with other key studies related to this Thesis. The general discussion emphasizes the ecological implications of the results obtained in each chapter.

Through this PhD thesis, the interactions between coastal seagrass canopies, defined through characteristic structural parameters, and the hydrodynamics of coastal marine seascapes has been established. Furthermore, these interactions determine the vertical and horizontal distribution of sediment transport within seagrass canopies from external sources, impacting on the sediment balance and therefore to other particle associate components. Therefore, its is expected that from the findings of the current PhD thesis several ecological implications can be derived.

Among the ecological services expected for coastal seagrass canopies, the retention or accumulation of sediments is considered a major role (Casal-Porras et al., 2022; Gacia and Duarte, 2001; Johannessen, 2022; Lopez-y-Royo et al., 2011; Trevathan-Tackett et al., 2015), reduce the suspended sediment and enhance the sedimentation to the seabed (Gacia et al., 1999; Gacia and Duarte, 2001). Furthermore, asa consequence of their impact in the turbidity, seagrass meadows are used as a biological indicators of water quality (Güreşen et al., 2020; Malea et al., 2019). Also their role in the sediment balance represents also a major issue, as they play a crucial role in blue carbon sequestration (Ricart et al., 2017). Climate change, on the other hand, has been shown to increase the frequency and severity of severe rainfall, resulting in higher episodic river and runoff flows that may reach seagrass meadows

(Vautard et al., 2014). Other external sediment sources that can reach seagrass meadows as sediment plumes include subglacial transported meltwater (Hallet et al., 1996), meltwater run-off (Chu et al., 2009), iceberg submarine melting (Fried et al., 2015), and iceberg calving (Koppes et al., 2010). Furthermore, Asplund et al. (2021) reported greater carbon burial in seagrass meadows near deforested mangroves, implying that mangrove material can be washed into seagrass meadows. Furthermore, anthropogenic activities such as urban and industrial runoff, aquaculture and agriculture runoff can all produce sediment outputs that can reach seagrass meadows as sediment plumes (Abadie et al., 2016; Grech et al., 2012; Montefalcone, 2009). A high inflow of sediment on seagrass meadows may have a negative impact on its quality status as the sediment captured on the leaves surface may diminish the light availability and also increase the diffusion layer between the leaves and the surrounding water (Brodersen and Kühl, 2022; Pujol et al., 2019). Since the majority of sediment dispersal studies are focused on the sediment resuspension from the meadow itself (Gacia et al., 1999; Gacia and Duarte, 2001; Ros et al., 2014), the current PhD is focussed on determining the capacity of seagrasses in capturing sediment from other sources. Thus, this PhD fulfil the lack of knowledge on the how structural canopy parameters and hydrodynamics impact on the sediment distribution from external sources.

This PhD also proves that coastal hydrodynamics also plays a crucial role on the structural canopy parameters, effecting the major structural parameters as the plant density (especially at canopy edges) and the stiffness of the plants, which in consequence will alter the plant height. The hydrodynamics through both the wave velocity (U_w) and the turbulent kinetic energy (TKE), coupled with the structural parameters defining a seagrass canopy through the plant density, the patch length, the plant height and the epiphyte colonization, together with the gap sizes within a meadow impact on the sediment balance.

That is, they will determine the distribution of sediment in the different compartments: deposited to the seabed, remaining in suspension, and captured on the leaves surface. The interaction between the structural parameters and the local hydrodynamics within a seagrass canopy may determine the level of patchiness of the meadow, resulting in a wide range of meadow types, i.e. from fragmented to continuous seagrass meadows (Spalding et al. 2003). Not only this, seagrass canopies can present interspersed gaps, that is, areas without plants, due to either natural (Infantes et al., 2009) or anthropogenic disturbances (Colomer et al., 2017). The relationship between the gap sizes and the patch lengths has been found to impact on the level of 'patchiness', which is expected to vary with time. This thesis proves that the level of fragmentation is crucial at understanding the equipartition of sediment within a fragmented canopy.

All in all, the chapters presented in the current thesis are directed to determine the interactions between the structural canopy parameters and the coastal hydrodynamics and discuss on the possible ecological implications through some structural thresholds.

8.1 Interaction between the structural canopy parameters and the local hydrodynamics

To classify the seagrass meadows by a parameter that encompasses both the canopy structural parameters and the hydrodynamics, this thesis has used the ratio A_w/S, where A_w is the orbital length and S is the plant-to-plant distance, which is first described in Chapter 1, and later used in chapters 3, 4, 5, 6 and 7. Results in Chapters 3 and 4 showed that for all the cases of A_w/S the wave velocity attenuation depends on the plant density and wave frequency. For all the cases studied encompassing canopies with a range of plant densities, denser canopies were found to present a higher wave attenuation. These results

align with Pujol et al. (2013b), Hendriks et al. (2008) and Gacia et al. (1999) who found a decrease in the wave velocity as the plant density increased. Also, experimental laboratory results in the wave flume demonstrate that the wave attenuation is greater for lower wave frequencies, with agrees with the findings by Hansen and Reidenbach (2012).

However, the TKE attenuation presents a more complex behaviour (Chapters 3, 4 and 6). It is important to distinguish between the vertical TKE attenuation (from the top layer of the plant to the bottom) and the TKE attenuation comparing vegetated areas with bare soil areas. Both, A_w/S and the plant stiffness are key parameters to understand TKE attenuation. Rigid canopies attenuate vertically the TKE, as the TKE within the canopy is always lower than the one measured on the top layer of the canopy due to the drag produced by the rigid stems. On the contrary, for flexible vegetation a threshold at $A_w/S = 0.35$ has been proved. Flexible canopies only attenuate TKE for $A_w/S < 0.35$ as the plants do not interact with the flow as they are mostly under low wave frequencies condition allowing a greater oscillatory excursion length on the top of the plant, which do not produce wakes around the blades. For $A_w/S > 0.35$ flexible canopies produce TKE, as they are under higher wave frequencies allowing less motion of the plants, so under such conditions, plants remain stiffer and in consequence plants interact efficiently with waves producing TKE along the entire plant through the generation of wakes. These results align with the findings by van Veelen et al. (2020) who found that flexible plants swayed with the flow and did not dampen wave velocities, while rigid vegetations produced greater resistance to the flow and dumped wave velocities. Also, Granata et al., (2001) found a vertical attenuation of the TKE in *P. oceanica* meadows.

In contrast, rigid vegetation produces TKE, resulting in greater TKE compared to bare soil for all cases studied due to the generation of stem-wake turbulence associated to a large reduction in the wave velocity (Pujol et al., 2013a). Flexible canopies dissipate the TKE in the lower canopy layer for $A_w/S < 0.35$, under these conditions single stems do not contribute to TKE generation, instead, stems dampen the near-bed generated TKE. However, for $A_w/S > 0.35$ the TKE will be enhanced within the canopy. This threshold is concurrent with the results of Zhang et al. (2018) who also found this transition for the inner canopy layer in flexible plants.

In Chapters 4 and 6 a non-dimensional model was defined in order to establish that the production on the TKE within a modelled seagrass canopy depends not only on the wave velocity, canopy density and plant stiffness but also on the patch length. Here, the behaviour of fragmented canopies might shift from the behaviour of continuous ones. While rigid plants required $\left[C_{D-Patch}\frac{nd^2}{2(1-\emptyset)}\right]^{\frac{2}{3}}U_w{}^2 > 2$, flexible plants required $\left[C_{D-Patch}\frac{nd^2}{2(1-\emptyset)}\right]^{\frac{2}{3}}U_w{}^2 > 4$, where $C_{D\text{-}patch}$ is the drag generated by the patch, n is the plant density, d is the stem diameter and ϕ is the solid volume fraction. The fact that the threshold is lower for rigid vegetation is due to the fact that flexible plants move with the flow, so the drag produced by the canopy varies depending on the stiffness of the vegetation (van Veelen et al., 2020). These studies demonstrated that a minimum of plant density is required to produce TKE, which can be defined in terms of both the plant density and the patch length. Moreover, the vegetation stiffness will affect the effective plant height which will affect the wave and TKE attenuation as well, as an increase in the plant height enhances the wave attenuation (Koftis and Prinos, 2011; Pujol et al., 2013a). Small patches with patch lengths below 6 times the effective plant height under high wave frequencies has been proven to not provide any

reduction in the wave velocity compared with the bare soil areas, while patches larger than these dimensions reduce the wave velocity as the plant density increase. Moreover, a moderate TKE production is needed by the meadow to diminish the diffusive boundary layer on the leaves. Reducing the diffusive boundary layer, the oxygen exchange will be enhanced (Pujol et al., 2019). Pujol et al. (2019) found that for $U_w < 6$ cm s^{-1}, the gas exchange through the diffusive boundary layer is reduced, aligning with the results found in this PhD.

Here, the structural canopy parameters impact on the local hydrodynamics, but the contrary also holds. That is hydrodynamics also impact on the canopy structure. Serra et al. (2020) determined that the level of fragmentation, in terms of gap size (non-vegetated areas within a meadow) impacts on the wave velocity attenuation. They demonstrated that the higher the gap the lower is the wave attenuation within the gap. Also, Colomer et al. (2017) found that the attenuation on the wave velocity and the TKE increased up to 1 m away from the edge of a vegetated patch, indicating that the hydrodynamic parameters are attenuated at distances of 1 m within the meadow. Therefore, patchy meadows will have higher wave velocities and turbulence (El Allaoui et al., 2016) than continuous meadows. These results align with those demonstrated in Chapter 2. This study proved the effect of the level of fragmentation on the plant density in both gap-scale and meadow-scale. At gap-scale (gap size), this study determined that the larger the gap the lower the plant density of the vegetation surrounding the gap. Then, the results found in Chapter 2, aligns with those of Colomer et al. (2017), who found lower vegetation covers near larger gaps. Thus, these differences in plant densities according to the gap size could compromise the meadow resistance due to an increase in seabed erosion, enhancing the generation of further gaps accelerating the transition from continuous to patchy meadows. Moreover, at

meadow-scale (percentage of gaps area), the higher the fragmentation degree of the meadow, the lower the plant density is in the surrounding vegetation near the gap. Therefore, the overall degree of fragmentation is a crucial parameter for the vulnerability of the seagrass meadow. For the same gap size, meadows with higher fragmentation will present lower plant densities at the edge of the gaps.

8.2 Canopy structural characteristics and hydrodynamic parameters effects on the sediment distribution within vegetated coastal systems

The results from Chapters 3, 5 and 7 demonstrated that flexible canopies represent new surfaces were particles can deposit. Findings here demonstrate that seagrasses enhance both the deposition to the seabed and the trapping on the surface of the leaves, reducing the suspended sediment from external sources . The amount of sediment remaining in suspension, deposited to the seabed, or captured on the leaves surface has been demonstrated to depend on the structural canopy parameters: the plant density of the canopy, patch size, effective plant height and the total amount of epiphytes on the leaves; and on the hydrodynamic conditions in terms of the local U_w and TKE.

Chapter 3 demonstrated that denser canopies reduce the suspended sediment within the canopy, which agrees with Short et al. (1984) who found a reduction in turbidity for vegetated beds, which might be a positive feedback for the plant productivity. The suspended sediment is captured on the seabed and trapped on the leaves surface. The study performed in Chapter 3 showed that the plant density has an impact on the amount of coarse sediment particles (between 6 to 122 μm) trapped on the leaf surface of each plant. While, fine sediment particles captured by each plant do not show any changes with the plant density, for coarse sediment particles, the lower the plant density the

greater the amount of coarse sediment particles trapped on the leaves. These results could be explained by the fact that in sparse canopies there is a reduction in the interaction between leaves, whereas in dense canopies the contact between leaves can wash off the sediment deposited on the neighbouring plants by the leaves friction (Gacia et al., 1999; Hendriks et al., 2008), resulting in cleaner leaves. However, the effect of the overall canopy showed that the trapping of both fine and coarse sediment particles on the leaves increases with the plant density. An increase in the plant density implies an increase in the available surface for the sediment, being trapped. Thus, this study demonstrated that while denser canopies have fewer particles per leaf, the higher density of the canopies balances this result, producing the greater overall particle trapping on the leaves. These results provide a quantification of what other authors have pointed out, that a significant portion of the suspended particles transported inside the seagrass meadows collides with the leaves (Ackerman, 2002; Hendriks et al., 2008), increasing the probability of collision in denser canopies. Thus, sparse canopies will be more vulnerable as the sediment layer in each plant will be thicker and may produce negative effects on the activity and efficiency of photosynthesis and on the night-time oxygen exchange. Also, the suspended sediment within the spare canopies will be greater, thus the level of turbidity will be higher, reducing the light availability (Lopez-y-Royo et al., 2011). Moreover, the sediment deposition on the seabed of spare canopies will be lower, and in consequence the storage and preservation of carbon in the seabed.

The results of Chapter 5 demonstrated the importance of both the patch size and the hydrodynamics on the sediment distribution. Here, a decrease in the concentration of suspended sediment by increasing the patch length was observed for all the hydrodynamic conditions tested. In consequence, the water quality within the patch improves as the patch length increases.

However, for the sediment deposited to seabed and trapped by the leaves surface, a threshold that determines the capacity of the canopy in trapping sediment was obtained. This threshold indicates the transition in the capacity of the canopy in increasing both the sediment deposited to the seabed and trapped on the leaves. For $(A_w/S)\,(L_p/h_v) > 8$ (where L_p is the patch length and h_v is the plant height), the sediment trapped by the leaves and deposited to the seabed increase. While, for $(A_w/S)\,(L_p/h_v) < 8$, both the sediment deposited to the seabed and trapped on the leaves remains constant, indicating that the meadow does not produce any effect on either the sedimentation or the leaf trapping. As shown in Chapter 6, when $A_w/S > 0.35$ the system dissipates the mean wave energy by producing TKE, which also corresponds to $(A_w/S)\,(L_p/h_v) > 8$. Under such conditions, seagrass patches have the role of both increasing the sediment captured by plant leaves and the sedimentation to the bottom. Thus, under these conditions, the canopy protects the bed from the oscillatory flow, and the larger the patch (i.e., L_p/h_v), the greater its effect on the bed will be. This threshold aligns with Zhu et al. (2021), who found higher sediment trapping on denser *P. oceanica* meadow due to the reduction of the mean energy of the flow. Therefore, the threshold for when seagrass patch preserves canopy characteristics depends on the hydrodynamics (through A_w), the plant density (through S) and the effective plant height. Small patches produce lower deposition rates on the seabed and on their leaves, thus presenting higher concentrations of suspended sediment, increasing the water turbidity and being more vulnerable in low light conditions. This may agree with the high rates of *Z. marina* mortality for small and sparse patches observed by Olesen and Sand-Jensen (1994). This study proved that spare patches required larger dimensions in order to accomplish the ecological services compared to dense seagrass patches.

Despite all the structural parameters of the canopy, seagrass leaves are naturally covered by epiphytes (Trautman and Borowitzka, 1999), providing an additional functionality to the system. Epiphytes increase the available surface of leaves where sediment can be trapped may vary. In consequence the amount of sediment captured in the plant surface will be modified. The results in Chapter 7 demonstrated that the sediment distribution also depends on the total epiphytic area of the meadow and the effective plant height. Canopies with greater epiphytic areas and taller plants reduce the suspended sediment by increasing the sediment trapping by plant leaves. These meadows capture part of the sediment that would be deposited to the seabed or remain in suspension in the water column. Thus, larger epiphytic areas increase the capture of sediment by plant leaves, reducing the sediment reaching the bottom. However, the sediment settling at the seabed increased with the effective plant height, indicating that taller plant leaves provide a greater surface area for particle capture (Borum, 1987; Ruesink, 2016). However, the accumulation of sediment on plant leaves might produce a negative feedback on seagrasses. That is, sediment is expected to reduce the capacity of their gas exchange (Pujol et al., 2019) and their ability to meet light requirements (Brodersen and Kühl, 2022) . In addition, this capacity might also be reduced by the presence of epiphytes leading to a build-up on the diffusive boundary layer which may impeded oxygen transfer between the seagrass leaf and the surrounding water (Noisette et al., 2020). However, this negative effect of epiphytes might be counteracted in dense canopies, which capture less sediment per plant leaf, as shown in Chapter 2. Moreover, this is not the only effect of epiphytes. The amount of epiphytes on the seagrass leaves may also impact on the flexural capacity of plants, resulting in more rigid or more flexible structures which can modify plant behaviour under different hydrodynamic conditions. As determined in Chapter 6, rigid plants can

produce more TKE than flexible plants, which subsequently reduces the thickness of the diffuse boundary layer through increased flow velocity (Pujol et al., 2019) and potentially alters nutrient uptake (Cornelisen and Thomas, 2004).

Therefore, this PhD thesis demonstrates that the sediment distribution depends on the morphometric parameters of the canopy (plant density, plant height, plant stiffness, patch length and the presence of epiphytes and its area) and on the local hydrodynamic parameters (U_w and TKE). This PhD also sets the conditions for understanding the fate sediment from external sediment sources impacting on coastal seagrass canopies. The two main objectives (defined in Chapter 1) of the PhD thesis have been demonstrated though a set of specific objectives detailed in each of the 7 parameters. Thresholds of the main parameters are presented and the ecological implications of the findings are presented and discussed in terms of both the behavior of the seagrass and the water quality.

8.3 Future implications

This PhD thesis studied the effect of the morphometric parameters of a seagrass meadow on both hydrodynamics and sediment distribution. However, the accumulation of sediment on the leaves may produce negative feedbacks to the meadow, and on the impact on the seagrass growth, as well higher amount of sediment captured on the seagrass leaves or on the epiphyte surface will decrease the gas exchange and the light availability, impacting on the growth or even on the survival of seagrasses. Also, higher amounts of sediment trapped on the seagrass leaves may modify the bending and stiffness of the plants, which will modify the local hydrodynamics, such as the

production of TKE. Also, higher sediment deposition rates to the seabed may compromise the survival of the meadow by the burial of plants. Therefore, there is a need to establish thresholds for the survival and/or guarantee healthy conditions for the seagrass meadow.

This PhD brought knowledge on the effect of several seagrass morphometric parameters (plant density, patch length, plant height, plant stiffness and the amount of epiphytes) on both the hydrodynamics and the sediment distribution through a non-dimensional model based on scaling parameters. The characteristic parameters able to describe the model were not the same than those used to describe the sediment capture, sedimentation and suspension. Therefore, future work needs to be conducted to establish a general model that contemplates all the structural parameters tested and the hydrodynamic parameters (U_w and TKE) to determine the sediment distribution in seagrass canopies for better coastal system management. In addition, based on the results obtained Chapter 7, the morphometry is modified by the presence of epiphytes, introducing a new parameter to be considered in the future model.

In addition, local hydrodynamic conditions represent a potential risk to the motile benthic fauna in coastal areas as they can dislodge them and restrict their movements, affecting their horizontal distribution within the environment. Seagrass meadows are important ecosystems that protect many organisms from predators and adverse hydrodynamic conditions. Therefore, the morphometric parameters of the canopy may influence on the dislodgement and survival of these species. as Also, the structural parameters of the seagrass can determine the hydrodynamic conditions produced by the canopy itself, such as the production of the TKE and the attenuation of the mean wave energy. Thus, future studies on the effect of the structural parameters on the motile benthic fauna dislodgement could be performed. In

order to address this lack of knowledge, a study about the effect of both patch length and flow velocity on the dislodgment of the shrimp *Palaemon adspersus*, an epifaunal species that thrives in *Zostera marina* seagrass, have been carried out in a laboratory flume and is currently under review on the journal *Limnology and Oceanography*.

Moreover, local hydrodynamics can be modified along the year by weather conditions and also for the local climate of the area. For instance, the summer season is characterized by low precipitation and low wind events, producing a decrease in the energy of the currents and waves. Thus, several macroalgal species may be trapped in the seagrass canopies during this season, resulting in a possible decrease in the oxygen uptake by seagrass plants. Therefore, the influence of the morphometric parameters on the macroalgal trapping is crucial to the survival of the seagrass canopies. A study to understand the effect of gap size and fragmentation level on the macroalgal trapping by seagrass meadows is currently being performed in order to establish management strategies to prevent the seagrass burial by macroalgae.

CHAPTER 9

Conclusions

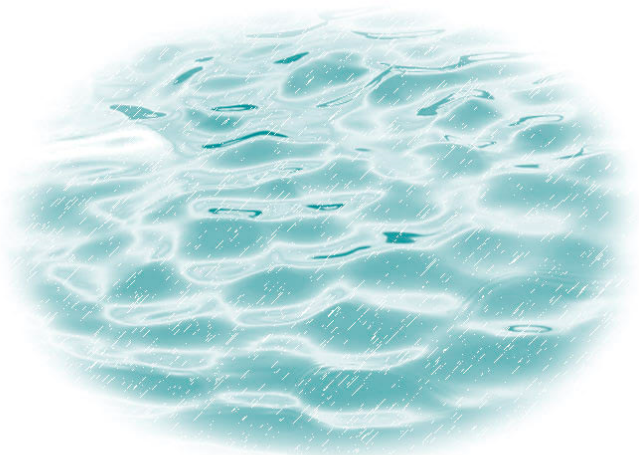

Cover design: Carles Arbat

This PhD presents the interaction between seagrass meadows and sediment particles. Different structures of the seagrass meadows were considered and analysed to determine their impact on the capacity of sediment capture by seagrass canopies. The structural parameters considered were:. The behaviour of the canopy was studied under oscillatory flow conditions through the analysis of the wave velocity and the turbulent kinetic energy.

9.1 Chapter 2

- In coastal areas exposed to currents and waves, the impact of the wave on the meadow fragmentation is two-fold: one on the local scale of the gap (gap-scale) and the other on the scale of the meadow (meadow-scale).
- At gap-scales, the gap size negatively influences the canopy density of the nearby vegetation. The larger the gap size the lower the shoot density of the nearby vegetation.
- At the meadow-scale, the overall degree of fragmentation of the meadow is a crucial parameter for the vulnerability of the seagrass meadows. Higher fragmented meadows present lower shoot density in the vegetation surrounding the gaps than less fragmented meadows, but with the same sized gaps.
- The fragmentation of a seagrass meadow may compromise the ecological services it provides, such as the sheltering of the seabed, negatively impacting on possible seagrass recolonization and therefore threatening any potential future restoration intervention.

9.2 Chapter 3

- Seagrasses decreases the amount of suspended sediment from external sources compared to unvegetated beds through two processes: the capture of sediment particles by plant leaves, and the enhancement of particle sedimentation onto the seabed.
- The plant leaves captured suspended particles settling through the water column. The denser the canopy the lower the percentage of particles trapped by the blades individually, but the greater the percentage trapped by the whole canopy.
- An increase in canopy cover increases sedimentation and particle capture by the leaves of the plants and, therefore, decreasing the suspended sediment remaining in the water column inside the canopy and improving the water clarity in these canopies.
- The concentration of fine particles trapped by individual leaf blades does not vary neither with the canopy cover nor with the TKE. In contrast, the concentration of coarse particles trapped by individual blades decreased as the canopy cover increased.
- The overall trapping of particles by seagrasses, either through settling on the bed or being trapped by their leaves, produces a decrease in the suspended sediment concentration, enhancing the water quality and resulting in positive feedback for the seagrass itself.

9.3 Chapter 4

- Under low wave velocities, plants do not interact with waves and dissipate the near-bed generated turbulence.

- For moderate wave velocities, plants interact with waves through the production of TKE.
- High canopy densities are expected to produce greater TKE than low canopy densities.
- The production of TKE holds for small patches under moderate wave velocities or, conversely, for low wave velocities acting on large canopy areas. These results indicate a threshold in the patch length (the minimum patch) that is capable of producing TKE. In such cases, vegetated patches will provide the functional dynamics to optimize the ecosystem services required.
- The resilience and resistance of seagrass canopies undergoing patchiness might be compromised when vegetated patches do not interact with the flow, since their length scale is lower than the required minimum patch scale that provide patch/flow interaction.

9.4 Chapter 5

- Patches of vegetation decreased the amount of suspended sediment concentration, compared with continuous vegetation landscapes. The larger and denser the patch is, the lower the concentration levels of suspended sediment are.
- Seagrass patches reduce the suspended sediment concentration by trapping sediment particles on plant leaves and enhancing the sedimentation by the presence of vegetation.
- Seagrass patches are able to increase the settling of particles to the bottom and also to capture particles on their leaves when $(A_w/S)\,(L_p/h_v) > 8$. This, holds for both large or dense seagrass patches (i.e., large L_p

and low S) and provides the limit for when seagrass patches become vulnerable to external pressures.

- Seagrass patches in wave frequencies of 0.5 Hz present greater sediment deposition at the edges compared to the inner canopy region, resulting in spatial heterogeneous sediment deposition patterns. In contrast, sediment deposition rates in seagrass patches in wave frequency environments of 1.2 Hz present a spatial homogeneous distribution.

9.5 Chapter 6

- Flexible plants move with the flow in the upper part of the canopy layer but present a more rigid structure in the inner canopy layer. In contrast, the canopies of rigid plants produce a high drag on the flow all along their stem, producing turbulent kinetic energy along the whole of their plant stem.
- Rigid and flexible vegetation presents a similar stem-like behaviour in the inner part of the canopy for $\left[C_{D-Patch}\frac{nd^2}{2(1-\emptyset)}\right]^{\frac{2}{3}}U_w{}^2 > 2$ and $\left[C_{D-Patch}\frac{nd^2}{2(1-\emptyset)}\right]^{\frac{2}{3}}U_w{}^2 > 4$, respectively, whereas in the canopy top layer flexible plants move with the flow to cope with the hydrodynamics, presenting a blade-like behaviour. In contrast, neither rigid nor flexible plants for $\left[C_{D-Patch}\frac{nd^2}{2(1-\emptyset)}\right]^{\frac{2}{3}}U_w{}^2 < 2$ or $\left[C_{D-Patch}\frac{nd^2}{2(1-\emptyset)}\right]^{\frac{2}{3}}U_w{}^2 < 4$, respectively, produce turbulent kinetic energy.

- The behaviour of flexible plants might shift to being closer to that of rigid plants for high wave frequencies. In contrast, flexible plants produce a larger sway movement when they are under low oscillatory frequencies.

9.6 Chapter 7

- Sediment particles originating from an external source interacted with the canopy, either becoming trapped on the epiphytic surfaces of plant leaves, remaining suspended within the canopy, or settling to the bottom bed.
- The mass of sediment trapped by the epiphytic leaves accumulated within the canopy bed, and remaining in suspension were found to be a function of the effective plant height (h_v) and the total epiphytic area (A).
- Eelgrass canopies with higher epiphytic leaf areas and longer effective leaf lengths (h_v) are prone to increase the mass sediment captured by the epiphyted plants.
- Longer plant leaves are expected to provide a greater surface area for epiphyte attachment compared to shorter leaves.
- Canopies with higher epiphyted cover would promote an increase in the sediment capture by plants, thereby reducing the amount of sediment that reaches the seabed.
- For the epiphyte with the greatest surface area, the sediment mass trapped within the leaves can be 10 times greater than that captured by leaves without epiphytes.

9.7 General conclusions

This PhD thesis has fulfilled the two main objectives to understand how the morphometric parameters (plant density, patch length, plant stiffness, plant height and epiphyte colonization) influence the hydrodynamics and sediment distribution within seagrass meadows, and to establish morphometric thresholds for hydrodynamics and sediment capture for seagrass meadows to maintain ecosystem services.

In reference on the first aim, the effects of structural parameters on seagrass canopies have been determined separately, and also in combination in a non-dimensional model. The main conclusions for the first aim are:

- The meadow fragmentation has a two-fold impact: one on local scale of the gap (gap-scale) and the other on the scale of the meadow (meadow-scale). The gap size diminishes canopy density of the nearby vegetation. And higher fragmentation levels result in lower shoot density in the vegetation surrounding the gaps, increasing the vulnerability of the meadow.
- Canopies with higher plant densities, patch lengths, stiffer plants, larger plants and/or moderate local wave velocities enhance the production of turbulent kinetic energy.
- Externally sourced sediment particles interact with the canopy, becoming trapped on the epiphytic surfaces of plant leaves, remaining suspended within the canopy, or settling to the bottom bed.
- Canopies with higher plant densities, patch lengths, larger plants and/or higher amount of epiphytes reduce the suspended sediment by enhancing the balance between trapping on the leaves surface and the settling to the seabed.

In reference to the second aim, non-dimensional models have been established in order to determine hydrodynamics and sediment distribution thresholds. The main conclusions for the second aim are:

- Flexible plants, such as seagrasses do not produce turbulent kinetic energy, instead attenuate the turbulence produced by the interaction of the current with the seabed for $\left[C_{D-Patch}\frac{nd^2}{2(1-\emptyset)}\right]^{\frac{2}{3}}U_w{}^2 < 4$, whereas for $\left[C_{D-Patch}\frac{nd^2}{2(1-\emptyset)}\right]^{\frac{2}{3}}U_w{}^2 > 4$, produce turbulent kinetic energy.
- Seagrass canopies enhance the settling of particles to the bottom and the capture of particles on their leaves when $(A_w/S)\,(L_p/h_v) > 8$.

In summary, this PhD thesis has established thresholds on hydrodynamics and sediment capture to guarantee the ecosystem services provided by seagrass meadows. Seagrasses generate turbulent kinetic energy within the canopy and therefore attenuating the mean wave velocity of the flow, providing sheltering and refuge for all the fauna inhabiting in there. The seagrass morphometric parameters have been determined to guarantee a good quality of the ecosystem, such as provide the reduction of the suspended sediment, which will allow greater penetration of light into the canopies improving the water quality. Also, healthy canopies will enhance the sediment deposition to the seabed and the capture on the seagrass leaves, which provide a positive feedback for the canopy. The sum of these factors will provide higher quality of the water and greater light penetration by the reduction of the suspended sediment. Also, greater nutrient deposition to the seabed by the increase in the sediment deposition. Finally, denser seagrass meadows, larger patches or higher epiphyted canopies may capture higher amount of sediment on the

leaves but the capture by each plant will be reduced. These processes together with the production of the TKE will enhance the gas and light exchange, which will generate a positive feedback for the meadow development.

CHAPTER 10

Bibliography

Cover design: Carles Arbat

Abadie, A., Borges, A. V, Champenois, W., Gobert, S., 2017. Natural patches in Posidonia oceanica meadows: the seasonal biogeochemical pore water characteristics of two edge types. Mar Biol 164, 166. https://doi.org/10.1007/s00227-017-3199-5

Abadie, A., Gobert, S., Bonacorsi, M., Lejeune, P., Pergent, G., Pergent-Martini, C., 2015. Marine space ecology and seagrasses. Does patch type matter in Posidonia oceanica seascapes? Ecol Indic 57, 435–446. https://doi.org/10.1016/j.ecolind.2015.05.020

Abadie, A., Lejeune, P., Pergent, G., Gobert, S., 2016. From mechanical to chemical impact of anchoring in seagrasses: The premises of anthropogenic patch generation in Posidonia oceanica meadows. Mar Pollut Bull 109, 61–71. https://doi.org/10.1016/j.marpolbul.2016.06.022

Abadie, A., Pace, M., Gobert, S., Borg, J.A., 2018. Seascape ecology in Posidonia oceanica seagrass meadows: Linking structure and ecological processes for management. Ecol Indic 87, 1–13. https://doi.org/10.1016/j.ecolind.2017.12.029

Ackerman, J.D., 2002. Diffusivity in a marine macrophyte canopy: implications for submarine pollination and dispersal. Am J Bot 89, 1119–1127. https://doi.org/10.3732/ajb.89.7.1119

Agawin, N.S.R., Duarte, C.M., 2002. Evidence of direct particle trapping by a tropical seagrass meadow. Estuaries 25, 1205–1209. https://doi.org/10.1007/BF02692217

Armitage, A.R., Fourqurean, J.W., 2016. Carbon storage in seagrass soils: long-term nutrient history exceeds the effects of near-term nutrient

enrichment. Biogeosciences 13, 313–321. https://doi.org/10.5194/bg-13-313-2016

Asplund, M.E., Dahl, M., Ismail, R.O., Arias-Ortiz, A., Deyanova, D., Franco, J.N., Hammar, L., Hoamby, A.I., Linderholm, H.W., Lyimo, L.D., Perry, D., Rasmusson, L.M., Ridgway, S.N., Salgado Gispert, G., D'Agata, S., Glass, L., Mahafina, J.A., Ramahery, V., Masque, P., Björk, M., Gullström, M., 2021. Dynamics and fate of blue carbon in a mangrove–seagrass seascape: influence of landscape configuration and land-use change. Landsc Ecol 36, 1489–1509. https://doi.org/10.1007/s10980-021-01216-8

Bacci, T., Rende, F.S., Scardi, M., 2017. Shoot micro-distribution patterns in the Mediterranean seagrass Posidonia oceanica. Mar Biol 164, 85. https://doi.org/10.1007/s00227-017-3121-1

Baggett, L.P., Heck, K.L.J., Frankovich, T.A., Armitage, A.R., Fourqurean, J.W., 2010. Nutrient enrichment, grazer identity, and their effects on epiphytic algal assemblages: field experiments in subtropical turtlegrass Thalassia testudinum meadows. Mar Ecol Prog Ser 406, 33–45. https://doi.org/10.3354/meps08533

Balata, D., Bertocci, I., Piazzi, L., Nesti, U., 2008. Comparison between epiphyte assemblages of leaves and rhizomes of the seagrass Posidonia oceanica subjected to different levels of anthropogenic eutrophication. Estuar Coast Shelf Sci 79, 533–540. https://doi.org/10.1016/j.ecss.2008.05.009

Barcelona, A., Colomer, J., Serra, T., 2023a. Stem stiffness functionality in a submerged canopy patch under oscillatory flow. Sci Rep 13, 1904. https://doi.org/10.1038/s41598-023-28077-2

Barcelona, A., Colomer, J., Serra, T., 2023b. Spatial sedimentation and plant captured sediment within seagrass patches. Mar Environ Res 188, 105997. https://doi.org/10.1016/j.marenvres.2023.105997

Barcelona, A., Colomer, J., Soler, M., Gracias, N., Serra, T., 2021a. Meadow fragmentation influences Posidonia oceanica density at the edge of nearby gaps. Estuar Coast Shelf Sci 249, 107106. https://doi.org/10.1016/j.ecss.2020.107106

Barcelona, A., Oldham, C., Colomer, J., Garcia-Orellana, J., Serra, T., 2021b. Particle capture by seagrass canopies under an oscillatory flow. Coastal Engineering 169, 103972. https://doi.org/10.1016/j.coastaleng.2021.103972

Barcelona, A., Oldham, C., Colomer, J., Serra, T., 2021c. Functional dynamics of vegetated model patches: The minimum patch size effect for canopy restoration. Science of The Total Environment 795, 148854. https://doi.org/10.1016/j.scitotenv.2021.148854

Barsanti, M., Delbono, I., Ferretti, O., Peirano, A., Bianchi, C.N., Morri, C., 2007. Measuring change of Mediterranean coastal biodiversity: diachronic mapping of the meadow of the seagrass Cymodocea nodosa (Ucria) Ascherson in the Gulf of Tigullio (Ligurian Sea, NW Mediterranean). Hydrobiologia 580, 35–41. https://doi.org/10.1007/s10750-006-0467-7

Bell, S.S., Brooks, R.A., Robbins, B.D., Fonseca, M.S., Hall, M.O., 2001. Faunal response to fragmentation in seagrass habitats: implications for seagrass conservation. Biol Conserv 100, 115–123. https://doi.org/10.1016/S0006-3207(00)00212-3

Ben Brahim, M., Hamza, A., Hannachi, I., Rebai, A., Jarboui, O., Bouain, A., Aleya, L., 2010. Variability in the structure of epiphytic assemblages of Posidonia oceanica in relation to human interferences in the Gulf of Gabes, Tunisia. Mar Environ Res 70, 411–421. https://doi.org/10.1016/j.marenvres.2010.08.005

Ben Brahim, M., Mabrouk, L., Hamza, A., Jribi, I., 2020. Comparison of spatial scale variability of shoot density and epiphytic leaf assemblages of Halophila stipulacea and Cymodocea nodosa on the Eastern Coast of Tunisia. Plant Biosystems - An International Journal Dealing with all Aspects of Plant Biology 154, 413–426. https://doi.org/10.1080/11263504.2019.1674399

Borfecchia, F., Micheli, C., Cecco, L. De, Sannino, G., Struglia, M.V., Sarra, A.G. Di, Gomez, C., Mattiazzo, G., 2021. Satellite Multi/Hyper Spectral HR Sensors for Mapping the Posidonia oceanica in South Mediterranean Islands. Sustainability 13, 13715. https://doi.org/10.3390/su132413715

Borg, J.A., Attrill, M.J., Rowden, A.A., Schembri, P.J., Jones, M.B., 2005. Architectural characteristics of two bed types of the seagrass Posidonia oceanica over different spatial scales. Estuar Coast Shelf Sci 62, 667–678. https://doi.org/10.1016/j.ecss.2004.10.003

Borowitzka, M.A., Lavery, P.S., van Keulen, M., 2005. Epiphytes of Seagrasses, in: Seagrass:Biology, Ecologyl and Conservation. Springer Netherlands, Dordrecht, pp. 441–461. https://doi.org/10.1007/978-1-4020-2983-7_19

Borum, J., 1987. Dynamics of epiphyton on eelgrass (Zostera marina L.) leaves: Relative roles of algal growth, herbivory, and substratum

turnover. Limnol Oceanogr 32, 986–992. https://doi.org/10.4319/lo.1987.32.4.0986

Bos, A.R., Bouma, T.J., de Kort, G.L.J., van Katwijk, M.M., 2007. Ecosystem engineering by annual intertidal seagrass beds: Sediment accretion and modification. Estuar Coast Shelf Sci 74, 344–348. https://doi.org/10.1016/j.ecss.2007.04.006

Boström, C., Baden, S., Bockelmann, A., Dromph, K., Fredriksen, S., Gustafsson, C., Krause-Jensen, D., Möller, T., Nielsen, S.L., Olesen, B., Olsen, J., Pihl, L., Rinde, E., 2014. Distribution, structure and function of Nordic eelgrass *(Zostera marina)* ecosystems: implications for coastal management and conservation. Aquat Conserv 24, 410–434. https://doi.org/10.1002/aqc.2424

Boudouresque, C.F., Bernard, G., Pergent, G., Shili, A., Verlaque, M., 2009. Regression of Mediterranean seagrasses caused by natural processes and anthropogenic disturbances and stress: a critical review. Botanica Marina 52, 395–418. https://doi.org/10.1515/BOT.2009.057

Bouma, T.J., De Vries, M.B., Low, E., Peralta, G., Tánczos, I.C., van de Koppel, J., Herman, P.M.J., 2005. TRADE-OFFS RELATED TO ECOSYSTEM ENGINEERING: A CASE STUDY ON STIFFNESS OF EMERGING MACROPHYTES. Ecology 86, 2187–2199. https://doi.org/10.1890/04-1588

Bouma, T.J., Friedrichs, M., Klaassen, P., van Wesenbeeck, B.K., Brun, F.G., Temmerman, S., van Katwijk, M.M., Graf, G., Herman, P.M.J., 2009. Effects of shoot stiffness, shoot size and current velocity on

scouring sediment from around seedlings and propagules. Mar Ecol Prog Ser 388, 293–297. https://doi.org/10.3354/meps08130

Bouma, T.J., van Duren, L.A., Temmerman, S., Claverie, T., Blanco-Garcia, A., Ysebaert, T., Herman, P.M.J., 2007. Spatial flow and sedimentation patterns within patches of epibenthic structures: Combining field, flume and modelling experiments. Cont Shelf Res 27, 1020–1045. https://doi.org/10.1016/j.csr.2005.12.019

Bradley, K., Houser, C., 2009. Relative velocity of seagrass blades: Implications for wave attenuation in low-energy environments. J Geophys Res 114, F01004. https://doi.org/10.1029/2007JF000951

Brodersen, K.E., Hammer, K.J., Schrameyer, V., Floytrup, A., Rasheed, M.A., Ralph, P.J., Kühl, M., Pedersen, O., 2017. Sediment Resuspension and Deposition on Seagrass Leaves Impedes Internal Plant Aeration and Promotes Phytotoxic H2S Intrusion. Front Plant Sci 8. https://doi.org/10.3389/fpls.2017.00657

Brodersen, K.E., Kühl, M., 2022. Effects of Epiphytes on the Seagrass Phyllosphere. Front Mar Sci 9. https://doi.org/10.3389/fmars.2022.821614

Brodersen, M.M., Pantazi, M., Kokkali, A., Panayotidis, P., Gerakaris, V., Maina, I., Kavadas, S., Kaberi, H., Vassilopoulou, V., 2018. Cumulative impacts from multiple human activities on seagrass meadows in eastern Mediterranean waters: the case of Saronikos Gulf (Aegean Sea, Greece). Environmental Science and Pollution Research 25, 26809–26822. https://doi.org/10.1007/s11356-017-0848-7

Brouwer, S., Humphries, P., Holland, A., McCasker, N., 2023. Effect of suspended sediment concentration on the clearance and biodeposition rates of an Australian freshwater mussel (Hyriidae: Alathyria jacksoni). Freshw Biol. https://doi.org/10.1111/fwb.14137

Cabaço, S., Santos, R., Duarte, C.M., 2008. The impact of sediment burial and erosion on seagrasses: A review. Estuar Coast Shelf Sci 79, 354–366. https://doi.org/10.1016/j.ecss.2008.04.021

Cacabelos, E., Gestoso, I., Ramalhosa, P., Canning-Clode, J., 2022. Role of non-indigenous species in structuring benthic communities after fragmentation events: an experimental approach. Biol Invasions 24, 2181–2199. https://doi.org/10.1007/s10530-022-02768-9

Cambridge, M., How, J., Lavery, P., Vanderklift, M., 2007. Retrospective analysis of epiphyte assemblages in relation to seagrass loss in a eutrophic coastal embayment. Mar Ecol Prog Ser 346, 97–107. https://doi.org/10.3354/meps06993

Carr, J., D'Odorico, P., McGlathery, K., Wiberg, P., 2010. Stability and bistability of seagrass ecosystems in shallow coastal lagoons: Role of feedbacks with sediment resuspension and light attenuation. J Geophys Res 115, G03011. https://doi.org/10.1029/2009JG001103

Casal-Porras, I., de los Santos, C.B., Martins, M., Santos, R., Pérez-Lloréns, J.L., Brun, F.G., 2022. Sedimentary organic carbon and nitrogen stocks of intertidal seagrass meadows in a dynamic and impacted wetland: Effects of coastal infrastructure constructions and meadow establishment time. J Environ Manage 322, 115841. https://doi.org/10.1016/j.jenvman.2022.115841

Chatting, M., Al-Maslamani, I., Walton, M., Skov, M.W., Kennedy, H., Husrevoglu, Y.S., Vay, L. Le, 2022. Future Mangrove Carbon Storage Under Climate Change and Deforestation. Front Mar Sci 9. https://doi.org/10.3389/fmars.2022.781876

Chen, M., Lou, S., Liu, S., Ma, G., Liu, H., Zhong, G., Zhang, H., 2020. Velocity and turbulence affected by submerged rigid vegetation under waves, currents and combined wave–current flows. Coastal Engineering 159, 103727. https://doi.org/10.1016/j.coastaleng.2020.103727

Chen, Z., Jiang, C., Nepf, H., 2013. Flow adjustment at the leading edge of a submerged aquatic canopy. Water Resour Res 49, 5537–5551. https://doi.org/10.1002/wrcr.20403

Chu, V.W., Smith, L.C., Rennermalm, A.K., Forster, R.R., Box, J.E., Reeh, N., 2009. Sediment plume response to surface melting and supraglacial lake drainages on the Greenland ice sheet. Journal of Glaciology 55, 1072–1082. https://doi.org/10.3189/002214309790794904

Colomer, J., Boubnov, B.M., Fernando, H.J.S., 1999. Turbulent convection from isolated sources. Dynamics of Atmospheres and Oceans 30, 125–148. https://doi.org/10.1016/S0377-0265(99)00023-8

Colomer, J., Ross, J.A., Casamitjana, X., 1998. Sediment entrainment in karst basins. Aquat Sci 60, 338. https://doi.org/10.1007/s000270050045

Colomer, J., Serra, T., 2021. The World of Edges in Submerged Vegetated Marine Canopies: From Patch to Canopy Scale. Water (Basel) 13, 2430. https://doi.org/10.3390/w13172430

Colomer, J., Soler, M., Serra, T., Casamitjana, X., Oldham, C., 2017. Impact of anthropogenically created canopy gaps on wave attenuation in a Posidonia oceanica seagrass meadow. Mar Ecol Prog Ser 569, 103–116. https://doi.org/10.3354/meps12090

Cornacchia, L., Licci, S., Nepf, H., Folkard, A., Wal, D., Koppel, J., Puijalon, S., Bouma, T.J., 2019. Turbulence-mediated facilitation of resource uptake in patchy stream macrophytes. Limnol Oceanogr 64, 714–727. https://doi.org/10.1002/lno.11070

Cornelisen, C.D., Thomas, F.I.M., 2004. Ammonium and nitrate uptake by leaves of the seagrass Thalassia testudinum: impact of hydrodynamic regime and epiphyte cover on uptake rates. Journal of Marine Systems 49, 177–194. https://doi.org/10.1016/j.jmarsys.2003.05.008

Cox, J.R., Paauw, M., Nienhuis, J.H., Dunn, F.E., van der Deijl, E., Esposito, C., Goichot, M., Leuven, J.R.F.W., van Maren, D.S., Middelkoop, H., Naffaa, S., Rahman, M., Schwarz, C., Sieben, E., Triyanti, A., Yuill, B., 2022. A global synthesis of the effectiveness of sedimentation-enhancing strategies for river deltas and estuaries. Glob Planet Change 214, 103796. https://doi.org/10.1016/j.gloplacha.2022.103796

de los Santos, C.B., Krång, A.-S., Infantes, E., 2021. Microplastic retention by marine vegetated canopies: Simulations with seagrass

meadows in a hydraulic flume. Environmental Pollution 269, 116050. https://doi.org/10.1016/j.envpol.2020.116050

Devi, T.B., Kumar, B., 2016. Experimentation on submerged flow over flexible vegetation patches with downward seepage. Ecol Eng 91, 158–168. https://doi.org/10.1016/j.ecoleng.2016.02.045

Di Maida, G., Tomasello, A., Sciandra, M., Pirrotta, M., Milazzo, M., Calvo, S., 2013. Effect of different substrata on rhizome growth, leaf biometry and shoot density of Posidonia oceanica. Mar Environ Res 87–88, 96–102. https://doi.org/10.1016/j.marenvres.2013.04.001

Duarte, C.M., 2002. The future of seagrass meadows. Environ Conserv 29, 192–206. https://doi.org/10.1017/S0376892902000127

Duarte, C.M., 1991. Seagrass depth limits. Aquat Bot 40, 363–377. https://doi.org/10.1016/0304-3770(91)90081-F

Duarte, C.M., Borja, A., Carstensen, J., Elliott, M., Krause-Jensen, D., Marbà, N., 2015. Paradigms in the Recovery of Estuarine and Coastal Ecosystems. Estuaries and Coasts 38, 1202–1212. https://doi.org/10.1007/s12237-013-9750-9

Duarte, C.M., Losada, I.J., Hendriks, I.E., Mazarrasa, I., Marbà, N., 2013. The role of coastal plant communities for climate change mitigation and adaptation. Nat Clim Chang 3, 961–968. https://doi.org/10.1038/nclimate1970

Duarte, C.M., Middelburg, J.J., Caraco, N., 2005. Major role of marine vegetation on the oceanic carbon cycle. Biogeosciences 2, 1–8. https://doi.org/10.5194/bg-2-1-2005

Dunn, F.E., Darby, S.E., Nicholls, R.J., Cohen, S., Zarfl, C., Fekete, B.M., 2019. Projections of declining fluvial sediment delivery to major deltas worldwide in response to climate change and anthropogenic stress. Environmental Research Letters 14, 84034. https://doi.org/10.1088/1748-9326/ab304e

Eckardt, N.A., Ainsworth, E.A., Bahuguna, R.N., Broadley, M.R., Busch, W., Carpita, N.C., Castrillo, G., Chory, J., DeHaan, L.R., Duarte, C.M., Henry, A., Jagadish, S.V.K., Langdale, J.A., Leakey, A.D.B., Liao, J.C., Lu, K.-J., McCann, M.C., McKay, J.K., Odeny, D.A., Jorge de Oliveira, E., Platten, J.D., Rabbi, I., Rim, E.Y., Ronald, P.C., Salt, D.E., Shigenaga, A.M., Wang, E., Wolfe, M., Zhang, X., 2023. Climate change challenges, plant science solutions. Plant Cell 35, 24–66. https://doi.org/10.1093/plcell/koac303

El Allaoui, N., Serra, T., Colomer, J., Soler, M., Casamitjana, X., Oldham, C., 2016. Interactions between Fragmented Seagrass Canopies and the Local Hydrodynamics. PLoS One 11, e0156264. https://doi.org/10.1371/journal.pone.0156264

El Allaoui, N., Serra, T., Soler, M., Colomer, J., Pujol, D., Oldham, C., 2015. Modified hydrodynamics in canopies with longitudinal gaps exposed to oscillatory flows. J Hydrol (Amst) 531, 840–849. https://doi.org/10.1016/j.jhydrol.2015.10.041

Elibol, A., Garcia, R., Gracias, N., 2011. A new global alignment approach for underwater optical mapping. Ocean Engineering 38, 1207–1219. https://doi.org/10.1016/j.oceaneng.2011.05.013

Espel, D., Diepens, N.J., Boutron, O., Buffan-Dubau, E., Chérain, Y., Coulet, E., Grillas, P., Probst, A., Silvestre, J., Elger, A., 2019.

Dynamics of the seagrass Zostera noltei in a shallow Mediterranean lagoon exposed to chemical contamination and other stressors. Estuar Coast Shelf Sci 222, 1–12. https://doi.org/10.1016/j.ecss.2019.03.019

Ettinger, C.L., Voerman, S.E., Lang, J.M., Stachowicz, J.J., Eisen, J.A., 2017. Microbial communities in sediment from Zostera marina patches, but not the Z. marina leaf or root microbiomes, vary in relation to distance from patch edge. PeerJ 5, e3246. https://doi.org/10.7717/peerj.3246

Evans, S.M., Griffin, K.J., Blick, R.A.J., Poore, A.G.B., Vergés, A., 2018. Seagrass on the brink: Decline of threatened seagrass Posidonia australis continues following protection. PLoS One 13, e0190370. https://doi.org/10.1371/journal.pone.0190370

Folkard, A.M., 2019. Biophysical Interactions in Fragmented Marine Canopies: Fundamental Processes, Consequences, and Upscaling. Front Mar Sci 6. https://doi.org/10.3389/fmars.2019.00279

Folkard, A.M., 2005. Hydrodynamics of model Posidonia oceanica patches in shallow water. Limnol Oceanogr 50, 1592–1600. https://doi.org/10.4319/lo.2005.50.5.1592

Fonseca, M., Bell, S., 1998. Influence of physical setting on seagrass landscapes near Beaufort, North Carolina, USA. Mar Ecol Prog Ser 171, 109–121. https://doi.org/10.3354/meps171109

Fonseca, M.S., Koehl, M.A.R., 2006. Flow in seagrass canopies: The influence of patch width. Estuar Coast Shelf Sci 67, 1–9. https://doi.org/10.1016/j.ecss.2005.09.018

Fonseca, M.S., Zieman, J.C., Thayer, G.W., Fisher, J.S., 1983. The role of current velocity in structuring eelgrass (Zostera marina L.) meadows. Estuar Coast Shelf Sci 17, 367–380. https://doi.org/10.1016/0272-7714(83)90123-3

Fourqurean, J.W., Duarte, C.M., Kennedy, H., Marbà, N., Holmer, M., Mateo, M.A., Apostolaki, E.T., Kendrick, G.A., Krause-Jensen, D., McGlathery, K.J., Serrano, O., 2012. Seagrass ecosystems as a globally significant carbon stock. Nat Geosci 5, 505–509. https://doi.org/10.1038/ngeo1477

Francalanci, S., Paris, E., Solari, L., 2021. On the prediction of settling velocity for plastic particles of different shapes. Environmental Pollution 290, 118068. https://doi.org/10.1016/j.envpol.2021.118068

Fraser, M.W., Short, J., Kendrick, G., McLean, D., Keesing, J., Byrne, M., Caley, M.J., Clarke, D., Davis, A.R., Erftemeijer, P.L.A., Field, S., Gustin-Craig, S., Huisman, J., Keough, M., Lavery, P.S., Masini, R., McMahon, K., Mengersen, K., Rasheed, M., Statton, J., Stoddart, J., Wu, P., 2017. Effects of dredging on critical ecological processes for marine invertebrates, seagrasses and macroalgae, and the potential for management with environmental windows using Western Australia as a case study. Ecol Indic 78, 229–242. https://doi.org/10.1016/j.ecolind.2017.03.026

Fried, M.J., Catania, G.A., Bartholomaus, T.C., Duncan, D., Davis, M., Stearns, L.A., Nash, J., Shroyer, E., Sutherland, D., 2015. Distributed subglacial discharge drives significant submarine melt at a Greenland tidewater glacier. Geophys Res Lett 42, 9328–9336. https://doi.org/10.1002/2015GL065806

Gacia, E., Duarte, C.M., 2001. Sediment Retention by a Mediterranean Posidonia oceanica Meadow: The Balance between Deposition and Resuspension. Estuar Coast Shelf Sci 52, 505–514. https://doi.org/10.1006/ecss.2000.0753

Gacia, E., Granata, T.C., Duarte, C.M., 1999. An approach to measurement of particle flux and sediment retention within seagrass (Posidonia oceanica) meadows. Aquat Bot 65, 255–268. https://doi.org/10.1016/S0304-3770(99)00044-3

Ganthy, F., Soissons, L., Sauriau, P.-G., Verney, R., Sottolichio, A., 2015. Effects of short flexible seagrass *Zostera noltei* on flow, erosion and deposition processes determined using flume experiments. Sedimentology 62, 997–1023. https://doi.org/10.1111/sed.12170

García-Redondo, V., Bárbara, I., Díaz-Tapia, P., 2019a. Zostera marina meadows in the northwestern Spain: distribution, characteristics and anthropogenic pressures. Biodivers Conserv 28, 1743–1757. https://doi.org/10.1007/s10531-019-01753-4

García-Redondo, V., Bárbara, I., Díaz-Tapia, P., 2019b. Biodiversity of epiphytic macroalgae (Chlorophyta, Ochrophyta and Rhodophyta) on leaves of Zostera marina in the northwestern Iberian Peninsula. Anales del Jardín Botánico de Madrid 76, 078. https://doi.org/10.3989/ajbm.2502

Gera, A., Pagès, J.F., Romero, J., Alcoverro, T., 2013. Combined effects of fragmentation and herbivory on *Posidonia oceanica* seagrass ecosystems. Journal of Ecology 101, 1053–1061. https://doi.org/10.1111/1365-2745.12109

Ghisalberti, M., 2002. Mixing layers and coherent structures in vegetated aquatic flows. J Geophys Res 107, 3011. https://doi.org/10.1029/2001JC000871

Gilby, B.L., Olds, A.D., Duncan, C.K., Ortodossi, N.L., Henderson, C.J., Schlacher, T.A., 2020. Identifying restoration hotspots that deliver multiple ecological benefits. Restor Ecol 28, 222–232. https://doi.org/10.1111/rec.13046

Gleason, A.C.R., Lirman, D., Williams, D., Gracias, N.R., Gintert, B.E., Madjidi, H., Reid, R.P., Boynton, G.C., Negahdaripour, S., Miller, M., Kramer, P., 2007. Documenting hurricane impacts on coral reefs using two-dimensional video-mosaic technology. Marine Ecology 28, 254–258. https://doi.org/10.1111/j.1439-0485.2006.00140.x

González-Ortiz, V., Egea, L.G., Jiménez-Ramos, R., Moreno-Marín, F., Pérez-Lloréns, J.L., Bouma, T., Brun, F., 2016. Submerged vegetation complexity modifies benthic infauna communities: the hidden role of the belowground system. Marine Ecology 37, 543–552. https://doi.org/10.1111/maec.12292

Goring, D.G., Nikora, V.I., 2002. Despiking Acoustic Doppler Velocimeter Data. Journal of Hydraulic Engineering 128, 117–126. https://doi.org/10.1061/(ASCE)0733-9429(2002)128:1(117)

Grabowski, R.C., Droppo, I.G., Wharton, G., 2011. Erodibility of cohesive sediment: The importance of sediment properties. Earth Sci Rev 105, 101–120. https://doi.org/10.1016/j.earscirev.2011.01.008

Granata, T.C., Serra, T., Colomer, J., Casamitjana, X., Duarte, C., Gacia, E., 2001. Flow and particle distributions in a nearshore seagrass

meadow before and after a storm. Mar Ecol Prog Ser 218, 95–106. https://doi.org/10.3354/meps218095

Grech, A., Chartrand-Miller, K., Erftemeijer, P., Fonseca, M., McKenzie, L., Rasheed, M., Taylor, H., Coles, R., 2012. A comparison of threats, vulnerabilities and management approaches in global seagrass bioregions. Environmental Research Letters 7, 24006. https://doi.org/10.1088/1748-9326/7/2/024006

Greiner, J.T., Wilkinson, G.M., McGlathery, K.J., Emery, K.A., 2016. Sources of sediment carbon sequestered in restored seagrass meadows. Mar Ecol Prog Ser 551, 95–105. https://doi.org/10.3354/meps11722

Gruber, R.K., Kemp, W.M., 2010. Feedback effects in a coastal canopy-forming submersed plant bed. Limnol Oceanogr 55, 2285–2298. https://doi.org/10.4319/lo.2010.55.6.2285

Guidetti, P., 2000. Leaf primary production in Posidonia oceanica: two reconstructive aging techniques give similar results. Aquat Bot 68, 337–343. https://doi.org/10.1016/S0304-3770(00)00129-7

Güreşen, A., Güreşen, S.O., Aktan, Y., 2020. Combined synthetic and biotic indices of Posidonia oceanica to qualify the status of coastal ecosystems in the North Aegean. Ecol Indic 113, 106149. https://doi.org/10.1016/j.ecolind.2020.106149

Hallet, B., Hunter, L., Bogen, J., 1996. Rates of erosion and sediment evacuation by glaciers: A review of field data and their implications. Glob Planet Change 12, 213–235. https://doi.org/10.1016/0921-8181(95)00021-6

Hansen, J., Reidenbach, M., 2012. Wave and tidally driven flows in eelgrass beds and their effect on sediment suspension. Mar Ecol Prog Ser 448, 271–287. https://doi.org/10.3354/meps09225

Hendriks, I.E., Bouma, T.J., Morris, E.P., Duarte, C.M., 2010. Effects of seagrasses and algae of the Caulerpa family on hydrodynamics and particle-trapping rates. Mar Biol 157, 473–481. https://doi.org/10.1007/s00227-009-1333-8

Hendriks, I., Sintes, T., Bouma, T., Duarte, C., 2008. Experimental assessment and modeling evaluation of the effects of the seagrass Posidonia oceanica on flow and particle trapping. Mar Ecol Prog Ser 356, 163–173. https://doi.org/10.3354/meps07316

Hovel, K.A., Duffy, J.E., Stachowicz, J.J., Reynolds, P., Boström, C., Boyer, K.E., Cimon, S., Cusson, M., Fodrie, F.J., Gagnon, K., Hereu, C.M., Hori, M., Jorgensen, P., Kruschel, C., Lee, K., Nakaoka, M., O'Connor, N.E., Rossi, F., Ruesink, J., Tomas, F., Ziegler, S., 2021. Joint effects of patch edges and habitat degradation on faunal predation risk in a widespread marine foundation species. Ecology 102. https://doi.org/10.1002/ecy.3316

Howe, A.J., Rodríguez, J.F., Saco, P.M., 2009. Surface evolution and carbon sequestration in disturbed and undisturbed wetland soils of the Hunter estuary, southeast Australia. Estuar Coast Shelf Sci 84, 75–83. https://doi.org/10.1016/j.ecss.2009.06.006

Howley, C., Devlin, M., Burford, M., 2018. Assessment of water quality from the Normanby River catchment to coastal flood plumes on the northern Great Barrier Reef, Australia. Mar Freshw Res 69, 859. https://doi.org/10.1071/MF17009

Hughes, A.R., Williams, S.L., Duarte, C.M., Heck, K.L., Waycott, M., 2009. Associations of concern: declining seagrasses and threatened dependent species. Front Ecol Environ 7, 242–246. https://doi.org/10.1890/080041

Iafrati, A., 2011. Energy dissipation mechanisms in wave breaking processes: Spilling and highly aerated plunging breaking events. J Geophys Res Oceans 116, 2011JC007038. https://doi.org/10.1029/2011JC007038

Infantes, E., Hoeks, S., Adams, M., van der Heide, T., van Katwijk, M., Bouma, T., 2022. Seagrass roots strongly reduce cliff erosion rates in sandy sediments. Mar Ecol Prog Ser 700, 1–12. https://doi.org/10.3354/meps14196

Infantes, E., Orfila, A., Simarro, G., Terrados, J., Luhar, M., Nepf, H., 2012. Effect of a seagrass (Posidonia oceanica) meadow on wave propagation. Mar Ecol Prog Ser 456, 63–72. https://doi.org/10.3354/meps09754

Infantes, E., Terrados, J., Orfila, A., Cañellas, B., Álvarez-Ellacuria, A., 2009. Wave energy and the upper depth limit distribution of *Posidonia oceanica*. botm 52, 419–427. https://doi.org/10.1515/BOT.2009.050

Islam, M., Jahra, F., Hiscock, S., 2016. Data analysis methodologies for hydrodynamic experiments in waves. Journal of Naval Architecture and Marine Engineering 13, 1–15. https://doi.org/10.3329/jname.v13i1.25347

Jankowska, E., Michel, L.N., Zaborska, A., Włodarska-Kowalczuk, M., 2016. Sediment carbon sink in low-density temperate eelgrass

meadows (Baltic Sea). J Geophys Res Biogeosci 121, 2918–2934. https://doi.org/10.1002/2016JG003424

Johannessen, S.C., 2022. How can blue carbon burial in seagrass meadows increase long-term, net sequestration of carbon? A critical review. Environmental Research Letters 17, 093004. https://doi.org/10.1088/1748-9326/ac8ab4

Kendrick, G.A., Eckersley, J., Walker, D.I., 1999. Landscape-scale changes in seagrass distribution over time: a case study from Success Bank, Western Australia. Aquat Bot 65, 293–309. https://doi.org/10.1016/S0304-3770(99)00047-9

Koch, E.W., 2001. Beyond Light: Physical, Geological, and Geochemical Parameters as Possible Submersed Aquatic Vegetation Habitat Requirements. Estuaries 24, 1. https://doi.org/10.2307/1352808

Koftis, T., Prinos, P., 2011. Estimation of wave attenuation over Posidonia Oceanica, in: 5th International Short Conference on Applied Coastal Research. RWTH Aachen University, pp. 264–271.

Koppes, M., Sylwester, R., Rivera, A., Hallet, B., 2010. Variations in Sediment yield Over the Advance and Retreat of a Calving Glacier, Laguna San Rafael, North Patagonian Icefield. Quat Res 73, 84–95. https://doi.org/10.1016/j.yqres.2009.07.006

Kupsky, B.G., Dornbush, M.E., 2019. Experimental test of abiotic and biotic factors driving restoration success of Vallisneria americana in the Lower Bay of Green Bay. J Great Lakes Res 45, 340–349. https://doi.org/10.1016/j.jglr.2019.01.006

Lara, M., Peralta, G., Alonso, J.J., Morris, E.P., González-Ortiz, V., Rueda-Márquez, J.J., Pérez-Lloréns, J.L., 2012. Effects of intertidal seagrass habitat fragmentation on turbulent diffusion and retention time of solutes. Mar Pollut Bull 64, 2471–2479. https://doi.org/10.1016/j.marpolbul.2012.07.044

Lawson, S.E., McGlathery, K.J., Wiberg, P.L., 2012. Enhancement of sediment suspension and nutrient flux by benthic macrophytes at low biomass. Mar Ecol Prog Ser 448, 259–270. https://doi.org/10.3354/meps09579

Le Méhauté, B., 1976. An Introduction to Hydrodynamics & Water Waves, First Edition. ed.

Lee, S.Y., Kim, J.B., Lee, S.M., 2006. Temporal dynamics of subtidal Zostera marina and intertidal Zostera japonica on the southern coast of Korea. Marine Ecology 27, 133–144. https://doi.org/10.1111/j.1439-0485.2006.00089.x

Lefebvre, L., Provancha, J., Slone, D., Kenworthy, W., 2017. Manatee grazing impacts on a mixed species seagrass bed. Mar Ecol Prog Ser 564, 29–45. https://doi.org/10.3354/meps11986

Lera, S., Nardin, W., Sanford, L., Palinkas, C., Guercio, R., 2019. The impact of submersed aquatic vegetation on the development of river mouth bars. Earth Surf Process Landf 44, 1494–1506. https://doi.org/10.1002/esp.4585

Leriche, A., Pasqualini, V., Boudouresque, C.-F., Bernard, G., Bonhomme, P., Clabaut, P., Denis, J., 2006. Spatial, temporal and structural variations of a Posidonia oceanica seagrass meadow facing

human activities. Aquat Bot 84, 287–293. https://doi.org/10.1016/j.aquabot.2005.10.001

Li, W., Wang, D., Jiao, J., Yang, K., 2019. Effects of vegetation patch density on flow velocity characteristics in an open channel. Journal of Hydrodynamics 31, 1052–1059. https://doi.org/10.1007/s42241-018-0086-6

Licci, S., Nepf, H., Delolme, C., Marmonier, P., Bouma, T.J., Puijalon, S., 2019. The role of patch size in ecosystem engineering capacity: a case study of aquatic vegetation. Aquat Sci 81, 41. https://doi.org/10.1007/s00027-019-0635-2

Lirman, D., Gracias, N., Gintert, B., Gleason, A.C.R., Deangelo, G., Dick, M., Martinez, E., Reid, R.P., 2010. Damage and recovery assessment of vessel grounding injuries on coral reef habitats by use of georeferenced landscape video mosaics. Limnol Oceanogr Methods 8, 88–97. https://doi.org/10.4319/lom.2010.8.0088

Liu, W.-C., Liu, H.-M., Young, C.-C., 2022. Effects of Environmental Factors on Suspended Sediment Plumes in the Continental Shelf Out of Danshuei River Estuary. Water (Basel) 14, 2755. https://doi.org/10.3390/w14172755

Longstaff, B.J., Dennison, W.C., 1999. Seagrass survival during pulsed turbidity events: the effects of light deprivation on the seagrasses Halodule pinifolia and Halophila ovalis. Aquat Bot 65, 105–121. https://doi.org/10.1016/S0304-3770(99)00035-2

Lopez-y-Royo, C., Pergent, G., Alcoverro, T., Buia, M.C., Casazza, G., Martínez-Crego, B., Pérez, M., Silvestre, F., Romero, J., 2011. The seagrass Posidonia oceanica as indicator of coastal water quality:

Experimental intercalibration of classification systems. Ecol Indic 11, 557–563. https://doi.org/10.1016/j.ecolind.2010.07.012

Lovelock, C.E., Adame, M.F., Bennion, V., Hayes, M., O'Mara, J., Reef, R., Santini, N.S., 2014. Contemporary Rates of Carbon Sequestration Through Vertical Accretion of Sediments in Mangrove Forests and Saltmarshes of South East Queensland, Australia. Estuaries and Coasts 37, 763–771. https://doi.org/10.1007/s12237-013-9702-4

Lowe, R.J., Koseff, J.R., Monismith, S.G., Falter, J.L., 2005. Oscillatory flow through submerged canopies: 2. Canopy mass transfer. J Geophys Res 110, C10017. https://doi.org/10.1029/2004JC002789

Luhar, M., Coutu, S., Infantes, E., Fox, S., Nepf, H., 2010. Wave-induced velocities inside a model seagrass bed. J Geophys Res Oceans 115. https://doi.org/10.1029/2010JC006345

Mabrouk, L., Hamza, A., Ben Brahim, M., Bradai, M.-N., 2013. Variability in the structure of epiphyte assemblages on leaves and rhizomes of Posidonia oceanica in relation to human disturbances in a seagrass meadow off Tunisia. Aquat Bot 108, 33–40. https://doi.org/10.1016/j.aquabot.2013.03.002

Madsen, J.D., Chambers, P.A., James, W.F., Koch, E.W., Westlake, D.F., 2001. The interaction between water movement, sediment dynamics and submersed macrophytes. Hydrobiologia 444, 71–84. https://doi.org/10.1023/A:1017520800568

Malea, P., Mylona, Z., Kevrekidis, T., 2019. Improving the utility of the seagrass Posidonia oceanica as a biological indicator of past trace element contamination. Ecol Indic 107, 105596. https://doi.org/10.1016/j.ecolind.2019.105596

Mancini, M., Serra, T., Colomer, J., Solari, L., 2023. Suspended sediments mediate microplastic sedimentation in unidirectional flows. Science of the Total Environment 890. https://doi.org/10.1016/j.scitotenv.2023.164363

Manzanera, M., Pérez, M., Romero, J., 1998. Seagrass mortality due to oversedimentation: an experimental approach. J Coast Conserv 4, 67–70. https://doi.org/10.1007/BF02806491

Marbà, N., Arias-Ortiz, A., Masqué, P., Kendrick, G.A., Mazarrasa, I., Bastyan, G.R., Garcia-Orellana, J., Duarte, C.M., 2015. Impact of seagrass loss and subsequent revegetation on carbon sequestration and stocks. Journal of Ecology 103, 296–302. https://doi.org/10.1111/1365-2745.12370

Marin-Diaz, B., Bouma, T.J., Infantes, E., 2020. Role of eelgrass on bed-load transport and sediment resuspension under oscillatory flow. Limnol Oceanogr 65, 426–436. https://doi.org/10.1002/lno.11312

Mateo, M.A., Romero, J., Pérez, M., Littler, M.M., Littler, D.S., 1997. Dynamics of Millenary Organic Deposits Resulting from the Growth of the Mediterranean SeagrassPosidonia oceanica. Estuar Coast Shelf Sci 44, 103–110. https://doi.org/10.1006/ecss.1996.0116

Mazarrasa, I., Marbà, N., Garcia-Orellana, J., Masqué, P., Arias-Ortiz, A., Duarte, C.M., 2017. Dynamics of carbon sources supporting burial in seagrass sediments under increasing anthropogenic pressure. Limnol Oceanogr 62, 1451–1465. https://doi.org/10.1002/lno.10509

Mazarrasa, I., Samper-Villarreal, J., Serrano, O., Lavery, P.S., Lovelock, C.E., Marbà, N., Duarte, C.M., Cortés, J., 2018. Habitat characteristics provide insights of carbon storage in seagrass

meadows. Mar Pollut Bull 134, 106–117. https://doi.org/10.1016/j.marpolbul.2018.01.059

Metz, J.L., Harris, R.J., Arrington, D.A., 2020. Seasonal occurrence patterns of seagrass should influence resource assessment and management decisions: A case study in the Indian River Lagoon and Loxahatchee River Estuary, Florida. Reg Stud Mar Sci 34, 101093. https://doi.org/10.1016/j.rsma.2020.101093

Montefalcone, M., 2009. Ecosystem health assessment using the Mediterranean seagrass Posidonia oceanica: A review. Ecol Indic 9, 595–604. https://doi.org/10.1016/j.ecolind.2008.09.013

Montefalcone, M., Bianchi, C.N., Morri, C., Peirano, A., Albertelli, G., 2006. Lower limit typology and functioning of six Posidonia oceanica meadows in the Ligurian Sea (NW Mediterranean). Biol Mar Mediterr 13, 262–266.

Montefalcone, M., Parravicini, V., Vacchi, M., Albertelli, G., Ferrari, M., Morri, C., Bianchi, C.N., 2010. Human influence on seagrass habitat fragmentation in NW Mediterranean Sea. Estuar Coast Shelf Sci 86, 292–298. https://doi.org/10.1016/j.ecss.2009.11.018

Montefalcone, M., Vacchi, M., Archetti, R., Ardizzone, G., Astruch, P., Bianchi, C.N., Calvo, S., Criscoli, A., Fernández-Torquemada, Y., Luzzu, F., Misson, G., Morri, C., Pergent, G., Tomasello, A., Ferrari, M., 2019. Geospatial modelling and map analysis allowed measuring regression of the upper limit of Posidonia oceanica seagrass meadows under human pressure. Estuar Coast Shelf Sci 217, 148–157. https://doi.org/10.1016/j.ecss.2018.11.006

Moore, E.C., Hovel, K.A., 2010. Relative influence of habitat complexity and proximity to patch edges on seagrass epifaunal communities. Oikos 119, 1299–1311. https://doi.org/10.1111/j.1600-0706.2009.17909.x

Mulder, T., Syvitski, J.P.M., 1995. Turbidity Currents Generated at River Mouths during Exceptional Discharges to the World Oceans. J Geol 103, 285–299. https://doi.org/10.1086/629747

Mutlu, E., Karaca, D., Duman, G.S., Şahin, A., Özvarol, Y., Olguner, C., 2022. Seasonality and phenology of an epiphytic calcareous red alga, Hydrolithon boreale, on the leaves of Posidonia oceanica (L) Delile in the Turkish water. Environmental Science and Pollution Research 30, 17193–17213. https://doi.org/10.1007/s11356-022-23333-w

Nakaoka, M., Aioi, K., 1999. Growth of seagrass Halophila ovalis at dugong trails compared to existing within-patch variation in a Thailand intertidal flat. Mar Ecol Prog Ser 184, 97–103. https://doi.org/10.3354/meps184097

Navarrete-Fernández, T., Bermejo, R., Hernández, I., Deidun, A., Andreu-Cazenave, M., Cózar, A., 2022. The role of seagrass meadows in the coastal trapping of litter. Mar Pollut Bull 174, 113299. https://doi.org/10.1016/j.marpolbul.2021.113299

Nepf, H.M., 1999. Drag, turbulence, and diffusion in flow through emergent vegetation. Water Resour Res 35, 479–489. https://doi.org/10.1029/1998WR900069

Nepf, H.M., Sullivan, J.A., Zavistoski, R.A., 1997. A model for diffusion within emergent vegetation. Limnol Oceanogr 42, 1735–1745. https://doi.org/10.4319/lo.1997.42.8.1735

Nepf, H.M., Vivoni, E.R., 2000. Flow structure in depth-limited, vegetated flow. J Geophys Res Oceans 105, 28547–28557. https://doi.org/10.1029/2000JC900145

Newell, R.I.E., Koch, E.W., 2004. Modeling seagrass density and distribution in response to changes in turbidity stemming from bivalve filtration and seagrass sediment stabilization. Estuaries 27, 793–806. https://doi.org/10.1007/BF02912041

Noisette, F., Depetris, A., Kühl, M., Brodersen, K.E., 2020. Flow and epiphyte growth effects on the thermal, optical and chemical microenvironment in the leaf phyllosphere of seagrass (Zostera marina). J R Soc Interface 17, 20200485. https://doi.org/10.1098/rsif.2020.0485

Oey, L.-Y., Mellor, G.L., 1993. Subtidal Variability of Estuarine Outflow, Plume, and Coastal Current: A Model Study. J Phys Oceanogr 23, 164–171. https://doi.org/10.1175/1520-0485(1993)023<0164:SVOEOP>2.0.CO;2

Olesen, B, Sand-Jensen, K., 1994. Patch dynamics of eelgrass Zostera marina. Mar Ecol Prog Ser 106, 147–156. https://doi.org/10.3354/meps106147

Olesen, Birgit, Sand-Jensen, K., 1994. Demography of Shallow Eelgrass (Zostera Marina) Populations--Shoot Dynamics and Biomass Development. J Ecol 82, 379. https://doi.org/10.2307/2261305

Oreska, M.P.J., McGlathery, K.J., Porter, J.H., 2017. Seagrass blue carbon spatial patterns at the meadow-scale. PLoS One 12, e0176630. https://doi.org/10.1371/journal.pone.0176630

Paladini de Mendoza, F., Fontolan, G., Mancini, E., Scanu, E., Scanu, S., Bonamano, S., Marcelli, M., 2018. Sediment dynamics and resuspension processes in a shallow-water Posidonia oceanica meadow. Mar Geol 404, 174–186. https://doi.org/10.1016/j.margeo.2018.07.006

Paling, E.I., Fonseca, M., van Katwijk, M.M., van Keulen, M., 2009. Seagrass restoration. Elsevier.

Paling, E.I., van Keulen, M., Wheeler, K.D., Phillips, J., Dyhrberg, R., 2003. Influence of Spacing on Mechanically Transplanted Seagrass Survival in a High Wave Energy Regime. Restor Ecol 11, 56–61. https://doi.org/10.1046/j.1526-100X.2003.00072.x

Palmer, M.R., Nepf, H.M., Pettersson, T.J.R., Ackerman, J.D., 2004. Observations of particle capture on a cylindrical collector: Implications for particle accumulation and removal in aquatic systems. Limnol Oceanogr 49, 76–85. https://doi.org/10.4319/lo.2004.49.1.0076

Paquier, A.-E., Meulé, S., Anthony, E.J., Larroudé, P., Bernard, G., 2019. Wind-Induced Hydrodynamic Interactions With Aquatic Vegetation in a Fetch-Limited Setting: Implications for Coastal Sedimentation and Protection. Estuaries and Coasts 42, 688–707. https://doi.org/10.1007/s12237-018-00487-w

Pascolo, S., Petti, M., Bosa, S., 2019. Wave Forecasting in Shallow Water: A New Set of Growth Curves Depending on Bed Roughness. Water (Basel) 11, 2313. https://doi.org/10.3390/w11112313

Pastor, A., Ospina-Alvarez, A., Larsen, J., Hansen, F.T., Krause-Jensen, D., Maar, M., 2022. A network analysis of connected biophysical

pathways to advice eelgrass (Zostera marina) restoration. Mar Environ Res 179, 105690. https://doi.org/10.1016/j.marenvres.2022.105690

Paul, M., Amos, C.L., 2011. Spatial and seasonal variation in wave attenuation over *Zostera noltii*. J Geophys Res 116, C08019. https://doi.org/10.1029/2010JC006797

Paul, M., de los Santos, C.B., 2019. Variation in flexural, morphological, and biochemical leaf properties of eelgrass (Zostera marina) along the European Atlantic climate regions. Mar Biol 166, 127. https://doi.org/10.1007/s00227-019-3577-2

Pineda, M.-C., Strehlow, B., Kamp, J., Duckworth, A., Jones, R., Webster, N.S., 2017. Effects of combined dredging-related stressors on sponges: a laboratory approach using realistic scenarios. Sci Rep 7, 5155. https://doi.org/10.1038/s41598-017-05251-x

Pinheiro, L.M., Britz, L.M.K., Agostini, V.O., Pérez-Parada, A., García-Rodríguez, F., Galloway, T.S., Pinho, G.L.L., 2022. Salt marshes as the final watershed fate for meso- and microplastic contamination: A case study from Southern Brazil. Science of The Total Environment 838, 156077. https://doi.org/10.1016/j.scitotenv.2022.156077

Piovano, S., Lemons, G., Ciriyawa, A., Batibasaga, A., Seminoff, J., 2020. Diet and recruitment of green turtles in Fiji, South Pacific, inferred from in-water capture and stable isotope analysis. Mar Ecol Prog Ser 640, 201–213. https://doi.org/10.3354/meps13287

Pitarch, J., Falcini, F., Nardin, W., Brando, V.E., Cicco, A. Di, Marullo, S., 2019. Linking flow-stream variability to grain size distribution of suspended sediment from a satellite-based analysis of the Tiber River

plume (Tyrrhenian Sea). Sci Rep 9, 19729. https://doi.org/10.1038/s41598-019-56409-8

Pujol, D., Abdolahpour, M., Lavery, P.S., McMahon, K., Oldham, C., 2019. Flow velocity and nutrient uptake in marine canopies. Mar Ecol Prog Ser 622, 17–30. https://doi.org/10.3354/meps12987

Pujol, D., Casamitjana, X., Serra, T., Colomer, J., 2013a. Canopy-scale turbulence under oscillatory flow. Cont Shelf Res 66, 9–18. https://doi.org/10.1016/j.csr.2013.06.012

Pujol, D., Colomer, J., Serra, T., Casamitjana, X., 2010. Effect of submerged aquatic vegetation on turbulence induced by an oscillating grid. Cont Shelf Res 30, 1019–1029. https://doi.org/10.1016/j.csr.2010.02.014

Pujol, D., Nepf, H., 2012. Breaker-generated turbulence in and above a seagrass meadow. Cont Shelf Res 49, 1–9. https://doi.org/10.1016/j.csr.2012.09.004

Pujol, D., Serra, T., Colomer, J., Casamitjana, X., 2013b. Flow structure in canopy models dominated by progressive waves. J Hydrol (Amst) 486, 281–292. https://doi.org/10.1016/j.jhydrol.2013.01.024

Reyes, J., Sanson, M., Afonso-Carrillo, J., 1998. Distribution of the Epiphytes along the Leaves of Cymodocea nodosa in the Canary Islands, Botanica Marina.

Reynolds, P.L., Richardson, J.P., Duffy, J.E., 2014. Field experimental evidence that grazers mediate transition between microalgal and seagrass dominance. Limnol Oceanogr 59, 1053–1064. https://doi.org/10.4319/lo.2014.59.3.1053

Ricart, A.M., Pérez, M., Romero, J., 2017. Landscape configuration modulates carbon storage in seagrass sediments. Estuar Coast Shelf Sci 185, 69–76. https://doi.org/10.1016/j.ecss.2016.12.011

Ricart, A.M., York, P.H., Rasheed, M.A., Pérez, M., Romero, J., Bryant, C. V, Macreadie, P.I., 2015. Variability of sedimentary organic carbon in patchy seagrass landscapes. Mar Pollut Bull 100, 476–482. https://doi.org/10.1016/j.marpolbul.2015.09.032

Robbins, B.D., Bell, S.S., 1994. Seagrass landscapes: a terrestrial approach to the marine subtidal environment. Trends Ecol Evol 9, 301–304. https://doi.org/10.1016/0169-5347(94)90041-8

Röhr, M.E., Holmer, M., Baum, J.K., Björk, M., Boyer, K., Chin, D., Chalifour, L., Cimon, S., Cusson, M., Dahl, M., Deyanova, D., Duffy, J.E., Eklöf, J.S., Geyer, J.K., Griffin, J.N., Gullström, M., Hereu, C.M., Hori, M., Hovel, K.A., Hughes, A.R., Jorgensen, P., Kiriakopolos, S., Moksnes, P.-O., Nakaoka, M., O'Connor, M.I., Peterson, B., Reiss, K., Reynolds, P.L., Rossi, F., Ruesink, J., Santos, R., Stachowicz, J.J., Tomas, F., Lee, K.-S., Unsworth, R.K.F., Boström, C., 2018. Blue Carbon Storage Capacity of Temperate Eelgrass (Zostera marina) Meadows. Global Biogeochem Cycles 32, 1457–1475. https://doi.org/10.1029/2018GB005941

Ros, À., Colomer, J., Serra, T., Pujol, D., Soler, M., Casamitjana, X., 2014. Experimental observations on sediment resuspension within submerged model canopies under oscillatory flow. Cont Shelf Res 91, 220–231. https://doi.org/10.1016/j.csr.2014.10.004

Roy, E.D., White, J.R., Smith, E.A., Bargu, S., Li, C., 2013. Estuarine ecosystem response to three large-scale Mississippi River flood

diversion events. Science of The Total Environment 458–460, 374–387. https://doi.org/10.1016/j.scitotenv.2013.04.046

Ruesink, J.L., 2016. Epiphyte load and seagrass performance are decoupled in an estuary with low eutrophication risk. J Exp Mar Biol Ecol 481, 1–8. https://doi.org/10.1016/j.jembe.2016.03.022

Sagerman, J., Hansen, J.P., Wikström, S.A., 2020. Effects of boat traffic and mooring infrastructure on aquatic vegetation: A systematic review and meta-analysis. Ambio. https://doi.org/10.1007/s13280-019-01215-9

Sand-Jensen, K., 1977. Effect of epiphytes on eelgrass photosynthesis. Aquat Bot 3, 55–63. https://doi.org/10.1016/0304-3770(77)90004-3

Sand-Jensen, K., Mebus, J.R., 1996. Fine-Scale Patterns of Water Velocity within Macrophyte Patches in Streams. Oikos 76, 169. https://doi.org/10.2307/3545759

Sand-Jensen, K., Pedersen, M.L., 2008. Streamlining of plant patches in streams. Freshw Biol 53, 714–726. https://doi.org/10.1111/j.1365-2427.2007.01928.x

Schaefer, R.B., Nepf, H.M., 2022. Flow Structure in an Artificial Seagrass Meadow in Combined Wave-Current Conditions. Front Mar Sci 9. https://doi.org/10.3389/fmars.2022.836901

Schoelynck, J., Creëlle, S., Buis, K., Mulder, T. De, Emsens, W.-J., Hein, T., Meire, D., Meire, P., Okruszko, T., Preiner, S., Gonzalez, R.R., Silinski, A., Temmerman, S., Troch, P., Oyen, T. Van, Verschoren, V., Visser, F., Wang, C., Wolters, J.-W., Folkard, A., 2018. What is a macrophyte patch? Patch identification in aquatic ecosystems and

guidelines for consistent delineation. Ecohydrology & Hydrobiology 18, 1–9. https://doi.org/10.1016/j.ecohyd.2017.10.005

Schotanus, J., Walles, B., Capelle, J.J., van Belzen, J., van de Koppel, J., Bouma, T.J., 2020. Promoting self-facilitating feedback processes in coastal ecosystem engineers to increase restoration success: Testing engineering measures. Journal of Applied Ecology 57, 1958–1968. https://doi.org/10.1111/1365-2664.13709

Serra, T., Colomer, J., Cristina, X.P., Vila, X., Arellano, J.B., Casamitjana, X., 2001. Evaluation of Laser In Situ Scattering Instrument for Measuring Concentration of Phytoplankton, Purple Sulfur Bacteria, and Suspended Inorganic Sediments in Lakes. Journal of Environmental Engineering 127, 1023–1030. https://doi.org/10.1061/(ASCE)0733-9372(2001)127:11(1023)

Serra, T., Colomer, J., Gacia, E., Soler, M., Casamitjana, X., 2002a. Effects of a turbid hydrothermal plume on the sedimentation rates in a karstic lake. Geophys Res Lett 29, 2029. https://doi.org/10.1029/2002GL015368

Serra, T., Colomer, J., Zamora, L., Moreno-Amich, R., Casamitjana, X., 2002b. Seasonal development of a turbid hydrothermal lake plume and the effects on the fish distribution. Water Res 36, 2753–2760. https://doi.org/10.1016/S0043-1354(01)00510-3

Serra, T., Gracias, N., Hendriks, I.E., 2020. Fragmentation in Seagrass Canopies Can Alter Hydrodynamics and Sediment Deposition Rates. Water (Basel) 12, 3473. https://doi.org/10.3390/w12123473

Serra, T., Oldham, C., Colomer, J., 2018. Local hydrodynamics at edges of marine canopies under oscillatory flows. PLoS One 13. https://doi.org/10.1371/journal.pone.0201737

Short, F.T., Short, C.A., 1984. The seagrass filter: purification of estuarine and coastal waters, in: Kennedy, V.S. (Ed.), The Estuary As a Filter. Elsevier, pp. 395–413. https://doi.org/10.1016/B978-0-12-405070-9.50024-4

Sleeman, J.C., Kendrick, G.A., Boggs, G.S., Hegge, B.J., 2005. Measuring fragmentation of seagrass landscapes: which indices are most appropriate for detecting change? Mar Freshw Res 56, 851. https://doi.org/10.1071/MF04300

Smith, T.M., Hindell, J.S., Jenkins, G.P., Connolly, R.M., 2010. Seagrass patch size affects fish responses to edges. Journal of Animal Ecology 79, 275–281. https://doi.org/10.1111/j.1365-2656.2009.01605.x

Soler, M., Serra, T., Folkard, A., Colomer, J., 2021. Hydrodynamics and sediment deposition in turbidity currents: Comparing continuous and patchy vegetation canopies, and the effects of water depth. J Hydrol (Amst) 594, 125750. https://doi.org/10.1016/j.jhydrol.2020.125750

Somma, E., Terlizzi, A., Costantini, M., Madeira, M., Zupo, V., 2023. Global Changes Alter the Successions of Early Colonizers of Benthic Surfaces. J Mar Sci Eng 11, 1232. https://doi.org/10.3390/jmse11061232

Sridhar, P.N., Ali, M.M., Vethamony, P., Babu, M.T., Ramana, I. V, Jayakumar, S., 2008. Seasonal Occurrence of Unique Sediment Plume in the Bay of Bengal. Eos, Transactions American Geophysical Union 89, 22. https://doi.org/10.1029/2008EO030002

Stankovic, M., Kaewsrikhaw, R., Rattanachot, E., Prathep, A., 2019. Modeling of suitable habitat for small-scale seagrass restoration in tropical ecosystems. Estuar Coast Shelf Sci 231, 106465. https://doi.org/10.1016/j.ecss.2019.106465

Stipek, C., Santos, R., Babcock, E., Lirman, D., 2020. Modelling the resilience of seagrass communities exposed to pulsed freshwater discharges: A seascape approach. PLoS One 15, e0229147. https://doi.org/10.1371/journal.pone.0229147

Sweatman, J.L., Layman, C.A., Fourqurean, J.W., 2017. Habitat fragmentation has some impacts on aspects of ecosystem functioning in a sub-tropical seagrass bed. Mar Environ Res 126, 95–108. https://doi.org/10.1016/j.marenvres.2017.02.003

Tang, C., Lei, J., Nepf, H.M., 2019. Impact of Vegetation-Generated Turbulence on the Critical, Near-Bed, Wave-Velocity for Sediment Resuspension. Water Resour Res 55, 5904–5917. https://doi.org/10.1029/2018WR024335

Tanner, J.E., 2005. Edge effects on fauna in fragmented seagrass meadows. Austral Ecol 30, 210–218. https://doi.org/10.1111/j.1442-9993.2005.01438.x

Tanner, J.E., 2003. Patch shape and orientation influences on seagrass epifauna are mediated by dispersal abilities. Oikos 100, 517–524. https://doi.org/10.1034/j.1600-0706.2003.12060.x

Tassan, S., 1997. A numerical model for the detection of sediment concentration in stratified river plumes using Thematic Mapper data. Int J Remote Sens 18, 2699–2705. https://doi.org/10.1080/014311697217567

Terrados, J., Duarte, C.M., 2000. Experimental evidence of reduced particle resuspension within a seagrass (Posidonia oceanica L.) meadow. J Exp Mar Biol Ecol 243, 45–53. https://doi.org/10.1016/S0022-0981(99)00110-0

Tinoco, R.O., Coco, G., 2014. Observations of the effect of emergent vegetation on sediment resuspension under unidirectional currents and waves. Earth Surface Dynamics 2, 83–96. https://doi.org/10.5194/esurf-2-83-2014

Todo, K., Sato, K., 2002. Directive 2000/60/EC of the European Parliament and of the Council of 23 October 2000 establishing a framework for Community action in the field of water policy. Environmental Research Quarterly 66–106.

Trautman, D., Borowitzka, M., 1999. Distribution of the epiphytic organisms on Posidonia australis and P. sinuosa, two seagrasses with differing leaf morphology. Mar Ecol Prog Ser 179, 215–229. https://doi.org/10.3354/meps179215

Trevathan-Tackett, S.M., Kelleway, J., Macreadie, P.I., Beardall, J., Ralph, P., Bellgrove, A., 2015. Comparison of marine macrophytes for their contributions to blue carbon sequestration. Ecology 96, 3043–3057. https://doi.org/10.1890/15-0149.1

Tuck, M.E., Ford, M.R., Kench, P.S., Masselink, G., 2021. Sediment supply dampens the erosive effects of sea-level rise on reef islands. Sci Rep 11, 5523. https://doi.org/10.1038/s41598-021-85076-x

Turner, S.J., 2007. Growth and productivity of intertidal Zostera capricorni in New Zealand estuaries. N Z J Mar Freshwater Res 41, 77–90. https://doi.org/10.1080/00288330709509897

Unsworth, R.K.F., McKenzie, L.J., Collier, C.J., Cullen-Unsworth, L.C., Duarte, C.M., Eklöf, J.S., Jarvis, J.C., Jones, B.L., Nordlund, L.M., 2019. Global challenges for seagrass conservation. Ambio 48, 801–815. https://doi.org/10.1007/s13280-018-1115-y

Unsworth, R.K.F., Williams, B., Jones, B.L., Cullen-Unsworth, L.C., 2017. Rocking the boat: Damage to eelgrass by swinging boat moorings. Front Plant Sci 8. https://doi.org/10.3389/fpls.2017.01309

Valdemarsen, T., Canal-Verges, P., Kristensen, E., Holmer, M., Kristiansen, M.D., Flindt, M.R., 2010. Vulnerability of Zostera marina seedlings to physical stress. Mar Ecol Prog Ser 418, 119–130. https://doi.org/10.3354/meps08828

Valdez, S.R., Zhang, Y.S., van der Heide, T., Vanderklift, M.A., Tarquinio, F., Orth, R.J., Silliman, B.R., 2020. Positive Ecological Interactions and the Success of Seagrass Restoration. Front Mar Sci. https://doi.org/10.3389/fmars.2020.00091

Valero, M., Tena, J., Torres, J., Royo, M., 2009. Estudio de la Pradera de Posidonia oceanica (L.) Delile del ´Area Litoral del Municipio de Teulada (Alicante). Nereis 2, 29–39.

van de Koppel, J., Bouma, T.J., Herman, P.M.J., 2012. The influence of local- and landscape-scale processes on spatial self-organization in estuarine ecosystems. Journal of Experimental Biology 215, 962–967. https://doi.org/10.1242/jeb.060467

van Katwijk, M.M., Bos, A.R., Hermus, D.C.R., Suykerbuyk, W., 2010. Sediment modification by seagrass beds: Muddification and sandification induced by plant cover and environmental conditions.

Estuar Coast Shelf Sci 89, 175–181. https://doi.org/10.1016/j.ecss.2010.06.008

van Katwijk, M.M., Thorhaug, A., Marbà, N., Orth, R.J., Duarte, C.M., Kendrick, G.A., Althuizen, I.H.J., Balestri, E., Bernard, G., Cambridge, M.L., Cunha, A., Durance, C., Giesen, W., Han, Q., Hosokawa, S., Kiswara, W., Komatsu, T., Lardicci, C., Lee, K., Meinesz, A., Nakaoka, M., O'Brien, K.R., Paling, E.I., Pickerell, C., Ransijn, A.M.A., Verduin, J.J., 2016. Global analysis of seagrass restoration: the importance of large-scale planting. Journal of Applied Ecology 53, 567–578. https://doi.org/10.1111/1365-2664.12562

van Veelen, T.J., Fairchild, T.P., Reeve, D.E., Karunarathna, H., 2020. Experimental study on vegetation flexibility as control parameter for wave damping and velocity structure. Coastal Engineering 157, 103648. https://doi.org/10.1016/j.coastaleng.2020.103648

Vanderploeg, H.A., Johengen, T.H., Lavrentyev, P.J., Chen, C., Lang, G.A., Agy, M.A., Bundy, M.H., Cavaletto, J.F., Eadie, B.J., Liebig, J.R., Miller, G.S., Ruberg, S.A., McCormick, M.J., 2007. Anatomy of the recurrent coastal sediment plume in Lake Michigan and its impacts on light climate, nutrients, and plankton. J Geophys Res 112, C03S90. https://doi.org/10.1029/2004JC002379

Vautard, R., Gobiet, A., Sobolowski, S., Kjellström, E., Stegehuis, A., Watkiss, P., Mendlik, T., Landgren, O., Nikulin, G., Teichmann, C., Jacob, D., 2014. The European climate under a 2 °C global warming. Environmental Research Letters 9, 034006. https://doi.org/10.1088/1748-9326/9/3/034006

Verdura, J., Santamaría, J., Ballesteros, E., Smale, D.A., Cefalì, M.E., Golo, R., Caralt, S., Vergés, A., Cebrian, E., 2021. Local-scale climatic refugia offer sanctuary for a habitat-forming species during a marine heatwave. Journal of Ecology 109, 1758–1773. https://doi.org/10.1111/1365-2745.13599

Virnstein, R.W., Hall, L.M., 2009. Northern range extension of the seagrasses Halophila johnsonii and Halophila decipiens along the east coast of Florida, USA. Aquat Bot 90, 89–92. https://doi.org/10.1016/j.aquabot.2008.05.007

Ward, E.A., Aldis, C., Wade, T., Miliou, A., Tsimpidis, T., Cameron, T.C., 2022. Is All Seagrass Habitat Equal? Seasonal, Spatial, and Interspecific Variation in Productivity Dynamics Within Mediterranean Seagrass Habitat. Front Mar Sci 9. https://doi.org/10.3389/fmars.2022.891467

Warrick, J.A., Mertes, L.A.K., Siegel, D.A., Mackenzie, C., 2004. Estimating suspended sediment concentrations in turbid coastal waters of the Santa Barbara Channel with SeaWiFS. Int J Remote Sens 25, 1995–2002. https://doi.org/10.1080/01431160310001619535

Waycott, M., Duarte, C.M., Carruthers, T.J.B., Orth, R.J., Dennison, W.C., Olyarnik, S., Calladine, A., Fourqurean, J.W., Heck, K.L., Hughes, A.R., Kendrick, G.A., Kenworthy, W.J., Short, F.T., Williams, S.L., 2009. Accelerating loss of seagrasses across the globe threatens coastal ecosystems. Proceedings of the National Academy of Sciences 106, 12377–12381. https://doi.org/10.1073/pnas.0905620106

West, R.J., Jacobs, N.E., Roberts, D.E., 1990. Experimental transplanting of seagrasses in Botany Bay, Australia. Mar Pollut Bull 21, 197–203. https://doi.org/10.1016/0025-326X(90)90502-Y

Whalen, M.A., Duffy, J.E., Grace, J.B., 2013. Temporal shifts in top-down vs. bottom-up control of epiphytic algae in a seagrass ecosystem. Ecology 94, 510–520. https://doi.org/10.1890/12-0156.1

Wilkie, L., O'Hare, M.T., Davidson, I., Dudley, B., Paterson, D.M., 2012. Particle trapping and retention by Zostera noltii: A flume and field study. Aquat Bot 102, 15–22. https://doi.org/10.1016/j.aquabot.2012.04.004

Williams, S.L., 2007. Introduced species in seagrass ecosystems: Status and concerns. J Exp Mar Biol Ecol 350, 89–110. https://doi.org/10.1016/j.jembe.2007.05.032

Wu, P.P.-Y., McMahon, K., Rasheed, M.A., Kendrick, G.A., York, P.H., Chartrand, K., Caley, M.J., Mengersen, K., 2018. Managing seagrass resilience under cumulative dredging affecting light: Predicting risk using dynamic Bayesian networks. Journal of Applied Ecology 55, 1339–1350. https://doi.org/10.1111/1365-2664.13037

Zhang, X., Nepf, H.M., 2008. Density-driven exchange flow between open water and an aquatic canopy. Water Resour Res 44. https://doi.org/10.1029/2007WR006676

Zhang, Y., Nepf, H., 2019. Wave-Driven Sediment Resuspension Within a Model Eelgrass Meadow. J Geophys Res Earth Surf 124, 1035–1053. https://doi.org/10.1029/2018JF004984

Zhang, Y., Tang, C., Nepf, H., 2018. Turbulent Kinetic Energy in Submerged Model Canopies Under Oscillatory Flow. Water Resour Res 54, 1734–1750. https://doi.org/10.1002/2017WR021732

Zhao, L., Ru, S., He, J., Zhang, Z., Song, X., Wang, D., Li, X., Wang, J., 2022. Eelgrass (Zostera marina) and its epiphytic bacteria facilitate the sinking of microplastics in the seawater. Environmental Pollution 292, 118337. https://doi.org/10.1016/j.envpol.2021.118337

Zhu, L., Zou, Q., Huguenard, K., Fredriksson, D.W., 2020. Mechanisms for the Asymmetric Motion of Submerged Aquatic Vegetation in Waves: A Consistent-Mass Cable Model. J Geophys Res Oceans 125. https://doi.org/10.1029/2019JC015517

Zhu, Q., Wiberg, P.L., Reidenbach, M.A., 2021. Quantifying Seasonal Seagrass Effects on Flow and Sediment Dynamics in a Back-Barrier Bay. J Geophys Res Oceans 126. https://doi.org/10.1029/2020JC016547

Zong, L., Nepf, H., 2011. Spatial distribution of deposition within a patch of vegetation. Water Resour Res 47. https://doi.org/10.1029/2010WR009516

Zucchetta, M., Venier, C., Taji, M.A., Mangin, A., Pastres, R., 2016. Modelling the spatial distribution of the seagrass Posidonia oceanica along the North African coast: Implications for the assessment of Good Environmental Status. Ecol Indic 61, 1011–1023. https://doi.org/10.1016/j.ecolind.2015.10.059

Estuarine, Coastal and Shelf Science 249 (2021) 107106

Contents lists available at ScienceDirect

Estuarine, Coastal and Shelf Science

journal homepage: http://www.elsevier.com/locate/ecss

Meadow fragmentation influences *Posidonia oceanica* density at the edge of nearby gaps

Aina Barcelona [a,*], Jordi Colomer [a], Marianna Soler [a], Nuno Gracias [b], Teresa Serra [a]

[a] Department of Physics, University of Girona, 17071, Girona, Spain
[b] Computer Vision and Robotics Institute, University of Girona, 17071, Girona, Spain

ARTICLE INFO

Keywords:
Seagrass meadows
Posidonia oceanica
Fragmentation
Canopy density
Gap-scale
Meadow-scale

ABSTRACT

Seagrass meadows are globally threatened by anthropogenic and natural pressures that cause habitat fragmentation and ecosystem degradation. Seagrass fragmentation is manidested by the loss of vegetation in gaps within a meadow. Depending on the degree of fragmentation, the ecological services provided by theseagrass meadows may be compromised. This study aims to understand the effect meadow fragmentation hason the shoot density of the canopy (large-scale or meadow-scale effect), as well as the effect the local gap size has on the shoot density at the edge of the gap (local-scale or gap-scale effect). In other woerd, determine whether the effects on the large scale can impact the local scales of the gap. This study demonstrates that the greater the gap area is, the lower the shoot density of the vegetation surrounding the gap. Moreover, the effect of fragmentation at the meadow-scale has been proved: the higher the fragmentation degree of the meadow is, the lower the shoot density is in the surrounding vegetation near the gap. Hence, the differences in shoot density at the edges of a gap are proven to be produced by both meadow fragmentation and gap characteristics.

1. Introduction

Seagrass meadows are globally extensive nearshore eosystems (Waycott et al., 2009; Smith et al., 2010; Unsworth et al., 2018) and provide significant ecosystem services such as the stabilization of habitats for fish feeding and predation (Unsworth et al., 2018), wave and turbulence attenuation (Gacia et al., 1999; Pujol and Nepf, 2012; Pujol et al., 2013), and sediment deposition (Zong and Nepf, 2011), which creates new substrates, that will enhance the canopy growth (Folkard, 2019). Seagrass meadows provide an immensely rich fauna diversity and a high water quality and ensure carbon storage and sequestration (Grech et al., 2012; Duarte et al., 2013; Ricart et al., 2015). Organic carbon can be accumulated, buried and preserved for millennia by seagrass meadows (Mateo et al., 1997), thus contributing to mitigating the effects of climate change (Mazarrasa et al., 2017).

Seagrass meadows are threatened by natural and anthropogenic pressures, which result in meadows with differing degrees of habitat fragmentation. The principal causes for the increase in seagrass fragmentation are coastal development and overexploitation, both of which have a major impact on the seafloor where the meadows grow. Destructive fishing activities, anchoring and boat moorings have also resulted in the direct loss of seagrass meadow biomass; as has the ever-increasing nutrient and sediment pollution in the coastal waters (Colomer et al., 2017; Unsworth et al., 2017). These practices have been reported to decrease the number of herbivores that predate over the fouling algae in seagrass leaves, resulting in a reduced quality of seagrass meadows (Waycott et al., 2009). Furthermore, trawling and aquaculture have led to the introduction and dispersion of non-native species like *Caulerpa taxifolia* (M.Vahl) C. Agardh, *Caulerpa cylindracea* Sonder, *Codium fragile* subsp. *Fragile* (Suringar) Hariot, among others (Williams 2007). Global change has also triggered an increase in the salinity and temperature of the water which, in turn, generates a regression of the coastal seagrass meadows (Boudouresque et al., 2009; Grech et al., 2012; Unsworth et al., 2018; Espel et al., 2019). All these pressures are accompanied by the rapid degradation of the coastal sea-floor and by the continuous increase in seagrass meadow fragmentation worldwide (Montefalcone et al., 2010; Abadie et al., 2015). Patchy seagrass meadows are the result of the loss of both their stability and their shoot density (Smith et al., 2010; Colomer et al., 2017). In the Mediterranean *Posidonia oceanica* (Linnaeus) Delile seagrass meadows, Montefalcone et al. (2019) found that the extent of the regressed upper limits ranges between 18% and 99%. Therefore, continuous meadows

* Corresponding author.
E-mail address: ainabarcelonaarbat@gmail.com (A. Barcelona).

https://doi.org/10.1016/j.ecss.2020.107106
Received 2 March 2020; Received in revised form 10 November 2020; Accepted 16 November 2020
Available online 20 November 2020

shift to fragmented meadows where gap of vegetation (where the seabed remains exposed to the hydrodynamics) are interspersed within the meadow (where the vegetation shelters the seabed). The resulting habitat patchiness, where large areas of habitat are removed or damaged, influences the ecosystem's integrity to the point that its ecological functions are compromised. Reversing the vegetation loss is difficult because of complicated feed-back mechanisms that either reinforce vegetation dominance or threaten its resilience. For example, in the absence of seagrass vegetation, a drift to macroalgae proliferation can occur (Valdemarsen et al., 2010). Also, the reduction in sheltering (caused by the decrease in the density of vegetation) can lead to a decrease in seabed protection. A decrease in the seabed sheltering will lead to a high sediment resuspension which in turn might result in a further decrease in the vegetation density (Valdez et al., 2020).

Seagrass habitat fragmentation increases the number of gaps and edges in meadows, which then influence the physical and biological patterns of the meadow's structure (Ricart et al., 2015). El Allaoui et al. (2016) found lower wave and turbulent kinetic energy attenuation in fragmented canopy areas with large vegetation gaps than in canopies with small gaps albeit with the same degree of fragmentation. They also found that the overall turbulence in a canopy will increase with the degree of fragmentation in the canopy, thus highlighting the roles vegetation and gaps play at the meadow-scale. Likewise, an increase in the turbulent diffusion in the fragmented canopies of *Zostera noltei* Hornemann, indicated that fragmented habitats are more susceptible to dissolving pollutants (Lara et al., 2012). The physical modifications resulting from the gaps in fragmented canopies have been found to alter the carbon sequestring abilities of the seagrass. For instance, Ricart et al. (2015) found lower carbon storage in sediments within fragmented *Zostera muelleri* Irmisch ex Ascherson meadows. Edges can also have a negative effect on the a seagrass meadow by increasing the risk of predation and/or encouraging invasions by exotic species. Habitat fragmentation can also endanger species that require interior habitats (Tanner, 2005), thus reducing their abundance at the edges and within the meadow itself (Smith et al., 2010).

How canopy fragmentationaffects seagrass meadow morphology and functionality is still unclear. In particular, the impact that global fragmentation (meadow-scale fragmentation) or the local presence of a

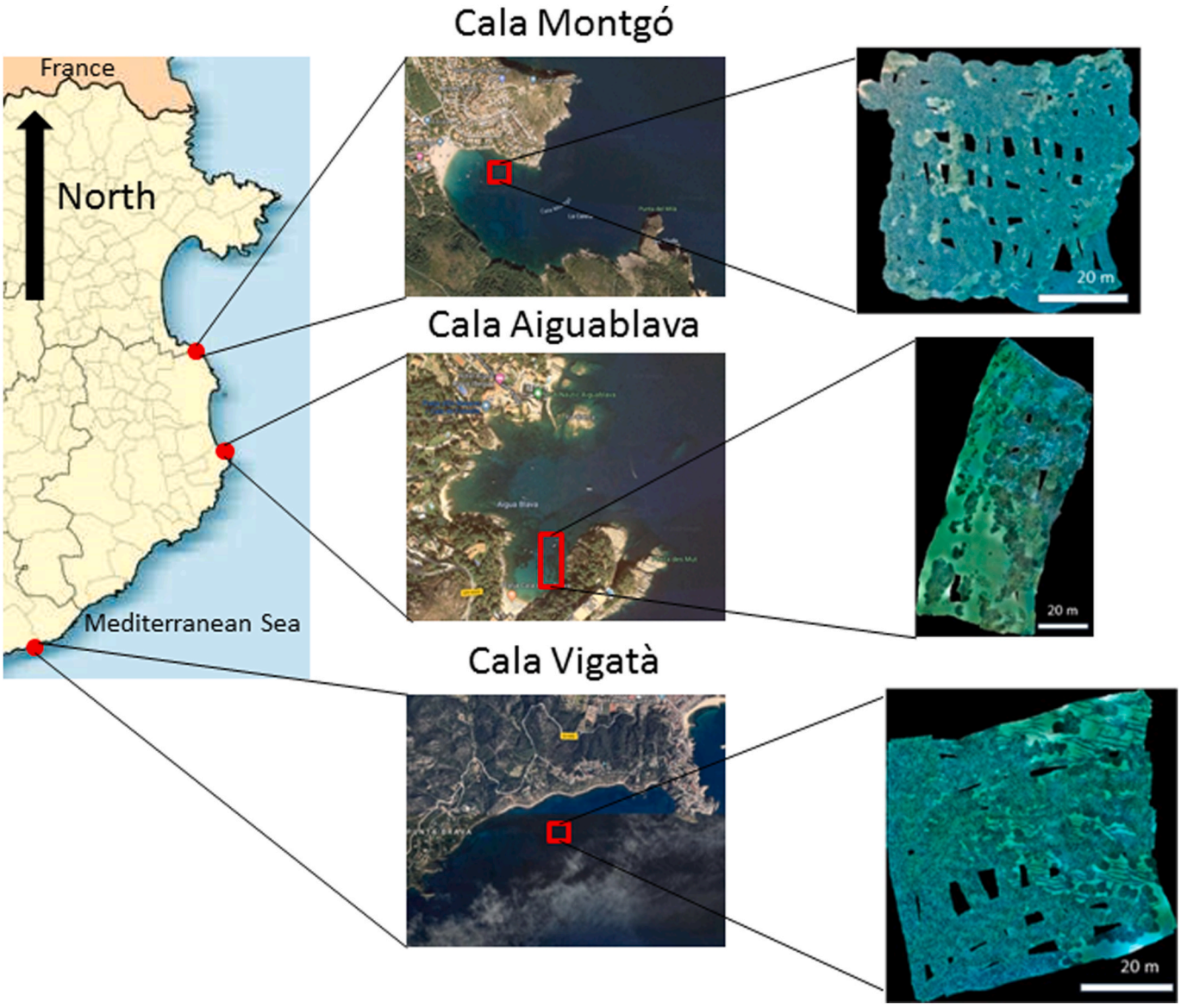

Fig. 1. Study sites located in Cala Montgó (42°6.305′N, 3°10.308′′E), Cala Aiguablava (41°56.118′N, 3°13.034′E) and Cala Vigatà (41°46.389′N, 3°1.554′E), on the NE coast of Spain (NW Mediterranean Sea). Figures on the right represent reconstructed images (photomosaics) of the studied seagrass meadows. Dark zones correspond to missing data due to no overlapping data images being captured during the video trajectories.

nearby gap (gap-scale characteristics) affect the shoot density of the edges of the canopy or the canopy density itself, are still to be fully determined. Therefore, using extensive field measurements from three *Posidonia oceanica* meadows on the northeast coast of Spain monitored over two consecutive years this manuscript aims to determine how both gap-scale characteristics and meadow-scale fragmentation impact canopy density. Two hypotheses are tested in this study: i) anincrease in gap size is expected to affect shoot density at the edges of the gap (the surrounding vegetation of the gaps) and ii) an increase in the degree of meadow fragmentation is expected to reduce shoot density at both the edge of the gaps and within the fully vegetated zone.

2. Methodology

Three *Posidonia oceanica* seagrass meadows on the NE coast of Spain (NW Mediterranean Sea) were studied over two consecutive years. The meadows were located 7 m deep off the bay of Cala Aiguablava and, 10 m deep off the Cala Montgó and Cala Vigatà bays (Fig. 1). Cala Aiguablava and Cala Montgó are semi-closed bays exposed to incoming winds and waves from the east i.e., the onshore is the exposed direction and the longshore the sheltered direction. On the contrary, Cala Vigatà is an open bay exposed to southerly and easterly winds and waves, i.e., both the onshore and the longshore are exposed to waves and currents. The three sites were surveyed in October 2018 and then again in October 2019.

The three *Posidonia oceanica* seagrass meadows were mapped over a prefixed area of analysis through video transects recorded by a scuba diver with a GoPro action camera and swimming 2 m above the meadows. The diver swam back and forth in both onshore and longshore directions to obtain the seascape view (photomosaic) of each meadow. The diver's trajectories were such that each sequential path (back and forth) ensured a 30% overlap between the recorded images in order to minimize the presence of holes in the photomosaics. The photomosaics were obtained by joining the images from the videos using the technique described in Gleason et al. (2007) and Elibol et al. (2011). The regions mapped presented outlined rectangular or quadrat shapes, consistent with the specific positions of the meadows (Fig. 1). Georeferencing was added during the photomosaic optimization process by using the fixed GPS coordinates of a set of seafloor features that were easily identifiable and manually annotated to create additional information in the analysis of the video images (Lirman et al., 2010), mainly by distinguishing the vegetated areas from the non-vegetated gaps. Three seascape photomosaics were created covering an area of 2247, 2622 and 2442 m^2 for Cala Aiguablava, Cala Montgó and Cala Vigatà, respectively (Fig. 1).

Gaps were classified in three classes (i.e., GAP1, GAP2, and GAP3), according to the ratio between their maximum lengths and the *Posidonia oceanica* leaf length. Since the mean leaf length of the plant (h_v) was 0.53 m, GAP1 includes gaps with a maximum size of $2h_v$, i.e., <1.06 m; GAP2 are gaps with between $3h_v$ and $2h_v$, i.e., 1.06< size <1.59 m andGAP3 have a size greater than$3h_v$, i.e., >1.59 m. Since the gaps in the field were not exactly circular, but often elliptical, their final classification was made based on their area. The area (in m^2) of each gap was calculated by considering an ellipse-shaped area around the two axes $L_{onshore}$ and $L_{longshore}$, and using equation (1):

$$A_{gap} = \pi \cdot \frac{L_{onshore}}{2} \cdot \frac{L_{longshore}}{2} \quad (1)$$

Therefore, GAP1 has a gap area $A_{gap} < 0.9\ m^2$, GAP2 in the range of $0.9\ m^2 < A_{gap} < 2\ m^2$, and GAP3 in the range of $2\ m^2 < A_{gap} < 3.5\ m^2$, whilst gaps $> 3.5\ m^2$ were discarded. A total of twenty one gaps were categorised, ten gaps in the GAP1 class, seven in GAP2, and four in GAP3 (Table 1). In correspondence with each gap, four transects in the vegetation surrounding the gap were established: two in the longshore and two in the onshore directions (see scheme in Fig. 2). Considering the starting point of each transect at the edge of the gap (corresponding to $x_1 = 0$ m), the subsequent longshore and onshore positions identified in the adjacent vegetation surrounding the gap were $x_2 = 0.5$ m, $x_3 = 1$ m and $x_4 = 2$ m, where the shoot density of the vegetation was measured. Therefore, for each gap, a total of sixteen positions in the vegetation were established and studied, four at the very edge of the gap and twelve in the vegetation adjacent to the gap, totalling 336 measurement points in the three meadows investigated. All the gaps in the analysis were chosen by considering that the inter-gap distances, (i.e., the distance between gap edges), were greater than 4 m to ensure that, the furthest position of analysis (2 m from the edge) in each gap, did not overlap with the adjacent gap. From the total number of gaps observed in the three meadows over both years, 25% of them would be included in the study (Table 1).

Table 1
Classes and characteristics of the gaps measured in the three meadows investigated in the two survey periods (2018, 2019). A_{gap} is the area of the gap, $L_{onshore}$ and $L_{longshore}$ are the two axes in the ellipse-shaped area of the gap.

Meadow	Year	GAP class	A_{gap} (m^2)	$L_{onshore}$ (m)	$L_{longshore}$ (m)
Aiguablava	2019	1	0.55	0.70	1.00
		1	0.50	0.40	1.60
		2	1.80	1.00	2.30
	2018	1	0.69	0.80	1.10
		1	0.94	0.75	1.60
		2	2.04	1.00	2.60
Montgó	2019	1	0.35	0.40	1.10
		1	0.94	1.50	0.80
		2	1.63	2.60	0.80
	2018	1	0.82	1.10	0.95
		2	1.84	1.18	1.30
		3	2.76	2.70	1.30
		1	0.71	0.70	1.30
		2	1.48	0.90	2.10
		3	2.76	1.30	2.70
Vigatà	2019	1	0.75	1.20	0.80
		2	1.56	0.90	2.20
		3	2.83	1.50	2.40
	2018	1	0.85	1.05	1.03
		2	1.51	1.60	1.20
		3	2.68	3.10	1.10

The ratio between the area of the gaps and the whole area of the studied meadow (in %) corresponded to the degree of fragmentation (I_{Frag}) of the meadow in each bay. In their study, Sleeman et al. (2005) used five categories (from highly fragmented to continuous seagrass seascapes) to classify meadow fragmentation: many/small patches for seagrass cover less than 7%, medium patches for 16%–37% of seagrass cover, few/large patches for 32–45% of seagrass cover, perforated continuous meadows to 45%–86% and continuous meadows for seagrass

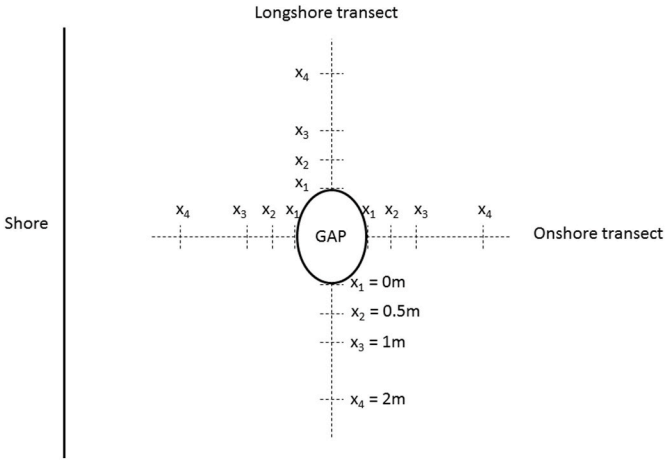

Fig. 2. Schematic representation of the measurement positions (x_1 to x_4) on both longshore and onshore transects.

cover greater than 93%. For each gap and at each measurement point the shoot density (SD, hereafter) was measured and considered to be as the key parameter with which to characterise the structural condition of the vegetation surrounding the gap. SD was measured following Colomer et al. (2017), by counting shoots within a 40 cm × 40 cm square subdivided into four 20 cm × 20 cm sub-quadrates, and placed on the top of the canopy. SD data at each gap edge distance for the two longshore and the two onshore directions were averaged in each gap and then averaged in all the gaps in Cala Aiguablava and Cala Montgó. In contrast, in Cala Vigatà, all SD data were averaged independent of the direction of the transect (i.e., longshore or onshore) because, due to the particular orientation of the bay, the gaps in Cala Vigatà were equally exposed to the incoming winds and waves from the south and the east (see Fig. 1). For this reason, all transects in Cala Vigatà have been considered to have the same characteristics and have been averaged all together and named "onshore".

For a suitable comparison of shoot density data among the three meadows, the non-dimensional parameter, ε, was calculated using equation (2):

$$\varepsilon = \frac{SD}{SD_{max}} \tag{2}$$

where SD is the shoot density averaged for longshore or onshore positions in each transect of each gap, and SD_{max} is the mean value of the four highest shoot densities measured at the position x = 2 m of longshore or onshore directions for each gap. ε represents the local density of the meadow compared to the maximum density of the canopy. ε < 1 indicates that the vegetation at the local scale has a density lower than the mean shoot density of the inner canopy areas for the study site. Maximum shoot density for each year in each meadow (Year SD_{max}) was calculated by averaging SD_{max} in each meadow during each survey period.

The porosity of the vegetation at the edge of the gap (P), measured in the position $x_1 = 0$ m (see Fig. 2), was calculated according to equation (3):

$$P_{\substack{edge \\ x_1 = 0}} = 1 - \varepsilon_{edge} \tag{3}$$

The porosity at the edge of the gap (at $x_1 = 0$ m) represents the part of the edge adjacent to the seafloor region without plants. Porosity was also related to the parameter L/S, where L is the characteristic length of the gap in both longshore ($L_{Longshore}$) and onshore ($L_{Onshore}$) directions and S is the plant-to-plant distance at the gap edge. The parameter δ50, which is the $L_{Onshore}/S$ value corresponding to a distance with porosity of 0.5 (50%), has been computed in each meadow.

3. Results

The degree of I_{Frag} was 63.4%, 22.1% and 13.6%, for Cala Aiguablava, Cala Vigatà and Cala Montgó meadows, respectively. The lowest fragmented meadows were at Cala Montgó and Cala Vigatà which corresponded to the category "perforated continuous meadow", while the highest fragmented meadow was found at Cala Aiguablava corresponded to the "medium patches" category. Year SD_{max} did not change consistently with I_{Frag} (Table 2).

Table 2
Meadow characteristics: mean values (±standard deviations) of the maximum shoot density (Year SD_{max}) for each year in each meadow, depth where the measurements were taken and degree of meadow fragmentation (I_{Frag}).

Year	Meadow	Year SD_{max} (shoots·m^{-2})	Depth (m)	I_{Frag} (%)
2018	Aiguablava	449 ± 36	7.1 ± 0.6	63.36
2018	Vigatà	353 ± 89	10.4 ± 0.2	22.06
2018	Montgó	332 ± 50	9.5 ± 0.2	13.60
2019	Aiguablava	105 ± 7	4.9 ± 0.4	63.36
2019	Vigatà	119 ± 6	5.2 ± 0.3	22.06
2019	Montgó	122 ± 3	4.9 ± 0.9	13.60

3.1. Structural analysis of vegetation adjacent to the gaps at the gap scale

With distance from the edge of the gap towards the fully vegetated canopy, ε increased until reaching a plateau (ε ≈ 1) at a distance x between 1 and 2 m from the gap edge in all cases (Fig. 3a). Two regions can be differentiated: the edge of the vegetation (where ε < 1) and within the canopy (where ε ≈ 1). The decrease in ε values with distance from within the meadow to the edge of the vegetation was more accentuated for large gaps than for small ones. Furthermore, ε decreased with the area of the gap, ranging from 0.92 for GAP1 to 0.38 for GAP3 (Fig. 3a). Cala Montgó, which is the least fragmented meadow, exhibited higher ε at the edge of the gaps (at $x_1 = 0$ m) than the most fragmented meadow at Cala Aiguablava, In Cala Montgó ε was higher than in Cala Aiguablava (Fig. 3b).

The porosity (P) at edge of the meadow, showed a linear relation with $L_{Onshore}/S$ in all three meadows (Fig. 4a). In contrast, for Cala Aiguablava and Cala Montgó, P did not show any dependence with $L_{Longshore}/S$ (Fig. 4b). Cala Aiguablava showed the highest relationship with P, increasing with $L_{Onshore}/S$, followed by Cala Vigatà and then Cala Montgó, showing the smoothest increase (Fig. 4a).

3.2. Structural analysis of vegetation near gaps at the canopy scale

I_{Frag} presented an inverse relationship with δ50 (Fig. 5). For a porosity level of 50%, the gap dimension ($L_{Onshore}/S$) expressed as δ50 was higher as the fragmentation was lower; as observed in Cala Montgó (Fig. 5a and b). Cala Aiguablava showed the highest I_{Frag} (63.4%, Fig. 5a) and the lowest δ50 (19.8, Fig. 5b). In Cala Montgó, displaying the lowest fragmentation (13.60%, Fig. 5a), fragmentation was inversely correlated with δ50.

4. Discussion

Meadow shoot density increased from the edge of a gap towards the fully-vegetated area to reach the highest canopy densities, whereby plant density stabilized. For all gap sizes and for all three meadows investigated, the highest canopy density was reached within 1–2 m from the edge of the gap. These results agree with Tanner (2005) who found that at the distance of 1 m from the *Zostera muelleri* and *Zostera muelleri* subsp. *macronuta* (Hartog) S.W.L. Jacobs meadows edges, the biomass of both seagrass species stabilized to the highest value of biomass (i.e., the biomass characteristic of the meadows). Colomer et al. (2017) found that the reduction in wave velocity and turbulent kinetic energy increased up to 1 m away from the edge of a vegetated patch, indicating that within a meadow at distances greater than 1 m from a meadow edge, the hydrodynamic parameters are attenuated. Unsworth et al. (2017) also found an increase in cover and canopy height for *Zostera marina* Linnaeus with increasing distance away from vegetation gaps. The present study proves that differences in vegetation gap sizes influence meadow density at the edge of a gap. On a local scale (i.e. gap-scale), larger gaps showed lower shoot density at the edge, while smaller gaps presented higher values of shoot density, which agrees with Colomer et al. (2017) where lower values of vegetation covers were found near larger gaps. A reduction in the canopy density is expected to lead to an increase in sediment resuspension (Gacia et al., 1999). Therefore, patchy meadows will have higher wave velocities and turbulence (El Allaoui et al., 2016), with higher sediment resuspension and erosion (El Allaoui et al., 2015) depending on the shoot density at the edges (Serra et al., 2018). These differences in canopy densities according to gap sizes could compromise meadow resistance due to an increase in seabed erosion, thus enhancing the generation of further gaps and the change from a continuous to patchy meadows (Abadie et al., 2018).

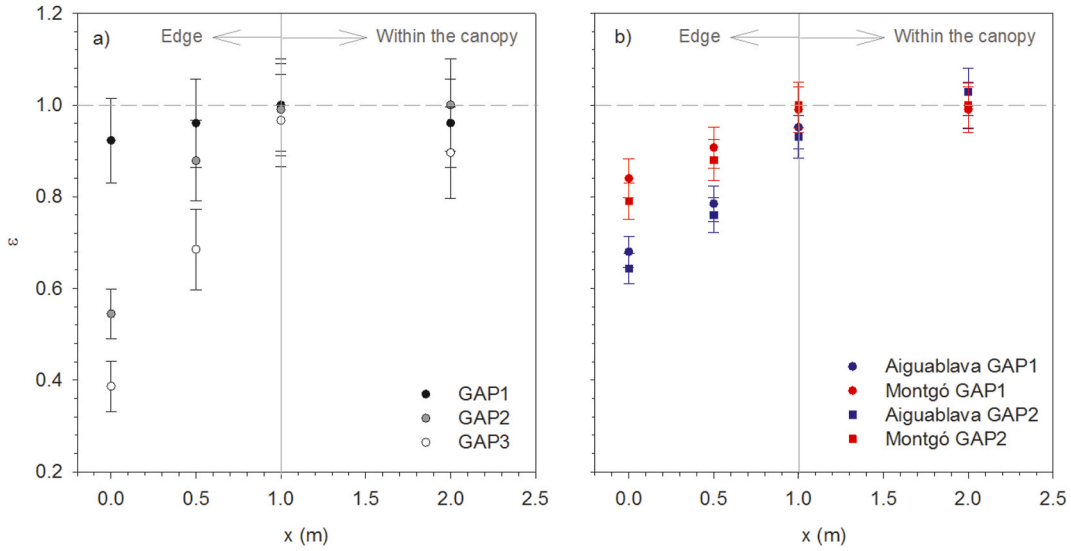

Fig. 3. a) Mean ε values for Cala Montgó in the 2019 survey along the onshore transect. Black filled circles correspond to GAP1 measurements, grey filled circles to GAP2 measurements and unfilled circles to GAP3 measurements. Error bars represent the standard deviation of the two transects with the same directions in each gap. b) Mean ε values for all surveys in Cala Montgó and Cala Aiguablava for each gap size along the onshore transects. Blue symbols correspond to Cala Aiguablava and red to Cala Montgó. Circles correspond to measurements from GAP1 and squares from GAP2. The dashed horizontal line symbolizes the maximum ε value ($\varepsilon \approx 1$), whilst the continuous vertical lines the distance (x) at which the gap edge reaches the maximum ε value.

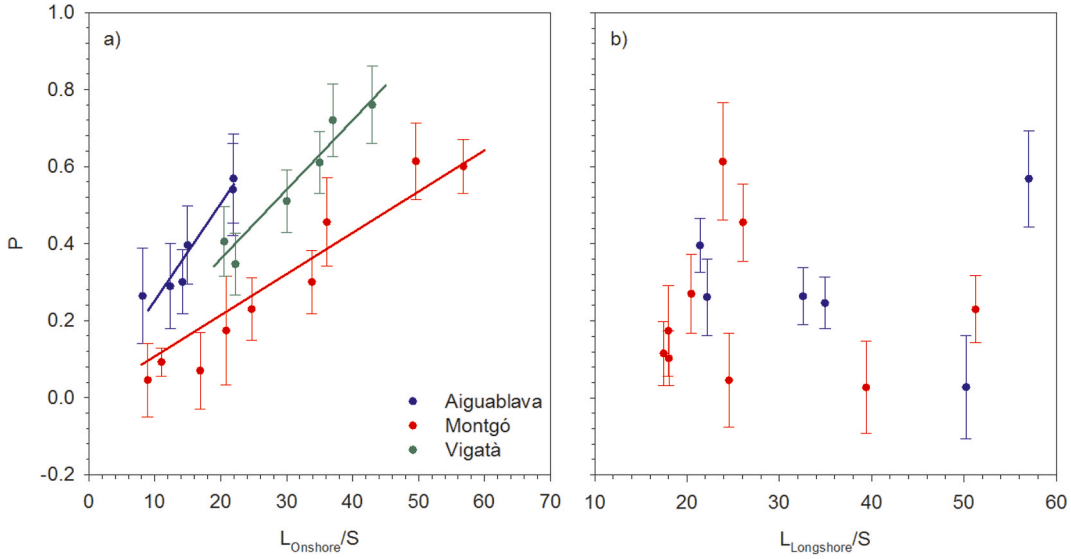

Figure 4. a) Relationships between the porosity (P) at the edge of the gaps and the ratio between $L_{Onshore}$ and plant-to-plant distance (S), for Cala Aiguablava (blue filled circles), Cala Montgó (red filled circles) and Cala Vigatà (green filled circles). The equations of the linear tendencies are: $P = 0.03$ ($L_{Onshore}/S$) with $R^2 = 0.911$ (for Cala Aiguablava), *p-value* $= 0.01$ ($L_{Onshore}/S$) with $R^2 = 0.912$ (for Cala Montgó);*p-value* $= 0.02$ ($L_{Onshore}/S$) with $R^2 = 0.939$ (for Cala Vigatà). b) Relationships between the porosity (P) at the edge of the gaps and the ratio between $L_{Longshore}$ and plant-to-plant distance (S), for Cala Aiguablava (blue filled circles) and Cala Montgó (red filled circles). Note that for Cala Vigatà, the longshore and onshore values of P were averaged since the of Cala Vigatà meadow is situated in an open bay with both directions exposed to waves and currents.

At the meadow scale, the degree of fragmentation of each zone has also been demonstrated to influence canopy density at the edge of gaps. This result agrees with the model by El Allaoui et al. (2016), who found that highly fragmented meadows have greater turbulent kinetic energy in the overall canopy, consequently reducing the shelter offered by the vegetation. Therefore, for the same gap size, the higher the overall meadow fragmentation is, the lower the meadow density at the edge. This result indicates that, given the same gap size, the gap remains more protected by the vegetated canopy in a continuous meadow than in a more fragmented meadow. These results confirm - in the field - the model created by El Allaoui et al. (2016), which hypothesised that fragmented canopies with smaller gaps produced higher shelter than fragmented canopies with larger gaps but with the same total fragmentation.

The degree of meadow fragmentation only affected the vegetation found in the onshore side of the gaps. In Cala Aiguablava and in Cala Montgó, only the edges of the gaps perpendicular to the coast are exposed to incoming winds and waves from the east, with the canopy responding at a gap scale through changes in canopy density in the onshore direction. Meanwhile, north-south gap edges did not present any relationship with canopy density. In contrast, in Cala Vigatà, which is exposed to easterly and southerly winds and waves, all the vegetation

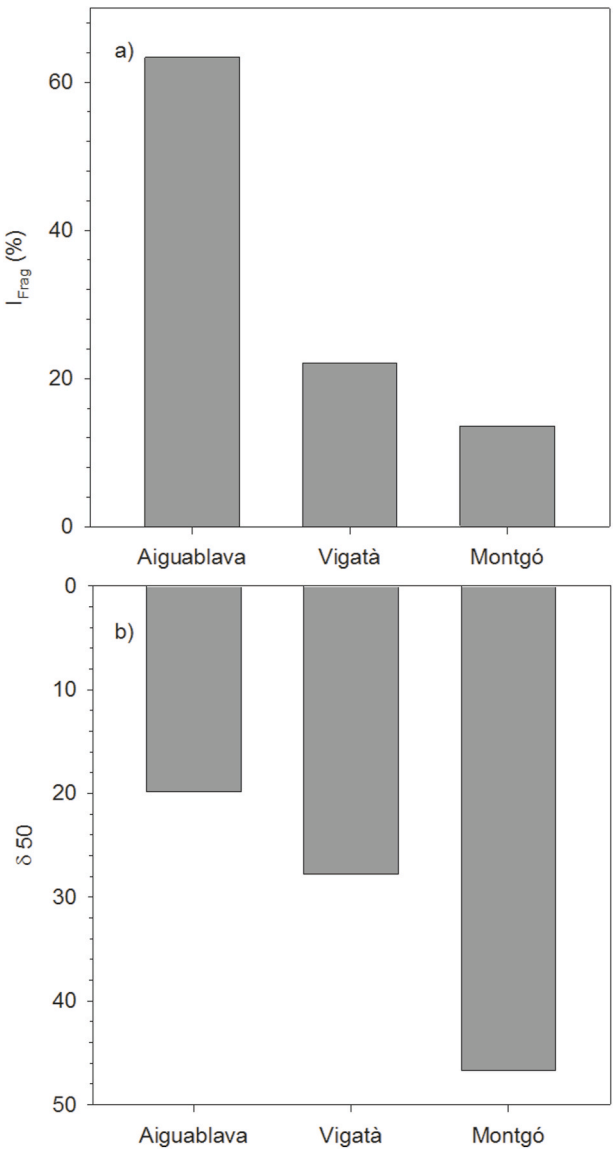

Fig. 5. a) Degree of meadow fragmentation, I_{Frag}, for Cala Aiguablava, Cala Montgó and Cala Vigatà. b) $L_{Onshore}/S$ value corresponding to a distance with porosity of 50%, δ 50 for the meadows of Cala Aiguablava, Cala Montgó and Cala Vigatà.

surrounding the gaps presented canopy densities that depend on the size of the gaps. Likewise, Tanner (2003) found that the abundance of animal groups was distributed depending on the orientation of vegetation patches to currents. For instance, greater numbers of adult and juvenile fishes were found in vegetated patches oriented parallel to the current; probably because they received a greater flux of feeding material. In contrast, larval forms, which are easily dispersed by higher currents, found refuge in patches perpendicular to the flow, i.e., in patches that provide a large extension of vegetation and hence higher protection.

The function of protection provided by seagrass is clearly conditioned by the local degree of fragmentation of each meadow. Thus, highly fragmented meadows like Cala Aiguablava, which corresponded to medium patch vegetation, will present vegetation gaps with lower surrounding canopy densities than zones that present lower fragmentation such as the Cala Vigatà or Cala Montgó meadows, both of which correspond to perforated meadows (Sleeman et al., 2005). Differences in canopy densities at the gap edges may imply changes in the vulnerability of the meadow to external pressures. For instance, Paquier et al. (2019) found that patchy meadows are not able to attenuate small and short waves. Higher canopy densities, however, are capable of attenuating not only wave velocity but also turbulent kinetic energy, thus providing greater protection (Hansen and Reidenbach, 2012; Hendricks et al., 2008; Granata et al., 2001). Colomer et al. (2017) found that vegetation gaps with greater surrounding plant cover present higher wave attenuation than gaps with lower surrounding plant cover. Lara et al. (2012) found an increase in turbulent diffusion in fragmented habitats of *Z. noltei*. Hence, higher fragmented seagrass meadows may present gap edges with low canopy density which might be more exposed to hydrodynamic processes and, in turn, make them more vulnerable. In contrast, gaps in less fragmented meadows may be more easily recolonized than gaps in higher fragmented meadows because of the greater shelter provided by the greater density at the gap edges. However, in mixed-species communities, the increase in the resuspended sediments due to the decrease in the shoot density could imply a shift in the associated community composition, with an increase in turbidity tolerant species when the pressure persists over time (Ros et al., 2014; Sagerman et al., 2020). While some authors (Smith et al., 2010) have hypothesised that vegetated patch sizes can influence the magnitude and patterns of the edge effects, this study has proved that gap size modifies the structural vegetation characteristics found at the edges of gaps. In fact, the results of the present study have also proved that the fragmentation of meadows at the meadow-scale produced differential effects at the local scale; in particular, high fragmentation negatively impacted the vegetation around the gaps, especially in the directions where the canopy edge was more exposed to currents and waves. In contrast, because they were sheltered, non-exposed canopy edges remained the same.

5. Conclusions

This study demonstrates that in the flow directions exposed to currents and waves, the impact meadow fragmentation has is two-fold effect: one on the local scale of the gap (gap-scale) and the other on the scale of the meadow (meadow-scale). At gap-scales, the gap size negatively influences the canopy density of the nearby vegetation. The larger the gap size is, the lower the shoot density of the nearby vegetation will be, thus allowing higher wave penetration At the meadow-scale, more fragmented meadows present lower shoot density in the vegetation surrounding the gaps than less fragmented meadows, but with the same sized gaps. Therefore, the overall degree of fragmentation of the meadow is a crucial parameter for the vulnerability of the seagrass meadows. The findings from this study also prove the impact of large-scale features (i.e., meadow scale fragmentation) or local-scale (i.e., gap-scale) processes. .

These results reveal that the fragmentation of a seagrass meadow may compromise the ecological services (such as the sheltering of the seabed) it provides, negatively impacting on possible seagrass recolonization and therefore threatening any potential future restoration intervention. In addition, the presence of gaps will leave the seabed exposed to waves and currents, increasing the sediment resuspension and therefore reducing their function in mitigating the effects of climate change and producing a negative feedback on the meadow's stability.

CRediT authorship contribution statement

Aina Barcelona: Methodology, Investigation, Formal analysis, Data curation, Writing - original draft. **Jordi Colomer:** Conceptualization, Methodology, Investigation, Data curation, Writing - review & editing. **Marianna Soler:** Conceptualization, Data curation, Writing - review & editing. **Nuno Gracias:** Image analysis, Methodology. **Teresa Serra:** Conceptualization, Methodology, Investigation, Data curation, Writing - review & editing, Supervision.

Declaration of competing interest

The authors declare that they have no known competing financial interests or personal relationships that could have appeared to influence the work reported in this paper.

Acknowledgments

This research was funded by the "Ministerio de Economía, Industria y Competitividad" of the Spanish Government through the grant CGL 2017-86515-P.

References

Abadie, A., Gobert, S., Bonacorsi, M., Lejeune, P., Pergent, G., Pergent-Martini, C., 2015. Marine space ecology and seagrasses. Does patch type matter in *Posidonia oceanica* seascapes? Ecol. Indicat. 57, 435–446. https://doi.org/10.1016/j.ecolind.2015.05.020.

Abadie, A., Pace, M., Gobert, S., Borg, J.A., 2018. Seascape ecology in *Posidonia oceanica* seagrass meadows: linking structure and ecological processes for management. Ecol. Indicat. 87, 1–13. https://doi.org/10.1016/j.ecolind.2017.12.029.

Boudouresque, C.F., Bernard, G., Pergent, G., Shill, A., Verlaque, M., 2009. Regression of Mediterranean seagrasses caused by natural processes and anthropogenic disturbances and stress: a critical review. Bot. Mar. 52, 395–418. https://doi.org/10.1515/BOT.2009.057.

Colomer, J., Soler, M., Serra, T., Casamitjana, X., Oldham, C., 2017. Impact of anthropogenically created canopy gaps on wave attenuation in a Posidonia oceanica seagrass meadow. Mar. Ecol. Prog. Ser. 569, 103–116. https://doi.org/10.3354/meps12090.

Duarte, C.M., Losada, I.J., Hendriks, I.E., Mazarrasa, I., Marbà, N., 2013. The role of coastal plant communities for climate change mitigation and adaptation. Nat. Clim. Change 3, 961–968. https://doi.org/10.1038/NCLIMATE1970.

El Allaoui, N., Serra, T., Colomer, J., Soler, M., Casamitjana, X., Oldham, C., 2016. Interactions between fragmented seagrass canopies and the local hydrodynamics. PloS One 11 (5), e0156264. https://doi.org/10.1371/journal.pone.0156264.

El Allaoui, N., Serra, T., Soler, M., Colomer, J., Pujol, D., Oldham, C., 2015. Modified hydrodynamics in canopies with longitudinal gaps exposed to oscillatory flows. J. Hydrol. 531, 840–849. https://doi.org/10.1016/j.jhydrol.2015.10.041.

Elibol, A., Garcia, R., Gracias, N., 2011. A new global alignment approach for underwater optical mapping. Ocean. Eng. 38 (10), 1207–1219. https://doi.org/10.1016//j.oceaneng.2011.02.013.

Espel, D., Diepens, N.J., Boutron, O., Buffan-Dubau, E., Chérain, Y., Coulet, E., Grillas, P., Probst, A., Silvestre, J., Elger, A., 2019. Dynamics of the seagrass *Zostera noltei* in a shallow Mediterranean lagoon exposed to chemical contamination and other stressors. Estuar. Coast Shelf Sci. 222, 1–12. https://doi.org/10.1016/j.ecss.2019.03.019.

Folkard, A.M., 2019. Biophysical interactions in fragmented marine canopies: fundamental processes, consequences, and upscaling. Frontiers in Marine Science 6, 279. https://doi.org/10.3389/fmars.2019.00279.

Gacia, E., Granata, T.C., Duarte, C.M., 1999. An approach to measurement of particle flux and sediment retention within seagrass (*Posidonia oceanica*) meadows. Aquat. Bot. 65, 255–268.

Gleason, A.C.R., Lirman, D., Williams, D., Gracias, N.R., Gintert, B.E., Madjidi, H., Reid, R.P., Boyton, G.C., Negahdaripour, S., Miller, M., Kramer, P., 2007. Documenting hurricane impacts on coral reefs using two-dimensional video-mosaic technology. Mar. Ecol. 28 (2), 254–258. https://doi.org/10.1111/j.1439-0485.2006.00140.x.

Granata, T.C., Serra, T., Colomer, J., Casamitjana, X., Duarte, C.M., Gacia, E., 2001. Flow and particle distributions in a nearshore seagrass meadow before and after a storm. Mar. Ecol. Prog. Ser. 218, 95–106. https://doi.org/10.3354/meps218095.

Grech, A., Chartrand-Miller, K., Erftemeijer, P., Fonseca, M., McKenzie, L., Rasheed, M., Taylor, H., Coles, R., 2012. A comparison of threats, vulnerabilities and management approaches in global seagrass bioregions. Environ. Res. Lett. 7, 024006 https://doi.org/10.1088/1748-9326/7/1/024006.

Hansen, C.R., Reidenbach, M.A., 2012. Wave and tidally driven flows in eelgrass beds and their effect on sediment suspension. Mar. Ecol. Prog. Ser. 448, 271–287. https://doi.org/10.3354/meps09225.

Hendriks, I.E., Sintes, T., Bouma, T.J., Duarte, C.M., 2008. Experimental assessment and modeling evaluation of the seagrass Posidonia oceanica on flow and particle trapping. Mar. Ecol. Prog. Ser. 356, 163–173. https://doi.org/10.3354/meps07316.

Lara, M., Peralta, G., Alonso, J.J., Morris, E.P., González-Ortiz, V., Rueda-Márquez, J.J., Pérez-Lloréns, J.L., 2012. Effects on intertidal seagrass habitat fragmentation on turbulent diffusion and retention time of solutes. Mar. Pollut. Bull. 64, 2471–2479. https://doi.org/10.1016/j.marpolbul.201.07.044.

Lirman, D., Gracias, N., Gintert, B., Gleason, A.C.R., Deangelo, G., Dick, M., Martinez, E., Ried, R.P., 2010. Damage and recovery assessment of vessel grounding injuries on coral reef habitats by use of georeferenced landscape video mosaics. Limnol Oceanogr. Methods 8, 88–97. https://doi.org/10.4319/lom.2010.8.0088.

Mateo, M.A., Romero, J., Pérez, M., Litter, M.M., Litter, D.S., 1997. Dynamics of millenary organic deposits resulting from the growth of the Mediterranean seagrass *Posidonia oceanica*. Estuar. Coast Shelf Sci. 44, 103–110. https://doi.org/10.1016/ecss.1996.0116.

Mazarrasa, I., Marbà, N., Garcia-Orellana, J., Masqué, P., Arias-Ortiz, A., Duarte, C.M., 2017. Dynamics of carbon sources supporting burial in seagrass sediments under increasing anthropogenic pressure. Limnol. Oceanogr. 62, 1451–1465. https://doi.org/10.1002/lno.10509.

Montefalcone, M., Parravicini, V., Vacchi, M., Albertelli, G., Ferrari, M., Morri, C., Bianchi, C.N., 2010. Human influence on seagrass habitat fragmentation in NW Mediterranean Sea. Estuar. Coast Shelf Sci. 86, 292–298. https://doi.org/10.1016/j.ecss.2009.11.018.

Montefalcone, M., Vacchi, M., Archetti, R., Ardizone, G., Astruch, P., Bianchi, C.N., Calvo, S., Criscoli, A., Fernández-Torquemada, Y., Luzzu, F., Misson, G., Morri, C., Pergent, G., Tomasello, A., Ferrari, M., 2019. Geospatial modelling and map analysis allowed measuring regression of the upper limit of *Posidonia oceanica* seagrass meadows under human pressure. Estuar. Coast Shelf Sci. 217, 148–157. https://doi.org/10.1016/j.ecss.2018.11.006.

Paquier, A., Meulé, S., Anthony, E.J., Larroudé, P., Bernard, G., 2019. Wind induced hydrodynamics interactions with aquatic vegetation in a fetch-limited setting: implications for coastal sedimentation and protection. Estuar. Coast 42, 688–707. https://doi.org/10.1007/s12237-018-00487-w.

Pujol, D., Nepf, H., 2012. Breaker-generated turbulence in and above a seagrass meadow. Continent. Shelf Res. 49, 1–9. https://doi.org/10.1016/j.csr.2012.09.004.

Pujol, D., Serra, T., Colomer, J., Casamitjana, X., 2013. Flow structure in canopy models dominated by progressive waves. J. Hydrol. 486, 281–292. https://doi.org/10.1016/j.jhydrol.2013.01.024.

Ricart, A.M., York, P.H., Rasheed, M.A., Pérez, M., Romero, J., Bryant, C.V., Marcedie, P. I., 2015. Variability of sedimentary organic carbon in patchy seagrass landscapes. Mar. Pollut. Bull. 100, 476–482. https://doi.org/10.1016/j.marpolbul.2015.09.03.

Ros, A., Colomer, J., Serra, T., Pujol, D., Soler, M., Casamitjana, X., 2014. Experimental observations on sediment resuspension within submerged model canopies under oscillatory flow. Continent. Shelf Res. 91, 220–231. https://doi.org/10.1016/j.csr.2014.10.004.

Sagerman, J., Hansen, J.P., Wikström, S.A., 2020. Effects of boat traffic and mooring infrastructure on aquatic vegetation: a systematic review and meta-analysis. Ambio 49, 517–530. https://doi.org/10.1007/s13280-019-01212-9.

Serra, T., Oldham, C., Colomer, J., 2018. Local hydrodynamics at edges of marine canopies under oscillatory flows. PloS One 13 (8), e0201737. https://doi.org/10.1371/jounal.pone.0201737.

Sleeman, J.C., Kendrick, G.A., Boggs, G.S., Hegge, B.J., 2005. Measuring fragmentation of seagrass landscapes: which indices are most appropriate for detecting change? Mar. Freshw. Res. 58, 851–864. https://doi.org/10.1071/MF04300.

Smith, T.M., Hindell, J.S., Jenkins, G.P., Connolly, R.M., 2010. Seagrass patch size affects fish responses to edges. J. Anim. Ecol. 79, 275–281. https://doi.org/10.1111/j.1365-2656.2009.01605.x.

Tanner, J.E., 2003. Patch shape and orientation influences on seagrass epifauna are mediated by dispersal abilities. Oikos 100, 517–524. https://doi.org/10.1034/j.1600-0706.2003.12060.x.

Tanner, J.E., 2005. Edge effects on fauna in fragmented seagrass meadows. Austral Ecol. 20, 210–218. https://doi.org/10.1111/j.1441-9993.2005.01438.x.

Unsworth, R.K.F., McKenzie, L.J., Collier, C.J., Cullen-Unsworth, L.C., Duarte, C.M., Eklöf, J.S., Jarvis, J.C., Jones, B.L., Nordlund, L.M., 2018. Global challenges for seagrass conservation. Ambio 48, 801–815. https://doi.org/10.1007/s13280-018-1115-y.

Unsworth, R.K.F., Williams, B., Jones, B.L., Cullen-Unsworth, L.C., 2017. Rocking the boat: damage to eelgrass by swimming boat moorings. Front. Plant Sci. 8, 1309. https://doi.org/10.3389/fpls.2017.01309.

Valdemarsen, T., Canal-Vergés, P., Kritersen, E., Holmer, M., Kristiansen, M.D., Flindt, M. R., 2010. Vulnerability of *Zostera marina* seedlings to physical stress. Mar. Ecol. Prog. Ser. 418, 119–130. https://doi.org/10.3354/meps08828.

Valdez, S.R., Zhang, Y.S., van der Heide, T., Vanderklift, M.A., Tarquino, F., Orth, R.J., Silliman, B.R., 2020. Positive ecological interactions and success of seagrass restoration. Frontiers in Marine Science 7, 91. https://doi.org/10.3389/fmars.2020.00091.

Waycott, M., Duarte, C.M., Carruthers, T.J.B., Orth, R.j., Dennison, W.C., Olyarnik, S., Calladine, A., Fourqurean, J.W., Heck Jr., k. l., Hughes, A.R., Kendrick, G.A., Kenworthy, W.J., Short, F.T., Williams, S.L., 2009. Accelerating loss of seagrasses across the global threatens coastal ecosystems. Proc. Natl. Acad. Sci. Unit. States Am. 106 (30), 12377–12381. https://doi.org/10.1073/pnas.0905620106.

Williams, S.L., 2007. Introduced species in seagrass ecosystems: status and concerns. J. Exp. Mar. Biol. Ecol. 350, 89–110. https://doi.org/10.1016/j.jembe.2007.05.032.

Zong, L., Nepf, H., 2011. Spatial distribution of deposition within a patch of vegetation. Water Resour. Res. 47, W03516. https://doi.org/10.1029/2010WR009516.

Coastal Engineering 169 (2021) 103972

Contents lists available at ScienceDirect

Coastal Engineering

journal homepage: www.elsevier.com/locate/coastaleng

Particle capture by seagrass canopies under an oscillatory flow

Aina Barcelona [a,*], Carolyn Oldham [b], Jordi Colomer [a], Jordi Garcia-Orellana [c,d], Teresa Serra [a]

[a] Department of Physics, University of Girona, 17071, Girona, Spain
[b] School of Engineering, The University of Western Australia, Perth, WA, 6009, Australia
[c] Departament of Física, Universitat Autònoma de Barcelona (UAB), Campus UAB, 08193, Bellaterra, Barcelona, Spain
[d] Institut de Ciència i Tecnologia Ambientals, Z Building, Universitat Autònoma de Barcelona (UAB), Campus UAB, 08193, Bellaterra, Barcelona, Spain

ARTICLE INFO

Keywords:
Seagrass
Sediment transport
Oscillatory flow
Turbulent kinetic energy
Sediment capture
Sedimentation

ABSTRACT

Although seagrass canopies are known to enhance particle sedimentation, there is still limited knowledge about how seagrasses modify the vertical distribution of sediment particles; especially when particles come from allochthonous sources. This study determined the volume of particles trapped by the seagrass leaves, the amount that remains in suspension both within and above the canopy, and the amount deposited onto the seabed. A set of laboratory experiments were conducted in which hydrodynamic conditions and canopy densities were varied to mimic real field conditions. This study demonstrated and quantified previously recorded observations concerning the fate of sediment in seagrass meadows. Seagrass meadows decreased the amount of suspended sediment by capturing the sediment on the blades of the seagrass and by enhancing particle sedimentation on the seabed. However, particles trapped by the blades of seagrass in the whole canopy increased with canopy density and reduced the number of particles in suspension within the canopy. The ecological implications were significant, since a seabed covered by vegetation, when compared to a bare seabed, produced a reduction in the suspended sediment particles within the canopy, improving water clarity. Furthermore, canopies (compared to bare substrates) enhanced seabed sedimentation and the denser the canopy was, the greater the amount of sediment deposited on the seabed.

1. Introduction

Seagrass canopies formed by *Posidonia oceanica* (Linnaeus) Delile or *Cymodocea nodosa* (Ucria) Ascherson are recognized in the EU Water Framework Directive (Community, 2000) as water quality indicators as they provide many ecosystem functions and services and maintain the complex structure of habitats (Brodersen et al., 2017b; Zucchetta et al., 2016). Species diversity in seagrasses increases with the structural complexity of the seagrass canopies (González-Ortiz et al., 2016). Seagrass meadows also play a role in 'blue carbon' sequestration because suspended particulate organic carbon can be trapped and buried by canopy action, thus mitigating the effect of the ongoing increase in CO_2 (Armitage and Fourqurean, 2016; Ricart et al., 2017). Furthermore, because damage to or the destruction of seagrass meadows can cause a release of carbon to the environment (Fourqurean et al., 2012), in developing 'blue carbon' strategies, management authorities and stakeholders could restore carbon sequestration capacities through coastal restoration projects (Duarte et al., 2013, 2015).

Allochthonous sediment particles transported by currents can impact coastal seagrass meadows negatively and consequently reduce the services they provide (Fraser et al., 2017). Some natural origins of the allochthonous sediment input can be coastal runoff, river plumes or natural resuspension (Pineda et al., 2016). Climate change has led to an increase in the frequency and intensity of heavy precipitation episodes which, in turn, has increased episodic river and runoff outflow (Vautard et al., 2014). Coastal development is also responsible for moving large amounts of sediment that can impact seagrass meadows (Wu et al., 2017). Suspended sediment input increases turbidity in the water column (Pineda et al., 2016; Wu et al., 2017; Roy et al., 2013), leading to a decrease in light intensity that then limits phytoplankton and seagrass growth, and buries benthic communities (Fraser et al., 2017; Vanderploeg et al., 2007; Longstaff and DennisonW.C., 1999).

Seagrass beds are one of the most valuable habitats in coastal zones because they promote the reduction of suspended particles within the seagrass meadows. Seagrasses affect particle sediment fluxes by reducing flow velocity, increasing sediment deposition and, via the plant

* Corresponding author.
E-mail addresses: aina.barcelona@udg.edu (A. Barcelona), carolyn.oldham@uwa.edu.au (C. Oldham), jordi.colomer@udg.edu (J. Colomer), jordi.garcia@uab.cat (J. Garcia-Orellana), teresa.serra@udg.edu (T. Serra).

https://doi.org/10.1016/j.coastaleng.2021.103972
Received 15 July 2020; Received in revised form 10 June 2021; Accepted 4 August 2021
Available online 4 August 2021

leaves themselves within the seagrass canopy capturing particles (Granata et al., 2001; Hendriks et al., 2008), decreasing sediment resuspension (Gacia et al., 1999; Zong and Nepf, 2011). Hence, the allochthonous suspended sediment that is advected over a canopy can remain in suspension in the water column inside the canopy, or settle to the seabed and possibly be resuspended, or be captured by the seagrass. That said, little information is available about the physical role the canopy densities play in trapping particles and thus improving carbon sequestration in coastal waters (Greiner et al., 2016; Marbà et al., 2015). Until now, the effect seagrasses have on the fate of particles from allochthonous sources in coastal areas has been studied observationally. For instance, Lawson et al. (2012) found an increase in the sediment suspended from the seabed in low densities of *Agarophyton vermiculophylla* (Ohmi) Gurgel, although J.N Norris & Fredericq compared this with higher densities. Through field observations, Gacia et al. (1999) determined that, when compared to bare substrates, seagrass meadows promote sediment accretion. Other authors have studied sediment resuspension in laboratory experiments (Ros et al., 2014; Zhang et al., 2018; Zhang and Nepf, 2019). Ros et al. (2014), for example, found that the presence of vegetation produced a decrease in resuspension and an increase in sediment deposition compared to bare seabeds. Sediment resuspension is reduced in dense model canopies because of the attenuation of the turbulent kinetic energy (*TKE*) (Gacia et al., 1999; Ros et al., 2014; Zhang et al., 2018; Bos et al., 2007). However, none of these studies quantifies the amount of sediment particles captured by plant leaves or how particles settling onto the seabed is enhanced by the presence of vegetation.

Hendricks et al. (Hendriks et al., 2008) did, however, find that there was a reduction in resuspended sediments within a seagrass canopy compared to bare or eroded grasslands, not only because of reduced hydrodynamic energy, but also because of reduced particle transport due to the energy loss caused by collisions with seagrass leaves. Different rates of reduction in the suspended sediment were also found for different types of *Caulerpa* sp. And seagrass canopies (Hendriks et al., 2010), indicating the role the distinct architectures found within the canopy has in the behaviour of suspended particles. Furthermore, the particle retention by a single cylindrical collector was also quantified and found to increase as the diameter of the collector increased (Palmer et al., 2004). Short and Short (Short et al., 1984) also found a smaller overall turbidity in seagrasses with higher leaf surface area, indicating the potential role the leaves have in reducing water turbidity. In their study, however, no quantification of the sediment deposited on the leaves was carried out. Terrados and Duarte (2000) conducted experiments with leaf detritus samples situated within a seagrass bed and on an unvegetated bed and demonstrated that seagrasses reduce particle resuspension compared to bare sandy beds. Lovelock et al. (2014) found that, because of a higher sediment input in saltmarshes compared to areas of mangroves, a greater accumulation of carbon occurred in the saltmarshes. Howe et al. (2009) also found a higher carbon sequestration in undisturbed saltmarshes compared to disturbed saltmarshes, with the increase in the carbon sequestration in undisturbed saltmarshes being driven by greater rates of vertical accretion. Finally, Agawin and Duarte (2002) studied the capture of particles by seagrass leaves in the field and observed that some of the suspended particles were phagocyted by the seagrass epiphytes found on the leaves of the plants (Agawin and Duarte, 2002). However, in their study they did not explore the role hydrodynamics play in capturing particles.

Despite the availability of all these studies concerning particle dynamics within a seagrass meadow, there are still no studies that address and quantify the effect of the canopy density and the trapping (capturing) of particles by seagrass leaves from allochthonous sources under different hydrodynamic conditions. Therefore, and considering that the fate of allochthonous particle sedimentation in seagrass canopies is not yet fully understood, or that most current findings have been obtained from field observations, the aim of this study was to identify and quantify the role seagrasses have in capturing sediments. To understand the ecological implications, laboratory experiments were carried out to: i) study how sediment particles of different sizes are trapped by plant leaves under different hydrodynamic conditions, ii) examine the suspended sediment concentration within and above the canopy and iii) determine the sedimentation on the seabed of different sized particles. Special attention was paid to the behaviour of the particle sizes for both particle trapping by plant blades, and sedimentation onto the seabed.

2. Methodology

2.1. The flume

The study was carried out in a methacrylate flume (600 × 50 × 50 cm; Fig. 1) with a mean water depth of $h = 30$ cm (Table 1). A vertical flap-type wavemaker was driven by a variable-speed motor at two frequencies (0.7, 1.2 Hz) and four strokes (12, 14, 16, and 18 cm). The wave lengths (λ) were calculated using the dispersion equation by Lowe et al. (Le Méhauté, 1976), as $\lambda = 2.43$ m for $f = 0.7$ Hz and $\lambda = 1.03$ m for $f = 1.2$ Hz. These wave conditions, $\lambda/20 < h < \lambda/2$, corresponded to transitional water waves like those typically found in coastal regions (Serra et al., 2018) with the presence of seagrasses. The waves produced had amplitudes in the range A = 2–4 cm. Therefore, $2A/\lambda = 0.08$, which is below the threshold of 0.14 and corresponds to breaking waves. However, while these waves fell far from the linear Stokes waves, they did correspond to third order Stokes waves, i.e., closer to the breaking limit than linear waves (Le Méhauté, 1976). Third order Stokes waves have been found to produce instabilities at the water surface (in the form of spilling) for $2A/\lambda = 0.10$, thus producing turbulence that is transported downwards in the water column (Iafrati, 2011). The waves used here had $2A/\lambda = 0.08$; close to the threshold found by Iafrati (2011). Therefore, although spilling was not observed through visual inspection, some *TKE* production at the surface could hold. The presence of seagrasses has been found from 1 m to nearly 18 m depths depending on the light attenuation (Duarte, 1991). From these above-mentioned considerations, the scaling of the vegetation in the flume could represent the behaviour of seagrasses in coastal areas. The combination of frequencies and strokes yielded eight wave amplitudes (A = 1.5, 2.0, 2.2, 3.0, 5.0, 5.6 cm). A plywood beach with a slope of 1:3 and covered with a 7 cm thick layer of foam rubber was positioned at the end of the flume to eliminate wave reflection (Pujol et al., 2013b; Pujol and Nepf, 2012). The wavemaker was situated at x = 0 cm in the longitudinal direction, the centre of the tank at y = 0 cm in the lateral direction, and the flume bed at z = 0 cm in the vertical direction.

To mimic the injection of sediment particles from an allochthonous source, a methacrylate pipe (*Internal diameter, ID* = 3 cm, length = 300 cm) with 43 evenly distributed injectors (*ID* = 0.5 cm, length = 8.6 cm, 7 cm apart) was used to inject sediment-laden water (see Section 2.3) into the flume. The end of each injector was covered with a 1 mm mesh to slow down injection rates. The injection pipe was situated outside the water column so that the injectors protruded 5 cm into the water surface as the injection was carried out.

Throughout this study, an allochthonous sediment source is considered as the sediment input from outside the meadow. In the discussion, the results obtained will be compared to other studies carried out on the resuspension of sediment already deposited on the seabed, i.e., not coming from outside the meadow and therefore considered as autochthonous sediment.

2.2. The canopy

Each plant in the canopy was made up of eight 0.075 mm-thick polyethylene canopy leaf blades attached to PVC dowels that had been randomly inserted into a perforated baseboard ($L = 250$ cm (Pujol et al., 2013a),). The rigid dowel extended 1 cm above the bed (Zhang et al., 2018) and the canopy leaf blades were geometrically and dynamically

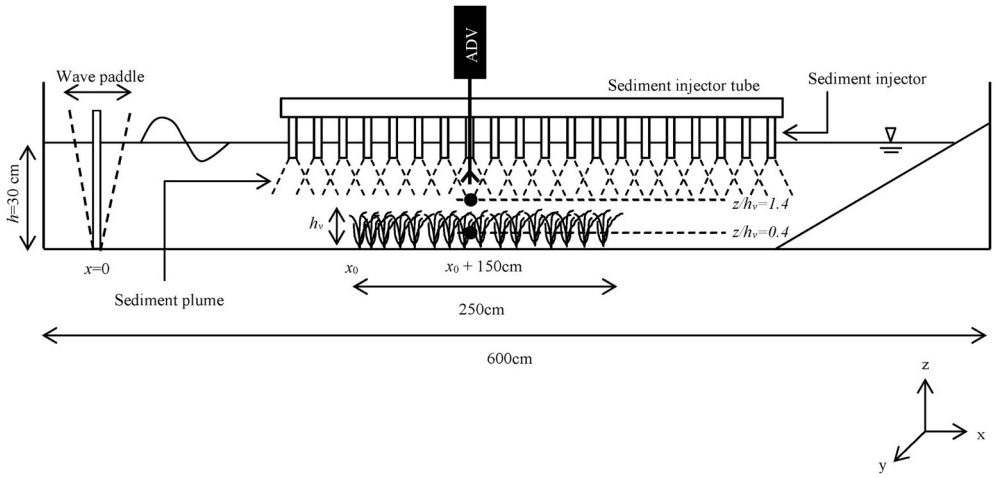

Fig. 1. A lateral view of the experimental setup. Experiments were conducted in a 600 × 50 × 50 cm long flume, with a mean water depth of 30 cm. The model canopy was 250 cm long and canopy height was $h_v = 14$ cm. Filled circles show where both hydrodynamics and sediment measurements were taken. The triangle at the water-air interface represents the water level in the flume.

Table 1
Nomenclature table.

Variable	Units	Definition	Variable	Units	Definition
A	cm	wave amplitude	SPF	%	solid plant fraction
a	cm^2	frontal area	SW	μL	suspended sediment within the canopy ($z/h_v = 1.4$)
ad	non-dimensional	fractional volume occupied by plants	t	min	time
A_{inj}	m^2	injection area	TKE	$cm^2 \cdot s^{-2}$	turbulent kinetic energy
A_w	cm	wave excursion length	T_s	min	time of the steady state
A_w/S_b	non-dimensional	ratio of wave excursion to plant-to-plant distance between blades	u	$cm \cdot s^{-1}$	Eulerian velocity in the x direction
B_o	$m^2 \cdot s^{-3}$	buoyancy flux	u'	$cm \cdot s^{-1}$	turbulent velocity
c	%	particle concentration	U_c	$cm \cdot s^{-1}$	steady velocity associated with the current
c_0	$\mu L \cdot L^{-1}$	initial sediment concentration	U_i	$cm \cdot s^{-1}$	instantaneous velocity
c_p	$\mu L \cdot L^{-1}$	concentration of sediment attached to blades	$U_i(\phi)$	$cm \cdot s^{-1}$	instantaneous velocity according to the phase
c_s	$\mu L \cdot L^{-1}$	suspended sediment concentration at steady state	U_w	$cm \cdot s^{-1}$	wave velocity
c_t	$\mu L \cdot L^{-1}$	suspended sediment concentration with time	U_w^{rms}	$cm \cdot s^{-1}$	orbital velocity
d	cm	blade diameter	v	$cm \cdot s^{-1}$	Eulerian velocity in the y direction
D	m	Injector ID	V_{IN}	%	total volume of particles injected into the flume
$D50$	μm	representative particle diameter	V_{SB}	%	volume of sediment settled to the bed
d_p	μm	particle diameter	V_{SC}	%	volume of suspended sediment inside the canopy ($z/h_v = 0.4$)
f	Hz	wave frequency	Vs_P	%	volume of sediment captured by the plants
g	$m \cdot s^{-2}$	gravitational acceleration	V_{SW}	%	volume of suspended sediment above the canopy ($z/h_v = 1.4$)
h	cm	water height	w	$cm \cdot s^{-1}$	Eulerian velocity in the z direction
h_v	cm	canopy height	w_o	cm·s	injection velocity
ID	cm	inner diameter	x	cm	longitudinal direction
L	cm	canopy length	$x=0$	cm	position of the wave paddle
L_M	cm	length scale	x_0	cm	initial position of the canopy
M_o	$m^4 \cdot s^{-2}$	volume flux	y	cm	lateral direction
n	$stems \cdot m^{-2}$	canopy density	z	cm	vertical direction
n_b	blades	number of blades	z/h_v	non-dimensional	measurement position
n_{inj}	injectors	number of injectors	α_w	non-dimensional	ratio of U_w
P_C	%	partition coefficient of V_{SP} and V_{SC}	β_w	non-dimensional	ratio of TKE
Q	$m^3 \cdot s^{-1}$	injection flow	Δb_o	$m \cdot s^{-2}$	buoyancy of the resting plume fluid
Q_o	$m^4 \cdot s^{-3}$	momentum flux	λ	m	wave length
S_b	cm	blade-to-blade distance	ρ_s	$kg \cdot m^{-3}$	water density
SB	μL	sediment settled to the bed	ρ_w	$kg \cdot m^{-3}$	sediment density
SC	μL	suspended sediment within the canopy ($z/h_v = 0.4$)	ϕ	radians	wave phase
SP	μL	sediment attached to plants	ω	$radians \cdot s^{-1}$	angular frequency
			k	$radians \cdot cm^{-1}$	spatial frequency

similar to those of *Posidonia oceanica* (Pujol et al., 2013a; Ghisalberti and Nepf, 2002; Folkard, 2005). The canopy height was $h_v = 14$ cm, however, the effective height when the leaf blades were bent by the waves was $h_v = 13 \pm 1$ cm. The initial position of the vegetation (x_0) was situated 100 cm from the wavemaker (Fig. 1). The canopy density was quantified using the solid plant fraction (SPF) defined as:

$$SPF\ (\%) = 100n\pi\left(\frac{d}{2}\right)^2 \quad (1)$$

where n is the number of stems per unit area and d is the stem diameter (1 cm). Five *SPF*s were used (0%, 1%, 2.5%, 5% and 7.5%), which corresponded to canopy densities n = 0, 127, 318, 637 and 955 stems·m^{-2} (Fig. 2) which fall within the range 78–1000 stems·m^{-2} found in the field (Hendriks et al., 2008; Ghisalberti and Nepf, 2002; Folkard, 2005; Zhang and Nepf, 2008; Goring and Nikora, 2002). *SPF* = 0% corresponded to unvegetated beds. Two frequencies and eight wave amplitudes varied across the five *SPF*s resulted in a total of 40 experiments (Table 2), each 90 min in duration.

The fractional volume occupied by the plants (ad) for each canopy density was calculated as the frontal area of the plant per unit volume, a, multiplied by the stem diameter, d (Zhang and Nepf, 2008). Greyscale photographs taken from the top of the canopy were analysed to calculate canopy cover in the absence of wave motion (Serra et al., 2018). The five canopy densities corresponded to a canopy cover of 0, 37.4, 52.1, 70.6 and 80.9% (Fig. 2) and the photographs determining the cover were taken in the absence of wave motion. Canopy cover followed a non-linear trend with the fractional volume (Fig. 2e) cover = 207*$ad^{0.4}$, indicating that full cover (100%) occurred at ad = 0.16, corresponding to an *SPF* of 12.5% and a canopy density of 1592 stems·m^{-2}.

2.3. Measuring velocities

The Eulerian velocity field was defined as (u, v, w) in the (x, y, z) directions, respectively. The three components of velocity were recorded (at a frequency of 50 Hz over 10 min) with a downwards-looking Acoustic Doppler Velocimeter (16-MHz MicroADV, Sontek). The ADV measures at a distance of 5 cm from the probe tip, and with a sampling volume of 0.09 cm^3. Beam correlations less than 80% were discarded and spikes were removed (Pujol et al., 2013a; Goring and Nikora, 2002). The number of spikes increased slightly with the presence of the plants and the canopy density compared with the unvegetated case. The percentage of spikes was from 0.33% for the unvegetated case to 0.77% for the most densely vegetated case.

To eliminate the lower order spatially periodic variation in wave and velocity amplitude associated with wave reflection (Pujol et al., 2013a; Luhar et al., 2010), the longitudinal velocity was measured at an antinode. The model canopy was then shifted longitudinally along the flume to ensure measurements were taken 150 cm from the canopy edge. For the densest canopy experiments, some plants were removed and re-inserted into nearby holes to avoid blocking the ADV beams (Zhang et al., 2018; Zhang and Nepf, 2019; Pujol et al., 2010, 2013b; Colomer et al., 2017).

2.4. Velocity and turbulent kinetic energy analysis

For oscillatory flows, the instantaneous velocity, $U_i(t)$, can be decomposed as:

$$U_i(t) = U_c + U_w + u'. \quad (2)$$

where U_c is the steady velocity associated with the current, U_w is the unsteady wave motion which represents spatial variations in the phase-averaged velocity field, and u' is the turbulent velocity, that is, the instantaneous velocity fluctuation in the x-direction. U_c is the phase-averaged velocity:

$$U_c = \frac{1}{2\pi}\int_0^{2\pi} U_i(\phi)\partial\phi \quad (3)$$

where $U_i(\phi)$ is the instantaneous velocity according to the phase (Luhar et al., 2010; Lowe et al., 2005). Wave velocity, U_w, was obtained by using a phase averaging technique. The Hilbert transform was used to average oscillatory flow velocities with a common phase (Ros et al., 2014; Pujol et al., 2013b). The root mean square (rms) of $U_i(\phi)$ was considered as the characteristic value of the orbital velocity U_w^{rms} (U_w hereafter) at each depth, and was calculated according to:

$$U_w^{rms} = \sqrt{\frac{1}{2\pi}\int_0^{2\pi}(U_i(\phi) - U_c)^2\partial\phi} \quad (4)$$

For cases WP5 and SFV37, vertical profiles of the velocity were taken from which the wave velocity and turbulent kinetic energy profiles were calculated (Fig. 3). The wave velocity decreased from the layer above the canopy to the bed. From the vertical profile of the wave velocity, two vertical regions were differentiated: the above-canopy layer and the within-canopy layer (Fig. 3a). In the above-canopy layer, the wave velocity was the highest with similar results compared to the without-

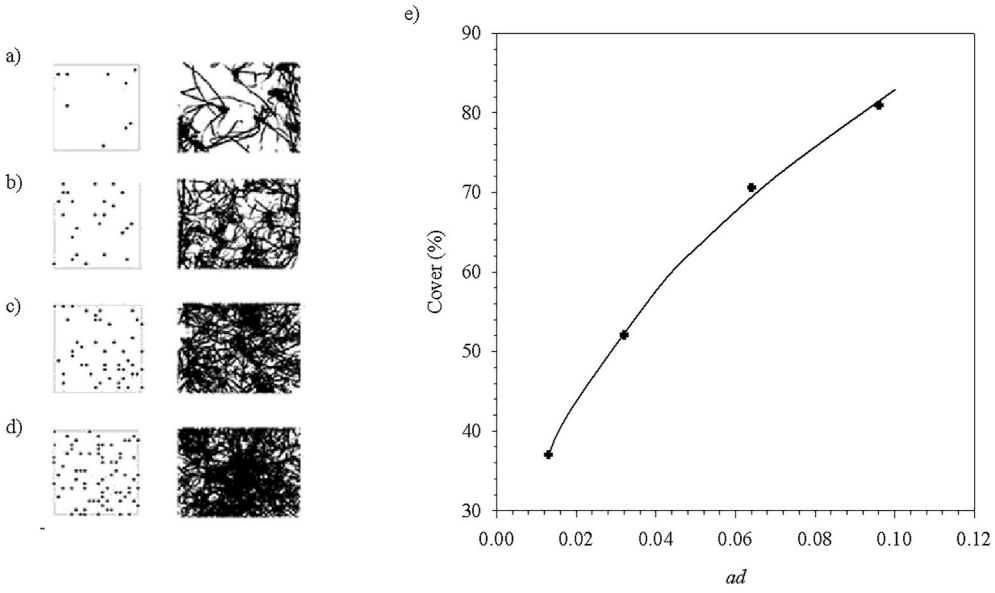

Fig. 2. Plant distribution for the different *SPF*s a) 1%, b) 2.5%, c) 5%, and d) 7.5% on the PVC bases (left panels) and black and white digitized photography (right panels). e) is the relationship between the canopy cover (%) and the volume plant fraction (ad).

Table 2
Summary of the wave and vegetation parameters for each experiment.

Run	Canopy model	*SPF* (%)	*n* (stems·m^{-2})	Coverage (%)	*ad*	S_b (cm)	*F* (Hz)	λ (m)	*A* (cm)	A_w (cm)
WP1	Without vegetation	0	0	0	0		0.7	2.43	2.0	0.91
WP2									2.2	1.43
WP3									2.0	2.02
WP4									1.5	2.16
WP5							1.2	1.03	3.0	1.82
WP6									3.2	1.63
WP7									5.0	1.96
WP8									5.6	2.55
SFV9	Submerged flexible vegetation model	1	127	37	0.013	3.14	0.7	2.43	2.0	0.98
SFV10									2.2	0.65
SFV11									2.0	2.70
SFV12									1.5	2.18
SFV13							1.2	1.03	3.0	2.70
SFV14									3.2	1.24
SFV15									5.0	1.21
SFV16									5.6	1.11
SFV17		2.5	318	52	0.032	1.98	0.7	2.43	2.0	1.43
SFV18									2.2	0.80
SFV19									2.0	2.82
SFV20									1.5	2.83
SFV21							1.2	1.03	3.0	1.52
SFV22									3.2	1.39
SFV23									5.0	1.66
SFV24									5.6	1.77
SFV25		5	637	71	0.064	1.40	0.7	2.43	2.0	0.45
SFV26									2.2	1.18
SFV27									2.0	1.54
SFV28									1.5	1.51
SFV29							1.2	1.03	3.0	1.39
SFV30									3.2	1.61
SFV31									5.0	1.55
SFV32									5.6	1.96
SFV33		7.5	955	81	0.096	1.14	0.7	2.43	2.0	1.09
SFV34									2.2	0.61
SFV35									2.0	0.75
SFV36									1.5	1.56
SFV37							1.2	1.03	3.0	1.67
SFV38									3.2	1.82
SFV39									5.0	1.69
SFV40									5.6	1.72

plants case. In the within-canopy layer, the velocity decreased gradually with depth until $z = 5$ cm ($z/h_v = 0.4$) where the wave velocity remained nearly constant down to the bottom. In this layer, the velocity in the presence of plants was lower than that in the without-plants case.

The turbulent velocity was obtained by:

$$u' = U_i - U_c - U_w \tag{6}$$

where U_c and U_w were calculated by Eqs. (3) and (4). The same methodology was used to calculate the other two turbulent velocity components (v' and w').

The turbulent kinetic energy (*TKE*) was calculated following Ros et al. (2014) as:

$$TKE = \frac{1}{2}\left(u'^2 + v'^2 + w'^2\right) \tag{7}$$

where $< >$ denotes the time average.

Like U_w, the *TKE* decreased with depth (Fig. 3b) and the same two vertical layers (above-canopy and within-canopy) can be distinguished. The above-canopy layer presented similar *TKE* for both the with and without-plants experiments. Within the canopy, the *TKE* decreased compared to the without-plants experiments. From the results of the vertical profiles of both U_w and *TKE*, the depth of $z = 5$ cm was considered representative of the hydrodynamics of the within-canopy layer, and the depth of $z = 20$ cm representative of the hydrodynamics of the above-canopy layer. Therefore, for the rest of the experiments carried out, the current velocity was measured at these two vertical positions: $z = 20$ cm ($z/h_v = 1.4$, above the canopy) and $z = 5$ cm ($z/h_v = 0.4$, within the canopy). Within the canopy layer (at $z/h_v = 0.4$), the mean flow velocity was $U_c = -0.04$ cm s^{-1} and -0.10 cm s^{-1} for non-vegetated experiments and for the wave frequencies of $f = 0.7$ Hz and $f = 1.2$ Hz, respectively. For experiments with vegetation, and at the same depth, the mean flow velocity among all the experiments as $U_c = -0.22$ cm s^{-1} for $f = 0.7$ Hz and -0.25 cm s^{-1} for wave frequencies $f = 1.2$ Hz. These flow velocities were negative in all the cases, indicating that they were directed towards the wave maker. They have lower values than those found in the experiments of (Luhar et al., 2010), where they used a paddle type wave maker with frequencies of 0.5 Hz and U_c at this depth was directed towards the beach. In this present study, a flap-type wave maker was used, and higher wave frequencies were considered. This study gives similar results and directions for U_c as those found by (Pujol et al., 2013b) for the same type of wave maker and frequencies of 1 Hz and 1.4 Hz.

2.5. Sediment-laden injection

A synthetic dust powder (ISO 12103–1. A4 Coarse, Powder Technology Inc. Burnsville) was used as the sediment in the experiments. The volumetric concentrations of suspended sediment (in μL·L^{-1}) were analysed using the LISST-100X (Laser In-Situ Scattering and Transmissometry, Sequoia Scientific, Inc, Bellevue, WA) particle size analyser. The LISST-100X consists of a laser beam and an array of detector rings of progressive diameters which allow the light received at the scattering angles of the beam to be analysed. The device measures particle volume concentrations for 32 size-classes, (logarithmically distributed in the size range of 2.5–500.0 μm), using a procedure based on the diffraction

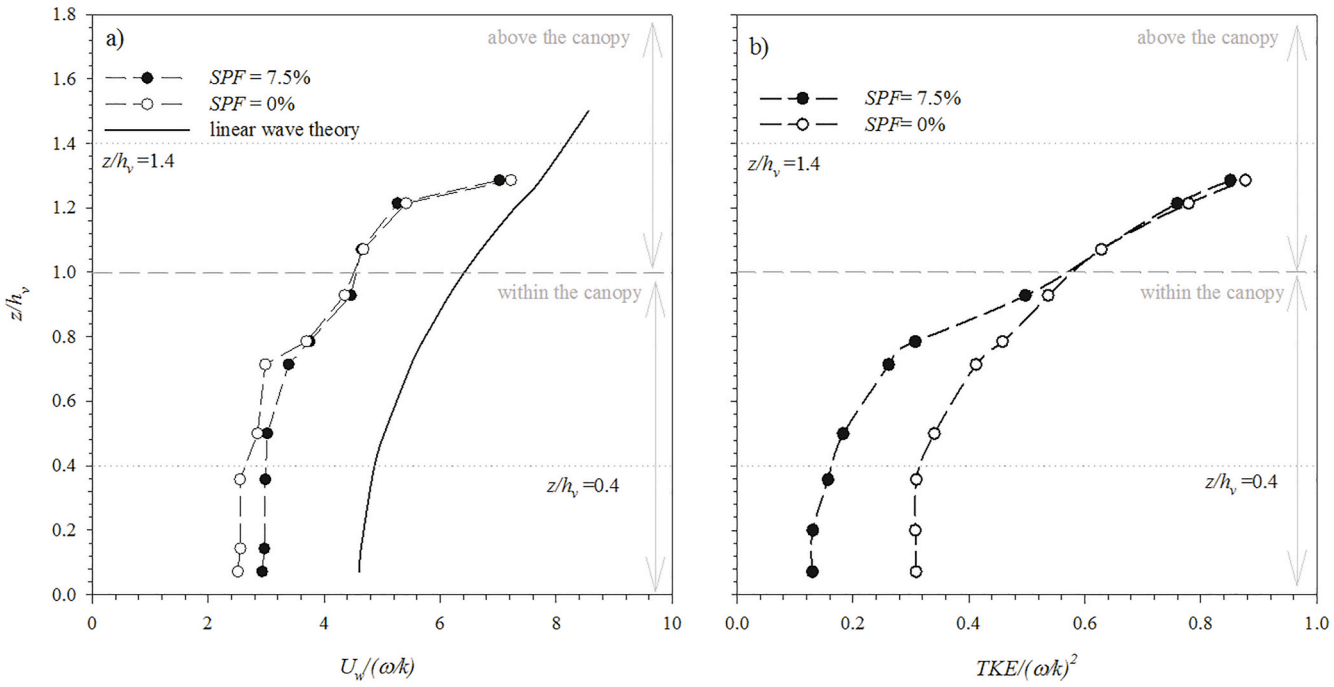

Fig. 3. Vertical profiles of both the wave velocity $U_w/(\omega/k)$, where $\omega = 2\pi f$ and $k = 2\pi/\lambda$(a) and the turbulent kinetic energy $TKE/(\omega/k)^2$ (b) for $SPF = 0\%$ (unfilled circles), $SPF = 7.5\%$ (filled circles) and the linear wave theory (solid line). The dashed line shows the top of the plant blades and the dotted lines show the level where the measurements were taken. The vertical axis represents the non-dimensional depth z/h_v.

theory of light. The LISST-100X has been found to perform well when determining particle size distribution and concentration for both organic (Serra et al., 2001) and inorganic particles (Serra et al., 2002a, 2002b) suspended in water. This instrument can be used *in situ* in the field, where it can be submerged in the water, or it can be employed in the laboratory to measure small samples by using a measuring chamber. For laboratory use, the water sample has to have a volume between a minimum of 80 ml (to ensure the detector is completely covered) and a maximum of 100 ml (the maximum volume of the measuring chamber). The particle size distribution of the sediment used was bimodal, with fine particles, 2.5–6.0 μm in diameter, corresponding to strongly cohesive clay and very fine silts with a median $D50 = 3.78$ μm and making up 30% of the sediment, and coarse particles, 6.0–122 μm in diameter, corresponding to weakly cohesive fine to coarse silts and small sand

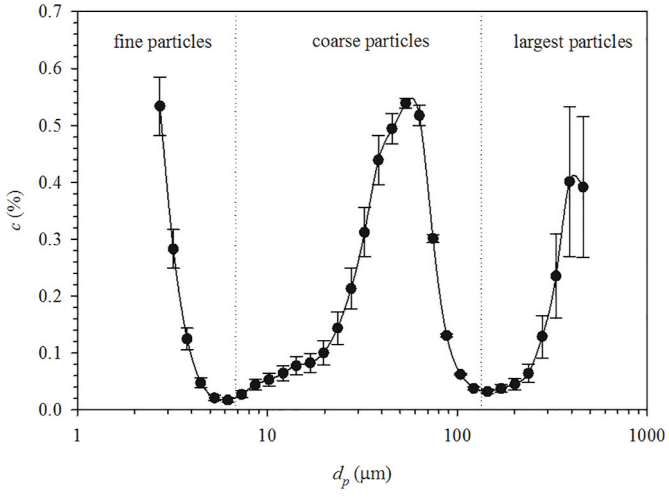

Fig. 4. Sediment particle distribution in %. Three different particle sizes are shown: fine particles below 6 μm, coarse particles between 6 and 122 μm, and the largest size particles over 122.0 μm.

particles with a median of $D50 = 27.6$ μm making up 70% of the sediment (Fig. 4). The concentration of the particles in each size-class was calculated by the sum of the volume concentrations of the particles ranging between 2.5 and 6.0 μm for the fine particles and between 6.0 and 122.0 μm for coarse particles (Fig. 4). The particle concentration will be expressed in volume concentrations in the whole manuscript to mitigate for the quantity of fine particles in every sediment mixture being higher than the coarse particles.

Before the injection, the wavemaker was started and left to run for 60 min to allow the system to reach equilibrium. After this time had elapsed, the particle-laden flow to be used in the injection was prepared with an initial volume (2 L) of sediment suspension (with a concentration of 40 g L^{-1}) introduced into one end of the sediment-injection pipe. The injection pipe was situated at $y = 0$ along the axis of the flume (Fig. 1). While introducing the sediment into the pipe, the injectors faced upwards to avoid any uncontrolled spillage. Once the pipes had been filled with the sediment suspension, they were closed and then turned to face downwards with their ends protruding 5 cm below the water surface, thus producing an even release of suspended sediment along the flume. After 18 s, individual injector plumes started to merge. The injection of sediment lasted less than 1.5 min. The sediment mass from the injection produced a total suspended sediment concentration (c_s) in the flume within the range 5–14 μL L^{-1}, which coincides with the typical sediment concentration discharges, 4–400 μL L^{-1}, of river plumes in coastal waters (Mulder and Syvitski, 1995). A river plume in the Bay of Bengal was found to discharge concentrations in the range of 0.4 μL L^{-1} to 20.7 μL L^{-1} (Sridhar et al., 2014), also in a range similar to that in the present study.

The length scale, L_M (Colomer et al., 1999), was used to calculate the 'plume' or 'jet' nature of the injection. L_M indicates the distance up to where the injected fluid behaves as a jet and was calculated as:

$$L_M = \frac{M_O^{3/4}}{Q_O^{1/2}} \tag{9}$$

where M_o was the volume flux and Q_o was the momentum flux. *Mo* was calculated as:

$$M_O = \frac{\pi D^2 w_o^2}{4}. \quad (10)$$

where D is the inner diameter of the injectors and w_o is the injection velocity, calculated as:

$$w_o = \frac{Q}{n_{inj}\, A_{inj}}. \quad (11)$$

where Q is the injection flow, n_{inj} is the number of injectors and A_{inj} is the injector area.

Q_o was calculated as:

$$Q_o = \frac{\pi D^2 B_o}{4} \quad (12)$$

where Bo is the buoyancy flux per unit area, calculated as:

$$B_o = \Delta b_o w_o \quad (13)$$

where Δb_o is the buoyancy of the resulting plume fluid, calculated as:

$$\Delta b_o = \frac{(\rho_s - \rho_w) g}{\rho_w} \quad (14)$$

where $\rho_s = 2500$ kg m^{-3} is the sediment density, $\rho_w = 1000$ kg m^{-3} is the water density and $g = 9.8$ m s^{-2} is the gravitational acceleration.

Merging equations (9)–(14) resulted in $L_M = 0.025$ cm. Therefore, the injection behaved like a jet for distances up to 0.025 cm from the injector and then plume-like once it got further away than that. As the water depth was 30 cm and the plants extended up 14 cm, the possibility the injectors being a source of turbulence within the canopy was discarded and the plume character of the injector was demonstrated. In addition, a test for the effect the injection has on the *TKE* measurements was carried out. That is, the *TKE* was measured with and without the injection. The *TKE* with the injection increased by 5.5%, which is within the standard deviation measured for the *TKE*. In addition, the injection time was less than 1.5 min, representing 1.2% of the total running period of the sediment study. Therefore, any effect the injection might have had on the measuring point was disregarded.

2.6. Sediment measurements

In the first test, two transversal points (situated 25 cm apart) and two longitudinal (1 m apart) were considered for the particle concentration measurements and confirmed that, after 1.5 min of injection, the suspended sediment was not only homogeneously mixed in both the longitudinal and transversal directions of the flume with maximum differences of 0.06 μL L^{-1} but was also below the standard deviation obtained for the measurements of the concentration at one single point (of 0.20 μL L^{-1}). Therefore, the samples of sediment were taken at $y = 0$ and at the same x-position where the hydrodynamics were measured (x = 150 cm from the edge of the canopy). The concentration of suspended sediment c_t (μL·L^{-1}), was measured at the same water depths ($z/h_v = 0.4$ and at $z/h_v = 1.4$) considered representative for the hydrodynamics in both the above-canopy and the within-canopy layers (Fig. 3a and b). Water samples, 20 mL in volume, were collected with a pipette from these two depths at different time steps $t = 1$, 5, 15, 30, 45, 60 and 90 min, and analysed for suspended sediment concentration. As the samples were not returned to the flume, this represented a total volume decrease of 280 mL (a 0.03% decrease in the total volume of the water volume) during the running time of the experiment. This change in the water volume produced a negligible change in the water height (<0.05 cm). The time evolution for the sediment concentration, c_t, decreased and reached the steady state (c_s) at $t = 60$ min (T_s, Fig. 5). At the end of the experiment ($t = 90$ min), ten model plants were gently removed from different evenly separated positions within the meadow and introduced into a beaker with a volume of 80 mL of water. The plants were then stirred in the fluid to remove the sediment trapped by the surface of the blades, after which particle concentration (c_p) was analysed with the particle size analyser (LISST-100X).

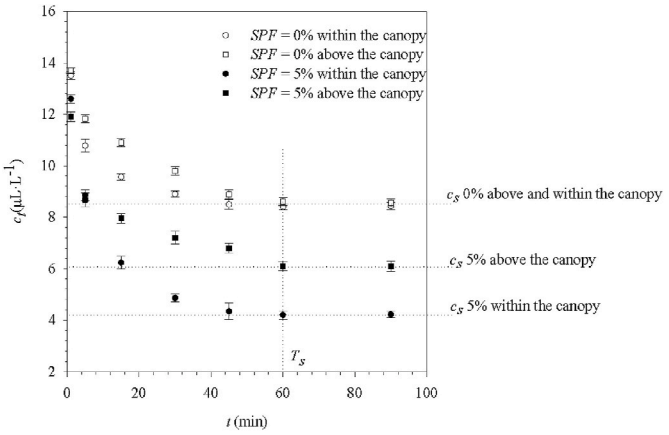

Fig. 5. Decline in suspended sediment concentration, c_t, with time, comparing experiments with canopy (*SPF* 5%) and at the equivalent heights in experiments without canopy (*SPF* 0%). Sediment concentrations were measured above the canopy ($z/h_v = 1.4$) and inside the canopy ($z/h_v = 0.4$). The vertical dashed line indicates the time (T_S) to reach steady state conditions, while the horizontal dashed lines indicate steady state sediment concentrations (c_s).

2.7. Sediment mass balance

A conceptual model was developed for the canopy system with four sediment compartments based on the hydrodynamics (Fig. 3): sediment suspended within the canopy (*SC*), sediment suspended in the water above the canopy (*SW*), sediment attached to the leaf blades (*SP*), and sediment settled at the bottom of the tank (*SB*). For suspended sediments, the concentrations measured within each compartment were mutiplied by the volume of the compartment to estimate the volume (in μL) of the suspended sediments in that compartment. To determine the total volume of sediment attached to the plant blades (μL), measured particle concentrations were normalised per plant and then multiplied by the total number of plants in the canopy (which varied with *SPF*). The volume of particles settled to the bottom was not directly measured, instead it was calculated as the difference between the total volume injected and the sum of the suspended particle volume and the volume attached to plants.

V_{IN} is the total volume injected, distributed in the region occupied by the canopy, calculated by multiplying the injected sediment mass by the volume of the canopy and divided by the total volume of the flume. Finally, the injected mass was converted to volume units using the sediment density (2500 kg m^{-3}). The injected volume was fractionated into fine and coarse particles using the previously-determined particle size distribution.

A volume balance was then determined as:

$$V_{IN}^F = V_{SC}^F + V_{SW}^F + V_{SP}^F + V_{SB}^F \quad (15)$$

where V_{IN}^F is the volume of fine particles injected above the canopy, V_{SC}^F is the volume of suspended fine sediment inside the canopy, determined at $z/h_v = 0.4$, the volume inside the canopy corresponded to the water volume, which is inside the area and height of the vegetation, V_{SW}^F is the volume of suspended fine sediment in the water above the canopy, determined at $z/h_v = 1.4$, V_{SP}^F is the volume of sediment captured by the plants, and V_{SB}^F is the volume of fine sediment settled to the bottom. An equivalent volume balance was made for coarse sediments:

$$V_{IN}^C = V_{SC}^C + V_{SW}^C + V_{SP}^C + V_{SB}^C \quad (16)$$

3. Results

Differences in the turbulent kinetic energies were found between the bare substrate and sparse and dense canopies. The results of the turbulent kinetic energy averaged over all the experiments carried out with different wave amplitudes and the same frequency and *SPF* are referred to as the mean turbulent kinetic energy (*<TKE>*). The *<TKE>* decreased gradually with the canopy cover for both wave frequencies. Considering the error margin, no differences in the *TKE* were obtained between the two frequencies studied (0.7 and 1.2 Hz) (Fig. 6). The reduction in the *<TKE>* for sparse canopies and dense canopies ranged from 14% to 35% to that of the *<TKE>* of the bare substrate.

The suspended sediment concentrations at steady state, c_s, for both fine and coarse particles, were linearly dependent on *TKE* (Fig. 7a). Since the *TKE* depended on the cover, the average of the steady state concentrations ($<c_s>$) over the same cover experiments for both fine and coarse particles decreased as canopy cover increased (Fig. 7b). The sediment trapped by the surface of the blades of each plant, c_p, was also analysed, (as described in Methods), and quantified as the concentration of sediment in the wash-off liquid. The coarse particles captured by each plant showed similar linear relationships with *TKE* as those observed for the steady state suspended sediment concentrations (Fig. 7c) In contrast, the concentration of fine particles trapped by the blades of the plants was independent of the *TKE* (Fig. 7c). The average of the particle concentration trapped by the plants in the whole canopy ($<c_p>$) was calculated for each canopy cover and increased as the canopy cover increased (Fig. 7d).

For all the experiments, the volume of fine and coarse sediment particles was calculated as outlined in the methodology. For example, the volume of particles suspended within the canopy was calculated by multiplying the concentration of suspended particles at $z = 0.4\ h_v$ by the volume of the region occupied by the canopy. For the non-vegetated case, the volumes of the fine V_{SC}^F(Fig. 8a), and coarse, V_{SC}^C (Fig. 8b) particles that remained in suspension in the bottom portion of the water where the canopy was present for the vegetated cases, were greater than those of the vegetated cases. Also, in both cases the volumes of the fine V_{SP}^F (Fig. 8a) and coarse V_{SP}^C (Fig. 8b) particles trapped by plant blades increased as the cover increased. The increase in the particles trapped by plant blades in the whole canopy, V_{SP}, coincided with a decrease in V_{SC}. The volume of suspended sediment above the canopy for both the fine and coarse particles (V_{SW}^F and V_{SW}^C) decreased with the increase in canopy cover. Finally, the sedimentation (V_{SB}) to the bottom increased as the canopy density increased and ranged from 75% to 80% for fine particles over the total volume of fine particles and from 57% to 60% for coarse particles over the total volume of coarse particles (following equations (15) and (16)). For the non-vegetated cases, the sedimentation to the bottom was lower than that for vegetated cases, around 70% for fine particles and around 46% for coarse particles (Fig. 8a and b). In each case, the percentage is given over the total amount per each particle range.

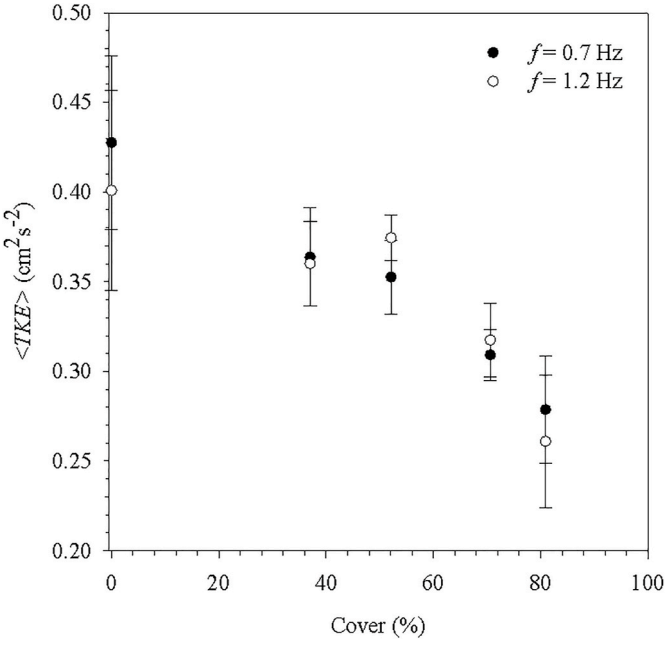

Fig. 6. *TKE* values within the canopy averaged over the experiments, *<TKE>* with the same canopy density (*SPF*) versus the canopy cover for both the high frequency (1.2 Hz, unfilled circles) and the low frequency (0.7 Hz, filled circles) experiments.

The partition coefficient (P_C) between the sediment trapped by the plant blades and the suspended sediment inside the canopy (V_{SC}) was calculated as:

$$P_C = \frac{V_{SP}}{V_{SC}} * 100 \tag{17}$$

P_C decreased linearly with *<TKE>* for both fine and coarse particles (Fig. 9a). For *<TKE>* above 0.36 $cm^2 s^{-2}$, corresponding to cover percentages <52%, the P_C for fine and coarse particles did not present any differences. For high canopy covers, the partition coefficient was greater for fine particles (Fig. 9b) than for coarse particles. For the highest cover, P_C was 50% for fine particles, i.e., $V_{SP}^F = 0.5 V_{SC}^F$, which indicates that the volume of particles captured by the leaf blades is half that remaining in suspension inside the canopy. P_C was 30% for coarse particles, i.e., $V_{SP}^C = 0.3 V_{SC}^C$ (Fig. 9b).

4. Discussion

Experiments performed in the laboratory flume showed that allochthonous sediment encountering seagrass canopies can undergo different fates, namely be: i) maintained in suspension above the canopy, ii) maintained in suspension within the canopy, iii) captured by plant blades or iv) settle to the seabed. However, results show that submerged seagrass canopies under oscillatory conditions affect the hydrodynamics and the distribution and transport of sediments mainly by reducing the wave velocity and the turbulent kinetic energy that depends on both canopy density and wave frequency.

4.1. Submerged model vegetation hydrodynamics by oscillatory flow

Submerged canopies were found to attenuate both wave velocity and *TKE* within the canopy, in agreement with (Pujol et al., 2013b) in their laboratory study and the results observed by Gacia et al. (1999) and by Hendriks et al. (2008) in their field studies. The *TKE* attenuation of between 14 and 35% found in this laboratory study, agrees with the 25% reduction in turbulence between bare substrate and *P. oceanica* bed found by Granata et al. (2001) in their field study. The fact that the *TKE* decreased with the canopy cover indicates that dense canopies shelter the seabed. This reduction in the *TKE* produces different distributions of sediment depending on the density of the cover. The decrease in the *TKE* with depth was also found by Zhang et al. (2018), but in their case, the *TKE* in the upper without-plant water layer was lower than in the present study. In laboratory conditions the plant height was $h_v = 14$ cm, wave amplitudes were A = 1.5 cm and 5.6 cm and the periods were $T =$ 1.43 s and 0.83 s. Considering the flume height $H = 30$ cm and shallow field depth cases with $H = 100$ cm a scale factor of 3.3 would apply by using Froude scaling (Islam et al., 2016). Using the Froude scaling, the laboratory studied conditions would represent field waves with amplitudes of $A = 4.95$ and 18.48 cm and periods of $T = 2.59$ s and 1.51 s. Such field conditions might be found in river or lake environments and closed basin estuaries in marine systems (Pascolo et al., 2019; Smith et al., 2001), where particle laden river plumes may have a significant

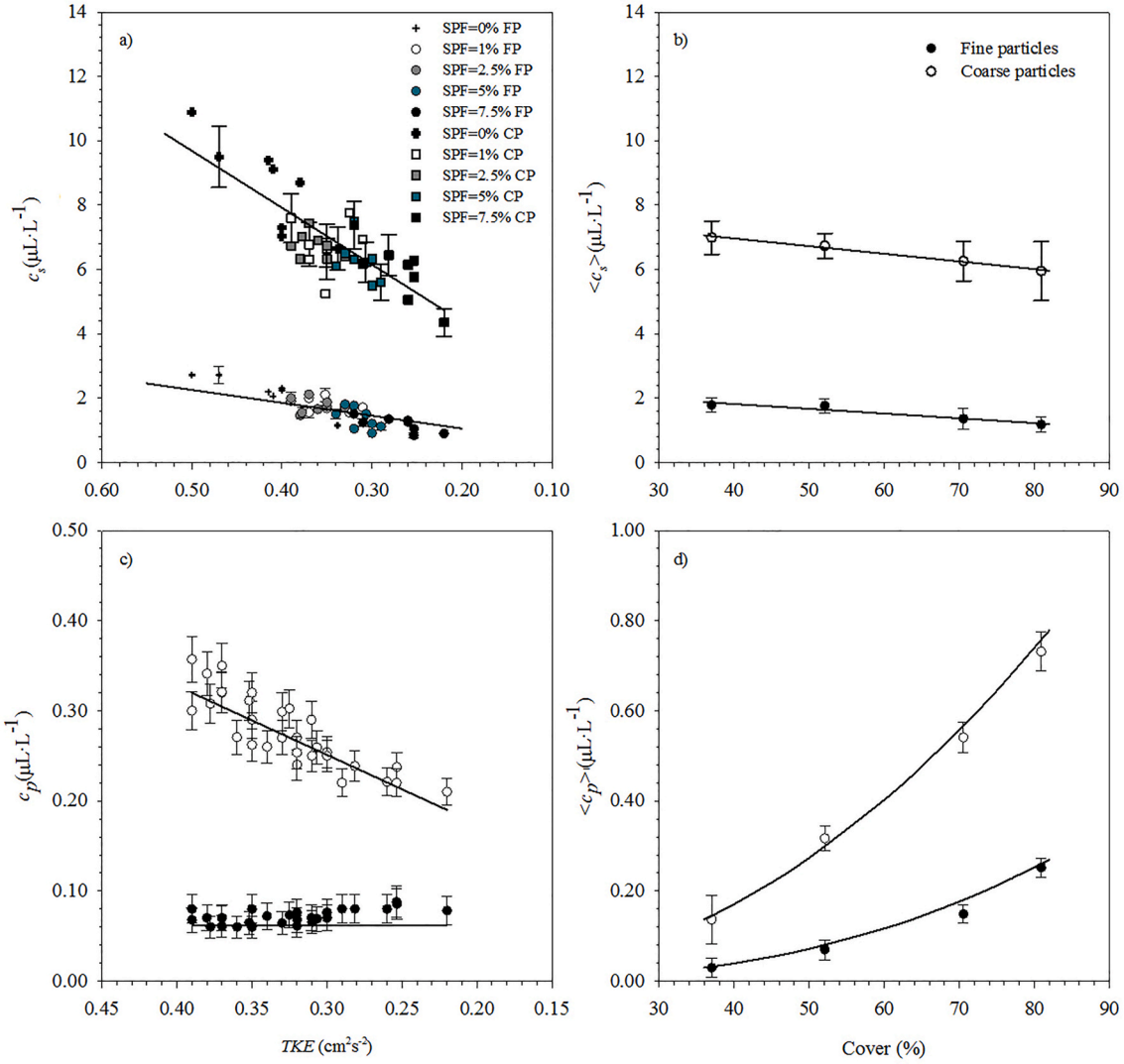

Fig. 7. a) Steady state suspended sediment concentration, c_s, versus *TKE*, with variable *SPF*. Circles correspond to fine particles (FP) and squares to coarse particles (CP). Fine and coarse particles follow a linear trend with the expressions: $c_s = 17.69*TKE+0.84$ (with a $R^2 = 0.681$ and 99% of confidence) and $c_s = 6.69*TKE-0.74$ (with a $R^2 = 0.742$ and 99% of confidence), respectively; b) Steady state suspended sediment concentration averaged over the experiments with the same canopy cover versus canopy cover for fine particles (filled circles) and coarse particles (unfilled circles). The linear trends for fine and coarse particles are: $<c_s> = -0.01*Cover+2.41$ (with a $R^2 = 0.919$ and 95% of confidence) and $<c_s> = -0.02*Cover+7.91$ (with a $R^2 = 0.988$ and 99% of confidence), respectively; c) Sediment captured by each plant c_p, for fine and coarse particles versus *TKE*. Coarse particles follow the linear trend expression: $c_p = 1.23*TKE–0.13$ (with $R^2 = 0.673$ and 99% of confidence); d) Mean sediment concentration captured by all the plants in the canopy averaged over all the experiments with the same canopy cover versus canopy cover for fine and coarse particles. The potential trend expression followed by coarse particles is: $<c_p> = 7*10^{-5}*Cover^{2.11}$ (with $R^2 = 0.994$ and 99% of confidence) and fine particles follow the expression: $<c_p> = 2*10^{-6}*Cover^{2.68}$ (with $R^2 = 0.994$ and 99% of confidence). Vertical error bars represent the standard deviation in the concentration obtained by different measurements of the concentration for the same experiments. In Fig. 7a, only some error bars have been shown to provide a clear plot of the data.

impact (Oey and L Mellor, 1993; Howley et al., 2018).

4.2. Effect of the canopy on the suspended sediment from the allochthonous plume

The concentration of suspended sediment in the water column follows a linear relationship with the *TKE*. High *TKE* corresponds to the sparsest canopies, whereas low *TKE* corresponds to the densest. Therefore, the decrease in the suspended sediment concentration corresponded to the densest canopies. This result is in agreement with the reduction of turbidity found by Short and Short (Short et al., 1984) for a vegetated bed. Consequently, the presence of a seagrass canopy protects seagrass meadows in coastal regions by enhancing the sedimentation. This result has been observed in the field, where a greater sediment deposition was found on the seabeds sheltered by *P. oceanica* in the NE Spanish Mediterranean (Grabowski et al., 2011; Gacia et al., 1999).

4.3. Allochthonous sediment trapped by the blades of an individual plant

This study demonstrated that plant blades trap sediment particles. Sediment trapped by blades in sparse canopies was quantified and compared to that in dense canopies. The sediment concentration trapped by the blades of each plant, (c_p), was higher for coarse particles than it was for fine ones. The concentration of fine particles trapped on the leaf blades of each plant remained constant with the *TKE* and with the canopy density, which may be due to the leaves of the plants easily trapping fine particles until the surfaces become saturated. In contrast, the concentration of coarse particles trapped on the leaf blades of each plant increased with the *TKE*, i.e., decreased with cover. Therefore, for coarse particles the greatest concentration of particles trapped by plant

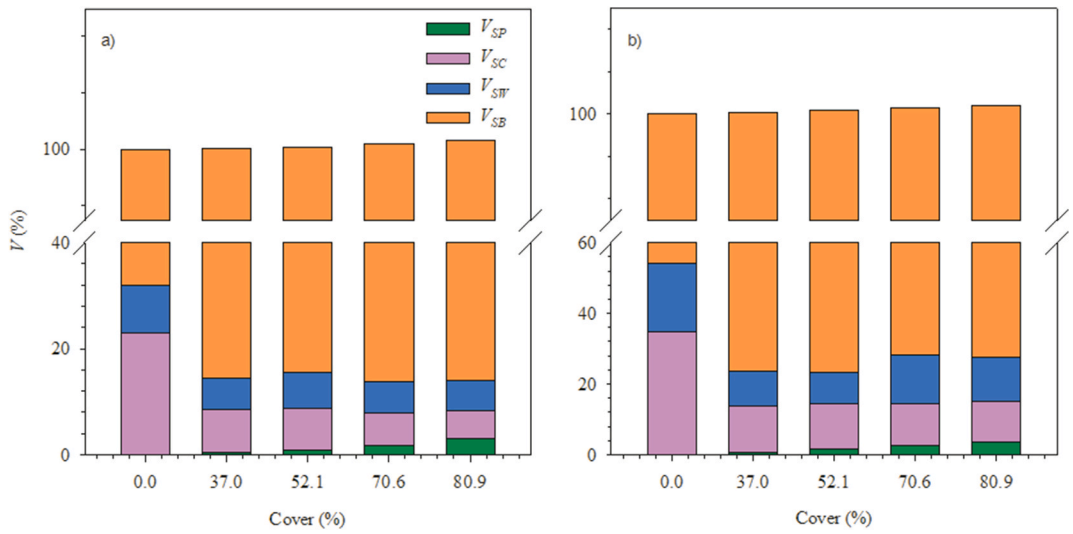

Fig. 8. Sediment volume balance (V) of the volume trapped by the blades (V_{SP}), volume inside the canopy (at $z/h_v = 0.4$) (V_{SC}), volume above the canopy (at $z/h_v = 1.4$) (V_{SW}) for different covers for fine particles (a) and for coarse particles (b), and volume deposited to the bottom (V_{SB}).

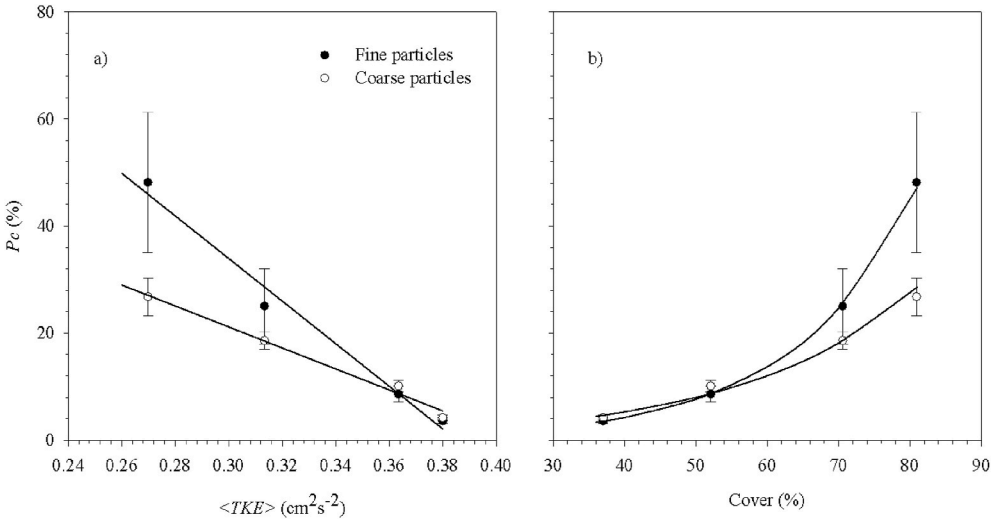

Fig. 9. a) Partition coefficient of the sediment trapped by the blades versus the $<TKE>$ for fine particles (filled circles) and for coarse particles (unfilled circles). $<TKE>$ is the mean value of the *TKE* averaged over the experiments with the same cover. Fine and coarse particles follow a linear trend with the expressions: $Pc = -397.8*<TKE>+153.3$ ($R^2 = 0.981$ and 99% of confidence) and $Pc = -196.2*<TKE>+80.0$ ($R^2 = 0.995$ and 99% of confidence), respectively; b) Partition coefficient for the sediment trapped by blades for the two particle size ranges versus the cover. The relationship between *Pc* and the cover showed an exponential tendency ($Pc = 0.4e^{0.06cover}$, $R^2 = 0.994$ and $Pc = e^{0.04cover}$, $R^2 = 0.987$ for fine and coarse particles, respectively). Error bars represent the standard deviation between the different experiments carried out at the same $<TKE>$ (Fig. 9a) and for the same cover (Fig. 9b).

leaves corresponded to the lowest canopy density. Two possible reasons could explain this result. A first hypothesis is that in sparse canopies there is a reduction in the interaction between leaf blades, whereas in dense canopies the contact between blades can wash off the sediment deposited on the blades of neighbouring plants, thus resulting in cleaner blades. As reported by Gacia et al. (1999) and Hendricks et al. (Hendriks et al., 2008), an increase in the canopy density generates an increase in plant blade friction. The second hypothesis is that sparser canopies have higher *TKE*, thus favouring the contact between particles and blades and resulting in a greater amount of sediment being trapped on the surface of the plant blades. Short and Short (Short et al., 1984) also observed that seabeds covered by plants with blades of leaves with large surface areas produced a greater reduction in the turbidity of the water column compared to seabeds covered by plants with blades that have a small surface area.

4.4. Allochthonous sediment trapped by the overall canopy

Therefore, the decrease in the within-canopy suspended sediment could be attributed to two factors: the capture of suspended particles by plant blades or the particles settling onto the bed. This is consistent with the fact that the presence of plants increases the available surface where particles can settle and so an increase in plant density implies an increase in the available surface.

Agawin and Duarte (2002) observed that particles with diameters around 15 μm were trapped faster by canopy blades than those particles around 1–3 μm. The trapping rates were 0.24 d^{-1} and 0.50 d^{-1} for 15 μm and 3 μm, respectively. At first glance, it would seem that their results do not agree with the results obtained in this study, where a greater sediment volume was found for the coarse particles, however, in converting the volume of particles to the number of particles for a canopy cover of 80.9%, the volume trapped by plants corresponds to a number of particles of 9.44×10^9 and 8.13×10^6 for fine and coarse particles, respectively. Therefore, a larger number of fine particles (as opposed to coarse particles) are trapped by the leaf blades, which is consistent with Agawin and Duarte (2002). This may be caused by the greater cohesiveness of fine particles compared to coarse particles (Grabowski et al., 2011).

In terms of mass balance, the total volume of particles settled to the bed in 1 h ranged from 5000 μlL to 6000 μlL, i.e., a mass of sediment from 12.5 g to 15 g, when considering a sediment density of 2500 g L^{-1}. This mass settled in the area under study equalling 2.5 m of in length per

0.5 m in width. This results in a range in the sedimentation rate of 240–288 g m^{-2}·day^{-1}. This sedimentation rate within seagrass beds is greater than that found by some authors (Granata et al., 2001; Serra et al., 2020). However, sedimentation rates in seagrass beds varies through the year in the range of 1.5–500 g m^{-2}·day^{-1} (Gacia and Duarte, 2001). These sedimentation rate values align with those in the present study. However, note that high sedimentation rates might cause plant burial that can negatively affect the growth of plants, thus compromising their survival (Cabaço et al., 2008; Manzanera et al., 1998). Manzanera et al. (1998) found that an increase in sediment deposition producing a 15 cm change in sediment height produced total mortality of the seagrass after 200–300 days. In the present study, considering a volume of 5000 μL of sediment deposited after 1 h, it would require 37500 h (i.e., 10.4 days) to reach such a change (i.e.15 cm) in the height of the sediment.

Particle sedimentation onto the seabed was affected by the presence of canopies and had a greater impact on coarse, rather than fine, particles, between 5.7 - 10.9% and 11.0–14.4% higher in the presence of vegetation, respectively. The annual cycle of the seagrasses could imply different regimes of sedimentation due to the continuous loss and renewal of leaves. *Posidonia oceanica* leaves grow progressively from winter to summer, when they obtain their maximum extension (Gruber and Kemp, 2010). In contrast, from late summer to autumn they shed their leaves, causing an accumulation of leaf litter on the seabed until the energy flow is able to transport them away (Paladini de Mendoza et al., 2018). This indicates that, at the end of the plant cycle, a portion of the dead leaves is likely to ultimately be transported to the bottom. Therefore, this study states that the presence of the canopy enhances the flux of allochthonous particles down to the bed in two different ways: it increases the direct sedimentation to the bed (through a reduction in the *TKE*) and it captures particles on its blades that may eventually end up on the seabed when the blades die.

This study demonstrated that under oscillatory flow for both fine and coarse sediment particles, shoot density also increased the sediment deposited to the seabed and reduced the suspended sediment particles. This aligns with the results found by Wilkie et al. (2012), who claimed that under a unidirectional flow, sediment deposition increased with seagrass density.

4.5. Sediment balance between sediment trapped by plant blades and by the canopy

A partition coefficient higher than 18.5% for fine particles and 25.0% for coarse particles was found for low values of *TKE*, and which correspond to the highest canopy cover. This result indicates that a larger volume of suspended sediment was trapped on the surface of the plant leaves compared to the volume of suspended sediment that remained in suspension inside the canopy in denser canopies. This demonstrates the fact that, while denser canopies have fewer particles per blade, the higher density of the canopies balances this result, producing the greater overall particle trapping observed on blades in the denser canopies. These results show that, as has been pointed out by other authors (Hendriks et al., 2008; Short et al., 1984; Ackerman, 2002), a significant portion of the suspended particles transported inside the seagrass canopies collides with the leaves. For canopy covers over 52.1%, the trapping of fine particles on plant blades was greater than that for coarse particles, while with lower covers, the blades had the same ability to trap both fine and coarse particles. So, a threshold of $TKE = 0.36\ cm^2\ s^{-2}$ indicates that for *TKE* below this value, leaf blades are able to trap the different sized suspended sediment particles. In addition to canopy density, plant height might also impact the canopy cover because longer leaves can bend more and produce a greater cover under certain hydrodynamic conditions. This increase in the cover by larger plants can have an impact on the TKE. An increase in plant height has been found to increase wave attenuation (Pujol et al., 2013a; Koftis et al., 2011). Furthermore, during the leaf growth, leaves might shift from a more rigid to a more flexible structure which can also impact the canopy cover. Rigid canopy structures can reduce the energy of the flow by three times that of flexible canopies (Bouma et al., 2005). Therefore, more work should be done to assess the effect both plant height and flexibility have on the hydrodynamics and the ability to capture particles on the leaves.

4.6. Ecological implications

Through the flume laboratory experiments carried out in this study, results contribute to confirming those obtained in field surveys where the importance of preserving seagrass meadows has been clearly demonstrated. The laboratory results allow us to demonstrate that the presence of seagrass in coastal areas does in fact have direct ecological implications on marine ecosystems since it favours the preservation of marine coastal seabeds and, therefore, the accumulation of sediments that contribute to storing and preserving carbon from autochthonous and allochthonous sources within the context of climate change.

Seagrass canopies play a crucial role in determining the characteristics of the seabed. Van Katwijk et al. (van Katwijk et al., 2010) found, on the one hand, muddification (an increase in fine sediment on the seabed), in high density canopies and, on the other hand, sandification in sparse canopies which tended to have a greater concentration of large sized particles. These results agree with the increase in the ratio between the mass of fine to coarse particles attached to blades from sparse (with $\frac{V^F_{SP}}{V^C_{SP}} = 0.5\%$ for $SPF = 1\%$) to dense canopies ($\frac{V^F_{SP}}{V^C_{SP}} = 0.8\%$ for $SPF = 7.5\%$). A high level of attachment of fine particles to blades results from the increase in the available surface where particles can be deposited.

Brodersen et al. (2017a) found that the silt/clay sediment attached to leaves of *Zostera muelleri* Irmisch ex Ascherson, has negative effects on the activity and efficiency of photosynthesis and on the night-time O_2 exchange between the leaf tissue and the surrounding water. According to our study, seagrass meadows with high canopy cover values will reduce the sediment trapped by each plant, thus favouring photosynthetic activity and O_2 exchange, while the sediment trapped by the whole canopy will be greater, thus reducing turbidity. Therefore, the overall effect of dense canopies will be twofold, less suspended sediment and cleaner leaves, which result in water of a better quality with greater clarity that can fulfil the photosynthetic requirements of the vegetation. This result may explain the existence of a potential threshold for the status of the water quality due to the effect canopies have. From Lopez-y-Royo et al. (Lopez-y-Royo et al., 2011), the threshold for moderate to good status water quality in seagrasses was for a shoot density of 210 shoots m^{-2}. From the present study, such a shoot density corresponds to a canopy cover of 46.3%; which coincides with the threshold where the *Pc* became differential for fine and coarse particles, i.e., to the greater cover of 50%. Therefore, the fact that plant blades trap a smaller portion of coarse than fine particles, may be related to water quality. Since fine particles trapped by each plant remain constant, the effect on plant fitness is as a result of the coarse particles trapped by plants. We hypothesize that those lower values of coarse particles attached to the leaf blades of the plants will result in a thinner layer of sediment on the blades, thus allowing for a better gas exchange. Hence, photosynthetic activity is improved and so too the meadow's fitness. In addition, the reduction of suspended sediment within the canopy in the case of dense canopies, will improve the water quality of the ecosystem, producing positive feedback to the canopy.

Another important aspect of sediment deposition on seagrass meadows is the storage and preservation of carbon in the seabed which, by managing these ecosystems, would be a potential mechanism for mitigating CO_2 emissions. Ricart et al. (2015b) found a higher content of organic carbon inside the seagrass canopies than at the edges of the canopy. The results presented here substantiate the argument for the seagrass restoration programmes conducted world-wide since the mid-20th century to mitigate climate change (Paling et al., 2009), help

rebuild the lost carbon sink and conserve the remaining stores due to the ability of seagrass canopies to capture particles in an oscillatory flow.

5. Conclusions

Seagrasses impacted by allochthonous sediment sources decreased the amount of suspended sediment compared to unvegetated beds through two processes: the capture of sediment particles by plant blades, and the enhancement of particle sedimentation onto the seabed. The plant blades captured suspended particles settling through the water column. The denser the canopy was, the lower the percentage of particles trapped by the blades individually, but the greater the percentage trapped by the whole canopy. As a result, estimates of particle sedimentation onto the seabed increased with canopy cover, coinciding with a decrease in the *TKE*. Therefore, this study reports that an increase in canopy cover increases sedimentation and particle capture by the leaves of the plants and, therefore, impacts on the suspended sediment remaining in the water column inside the canopy in such a way that water clarity in dense seagrass canopies improves.

This study also reports that the sediment concentration obtained for coarse particles, either in suspension or trapped by the canopy, is greater than that for fine particles. The concentration of fine particles trapped by individual leaf blades, however, does not vary with canopy cover or with the *TKE*. In contrast, the concentration of coarse particles trapped by individual blades decreased as the canopy cover increased, i.e., as the *TKE* decreased. This means that for all the *TKE* ratios studied, plants were equally able to capture fine particles in suspension but not the coarse particle fractions, where a threshold for the *TKE* was observed. For canopy covers over 52%, the trapping of fine particles on the blades is greater than that for coarse particles. This canopy cover value represents a threshold for the maximum volume of particles blades in sparse canopies can capture, which might impact on their fitness.

To conclude, the presence of vegetation in seagrass beds increased the available surface on which particles can be deposited. In addition, the reduction of turbulence and flow velocities was enhanced by the presence of vegetation and increased with canopy density. Therefore, the overall trapping of particles by seagrasses, either through settling on the bed or being trapped by their leaves, produced a decrease in the suspended sediment concentration, enhancing the water quality and resulting in positive feedback for the seagrass itself.

CRediT authorship contribution statement

Aina Barcelona: Methodology, Investigation, Formal analysis, Data curation, Writing – original draft. **Carolyn Oldham:** Data curation, Writing – review & editing, Supervision. **Jordi Colomer:** Conceptualization, Methodology, Investigation, Data curation, Writing – review & editing. **Jordi Garcia-Orellana:** Conceptualization, Writing – review & editing. **Teresa Serra:** Conceptualization, Methodology, Investigation, Data curation, Writing – review & editing, Supervision.

Declaration of competing interest

The authors declare that they have no known competing financial interests or personal relationships that could have appeared to influence the work reported in this paper.

Acknowledgments

This research was funded by the University of Girona, through the grant MPCUdG2016-006 and by the Ministerio de Economía, Industria y Competitividad of the Spanish Government through the grant CGL2017-86515-P. This work contributes to the ICTA 'Unit of Excellence' (MinECo, MDM2015-0552) and the Generalitat de Catalunya research program (2017 SGR-1588). Aina Barcelona was funded by the pre-doctoral grant 2020 FI SDUR 00043 by the "Generalitat de Catalunya".

References

Ackerman, J.D., 2002. Diffusivity in a Marine macrophyte canopy: implications for submarine pollination and dispersal. Am. J. Bot. 89, 1119–1127.
Agawin, N.S.R., Duarte, C.M., 2002. Evidence of direct particle trapping by a tropical seagrass meadow. Estuaries 25, 1205–1209.
Armitage, A.R., Fourqurean, J.W., 2016. Carbon storage in seagrass soils: long-term nutrient history exceeds the effects of near-term nutrient enrichment. Biogeosciences 13, 313–321.
Bos, A.R., Bouma, T.J., de Kort, G.L.J., van Katwijk, M.M., 2007. Ecosystem engineering by annual intertidal seagrass beds: sediment accretion and modification. Estuar. Coast Shelf Sci. 74, 344–348.
Bouma, T.J., de Vries, M.B., Low, E., Peralta, G., T Nczos, I.C., van de Koppel, J., J Herman, P.M., 2005. Trade-off related to ecosystem engineering: a case study on stiffness of emerging macrophytes. Ecology 86 (8), 2187–2199.
Brodersen, K.E., Hammer, K.J., Schrameyer, V., Floytrup, A., Rasheed, M.A., Ralph, P.J., Kühl, M., Pedersen, O., 2017a. Sediment resuspension and deposition on seagrass leaves impedes internal plant aeration and promotes phytotoxic H_2S intrusion. Front. Plant Sci. 8, 1–13.
Brodersen, M.M., Panatzi, M., Kokkali, A., Panayotidis, P., Gerakaris, V., Maina, I., Kavadas, S., Kaber, H., Vassilopoulou, V., 2017b. Cumulative impacts from multiple human activities on seagrass meadow in eastern Mediterranean waters: the case of Saronikos Gulf (Aegean Sea, Greece). Environ. Sci. Pollut. Res. 25, 26809–29822.
Cabaço, S., Santos, R., Duarte, C.M., 2008. The impact of sediment burial and erosion on seagrasses: a review. Estuar. Coast Shelf Sci. 79, 354–366.
Colomer, J., Boubnov, B.M., Fernando, H.J.S., 1999. Turbulent convection from isolated sources. Dynam. Atmos. Oceans 30, 125–148.
Colomer, J., Soler, M., Serra, T., Casamitjana, X., Oldham, C., 2017. Impact of anthropogenically created canopy gaps on wave attenuation in a *Posidonia oceanica* seagrass meadow. Mar. Ecol. Prog. Ser. 569, 103–116.
Community, European, 2000. Directive 2000/60/EC of the European Parliament and of the Council of 23 October 2000 establishing a framework for Community action in the field of water policy. Off J Eur Communities L327.
Duarte, C.M., 1991. Seagrass depth limits. Aquat. Bot. 40 (4), 363–377.
Duarte, C.M., Sintes, T., Marbà, N., 2013. Assessing the CO_2 capture potential of seagrass restoration projects. J. Appl. Ecol. 50, 1341–1349.
Duarte, C.M., Borja, A., Carstensen, J., Elliott, M., Krause-Jensen, D., Marbà, N., 2015. Paradigms in the recovery of estuarine and coastal ecosystems. Estuar. Coast 38, 1202–1212.
Folkard, A., 2005. Hydrodynamics of model *Posidonia oceanica* patches in shallow water. Limnol. Oceanogr. 50, 1592–1600.
Fourqurean, J.W., Duarte, C.M., Kennedy, H., Marbà, N., Holmer, M., Mateo, M.A., Apostolaki, E.T., Kendrick, G.A., Krause-Jensen, D., McGathery, K.J., Serrano, O., 2012. Seagrass ecosystems as a globally significant carbon stock. Nat. Geosci. 5, 505–509.
Fraser, M.W., Short, J., Kendrick, G., McLean, D., Keesing, J., Byrne, M., Caley, M.J., Clarke, D., Davis, A.R., Erftemeijer, P.L.A., Field, S., Gustin-Craig, S., Huisman, J., Keough, M., Lavery, P.S., Masini, R., McMahon, K., Mengersen, K., Rasheed, M., Statton, J., Stoddart, J., Wu, P., 2017. Effects of dredging on critical ecological processes for marine invertebrates, seagrasses and macroalgae, and the potential for management with environmental windows using Western Australia as a case study. Ecol. Indicat. 78, 229–242.
Gacia, E., Duarte, C.M., 2001. Sediment retention by a Mediterranean *Posidonia oceanica* meadow: the balance between deposition and resuspension. Estuar. Coast Shelf Sci. 52, 505–514.
Gacia, E., Granata, T.C., Duarte, C.M., 1999. An approach to measurement of particle flux and sediment retention within seagrass (*Posidonia oceanica*) meadows. Aquat. Bot. 65, 255–268.
Ghisalberti, M., Nepf, H., 2002. Mixing layers and coherent structures in vegetated aquatic flows. J. Geophys. Res. 107, C23011.
González-Ortiz, V., Egea, L.G., Jiménez-Ramos, R., Moreno-Marín, F., Pérez-Lloréns, J.L., Bouma, T., Brun, F., 2016. Submerged vegetation complexity modifies benthic infauna communities: the hidden role of the belowground system. Mar. Ecol. 37, 543–552.
Goring, D.G., Nikora, V.I., 2002. Despiking acoustic Doppler velocimeter data. J. Hydraul. Eng. 128, 117–126.
Grabowski, R.C., Droppo, I.G., Wharton, G., 2011. Erodibility of cohesive sediment: the importance of sediment properties. Earth Sci. Rev. 105 (3–4), 101–120.
Granata, T.C., Serra, T., Colomer, J., Casamitjana, X., Duarte, C.M., Gacia, E., 2001. Flow and particle distributions in a nearshore seagrass meadow before and after a storm. Mar. Ecol. Prog. Ser. 218, 95–106.
Greiner, J.T., Wilkinson, G.M., McGlathery, K.J., Emery, K.A., 2016. Sources of sediment carbon sequestered in restored seagrass meadows. Mar. Ecol. Prog. Ser. 551, 95–105.
Gruber, R.K., Kemp, W.M., 2010. Feedback effects in a coastal canopy-forming submersed plant bed. Limnol. Oceanogr. 55, 2285–2298.
Hendriks, I.E., Sintes, T., Bouma, T.J., Duarte, C.M., 2008. Experimental assessment and modeling evaluation of the seagrass *Posidonia oceanica* on flow and particle trapping. Mar. Ecol. Prog. Ser. 356, 163–173.
Hendriks, I.E., Bouma, T.J., Morris, E.P., Duarte, C.M., 2010. Effects of seagrass and algae of the *Caulerpa* family on hydrodynamics and particle-trapping rates. Mar. Biol. 157, 473–481.
Howe, A.J., Rodríguez, J.F., Saco, P.M., 2009. Surface evolution and carbon sequestration in disturbed and undisturbed wetland soils of the Hunter estuary, southeast Australia. Estuar. Coast Shelf Sci. 84, 75–83.

Howley, C., Devlin, M., Burford, M., 2018. Assessment of water quality from the Normanby River catchment to coastal flood plumes on the northern Great Barrier Reef, Australia. Mar. Freshw. Res. 69 (6), 859–873.
Iafrati, A., 2011. Energy dissipation mechanisms in wave breaking process: spilling and highly aerated plunging breaking events. J. Geophys. Res. 16, C07024.
Islam, M., Jahra, F., Hiscock, S., 2016. Data analysis methodologies for hydrodynamic experiments in waves. J. Nav. Architect. Mar. Eng. 13 (1), 1–15.
Koftis, T., Prinos, P., January, (, 2011. Estimation of wave attenuation over *Posidonia oceanica*. In: 5th International Short Conference on Applied Coastal Research. Aachen, Germany.
Lawson, S.E., McGlathery, K.J., Wilberg, P.L., 2012. Enhancement of sediment suspension and nutrient flux by benthic macrophytes at low biomass. Mar. Ecol. Prog. Ser. 448, 259–270.
Le Méhauté, B., 1976. An Introduction to Hydrodynamics & Water Waves, first ed. (California: Pasadena).
Longstaff, B.J., Dennison, W.C., 1999. Seagrass survival during pulsed turbidity events: the effects of light deprivation on the seagrasses *Halodule pinifolia* and *Halophila ovalis*. Aquat. Bot. 65, 105–121.
Lopez-y-Royo, C., Pergent, G., Alcoverro, T., Buia, M.C., Casazza, G., Martínez-Crego, B., Pérez, M., Silvestre, F., Romero, J., 2011. The seagrass *Posidonia oceanica* as indicator of coastal water quality: experimental intercalibration of classification systems. Ecol. Indicat. 11, 557–563.
Lovelock, C.E., Adame, M.F., Bennion, V., Hayes, M., O'Mara, J., Reef, R., Santini, N.S., 2014. Contemporary rates of carbon sequestration through vertical accretion of sediments in mangrove forest and saltmarshes of South East Queensland, Australia. Estuar. Coast 37, 763–771.
Lowe, R.J., Koseff, J.R., Monismith, S.G., 2005. Oscillatory flow through submerged canopies: 2. Canopy mass transfer. J. Geophys. Res. 110, C10017.
Luhar, M., Coutu, S., Infantes, E., Fox, S., Nepf, H., 2010. Wave-induced velocities inside a model seagrass bed. J. Geophys. Res. 115, C12005.
Manzanera, M., Pérez, M., Romero, J., 1998. Seagrass mortality due to over sedimentation: an experimental approach. J. Coast Conserv. 4 (1), 67–70.
Marbà, N., Arias-Ortiz, A., Masqué, P., Kendrick, G.A., Mazarrassa, I., Bastyan, G.R., Garcia-Orellana, J., Duarte, C.M., 2015. Impact on seagrass loss and subsequent revegetation on carbon sequestration and stocks. J. Ecol. 103, 296–302.
Mulder, T., Syvitski, J.P.M., 1995. Turbidity currents generated at river mouths during exceptional discharges to the world oceans. J. Geol. 103, 285–299.
Oey, L., L Mellor, G., 1993. Subtidal variability of estuarine outflow, plume, and coastal current: a model study. J. Phys. Oceanogr. 23, 164–171.
Paladini de Mendoza, F., Fontolan, G., Mancini, E., Scanu, E., Scanu, S., Bonamano, S., Marcelli, M., 2018. Sediment dynamics and resuspension processes in a shallow-water *Posidonia oceanica* meadow. Mar. Geol. 404, 174–186.
Paling, E.I., Fonseca, M., van Katwijk, M.M., van Keulen, M., 2009. Seagrass restoration. In: Perillo, G., Wolanski, E., Cahoon, D., Brinson, M. (Eds.), Coastal Wetlands: an Integrated Ecosystems Approach. Elsevier, Amsterdam, pp. pp687–713.
Palmer, M.R., Nepf, H., Ackerman, J.D., 2004. Observations of particle capture on a cylindrical collector: implications for particle accumulation and removal in aquatic systems. Limnol. Oceanogr. 49, 76–85.
Pascolo, S., Petti, M., Bosa, S., 2019. Wave forecasting in shallow water: a new set of growth curves depending on bed roughness. Water 11, 2313.
Pineda, M.-C., Strehlow, B., Kamp, J., Duckworth, A., Jones, R., Webster, N.S., 2016. Effects of combined dredging-related stressors on sponges: a laboratory approach using realistic scenarios. Sci. Rep. 7, 5155.
Pujol, D., Nepf, H., 2012. Breaker-generated turbulence in and above a seagrass meadow. Continent. Shelf Res. 49, 1–9.
Pujol, D., Colomer, J., Serra, T., Casamitjana, X., 2010. Effect of submerged aquatic vegetation on turbulence induced by an oscillatory grid. Continent. Shelf Res. 30, 1019–1029.
Pujol, D., Casamitjana, X., Serra, T., Colomer, J., 2013a. Canopy-scale turbulence under oscillatory flow. Continent. Shelf Res. 66, 9–18.
Pujol, D., Serra, T., Colomer, J., Casamitjana, X., 2013b. Flow structure in canopy models dominated by progressive waves. J. Hydrol. 486, 281–292.
Ricart, A.M., York, P.H., Rasheed, M.A., Pérez, M., Romero, J., Bryant, C.V., Macreadie, P.I., 2015. Variability of sedimentary organic carbon in patchy seagrass landscapes. Mar. Pollut. Bull. 100, 476–482.
Ricart, A.M., Pérez, M., Romero, J., 2017. Landscape configuration modulates carbon storage in seagrass sediments. Estuar. Coast Shelf Sci. 185, 69–76.
Ros, À., Colomer, J., Serra, T., Pujol, D., Soler, M., Casamitjana, X., 2014. Experimental observations on sediment resuspension within submerged model canopies under oscillatory flow. Continent. Shelf Res. 91, 220–231.
Roy, E.D., White, J.R., Smith, E.A., Bargu, S., Li, C., 2013. Estuarine ecosystem response to three large-scale Mississippi River flood diversion events. Sci. Total Environ. 458, 374–387.
Serra, T., Colomer, J., Cristina, X., Vila, X., Arellano, J.B., Casamitjana, X., 2001. Evaluation of a laser in situ scattering instrument for measuring the concentration of phytoplankton, purple sulphur bacteria and suspended inorganic sediments in lakes. J. Environ. Eng. 127, 1023–1030.
Serra, T., Colomer, J., Gacia, E., Soler, M., Casamitjana, X., 2002a. Effects of a turbid hydrothermal plume on the sedimentation rates in a karstic lake. Geophys. Res. Lett. 29, 1–5.
Serra, T., Colomer, J., Zamora, L., Moreno-Amich, R., Casamitjana, X., 2002b. Seasonal development of a turbid hydrothermal lake plume and the effects on the fish distribution. Water Res. 36, 2753–2760.
Serra, T., Oldham, C., Colomer, J., 2018. Local hydrodynamics at edges of marine canopies under oscillatory flows. PloS One 13, e0201737.
Serra, T., Gracias, N., Hendriks, I., 2020. Fragmentation in seagrass canopies can alter hydrodynamics and sediment deposition rates. Water 12 (12), 3473.
Short, F.T., Short, C.A., 1984. The seagrass filter: purification of estuarine and coastal waters. In: Kennedy, V.S. (Ed.), The Estuary as a Filter, pp. pp395–413.
Smith, M.J., Stevens, C.L., Gorman, R.A., McGregor, J.A., Neilson, C.G., 2001. Wind-wave development across a large shallow intertidal estuary: a case study of Manukau Harbour, New Zealand. N.Z.J. Mar. Freshwater. Res. NEW ZEAL J MAR FRESH. 35 (5), 985–1000.
Sridhar, P.N., Ramana, I.V., Jaya Kumar, S., 2014. Seasonal occurrence of unique sediment plume in the Bay of Bengal. Eos Transactions American Geophysical Union 89 (3), 22–23.
Terrados, J., Duarte, C.M., 2000. Experimental evidence of reduced particle resuspension within a seagrass (*Posidonia oceanica* L.) meadow. J. Exp. Mar. Biol. Ecol. 243, 45–53.
van Katwijk, M.M., Bos, A.R., Hermus, D.C.R., Suykerbuyk, W., 2010. Ediment modification by seagrass beds: muddification and sandification induced by plant cover and environmental conditions. Estuar. Coast Shelf Sci. 89, 175–181.
Vanderploeg, H.A., Johenger, T.H., Lavrentyev, P.J., Chen, C., Lang, G.A., Agy, M.A., Bundy, M.H., Cavaletto, J.F., Eadie, B.J., Liebig, J.R., Miller, G.S., Ruberg, S.A., McCormick, M.J., 2007. Anatomy of the recurrent coastal sediment plume in Lake Michigan and its impacts on light climate, nutrients, and plankton. J. Geophys. Res. 112, C03S90.
Vautard, R., Bobiet, A., Sobolowski, S., Kjellström, E., Stegehuis, A., Watkiss, P., Mendlik, T., Landgren, O., Nikulin, G., Teichmann, C., Jacob, D., 2014. The European climate under a 2°C global warming. Environ. Res. Lett. 9, 034006.
Wilkie, L., O'Hare, M.T., Davidson, I., Dudley, B., Paterson, D.M., 2012. Particle trapping and retention by *Zostera noltii*: a flume and field study. Aquat. Bot. 102, 15–22.
Wu, P.P.-Y., McMahon, K., Rasheed, M.A., Kendrick, G.A., York, P.H., Chartrand, K., Caley, M.J., Mengersen, K., 2017. Managing seagrass resilience under cumulative dredging affecting light: predicting risk using dynamic Bayesian networks. J. Appl. Ecol. 55, 1339–1350.
Zhang, X., Nepf, H., 2008. Density-driven exchange flow between on water and an aquatic canopy, Water. Resour. Res. 44, W08417.
Zhang, Y., Nepf, H., 2019. Wave-driven sediment resuspension within a model eelgrass meadow. J. Geophys. Res.-Earth 124, 1035–1053.
Zhang, Y., Tang, C., Nepf, H., 2018. Turbulent kinetic energy in submerged model canopies under oscillatory flow, Water. Resour. Res. 54, 1734–1750.
Zong, L., Nepf, H., 2011. Spatial distribution of deposition within a patch of vegetation. Water Resour. Res. 47, W03516.
Zucchetta, M., Veiner, C., Taji, M.A., Mangin, A., Pastres, R., 2016. Modelling the spatial distribution of the seagrass *Posidonia oceanica* along the north african coast: implications for the assessment of good environmental status. Ecol. Indicat. 61, 1011–1023.

Science of the Total Environment 795 (2021) 148854

Contents lists available at ScienceDirect

Science of the Total Environment

journal homepage: www.elsevier.com/locate/scitotenv

Functional dynamics of vegetated model patches: The minimum patch size effect for canopy restoration

Aina Barcelona [a,*], Carolyn Oldham [b], Jordi Colomer [a], Teresa Serra [a]

[a] Department of Physics, University of Girona, 17071 Girona, Spain
[b] School of Engineering, The University of Western Australia, Perth, WA 6009, Australia

HIGHLIGHTS

- A minimum seagrass patch size is needed for successful canopy restoration
- The response of seagrass patches depends on wave velocity and canopy density.
- Under low velocities seagrasses do not interact with waves, but attenuate seabed *TKE*.
- Under moderate to high wave velocities seagrasses interact with waves producing *TKE*.

GRAPHICAL ABSTRACT

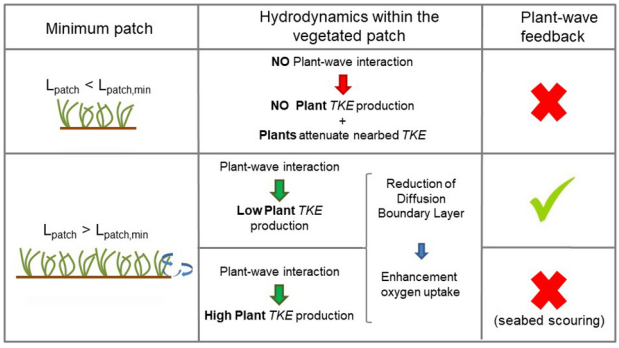

ARTICLE INFO

Article history:
Received 30 January 2021
Received in revised form 31 May 2021
Accepted 30 June 2021
Available online 3 July 2021

Editor: Martin Drews

Keywords:
Seagrass patch length
Turbulent kinetic energy
Wave velocity
Canopy density

ABSTRACT

For the past two centuries coastal zones have been suffering seagrass loss resulting in a network of vegetated patches which are barely interconnected and which may compromise the ecological services provided by the canopy. To optimize management efforts for successful restoration strategies, questions need to be addressed about what appropriate canopy architectural considerations are required under certain hydrodynamic conditions. In this study, a set of laboratory experiments were conducted in which hydrodynamic conditions, plant densities and vegetated patch lengths were varied to determine minimum patch lengths for successful management strategies. Based on the *TKE* production, this study finds two possible canopy behaviours of seagrasses under oscillating flows: one where plants do not interact with the flow and the other where they interact with waves and produce *TKE*. A threshold from the first to second behaviour occurs for $[C_{D-Patch}\frac{nd^2}{2(1-\phi)}]^{\frac{1}{3}}U_w = 2$, where C_D is the drag of the vegetated patch, n is the number of stems per m^2, d is the stem diameter and ϕ is the solid plant fraction. Therefore, high canopy densities, large patches of vegetation or moderate wave velocities will produce plant-wave interaction, whereas low canopy densities, small vegetation patches or slow wave velocities will produce a behaviour akin to the non-vegetated cases.

1. Introduction

Seagrass meadows are seascape ecosystems providing key ecological services in coastal areas such as providing habitats for thousands of fish, bird and invertebrate species (Hughes et al., 2009), supporting commercial fisheries (Metz et al., 2020), regulating nutrient cycling (Montefalcone, 2009), stabilizing seabed sediments (Bouma et al., 2007; Waycott et al., 2009) and mitigating climate change through both carbon storage and sequestration (Fourqurean et al., 2012; Unsworth et al., 2018).

Seagrasses are found in shallow coastal waters (most less than 10 m deep), making them vulnerable to human pressure which can cause direct physical damage to the meadow itself through anchoring, trawling,

* Corresponding author.
E-mail address: aina.barcelona@udg.edu (A. Barcelona).

https://doi.org/10.1016/j.scitotenv.2021.148854
0048-9697/

dredging or urban/port infrastructure development, or indirect damage through nutrient over-enriched waters and/or high sediment loads coming from urban/industrial runoff, aquaculture, and agricultural runoff (Abadie et al., 2016; Grech et al., 2012; Montefalcone, 2009). Consequently, almost 15% of seagrass species worldwide are threatened (Hughes et al., 2009). Waycott et al. (2009) reported that since 1879, 29% of the world's seagrasses have been lost. Furthermore, since 1980 seagrass meadows have disappeared at a rate of 110 km^2 yr^{-1} which, in turn, results in sea soil remineralization and consequently a stock carbon release of up to 299 Tg C yr^{-1} (Fourqurean et al., 2012). Some of the less affected seagrass canopies end with gaps within vegetation patches, contributing to the meadow heterogeneity, while the most endangered seagrass canopies end up as a group of interconnected patches (Sleeman et al., 2005).

Seagrass loss is presented either by an increase in habitat fragmentation that transforms a continuous tract of vegetation into canopies with interspersed gaps (i.e., areas of bare soil interspersed within the meadow) or by a network of vegetated patches in which interconnections are compromised (Robbins and Bell, 1994; Tanner, 2003). Compared with continuous canopies and given their difficulties in coping with hydrodynamical stressors, vegetation patches are usually described as having lower plant densities, shorter leaves and lower nutrient storage (Gera et al., 2013). The functional dynamics of seagrass canopies depend on attenuating the wave velocity (Newell and Koch, 2004) and the turbulent kinetic energy (*TKE*) (Pujol et al., 2013a) which both hinge on plant density and flexibility and the submergence ratio and distance from the meadow edge. As such, the ecological services of fragmented seagrass canopies are expected to be compromised (Paul and Amos, 2011; Serra et al., 2018) because fragmented seagrasses are not fully able to reduce the energy of the flow and therefore the sheltering effect of vegetation is reduced (El Allaoui et al., 2016). Not only this, as the increase in seagrass fragmentation will result in an increase in edges over the canopy areas then the attenuation of the hydrodynamics is also reduced (Granata et al., 2001). Edges are transitional areas between the bare soil and the canopy and represent transition zones for local hydrodynamics. They are mainly a region of the canopy with low wave velocity and *TKE* attenuation compared to a bare bed and where both wave velocity and *TKE* decrease gradually towards the inner canopy region (Serra et al., 2018).

Most studies have focused on the patch size effect on unidirectional flows to discern the structural characteristic of patches and their role in optimising the ecological services provided. For instance, Licci et al. (2019) evaluated the effects of patches of *Callitriche platycarpa* Kütz in lotic ecosystems and found that small patches induced little to no modification to physical parameters. Patches, however, as noted by Folkard (2005), can significantly modify hydrodynamic patterns depending on the distance between them. Likewise, Li et al. (2019) found that vegetated patches greatly impacted the downstream flow: the greater the plant density was, the lower the depth-averaged velocity adjacent to the patch. Concurrent with these results but under oscillatory wave conditions, El Allaoui et al. (2016) found that at the edges of vegetation the sheltering provided was reduced compared to within the canopy, although denser fragmented canopies produced greater sheltering than sparser ones did. The structural characteristics, such as plant density and leaf length, of *Posidonia oceanica* (Linnaeus) Delile meadows determine flow attenuation, with vegetation sheltering nearby gaps (depending on the length of the gaps) in such a way that larger gaps were less protected by the nearby canopy (Colomer et al., 2017). Therefore, fragmented seagrasses that undergo patchiness result in more vulnerable meadows that are then exposed to higher levels of energy which may amplify sediment resuspension and turbidity and produce negative feedback on the canopies (Zhang et al., 2018; Carr et al., 2010).

All of these results have strong implications for seagrass ecosystem restoration strategies which are designed to recover seascapes, their ecosystem biodiversity and the services they provide (Gilby et al., 2020; van Katwijk et al., 2016). Although the first trials for seagrass restoration started during the first half of the twentieth century, it was not until 1970 that interest in restoring seagrass ecosystems increased (van Katwijk et al., 2016). Furthermore, the increased effect that anthropogenic emissions and activities have on the fate of fragmented canopies has meant there is an urgent need to restore world's seascapes, among which include seagrass canopies. Some studies have also modelled seagrass restoration efficiency using chemical and physical abiotic variables such as light, temperature and salinity (Stankovic et al., 2019). For successful restorations, strategies such as improving water quality, removing exotic species, and ensuring the minimum number of shoots planted is within the range of 1000–10,000 shoots/seeds have been implemented (Kupsky and Dornbush, 2019). Many attempts to transplant plants into fragmented canopies have resulted in limited survival rates varying from 9% to 40% according to Paling et al. (2003), while van Katwijk et al. (2016) found that the survival rate was estimated at 37% for the majority of the seagrass restoration trials. Such results indicate the importance of establishing functional dynamic criteria for the patch length scales required if plants are to be successfully replanted in the canopies. Infantes et al. (2009) indicated that high wave velocities produce a loss in the *Posidonia oceanica*' cover. Therefore, despite all the studies carried out, none of them focus on the functional dynamics of the patch, which is dependent on the patch scale; therefore there is a need to include hydrodynamics in the parametrization for future projects of plant restoration.

This study, then, is focused on determining whether there is (or not) an optimal patch length in which the hydrodynamics of the patch mimics those of a canopy without fragmentation. The objective of this study is to determine whether (or not) a single patch behaves dynamically as a canopy. As such, the minimum patch size was defined as the critical length over which a single patch was dynamically mimicking a continuous canopy under a certain oscillatory flow regime. It is expected that a patch with functional dynamics akin to those of a canopy might be optimal for successful replantation. Thus, different patches with different lengths and vegetation densities were combined to obtain the structural scale that can guarantee successful seagrass canopy restoration.

2. Methodology

2.1. The flume

The study was carried out in a laboratory methacrylate flume (600 cm long, 50 cm wide and 60 cm deep, Fig. 1) with a mean water height of $h = 30$ cm (Table 1). The flume was equipped with a vertical paddle-type wavemaker at the entrance. The wavemaker was driven by a variable-speed motor at two frequencies ($f = 0.50$, 1.12 Hz). A plywood beach (slope = 1:2) covered with foam rubber to eliminate wave reflection was placed at the end of the flume (Pujol et al., 2013a; Serra et al., 2018). At the measurement depth, the percentage of U_c reduction was 39% and 59% for the wave frequencies of 1.12 Hz and 0.5 Hz, respectively. There was also a reduction of 3.0% and 2.9% for the wave velocity for frequencies of 1.12 Hz and 0.5 Hz, respectively. In the longitudinal direction, $x = 0$ cm was situated at the wavemaker, in the lateral direction, $y = 0$ cm was at the centre of the tank, and in the vertical direction, $z = 0$ cm was situated at the flume bed.

2.2. Patches of flexible vegetation

The system of laboratory model vegetation consisted of a series of flexible plants made from eight 0.075 mm thick polyethylene canopy blades attached to PVC dowels that had been randomly inserted into a perforated baseboard ($L_{base\text{-board}} = 250$ cm, Pujol et al., 2013a), with a rigid dowel extending 1 cm above the bed (Zhang et al., 2018). The model plants were geometrically and dynamically similar to *Posidonia oceanica* plants (Ghisalberti and Nepf, 2002; Pujol et al., 2013a). The leaf length was 14 cm, and the effective height when the leaves were

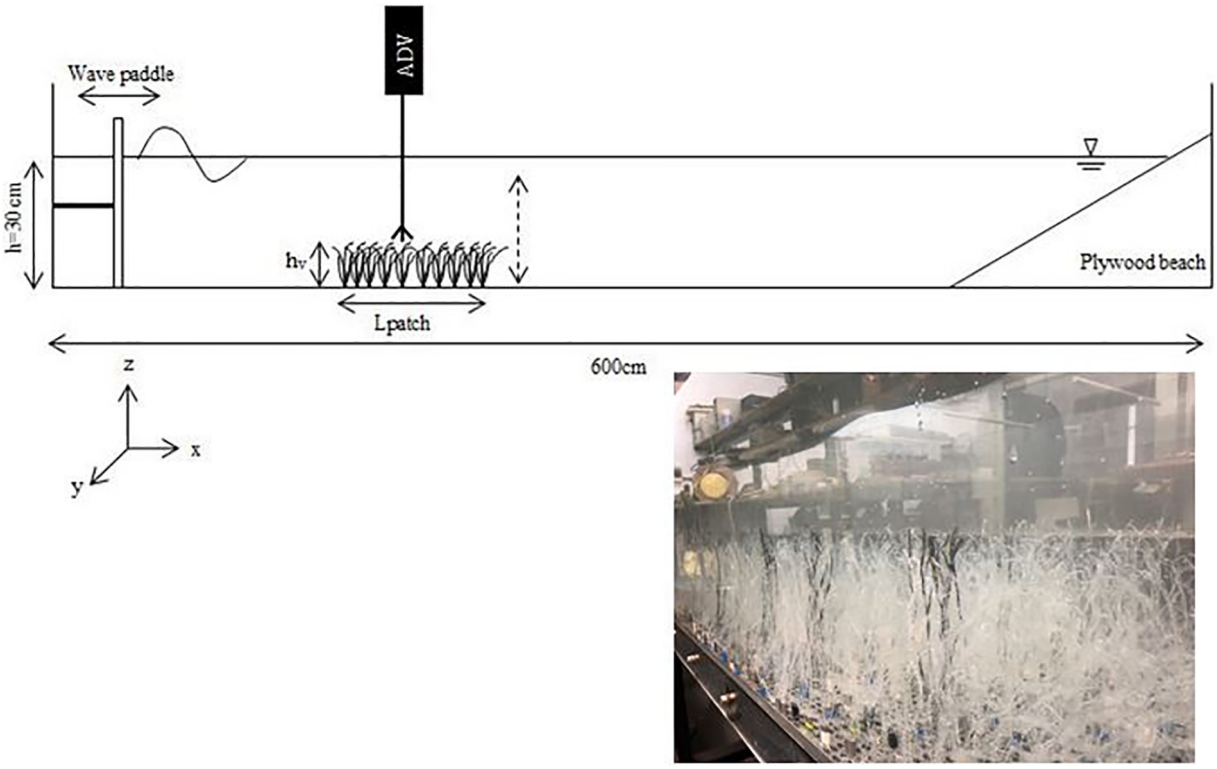

Fig. 1. A lateral view of the experimental setup (top), with the wave paddle on the left to provide waves from left to right. Experiments were conducted in a 600x50x50 cm long flume, with a mean water depth of 30 cm. The model patch had patch lengths that ranged from 2.8 cm to 42 cm. The triangle at the water-air interface represents the water level in the flume. An ADV was vertically mounted to measure the instantaneous velocities at selected vertical heights. A photograph of the experimental setup (bottom), with the simulated vegetation.

bent by the waves was $h_v = 8.5$ cm for $f = 1.12$ Hz and $h_v = 10.5$ cm for $f = 0.5$ Hz. The effective heights were calculated by the mean between both the maximum and the minimum bending heights of the plants for 25 oscillations The initial position of the vegetation (x_0) was situated 100 cm from the wavemaker (Fig. 1). The vegetation density of patches was quantified using the solid plant fraction (*SPF*) defined as:

$$\mathrm{SPF}\ (\%) = 100n\pi\left(\frac{d}{2}\right)^2 \quad (1)$$

where n is the number of stems per unit area and d is the stem diameter (1 cm). Six *SPF*s were used (0%, 2.5%, 3.5%, 5%, 7.5% and 10%), which corresponded to vegetation densities of $n = 0$, 318, 446, 637, 955 and 1273 stems·m^{-2} (Fig. 2) and similar to the canopy densities between 78 to 1000 stems·m^{-2} found in coastal areas (Bacci et al., 2017; Colomer et al., 2017; Gera et al., 2013; van Katwijk et al., 2010); *SPF* = 0% corresponded to the case with no vegetation. For each *SPF*, different patch sizes, L_{patch}, ranging from 32 to 240 cm were considered (Table 2). In this study, the longest patch $L_{patch} = 240$ cm. A total of 67 experiments were performed for the different *SPF*s, patch lengths and wave frequencies (Table 2). In the experiments, the patch edge was considered as the interface from the vegetated region and the non-vegetated region (Schoelynck et al., 2018). For all patch lengths, flow velocity profiles were measured at the centre of the patch. The length of the patch increased from this centre point outwards (i.e., to the wave maker and to the beach, see Fig. 1) so that the measuring point was always the same for all patches.

Table 1
Nomenclature table.

Variable	Units	Definition
a	cm^2	Frontal area
A_w	cm	Wave excursion length
A_w/S_b	Non-dimensional	Ratio between wave excursion to plant-to-plant distance between blades
f	Hz	Wave frequency
h	cm	Water height
h_v	cm	Effective plant height
L	cm	Vegetation length
L_{canopy}	cm	Canopy length
L_{patch}	cm	Patch length
n	stems·m^{-2}	Canopy density
n_b	Blades	Blade density
S_b	cm	Plant-to-plant distance between blades
SPF	%	Solid plant fraction
TKE	cm^2·s^{-2}	Turbulent kinetic energy
u	cm·s^{-1}	Eulerian velocity in the x direction
u'	cm·s^{-1}	Turbulent velocity
U_c	cm·s^{-1}	Steady velocity associated with the current
U_i	cm·s^{-1}	Instantaneous velocity
$U_i(\varphi)$	cm·s^{-1}	Instantaneous velocity according to the phase
U_w	cm·s^{-1}	Wave velocity
U_w^{rms}	cm·s^{-1}	Orbital velocity
v	cm·s^{-1}	Eulerian velocity in the y direction
w	cm·s^{-1}	Eulerian velocity in the z direction
x	cm	Longitudinal direction
$x = 0$	cm	Position of the wave paddle
y	cm	Lateral direction
z	cm	Vertical direction
α_w	Non-dimensional	Ratio of vegetated to non-vegetated U_w
β_w	Non-dimensional	Ratio of vegetated to non-vegetated *TKE*
φ	Radians	Wave phase
ϕ	Non-dimensional	Solid plant fraction

2.3. Measuring velocities

The Eulerian velocity field was defined as (u, v, w) in the (x, y, z) directions, respectively. The three components of velocity were recorded (50 Hz over 5 min) with a downwards looking Acoustic Doppler Velocimeter (16-MHz MicroADV, Sontek). The ADV measured at a distance of 5 cm from the probe tip and with a sampling volume of 0.09 cm^3. Beam correlations less than 70% were discarded and spikes were removed (Goring and Nikora, 2002; Pujol et al., 2013a). The longitudinal

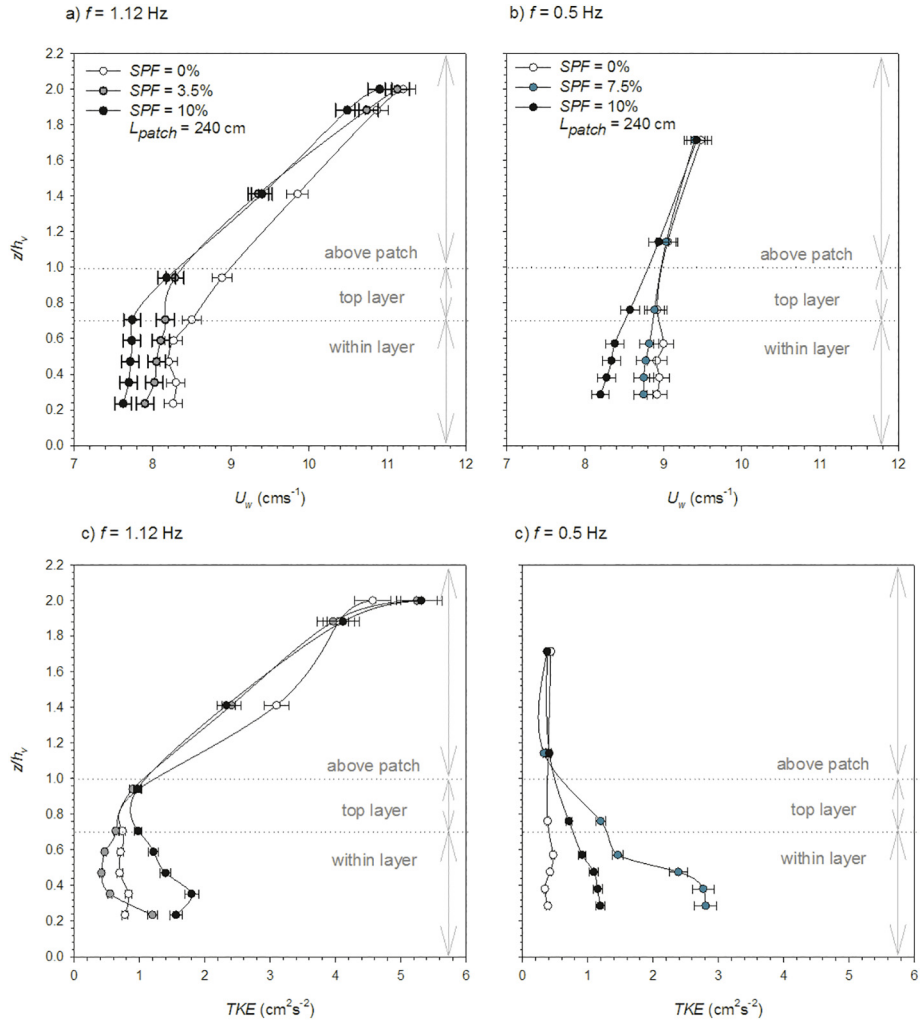

Fig. 2. Wave velocity (U_w) vertical profiles for a) $f = 1.12$ Hz, b) $f = 0.5$ Hz and *TKE* vertical profiles for c) $f = 1.12$ Hz and d) $f = 0.5$ Hz. Unfilled circles correspond to the cases of $SPF = 0\%$, whereas black, blue and grey filled symbols correspond to $SPF = 10\%$, 7.5%, and 3.5% respectively. The experiments presented here correspond to the $L_{patch} = 240$ cm patch length case. (For interpretation of the references to colour in this figure legend, the reader is referred to the web version of this article.)

velocity was measured at an antinode to eliminate the lower order spatially periodic variation in wave and velocity amplitude associated with wave reflection (Luhar et al., 2010; Pujol et al., 2013a). The ADV was mounted on a movable vertical frame (at y = 0 cm, Fig. 1) and manually adjusted to measure a vertical profile. Some plants were removed to avoid blocking the ADV beams (Ros et al., 2014; Zhang et al., 2018), and were re-inserted into nearby holes.

2.4. Hydrodynamic analysis

For oscillatory flows, the instantaneous velocity in the *x* direction, $U_i(t)$, can be decomposed as:

$$U_i(t) = U_c + U_w + u' \tag{2}$$

where U_c is the steady velocity associated with the wave, U_w is the unsteady wave motion in the *x* direction which represents spatial variations in the phase-averaged velocity field, and u' is the turbulent velocity, that is, the instantaneous velocity fluctuation in the x-direction. U_c is the phase-averaged velocity:

$$U_c = \frac{1}{2\pi}\int_0^{2\pi} U_i(\varphi)\partial\varphi \tag{3}$$

where $U_i(\varphi)$ is the instantaneous velocity according to the phase (Lowe et al., 2005; Luhar et al., 2010). Wave velocity, U_w, was obtained by using a phase averaging technique. The Hilbert transform was used to average oscillatory flow velocities with a common phase (Pujol et al., 2013b; Ros et al., 2014). The root mean square (rms) of $U_i(\varphi)$ was considered as the characteristic value of the orbital velocity U_w^{rms} (U_w hereafter) at each depth and was calculated according to:

$$U_w^{rms} = \sqrt{\frac{1}{2\pi}\int_0^{2\pi} (U_i(\varphi) - U_c)^2 \partial\varphi} \tag{4}$$

The ratio α_w of the wave velocity (U_w) was calculated following Lowe et al. (2005):

$$\alpha_w = \frac{U_w}{U_{w,WP}} \tag{5}$$

where U_w is the wave velocity within the patch at z = 4 cm for vegetated cases and $U_{w,WP}$ is the wave velocity at z = 4 cm for non-vegetated cases. The measurements within the vegetation at $z = 4$ cm corresponded to $z/h_v = 0.47$ for $f = 1.12$ Hz and $z/h_v = 0.38$ for $f = 0.5$ Hz. This depth was chosen from the wave velocity profile, shown later on in the results section so that it was situated out of the shear region situated at the top of the vegetation and also far from the bed of the flume. Therefore, α_w provided a measure of the wave velocity attenuation within the patch for vegetated cases compared to non-vegetated cases. Consequently, values of $\alpha_w \approx 1$ indicated a weak or negligible

Table 2
Summary of the experiment characteristics.

Run	f (Hz)	SPF (%)	n (stems·m^{-2})	L_{patch} (cm)	aL	Aw/S_b	Run	f (Hz)	SPF (%)	n (stems·m^{-2})	L_{patch} (cm)	aL	Aw/S_b
WP1	0.5	0	0		0		SFV34	1.12	3.5	446	70	3.12	0.70
WP2	1.12	0	0		0		SFV35				112	5.00	0.69
SFV3	0.5	1	127	42	0.53	0.94	SFV36				126	5.62	0.69
SFV4				70	0.89	0.92	SFV37				140	6.24	0.70
SFV5				112	1.42	0.92	SFV38				154	6.87	0.68
SFV6				196	2.49	0.94	SFV39				168	7.49	0.68
SFV7		7.5	955	42	4.01	2.84	SFV40				196	8.74	0.68
SFV8				70	6.69	2.75	SFV41				240	10.61	0.67
SFV9				112	10.70	2.77	SFV42		5	637	42	2.68	0.83
SFV10				196	18.72	2.67	SFV43				70	4.46	0.83
SFV11		10	1273	42	5.35	3.11	SFV44				98	6.24	0.83
SFV12				70	8.91	3.08	SFV45				126	8.03	0.82
SFV13				84	10.69	2.97	SFV46				168	12.49	0.80
SFV14				98	12.48	2.96	SFV47				196	10.70	0.81
SFV15				112	14.26	2.92	SFV48				210	13.38	0.80
SFV16				133	16.93	2.98	SFV49				240	15.16	0.80
SFV17				140	17.82	2.84	SFV50		7.5	955	42	4.01	1.03
SFV18				154	19.60	2.97	SFV51				70	6.69	1.04
SFV19				182	23.17	3.04	SFV52				84	8.02	1.01
SFV20				224	28.52	2.89	SFV53				98	9.36	1.01
SFV21				240	30.30	2.86	SFV54				112	10.70	0.99
SFV22	1.12	2.5	318	42	1.34	0.59	SFV55				133	12.03	0.98
SFV23				70	2.23	0.60	SFV56				154	14.71	0.99
SFV24				84	2.67	0.59	SFV57				196	18.72	0.96
SFV25				98	3.12	0.59	SFV58				240	22.73	0.97
SFV26				112	3.56	0.58	SFV59		10	1273	42	5.35	1.18
SFV27				126	4.01	0.59	SFV60				70	8.91	1.18
SFV28				140	4.45	0.59	SFV61				84	10.69	1.15
SFV29				154	4.90	0.59	SFV62				98	12.48	1.15
SFV30				168	5.34	0.59	SFV63				112	16.04	1.13
SFV31				182	5.79	0.59	SFV64				133	24.95	1.10
SFV32				196	6.23	0.59	SFV65				168	19.60	1.12
SFV33				240	7.57	0.59	SFV66				196	21.39	1.12
							SFV67				240	30.30	1.11

attenuation of the wave velocity by the vegetation, whereas low values of $\alpha_w < 1$ indicated high wave velocity attenuation.

The turbulent velocity was obtained by:

$$u' = U_i - U_c - U_w \tag{6}$$

where U_c and U_w were calculated by Eqs. 3 and 4. The turbulent velocity was calculated for all directions (u', v' and w') for z = 4 cm.

Turbulent kinetic energy (TKE) was calculated following Ros et al. (2014) as:

$$TKE = \frac{1}{2}\left(\left\langle u'^2\right\rangle + \left\langle v'^2\right\rangle + \left\langle w'^2\right\rangle\right) \tag{7}$$

where $< >$ denotes the time average.

The ratio, β_w, was calculated following Colomer et al. (2017):

$$\beta_w = \frac{TKE}{TKE_{WP}} \tag{8}$$

where TKE was the turbulent kinetic energy within the patch at z = 4 cm for vegetated cases and TKE_{WP} was the TKE measured at z = 4 cm for the non-vegetated case. Therefore, values of $\beta_w \approx 1$ indicated a weak or negligible attenuation of the TKE, whereas low values of $\beta_w < 1$ indicated a high TKE attenuation compared to the non-vegetated case.

In order to gain knowledge of the vertical distribution of TKE within the patch, a non-dimensional model was set following Zhang et al. (2018). For a full canopy, Zhang et al. (2018) found that the relationship between the TKE, U_w and the main canopy parameters followed:

$$\frac{\sqrt{TKE}}{U_w} = \delta\left[C_D \frac{l_t}{d}\frac{nd}{2(1-\phi)}\right]^{\frac{1}{3}} \tag{9}$$

where δ is the scale constant, ϕ is the solid volume fraction, $\phi = n\frac{\pi}{4}d^2$, l_t is characteristic eddy length-scale, and C_D is the drag of the form of the obstacle along the fluid patch, with $C_D = 1.4$ being used in both studies. In Eq. (9), the characteristic length scale, L_{patch} / L_{canopy}, for each frequency, is introduced to account for the volume of the patch in relation to the maximum canopy volume in the form of $\frac{V_{Patch}^{1/3}}{V_{Canopy}^{1/3}} = \left(\frac{aL_{patch}}{aL_{canopy}}\right)^{\frac{1}{3}} = \left(\frac{L_{patch}}{L_{canopy}}\right)^{\frac{1}{3}}$, therefore Eq. (9) is expressed following:

$$\frac{\sqrt{TKE}}{U_w} = \delta\left[C_D\left(\frac{L_{patch}}{L_{canopy}}\right)^{\frac{1}{3}}\frac{l_t}{d}\frac{nd^2}{2(1-\phi)}\right]^{\frac{1}{3}} \tag{10}$$

Zhang et al. (2018) considered $l_t = d$ for $S > 2d$ whereas $l_t = S$ for $S < 2d$. In the present study, since $S > 2d$, $l_t = d$, therefore:

$$\frac{\sqrt{TKE}}{U_w} = \delta\left[C_D\left(\frac{L_{patch}}{L_{canopy}}\right)^{\frac{1}{3}}\frac{nd^2}{2(1-\phi)}\right]^{\frac{1}{3}} \tag{11}$$

Defining $C_{D\text{-}Patch} = C_D(L_{patch}/L_{canopy})^{1/3}$ as the drag generated by the patch, Eq. (11) results:

$$\frac{\sqrt{TKE}}{U_w} = \delta\left[C_{D-Patch}\frac{nd^2}{2(1-\phi)}\right]^{\frac{1}{3}} \tag{12}$$

3. Results

For the longest patch considered (L_{patch} = 240 cm), the wave velocity U_w decreased with depth for all the experiments i.e., with and without plants (Fig. 2). Three vertical layers could be differentiated based on the vertical profile of U_w. A first layer above the patch ($z/h_v > 1$), where U_w for the vegetated case was similar to that of the without-plants case. A second layer within the patch ($0.7 < z/h_v < 1$), where U_w for the case with plants was lower than that for the non-vegetated case and decreased gradually with depth. A third layer within the patch, the inner vegetation layer ($z/h_v < 0.7$), where U_w was nearly constant with depth down to the bed. The vertical decrease of U_w for the higher frequency case (1.12 Hz) was stronger than for the low frequency (0.5 Hz) (Fig. 2a and b). For the higher frequency, a decrease in the U_w from the lowest to greatest depth was found for all the vegetated and non-vegetated cases (Fig. 2a), while for the lower frequency, U_w presented the slowest vertical reduction, especially for the non-vegetated cases (Fig. 2b). For the non-vegetated cases and for the high frequency, *TKE* decreased with depth down to $z/h_v = 0.7$. Below $z/h_v = 0.7$, the *TKE* remained constant down to the bed (Fig. 2c). In contrast, for the low frequency in non-vegetated cases, *TKE* was constant with depth (Fig. 2d). Unlike what had been obtained for U_w, the *TKE* was higher for vegetated than for non-vegetated cases, except for *SPF* = 3.5% at the higher frequency (Fig. 2c and d). For the higher frequency and the vegetated and non-vegetated cases, the *TKE* decreased with depth. However, for the vegetated cases, the *TKE* slightly increased with depth from $z/h_v =$ 0.7 down to the bed (Fig. 2c).

Both wave attenuation (α_w) and *TKE* attenuation (β_w) were calculated for the different non-dimensional patch length scales (L_{patch}/h_v) and for the different *SPF*s studied (Fig. 3). For both frequencies, the greater the *SPF* was, the lower α_w was (Fig. 3a and b). For the high frequency studied (f = 1.2 Hz) and for *SPF* = 2.5%, α_w remained constant with L_{patch}/h_v (Fig. 3a). For the other *SPF* studied (>2.5%), α_w was constant for low L_{patch}/h_v decreasing afterward as L_{patch}/h_v increased. Therefore, for the low frequency and all *SPF*s considered, the decrease in α_w started from a threshold in the patch length characterized by $L_{patch}/h_v = 4$ (Fig. 3b). For the low frequency studied, and for all *SPF*s considered, α_w decreased with an increase in L_{patch}/h_v (Fig. 3b), without any threshold in L_{patch}/h_v. For the high frequency, f = 1.12 Hz, α_w remained constant for $L_{patch}/h_v > 20$, whereas for f = 0.5 Hz, α_w remained constant for $L_{patch}/h_v > 10$. The value of α_w reached decreased as *SPF*s increased (Fig. 3a, b).

In contrast to U_w, β_w remained constant with L_{patch}/h_v for both frequencies (1.12 Hz and 0.5 Hz) and for all *SPF*s studied (Fig. 3c and d). However, for the high frequency studied, the low vegetation densities *SPF* = 2.5%, 3.5% and 5% showed values of $\beta_w < 1$, while β_w was above 1 for *SPF* = 7.5 and 10%, with β_w increasing with SPF (Fig. 3c). Contrary to this, for the low frequency studied, $\beta_w > 1$ except for the case of SPF = 1%, for which $\beta_w = 1$ (Fig. 3d). For this frequency, β_w for *SPF* = 10% was lower than that for *SPF* = 7.5%, contrary to what had been found for the high frequency.

Following Eq. (11), two behaviours could be distinguished when considering $TKE^{1/2}$ versus$[C_{D-Patch}\frac{nd^2}{2(1-\phi)}]^{\frac{1}{3}}U_w$, and deduced by applying the non-dimensional analysis, which is shown in Fig. 4. For $[C_{D-Patch}\frac{nd^2}{2(1-\phi)}]^{\frac{1}{3}}U_w < 2$, $TKE^{1/2}$ remained constant with $[C_{D-Patch}\frac{nd^2}{2(1-\phi)}]^{\frac{1}{3}}U_w$ at a value of $TKE^{1/2} = 0.56$, while for $[C_{D-Patch}\frac{nd^2}{2(1-\phi)}]^{\frac{1}{3}}U_w > 2$, $TKE^{1/2}$ presented a linear trend versus $[C_{D-Patch}\frac{nd^2}{2(1-\phi)}]^{\frac{1}{3}}U_w$ with a slope of 0.56 (Fig. 4). The first regime (on the left in Fig. 4) corresponded to the cases where the dynamics were governed by either single stems of

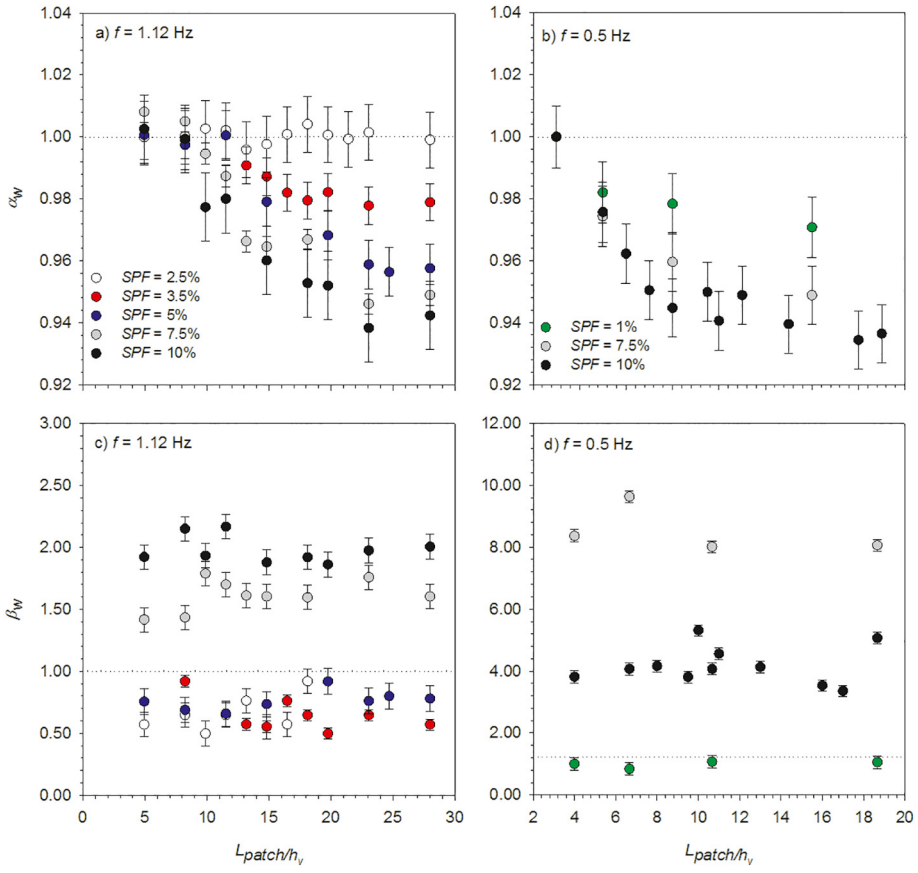

Fig. 3. Wave attenuation (α_w) versus L_{patch}/h_v for a) f = 1.12 Hz and b) f = 0.5 Hz, and *TKE* attenuation (β_w) for c) f = 1.12 Hz and d) f = 0.5 Hz at z = 4 cm, for different *SPF*s ranging from 1 to 10%.

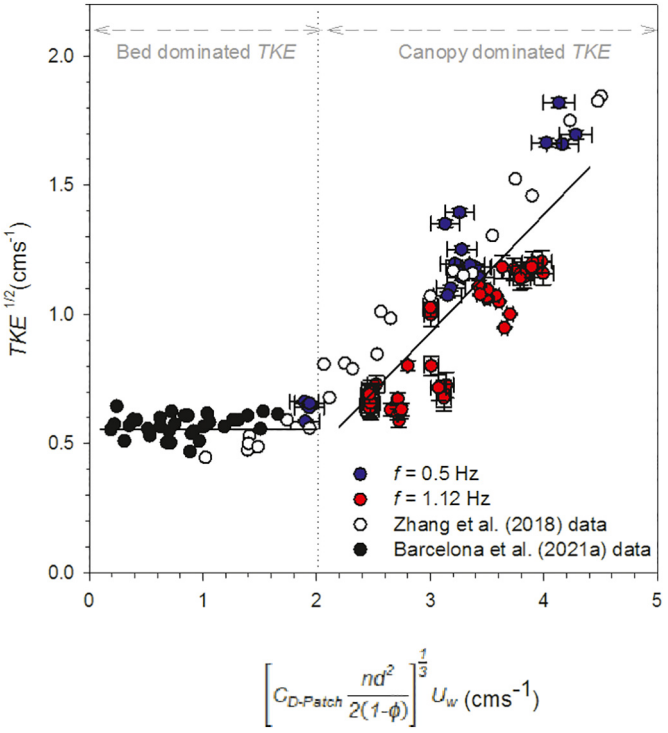

Fig. 4. Non-dimensional model for $TKE^{1/2}$ for high frequencies (red filled circles), low frequencies (blue filled circles), and Zhang et al. (2018) data (unfilled circles). H. Nepf (personal communication provided the original data from Zhang et al.'s (2018) and Barcelona et al. (2021a) data (black filled circles). The vertical dashed line represents the minimum value of $\left[C_{D-Patch}\frac{nd^2}{2(1-\phi)}\right]^{\frac{1}{3}}U_w$ that separates the different trends observed for $TKE^{1/2}$. The horizontal solid line at $TKE^{1/2} = 0.0056$ represents that for $\left[C_{D-Patch}\frac{nd^2}{2(1-\phi)}\right]^{\frac{1}{3}}U_w<2$, where $TKE^{1/2}$ remained constant. For $\left[C_{D-Patch}\frac{nd^2}{2(1-\phi)}\right]^{\frac{1}{3}}U_w> 2$ a linear tendency was found: $TKE^{1/2} = 0.47*\left[C_{D-Patch}\frac{nd^2}{2(1-\phi)}\right]^{\frac{1}{3}}U_w - 0.47$, with $R^2 = 0.73$ and 99% of confidence. (For interpretation of the references to colour in this figure legend, the reader is referred to the web version of this article.)

vegetation or the cases without vegetation. The second regime (on the right in Fig. 4) corresponded to the case where the dynamics were governed by the patch scale.

The transition of both regimes determines the minimum patch length $L_{patch,min}$, for which for $L_{patch} < L_{patch,\ min}$ the $TKE^{1/2}$ was independent of $[C_{D-Patch}\frac{nd^2}{2(1-\phi)}]^{\frac{1}{3}}U_w$. In this region $TKE^{1/2}$ was equal to that found for non-vegetated cases, indicating that the vegetation did not contribute to increasing the $TKE^{1/2}$. In contrast, for $L_{patch} > L_{patch,min}$ a linear trend between $TKE^{1/2}$ and $[C_{D-Patch}\frac{nd^2}{2(1-\phi)}]^{\frac{1}{3}}U_w$ was obtained. This result indicated that the experimental cases with high $L_{patch} > L_{patch,\ min}$ produced an increase in the $TKE^{1/2}$, therefore in this regime dominated by the patch scale the minimum patch length was calculated following Eq. (12), observing a dependence of the minimum patch length on L_{canopy}, canopy density and U_w, and calculated as follows:

$$L_{patch} = L_{canopy}\left[\frac{2(1-\phi)}{C_D n d^2}\left(\frac{2}{U_w}\right)^3\right]^3 \quad (13)$$

4. Discussion

In this study, the capacity of submerged patches of flexible plants to attenuate waves, in terms of their velocity and *TKE*, has been found to depend on the wave penetration within the patch and the volume occupied by the vegetation. The wave penetration was a function of the orbital excursion length scale and the plant-to-plant distance, while the volume of the vegetation patch was a function of its length and density. All of this information provides clues for determining the structural analysis of functional patches of seagrass that facilitate hydrodynamical services comparable to those of continuous seagrass meadows.

4.1. Effect of the canopy density of the patch

Here, the dynamics of functional patches that were observed to mimic the properties of a continuous vegetated canopy were characterized by the attenuation of the wave velocity with a magnitude that depended on the shoot density within the patch. This aligns with the results found previously by other authors (Gacia et al., 1999; Paul and Amos, 2011; Pujol et al., 2013b). According to the results from Ros et al. (2014) and Zhang et al. (2018), a continuous canopy also attenuates the turbulent kinetic energy generated by the bed when the wave can enter within the vegetation (i.e., $A_w/S_b < 1$, where A_w was the wave excursion length, S_b was the plant-to-plant distance between leaves, calculated as $S_b = (n_b)^{-1/2}$ (Zhang et al., 2018)). In these cases, the denser the canopy, the greater the sheltering provided. In contrast, when $A_w/S_b > 1$, the turbulent kinetic energy increases with A_w/S_b due to the interaction of the flow with the vegetation and the wakes generated by plant stems. Therefore, high canopy densities (i.e., small S_b and high A_w/S_b) result in higher *TKE* due to the production of stem wake turbulence. A range of A_w/S_b from 0.58 to 3.04 was considered in this study, covering cases with $A_w/S_b < 1$ where the *TKE* generated by the bed is attenuated and cases with $A_w/S_b > 1$ where *TKE* is generated by plant stems. In the case studied here, wave velocities at the vegetated patch ranged from 7 cm s^{-1} to 10 cm s^{-1}, resulting in stem Reynolds numbers between $Re_s = 700$ and 1000, respectively. Stem Reynolds numbers above 200 have been found to produce vortex shedding (Nepf et al., 1997) which is a source of turbulence in the system. The increase in the canopy density is expected to also produce an increase in the number of wakes generated and, in turn, an increase in the turbulent kinetic energy in the system. This aligns with the increase in the turbulent kinetic energy for the high patch densities observed in the present study.

However, this study demonstrates the contrary in that β_w remains constant with the patch size for both different *SPF*s and frequencies. Nevertheless, the results also show how patches, instead of reducing *TKE*, are capable of enhancing this energy for higher density patches (*SPF* ≤ 7.5%) for both frequencies ($f = 0.5$ and 1.12 Hz), while sparser patches attenuate the *TKE* in a range between β_w 0 to 0.5. These results agree with Zhang et al. (2018), who found that for $A_w/S_b > 1$ *TKE* was generated within the canopy. This coincides with the present study where, for both frequencies, the A_w/S_b was found to be greater than 1. These results are attributed to the increase in the number of wakes generated by the plant stems as the patch density increases which, in turn, is related to the reduction of the wave velocity (Tang et al., 2019). Folkard (2005) also found an increase of the Reynolds stress downstream of a single patch of flexible vegetation under unidirectional flow increasing with the flow velocity. Likewise, under the unidirectional flow, Tinoco and Coco (2014) also found higher *TKE* in denser canopies, thus agreeing with the results of this study even though they used emergent rigid stems.

4.2. Effect of wave velocity and frequency

Moreover, wave frequency plays a relevant and important role in wave attenuation within vegetated patches. Intermediate patch densities under oscillating flows provide greater wave attenuation for low frequencies than for high frequencies. This result is in accordance with Hansen and Reidenbach (2017) who found that lower frequencies produced a higher wave attenuation compared to higher frequencies. However, high patch densities of *SPF* = 10% produced equal wave attenuations for the two frequencies studied. These results agree with Paquier et al. (2018) who found that the attenuating capability of

waves of the patchy meadows is related to wave heights and frequencies. They also found that in the case of *Zostera noltei* Hornemann, patchy meadows are only capable of attenuating high frequency waves. These results are also in accordance with the concept that under low wave frequencies, a higher wave attenuation is produced than under high wave frequencies. Furthermore, for the low frequency case, the change from $SPF = 7.5\%$ to $SPF = 10\%$ did not produce a notable reduction in the U_w. This result might be because in high patch densities wakes are produced by stem overlap and occupy the entire region between plant stems. Therefore, a further increase in vegetation might not produce a subsequent increase in the turbulent kinetic energy locally. This result is in accordance with the definition of a patch of vegetation as described by Schoelynck et al. (2018).

4.3. Effect of the patch length scale

This study also demonstrates that the patch size plays a crucial role in determining the hydrodynamics within the vegetated patches. For low wave frequencies, the wave attenuation at the centre of the patch depended on its shoot density. These results may be related to the studies from Zong and Nepf (2010) and Devi and Kumar (2016), who found a lower linear velocity attenuation through sparse patches than through dense patches. In contrast, for high wave frequencies, small patches with $L_{patch} < 6h_v$, do not provide any reduction in the wave velocity compared with the without-plants case, whereas patches of $L_{patch} > 6h_v$ reduce the wave velocity as the canopy density increases. These results align with those from Licci et al. (2019), who found that the effect of small patches ($L_{patch}/h_v > 9$) of *Callitriche platycarpa,* Kütz in the attenuation of the linear velocity was little or negligible, while larger patches induced significant modifications in the linear velocity.

4.4. Patch length-scale thresholds

The non-dimensional model for the $TKE^{1/2}$ indicated that $TKE^{1/2}$ remains nearly constant for $[C_{D-Patch}\frac{nd^2}{2(1-\phi)}]^{\frac{1}{3}}U_w < 2$. Low values of $[C_{D-Patch}\frac{nd^2}{2(1-\phi)}]^{\frac{1}{3}}U_w$ can hold for both, low wave frequencies, sparse patches, or small patches. Therefore, a low volume of vegetation produces a constant value of $TKE^{1/2} = 0.56$, which is the same value obtained for the non-vegetated cases, hence the *TKE* source is generated by the bed friction. This threshold means that the minimum patch size required for a certain patch density and under certain hydrodynamical conditions to be dynamically functional as a continuous canopy can be determined. Conversely, it also means that the minimum density required for a certain patch length to play a role as a patch (instead of a non-vegetated case) can be determined, increasing the *TKE* by the interaction between the wave and the plants. That said, the results presented here not only show this, but also that the behaviour of a patch also depends on the hydrodynamics i.e., wave frequency and velocity. For cases of $[C_{D-Patch}\frac{nd^2}{2(1-\phi)}]^{\frac{1}{3}}U_w > 2$, the $TKE^{1/2}$ increased with $[C_{D-Patch}\frac{nd^2}{2(1-\phi)}]^{\frac{1}{3}}U_w$. It is interesting to notice that a certain patch with a certain canopy density might not generate *TKE* for low U_w i.e., $[C_{D-Patch}\frac{nd^2}{2(1-\phi)}]^{\frac{1}{3}}U_w < 2$, but after an increase in U_w it can interact with the wave field, producing *TKE* i.e., $[C_{D-Patch}\frac{nd^2}{2(1-\phi)}]^{\frac{1}{3}}U_w > 2$.

4.5. Management strategies

From a hydrodynamical point of view, a minimum patch size is required for the patch to interact with the wave flow and move from of a regime dominated by either the single stem scale or the non-vegetated case towards a regime dominated by the canopy. From this point of view, this study provides management strategies for potential successful seagrass meadow restoration. West et al. (1990) studied the survival of *Zostera muelleri* subsp., *capricorni* (Ascherson) S.W.L. Jacobs, and *Posidonia australis*, J.D. Hooker, transplants. For *P. australis* canopies, single shoots, or clumps of 2–3 shoots were transplanted, while for *Z. mulleri* subsp. *capricorni* about 20–30 shoots were used as transplanted units. The transplants were monitored and only very few survived under high energetic events, indicating that the parametrization of the transplanted shoots may have been incomplete. In addition, Infantes et al. (2009) reported that $U_w > 38$–42 cm·s^{-1} caused a decrease in the cover of the *Posidonia oceanica* meadows meaning that, for these velocities, the generation of *TKE* within the patch will become extremely high and will produce a sufficient level of seabed erosion to potentially cause irreversible plant loss. Therefore, hydrodynamics need to be included in the parameterization for future seagrass restoration projects.

Furthermore, Stipek et al. (2020) demonstrated that the mortality rate of seagrass patches depended on the size of the patch, with small patches (<50 m^2, $L_{patch} < 7.07$ m) undergoing a high annual mortality rate (of 57%) compared to the lower mortality rate (<5%) found for larger patches. If a mean leaf length of 0.8 m is considered (Gruber and Kemp, 2010), assuming that leaf would bend the same percentage like that in the current study for a typical frequency of 0.5 Hz ($h_v =$ 10.5 cm for a leaf length of 14 cm, 75% of the leaf length), h_v in the field would be 0.6 m. Then their small patches would correspond to lengths equal to or smaller than $L_{patch} = 7.07$ m $= 11.78\, h_v$. This finding aligns with the transition observed in this study, where for $L_{patch} > 10h_v$ and for typical ocean waves of $f = 0.5$ Hz, α_w remains constant, indicating that the patch behaves like a continuous canopy. In contrast, for $L_{patch} < 10h_v$, α_w increases towards the value for the non-vegetated case as L_{patch} decreases.

By applying the model found in the current study, the behaviour of patches found in natural seagrass meadows under different hydrodynamic conditions can be determined. In fact, two behaviours have been observed: one where plants do not interact with the wave field and another where they do, thus generating *TKE*. Considering the findings of the present study, the results found by Barcelona et al. (2021b) for Cala Aiguablava and Cala Vigatà - two fragmented meadows found on the northeast Spanish coast - have been analyzed. The meadow in Cala Aiguablava presents 66% fragmentation, with the smallest patch lengths being 0.64 m and the largest 8.06 m. The plant density oscillated between 449 and 105 plants·m^{-2} between the 2 years studied. Meanwhile, the meadow in Cala Vigatà presents 22% fragmentation, with the smallest patches being 5.23 m long and the largest 24.82 m. The plant density in Cala Vigatà oscillated between 353 and 119 plants·m^{-2} (Barcelona et al., 2021a). These meadows are categorized as a medium patch vegetation and a perforated meadow, respectively, following the classification by Sleeman et al., 2005, see Barcelona et al., 2021b). Using the model proposed in this study, the minimum patch size required for the vegetation to produce *TKE* for these bays has been determined by considering the typical wave frequency of the Mediterranean Sea (0.5 Hz) and a range of wave velocities between 0.5 and 30 cm·s^{-1}. For $h_v = 0.6$ m, $L_{canopy} = 10h_v$ would be $L_{canopy} = 6$ m For the high canopy densities and for $U_w < 5$ cm·s^{-1}, the minimum patch size required to produce *TKE* was $L_{patch} > 225$ m for Cala Aiguablava and $L_{patch} > 963$ m for Cala Vigatà, indicating unfavourable conditions for small patches under these wave velocities. In contrast, for $U_w > 5$ cm·s^{-1}, the minimum patch size required decreased to very low values in both bays (<0.06 m in Cala Aiguablava and <0.25 m in Cala Vigatà). In contrast, for low canopy densities and $U_w > 5$ cm·s^{-1} the minimum patch size was $L_{patch} = 36$ m for Cala Aiguablava and 24 m for Cala Vigatà, due to the different canopy densities in both meadows. Therefore, patches smaller than this threshold would be threatened. In the low-density canopy cases and $U_w < 5$ cm·s^{-1}, the minimum patch size required would be 194,606 m for Cala Aiguablava and 125,720 m for Cala Vigatà. Under such conditions all patches would be threatened. These results align with those found by Pujol et al. (2019) for oxygen transport

through the diffusive boundary layer (DBL). They found that by increasing the flow velocity, the DBL becomes thinner and the gas exchange by the plant is enhanced. They also found that for $U_w < 6\ cm \cdot s^{-1}$, the gas exchange through the DBL is reduced. This result is close to the velocity limit found for the two bays analyzed in the present study, where $U_w > 5\ cm \cdot s^{-1}$ produce plant-wave interactions, generating *TKE* and enhancing the particle mixing.

5. Conclusions

This study demonstrates that patches of seagrasses can respond to waves by adhering to two hydrodynamic behaviours that depend on wave velocity. The first behaviour corresponds to low wave velocities where plants do not interact with waves. In this case, plants dissipate the near-bed generated turbulence. The second behaviour corresponds to moderate wave velocities where plants interact with waves through the production of *TKE*. The two behaviours ultimately depend on the density of the canopy and the length of the patch. High canopy densities are expected to produce greater *TKE* than low canopy densities. In addition, the production of *TKE* holds for small patches under moderate wave velocities or, conversely, for low wave velocities acting on large canopy areas. In such cases, the production of *TKE* is guaranteed, providing vegetated patches with functional dynamics to optimize the ecosystems services they provide. For patches with length dimensions greater than the minimum patch scale, the production of *TKE* by the plants in the patch might enhance the gas exchange in plant leaves, which will favour patch resilience under wave activity. In contrast, the resilience and resistance of seagrass canopies undergoing patchiness might be compromised when vegetated patches do not interact with the flow, since their length scale is lower than the required minimum patch scale that provide patch/flow interaction.

CRediT authorship contribution statement

Aina Barcelona: Methodology, Investigation, Formal analysis, Data curation, Writing – original draft. **Carolyn Oldham:** Methodology, Writing – review & editing. **Jordi Colomer:** Conceptualization, Methodology, Data curation, Writing – review & editing. **Teresa Serra:** Conceptualization, Methodology, Data curation, Writing – review & editing, Supervision.

Declaration of competing interest

The authors declare that they have no known competing financial interests or personal relationships that could have appeared to influence the work reported in this paper.

Acknowledgements

This research was funded by the “Ministerio de Economía, Industria y Competitividad” of the Spanish Government through the grant CGL2017-86515-P. Aina Barcelona was funded by the pre-doctoral grant 2020 FI SDUR 00043 by the “Generalitat de Catalunya”.

References

Abadie, A., Lejeune, P., Pergent, G., Gobert, S., 2016. From mechanical to chemical impact of anchoring in seagrasses: the premises of anthropogenic patch generation in *Posidonia oceanica* meadows. Mar.Pollut.Bull. 109, 61–71. https://doi.org/10.1016/j.marpolbul.2016.06.022.

Bacci, T., Rende, F.S., Scardi, M., 2017. Shoot micro distribution patterns in the Mediterranean seagrass Posidonia oceanica. Mar.Biol. 164, 85. https://doi.org/10.1007/s00227-017-3121-1.

Barcelona, A., Colomer, J., Soler, M., Gracias, N., Serra, T., 2021a. Meadow fragmentation influences Posidonia oceanica density at the edge of nearby gaps. Estuar. Coast. Shelf. S. 249, 107106. https://doi.org/10.1016/j.ecss.2020.107106.

Barcelona, A., Oldham, C., Colomer, J., Garcia-Orellana, J., Serra, T., 2021b. Particle capture by seagrass canopies under an oscillatory flow. In Revision in Coastal Engineering.

Bouma, T.J., van Duren, L.A., Temmerman, S., Claverie, T., Blanco-Garcia, A., Ysebaert, T., Herman, P.M.J., 2007. Spatial flow and sedimentation patterns within patches of epibenthic structures: combining field, flume and modelling experiments. Cont. Shelf Res. 27, 1020–1045. https://doi.org/10.1016/j.csr.2005.12.019.

Carr, J., D'Odorico, P., McGlathery, K., Wiberg, P., 2010. Stability and biostability of seagrass ecosystems in shallow coastal lagoons: role of feedbacks with sediment resuspension and light attenuation. J Geophys Res-Biogeo 115, 1–14. https://doi.org/10.1029/2009JG001103.

Colomer, J., Soler, M., Serra, T., Casamitjana, X., Oldham, C., 2017. Impact of anthropogenically created canopy gaps on wave attenuation in a Posidonia oceanica seagrass meadow. Mar. Ecol. Prog. Ser. 569, 103–116. https://doi.org/10.3354/meps12090.

Devi, T.B., Kumar, B., 2016. Experimentation on submerged flow over flexible vegetation patches with downward seepage. Ecol. Eng. 91, 158–168. https://doi.org/10.1016/j.ecoleng.2016.02.045.

El Allaoui, N., Serra, T., Colomer, J., Soler, M., Casamitjana, X., Oldham, C., 2016. Interactions between fragmented seagrass canopies and the local hydrodynamics. PLoS One 11 (5), e0156264. https://doi.org/10.1371/journal.pone.0156264.

Folkard, A.M., 2005. Hydrodynamics of model *Posidonia oceanica* patches in shallow water. Limnol. Oceanogr. 50 (5), 1592–1600. https://doi.org/10.4319/lo.2005.50.5.1592.

Fourqurean, J.W., Duarte, C.M., Kennedy, H., Marbà, N., Holmer, M., Mateo, M.A., Apostolaki, E.T., Kendrick, G.A., Krause-Jensen, D., McGathery, K.J., Serrano, O., 2012. Seagrass ecosystems as a globally significant carbon stock. Nat. Geosci. 5 (7), 505–509. https://doi.org/10.1038/ngeo1477.

Gacia, E., Granata, T.C., Duarte, C.M., 1999. An approach to measurement of particle flux and sediment retention within seagrass (*Posidonia oceanica*) meadows. Aquat. Bot. 65, 255–268.

Gera, A., Pagès, J., Romero, J., Alcoverro, T., 2013. Combined effects of fragmentation and herbivory on *Posidonia oceanica* seagrass ecosystems. J. Ecol. 101, 1053–1061. https://doi.org/10.1111/1365-2745.12109.

Ghisalberti, M., Nepf, H., 2002. Mixing layers and coherent structures in vegetated aquatic flows. J. Geophys. Res. 107, C23011. https://doi.org/10.1029/2001JC000871.

Gilby, B.L., Olds, A.D., Duncan, C.K., Ortodossi, N.L., Henderson, C.J., Schlacher, T.A., 2020. Identifying restoration hotspots that deliver multiple ecological benefits. Restor. Ecol. 28 (1), 222–232. https://doi.org/10.1111/rec.13046.

Goring, D.G., Nikora, V.I., 2002. Despiking acoustinc Doppler velocimeter data. J. Hydraul. Eng. 128 (1), 117–126. https://doi.org/10.1061/(ASCE)0733-9429(2002)128:1(117).

Granata, T., Serra, T., Colomer, J., Casamitjana, X., Duarte, C.M., Gacia, E., 2001. Flow and particle distribution in a nearshore seagrass meadow before and after a storm. Mar. Ecol. Prog. Ser. 218, 95–106. https://doi.org/10.3354/meps218095.

Grech, A., Chartrand-Miller, K., Erftemeijer, P., Fonseca, M., McKenzie, L., Rasheed, M., Taylor, H., Coles, R., 2012. A comparison of threats, vulnerabilities and management approaches in global seagrass bioregions. Environ. Res. Lett. 7 (2), 024006. https://doi.org/10.1088/1748-9326/7/2/024006.

Gruber, R.K., Kemp, W.M., 2010. Feedback effects in a coastal canopy-forming submersed plant bed. Limnol. Oceanogr. 55 (6), 2285–2298. https://doi.org/10.4319/lo.2010.55.6.2285.

Hansen, J.C.R., Reidenbach, M.A., 2017. Turbulent mixing and fluid transport within Florida Bay seagrass meadows. Adv. Water Resour. 108, 205–215. https://doi.org/10.1016/j.advwaters.2017.08.001.

Hughes, A.R., Williams, S.L., Duarte, C.M., Heck Jr., K.L., Waycott, M., 2009. Associations of concern: declining seagrasses and threatened dependent species. Front. Ecol. Environ. 7 (5), 242–246. https://doi.org/10.1890/080041.

Infantes, E., Terrados, J., Orfila, A., Cañellas, B., Álvarez-Ellacuria, A., 2009. Wave energy and the upper depth limit distribution of *Posidonia oceanica*. Bot. Mar. 52, 419–427. https://doi.org/10.1515/BOT.2009.050.

Kupsky, B.G., Dornbush, M.E., 2019. Experimental test of abiotic and biotic factors driving restoration success of Vallisneria americana in the Lower Bay of Green Bay. J. Great Lakes Res. 45, 340–349. https://doi.org/10.1016/j.jglr.2019.01.006.

Li, W., Wang, D., Jiao, J., Yang, K., 2019. Effects of vegetation patch density on flow velocity characteristics in an open channel. J. Hydrodyn. 31 (5), 1052–1059. https://doi.org/10.1007/s42241-018-0086-6.

Licci, S., Nepf, H., Delome, C., Marmonier, P., Bouma, T.j., Puijalon, S., 2019. The role of patch size in ecosystem engineering capacity: a case study of aquatic vegetation. Aquat. Sci. 81 (3), 41. https://doi.org/10.1007/s00027-019-0635-2.

Lowe, R.J., Koseff, J.R., Monismith, S.G., 2005. Oscillatory flow through submerged canopies: 2. Canopy mass transfer. J. Geophys. Res. 110, C10017. https://doi.org/10.1029/2004JC002789.

Luhar, M., Coutu, S., Infantes, E., Fox, S., Nepf, H., 2010. Wave-induced velocities inside a model seagrass bed. J. Geophys. Res. 115, C12005. https://doi.org/10.1029/2010JC006345.

Metz, J.L., Harris, R.J., Arrington, D.A., 2020. Seasonal occurrence patterns of seagrass should influence resource assessment and management decisions: a case study in the Indian River Lagoon and Loxahatchee River Estuary, Florida. Reg. Stud. Mar. Sci. 34, 101093. https://doi.org/10.1016/j.rsma.2020.101093.

Montefalcone, M., 2009. Ecosystem health assessment using Mediterranean seagrass *Posidonia oceanica*. Ecol. Indic. 9, 595–604. https://doi.org/10.1016/j.ecolinf.2008.09.013.

Nepf, H.M., Sullivan, A., Zavistoski, R.A., 1997. A model for diffusion within emergent vegetation. Limnol. Oceanogr. 42 (8), 1735–1745. https://doi.org/10.4319/lo.1997.42.8.1735.

Newell, R.I.E., Koch, E.W., 2004. Modeling seagrass density and distribution in response to changes in turbidity stemming from bivalve filtration and seagrass sediment stabilization. Estuaries 27, 793–806. https://doi.org/10.1007/BF0912041.

Paling, E.I., van Keulen, M., Wheeler, K.D., Phillips, J., Dyhrberg, R., 2003. Influence of 593 spacing on mechanically transplanted seagrass survival in a high wave energy

regime. 594. Restor. Ecol. 11 (1), 5–61. https://doi.org/10.1046/j.1526-100X.2003.00072.x.

Paquier, A., Meulé, S., Anthony, E.J., Larroudé, P., Bernard, G., 2018. Wind-induced hydrodynamics interactions with aquatic vegetation in a fetch-limited setting: implications for coastal sedimentation and protection. Estuar. Coasts 42, 688–707. https://doi.org/10.1007/s12237-018-00487-w.

Paul, M., Amos, C.L., 2011. Spatial and seasonal variation in wave attenuation over *Zostera noltii*. J. Geophys. Res. 116, C08019. https://doi.org/10.1029/2010JC006797.

Pujol, D., Casamitjana, X., Serra, T., Colomer, J., 2013a. Canopy-scale turbulence under oscillatory flow. Cont. Shelf Res. 66, 9–18. https://doi.org/10.1016/j.csr.2013.06.012.

Pujol, D., Serra, T., Colomer, J., Casamitjana, X., 2013b. Flow structure in canopy models dominated by progressive waves. J. Hydrol. 486, 281–292. https://doi.org/10.1016/j.jhydrol.2013.01.024.

Pujol, D., Abdolahpour, M., Lavery, P.S., McMahon, K., Oldham, C., 2019. Flow velocity and nutrient uptake in marine canopies. Mar. Ecol. Prog. Ser. 622, 17–30. https://doi.org/10.3354/meps12987.

Robbins, B.D., Bell, S.S., 1994. Seagrass landscapes: a terrestrial approach to the marine subtidal environment. Trends Ecol. Evol. 9 (8), 301–304. https://doi.org/10.1016/0169-5347(94)90041-8.

Ros, À., Colomer, J., Serra, T., Pujol, D., Soler, M., Casamitjana, X., 2014. Experimental observations on sediment resuspension within submerged model canopies under oscillatory flow. Cont. Shelf Res. 91, 220–231. https://doi.org/10.1016/j.csr.2014.10.004.

Schoelynck, J., Creëlle, S., Buis, K., De Mulder, T., Emsens, W.J., Hein, T., Meire, D., Meire, P., Okrusko, T., Preiner, S., González, R.-R., Silinski, A., Temmerman, S., Troch, P., Van Oyen, T., Verschoren, V., Visser, F., Wang, C., Wolters, J.W., Folkard, A., 2018. What is a macrophyte patch? Patch identification in aquatic ecosystems and guidelines for consistent delineation. Ecohydrol.Hydrobiol. 18, 1–9. https://doi.org/10.1016/j.ecohyd.2017.10.005.

Serra, T., Oldham, C., Colomer, J., 2018. Local hydrodynamics at edges of marine canopies under oscillatory flows. PLoS One 13 (8), e0201737. https://doi.org/10.1371/journal.pone.0201737.

Sleeman, J.C., Kendrick, G.A., Boggs, G.S., Hegge, B.J., 2005. Measuring fragmentation of seagrass landscapes: which indices are most appropriate for detecting change? Mar.Freshwater.Res. 58, 851–864. https://doi.org/10.1071/MF04300.

Stankovic, M., Kaewsrikhaw, R., Rattanachot, E., Prathep, A., 2019. Modeling of suitable habitat of small-scale seagrass restoration in tropical ecosystems. Estuar. Coast. Shelf. S. 231, 106465. https://doi.org/10.1016/j.ecss.2019.106465.

Stipek, C., Santos, R., Barcock, E., Lirman, D., 2020. Modelling the resilience of seagrass communities exposed to pulsed freshwater discharges: a seascape approach. PLoS One 15 (2), e0229147. https://doi.org/10.1371/journal.pone.0229147.

Tang, C., Lei, J., Nepf, H.M., 2019. Impact of vegetation-generated turbulence on the critical, near-bed, wave-velocity for sediment resuspension. Water Resour. Res. 55, 5904–5917. https://doi.org/10.1029/2018WR024335.

Tanner, J.E., 2003. Patch shape and orientation influences on seagrass epifauna are mediated by dispersal abilities. Oikos 100 (3), 517–524. https://doi.org/10.1034/j.1600-0706.2003.12060.x.

Tinoco, R.O., Coco, G., 2014. Observation of the effect of emergent vegetation on sediment resuspension under unidirectional currents and waves. Earth. Surf. Dynam. 2, 83–96. https://doi.org/10.5194/esurf-2-83-2014.

Unsworth, R.K.F., McKenzie, L.J., Collier, C.J., Cullen-Unsworth, L.C., Duarte, C.M., Eklöf, J.S., Jarvis, J.C., Jones, B.L., Nordlund, L.M., 2018. Global challenges for seagrass conservation. Ambio 48 (8), 801–815. https://doi.org/10.1007/s13280-018-1115-y.

van Katwijk, M.M., Bos, A.R., Hermus, D.C.R., Suykerbuyk, W., 2010. Sediment modification by seagrass beds: Muddification and sandification induced by plant cover and environmental conditions. Estuar. Coast. Shelf. S. 89, 175–181. https://doi.org/10.1016/j.ecss.2010.06.008.

van Katwijk, M.M., Thorhaug, A., Marbà, N., Orth, R.J., Guarte, C.M., Kendrick, G.A., Althuizen, I.H.J., Balestri, E., Bernard, G., Cambridge, M.L., Cunha, A., Durance, C., Giesen, W., Han, Q., Hosokawa, S., Kiswara, W., Komatsu, T., Lardicci, C., Lee, K., Meinesz, A., Nakaoka, M., O'Brien, K.R., Paling, E.I., Pickerell, C., Ransijn, A.M.A., Verduin, J.J., 2016. Global analysis of seagrass restoration: the importance of large-scale planting. J. Appl. Ecol. 53, 567–578. https://doi.org/10.1111/1365-2664.12562.

Waycott, M., Duarte, C.M., Carruthers, T.J.B., Orth, R.J., Dennison, W.C., Olyarnik, S., Calladine, A., Fourqurean, J.W., Heck, K.L., Hughes, A.R., Kendrick, G.A., Kenworthy, W.J., Short, F.T., Williams, S.L., 2009. Accelerating loss of seagrasses across the globe threatens coastal ecosystems. PNAS 106 (30), 12377–12381. https://doi.org/10.1073/pnas.0905620106.

West, R.J., Jacobs, N.E., Roberts, D.E., 1990. Experimental transplanting of seagrasses in Botany Bay, Australia. Mar. Pollut. Bull. 21 (4), 197–203 (doi: 0025-326X/90).

Zhang, Y., Tang, C., Nepf, H., 2018. Turbulent kinetic energy in submerged model canopies under oscillatory flow. Water Resour. Res. 54, 1734–1750. https://doi.org/10.1002/2017WR021732.

Zong, L., Nepf, H., 2010. Flow and deposition in and around a finite patch of vegetation. Geomorphology 116, 363–372. https://doi.org/10.1016/j.geomorph.2009.11.020.

Marine Environmental Research 188 (2023) 105997

Contents lists available at ScienceDirect

Marine Environmental Research

journal homepage: www.elsevier.com/locate/marenvrev

Spatial sedimentation and plant captured sediment within seagrass patches

Aina Barcelona [a,*], Jordi Colomer [a], Teresa Serra [a]

[a] Department of Physics, University of Girona, 17071, Girona, Spain

ARTICLE INFO

Keywords:
Seagrass
Sedimentation
Leaves capture
Suspension
Seagrass patch
Fragmentation

ABSTRACT

Habitat degradation in coastal ecosystems has resulted in the fragmentation of coastal aquatic vegetation and compromised their role in supplying essential ecological services such as trapping sediment or sequestering carbon. Fragmentation has changed seagrass architecture by decreasing the density of the canopy or engendering small patches of vegetated areas. This study aims to quantify the role different patch sizes of vegetation with different canopy densities have in the spatial distribution of sediment within a patch. To this aim, two canopy densities, four different patch lengths, and two wave frequencies were considered. The amounts of sediment deposited onto the bed, captured by plant leaves, remaining in suspension within the canopy, and remaining in suspension above the canopy were used to understand the impact hydrodynamics has on sediment distribution patterns within seagrass patches. In all the cases studied, patches reduced the suspended sediment concentrations, increased the capture of particles in the leaves, and increased the sedimentation rates to the bed. For the lowest wave frequency studied (0.5 Hz), the sediment deposited to the bottom was enhanced at canopy edges, resulting in spatial heterogeneous sedimentation patterns. Therefore, restoration and preservation of coastal aquatic vegetation landscapes can help face future climate change scenarios where an increase in sedimentation can help mitigate predicted sea level rise in coastal areas.

1. Introduction

The maritime coastal seascape has suffered from both short and long-term structural changes because of increased anthropogenic impacts, population growth in coastal areas, habitat degradation, and the increasing impact of climate change (Barsanti et al., 2007; Cacabelos et al., 2022; Leriche et al., 2006; Montefalcone et al., 2019; Valero et al., 2009; Van De Koppel, 2015). Coastal seagrass meadows have been losing coverage over time, resulting in an increasingly fragmented landscape configuration (Montefalcone et al., 2010; Barcelona et al., 2021b). Therefore, coastal seagrasses can form large continuous meadows or more heterogeneous structures with different sized patches of vegetated areas mixed with assorted unvegetated sand or rocky beds. When a continuous seagrass meadow loses some of its vegetated area, it transforms into patchier areas with unvegetated bare soil and exhibits increasing gaps within the vegetation itself. The ability of coastal canopies to deal with both natural and anthropogenic disturbances has become a challenge for coastal marine ecosystem management and conservation as coastal canopies display patchiness that can persist over extended time scales (Bell et al., 2001; Colomer and Serra, 2021; Montefalcone et al., 2010). Consequently, individual patches of vegetation are now a typical sight in seascapes (Barcelona et al., 2021a; Borfecchia et al., 2021; Hovel et al., 2021; Pastor et al., 2022). High meadow fragmentation levels result in low shoot density in the surrounding area near gaps (Barcelona et al., 2021b), indicating the degrading effect fragmentation has.

Continuous coastal canopies are known to supply numerous ecological services such as reducing storm surges and marine heat waves, preventing the erosion of coastal beds (Madsen et al., 2001; Verdura et al., 2021), promoting sediment accretion (Granata et al., 2001) and heterogeneous litter decomposition, impacting carbon sequestration rates (Ettinger et al., 2017), influencing estuarine geomorphology (Lera et al., 2019) as well as providing refuge and nursery grounds for the local biota (Bell et al., 2001). However, when coastal seagrasses are fragmented, their role in supplying ecological services has been reported to be increasingly compromised. The ensuing levels of deterioration depend on the degree of local patchiness and the abiotic impacts (Colomer et al., 2017). The rise in sea levels predicted by future climate change scenarios, coupled with the low input of sediments from rivers, are expected to drown deltas (Dunn et al., 2019). Restauration of aquatic vegetation landscapes is a sedimentation enhancing strategy that can be used to compensate rising sea levels (Cox. et al., 2022). More

* Corresponding author.
E-mail address: aina.barcelona@udg.edu (A. Barcelona).

https://doi.org/10.1016/j.marenvres.2023.105997
Received 15 February 2023; Received in revised form 11 April 2023; Accepted 13 April 2023
Available online 23 April 2023

rigid submerged structures like coral reefs are also known to enhance sediment accretion and offset the erosive effects of rising sea levels (Tuck et al., 2021). Therefore, to cope with future climate change scenarios, preserving aquatic vegetation among other coastal landscapes is of special relevance.

Within canopies habitat complexity generally increases not only from patch edges to patch interiors (Moore and Hovel, 2010), patch-to-patch interactions (Abadie et al., 2017; Cornacchia et al., 2019) and fragmented to full canopies (Colomer and Serra 2021), but also in sparse to dense vegetation (Barcelona et al., 2021a) and in the differing leaf configurations of submerged and emergent plants (Barcelona et al., 2021b; Colomer et al., 2017; Montefalcone et al., 2006). Coastal canopies provide high flow resistance, and flow and waves are diverted and intensified above and/or next to the canopy, thus increasing water velocity and turbulence along the boundaries of the patch (Chen et al., 2013; Sand-Jensen and Mebus, 1996; Sand-Jensen and Pedersen, 2008). The balance between flow inertia, canopy drag, and canopy patch dimension determines, for example, particle deposition, which is laterally uniform (Zong and Nepf, 2011) and decreases inside the canopy patch (Zhu et al., 2021), indicating that within a patch sedimentation increases.

Gacia and Duarte (2001) reported that *Posidonia oceanica* meadows significantly buffer sediment resuspension. For instance, within the patch, sediment resuspension is three-fold lower than an area of bare sand. In their study, Serra et al. (2020) observed that constant sedimentation rates were found across gaps (zones without vegetation) of different sizes within a *Posidonia oceanica* meadow. They also found that sedimentation rates in the gaps within the meadow were close to those inside the canopy. In salt marshes, patches of vegetation have been found to participate in the sequestration and longstanding accumulation of sediments before they are then transported to the ocean (Pinheiro et al., 2002). Deposition of particle fluxes in patches of the seagrass *Zostera noltii* have been found higher within the patch than on bare sediments, i.e., the greater the vegetation density is, the higher the deposition rates are (Ganthy et al., 2015). Likewise, dense *Zostera marina* patches promoted the accumulation of fine sediments and organic content, therefore producing muddification in the interior of the patch. van Katwijk (2010) found that dense vegetated patches presented homogeneous sedimentation distribution, whereas although sparse vegetated patches presented a heterogeneous distribution of sediment, there was a decrease in fine particles compared to coarse particles. However, turbidity currents travelling through dense vegetated patches presented heterogeneous distributions of sediment, with fine sediment particles accumulating in the interior of a patch and coarse particles in its exterior (Soler et al., 2021). Barcelona et al. (2021c) reported that seagrass meadows may also capture sediment on the blades and thus enhance particle sedimentation on the seabed. The number of particles trapped by the blades of seagrass plants, and subsequently deposited on the seabed, increased with canopy density which, in turn, reduced the concentration of sediments in suspension within the canopy, thus improving the water clarity within the canopy. The impact meadows have on particle deposition and resuspension depends on the degree of current and wave attenuation, indicating that patches of vegetation can reduce particle resuspension from the bottom seabed, and enhance particle deposition and carbon burial (Gacia and Duarte, 2001; Oreska et al., 2017; Paladini de Mendoza et al., 2018). Deforestation of mangrove forests has also been shown to reduce blue carbon sequestration, showing the role that large continuous vegetation landscapes can play in facing future climate change scenarios (Chatting et al., 2022).

Nevertheless, both small and sparse vegetated patch behaviour has been found to deviate from large, dense seagrass patches. Pastor et al. (2022) pointed out that once seagrass degradation reaches a tipping point, functionality is lost and patches transition to a bare soil steady state, thus compromising potential restoration. Furthermore, Sweatman et al. (2017) suggested that fragmented seagrass beds shift their nutrient loads, which subsequently impacts their ecosystem functions in many ways by, for instance, reducing the availability of suitable habitats for animals or altering the available resources. Seagrass habitat fragmentation has also been found to threaten carbon sequestration (Mazarrasa et al., 2018). Continuous meadows are expected to be more efficient sequestering carbon than fragmented meadows. Previous experiments on the hydrodynamics of vegetated patches under oscillatory flows demonstrate that a minimum patch size is required to reduce the flow velocity through the turbulent kinetic energy being produced by plant stems (Barcelona et al., 2021a). A patch that is too small is unable to reduce waves and presents scouring at the meadow's edges (Marin-Diaz et al., 2020). However, there is still a lack of knowledge concerning the capacity seagrass patches have to capture sediment from allochthon sources. Therefore, this current study attempts to acquire knowledge as to the effect patch length and canopy density can have on the capture of sediment from allochthon sources under different hydrodynamic conditions. The sediment captured by leaves, the sediment deposited at the bottom and the sediment remaining in suspension will be studied for small (five times the leaf length) to large (14 times the leaf length) vegetated patch lengths, for two canopy densities (dense and sparse) and two different wave frequencies. The study was performed in a laboratory flume under conditions mimicking real field scenarios.

2. Methodology

2.1. The flume

The study was carried out in a methacrylate laboratory flume 600 cm long, 50 cm wide and 60 cm deep (Fig. 1) with a mean water height of h = 30 cm. The flume was equipped with a vertical piston-type wavemaker at the entrance. The wavemaker was driven by a variable-speed motor at two frequencies (f = 0.5, and 1.12 Hz). To eliminate wave reflection, a plywood beach (slope = 1:2) covered with foam rubber was placed at the end of the flume (Barcelona et al., 2021a; Serra et al., 2018).

2.2. Patches of flexible vegetation

The vegetation model consisted of a series of flexible plants made from eight 0.075 mm-thick polyethylene canopy blades attached to PVC dowels that had been randomly inserted into a 250-cm long perforated

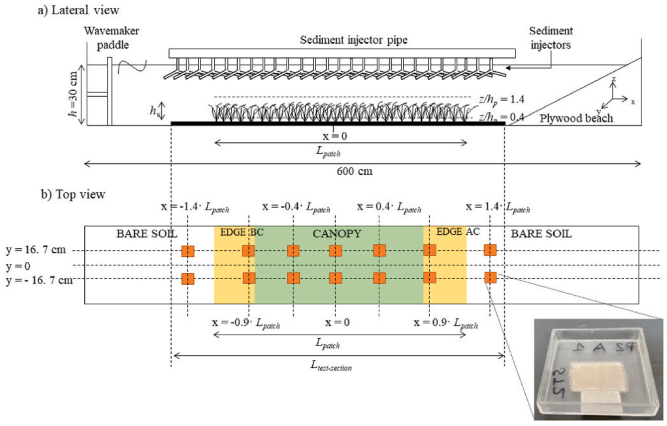

Fig. 1. Scheme of the experimental set-up a) Lateral view of the flume with the patch of flexible vegetation. The patch lengths ranged from L_{Patch} = 70–196 cm. b) Top view of the set-up. The region coloured in orange and green correspond to the patch. The green coloured area corresponds to the inner canopy region and the orange-coloured area corresponds to the edge region of the canopy. The Edge BC corresponds to the edge closest to the wavemaker and the Edge AC corresponds to the edge furthest from the wavemaker. Orange squares represent the sediment traps distributed along the flume bed.

baseboard (Pujol et al., 2013). PVC rigid dowels extended 1 cm above the bed (Zhang et al., 2018). The model plants were geometrically and dynamically close to *Posidonia oceanica* plants (Ghisalberti and Nepf, 2002). Leaf length, h_p, was 14 cm, and the effective height when the leaves were bent by the waves was $h_v = 8.4$ cm for $f = 1.12$ Hz and $h_v = 10.5$ cm for $f = 0.5$ Hz (Barcelona et al., 2021a). The vegetation density of patches was quantified using the solid plant fraction (*SPF*) defined as:

$$SPF\ (\%) = 100n\pi\left(\frac{d}{2}\right)^2 \quad (1)$$

where n is the number of shoots per unit area and d is the stem diameter (1 cm). Three SPFs were used (0%, 3.5% and 10%), which corresponded to vegetation densities of n = 0, 446 and 1273 stems·m^{-2}, according to the range of canopy densities (78–1000 stems·m^{-2}) found in coastal areas (Bacci et al., 2017; Boström et al., 2014; Colomer et al., 2017; Gera et al., 2013). *SPF* = 0% corresponded to the non-vegetated set-up. For each *SPF*, four patch sizes, L_{patch}, ranging from 70 to 196 cm in length were considered. A total of 18 experiments were performed for the different *SPFs*, L_{patch} and f (Table 1).

2.3. Sediment injection

The sediment used in the experiments was a synthetic dust powder (ISO 12103–1. A4 Coarse, Powder Technology Inc. Burnsville) with a median of 41.7 μm (Fig. 2) and a density of 2650 kg m^{-3}. The mean settling velocity for these sediment particles ($w_{settling} = 1.57 \times 10^{-3}$ m s^{-1}) was estimated by the Francalaci et al. (2021) formula assuming that sediment particles were nearly spherical (i.e., with a Corey shape factor equal to 1). Since the suspended sediment concentration in all the experiments was below 17.46 g L^{-1}, the sediment concentration was not expected to have any effect on the settling velocity (Colomer et al., 1998). The volumetric concentrations of suspended sediment (in μL·L^{-1}) were analysed using a LISST-100X (Laser In-Situ Scattering and Transmissometry, Sequoia Scientific, Inc, Bellevue, WA) particle size analyser. The LISST-100X consists of a laser beam and an array of detector rings of progressive diameters which allow the light received at the scattering angles of the beam to be analysed. The device measures particle volume concentrations for 32 size classes (logarithmically distributed in the size range of 2.5–500.0 μm), using the procedure based on the diffraction theory of light. This instrument has been widely used for organic (Serra et al., 2001) and inorganic particles (Ros et., 2014; Serra et al., 2002). The particle size distribution of the sediment used was bimodal, with fine particles being 2.5–6.0 μm in diameter, i.e., corresponding to strongly cohesive clay and very fine silts, and coarse particles were 6.0–122.0 μm in diameter, i.e., corresponding to weakly cohesive fine to coarse silts and small sand particles (Fig. 2). In this case, $d_{50} = 41.7$ μm, is of the order of the grain size of river plumes in coastal areas (40–65 μm, Pitarch et al., 2019). Pitarch et al. (2019) found that the largest non-cohesive particles settled at the mouth of the river and the finest sediment fractions were transported offshore.

The wavemaker was switched on and left to run for 15 min to allow

Table 1
Summary of the experimental conditions considered: each experimental run number (with the seagrass flexible vegetation as *SFV*), wave frequency (f, in Hz), solid plant fraction (*SPF*, in %), canopy density (n, in shoots m^{-2}), length of the vegetated patch (L_{patch}, in times the leaf length h_p), U_w (in cm s^{-1}) at $z/h_v = 0.4$ and the ratio between the orbital excursion length (A_w), and plant-to-plant distance (S).

Run	f (Hz)	*SPF* (%)	N (stems·m^{-2})	L_{patch}/h_p	U_w at $z/hv=0.4$ (cm s^{-1})	Aw/S
SFV 1	0.5	0	0		8.95	
SFV 2		3.5	446	0.36	9.40	0.63
SFV 3				0.64	9.37	0.63
SFV 4				0.86	8.93	0.60
SFV 5				1.00	9.22	0.62
SFV 6		10	1273	0.36	9.42	1.07
SFV 7				0.64	9.16	1.04
SFV 8				0.86	9.26	1.04
SFV 9				1.00	9.07	1.03
SFV 10	1.12	0	0		8.21	
SFV 11		3.5	446	0.36	8.33	0.25
SFV 12				0.64	7.99	0.24
SFV 13				0.86	8.02	0.24
SFV 14				1.00	8.01	0.24
SFV 15		10	1273	0.36	8.29	0.42
SFV 16				0.64	7.88	0.40
SFV 17				0.86	7.80	0.40
SFV 18				1.00	7.70	0.39

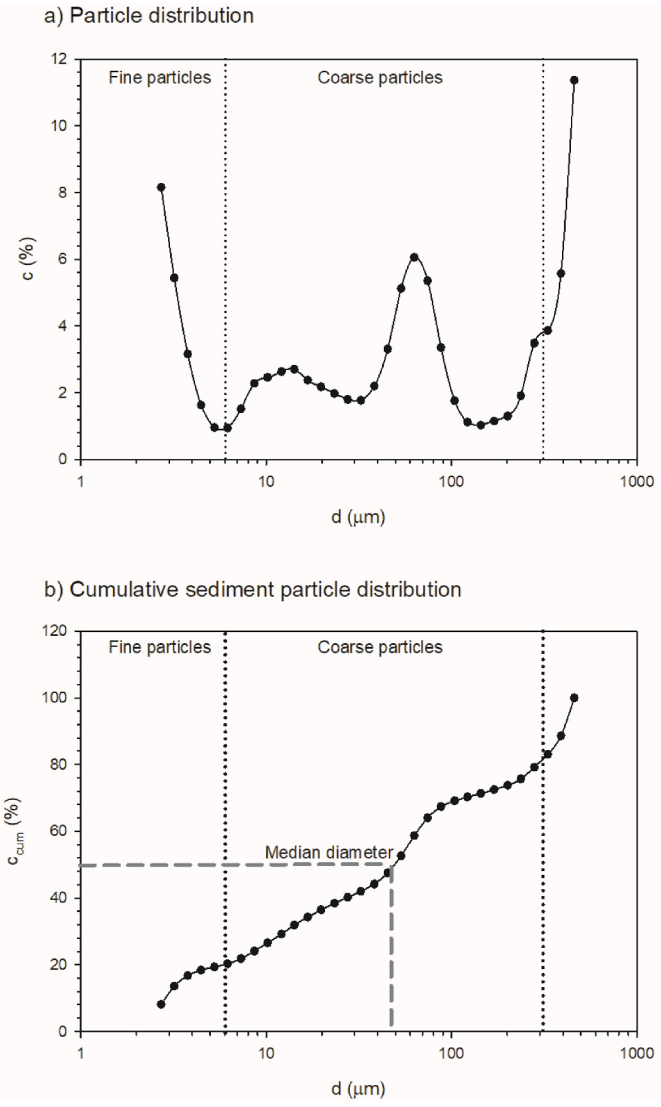

Fig. 2. a) Volumetric sediment particle size distribution (c, in %). b) Cumulative sediment particle size distribution (c_{cum}, in %). Dashed lines show the median diameter (i.e., the diameter where 50% of the cumulative distribution holds, $d_{50} = 41.7$ μm). In both figures, two different particle sizes are shown: fine particles below 6 μm, and coarse particles between 6 μm and 122 μm.

the system to reach equilibrium before sediment injection. The particle-laden flow used in the injection was prepared using an initial volume (2L) of sediment suspension (with a concentration of 80 g L^{-1}) and introduced into one end of the sediment-injector pipe. The injector pipe was situated at y = 0 cm along the axis of the flume (Fig. 1) While introducing the sediment into the pipe, the injectors faced upwards to avoid any uncontrolled spillage. Once the pipe had been filled with the sediment suspension, it was then closed and turned down so that injectors face downwards, protruding 5 cm below the water surface and therefore remaining at the very top of the water column and above the vegetated patch.

The sediment injector pipe consisted of a large 2.5 m-long pipe, with 42 sediment injectors evenly distributed 7 cm apart from each other. The Y-shape design of the sediment injectors was 26 cm long and each arm pipe was 22.5 cm long (see Fig. 1a). Each arm of the pipe had 12 holes, from where the sediment injected was released into the flume, thus resulting in a homogeneous injection along both the x-axis and the y-axis.

2.4. Sediment measurements

To obtain the sediment particle distribution along the canopy, three different types of sediment measurements were collected: sediment settled on the bed, suspended sediment, and sediment attached to plant leaves. To obtain the amount of sediment settled on the bed, fourteen sediment traps were distributed in two rows along the main axis of the flume and situated at y = ±16.7 cm (Fig. 1b). The traps' positions along the x-axis of the flume for each run were related to the patch length, x = ± 0, 0.4, 0.9 and 1.4·L_{patch} (Fig. 1b). Sediment traps were distributed into three subgroups: canopy, corresponding to the traps at x = ± 0 and 0.4·L_{patch}; edge, corresponding to the traps at x = ± 0.9·L_{patch}; and bare soil, corresponding to the traps outside the vegetated patch at x = ± 1.4·L_{patch}. The sediment samples from the sediment traps were collected at t = 60 min from the injection time. In order to obtain information on the suspended sediment, 80 mL of suspended sediment samples were pipetted at the same x position where the sediment traps were positioned for each run, at y = 0 cm, and at two water depths (at $z/h_v = 0.4$ and at $z/h_v = 1.4$). These samples were chosen as representative samples for within and above the canopy, respectively. In this case, samples were collected at different times (t = 2, 30 and 60 min) from the injection time, and analysed for suspended sediment concentration. To obtain information about the amount of sediment deposited on the plant leaves, at the end of each experiment (t = 60 min) five plants were gently removed at the same x positions within the vegetated patch as the sediment traps had been placed. They were then introduced into a beaker with 80 ml of water and the plants were stirred in the fluid to remove the sediment trapped by the surface of the leaves, after which particle concentration was analysed with the particle analyser LISST-100X.

2.5. Sediment capture distribution analysis

To calculate the amount of sediment collected in the different compartments of the system, a test section of 14h_p was considered. In other words, it coincided with the longest patch studied (see Fig. 1). The test section had different configurations depending on the presence or absence of vegetation. In the cases with vegetation, patch length and canopy density determined the amount of vegetation in the system. The test section had a vegetated vertical region within the canopy and an unvegetated vertical region above the canopy. In the non-vegetated experiments, the same two vertical layers were considered for the purpose of comparison.

The sediment trapped by the leaves, V_P (Fig. 3), corresponded to the sediment attached to the surface of the plant leaves. The concentration of sediment measured with the LISST -100x was divided by the number of plants collected for sampling and the volumetric concentration of sediment collected per plant was obtained. The concentration obtained was afterwards multiplied by the volume of the water used to rinse the plants (80 mL) and the total volume of sediment deposited was obtained (V_P, in μL).

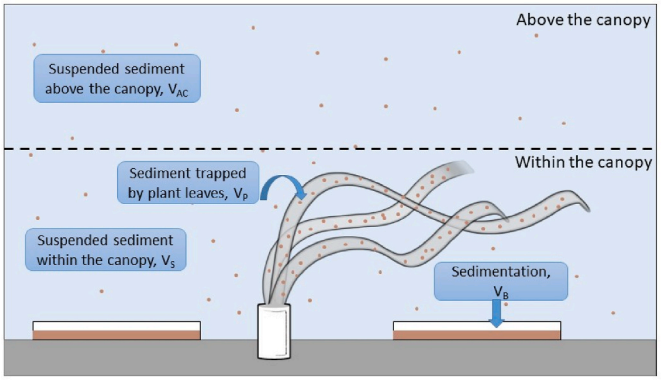

Fig. 3. Distribution of sediment in the four different compartments: on the plants (V_P), on the bed (V_B), in suspension within the canopy (V_S) and in suspension above the canopy (V_{AC}).

The amount of sediment in suspension within the canopy (V_S, Fig. 3) was calculated from the samples collected in suspension at a 5 cm depth above the bottom of the flume. The same depth was considered for the non-vegetated cases. For experiments carried out with vegetation, the test section had a vegetated part and a bare soil part. The volume of particles in suspension (V_S, in μL) was calculated by multiplying the concentration within the canopy by the volume of the patch ($L_p \times h_v \times$ W, where W is the width of the flume) plus the concentration in suspension in the bare soil multiplied by the volume of sediment collected in the bare soil (($L_{test\text{-}section}$-L_p) × h_v × W). In the case without vegetation, the volume of sediment in suspension was calculated by multiplying the concentration of sediment in suspension by the volume of the test section ($L_{test\text{-}section} \times h_v \times W$). The same calculation was carried out for the suspended sediment concentration above the canopy (at 20 cm above the bottom, V_{AC}, in μL). However, the vertical extension in this case was (h-h_v) instead of h_v used for the within canopy section.

The amount of sediment deposited at the bottom of the flume (V_B, in μL, Fig. 3) was calculated from the samples collected with the sediment traps. The concentration of sediment collected by the sediment traps was measured by the LISST-100X. The volume of sediment was obtained by multiplying the concentration obtained by the volume of the sample. Since the volume of sediment obtained corresponded to the area of the sediment trap (5 cm × 5 cm), the total volume of sediment deposited in the region where the trap was positioned was obtained by multiplying by the ratio of the total area of the region where the trap was situated (edge, bare soil, or vegetation) divided by the area of the test section. The total volume of sediment (V_B) at the bottom of the test section was calculated as the sum of the volume of sediment collected at the bottom of the bare soil plus the sediment collected at the edge and the sediment collected at the canopy regions.

The total volume of sediment was obtained by adding the volume of particles for each compartment in the test section (V_{TOTAL}=V_P + V_{AC} + V_S + V_B). From the total volume, the percentage of sediment particles in each compartment was calculated.

2.6. Measuring velocities

The Eulerian velocity field was defined as (u, v, w) in the (x, y, z) directions of the flume, respectively. The three components of velocity were recorded with a downwards looking Acoustic Doppler Velocimeter (16-MHz MicroADV, Sontek) at a frequency of 50 Hz over 10 min (obtaining a set of 30,000 data for each sampling point). Flow velocity profiles were measured at the centre of the patch and at z = 17 cm, 16

cm, 12 cm, 8 cm, 6 cm, 5 cm, 4 cm, 3 cm, and 2 cm from the bed of the flume. The ADV measures 5 cm from the probe tip with a sampling volume of 0.09 cm^3. Beam correlations less than 80% were discarded and spikes were removed (Goring and Nikora 2002; Pujol et al., 2013). For oscillatory flows, the instantaneous velocity, $U_i(t)$, can be decomposed as:

$$U_i(t) = U_c + U_w + u' \quad (2)$$

where U_c is the steady velocity associated with the current, U_w is the unsteady wave motion which represents spatial variations in the phase-averaged velocity field, and u' is the turbulent velocity, that is, the instantaneous velocity fluctuation in the x-direction. U_c is the phase-averaged velocity:

$$U_c = \frac{1}{2\pi}\int_0^{2\pi} U_i(\varphi)\partial\varphi \quad (3)$$

where $U_i(\varphi)$ is the instantaneous velocity according to the phase (Lowe et al., 2005b; Luhar et al., 2010). In the current study U_c at $z/h_v = 0.4$ above the bed (i.e. within the canopy layer) was always smaller than U_w, with mean values of 0.44 cm s^{-1} and -0.05 cm s^{-1} for the wave frequencies of 1.12 Hz and 0.5 Hz, respectively.

Wave velocity, U_w, was obtained by using a phase averaging technique. The Hilbert transform was used to average oscillatory flow velocities with a common phase (Pujol et al., 2013b; Ros et al., 2014). The root mean square (rms) of $U_i(\varphi)$ was considered as the characteristic

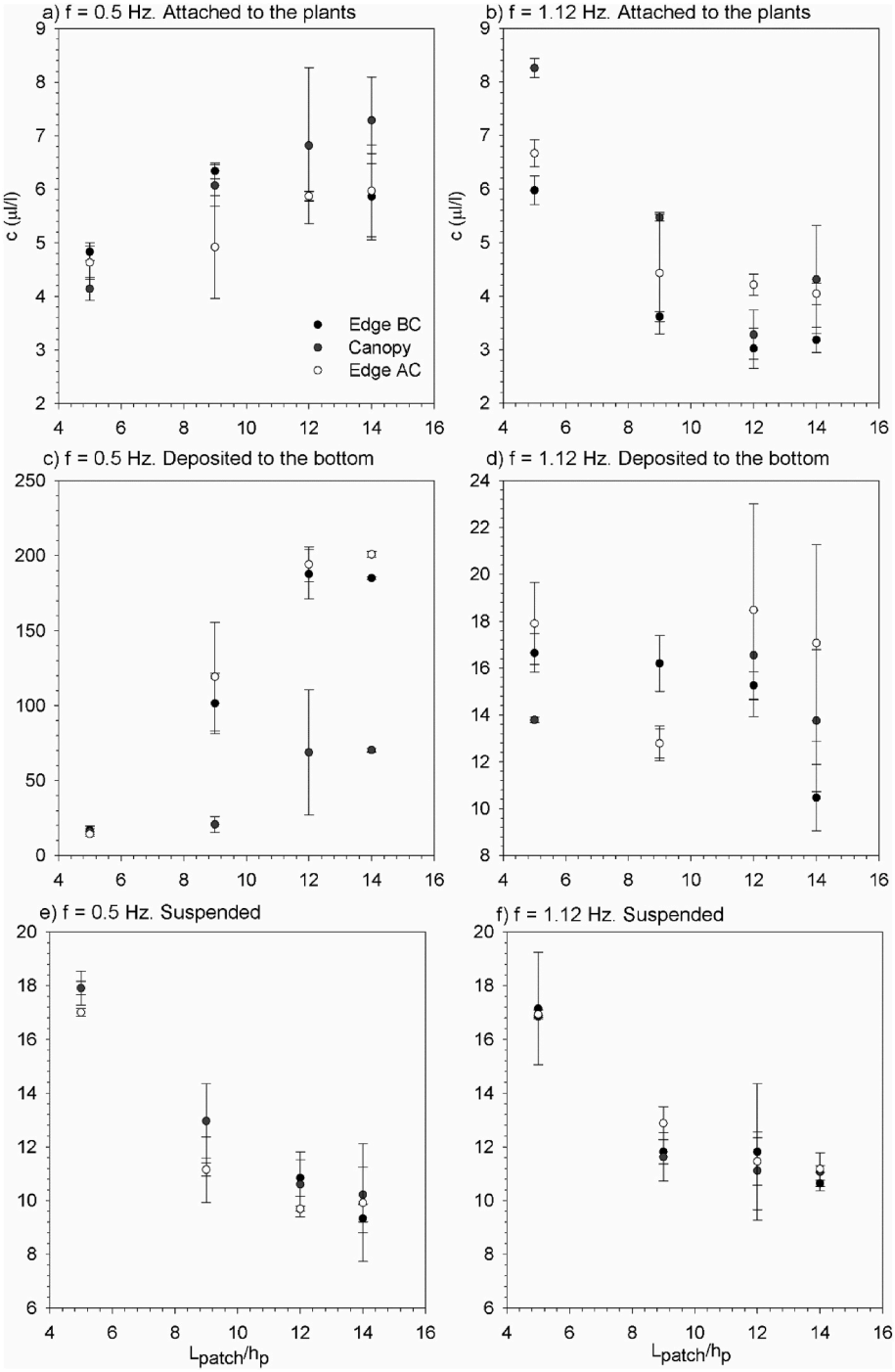

Fig. 4. Sediment concentration, c, trapped by the plant leaves vs. the ratio between patch length and plant height, L_{patch}/h_p for experiments carried out at SPF = 3.5%. Blue circles correspond to measurements taken at the edge BC (Fig. 1); red circles to the measurements taken in the inner canopy area; and unfilled circles to the measurements taken at the edge AC (Fig. 1). For a) f = 0.5 Hz and for d) f = 1.12 Hz. Sediment concentration, c, deposited at the bottom of the flume vs. L_{patch}/h_p, for b) f = 0.5 Hz and for e) f = 1.12 Hz. Suspended sediment concentration, c, remained in suspension within the canopy at z/h_p = 0.4, for c) f = 0.5 Hz and for f) f = 1.12 Hz.

value of the orbital velocity U_w^{rms} (U_w hereafter) at each depth, and was calculated according to:

$$U_w^{rms} = \sqrt{\frac{1}{2\pi}\int_0^{2\pi} (U_i(\varphi) - U_c)^2 \partial\varphi} \quad (4)$$

2.7. Theory

A non-dimensional model was constructed based on the Pi-Buckingham theorem. Four main variables and two dimensions were considered in this current study. The variables are the wave excursion length ($A_w = U_w/(2\pi f)$), the plant-to-plant distance ($S = n^{-1/2}$), the patch length (L_p) and the effective vegetation height (h_v). The effective vegetation height is the height of bent plants when they swing with the flow and will depend on the wave frequency (Barcelona et al., 2021c, 2023). The two dimensions are metres and seconds. Therefore, two governing non-dimensional parameters can be constructed to describe the results. First, A_w/S, i.e., the ratio between the wave excursion length and the plant-to-plant distance, accounts for the penetration of the wave within the vegetated patch. And second, L_p/h_v, which is the ratio between the length of the patch, L_p and the effective vegetation height h_v. Based on the above governing parameters, it is possible to expect that the percentage of sediment trapped by the leaves, the sediment in suspension and the sediment settled at the bottom of the tank, is a function of the dimensionless parameters, A_w/S and L_p/h_v (Zong and Nepf, 2011).

3. Results

After 60 min (from injection) had lapsed, the concentration levels of the sediment in suspension reached a steady state. In this steady state, the injected sediment was distributed into the four regions considered (Fig. 3): attached to the plant leaves, deposited at the bottom of the flume, or in suspension either above or within the canopy.

For each wave frequency considered, the concentration of particles trapped by individual plant leaves did not differ between the different regions (canopy and edges) (Fig. 4a and b). However, the behaviour of the sediment concentration with L_p/h_v was different depending on wave frequency. For the lower frequency (f = 0.5 Hz), the longer the patch length, the greater the amount of sediment trapped on the leaves (Fig. 4a). In contrast, for the highest frequency (f = 1.12 Hz), the longer the patch length, the lower the amount of sediment trapped by plant leaves (Fig. 4b).

The sediment concentration deposited at the bottom behaved differently depending on wave frequency. For the lowest wave frequency (f = 0.5 Hz), an increase in the patch length resulted in an increase in the sediment deposited at the bottom. Likewise, lower sediment concentrations were found within the canopy instead of at the edges (Fig. 4c). Meanwhile, for the highest frequency (f = 1.12 Hz), the sediment deposited at the bottom remained constant for all the patch lengths studied (Fig. 4d). In addition, for this wave frequency, there were no differences in sediment concentration levels between the edges and the canopy (Fig. 4d).

The suspended sediment concentration levels presented the same behaviour for the two wave frequencies studied: f = 0.5 and 1.12 Hz. The greater the patch length, the lower the sediment concentration that remained in suspension. In this case, there were no differences in suspended sediment concentration levels between the edge and the canopy (Fig. 4e and f).

Furthermore, it must be noted that, although both the sediment deposited on the leaves and the sediment remaining in suspension had the same range for the two wave frequencies studied (Fig. 4a, b, e and f), the range of the amount of sediment deposited at the bottom for f = 0.5 Hz was ten times that for f = 1.12 Hz (Fig. 4c and d).

The dependence of the percentage of the volume of sediment particles trapped by the leaves, V_P, with the non-dimensional parameter (A_w/S)/(L_p/h_v) presented two regimes (Fig. 5). For (A_w/S)/(L_p/h_v) < 8, a first regime where V_P remained constant with (A_w/S)/(L_p/h_v) with V_P = 4.7%. However, for (A_w/S)/(L_p/h_v) > 8, V_P increased linearly with (A_w/S)/(L_p/h_v) (Fig. 5). The first regime (left part of Fig. 5) mainly corresponded to cases with the highest frequency (f = 1.12 Hz). In contrast, the second regime (right part of Fig. 5) corresponded mainly to the experiments carried out with the lowest frequency (f = 0.5 Hz), independent of the canopy density.

The volume of particles remaining in suspension (in %) within the canopy was found to decrease linearly with (A_w/S)/(L_p/h_v) (Fig. 6).

The volume of the sediment deposited at the bottom (V_B, in %) versus (A_w/S)/(L_p/h_v) presented two regimes (Fig. 7). A first regime for (A_w/S)/(L_p/h_v) < 8, where V_B remained constant with (A_w/S)/(L_p/h_v) with V_p = 22.6%. A second regime for (A_w/S)/(L_p/h_v) > 8, where V_P increased linearly with (A_w/S)/(L_p/h_v) (Fig. 7). As with V_P, the first regime (left part of Fig. 7) mainly corresponded to the cases carried out with the highest frequency (f = 1.12 Hz) and the second regime (right part of Fig. 7) to the experiments carried out with the lowest frequency (f = 0.5 Hz).

4. Discussion

The current study demonstrates that both the architectural structure of a seagrass patch and the hydrodynamics impact sediment distribution. That is, the amount of sediment deposited on the bed and plant leaves, and the suspended sediment presents different percentages depending on the structural characteristics: patch length and plant density, and on the hydrodynamics, here the through-the-wave frequency.

Plant leaves captured sediment with a concentration that did not differ between whether the plants were situated within the canopy or at the edges of the canopy. However, it is interesting to notice that the sediment concentration captured by plant leaves increased with the

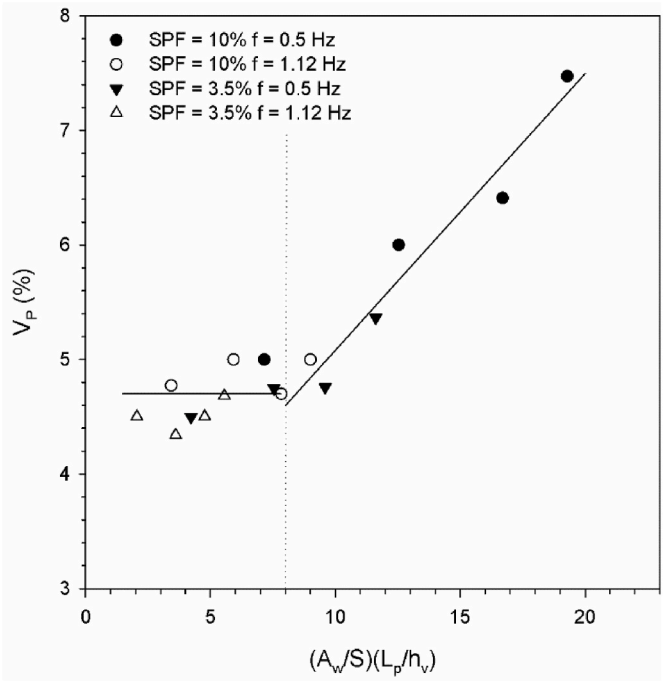

Fig. 5. Relationship between the volume of sediment trapped by the leaves, V_P, and (A_w/S)/(L_p/h_v) for all the experiments carried out. The vertical dashed line represents the minimum value of (A_w/S)/(L_p/h_v) that separated the different behaviours observed. The horizontal solid line at V_P = 4.7% represents the mean value of V_P for (A_w/S)/(L_p/h_v) < 8, where the V_P remained constant. For (A_w/S)/(L_p/h_v) > 8 a linear tendency was found with $V_P = 0.17 * (A_w/S)/(L_p/h_v) + 3.31$, with $R^2 = 0.80$ and 95% of confidence.

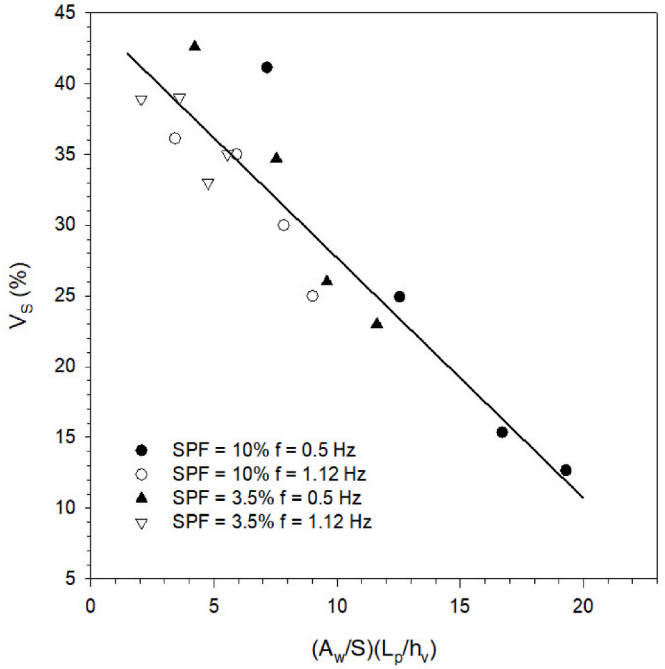

Fig. 6. Relationship between the sediment that remained in suspension, Vs, for all the experiments carried out. The solid line represents the linear tendency that was found Vs = −1.76 * $(A_w/S)/(L_p/h_v)$ + 44.60, with R^2 = 0.88 and 99% of confidence.

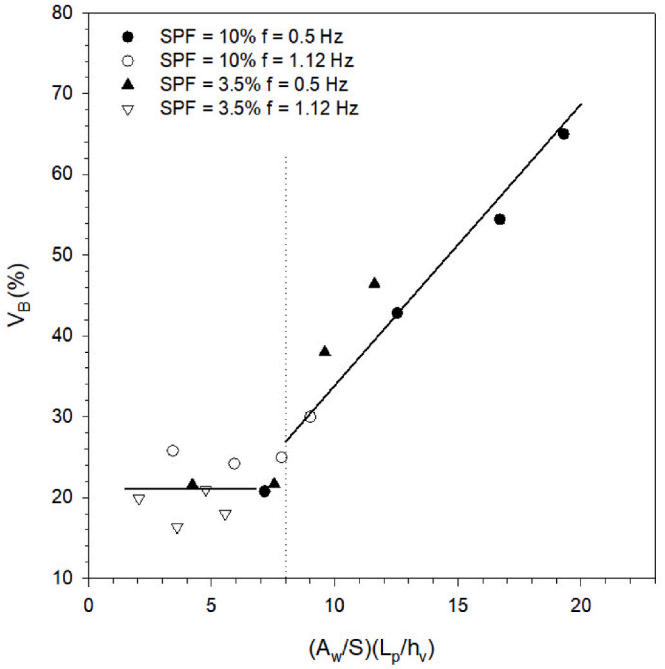

Fig. 7. Relationship between the volume of sediment deposited at the bottom, V_B, for all the experiments carried out. The vertical dashed line represents the minimum value of $(A_w/S)/(L_p/h_v)$ that separated the different trends observed for the V_B. The horizontal solid line at V_B = 22.58% represents that for $(A_w/S)/(L_p/h_v) < 8$, where the V_B remained constant. For $(A_w/S)/(L_p/h_v) > 8$, a linear tendency was found $V_B = 3.15^*$ $(A_w/S)/(L_p/h_v)$+ 3.92, with R^2 = 0.95 and 99% of confidence.

patch size for the wave frequency of 0.5 Hz and decreased with the patch size for 1.12 Hz. This difference might be because plants in large seagrass patches and low frequency wave environments have a large swing movement with a greater stroke, which would increase the chance of sediment particles being captured by single plants. On the other hand, the fast movement of the plant leaves in large seagrass patches and under a wave frequency of 1.12 Hz may increase the friction between leaves and cause the ejection of particles, thus reducing the chance of particles being potentially captured by plant leaves (Barcelona et al., 2021c).

Sediment particles deposited on the bottom also presented different behaviours depending on the wave frequency. In wave frequency environments of 0.5 Hz, plants in large seagrass patches played a synergistic role, consequently increasing by nearly ten times, the amount of sediment deposited onto the bottom from the smaller patch of $5h_p$ up to the largest patch of $14h_p$. In this case, sedimentation was maximized at the edges of large patches. This result agrees with those of Navarrete-Fernández et al. (2022) who found that microparticles presented the maximum sedimentation rates at the edges of the canopy, while decreasing towards the inner canopy. Zong and Nepf (2011) also found a heterogeneous distribution of sediment deposition in a patch of vegetation in a unidirectional flow. In their case, high deposition rates were observed at the edge of dense patches of vegetation, while also decreasing towards the patch interior. The sedimentation within the vegetation obtained for the case of wave frequencies of 1.12 Hz, was also lower than that for wave frequencies of 0.5 Hz. This can be attributed to the different movements of waves of different frequencies. In the case of 0.5 Hz, plants moved back and forth. In contrast, in the case of 1.12 Hz, plants were bent and oscillated asymmetrically to one side (see videos in the Supplementary Material). The different movements could cause different boundary layers for the different wave frequencies. Measurements of the suspended particle concentration levels above the canopy reveal that for the frequency of 0.5 Hz the suspended concentration levels was 25% lower than for 1.12 Hz. Therefore, the low sedimentation associated to 1.12 Hz could be because more particles accumulate above the canopy than in the case of 0.5 Hz. The different behaviour of the vegetation under different wave frequencies results in different boundary conditions being produced by the plants which can also explain why 0.5 Hz presents heterogeneous horizontal patterns compared 1.12 Hz, where a horizontal homogeneous sedimentation pattern holds. Likewise, note that the sediment concentration obtained in the non-vegetated experiment was 15.0 μL L^{-1}, i.e., close to that obtained for the small patch of $5h_p$. This indicates that the effect of the small patch of $5h_p$ on sedimentation does not deviate much from the non-vegetated case. This result is in accordance with the findings by Colomer et al. (2017), who found that $6.6h_p$ patches of *Posidonia Oceanica* produce low sheltering of the bed, i.e., close to bare soil conditions.

Under a wave frequency of 1.12 Hz, the concentration of sediment deposited onto the bottom for all the patches studied was close to that obtained for the smallest patch with the lower wave frequency, and to the sedimentation for the non-vegetated case for that same wave frequency (11.0 μL L^{-1}). Contrary to the wave frequency of 0.5 Hz, under the wave frequency of 1.12 Hz, the concentration of sediment deposited at the bottom of the patch did not depend on patch length. In this case, the sediment concentration was distributed homogeneously throughout the patch without any differences between canopy edges and the inner region. Therefore, the impact of a seagrass patch on the sedimentation rates also depends on the hydrodynamics of the flow, with heterogeneous distribution in wave frequencies of 0.5 Hz, and homogeneous distribution in wave frequencies of 1.12 Hz.

Contrary to what has been observed for the flux of sediment to the bottom and the capture of sediment by plant leaves, suspended sediment presents the same behaviour under both wave frequencies, 0.5 Hz and 1.12 Hz. In both cases, an increase in the patch length caused a decrease in the concentration levels of suspended sediment within the canopy. In addition, the suspended sediment concentration levels for the 1.12 Hz wave frequency was close to that obtained for 0.5 Hz. Therefore, the water quality within the patch, through a reduction in particle concentration, improves as the length of the patch increases. It must also be

noted that under both frequencies no differences in suspended sediment concentration levels were observed between canopy edges and patch interiors. The suspended sediment concentration ranged between 10 μL L^{-1} to 18 μL L^{-1}. The density of the sediment used in the current study was 2650 kg m^{-3}, which resulted in a suspended sediment concentration of 45 mg L^{-1}. This concentration is within the concentration range of river sediment plumes in natural environments (Tassan, 1997; Warrick et al., 2004; Liu et al., 2022).

The percentage of particles captured by plant leaves was nearly constant 4.7% versus the non-dimensional parameter (A_w/S) (L_p/h_v) up to a threshold of (A_w/S) $(L_p/h_v) = 8$. For (A_w/S) $(L_p/h_v) > 8$, the percentage of particles captured by plant leaves increased linearly with (A_w/S) (L_p/h_v). This second region indicates that more sediment particles are captured by plant leaves when A_w/S or L_p/h_v increase. The volume of sediment deposited on the bed presents the same threshold at (A_w/S) $(L_p/h_v) = 8$, from where the percentage of sedimentation increases with (A_w/S) (L_p/h_v) for (A_w/S) $(L_p/h_v) > 8$. In contrast, for (A_w/S) $(L_p/h_v) < 8$ the percentage of deposited particles on the bed remains constant at its lowest value of 22.6%, indicating that the vegetated patch does not produce any effect on the sedimentation.

For $A_w/S > 0.35$, seagrass patches dissipate wave velocity by generating turbulent kinetic energy (Barcelona et al., 2023). In this regime seagrass patches behave like canopies, in contrast, for $A_w/S < 0.35$ seagrass patches present a single stem-like behaviour and do not generate turbulent kinetic energy. In the current study, all cases with $A_w/S > 0.35$ correspond to (A_w/S) $(L_p/h_v) > 8$, where the seagrass patch has the role of both increasing sediment capture by plant leaves and sedimentation at the bottom. Therefore, from the results of the current study, seagrass patches behave as canopies when (A_w/S) $(L_p/h_v) > 8$. This case is expected to hold for both high A_w/S or L_p/h_v. High values of A_w/S indicate that waves interact with the canopy dissipating the mean energy of the flow, and it also means that the orbital excursion length of the wave is greater than the plant to plant distance. Therefore, the canopy protects the bed from the oscillatory flow. L_p/h_v represents the longitudinal extension of the vegetated patch. The larger the patch, the greater its effect on the bed will be. This result agrees with Zhu et al. (2021) who observed that seagrass meadows trapped sediment due to the reduction of the mean energy of the flow (waves and currents). They observed this result when seagrass meadow density was high. *Posidonia oceanica* seagrasses have been found to increase the deposition of sediment particles compared to bare soil (Gacia and Duarte, 2001). In their work, waves of frequencies between 0.33 s^{-1} and 0.07 s^{-1} lead to bed orbital velocities of 2–10 cm s^{-1}, and mean shoot densities of 200 shoots m^{-2}, resulting in $A_w/S = 0.672 > 0.35$. Therefore, this case corresponds to the case of a canopy that reduces the mean energy of the flow through the production of turbulent kinetic energy and, in turn, enhances the deposition of sediment to the bed.

Therefore, the current study demonstrates that the threshold for when a seagrass patch of length L_p preserves canopy characteristics depends on the hydrodynamics (through A_w), the seagrass density (through S) and the effective plant height h_v, which, in turn, depends on the hydrodynamics and the plant flexibility. From the current study, small patches of vegetation produce a low deposition of sediment on the bottom and on their leaves, thus presenting a high suspended sediment concentration. These patches of vegetation are expected to be more vulnerable under adverse conditions. These results might also explain how an increase in patchiness leads to small fragmented *Zostera marina* seagrass patches of 5.6–10 m long disappearing due to anthropogenic pressures (García-Redondo et al., 2019). Olesen and Sand-Jensen (1994) observed high rates of *Zostera marina* mortality for small and sparse seagrass patches. Moreover, López-y-Royo et al. (2011) used ecological indicators to categorize the water quality in the evolution of *Posidonia oceanica*. In their study, low water quality was associated with *Posidonia oceanica* densities below 200 shoots m^{-2}. The current study demonstrates that for a sparse canopy to provide the required ecological services compared to a dense canopy, it must have a large patch. Therefore, the current study highlights the fact that canopy density is not the only crucial parameter indicating meadow quality, as so too does the length of the seagrass patch. Long and continuous seagrass meadows are expected to provide seabed sediment stabilization and boost sediment trapping, thus providing a sediment enhancing strategy to cope with future sea level rises or improve carbon sequestration levels.

5. Conclusions

The current study demonstrates the role seagrass patch length plays in distributing sediment within the patch itself. Patches of vegetation decreased the amount of suspended sediment concentration, compared with continuous vegetation landscapes. The larger and denser the patch is, the lower the concentration levels of suspended sediment are. This reduction in the suspended sediment concentration is caused by two mechanisms: the trapping of sediment particles by plant leaves and the enhancement of sedimentation by the presence of vegetation. From the current study, a seagrass patch is able to increase the settling of particles to the bottom and also to capture particles on their leaves provided (A_w/S) $(L_p/h_v) > 8$. This condition holds for both large or dense seagrass patches and provides the limit for when seagrass patches become vulnerable to external pressures. From the results presented here, information can be obtained concerning the minimum length and density a vegetated patch under certain hydrodynamics has to have to maintain the functionality of its canopy and thus be less vulnerable.

The current study demonstrates that seagrass patches in wave frequencies of 0.5 Hz present greater sediment deposition at the edges compared to the inner canopy region, resulting in spatial heterogeneous sediment deposition patterns. In contrast, sediment deposition rates in seagrass patches in wave frequency environments of 1.2 Hz present a spatial homogeneous distribution.

This study presents the behaviour of a seagrass patch from the perspective of the sediment distribution patterns in the vegetated patch. The results indicate when a seagrass patch is no longer able to modify sediment distribution patterns or ensure the stabilization of the bed, thus losing part of its functionality. It also demonstrates the vulnerability of small and sparse seagrass patches under external pressures. This study provides information on the vital role aquatic vegetation plays in enhancing sedimentation within the canopy. Preserving the vegetation in these seascapes can help mitigate the future climate change scenarios that predict a decrease in the retention of sediments in coastal areas and the erosion and shrinking of deltas. Likewise, continuous seagrass landscapes fragmentation also predicts a reduction in the sedimentation and, therefore, a reduction in the carbon burial.

CRediT authorship contribution statement

Aina Barcelona: Conceptualization, Data curation, Formal analysis, Methodology, Writing-original draft, Writing-review & editing. Jordi Colomer: Conceptualization, Data curation, Writing-review & editing. Teresa Serra: Conceptualization, Writing-review & editing, Funding acquisition, Supervision.

Declaration of competing interest

The authors declare that they have no known competing financial interests or personal relationships that could have appeared to influence the work reported in this paper.

Data availability

Data will be made available on request.

Acknowledgments

This project has been funded by the Ministerio de Ciencia e

Innovación of the Spanish Government through the grant PID 2021-123860O3-100. Aina Barcelona was founded by the pre-doctoral grant 2020 FI SDUR 00043 by the "Generalitat de Catalunya".

Appendix A. Supplementary data

Supplementary data to this article can be found online at https://doi.org/10.1016/j.marenvres.2023.105997.

References

Abadie, A., Borges, A.V., Champenois, W., Gobert, S., 2017. Natural patches in *Posidonia oceanica* meadows: the seasonal biogeochemical pore water characteristics of two edge types. Mar. Biol. 164, 166. https://doi.org/10.1007/s00227-017-3199-5.

Bacci, T., Rende, F.S., Scardi, M., 2017. Shoot micro distribution patterns in the Mediterranean seagrass *Posidonia oceanica*. Mar. Biol. 164, 85. https://doi.org/10.1007/s00227-017-3121-1.

Barcelona, A., Oldham, C., Colomer, J., Serra, T., 2021a. Functional dynamics of vegetated model patches: the minimum patch size effect for canopy restoration. Sci. Total Environ., 148854 https://doi.org/10.1016/j.scitotenv.2021.148854.

Barcelona, A., Colomer, J., Soler, M., Gracias, N., Serra, T., 2021b. Meadow fragmentation influences *Posidonia oceanica* density at the edge of nearby gaps. Estuar. Coast Shelf Sci. 249, 107106 https://doi.org/10.1016/j.ecss.2020.107106.

Barcelona, A., Oldham, C., Colomer, J., Garcia-Orellana, J., Serra, T., 2021c. Particle capture by seagrass canopies under an oscillatory flow. Coast. Eng. 169, 103972 https://doi.org/10.1016/j.coastaleng.2021.103972.

Barcelona, A., Colomer, J., Serra, T., 2023. Stem stiffness functionality in a submerged canopy patch under oscillatory flow. Sci. Rep. (in press).

Barsanti, M., Delbono, I., Ferretti, O., Peirano, A., Bianchi, C.N., Morri, C., 2007. Measuring change of coastal biodiversity: diachronic mapping of the meadow of the seagrass *Cymodocea nodosa (ucria) ascherson* in the gulf of tigullio (ligurian sea, NW mediterranean). Hydrobiologia 580, 35–41. https://doi.org/10.1007/s10750-006-0467-7.

Bell, S.S., Brooks, R.A., Robbins, B.D., Fonseca, M.S., Hall, M.O., 2001. Faunal response to fragmentation in seagrass habitats: implications for seagrass conservation. Biol. Conserv. 100, 115–123. https://doi.org/10.1016/S0006-3207(00)00212-3.

Borfecchia, F., Micheli, C., De Cecco, L., Sannino, G., Struglia, M.V., Di Sarra, A.G., Gomez, C., Mattiazzo, G., 2021. Satellite multi/hyper spectral HR sensors for mapping the *Posidonia oceanica* in South Mediterranean islands. Sustainability 13, 13715. https://doi.org/10.3390/su132413715.

Boström, C., Baden, S., Bockelmann, A., Dromph, K., Frederiksen, S., Gustafsson, C., Krause-Jensen, D., Möller, T., Laurentis, S., Olesen, B., Olsen, J., Pihl, L., Rinde, E., 2014. Distribution, structure, and function of Nordic eelgrass (*Zostera marina*) ecosystems: implications for coastal management and conservation. Aquat. Conserv. 24 (3), 410–434. https://doi.org/10.1002/aqc.2424.

Cacabelos, E., Gestoso, I., Ramalhosa, P., Canning-Clode, J., 2022. Role of non-indigenous species in structuring benthic communities after fragmentation events: an experimental approach. Biol. Invasions 24, 2181–2199. https://doi.org/10.1007/s10530-022-02768-9.

Chatting, M., Al-Maslamani, I., Walton, M., Skov, M.W., Kennedy, H., Husrevoglu, Y.S., Le Vay, L., 2022. Future mangrove carbon storage under climate change and deforestation. Front. Mar. Sci. 9, 781876 https://doi.org/10.3389/fmars.2022.781876.

Chen, Z., Jiang, C., Nepf, H., 2013. Flow adjustment at the leading edge of a submerged aquatic canopy. Water Resour. Res. 49, 5537–5551. https://doi.org/10.1002/wrcr.20403.

Colomer, J., Ross, J.A., Casamitjana, X., 1998. Sediment entrainment in karst basins. Aquat. Sci. 60, 338–358. https://doi.org/10.1007/s000270050045.

Colomer, J., Soler, M., Serra, T., Casamitjana, X., Oldham, C., 2017. Impact of anthropogenically created canopy gaps on wave attenuation in a Posidonia oceanica seagrass meadow. Mar. Ecol. Prog. Ser. 569, 103–116. https://doi.org/10.3354/meps12090.

Colomer, J., Serra, T., 2021. The world of edges in submerged vegetated marine canopies: from patch to canopy scale. Water 13, 2430. https://doi.org/10.3390/w13172430.

Cornacchia, L., Licci, S., Nepf, H., Folkard, A., van der Wal, D., van de Koppel, J., Puijalon, S., Bouma, T.J., 2019. Turbulence-mediated facilitation of resource uptake in patchy stream macrophytes. Limnol. Oceanogr. 2, 714–727. https://doi.org/10.1002/lno.11070.

Cox, J.R., Paauw, M., Nienhuis, J.H., Dunn, F.E., van der Deijl, E., Espositio, C., Goichot, M., Leuven, J.R.F.W., van Maren, D.S., Middelkoop, H., Naffaa, S., Rahman, M., Schwarz, C., Sieben, E., Triyanti, A., Yuill, B., 2022. A global syntesis of the effectiveness of sedimentation-enchancing strategies for river deltas and estuaries. Global. Planet. Change. 214, 103796. https://doi.org/10.1016/j.gloplacha.2022.103796.

Dunn, F.E., Darby, S.E., Nicholls, R.J., Cohen, S., Zarfi, C., Fekete, B.M., 2019. Projections of declining fluvial sediment delivery to major deltas worldwide in respone to climate change and anthropogenic stress. Environ. Res. Lett. 14 (084034) https://doi.org/10.1088/1748-9326/ab304e.

Ettinger, C.L., Voerman, S.E., Lang, J.M., Stachowicz, J.J., Eisen, J.A., 2017. Microbial communities in sediment from *Zostera marina* patches, but not the Z. marina leaf or root microbiomes, vary in relation to distance from patch edge. PeerJ 5, e3246. https://doi.org/10.7717/peerj.3246.

Francalaci, S., Paris, E., Solari, L., 2021. On the prediction of settling velocity for plastic particles of different shapes. Environ. Pollut. 290, 118068 https://doi.org/10.1016/j.envpol.2021.118068.

Gacia, E., Duarte, C.M., 2001. Sediment retention by a mediterranean *Posidonia oceanica* meadow: the balance between deposition and resuspension. Estuar. Coast Shelf Sci. 52, 505–514. https://doi.org/10.1006/ecss.2000.0753.

Ganthy, F., Soissons, L., Sauriau, P.-G., Verney, R., Sottolichio, A., 2015. Effects of short flexible seagrass *Zostera noltei* on flow, erosion and deposition processes determined using flume experiments. Sedimentology 62, 997–1023. https://doi.org/10.1111/sed.12170.

García-Redondo, V., Bárbara, I., Díaz-Tapia, P., 2019. *Zostera marina* meadows in the northwestern Spain: distribution, characteristics, and anthropogenic pressures. Biodivers. Conserv. 28, 1743–1757. https://doi.org/10.1007/s10531-019-01753-4.

Gera, A., Pagès, J., Romero, J., Alcoverro, T., 2013. Combined effects of fragmentation and herbivory on *Posidonia oceanica* seagrass ecosystems. J. Ecol. 101, 1053–1061. https://doi.org/10.1111/1365-2745.12109.

Ghisalberti, M., Nepf, H., 2002. Mixing layers and coherent structures in vegetated aquatic flows. J. Geophys. Res. 107, C23011 https://doi.org/10.1029/2001JC000871.

Goring, D.G., Nikora, V.I., 2002. Despiking acoustic Doppler velocimeter data. J. Hydraul. Eng. 128 (1), 117–126.

Granata, T.C., Serra, T., Colomer, J., Casamitjana, X., Duarte, C.M., Gacia, E., 2001. Flow and particle distributions in a nearshore seagrass meadow before and after a storm. Mar. Ecol. Prog. Ser. 218, 95–106. https://doi.org/10.3354/meps218095.

Hovel, K.A., Duffy, J.E., Stachowicz, J.J., Reynolds, P., Boström, C., Boyer, K.E., Cimon, S., Cusson, M., Fodrie, F.J., Gagnon, K., Hereu, C.M., Hori, M., Jorgensen, P., Kruschel, C., Lee, K.-S., Nakaoka, M., O'Connor, N.E., Rossi, F., Ruesink, J., Tomas, F., Ziegler, S., 2021. Joint effects of patch edges and habitat degradation on faunal predation risk in a widespread marine foundation species. Ecology 102, e03316. https://doi.org/10.1002/ecy.3316, 2021.

Lera, S., Nardin, W., Sanford, L., Palinkas, C., Guercio, R., 2019. The impact of submersed aquatic vegetation on the development of river mouth bars. Earth Surf. Process. Landforms 44, 1494–1506. https://doi.org/10.1002/esp.4585.

Leriche, A., Pasqualini, V., Boudouresque, C.F., Bernard, G., Bonhomme, P., Clabaut, P., Denis, J., 2006. Spatial, temporal, and structural variations of a *Posidonia oceanica* seagrass meadow facing human activities. Aquat. Bot. 84, 287–293. https://doi.org/10.1016/j.aquabot.2005.10.001.

Liu, W.C., Liu, H.M., Young, C.C., 2022. Effects of environmental factors on suspended sediment plumes in the continental shelf out of Danshuei River Estuary. Water 14, 2755. https://doi.org/10.3390/w14172755.

López-y-Royo, C., Pergent, G., Alcoverro, T., Buia, M.C., Casazza, G., Martínez-Crego, B., Pérez, M., Silvestres, F., Romero, J., 2011. The seagrass *Posidonia oceanica* as an indicator of coastal water quality: experimental intercalibration of classification systems. Ecol. Indicat. 11, 557–563. https://doi.org/10.1016/j.ecolind.2010.07.012.

Lowe, R.J., Koseff, J.R., Monismith, S.G., 2005. Oscillatory flow through submerged canopies: 1. Velocity structure. J. Geophys. Res. 110, C10016 https://doi.org/10.1029/2004JC002788.

Luhar, M., Coutu, S., Infantes, E., Fox, S., Nepf, H., 2010. Wave-induced velocity inside a model seagrass bed. J. Geophys. Res. 115, C12005 https://doi.org/10.1029/2010JC006345.

Madsen, J.D., Chambers, P.A., James, W.F., Koch, E.W., Westlake, D.F., 2001. The interaction between water movement, sediment dynamics and submersed macrophytes. Hydrobiologia 444, 71–84. https://doi.org/10.1023/A:1017520800568.

Marin-Diaz, B., Bouma, T.J., Infantes, E., 2020. Role of eelgrass on bed-load transport and sediment resuspension under oscillatory flow. Limnol. Oceanogr. 65, 426–436. https://doi.org/10.1002/lno.11312.

Mazarrasa, I., Samper-Villareal, J., Serrano, O., Lavery, P.S., Lovelock, C.E., Marbà, N., Duarte, C.M., Cortés, J., 2018. Habitat characteristics provide insights of carbon storage in seagrass meadows. Mar. Pollut. Bull. 134, 106–117. https://doi.org/10.1016/j.marpolbul.2018.01.059.

Montefalcone, M., Bianchi, C.N., Morri, C., Peirano, A., Albertelli, G., 2006. Lower limit typology and functioning of six *Posidonia oceanica* meadows in the Ligurian Sea (NW Mediterranean). Biol. Mar. Mediterr. 13, 262–266.

Montefalcone, M., Parravicini, V., Vacchi, M., Albertelli, G., Ferrari, M., Morri, C., Bianchi, C.N., 2010. Human influence on seagrass habitat fragmentation in NW Mediterranean Sea. Estuar. Coast Shelf Sci. 86, 292–298. https://doi.org/10.1016/j.ecss.2009.11.018.

Montefalcone, M., Vacchi, M., Archetti, R., Ardizzone, G., Astruch, P., Bianchi, C.N., Calvo, S., Criscoli, A., Fernández-Torquemada, Y., Luzzu, F., Misson, G., Morri, C., Pergent, G., Tomasello, A., Ferrari, M., 2019. Geospatial modelling and map analysis allowed measuring regression of the upper limit of *Posidonia oceanica* seagrass meadows under human pressure. Estuar. Coast Shelf Sci. 217, 148–157. https://doi.org/10.1016/j.ecss.2018.11.006.

Moore, E.C., Hovel, K.A., 2010. Relative influence of habitat complexity and proximity to patch edges on seagrass epifaunal communities. Oikos 119, 1299–1311. https://doi.org/10.1111/j.1600-0706.2009.17909.x.

Navarrete-Fernández, T., Bermejo, R., Hernández, I., Deidun, A., Andreu-Cazenave, M., Cózar, A., 2022. The role of seagrass meadows in the coastal trapping of litter. Mar. Pollut. Bull. 174, 113299 https://doi.org/10.1016/j.marpolbul.2021.113299.

Olesen, B., Sand-Jensen, K., 1994. Patch dynamics of eelgrass *Zostera marina*. Mar. Ecol. Prog. Ser. 106, 147–156. https://doi.org/10.3354/meps106147.

Oreska, M.P.J., McGlathery, K.J., Porter, J.H., 2017. Seagrass blue carbon spatial patterns at the meadow-scale. PLoS One 12, e0176630. https://doi.org/10.1371/joucnal.pone.0176630.

Pastor, A., Ospina-Alvarez, A., Larsen, J., Hansen, F.T., Krause-Jensen, D., Maar, M., 2022. A network analysis of connected biophysical pathways to advice eelgrass (*Zostera marina*) restoration. Mar. Environ. Res. 179, 105690 https://doi.org/10.1010/j.marenvres.2022.105690.

Paladini de Mendoza, F., Fontolan, G., Mancini, E., Scanu, E., Scanu, S., Bonamano, S., Marcelli, M., 2018. Sediment dynamics and resuspension processes in a shallow-water *Posidonia oceanica* meadow. Mar. Geol. 404, 174–186. https://doi.org/10.1016/j.margeo.2018.07.006.

Pinheiro, L.M., Britz, L.M.K., Agostini, V.O., Pérez-Parada, A., García-Rodríguez, F., Galloway, T.S., Pinho, G.L.L., 2002. Salt marshes as the final watershed fate for meso- and microplastic contamination: a case study from Southern Brazil. Sci. Total Environ. 838, 156077 https://doi.org/10.1016/j.scitotenv.2022.156077.

Pitarch, J., Falcini, F., Nardin, W., Brando, V.E., Di Cicco, A., Marullo, S., 2019. Linking flow-stream variability to grain size distribution of suspended sediment from a satellite-based analysis of the Tiber River plume (Tyrrhenian Sea). Sci. Rep. 9, 19729 https://doi.org/10.1038/s41598-019-56409-8.

Pujol, D., Casamitjana, X., Serra, T., Colomer, J., 2013. Canopy-scale turbulence under oscillatory flow. Continent. Shelf Res. 66, 9–18. https://doi.org/10.1016/j.jhydrol.2013.01.024.

Ros, A., Colomer, J., Serra, T., Pujol, D., Soler, M., Casamitjana, X., 2014. Experimental observations on sediment resuspension within submerged model canopies under oscillatory flow. Continent. Shelf Res. 91, 220–231. https://doi.org/10.1016/j.csr.2014.10.004.

Sand-Jensen, K., Mebus, J.R., 1996. Fine-scale patterns of water velocity within macrophyte patches in streams. Oikos 76, 169–180. https://doi.org/10.2307/3545759.

Sand-Jensen, K., Pedersen, M.L., 2008. Streamlining of plant patches in streams. Freshw. Biol. 53, 714–726. https://doi.org/10.1111/j.1365-2427.2007.01928.x.

Serra, T., Colomer, J., Gacia, E., Soler, M., Casamitjana, X., 2002. Effects of a turbid hydrothermal plume on the sedimentation rates in a karstic lake. Geophys. Res. Lett. 29 (21), 1–4. https://doi.org/10.1029/2002GL015368.

Serra, T., Oldham, C., Colomer, J., 2018. Local hydrodynamics at edges of marine canopies under oscillatory flow. PLoS One 13 (8), e0201737. https://doi.org/10.1371/journal.pone.0201737.

Serra, T., Gracias, N., Hendriks, I.E., 2020. Fragmentation in seagrass canopies can alter hydrodynamics and sediment deposition rates. Water 12 (12), 3473. https://doi.org/10.3090/w12123473.

Serra, T., Colomer, J., Cristina, X., Vila, X., Arellano, J.B., Casamitjana, X., 2001. Evaluation of a laser in situ scattering instrument for measuring concentration of phytoplankton, purple sulfur bacteria, and suspended inorganic sediments in lakes. J. Environ. Eng. 127, 1023–1030. https://doi.org/10.1061/(ASCE)0733-9372(2001)127:11(1023).

Soler, M., Serra, T., Folkard, A., Colomer, J., 2021. Hydrodynamics and sediment deposition in turbidity currents: comparing continuous and patchy vegetation canopies, and the effects of water depth. J. Hydrol. 594, 125750 https://doi.org/10.1016/j.jhydrol.2020.125750.

Sweatman, J.L., Layman, C.A., Fourqurean, J.W., 2017. Habitat fragmentation has some impacts on aspects of ecosystem functioning in a sub-tropical seagrass bed. Mar. Environ. Res. 126, 95–108. https://doi.org/10.1016/j.marenvres.2017.02.003.

Tassan, S., 1997. A numerical model for the detection of sediment concentration in stratified river plumes using Thematic Mapper data. Int. J. Rem. Sens. 18 (12), 2699–2705. https://doi.org/10.1080/014311697217567.

Tuck, M.E., Ford, M.R., Kench, P.S., Masselink, G.M., 2021. Sediment supply dampens the erosive effects of sea-level rise on reef islands. Sci. Rep. 11, 5523. https://doi.org/10.1038/s41598-021-85076-x.

Valero, M., Tena, J., Torres, J., Royo, M., 2009. Estudio de la Pradera de *Posidonia oceanica (L.) Delile* del Área Litoral del Municipio de Teulada (Alicante). Nereis 2, 29–39.

van Katwijk, M.M., Bos, A.R., Hermus, D.C.R., Suykerbuyk, W., 2010. Sediment modification by seagrass beds: muddification and sandification induced by plant cover and environmental conditions. Estuar. Coast Shelf Sci. 89, 175–181. https://doi.org/10.1016/j.ecss.2010.06.008.

Van De Koppel, J., Bouma, T.J., Herman, P.M.J., 2015. The influence of local-and landscape-scale processes on spatial self-organization in estuarine ecosystems. J. Exp. Biol. 215, 962–967. https://doi.org/10.1242/jeb.060467, 2015.

Verdura, J., Santamarís, J., Ballesteros, E., Smale, D.A., Cefalì, M.E., Golo, R., de Caralt, S., Vergés, A., Cebrian, E., 2021. Local-scale climatic refugia offer sanctuary for a habitat-forming species during a marine heatwave. J. Ecol. 109, 1758–1773. https://doi.org/10.1111/1365-2745.13599.

Warrick, J.A., Mertes, L.A.K., Siegel, D.A., MacKenzie, C., 2004. Estimating suspended sediment concentrations in turbid coastal waters of the Santa Barbara Channel with SeaWiFS. J. Remote Sens. 25, 1995–2002. https://doi.org/10.1080/01431160310001619535.

Zhang, Y., Tang, C., Nepf, H., 2018. Turbulent kinetic energy in submerged model canopies under oscillatory flow. Water Resour. Res. 54, 1734–1750. https://doi.org/10.1002/2017WR021732.

Zhu, Q., Wiberg, Q., Reidenback, M.A., 2021. Quantifying seasonal seagrass effects on flow and sediment dynamics in a back-barrier bay. J. Geophys. Res.-Oceans 1, 126. https://doi.org/10.1029/2020JC016547 e2020JC016547.

Zong, L., Nepf, H., 2011. Spatial distribution of deposition within a patch of vegetation. Wat. Resour. Res 2011 47, W03516. https://doi.org/10.1029/2010WR009516.

scientific reports

Check for updates

OPEN

Stem stiffness functionality in a submerged canopy patch under oscillatory flow

Aina Barcelona, Jordi Colomer & Teresa Serra✉

Seagrass canopies are coastal ecosystems that are able to modify the abiotic environment through their architectural structure. They have different structural parameters, such as plant stem stiffness, patch length and canopy density, all of which determine their overall functionality in modifying the seafloor hydrodynamics within coastal areas. To determine the interaction between hydrodynamics and the canopy structure, a set of laboratory experiments were carried out with both rigid and flexible stems for different canopy densities, patch lengths and wave frequencies. In the upper part of the canopy, flexible plants move with the flow without generating drag or producing turbulent kinetic energy, while rigid plants generate drag and produce turbulent kinetic energy. In the inner canopy layer, both types of plants behave like rigid stems and produce turbulent kinetic energy. A non-dimensional model based on the turbulent kinetic energy, the wave velocity and the plant characteristics is presented to describe the behaviour of flexible and rigid plants under an oscillating flow. Flexible plants behave in a stiffer manner under high wave frequencies than under low wave frequencies, thus making their behaviour closer to that of rigid plant stems. This difference between both canopy structures can explain their distribution in the environment, with rigid canopies being more extended in more sheltered regions while flexible plants are characteristic of more exposed regions with high flow energy.

Seagrasses are valuable coastal ecosystems that protect the seabed from waves and currents[1,2]. They also provide habitats for aquatic life, improve water quality, sequester carbon, and stabilize sediment[3–5]. However, they are situated in regions where anthropogenic activities like anchoring, dredging, trawling, or sewage outflow cause their decline[6,7]. Human pressure has produced a 30–60% decline in seagrasses[8]. In some places, seagrasses have completely disappeared, while in others seagrass landscapes have changed from large continuous meadows to fragmented canopies[9], where a patchy distribution of plants dominates the seascape.

There is a lack of data concerning the hydrodynamics for all types of canopies, patch characteristics and the degree of landscape fragmentation[10]. While the hydrodynamics in continuous meadows is expected to be spatially homogeneous, in fragmented meadows[11] it is likely to be spatially heterogeneous. In addition, the increase in the degree of meadow's fragmentation also increases the overall turbulent kinetic energy, thus enhancing mixing for a greater sediment resuspension[11]. Therefore, it is expected that canopy fragmentation increases meadow vulnerability under external pressures[12].

Considering that fragmented landscape seagrasses are made up of patches of different sizes[13], patch length, then, is expected to determine the hydrodynamics in fragmented meadows. Interspersed within vegetation of fragmented meadows are gaps (i.e., zones without vegetation). The larger the gap, the greater the turbulent kinetic energy and wave velocity within that gap[14] is. However, for a certain gap size, the degree of meadow fragmentation has not been found to impact the hydrodynamics[14]. In contrast, the degree of fragmentation does impact canopy density at canopy interfaces near a gap[15]. These results reveal the need for more studies into the effect fragmentation has on the hydrodynamics within a fragmented meadow.

Vegetation produces a flow resistance that can differ depending on the plants' distinct structural characteristics, i.e., stem diameter, height, thickness, whether plants are submerged or emergent, their flexibility and horizontal distribution (density, staggered or random). Laboratory studies using models of rigid stems under oscillatory flows have shown that the wave velocity attenuation is greater for emergent stems than submerged ones[16]. Many of the studies into the hydrodynamics in rigid meadows under oscillatory and unidirectional flows have been conducted in laboratory flumes[2,17,18] in order to understand the role seagrasses play in sheltering the seabed. In addition, studies of the hydrodynamics in flexible meadows have also been carried out in the laboratory to better mimic seagrasses and understand the effect of flexibility. A flexible plant exhibits different

Department of Physics, University of Girona, 17071 Girona, Spain. ✉email: teresa.serra@udg.edu

configurations compared to rigid plant stems as they can remain erect, sway or be prone[19]. The turbulent kinetic energy within a meadow of submerged flexible plants has been found to depend on A_w/S, i.e., the ratio between the orbital wave excursion A_w and the plant-to-plant distance S[20]. For $A_w/S > 1$ the turbulent kinetic energy (*TKE*) increases with A_w/S whereas it remains constant for $A_w/S < 1$[20]. It must be pointed out that, despite the different structure of rigid and flexible stems, for low flow velocities the behaviour of flexible plant stems can be close to that of rigid plant stems due to the small amount of bending involved. However, the behaviour of patches of vegetation with different sizes of flexible and rigid plants has yet to be studied.

Understanding the relationship between all of the above-mentioned structural characteristics of the vegetation, along with the hydrodynamics might, offer clues as to what the optimal patch length scales, meadow densities or plant distributions are that could explain the resilience exhibited by some meadows. Some studies reveal that there are positive ecological interactions that favour the success of seagrass restoration[21]. The authors of these studies note that canopy density might play a positive dependence role, thus improving the survival of a seagrass population. Other structural parameters might likewise play critical roles in facilitating restoration projects, for instance, the minimum patch size that a patch of vegetation has to have or the arrangements of the stems in the patch. Hydrodynamics and plant characteristics have been found to determine sediment scouring that in turn can compromise seagrass restoration strategies[22]. High turbulent flows can lead to sediment scouring around plant stems.

Bouma et al.[23] compared the role of *Spartina alternifora* plants to that of *Zostera noltii*. (*Spartina alternifora* shoots are much stiffer than *Zostera noltii* shoots) in terms of their capacity to dissipate hydrodynamic forces) and found that dissipation was three times higher in vegetation with stiffer leaves than in vegetation with flexible leaves. They hypothesized that the drag exerted by the flow limits how far off the coast *Spartina* can grow. In more exposed areas, where the hydrodynamics are strong, other drag-minimizing species like *Zostera noltii* will grow, generating a sharp interface or transition between the extension of both types of ecological engineers. Therefore, seagrasses need to withstand hydrodynamic forces so that the costs (through drag) and benefits (their ability to modify the habitat conditions) are advantageous for their survival[23]. In addition, seagrasses have been found to have the capacity to adapt to certain environmental conditions by acclimation of their flexibility[23]. Paul and de los Santos[24] found that *Zostera marina* leaves were more rigid in summer than in winter and in deep sheltered zones than in shallow exposed zones where they presented more flexible leaves.

Hydrodynamics being modified by different types of plants (flexible or rigid) and patch lengths is still of concern and the role patch length plays for different plants' stiffness needs to be investigated. In the present study, the behaviour of single patches of different sizes formed by a random distribution of rigid or flexible plants under oscillatory conditions has been investigated. To this purpose, laboratory experiments were carried out in a flume using models of both rigid and flexible plants. To determine the behaviour of plants (rigid and flexible) under different hydrodynamic conditions two wave frequencies were considered. In addition, previous results obtained by other authors for a fixed patch length have been included in the study to provide a wider range of flow conditions and to compare between rigid and flexible plants. The modification of the hydrodynamics on the vertical axis by each type of plant and for each wave field was studied through the behaviour of the turbulent kinetic energy (*TKE*). The *TKE* can then be an indicator of the sediment resuspension in each set-up and provide clues on the possible resilience of seagrasses under different hydrodynamic conditions.

Results

The vertical profiles of TKE/U_w^2 presented different patterns depending on the wave frequency (Fig. 1a). For the non-vegetated set ups, and for the wave frequency of 1.12 Hz, TKE/U_w^2 presented a constant value at the top of the water column. Below this layer, a gradual decrease of TKE/U_w^2 was noted until a constant value situated at the bottom layer was observed. In contrast, for the wave frequency of 0.5 Hz, TKE/U_w^2 presented a constant value with z (Fig. 1a). From the vertical profiles of the normalized turbulent kinetic energy (TKE/U_w^2) in the vegetated set-ups, three layers could be distinguished. The above-canopy layer (ACL) corresponded to the layer above the maximum canopy height (h_p, determined as the leaf length for flexible plants and the stem length for the rigid canopy). In this layer TKE/U_w^2 presented three behaviours depending on the wave frequency. In the ACL, for the wave frequency of 1.12 Hz, TKE/U_w^2 tended to decrease (rigid, Fig. 1b) or remain constant (flexible, Fig. 1c) moving upwards from the canopy. In contrast, for the wave frequency of 0.5 Hz, TKE/U_w^2 increased with z/h_p for both rigid and flexible vegetation. From the TKE/U_w^2 profiles, a second interface could be observed. For the rigid canopy model, an interface between the upper-canopy layer (Fig. 1b), and which was situated at the same depth ($z/h_p = 0.44$) for both wave frequencies, was observed. In the lower-canopy layer (LCL), TKE/U_w^2 presented a smaller decrease with z/h_p in the case of the wave frequency of 1.12 Hz compared with the upper-canopy layer (UCL). In contrast, for the wave frequency of 0.5 Hz and for the LCL, TKE/U_w^2 decreased with z/h_p contrary to its behaviour in the UCL. For the flexible vegetation, the interface between the UCL and the LCL depended on the wave frequency (Fig. 1c), and the interface was situated at the depth of the effective plant height h_v (i.e., the height of the plant bent by the wave). In the LCL, for flexible vegetation and for a both wave frequencies, TKE/U_w^2 increased downwards as z/h_p decreased (Fig. 1c).

The *TKE* attenuations comparing vegetated with non-vegetated cases for both the UCL and LCL(β_{UCL} and β_{LCL}), were considered for all the rigid and flexible vegetation set-ups. For the flexible vegetation, β_{UCL} was found to be nearly 1 for all A_w/S (where $A_w = U_w/2\pi f$, U_w is the wave velocity and S is the plant to plant distance, see the "Methodology" section for more information) and both frequencies (Fig. 2a). However, for the rigid vegetation, β_{UCL} increased with A_w/S, from the threschold of $A_w/S > 0.35$ and followed a linear trend ($\beta_{UCL} = 9.08A_w/S\text{-}1.38$, $R^2 = 0.837$, $p < 0.05$) (Fig. 2b).

At the LCL for flexible vegetation, the same threshold at $A_w/S = 0.35$ was found for β_{LCL} (Fig. 2c). For $A_w/S < 0.35$ the values of β_{LCL} were close to 1, while for $A_w/S > 0.35$, β_{LCL} was higher than 1 (Fig. 2c). In this latter case, β_{LCL}

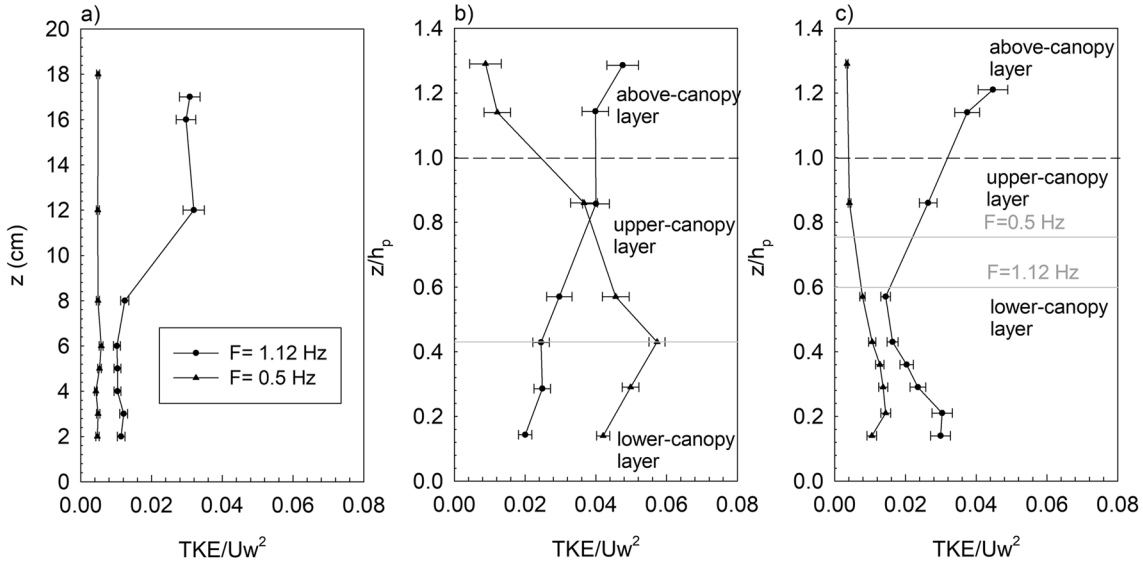

Figure 1. TKE/Uw^2 vertical profiles (**a**) versus z for non-vegetated set ups, and versus z/h_p for (**b**) rigid vegetation and (**c**) flexible vegetation for the two wave frequencies studied $f = 1.12$ Hz (circles) and (**b**) $f = 0.5$ Hz (triangles). The horizontal dashed lines in (**b**) and (**c**) represent the height of the plant leaf for flexible plants (h_p) or the height of the plant stem for rigid plants. The vegetated experiments presented here correspond to cases with a patch length of 238 cm and SPF = 10%. The horizontal grey lines represent the interface between the upper-canopy layer and the lower-canopy layer for both types of vegetation.

increased with A_w/S following a linear trend. Otherwise, for the rigid vegetation $\beta_{LCL} > 1$ was found for all A_w/S. In this case, β_{LCL} increased with A_w/S following a linear trend with a greater slople than for the flexible vegetaion case (Fig. 2d).

For the flexible vegetation, the vertical attenuation of the *TKE* (β', see the "Methodology" for its definition) was lower than 1 for $f = 1.12$ Hz, while for $f = 0.5$ Hz two different behaviours were found: for $A_w/S < 0.35$ $\boldsymbol{\beta'} \approx 1$ whereas for $A_w/S > 0.35$ $\boldsymbol{\beta'} > 1$ (Fig. 3a). For the rigid vegetation two behaviours were also found: for $A_w/S < 0.8$ $\boldsymbol{\beta'} < 1$, which included all the cases with $f = 1.12$ Hz and some cases of $f = 0.5$ Hz; meanwhile for $A_w/S > 0.8$ $\boldsymbol{\beta'} > 1$, which included the rest of the cases of $f = 0.5$ Hz (Fig. 3b).

The model from Eq. (12), was used to represent the *TKE* versus $\left[C_{D-Patch}\frac{nd^2}{2(1-\varnothing)}\right]^{\frac{2}{3}} U_w{}^2$ (where n is the canopy density, d the stem diameter and the solid plant fraction is $\phi = n\frac{\pi}{4}d^2$) for all experiments carried out with both the rigid and flexible models, where $C_{D-Patch} = C_D\left(\frac{L_{Patch}}{L_{Canopy}}\right)^{\frac{1}{3}}$, (see the "Methodology" section for a complete description of the model). For both the flexible and rigid vegetation models, two regions could be differentiated (Fig. 4a,b). For the flexible vegetation model (Fig. 4a), and for those cases with $\left[C_{D-Patch}\frac{nd^2}{2(1-\varnothing)}\right]^{\frac{2}{3}} U_w{}^2 < 4$, *TKE* was constant, at $TKE = 0.33$ cm^2 s^{-2}. In contrast, for $\left[C_{D-Patch}\frac{nd^2}{2(1-\varnothing)}\right]^{\frac{2}{3}} U_w{}^2 > 4$ two different behaviours were found. For the UCL, *TKE* for flexible vegetation was constant, with $TKE = 0.41$ cm^2 s^{-2} for $f = 0.5$ Hz and $TKE = 3.10$ cm^2 s^{-2} for $f = 1.12$ Hz, corresponding to the *TKE* measured without plants (SPF = 0%) for each frequency. For the LCL, the *TKE* increased linearly ($TKE = 0.20\left[C_{D-Patch}\frac{nd^2}{2(1-\varnothing)}\right]^{\frac{2}{3}} U_w{}^2 - 0.6$, $R^2 = 0.832$, $p < 0.05$) (Fig. 4a). For the rigid vegetation model (Fig. 5b), the threshold where *TKE* changed from being constant to increasing linearly from $\left[C_{D-Patch}\frac{nd^2}{2(1-\varnothing)}\right]^{\frac{2}{3}} U_w{}^2 = 2$. Therefore, for $\left[C_{D-Patch}\frac{nd^2}{2(1-\varnothing)}\right]^{\frac{2}{3}} U_w{}^2 > 2$, *TKE* followed a linear trend ($TKE = 0.27\left[C_{D-Patch}\frac{nd^2}{2(1-\varnothing)}\right]^{\frac{2}{3}} U_w{}^2 - 0.5$, $R^2 = 0.512$, $p < 0.05$), while for $\left[C_{D-Patch}\frac{nd^2}{2(1-\varnothing)}\right]^{\frac{2}{3}} U_w{}^2 < 2$, *TKE* remained constant with $TKE = 0.37$(Fig. 4b).

Discussion

In coastal zones, the structural characteristics of aquatic vegetation: stiffness, canopy density, height and patch length, play a crucial role in determining their functionality as ecological engineers. Rigid canopy patches provide greater drag than flexible canopy patches do under the same hydrodynamic conditions. This result might pose some limitations for rigid canopies if they are to sustain high energy flows.

Over bare soil, (i.e., without the presence of plants), the *TKE* declines with depth for all the wave frequencies studied. These results are in accordance with previous findings by Pujol et al.[16] and Zhang et al.[20] who found that *TKE* decreases with depth in non-vegetated beds. However, depending on the interaction between waves and plant stems, plants can reduce the *TKE* or in contrast, they can increase it due to the drag exerted by plant stems. In this case, the flexibility of the plant also determines the attenuation of the *TKE*. Rigid plants can produce drag

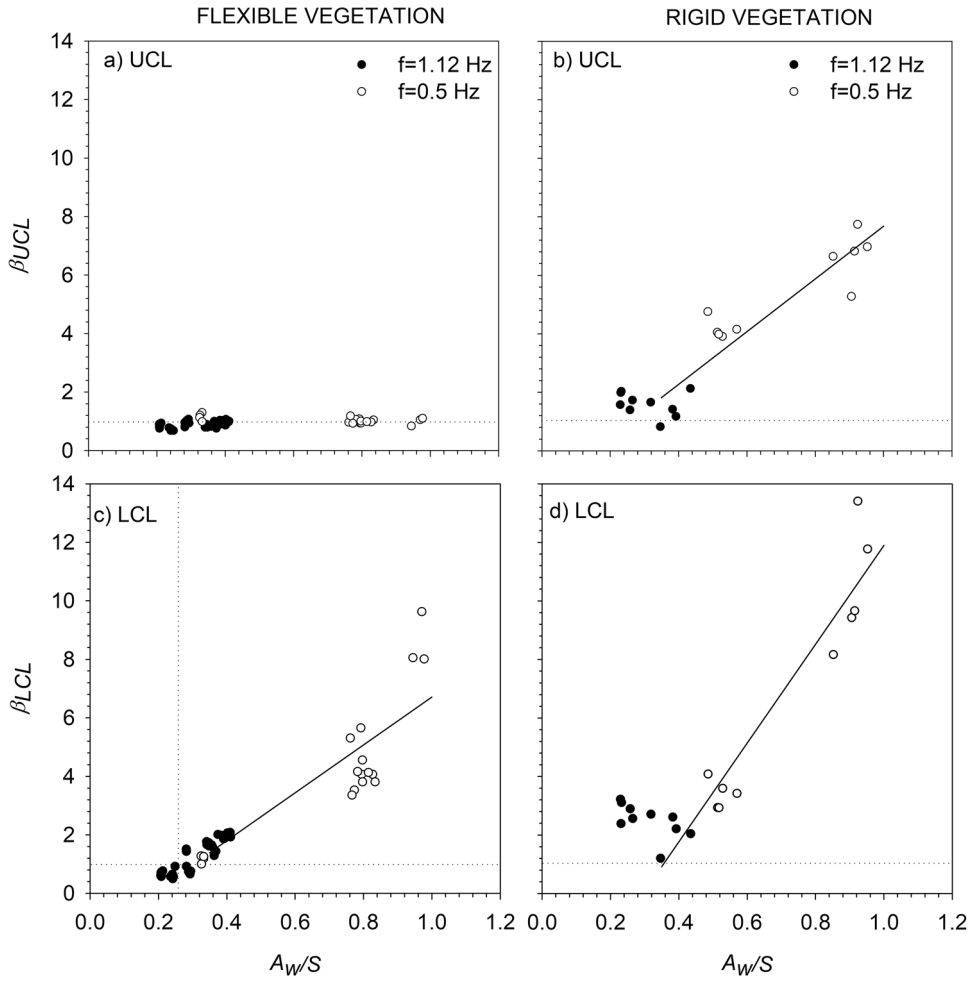

Figure 2. *TKE* attenuation in relation to the non-vegetated cases at the UCL (β_{UCL}) for (**a**) flexible vegetation (**a**) and for (**b**) rigid vegetation (**b**). *TKE* attenuation in relation to the non-vegetated cases at the LCL (β_{LCL}) for (**c**) flexible vegetation and for (**d**) rigid vegetation. Unfilled circles correspond to $f = 0.5$ Hz, and solid black circles to $f = 1.12$ Hz. Lines correspond to the linear best fit for the cases $A_w/S > 0.35$ when β increased linearly with A_w/S, independent of the wave frequency. In the UCL for rigid vegetation, $\beta = 9.02 \times A_w/S\text{-}1.34$ ($R^2 = 0.8625$, $p\text{-}value < 0.01$). In the LCL for rigid vegetation, $\beta = 16.90 \times A_w/S\text{-}5.00$ ($R^2 = 0.9224$, $p\text{-}value < 0.01$), and for the flexible vegetation $\beta = 8.19 \times A_w/S\text{-}1.48$ ($R^2 = 0.7819$, $p\text{-}value < 0.01$). Vertical dashed lines represent the x-axis position where $A_w/S = 0.35$, and horizontal dashed lines correspond to the y-axis position where $\beta = 1$.

along the entire plant stem, whereas flexible plants behave like a blade at the top, i.e. they move back and forth with the flow, thus reducing the relative motion between the flow and the blade[26]. However, they behave like a stem at the bottom, i.e., remain stiff with an increase in their relative motion.

In this study, the vertical attenuation of the *TKE* was studied by using two attenuation parameters: vertical attenuation (β') and attenuation by comparing the *TKE* with plants to the *TKE* without plants (β). For the rigid vegetation, the vertical attenuation β' is always below 1, indicating that the *TKE* in the LCL is lower than that at the UCL due to the drag produced by rigid stems in these two layers. However, for the flexible vegetation, β' is lower than 1 for those cases with $A_w/S < 0.35$, accounting for all the experiments carried out for $f = 1.12$ Hz and some at 0.5 Hz. In contrast, $\beta' > 1$ for all the experiments with $A_w/S > 0.35$, corresponding to some experiments carried out at $f = 0.5$ Hz. This result can be attributed to the fact that at high frequencies when $A_w/S > 0.35$, waves interact with the canopy of flexible plants producing *TKE* along the entire plant blade (due to the wakes generated) and so the plants remain stiff (i.e., behaving more like rigid plant stems). In contrast, low wave frequencies with $A_w/S < 0.35$ do not interact with the canopy, presenting a greater oscillatory excursion length at the top of the plant that at the bottom of it without producing wakes around the blades. In this case, flexible plants bend with the flow following a back and forth movement. These results align with the findings by van Veelen et al.[27] who studied wave damping by vegetation with differing flexibilities. In their study they found that flexible plants swayed with the flow and did not dampen wave velocities. In contrast, rigid plants produced a greater resistance, thus damping wave velocities. Wave damping is expected to be related to the production of *TKE*, thus coinciding with the results of the current study.

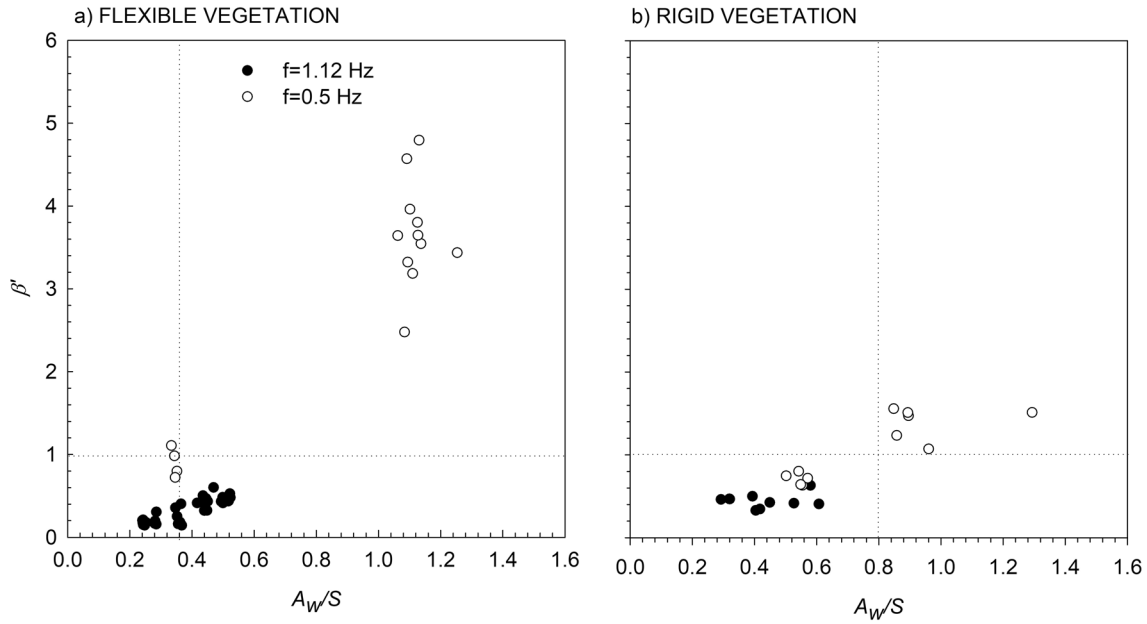

Figure 3. Vertical *TKE* attenuation, β', for the (**a**) flexible vegetation model and (**b**) rigid vegetation model. Unfilled circles correspond to $f = 0.5$ Hz, and solid black circles correspond to $f = 1.12$ Hz. The vertical dashed lines indicate the threshold of A_w/S for each type of plant, and the horizontal dashed line represents the y-axis value of $\beta' = 1$.

The attenuation of the *TKE* in both the UCL and LCL when compared to the without-plants experiments indicated that for the experiments carried out with rigid plants, and for all the wave frequencies studied $\beta_{UCL} > 1$ and $\beta_{UCL} > 1$ for both the UCL and LCL layers, also indicating that rigid plants produced *TKE* due to the greater relative motion between the waves and the rigid stems. These results align with the conclusions of Pujol et al.[2], who described the production of *TKE* by rigid canopies in the UCL due to the generation of stem-wake turbulence associated to a large reduction in wave velocity. For the case of a canopy of flexible plants, β_{UCL} was nearly 1 for the UCL since, at this depth, there is no plant-generated *TKE* because flexible plants swing with the flow and do not add any additional drag resistance to the movement; this behaviour could be described as a blade-like behaviour[20]. In this case, flexible plants reduce the drag to withstand the energy of the flow. This aligns with Paul and de los Santos[24] who found that the more rigid *Zostera marina* plants acclimatise in shallower regions far from energetic flow conditions while the more flexible *Zostera marina* plants extend far out from the coast.

This behaviour observed in the UCL changed in the LCL. For the case of a canopy of flexible plants and in the LCL, $\beta_{LCL} > 1$ for cases when $A_w/S > 0.35$, whereas $\beta_{LCL} < 1$ for cases when $A_w/S < 0.35$. This threshold obtained for $A_w/S = 0.35$ is equal to $A_w/S_b = 1$ (where S_b is the spacing considering that stems have eight blades, (i.e., $S_b = 1/(8\ N)^{1/2}$ and N is the stem density). This transition was also found by Zhang et al.[20] for the inner canopy layer of flexible plants. The experiments carried out by Pujol et al.[16] for flexible plants all corresponded to the cases $A_w/S < 0.35$. In such conditions, single stems do not contribute to *TKE* generation, instead, stems dampen the near-bed generated *TKE* relative to the non-vegetated cases. In contrast, for flexible meadows with $A_w/S > 0.35$, the *TKE* will be enhanced within the vegetated region relative to the non-vegetated cases. This *TKE* production determines that flexible vegetation in the LCL for $A_w/S > 0.35$ presents stem-like behaviour similar to rigid stems. A decrease in the *TKE* within a meadow of *Posidonia oceanica* was also found by Serra et al.[14] when compared to nearby gaps (areas without vegetation). In such cases, the canopy density was $N = 400$ stems m^{-2}, $T = 3.64$ s and $U_w = 0.01$ m s^{-1}, resulting in $A_w/S = 0.12 < 1$. Granata et al.[28] also found a vertical attenuation of *TKE* in a meadow of *Posidonia oceanica*. They compared the *TKE* above the canopy with the *TKE* within the canopy. In this case, the meadow sheltered the bed, i.e., stabilizing the sediment. Barcelona et al.[25] studied the capture of sediment particles via a model canopy of flexible plants in a flume and found that a meadow of flexible plants enhances sedimentation compared to non-vegetated conditions.

The present study demonstrates that *TKE* production by vegetation depends on wave velocity, canopy density, the plant flexibility and patch length for both rigid and flexible vegetation models. The thresholds $\left[C_{D-Patch}\frac{nd^2}{2(1-\varnothing)}\right]^{\frac{2}{3}} U_w{}^2 > 4$ (undefined for flexible plants[29]) and $\left[C_{D-Patch}\frac{nd^2}{2(1-\varnothing)}\right]^{\frac{2}{3}} U_w{}^2 > 2$ (for rigid plants, observed in the current study) is required for the canopy to produce *TKE*. It is important to notice that the production of *TKE* holds at a lower threshold for rigid than for flexible plants, because flexible plants move with the flow. Van Veelen et al.[27] also found that for low submergence ratios of the vegetation, like that in the current study ($h_p/H = 0.47$), the drag produced by the canopy varies depending on the type of plants (rigid or flexible). In their study, they found that the drag for flexible vegetation and for this submergence ratio was $C_D = 0.39$ compared to rigid plants, with $C_D = 1$. Considering this C_D for flexible plants, the threshold of

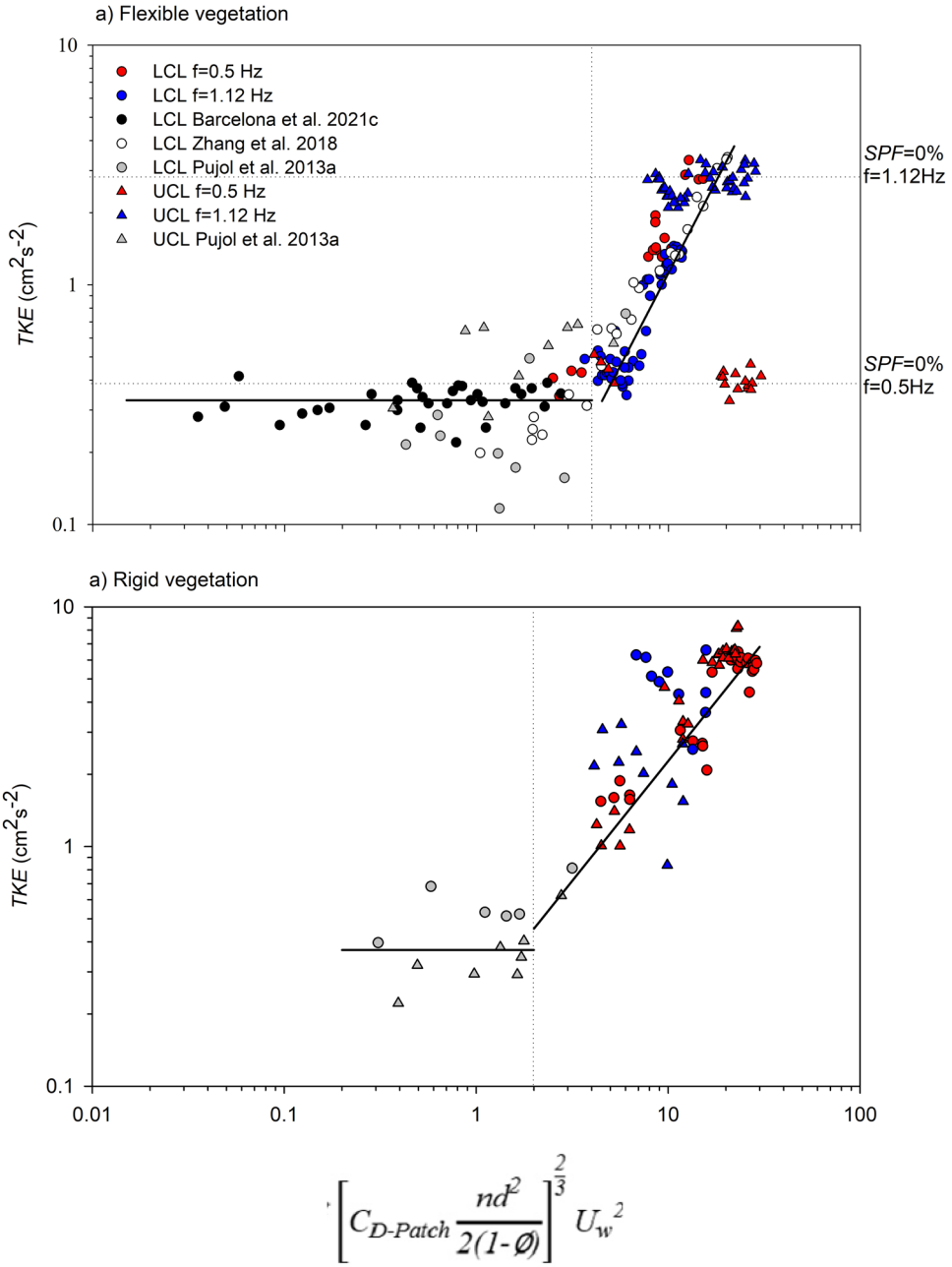

Figure 4. *TKE* versus $\left[C_{D-Patch}\frac{nd^2}{2(1-\varnothing)}\right]^{\frac{2}{3}}U_w{}^2$ for (**a**) flexible and (**b**) rigid vegetation. Data from Barcelona et al.[25], and Zhang et al.[20] for flexible vegetation have been included and data from Pujol et al.[16] for flexible vegetation and rigid vegetation have been included as well. The vertical dashed line indicates the threshold that separated the two behaviours. The solid line corresponds to the best fit line of the data points to the model for $\left[C_{D-Patch}\frac{nd^2}{2(1-\varnothing)}\right]^{\frac{2}{3}}U_w{}^2 > 2$ or $\left[C_{D-Patch}\frac{nd^2}{2(1-\varnothing)}\right]^{\frac{2}{3}}U_w{}^2 > 4$, for both flexible and rigid plants. Horizontal dashed lines in (**a**) correspond to the *TKE* for cases without plants and for both wave frequencies.

$\left[C_{D-Patch}\frac{nd^2}{2(1-\varnothing)}\right]^{\frac{2}{3}}U_w{}^2$=2 would increase to $\left[C_{D-Patch}\frac{nd^2}{2(1-\varnothing)}\right]^{\frac{2}{3}}U_w{}^2$=3.8, being closer, therefore, to that obtained for rigid plants $\left[C_{D-Patch}\frac{nd^2}{2(1-\varnothing)}\right]^{\frac{2}{3}}U_w{}^2 = 4$.

As Pujol et al.[30] pointed out, *TKE* production the correct diffusion of oxygen at the leaves' boundary layer. The current study demonstrates that the behaviour the seagrass not only depends on the hydrodynamics, but also on the structural characteristics of the canopy, i.e., canopy density, patch length, and plant stiffness. Below

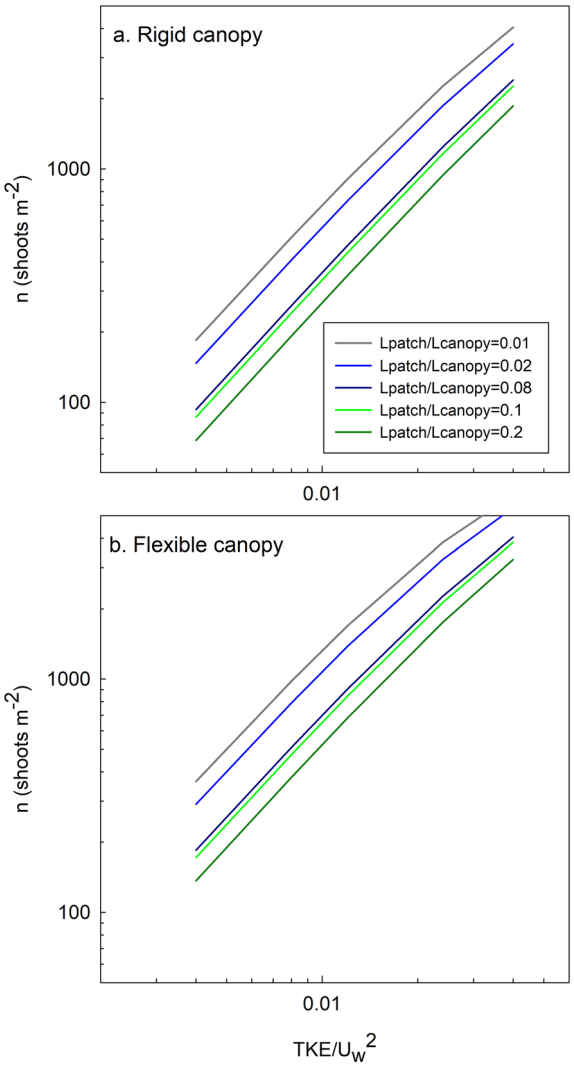

Figure 5. Number of shoots per m^2 (n) required to begin producing *TKE* versus TKE/U_w^2 for different patch lengths and for (**a**) rigid and (**b**) flexible plant structures.

the threshold of $\left[C_{D-Patch}\frac{nd^2}{2(1-\varnothing)}\right]^{\frac{2}{3}}U_w^2$, the behaviour of the canopy changes and its role is to reduce the seabed generated *TKE*. The current study also demonstrates that on the vertical axis, two regions can be differentiated for the flexible vegetation in terms of *TKE* behaviour. For the flexible vegetation and for $\left[C_{D-Patch}\frac{nd^2}{2(1-\varnothing)}\right]^{\frac{2}{3}}U_w^2 > 4$, the *TKE* in the UCL remains constant and is close to that for the non-vegetated cases. In this case, in the UCL the plants behave like blades, moving with the flow but not producing any additional *TKE* than that already present for the non-vegetated set-ups. In contrast, in the LCL, the *TKE* increases with $\left[C_{D-Patch}\frac{nd^2}{2(1-\varnothing)}\right]^{\frac{2}{3}}U_w^2$. In this case, plants in the LCL behave like stems, with small swaying movements, thus creating drag in the flow and producing *TKE*.

This result also aligns with that found by Bouma et al.[23] when comparing the dissipation of wave height by *Spartina alternifora* to that of *Zostera noltii*. In their case, greater wave height dissipation was obtained for the more rigid *Spartina alternifora* vegetation. This is in accordance with Zhang et al.[20] who divided the vertical structure of a flexible plant into two parts. The upper part was named the blade-like region and the lower part the stem-like region. In the stem-like region, they found a greater production of *TKE* compared with the blade-like region due to the greater relative motion between the flow velocity and the plant.

Contrary to flexible stems, rigid plants for $\left[C_{D-Patch}\frac{nd^2}{2(1-\varnothing)}\right]^{\frac{2}{3}}U_w^2 > 2$ present stem-like behaviour along the entire stem. In this case, *TKE* production is due to the greater relative motion between the flow and the rigid stem compared to the flexible blades. Contrary to flexible stems, in the UCL of rigid stems, *TKE* increases with $\left[C_{D-Patch}\frac{nd^2}{2(1-\varnothing)}\right]^{\frac{2}{3}}U_w^2$.From the results of the vertical attenuation of the *TKE* and the *TKE* attenuation compared

to the non-vegetated cases, rigid plants exhibit a similar behaviour to flexible plants for high wave frequencies ($f = 1.12$ Hz). In contrast, under low wave frequencies, when flexible plants have a large sway movement, the hydrodynamics are far from those obtained by rigid plants.

Considering the thresholds for both rigid and flexible vegetation, the required canopy density to begin to produce TKE could be determined in terms of either the length of the patch or the canopy density. The ratio TKE/Uw^2 was considered to range from 0.004 to 0.04 as was found in the laboratory tests. Four ratios L_{patch}/L_{canopy} (see the "Methodology" section for the definition of L_{patch} and L_{canopy}) will be considered, from 0.01 to 0.08. Considering these range of variation, flexible plants would require a canopy density ranging from 136 shoots m^{-2} to 6140 shoots m^{-2} (Fig. 5a). In contrast, a patch of rigid plants would require a density ranging from 69 shoots m^{-2} to 4046 shoots m^{-2} (Fig. 5b). Therefore, a patch of rigid plants would be capable of producing *TKE* in sparser canopy densities than a patch of flexible plants. This result might also have important implications for the sediment bed characteristics, with more provability of resuspension and scouring in regions covered with rigid canopies than in regions with flexible canopies when subject to high energetic conditions. This would align with the results of Bouma et al.[23] who found that for hydrodynamic exposed areas, the flexible shoots of *Zostera* caused far less scouring than the stiff shoots of *Puccinellia*. In addition, a small patch of flexible plants would require a denser vegetation to produce the same normalized TKE/U_w^2 than a larger patch but with sparser vegetation. Therefore, the parameter $\left[C_{D-Patch}\frac{nd^2}{2(1-\varnothing)}\right]^{\frac{2}{3}}$ is related to the total effect of the vegetation patch in terms of drag, length and density.

Conclusions

The current study presents the role plant flexibility plays, together with canopy density and patch length, in determining the hydrodynamics within a seagrass meadow. Flexible plants move with the flow in the upper part of the canopy layer but present a more rigid structure in the inner canopy layer. In contrast, canopies of rigid plants produce a high drag on the flow along the entire length of their stem, resulting in a turbulent kinetic energy production. This difference between the two canopy structures can explain their distribution in the environment, with rigid canopies being more extended in more sheltered regions, and flexible plants being more characteristic of more exposed regions with high flow energy. Rigid and flexible vegetation presents a similar stem-like behaviour in the inner part of the canopy for $\left[C_{D-Patch}\frac{nd^2}{2(1-\varnothing)}\right]^{\frac{2}{3}} U_w{}^2 > 2$ and $\left[C_{D-Patch}\frac{nd^2}{2(1-\varnothing)}\right]^{\frac{2}{3}} U_w{}^2 > 4$, respectively, whereas in the canopy top layer flexible plants move with the flow to cope with the hydrodynamics, presenting a blade-like behaviour. In contrast, neither rigid nor flexible plants for $\left[C_{D-Patch}\frac{nd^2}{2(1-\varnothing)}\right]^{\frac{2}{3}} U_w{}^2 < 2$ or $\left[C_{D-Patch}\frac{nd^2}{2(1-\varnothing)}\right]^{\frac{2}{3}} U_w{}^2 < 4$, respectively, produce turbulent kinetic energy. In addition, the behaviour of flexible plants might also move to being closer to that of rigid plants for high wave frequencies. In contrast, flexible plants produce a larger sway movement when they are under low oscillatory frequencies.

All in all, seagrass canopies are ecological engineers that modify the physical environment or, conversely, their distribution and extension depend on the trade-off between their physiological demands and their ability to withstand the energy of the system.

Methodology

The flume. The study was carried out in a laboratory methacrylate flume (600 cm long, 50 cm wide, and 60 cm deep, Fig. 6) with a mean water height of $h = 30$ cm (Table 1). The flume was equipped with a vertical paddle-type wavemaker at the entrance. The wavemaker was driven by a variable-speed motor at two frequencies ($f = 0.5$ Hz, 1.12 Hz). Wave heights measured by a wave gauge indicated that wave amplitudes were 6 cm and 3 cm for wave frequencies of 1.12 Hz and 0.5 Hz, respectively. A plywood beach (slope = 1:2) was placed at the end of the flume and covered with foam rubber to eliminate wave reflection[2,30]. In the longitudinal direction, $x = 0$ cm was situated at the wavemaker, in the lateral direction, $y = 0$ cm was in the centre of the tank, and in the vertical direction, $z = 0$ cm was situated at the flume bed.

Patches of flexible vegetation. Two types of submerged vegetation models, rigid and flexible, were used (Fig. 6). The rigid vegetation (SRV) consisted of a series of 1 cm thick 14 cm high PVC dowels. The flexible vegetation (SFV) consisted of a series of flexible plants of eight 0.075 mm thick polyethylene canopy blades attached to PVC dowels 1 cm in diameter and 2 cm high that had been randomly inserted into a perforated baseboard[2] (250 cm in length), with the rigid dowel extending 1 cm above the bed[20]. The plants in the flexible model were geometrically and dynamically similar to *Posidonia oceanica* plants[2,31]. The plant leaves in the flexible vegetation model were of 14 cm long. However, the effective height for the flexible vegetation when the leaves were bent by the waves was $h_v = 8.5$ cm for the wave frequency $f = 1.12$ Hz and $h_v = 10.5$ cm for the wave frequency $f = 0.5$ Hz. In contrast, the effective height for the rigid plants was the length of the PVC dowel, $h_p = 14$ cm. The effective heights were calculated as the mean between both the maximum and minimum bending heights of the plants for 25 oscillations. From the observations, the effective plant height increased as the wave frequency decreased. A linear fit between these two data points was made ($h_v = -3.23f + 12.11$). For the other studies considered here, the effective plant height was not always available, but it was estimated by the linear fit above between h_v and f.

The density of the vegetated patches was quantified using the solid plant fraction (*SPF*) defined as:

$$SPF(\%) = 100n\pi\left(\frac{d}{2}\right)^2 \quad (1)$$

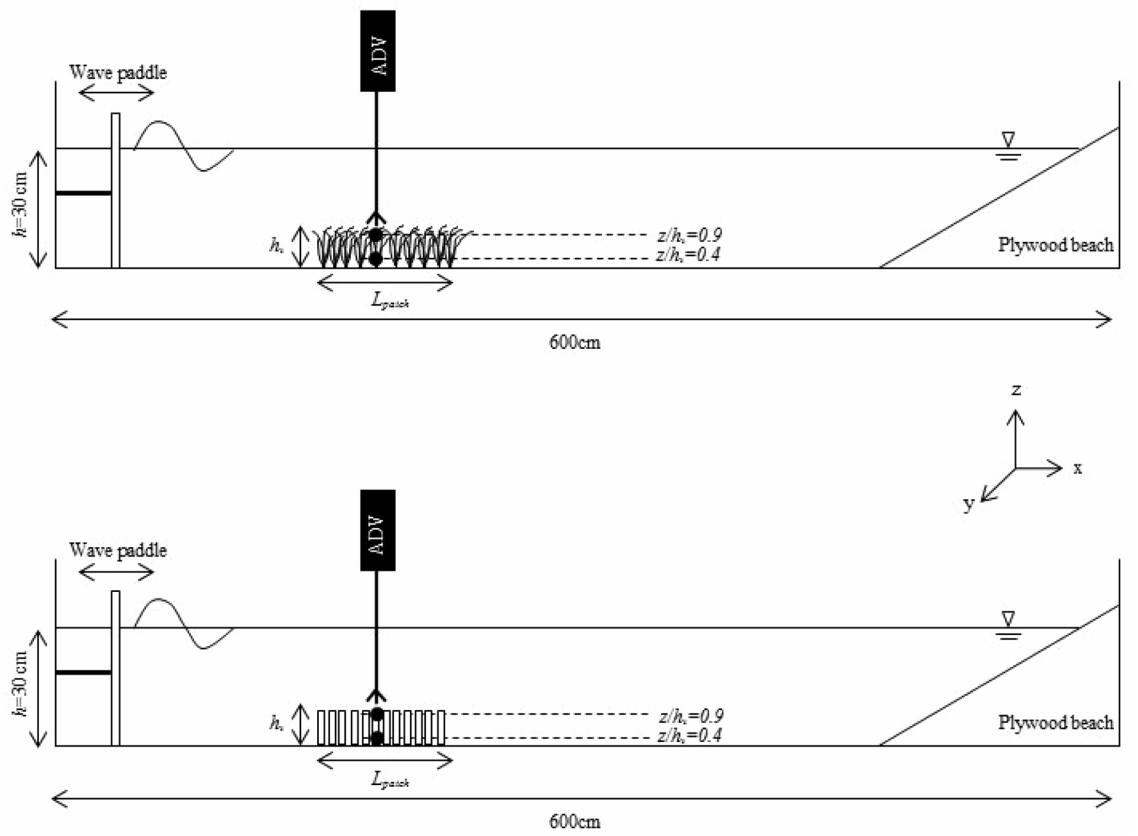

Figure 6. Lateral view of the experimental setup, with the wave paddle on the left. Experiments were conducted in a 600 × 50 × 50 cm long flume, with a mean water depth of 30 cm. The model patch had lengths that ranged from 2.8 to 42 cm and a patch height of effective height h_v. The triangle at the water–air interface represents the water level in the flume. An ADV was vertically mounted to measure the instantaneous velocities at selected vertical heights. The upper panel corresponds to the case of flexible plants and the bottom panel to rigid plants.

Variable	Units	Definition	Variable	Units	Definition
A_w	cm	Wave excursion length	u'	cm s^{-1}	Turbulent velocity
A_w/S	Non-dimensional	Ratio between wave excursion to plant-to-plant distance	U_c	cm s^{-1}	Steady velocity associated with the current
C_D	Non-dimensional	Drag of the obstacle along the fluid	U_i	cm s^{-1}	Instantaneous velocity
d	cm	Stem diameter	$U_i(\varphi)$	cm s^{-1}	Instantaneous velocity according to the phase
f	Hz	Wave frequency	U_w	cm s^{-1}	Wave velocity
h	cm	Water height	U_w^{rms}	cm s^{-1}	Orbital velocity
h_v	cm	Canopy height	v	cm s^{-1}	Eulerian velocity in the y direction
L_{canopy}	cm	Canopy length	x	cm	Longitudinal direction
L_{patch}	cm	Patch length	$x=0$	cm	Position of the wave paddle
n	stems m^{-2}	Canopy density	y	cm	Lateral direction
S	cm	Plant-to-plant distance	z	cm	Vertical direction
SPF	%	Solid plant fraction	β'	Non-dimensional	Vertical ratio between the TKE at the canopy top layer and the inner canopy layer
TKE	cm^2 s^{-2}	Turbulent kinetic energy	β_{UCL} and β_{LCL}	Non-dimensional	Ratio between the TKE with vegetation and without vegetation for both, the upper canopy layer, and the lower canopy layer
u	cm s^{-1}	Eulerian velocity in the x direction	ϕ	Non-dimensional	Solid volume fraction
LCL	–	Lower-canopy layer	UCL	–	Upper-canopy layer
ACL		Above-canopy layer	WP	–	Non-vegetation set up
h_p	cm	Leaf length for flexible vegetation and stem length for rigid vegetation			

Table 1. Nomenclature table.

where n is the number of stems per unit area and d is the stem diameter (1 cm). Therefore, *SPF* represents the percentage of vegetation covering the base to the flume. For the rigid vegetation three *SPFs* were used (0%, 3.5% and 10%) and for the flexible vegetation six *SPF*s were used (0%, 2.5%, 3.5%, 5%, 7.5% and 10%). These *SPF*s corresponded to vegetation densities of $n = 0$, 318, 446, 637, 955 and 1273 stems m^{-2} that are in the range of canopy densities found in coastal areas (78–1000 stems m^{-2})[6,12,32,33]. $SPF = 0\%$ corresponded to the case with no vegetation. For each *SPF* different patch sizes, L_{patch}, were considered, with L_{patch} ranging from 42 to 245 cm, corresponding to 2 to 17 time the leaf length (Table 2). To determine L_{patch} in the experiments, the patch edge was considered as the interface between the vegetated and the non-vegetated regions. Thus, for the different *SPF*s, L_{patch}, and the two wave frequencies, a total of 87 experiments were performed (Table 2).

Measuring velocities. The Eulerian velocity field was defined as (u, v, w) in the (x, y, z) directions, respectively. The three components of velocity were recorded for 5 min at a measuring frequency of 50 Hz with a downwards looking Acoustic Doppler Velocimeter (16-MHz MicroADV, Sontek). The ADV was mounted on a movable vertical frame (at $y = 0$ cm, Fig. 1) and manually adjusted to measure a vertical profile. Some plants were removed (and re-inserted into nearby holes) to avoid blocking the ADV beams[20,34,35]. The ADV measured at a 5 cm distance from the probe tip, and with a sampling volume of 0.09 cm^3. The longitudinal velocity was measured at an antinode to eliminate the lower order spatially periodic variation in wave and velocity amplitude associated with wave reflection[2,36]. Beam correlations less than 70% were discarded and spikes were removed[2,37].

Run	f (Hz)	*SPF* (%)	n (stems m^{-2})	L_{patch} (cm)	A_w/S LCL	A_w/S UTL	Run	f (Hz)	*SPF* (%)	n (stems m^{-2})	L_{patch} (cm)	A_w/S LCL	A_w/S UCL	Run	f (Hz)	*SPF* (%)	n (stems m^{-2})	L_{patch} (cm)	A_w/S LCL	A_w/S UCL
WP1	0.5	0	0				SFV35	1.12	3.5	446	112	0.24	0.28	SRV69	0.5			70	0.51	0.55
WP2	1.12	0	0				SFV36				126	0.24	0.28	SRV70				126	0.57	0.57
SFV3	0.5	1	127	42	0.33	0.35	SFV37				140	0.24	0.28	SRV71				182	0.52	0.55
SFV4				70	0.33	0.35	SFV38				154	0.24	0.28	SRV72				238	0.49	0.50
SFV5				112	0.33	0.34	SFV39				168	0.24	0.29	SRV73		10	1237	42	0.92	1.02
SFV6				196	0.33	0.33	SFV40				196	0.24	0.28	SRV74				70	0.95	1.04
SFV7		7.5	955	42	1.01		SFV41				238	0.24	0.28	SRV75				126	0.92	1.03
SFV8				70	0.97	0.99	SFV42		5	637	42	0.29	0.36	SRV76				182	0.91	1.01
SFV9				112	0.98	0.96	SFV43				70	0.29	0.37	SRV77				238	0.85	0.96
SFV10				196	0.94	0.94	SFV44				98	0.29	0.36	SRV78	1.12	3.5	446	42	0.23	0.30
SFV11		10	1273	42	0.83	1.11	SFV45				126	0.29	0.36	SRV79				70	0.23	0.30
SFV12				70	0.83	1.06	SFV46				168	0.28	0.36	SRV80				126	0.27	0.32
SFV13				84	0.79	1.13	SFV47				196	0.28	0.35	SRV81				182	0.23	0.29
SFV14				98	0.79	1.09	SFV48				210	0.28		SRV82				238	0.26	0.32
SFV15				112	0.78	1.25	SFV49				238	0.28	0.35	SRV83		10	1273	42	0.32	0.38
SFV16				133	0.80	1.14	SFV50		7.5	955	42	0.36	0.44	SRV84				70	0.43	0.50
SFV17				140	0.76	1.13	SFV51				70	0.37	0.45	SRV85				126	0.38	0.47
SFV18				154	0.80	1.10	SFV52				84	0.36	0.45	SRV86				182	0.39	0.45
SFV19				182	0.81	1.13	SFV53				98	0.36	0.44	SRV87				238	0.35	0.40
SFV20				224	0.77	1.09	SFV54				112	0.35	0.44							
SFV21				238	0.77	1.08	SFV55				126	0.35	0.45							
SFV22	1.12	2.5	318	42	0.21	0.25	SFV56				154	0.35	0.44							
SFV23				70	0.21	0.25	SFV57				196	0.34	0.44							
SFV24				84	0.21	0.25	SFV58				238	0.34	0.42							
SFV25				98	0.21	0.25	SFV59		10	1273	42	0.41	0.49							
SFV26				112	0.21	0.24	SFV60				70	0.41	0.52							
SFV27				126	0.21	0.24	SFV61				84	0.40	0.52							
SFV28				140	0.21	0.24	SFV62				98	0.39	0.52							
SFV29				154	0.21	0.24	SFV63				126	0.38	0.50							
SFV30				168	0.21	0.24	SFV64				154	0.39	0.50							
SFV31				182	0.21	0.24	SFV65				168	0.39	0.52							
SFV32				196	0.21	0.24	SFV66				196	0.40	0.51							
SFV33				238	0.21	0.24	SFV67				238	0.37	0.47							
SFV34	1.12	3.5	446	70	0.25	0.29	SRV68	0.5	3.5	446	42	0.53	0.54							

Table 2. Summary of the experimental conditions tested. Where SFV correspond to Submerged Flexible Vegetation and SRV to Submerged Rigid Vegetation. LCL denotes the lower canopy layer and UCL the upper canopy layer.

Hydrodynamic analysis. For oscillatory flows, the instantaneous velocity in the x direction, $U_i(t)$, can be decomposed as:

$$U_i(t) = U_c + U_w + u' \tag{2}$$

where U_c is the steady velocity associated with the wave, U_w is the unsteady wave motion in the x direction which represents spatial variations in the phase-averaged velocity field, and u' is the turbulent velocity, that is, the instantaneous velocity fluctuation in the x-direction. U_c is the phase-averaged velocity:

$$U_c = \frac{1}{2\pi}\int_0^{2\pi} U_i(\varphi)\partial\varphi \tag{3}$$

where $U_i(\varphi)$ is the instantaneous velocity according to the phase[36]. Wave velocity, U_w, was obtained by using a phase averaging technique. The Hilbert transform was used to average oscillatory flow velocities with a common phase[16,35]. The root mean square (rms) of $U_i(\varphi)$ was considered as the characteristic value of the orbital velocity ${U_w}^{rms}$ (U_w hereafter) at each depth, and was calculated according to:

$$U_w^{rms} = \sqrt{\frac{1}{2\pi}\int_0^{2\pi} (U_i(\varphi) - U_c)^2\partial\varphi} \tag{4}$$

The turbulent velocity was obtained by:

$$u' = U_i - U_c - U_w \tag{5}$$

where U_c and U_w were calculated by Eqs. (3) and (4). The turbulent velocity was calculated for all directions (u', v', and w') for z = 4 cm.

Following Ros et al.[35], turbulent kinetic energy (TKE) was calculated as:

$$TKE = \frac{1}{2}\left(\langle u'^2\rangle + \langle v'^2\rangle + \langle w'^2\rangle\right) \tag{6}$$

where < > denotes the average over the wave phase.

The ratio, β, was calculated following Colomer et al.[6] for both, the UCL and the LCL:

$$\beta_{UCL} = \frac{TKE_{UCL}}{TKE_{WP,UCL}} \quad \text{and} \quad \beta_{LCL} = \frac{TKE_{LCL}}{TKE_{WP,LCL}} \tag{7}$$

where TKE_{UCL} TKE_{LCL} were the turbulent kinetic energy values in the UCL and LCL, respectively. For the TKE_{UCL}, TKE at $z = 12$ cm was the characteristic TKE considered, whereas for the TKE_{LCL}, TKE at z = 4 cm was considered. For the non-vegetated cases and TKE_{WP},the TKE considered was also that measured at $z = 12$ cm and z = 4 cm, respectively. Therefore, the values of $\beta_{UCL} \approx 1$ and $\beta_{UCL} \approx 1$ indicated a weak or negligible attenuation of the TKE, whereas low values of $\beta_{UCL} < 1$ and $\beta_{UCL} < 1$ indicated a high TKE attenuation compared to the non-vegetated case.

The vertical TKE attenuation was calculated as β':

$$\beta' = \frac{TKE_{LCL}}{TKE_{LCL}} \tag{8}$$

where TKE_{LCL} and TKE_{UCL} were the turbulent kinetic energies in the LCL and UCL, respectively. For TKE_{UCL} , the TKE at $z = 4$ cm was considered the characteristic TKE of this layer, whereas the TKE measured at $z = 12$ cm was the characteristic TKE for the UCL. Therefore, values of $\beta' \approx 1$ indicated a weak or negligible vertical attenuation of the TKE, whereas low values of $\beta' < 1$ indicated a high TKE vertical attenuation, meaning greater TKE at $z = 4$ cm comparted to $z = 12$ cm.

To gain knowledge about the vertical distribution of TKE within the patch, a model was set up following Zhang et al.[20]. For a full canopy, Zhang et al.[20] found that the relationship between the TKE, $U_{w,}$ and the main canopy parameters followed:

$$\frac{TKE}{{U_w}^2} = \delta\left[C_D\frac{l_t}{d}\frac{nd^2}{2(1-\phi)}\right]^{\frac{2}{3}} \tag{9}$$

where δ is the scale constant, ϕ is the solid volume fraction, $\phi = n\frac{\pi}{4}d^2$, l_t is characteristic eddy length-scale, and C_D is the drag of the form of the obstacle along with the fluid patch, with $C_D = 1.4$ being considered in the study. In Eq. (9), the characteristic length scale, L_{patch}/L_{canopy} is introduced to account for the volume of the patch in relation to the maximum canopy volume in the form of $\left(\frac{L_{patch}}{L_{canopy}}\right)^{\frac{1}{3}}$. L_{canopy} was considered as the length of the vegetation patch from where the wave velocity did not change with a further increase in its length. Barcelona et al.[29] found that L_{canopy} depended on the wave frequency, f, with $L_{canopy} = 20h_v$ for $f = 1.12$ Hz and $L_{canopy} = 10h_v$ for $f = 0.5$ Hz. Therefore Eq. (9) is expressed following:

	Run	f (Hz)	*SPF* (%)	n (stems·m^{-2})	L_{patch} (cm)	*Aw/S UCL*		Run	f (Hz)	*SPF* (%)	n (stems·m^{-2})	L_{patch} (cm)	*Aw/S UCL*		Run	f (Hz)	*SPF* (%)	n (stems·m^{-2})	L_{patch} (cm)	*Aw/S UCL*	*Aw/S LCL*
Barcelona et al.[37]	B. SFV 1	0.7	1	127	245	0.03	Zhang et al.[20]	Z. SFV 1	1	1.1	280	200	1.21	Pujol et al.[16]	P. SRV 1	0.8	1	127	245	0.07	0.06
	B. SFV 2				245	0.04		Z. SFV 2				200	0.94		P. SRV 2		5	637	245	0.18	0.15
	B. SFV 3				245	0.11		Z. SFV 3				200	0.74		P. SRV 3		10	1280	245	0.25	0.18
	B. SFV 4				245	0.09		Z. SFV 4				200	0.54		P. SRV 4	1	1	127	245	0.05	0.07
	B. SFV 5		2.5	318	245	0.07		Z. SFV 5				200	0.42		P. SRV 5		5	637	245	0.13	0.14
	B. SFV 6				245	0.03		Z. SFV 6				200	0.29		P. SRV 6		10	1280	245	0.16	0.22
	B. SFV 7				245	0.15		Z. SFV 7		2.3	600	200	2.01		P. SRV 7	1.4	1	127	245	0.04	0.06
	B. SFV 8				245	0.17		Z. SFV 8				200	1.52		P. SRV 8		5	637	245	0.08	0.14
	B. SFV 9		5	637	245	0.04		Z. SFV 9				200	1.21		P. SRV 9		10	1280	245	0.11	0.17
	B. SFV 10				245	0.07		Z. SFV 10				200	0.88		P. SFV 1	0.8	1	127	245	0.06	0.06
	B. SFV 11				245	0.12		Z. SFV 11				200	0.68		P. SFV 2		5	637	245	0.14	0.15
	B. SFV 12				245	0.12		Z. SFV 12				200	0.46		P. SFV 3		10	1280	245	0.15	0.19
	B. SFV 13		7.5	955	245	0.11		Z. SFV 13		3.2	820	200	2.01		P. SFV 4	1	1	127	245	0.06	0.08
	B. SFV 14				245	0.06		Z. SFV 14				200	1.66		P. SFV 5		5	637	245	0.12	0.17
	B. SFV 15				245	0.07		Z. SFV 15				200	1.40		P. SFV 6		10	1280	245	0.26	0.21
	B. SFV 16				245	0.14		Z. SFV 16				200	1.06		P. SFV 7	1.4	1	127	245	0.04	0.06
	B. SFV 17	1.2	1	127	245	0.07		Z. SFV 17				200	0.80		P. SFV 8		5	637	245	0.10	0.14
	B. SFV 18				245	0.04		Z. SFV 18				200	0.49		P. SFV 9		10	1280	245	0.13	0.19
	B. SFV 19				245	0.05		Z. SFV 19		5.3	1370	200	2.22								
	B. SFV 20				245	0.04		Z. SFV 20				200	1.90								
	B. SFV 21		2.5	318	245	0.06		Z. SFV 21				200	1.57								
	B. SFV 22				245	0.07		Z. SFV 22				200	1.19								
	B. SFV 23				245	0.08		Z. SFV 23				200	0.91								
	B. SFV 24				245	0.08		Z. SFV 24				200	0.55								

Continued

	Run	f (Hz)	SPF (%)	n (stems·m^{-2})	L_{patch} (cm)	Aw/S UCL		Run	f (Hz)	SPF (%)	n (stems·m^{-2})	L_{patch} (cm)	Aw/S UCL		Run	f (Hz)	SPF (%)	n (stems·m^{-2})	L_{patch} (cm)	Aw/S UCL	Aw/S LCL
	B. SFV 25		5	637	245	0.08																
	B. SFV 26				245	0.10																
	B. SFV 27				245	0.15																
	B. SFV 28				245	0.12																
	B. SFV 29		7.5	955	245	0.13																
	B. SFV 30				245	0.14																
	B. SFV 31				245	0.15																
	B. SFV 32				245	0.15																

Table 3. Summary of the experimental conditions tested by Zhang et al.[20], Barcelona et al.[29] and Pujol et al.[16].

$$\frac{TKE}{{U_w}^2} = \delta\left[C_D\left(\frac{L_{patch}}{L_{canopy}}\right)^{\frac{1}{3}}\frac{l_t}{d}\frac{nd^2}{2(1-\phi)}\right]^{\frac{2}{3}} \tag{10}$$

Zhang et al.[20] considered $l_t = d$ for $S > 2d$ whereas $l_t = S$ for $S < 2d$. In the present study, $S > 2d$, $l_t = d$. Therefore,

$$\frac{TKE}{{U_w}^2} = \delta\left[C_D\left(\frac{L_{patch}}{L_{canopy}}\right)^{\frac{1}{3}}\frac{nd^2}{2(1-\phi)}\right]^{\frac{2}{3}} \tag{11}$$

The parameter ϕ has been substituted by its definition to obtain two differentiated parameters (one related to patch length and the other to shoot density), as:

$$\frac{TKE}{{U_w}^2} = \delta\left[\left(\frac{L_{patch}}{L_{canopy}}\right)^{\frac{1}{3}}\frac{2C_D nd^2}{4-\pi nd^2}\right]^{\frac{2}{3}} \tag{12}$$

To obtain a more complete model the experiments from Zhang et al.[20], Barcelona et al.[29] and Pujol et al.[16] were added to the comparison (Table 3).

Data availability

Data will be accessible from the following public data repository link: https://doi.org/10.34810/data528.

Received: 18 July 2022; Accepted: 12 January 2023
Published online: 02 February 2023

References

1. Gacia, E., Granata, T. C. & Duarte, C. M. An approach to measurement of particle flux and sediment retention within seagrass (*Posidonia oceanica*) meadows. *Aquat. Bot.* **65**, 255–268 (1999).
2. Pujol, D., Casamitjana, X., Serra, T. & Colomer, J. Canopy-scale turbulence under oscillatory flow. *Cont. Shelf Res.* **66**, 9–18. https://doi.org/10.1016/j.csr.2013.06.012 (2013).
3. Ricart, A. M. *et al.* Variability of sedimentary organic carbon in patchy seagrass landscapes. *Mar. Pollut. Bull.* **100**, 476–482. https://doi.org/10.1016/j.marpolbul.2015.09.03 (2015).
4. Unsworth, R. K. F. *et al.* Global challenges for seagrass conservation. *Ambio* **48**, 801–815. https://doi.org/10.1007/s13280-018-1115-y (2018).
5. Zong, L. & Nepf, H. Spatial distribution of deposition within a patch of vegetation. *Water Resour. Res.* **47**, W03516. https://doi.org/10.1029/2010WR009516 (2011).
6. Colomer, J., Soler, M., Serra, T., Casamitjana, X. & Oldham, C. Impact of anthropogenically created canopy gaps on wave attenuation in a *Posidonia oceanica* seagrass meadow. *Mar. Ecol. Prog. Ser.* **569**, 103–116. https://doi.org/10.3354/meps12090 (2017).
7. Unsworth, R. K. F., Williams, B., Jones, B. L. & Cullen-Unsworth, L. C. Rocking the boat: Damage to eelgrass by swimming boat moorings. *Front. Plant Sci.* **8**, 1309. https://doi.org/10.3389/fpls.2017.01309 (2017).
8. Evans, S. M., Griffin, K. J., Blick, R. A. J., Poore, A. G. B. & Vergés, A. Seagrass on the brink: Decline of threatened seagrass *Posidonia australis* continues following protection. *PLoS ONE* **14**(4), e0216107. https://doi.org/10.1371/journal.pone.0190370 (2018).

9. Sleeman, J. C., Kendrick, G. A., Boggs, G. S. & Hegge, B. J. Measuring fragmentation of seagrass landscapes: Which indices are most appropriate for detecting change?. *Mar. Freshw. Res.* **58**, 851–864. https://doi.org/10.1071/MF04300 (2005).
10. Folkard, A. M. Biophysical interactions in fragmented marine canopies: Fundamental processes, consequences, and upscaling. *Front. Mar. Sci.* **6**, 279. https://doi.org/10.3389/fmars.2019.00279 (2019).
11. El Allaoui, N. *et al.* Interactions between fragmented seagrasses canopies and the local hydrodynamics. *PLoS ONE* **11**(5), e0156264. https://doi.org/10.1371/journal.pone.0156264 (2016).
12. Gera, A., Pagès, J., Romero, J. & Alcoverro, T. Combined effects of fragmentation and herbivory on *Posidonia oceanica* seagrass ecosystems. *J. Ecol.* **101**, 1053–1061. https://doi.org/10.1111/1365-2745.12109 (2013).
13. Robbins, B. D. & Bell, S. S. Seagrass landscapes: A terrestrial approach to the marine subtidal environment. *Trends Ecol. Evol.* **9**(8), 301–304. https://doi.org/10.1016/0169-5347(94)90041-8 (1994).
14. Serra, T., Gracias, N. & Hendriks, I. E. Fragmented in seagrass canopies can alter hydrodynamics and sediment deposition rates. *Water* **20**(12), 3473. https://doi.org/10.3390/w12123473 (2020).
15. Barcelona, A., Colomer, J., Soler, M., Gracias, N. & Serra, T. Meadow fragmentation influences *Posidonia oceanica* density at the edge of nearby gaps. *Estuarine Coast. Self Sci.* **249**, 107106. https://doi.org/10.1016/j.ecs.2020.107106 (2021).
16. Pujol, D., Serra, T., Colomer, J. & Casamitjana, X. Flow structure in canopy models dominated by progressive waves. *J. Hydrol.* **486**, 281–292. https://doi.org/10.1016/j.jhydrol.2013.01.024 (2013).
17. Chen, M. *et al. Coast. Eng.* **159** 103727. https://doi.org/10.1016/j.coastaleng.2020.103727 (2020).
18. Tinoco, R. O. & Coco, G. Turbulence as the main driver of resuspension in oscillatory flow through vegetation. *J. Geophys. Res. Earth Surf.* **123**, 891–904. https://doi.org/10.1002/2017JF004504 (2018).
19. Nepf, H. M. & Vivoni, E. R. Flow structure in depth-limited, vegetated flow. *J. Geophys. Res.* **105**(C15), 28547–28557. https://doi.org/10.1029/2000JC933145 (2000).
20. Zhang, Y., Tang, C. & Nepf, H. Turbulent kinetic energy in submerged model canopies under oscillatory flow. *Water Resour. Res.* **54**, 1734–1750. https://doi.org/10.1002/2017WR021732 (2018).
21. Valdez, S. R. *et al.* Positive ecological interactions and the success of seagrass restoration. *Front. Mar. Sci.* **7**, 91. https://doi.org/10.3389/fmars.2020.00091 (2020).
22. Bouma, T. J. *et al.* Effects of shoot stiffness, shoot size and current velocity on scouring sediment from around seedlings and propagules. *Mar. Ecol. Prog. Ser.* **388**, 293–297. https://doi.org/10.3354/meps08130 (2009).
23. Bouma, T. J. *et al.* Trade-offs related to ecosystem engineering: A case study on stiffness of emerging macrophytes. *Ecology* **86**(8), 2187–2199. https://doi.org/10.1890/04-1588 (2005).
24. Paul, M. & de los Santos, C. B.,. Variation in flexural, morphological, and biomechanical leaf properties of eelgrass (*Zostera marina*) along the European Atlantic climate regions. *Mar. Biol.* **166**, 127. https://doi.org/10.1007/s00227-019-3577-2 (2019).
25. Barcelona, A., Oldham, C., Colomer, J., Garcia-Orellana, J. & Serra, T. Particle capture by seagrass canopies under an oscillatory flow. *Coast. Eng.* **169**, 103972. https://doi.org/10.1016/j.coastaleng.2021.103972 (2021).
26. Schaefer, R. B. & Nepf, H. M. Flow structure in an artificial seagrass meadow in combined wave-current conditions. *Front. Mar. Sci.* **9**, 836901. https://doi.org/10.3389/fmars.2022.836901 (2022).
27. van Veelen, T. J., Farichild, T. P., Reeve, D. E. & Karanurathna, H. Experimental study on vegetation flexibility as control parameter for wave damping and velocity structure. *Coast. Eng.* **157**, 103648 (2020).
28. Granata, T. C. *et al.* Flow and particle distributions in a nearshore seagrass meadow before and after a storm. *Mar. Ecol. Prog. Ser.* **218**, 95–106. https://doi.org/10.3354/meps218095 (2001).
29. Barcelona, A., Oldham, C., Colomer, J. & Serra, T. Functional dynamics of vegetated model patches: The minimum patch size effect for canopy restoration. *Sci. Total Environ.* **795**, 148854. https://doi.org/10.1016/j.scitotenv.2021.148854 (2021).
30. Pujol, D., Abdolahpour, M., Lavery, P. S., McMahon, K. & Oldham, C. Flow velocity and nutrient uptake in marine canopies. *Mar. Ecol. Prog. Ser.* **622**, 17–20. https://doi.org/10.3354/meps12987 (2019).
31. Serra, T., Oldham, C. & Colomer, J. Local hydrodynamics at edges of marine canopies under oscillatory flows. *PLoS ONE* **13**(8), e0201737. https://doi.org/10.1371/journal.pone.0201737 (2018).
32. Ghisalberti, M. & Nepf, H. Mixing layers and coherent structures in vegetated aquatic flows. *J. Geophys. Res.* **107**, C23011. https://doi.org/10.1029/2001JC000871 (2002).
33. Bacci, T., Rende, F. S. & Scardi, M. Shoot micro distribution patterns in the Mediterranean seagrass *Posidonia oceanica*. *Mar. Biol.* **164**, 85. https://doi.org/10.1007/s00227-017-3121-1 (2017).
34. van Katwijk, M. M., Bos, A. R., Hermus, D. C. R. & Suykerbuyk, W. Sediment modification by seagrass beds: Muddification and sandification induced by plant cover and environmental conditions. *Estuar. Coast. Shelf Sci.* **89**, 175–181. https://doi.org/10.1016/j.ecss.2010.06.008 (2010).
35. Ros, À. *et al.* Experimental observations on sediment resuspension within submerged model canopies under oscillatory flow. *Cont. Shelf Res.* **91**, 220–231. https://doi.org/10.1016/j.csr.2014.10.004 (2014).
36. Luhar, M., Coutu, S., Infantes, E., Fox, S. & Nepf, H. Wave-induced velocities inside a model seagrass bed. *J. Geophys. Res.* **115**, C12005. https://doi.org/10.1029/2010JC006345 (2010).
37. Goring, D. G. & Nikora, V. I. Despiking acoustic Doppler velocimeter data. *J. Hydraul. Eng.* **128**(1), 117–126. https://doi.org/10.1061/(ASCE)0733-9429(2002)128:1(117) (2002).

Acknowledgements

This work was supported by the "Ministerio de Economía y Competitividad" of the Spanish Government through the grant PID2021-123860OB-I00. Aina Barcelona was funded by the pre-doctoral grant 2020 FI SDUR 00043 from the "Generalitat de Catalunya".

Author contributions

J.C. and T.S. conceived the ideas and designed methodology; A.B. collected the data; A.B. analysed the data; all authors were involved in the writing of the manuscript, contributed critically to the drafts, and gave their final approval for publication.

Competing interests

The authors declare no competing interests.

Additional information

Correspondence and requests for materials should be addressed to T.S.

Reprints and permissions information is available at www.nature.com/reprints.

Marine Environmental Research 192 (2023) 106238

Contents lists available at ScienceDirect

Marine Environmental Research

journal homepage: www.elsevier.com/locate/marenvrev

The role epiphytes play in particle capture of seagrass canopies

Aina Barcelona [a,*], Jordi Colomer [a], Teresa Serra [a], Damboia Cossa [b,c], Eduardo Infantes [d]

[a] Department of Physics, University of Girona, 17071, Girona, Spain
[b] Department of Marine Sciences, Kristineberg, University of Gothenburg, 45178, Sweden
[c] Eduardo Mondlane University, Department of Biological Sciences, Maputo, Mozambique
[d] Department of Biological and Environmental Sciences, Kristineberg, University of Gothenburg, 45178, Sweden

ARTICLE INFO

Keywords:
Seagrass
Eelgrass
Epiphyte
Sedimentation
Leaves capture
Suspension
Leaf length
Epiphytic area

ABSTRACT

Seagrass epiphytic communities act as ecological indicators of the quality status of vegetated coastal environments. This study aims to determine the effect leaf epiphytes has on the sediment capture and distribution from outside sources. Thirteen laboratory experiments were conducted under a wave frequency of 0.5 Hz. Three epiphyte models were attached to a *Zostera marina* canopy of 100 plants/m^2 density. The sediment deposited to the seabed, captured by the epiphytic leaf surface, and remaining in suspension within the canopy were quantified. This study demonstrated that the amount of epiphytes impacts on the sediment stocks. *Zostera marina* canopies with high epiphytic areas and long effective leaf heights may increase the sediment captured on the epiphyte surfaces. Also, reducing suspended sediment and increasing the deposition to the seabed, therefore enhancing the clarity of the water column. For largest epiphytic areas, a 34.5% increase of captured sediment mass is observed. The sediment trapped on the leaves can be 10 times greater for canopies with the highest epiphytic areas than those without epiphytes. Therefore, both the effective leaf length and the level of epiphytic colonization are found to determine the seagrass canopy ability at distributing sediment.

1. Introduction

Coastal ecosystems are colonized by seagrass meadows that provide significant ecological and physical ecosystem services. For example, they act as refuge and nursery habitats for fish and macroinvertebrates (Unsworth et al., 2017), attenuate waves and turbulence (Gacia et al., 1999; Infantes et al., 2012; Pujol et al., 2013), reduce erosion with the roots (Infantes et al., 2022), stabilize the bottom through decreasing sediment resuspension (Ros et al., 2014) and enhance sediment trapping (Barcelona et al., 2021b, 2023a). Seagrass plants have a complex structure, with invertebrates and macroalgae growing on the leaves and rhizomes forming assemblages named epiphytes (Trautman and Borowitzka, 1999). The abundance of epiphytes depends on the available leaf area of the seagrass and can impact the growth of the seagrass itself by decreasing the light reaching the canopy and reducing water fluxes (Cambridge et al., 2007).

The presence of epiphytes on seagrass leaves suggests ecological indications and signals the quality status of vegetated coastal environments (Mutlu et al., 2022). Overall, the quantity and quality of epiphytes serve as indicators of the level of intensity and the spatial distribution of ecological and anthropogenic processes such as eutrophication, productivity, herbivory, acidification, seasonality, turbidity, pollution, sedimentation, hydrodynamics, among others (Baggett et al., 2010; Balata et al., 2008; Ben Brahim et al., 2020; Mutlu et al., 2022). Likewise, leaf growth is regulated to maintain a proportion of uncolonized leaf surface, and epiphyte coverage plays a role in its regulation. In *Zostera marina,* the rate of leaf emergence positively correlates with epiphyte load (Ruesink, 2016). Additionally, epiphyte biomass increases exponentially with leaf age during the first days of colonization, whereas for older leaves epiphytes do not change in biomass (Borum, 1987). Among the key processes, the patterns of the spatial variability of macro-epiphyte assemblages on *Posidonia oceanica* leaves differ in relation to anthropogenic interference in the Gulf of Gabes, with both biomass and mean percentage cover decreasing near a sewage outlet point compared to control locations (Ben Brahim et al., 2010). In *Cymodocea nodosa* and the invasive species *Halophila stipulucea*, shoot density and epiphytic biomass cover decreased when exposed to high levels of hydrodynamic activity (Ben Brahim et al., 2020). Seagrass epiphytes have been shown to progressively enrich seawater with minerals and nutrients (Brodersen and Kühl, 2022). However, high epiphytic colonization decreases light availability for seagrass leaves, thus increasing the diffusion distance between the leaf and the surrounding water, which

* Corresponding author.
E-mail address: aina.barcelona@udg.edu (A. Barcelona).

https://doi.org/10.1016/j.marenvres.2023.106238
Received 7 July 2023; Received in revised form 28 September 2023; Accepted 19 October 2023
Available online 21 October 2023

may result in basification, warming and/or hypoxia for the seagrass (Brodersen and Kühl, 2022).

Seagrass meadows are highly productive habitats that can act as "blue carbon sinks" in coastal ecosystems by facilitating sedimentation and trapping particles (Jankowska et al., 2016; Röhr et al., 2018). Most of the variation in carbon stocks has been explained by sediment mud content, dry carbon density and degree of sorting, salinity, and water depth, along with plant attributes such as biomass and shoot density (Röhr et al., 2018). Settling particles within an artificial seagrass canopy can be trapped by the plant leaves or settle to the bottom, increasing with the canopy coverage (Barcelona et al., 2023a) and decreasing with the wave frequency (Barcelona et al., 2021b). However, the amount of sediment trapped by each single plant leaf was lower for high canopy densities compared to low canopy densities. Both processes can act synergistically to reduce the exchange of light and gases that could harm seagrass canopy development. Moreover, the total amount of sediment trapped on the seagrass leaves increased linearly with patch length (Barcelona et al., 2023a), demonstrating the importance of canopy fragmentation in the trapping of sediment particles.

Epiphyte distribution on plant leaves can also modify the structure of the plants, impacting their flexural stiffness by modifying the cross-sectional area of the leaf (Fonseca and Koehl, 2006). In this case, the behaviour of a canopy can approach that of a rigid canopy and produce more turbulent kinetic energy or can approach a flexible canopy, i.e., moving with the flow and without producing turbulent kinetic energy (Barcelona et al., 2023b). Since hydrodynamics drive the capacity of seagrass to capture sediment particles (Barcelona et al., 2021b), it is worth determining how large amounts of sediment not only from coastal runoff, river plumes, natural resuspension, and heavy rains (Pineda et al., 2017; Vautard et al., 2014) but also from anthropogenic sources such as coastal development (Wu et al., 2018) reach seagrass meadows and are finally redistributed through the meadows. Therefore, it is expected that the distribution of epiphytes growing on plant leaves modifies sediment trapping capacity, thus regulating the sedimentation stocks in each canopy compartment. Indeed, suspended particles may be phagocyted by some seagrass epiphytes found on the leaves (Agawin and Duarte, 2002). Additionally, settling microplastics have been found to be trapped by seagrass (de los Santos et al., 2021), or adhere to eelgrass leaves and form biofilms, i.e., a sink of microplastics (Zhao et al., 2022).

The aim of the present study is to understand the role epiphytes on seagrass leaves have in the capture of sediment particles. The hypothesis of this study is formulated as follows: the area of the epiphytes colonizing a coastal canopy has the potential to modify the distribution and balance of sediment, including sediment suspended within the canopy, trapped by leaves and found on the canopy bed.

2. Methodology

2.1. Flume set-up

This study was conducted in the hydraulic flume at the Kristineberg Marine Research Station, Sweden (Fig. 1). The flume was 800 cm long, 50 cm wide, 50 cm deep and equipped with an electronic piston that generated waves at a frequency of f = 0.5 Hz. To prevent wave reflection at the end of the flume, a PVC beach with a 20° slope covered by synthetic fibre was placed at the end of the flume (Marin-Diaz et al., 2020; Serra et al., 2018). To simulate the natural conditions of the seagrass in the field, the flume was filled with seawater, directly from Gullmarn Fjord with a salinity of S = 27.65°/$_{oo}$ and the water temperature was T = 15 °C (± 1 °C). The mean water working height in the flume was h = 23 cm, and the test section was 200 cm long (Fig. 1), starting 300 cm from the wave generator. The bottom of the test section was filled with sandy sediment with a diameter of d_{50} = 0.8–2 mm. To minimise additional turbidity from the sandy sediment bottom, the flume was filled with water and immediately discarded to remove the resuspended small particle content from the bed. This process was carried out three times before starting the experiment. Finally, prior to each experiment run, the flume was filled with water and left under the action of the waves for 5 min.

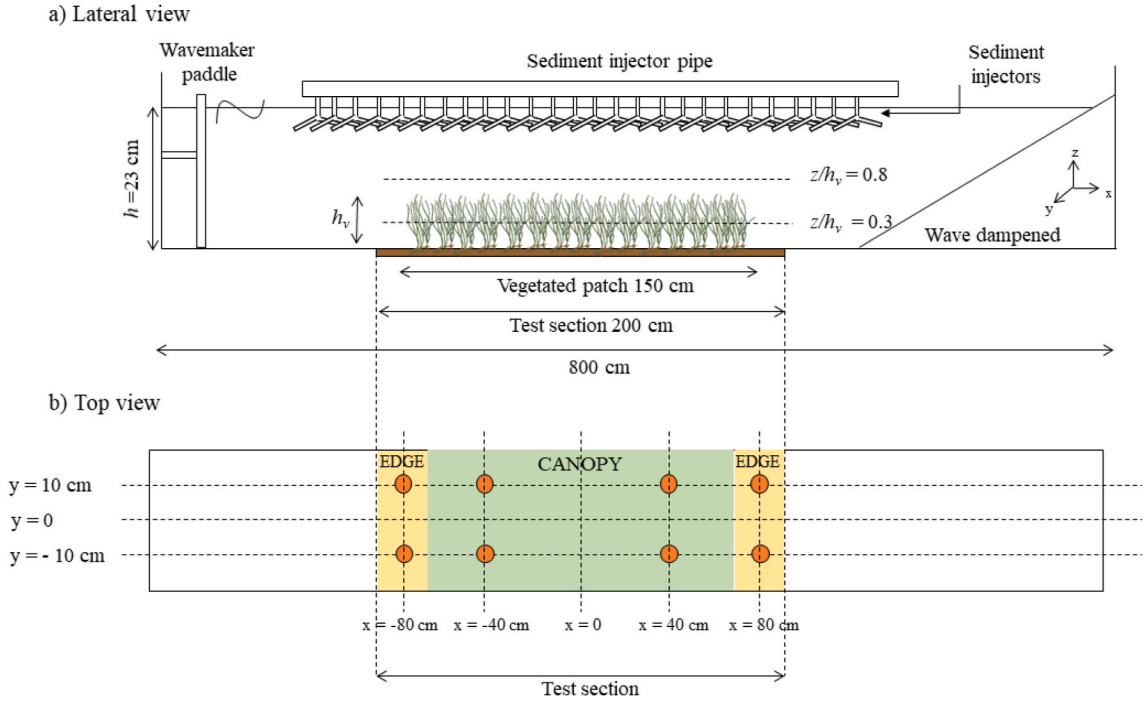

Fig. 1. Experimental setup and canopy regions with sediment trap locations, a) Lateral view of the experimental setup in the flume, with the wave paddle generator located on the left. Waves propagate from left to right. b) Top view of the setup illustrates two regions: the inner canopy region (in green) and the edge region of the canopy (in yellow). Additionally, orange circles indicate the position of sediment traps distributed along the flume bed in both the canopy and edge regions.

2.2. Vegetation

Eelgrass (*Zostera marina*) shoots were collected from the Gullmarn Fjord, located on the west coast of Sweden near the Kristineberg Marine Research Centre (58.25°N, 11.45° W). The seagrass meadows from the Gullmarn Fjord have been reported to be composed of *Z. marina* and *Zostera noltii* individuals, although, the eelgrass *Z. marina* is the most abundant one. Only *Z. marina* individuals were collected and used in the experiments. Since both *Zostera noltii* and *Z. marina* present the same morphology above ground, they are expected to behave similarly. Collection was carried out between June and August 2022 at a depth of 1–2 m. The eelgrass plants had an average of 3 ± 1 leaves·shoot^{-1}, with a shoot length of $h_p = 20 \pm 2$ cm, a shoot width of 0.4 ± 0.1 cm, and a thickness of 0.045 ± 0.005 cm. The plants were kept in laboratory tanks with flow-through seawater from the fjord. To prevent any scouring and uprooting of the plants in the flume, the rhizome and roots were separated, and each shoot was fixed to a wooden stick (3 cm long and 0.5 cm in diameter) with a cable tie. The stick and cable tie were then buried into the sediment. The vegetated area in the flume was 1.5 m long (Fig. 1a), with a plant density of $n = 100$ shoots·m^{-2} which falls within the range of shallow eelgrass densities found the west coast of Sweden (Boström et al., 2014).

2.3. Epiphyte distribution and treatments

To simulate the effect of the epiphyte cover, three macroalgae species, namely: *Fucus vesiculosus*, *Fucus serratus* and *Furcellaria lumbricalis* were used to represent three levels of epiphytic structure. *F. serratus* presents the simplest structure with laminar leaves, *F. vesiculosus* presents a greater complexity with laminar leaves but with aerocysts. In contrast, *F. lumbricalis* presents the most complex structure with a filamentous shape and with the greatest 3D morphology. These macroalgae species were chosen to represent various epiphyte morphology structures that can potentially be found attached to eelgrass leaves (García-Redondo et al., 2019). While these species may not commonly exist as epiphytes in eelgrass canopies, they were chosen due to their diverse morphologies which can be observed in actual epiphytes attached to eelgrass leaves. This selection allows for the simulation of different types of epiphytes that may occur naturally. Likewise, the constructed epiphyted covered the 35% of the plant leaf length according to the

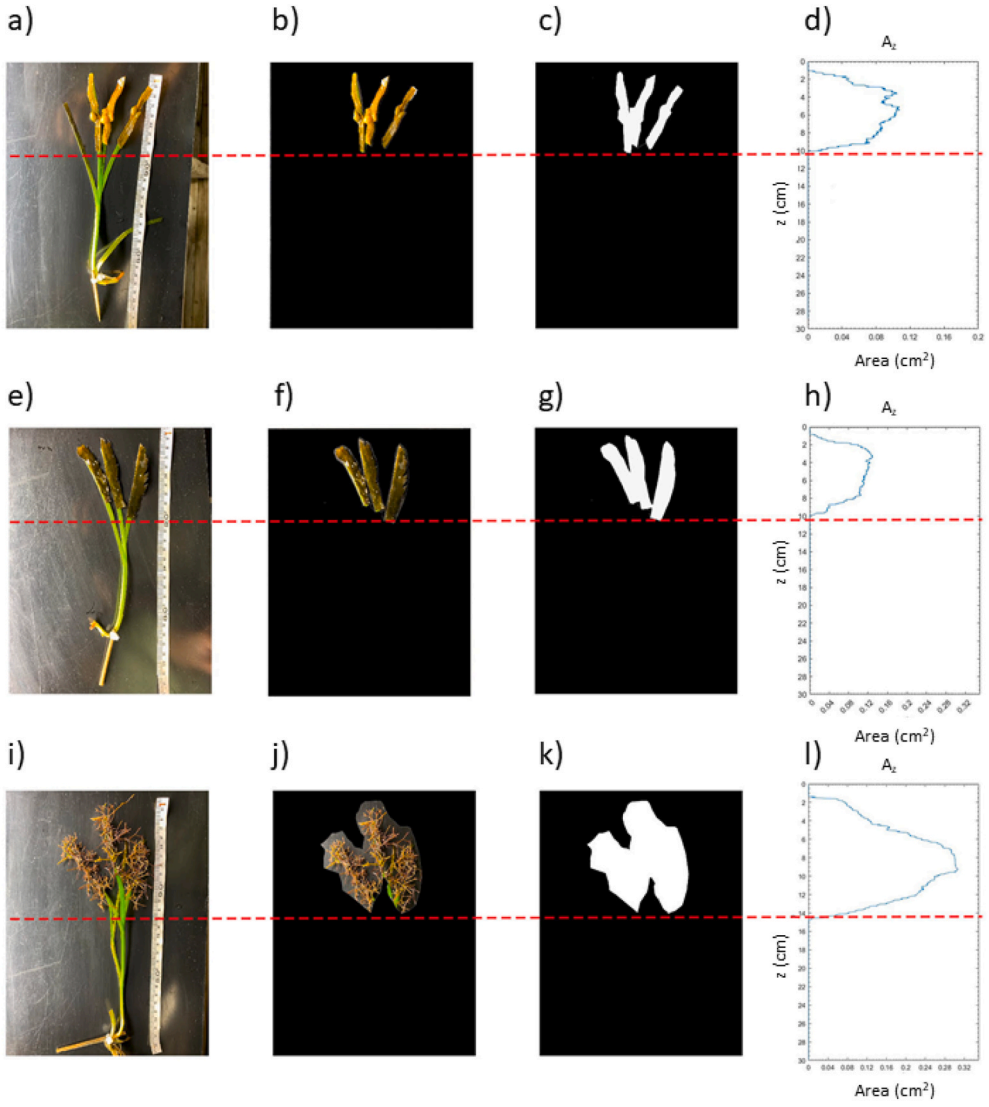

Fig. 2. Eelgrass shoots with epiphyted areas and vertical distribution of epiphyte coverage. Photograph of eelgrass shoots displaying the epiphytic area of a single plant located at the top of the leaves for the three epiphytes considered: *Fucus vesiculosus* (E1), *Fucus serratus* (E2, and *Furcellaria lumbricalis* (E3) (a, e, and i, respectively) (left panels). Furthermore, photographs of the epiphyte area for each type of species (central panels), and a plot illustrating the vertical distribution of the epiphyte area A_z with height for each type of epiphyte (d, h and l in the right panels) was generated.

percentages of epiphytes found in the field (Somma et al., 2023). This tries to mimic that in nature, epiphytes are more abundant in the apic part of the leaf than in the lower leaf sections (Reyes et al., 1998; Somma et al., 2023). The laboratory simulated epiphytic plants of epiphytic leaves with dimensions of 7 cm long x 0.5 cm wide piece of *F. serratus* or *F. vesiculosus* previously scraped with a scalpel to eliminate the epiphytic part on the algae, gently dried with a paper towel, and then glued to the eelgrass leaf with Loctite super glue. Therefore, each plant presented three epiphytic fragments; one for each leaf. In the case of *F. lumbricalis*, several 0.6 ± 0.1 cm fragments of *F. lumbricalis* were glued along the top 7-cm-long surface of the *Z. marina* leaves (Fig. 2). The simulated epiphytes covered the upper part of the leaves, which is considered the flexible portion of each plant (Barcelona et al., 2023b). From now on, the plants epiphyted with *F. vesiculosus, F. serratus* and *F. lumbricalis* will be referred to as E1, E2 and E3, respectively, because these algae species were used to model a natural epiphyte. Four epiphyted canopy distributions were used for each epiphyte type, E1, E2 and E3: 0 %, 25 %, 50 %, 75 % and 100% of the total number of plants of the canopy were epiphyted, resulting in 13 treatments (Table 1). Then, a total of 13 set ups were considered, one for each treatment.

The effective height of the eelgrass without epiphytes, which refers to the bending of leaves caused by the waves, was determined by calculating the mean of the maximum and minimum bending heights observed during 25 oscillations. This measurement was repeated three times. The effective heights measured for each epiphyted plant (E1, E2 and E3) were h_v = 16.00 ± 0.47, 17.13 ± 0.92, and 17.67 ± 1.05 respectively, and for the non-epiphyte plant experiment it was 17.96 ± 0.51 cm.

2.4. Sediment injection

The wavemaker was activated and allowed to operate for 15 min to establish equilibrium in the system before sediment injection. Synthetic dust powder (ISO 12103-1, A4 Coarse, Powder Technology Inc., Burnsville) was used as sediment in the experiment. The sediment A4 was composed by particles from 5 mm to 120 mm with a d50 = 41.7 μm (Barcelona et al., 2023a; Mancini et al., 2023). Therefore, it was composed from fine silts to fine sand particles. This is in accordance with the size of sediment particles composing river plumes (Grifoll et al., 2014).

The particle-laden flow for injection was prepared by taking an initial volume of sediment suspension (2 L), with a concentration of 120 g L^{-1}, which was then introduced into one end of the sediment-injector pipe. The injector pipe was positioned at y = 0 cm along the flume axis (Fig. 1a). During the sediment injection process, the injectors were oriented upwards to prevent any unintended spillage. Once the pipe was filled with the sediment suspension, it was closed and turned downward so that the injectors extended 5 cm below the water surface facing down. The injectors remained positioned at the top of the water column, above the vegetated patch, at a depth of 5 cm from the surface. Since the suspended sediment concentration in all the trials remained below 17.46 g L^{-1}, the sediment concentration was not expected to have any effect on the settling velocity of particles (Colomer et al., 1998).

The sediment injector pipe was a large 2.5 m-long pipe equipped with 42 sediment injectors evenly distributed 7 cm apart from each other. The design of the sediment injectors resembled a Y-shape, with a total length of 26 cm. Each arm of the injector pipe was 22.5 cm long (Fig. 1a). To ensure a uniform distribution of sediment, each arm of the pipe had 12 holes from which the sediment was released into the flume. This setup allowed for a homogeneous injection of sediment along both the x-axis and the y-axis of the flume.

Table 1
Summary of the conducted experiments.

Run	Epiphyted plants (%)	Epiphyte type
1	0%	non-epiphyted
2	25%	E1
3	50%	E1
4	75%	E1
5	100%	E1
6	25%	E2
7	50%	E2
8	75%	E2
9	100%	E2
10	25%	E3
11	50%	E3
12	75%	E3
13	100%	E3

2.5. Sediment measurements

To obtain the sediment concentration and distribution along the canopy, three types of sediment measurements were conducted: 1) sediment deposited on the bed, 2) suspended sediment, and 3) sediment attached to plant leaves with epiphytes.

Sediment deposition. To measure the sediment deposited on the bed, eight sediment traps were distributed in two rows along the main axis of the flume at y = ± 10 cm and x = 0 ± 40 cm, ±80 cm (Fig. 1b). Sediment samples from traps were collected at t = 60 min after the injection.

Suspended sediment. To measure suspended sediment, 50 mL water samples were pipetted at the same x position where the sediment traps were located for each run, at y = 0 cm, and at two water depths, at z/h_p = 0.3 (within the canopy) and at z/h_p = 0.8 (above the canopy). These sampling locations were chosen to provide representative measurements within and above the canopy. Water samples were collected at various time points (t = 2, 30 and 60 min) after the sediment injection, and were later analysed to determine the concentration levels of the suspended sediment.

Sediment trapping. To measure the influence of epiphytes on sediment trapping, five percentages of epiphyted seagrass leaves were considered in order to mimic natural occurrence observed in the field (Borowitzka et al., 2005). The following percentages of epiphyted leaves were examined: 0%, 25%, 50%, 75% and 100% of the plant leaves covered with epiphytes. For all the cases of 0% and 100%, three sets of five plants were collected for the analysis. For the cases of 25%, 50% and 75%, three sets of five epiphyted plants were collected, along with three sets of three epiphyted plants and two non-epiphyted for further analysis. In all cases, the plants were gently removed from the same x positions within the vegetated patch where the sediment traps had been placed at t = 60 min after the sediment injection. Afterwards, the plants were placed in a glass beaker with 100 mL of filtered seawater and stirred to remove the sediment trapped on the leaf surfaces or by the epiphytes.

To ensure the independency of the measurements a protocol was established. First, the suspended sediment samples were taken. Secondly, the sediment traps were covered with a lid. Thirdly, the fifteen plants were gently removed to measure the sediment trapped by the leaves and finally, the sediment traps were collected from the bottom of the flume and their content analysed.

The mass (in grams) of sediment in each sample was obtained by filtering them with glass microfiber filters (GF/F). The sediment traps and suspended sediment samples were filtered using filters with diameters of 50 mm and 25 mm, respectively. Firstly, the empty filters were weighted to obtain a zero weight. Then, the samples were filtered, dried at 60 °C over 24 h and then weighed again (Brouwer et al., 2023).

2.6. Measuring velocities

The Eulerian velocity field was defined as (u, v, w) in the (x, y, z) directions, respectively. The three components of the velocity were recorded with a downwards-facing Acoustic Doppler Velocimeter (ADV, Nortek, Vectrino) at a frequency of 25 Hz for 10 min, resulting in 15,000

measurements. Beam correlations less than 90% were discarded and spikes were removed (Goring and Nikora, 2002). The ADV was mounted on a movable vertical frame (at x = 0, Fig. 1b) and manually adjusted to measure at z = 5 cm, 6 cm, and 12 cm. Some plants were temporarily removed to prevent obstruction of the ADV beams (Zhang et al., 2018), and were re-inserted into the nearby area when measurements were completed.

For oscillatory flows, the instantaneous velocity, $U_i(t)$, can be decomposed as:

$$U_i(t) = U_c + Uw + u' \quad (1)$$

where, U_c is the mean current velocity associated to the wave, U_w is the unsteady wave motion which represents spatial variations in the phase-averaged velocity field, and u' is the turbulent velocity; that is, the instantaneous velocity fluctuation in the x-direction. U_c is the phase-averaged velocity:

$$U_c = \frac{1}{2\pi}\int_0^{2\pi} U_c(\varphi)\delta\varphi \quad (2)$$

where, $U_c(\varphi)$ is the instantaneous velocity according to the phase (Lowe et al., 2005; Luhar et al., 2010). In the current study, U_c at $z/h_v = 0.3$ above the bed (i.e., within the canopy layer) was always smaller than U_w, with mean values of -0.8 cm s^{-1}.

The wave velocity, U_w, was determined using a phase averaging technique. The Hilbert transform was used to average the oscillatory flow velocities with a common phase (Pujol et al., 2013; Ros et al., 2014). The root mean square (rms) of U_w was considered as the characteristic value of the orbital velocity U_w^{rms} (U_w hereafter) at each depth, and was calculated according to:

$$U_w^{rms} = \sqrt{\frac{1}{2\pi}\int_0^{2\pi} (U_i(\varphi) - Uc)^2\delta\varphi} \quad (3)$$

2.7. Theory

The sediment injected in the flume was distributed into four different compartments: captured by the epiphyted surface, deposited to the bottom, and remaining in suspension (above and within the canopy). A non-dimensional model was constructed based on the Pi-Buckingham theorem. Four variables and two dimensions were considered. The variables were the mass of sediment accumulated in each compartment (TM_i, where i = *b*, *s*, *p*, *ab*, where *b* represents sediment deposited at the bottom, *s* represents the sediment in suspension within the canopy, *p* represents the sediment deposited on the epiphyted surface of the plants and *ab* represents the sediment in suspension above the canopy), the sediment density (ρ), the total epiphyted area of the canopy (A) and the effective height (h_v). The dimensions were grams and metres. Therefore, two governing non-dimensional parameters can be constructed to describe the results. First, $TM_i/(A\rho h_v)$, representing the total mass of sediment captured by each compartment (TM_i) per total mass of the epiphyted canopy area, and second A/h_v^2, defined as the normalized area of the epiphyted meadow. This last parameter is a function of the normalized epiphyte length scale ($(L_{ep}/h_v)^2$), where L_{ep} is the epiphyte's length, which corresponded to the square root of A. A/h_v^2 indicates the increase in the frontal area between a non-epiphyted canopy and the different levels of epiphyted canopies. TM_p is the total mass of sediment collected by all plants in the canopy, obtained multiplying the mass of sediment collected by each single plant (M_p) by the number of plants in the canopy. TM_s is the total mass of sediment in suspension that was calculated by multiplying the mass of suspended sediment in the sample (M_s) by the ratio between the total volume within the canopy and the volume of the sample (100 mL). TM_b is the total mass of sediment deposited to the bottom that was calculated by multiplying the mass of sediment in the trap (M_b) by the ratio between the total area of the vegetated bottom and the area of a single trap (of 0.05×0.02 m^2).

Therefore, a non-dimensional model should consider the relationship between the above governing non-dimensional parameters. It is possible to expect:

$$\frac{TM_i}{A\rho hv} = f\left(\frac{A}{h_v^2}\right) = a\left(\frac{A}{h_v^2}\right)^c \quad (4)$$

where f is function of the dimensionless parameter A/h_v^2, and *a* and *c* are constants of the relationship.

The epiphyted area of each plant A_p was considered the effective area of the flow trapped inside the area of the epiphyte (Fig. 2). To obtain A_p, photographs of plants with epiphytes were converted to grayscale and later to black and white using MATLAB (MathWorks, Inc.). The threshold considered for the conversion to black and white corresponded to that representing the area of the region inside the epiphyte (Fig. 2a and b). The plant epiphyted area A_p was calculated as the vertical sum along the plant leaf of the area at each z (A_z) for each case (Fig. 2c). Therefore, the total epiphyted area of the canopy (A) was obtained multiplying A_p by the total number of epiphytes for each experiment.

2.8. Data analysis

TM_i was regressed against the percentage of epiphyted plant. The differences between the percentage of epiphyted plants and the epiphyted areas (A_p) were determined using ANOVA one-factor. The Shapiro-Wilk, and Levene's tests were performed to ensure normality and homogeneity.

3. Results

3.1. Distribution of sediment mass in the different compartments

The sediment was distributed into four compartments: sediment trapped by the seagrass leaves (Fig. 3a), sediment deposited on the bottom of the flume (Fig. 3b), sediment remaining in suspension within the canopy (Fig. 3c) and sediment remaining in suspension above the canopy (not considered). For the trials conducted with epiphytes E2 and E3, the mass of sediment, TM_p, trapped by all plant leaves increased linearly with the percentage of epiphyted plants (0%–100% epiphyted plants), following the tendencies for each epiphyte: $TM_p = 0.02$ (% epiphyted plants) + 0.75 for the E3 ($A_p = 94.51$ cm^2) and $TM_p = 0.01$ (% epiphyted plants) + 1.09 for the E2 ($A_p = 38.15$ cm^2) (Fig. 3a). However, for the lowest epiphyted area studied, corresponding to experiments with E1 ($A_p = 31.56$ cm^2), the mass of sediment trapped by plant leaves remained constant regardless of the percentage of epiphyted plants. In contrast, the mass of sediment deposited on the bottom did not show significant differences (p-value >0.05) between epiphyte types E1, E2 and E3, but did present a decreasing trend linearly correlated with the percentage of epiphyte plants, with a p-value <0.05 (Fig. 3b). In contrast, the sediment remaining in suspension did not show significant differences in relation to either the epiphyted area or the percentage of epiphyted plants (p-value >0.05, obtained by performing a one-way ANOVA) (Fig. 3c).

3.2. Non-dimensional model for sediment capture in each compartment

To quantify the sediment captured by the seagrass canopy, three non-dimensional models were developed to represent each compartment: sediment trapped by the plant leaves (Fig. 4), sediment deposited on the bottom (Fig. 5) and sediment remaining in suspension within the canopy (Fig. 6). These models were derived using Equation (4), as described in the Materials and Methods section.

For the sediment trapped by the plant leaves, a negative power trend

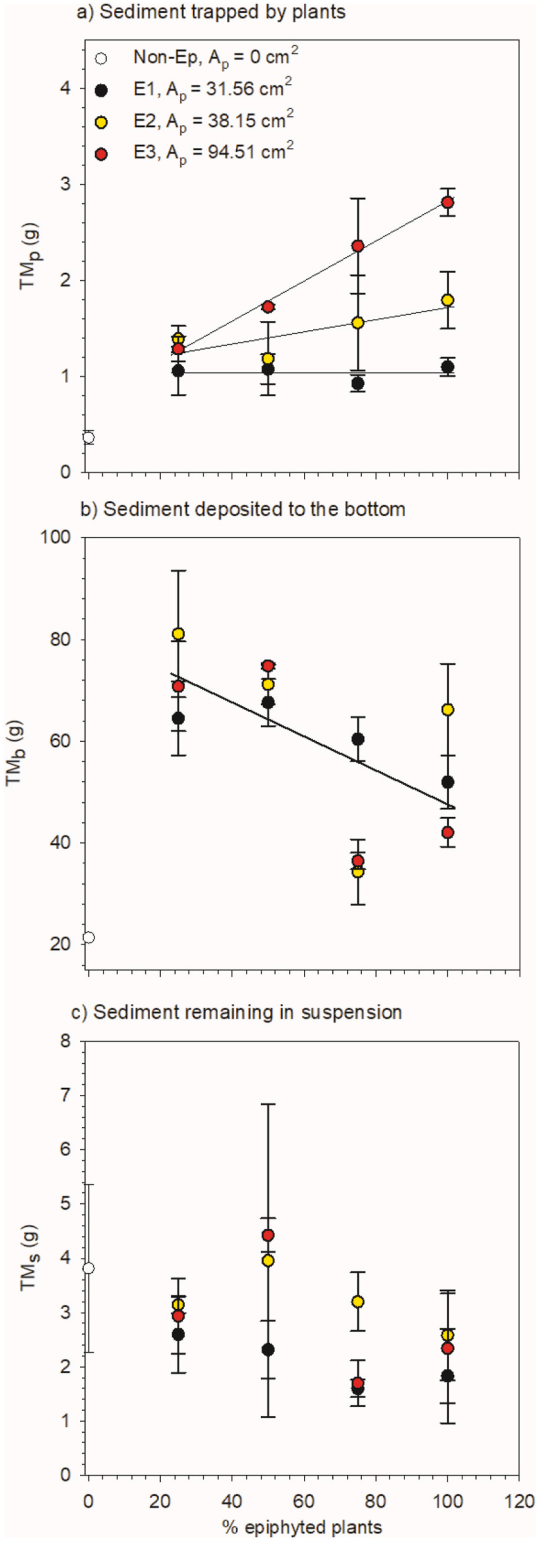

Fig. 3. Sediment distribution patterns associated with epiphyted plants. Mass of sediment a) trapped by plant leaves. The linear expressions for E2 and E3 found are: $TM_p = 0.02$ (% epiphyted plants) + 0.75 and $TM_p = 0.01$ (% epiphyted plants) + 1.09 respectively, p-value <0.05 in both cases, b) deposited to the bottom. The linear expression found is: $TM_b = -0.33$ (% epiphyted plants) + 81.00, p-value < 0.05 and c) remaining in suspension for the number epiphyted plants in the canopy (in percentage).

was found and is shown in Fig. 4. The expression has been solved for TM_p, following:

$$TM_p = 7{\cdot}10^{-5}\rho A^{0.27}h_v^{2.46}, \text{ with a } R^2 = 0.90 \quad [5]$$

and showing that the sediment trapped by the leaves increased with both the total epiphyted area A and the effective leaf length h_v (Fig. 4).

The non-dimensional mass deposited at the bottom in the complete area covered by vegetation, $TM_b/\rho Ah_v$, also presented a negative power trend with A/h_v^2 (Fig. 5). The dependence of the mass deposited at the bottom was obtained as a function of A and h_v, according to the following equation:

$$TM_b = 8.6{\cdot}10^{-3}\rho A^{-0.34}h_v^{3.68}, \text{ with a } R^2 = 0.94 \quad [6]$$

Therefore, the sediment deposited to the bottom depended negatively on the total epiphyted area (A) and positively on the effective height (h_v), as shown in Fig. 5. Equation (6) implies that the greater the epiphyted area, the lower the amount of sediment deposited to the bottom. However, the greater the effective height, the greater the amount of sediment deposited to the bottom (Fig. 5).

The sediment remaining in suspension within the total canopy region (TM_s), followed a negative power relationship (Fig. 6). The expression (as for the other compartments) was also solved by TM_s. TM_s decreased with the total epiphyted area (A) and increased with the effective height (h_v) with the following expression:

$$TM_s = 3{\cdot}10^{-4}\rho A^{-0.22}h_v^{3.43}, \text{ with a } R^2 = 0.92 \quad (7)$$

For the experiments conducted with 50% and 100% of epiphyted plants and for the different types of epiphytes, the total volume of sediment captured in each compartment (suspended, plant leaves, and bottom) was calculated. For the sediment trapped by the plant leaves, the total volume of sediment trapped was obtained as follows:

$$V_p = (M_{nep}\, N_{nep} + M_{ep}\, N_{ep}) / \rho \quad (8)$$

where N_{nep} and N_{ep} are the number of non-epiphyted and epiphyted plants, respectively. M_{nep} and M_{ep} are the mass of sediment captured by single both non-epiphyted and epiphyted plants, respectively.

For the sediment in suspension, the total volume of sediment within the canopy, V_s, was calculated as follows:

$$V_s = M_s\, L_p\, h_v / \rho \quad (9)$$

where L_p is the canopy length.

For the sediment deposited on the bottom, the total volume of sediment V_b was calculated as follows:

$$V_b = M_b\, L_p\, W \quad (10)$$

where W is the width of the flume.

The volume of particles deposited to the bottom (V_b) presented the largest percentage compared to the other two compartments (V_s and V_p). For the non-epiphytic case to the 100% of epiphyted plants (Fig. 7), the volume of sediment trapped by the plant leaves (V_p) increased with the total epiphyted area. The non-epiphytic case presented the lowest V_p = 0.6%, for the 50% of total epiphyted plants V_p increased from 1.5 to 2.1% with the total epiphyted area, and from 2.5 to 6.0% for the 100% of epiphyted plants (Fig. 7). In contrast, the volume of sediment deposited on the bottom (V_b) decreased with the total epiphyted area; being 93.5 for the non-epiphytic case, from 95% to 92.4% for the 50% epiphyted plants and from 93.8 to 90% for the 100% epiphyted plants (Fig. 7). V_s decreases with the presence of epiphytes, reaching a value of 5.9% for the non-epiphytic. However, V_s decreased as the total epiphytic area increased, from 3.3% to 5.1% for 50% of epiphyted plants and from 3.7% to 5.0% for experiments with 100% of epiphyted plants (Fig. 7).

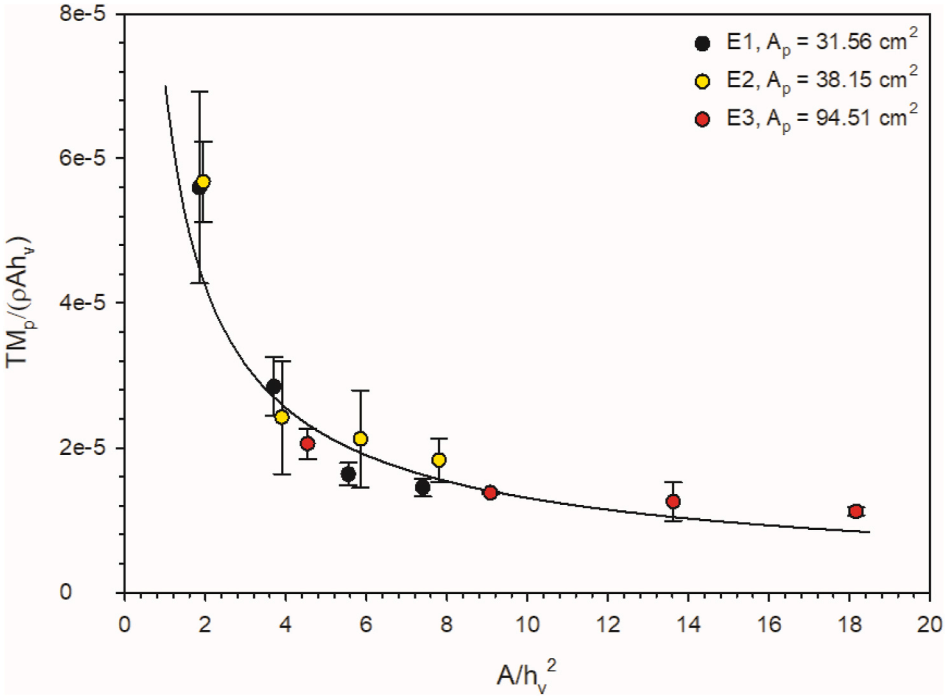

Fig. 4. Non-dimensional model for the mass sediment trapped by plant leaves, $TM_p/(\rho Ah_v)$ for the different A/h_v^2 tested. E1, A_p = 31.56 cm^2 (black filled circles), E2, A_p = 38.15 cm^2 (blue filled circles) and E3, A_p = 94.51 cm^2 (red filled circles). The power tendency found follows the expression: $TM_p/(\rho Ah_v) = 7{\cdot}10^{-5} (A/h_v^2)^{-0.73}$, with an $R^2 = 0.90$, p-value <0.05.

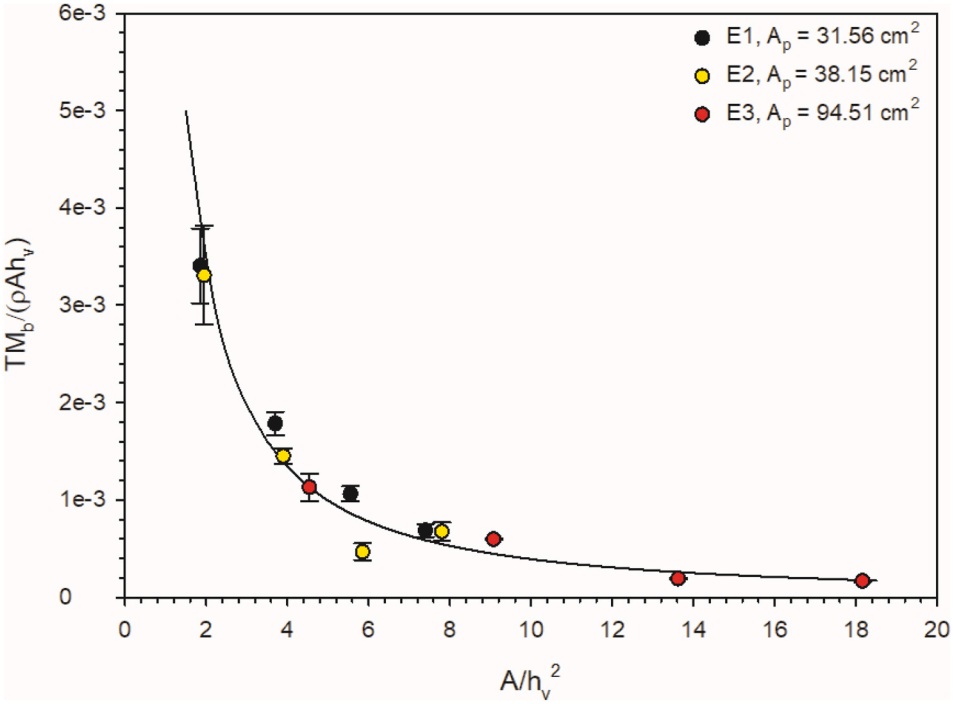

Fig. 5. Non-dimensional model for the mass sediment deposited to the bottom, $TM_b/(\rho Ah_v)$ for the different A/h_v^2 tested, E1, A_p = 31.56 cm^2 (black filled circles), E2, A_p = 38.15 cm^2 (blue filled circles) and E3, A_p = 94.51 cm^2 (red filled circles). The power tendency found follows the expression: $TM_p/(\rho Ah_v) = 8.6{\cdot}10^{-3} (A/h_v^2)^{-1.34}$, with an $R^2 = 0.94$, p-value <0.05.

4. Discussion

Seagrass habitats present a range of structural characteristics that affect the ecological services they provide (Ward et al., 2022). Factors such as plant stiffness, presence of bare sediment areas within seagrass canopies, leaf height, canopy density, stem diameter, patch length and presence of epiphytic communities, impact the functioning of seagrasses. This study demonstrates that sedimentation patterns at the bottom of epiphyted canopies and sediment capture by epiphyted leaves depend on both the effective height (h_v) of the plant and the total

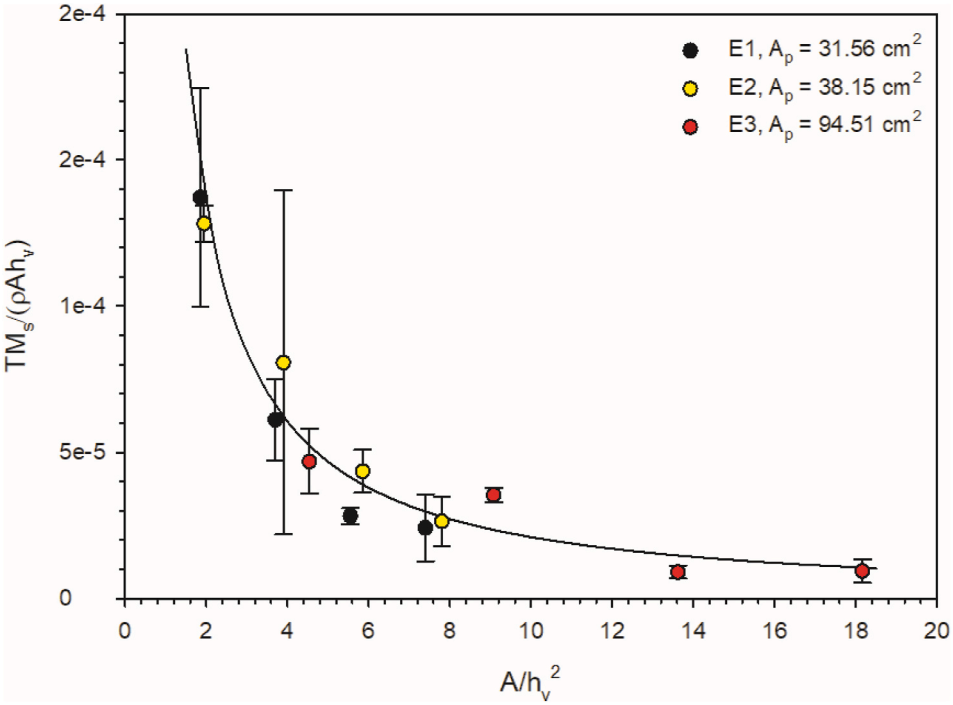

Fig. 6. Non-dimensional model for the mass sediment remained in suspension, $TM_s/(\rho Ah_v)$ for the different A/h_v^2 tested, E1, A_p = 31.56 cm^2 (black filled circles), E2, A_p = 38.15 cm^2 (blue filled circles) and E3, A_p = 94.51 cm^2 (red filled circles). The power tendency found follows the expression: $TM_s/(\rho Ah_v) = 3{\cdot}10^{-4}$ $(A/h_v^2)^{-1.22}$, with an R^2 = 0.92, p-value <0.05.

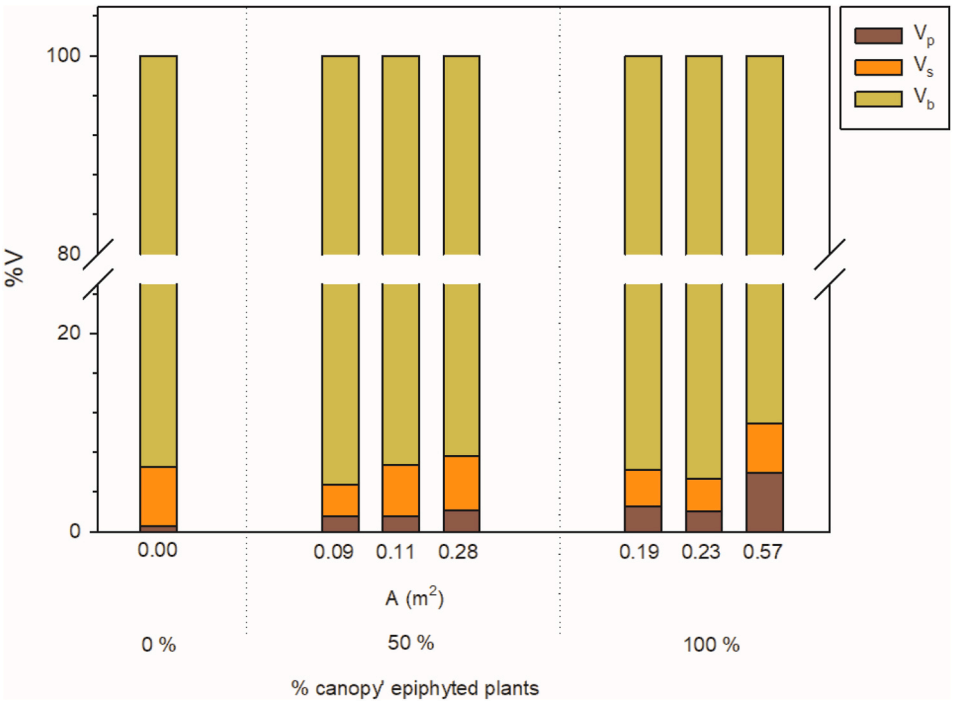

Fig. 7. Distribution of total sediment volume. Total sediment volume (V, in %) distributed in the different compartments: total volume of sediment trapped by the plant leaves (V_p), total volume of sediment, remaining in suspension within the canopy (V_s), and total volume of sediment deposited to the bottom (V_b) versus the total epiphytic area (A) for the cases 0%, 50% and 100% of epiphyted plants of the canopy. A (total epiphytic area), corresponds to each epiphyte used: E1 = 0.09; E2 = 0.11 and E3 = 0.28 m^2 for 50% of epiphyted plants and E1 = 0.19; E2 = 0.23 and E3 = 0.57 m^2 for 100% of epiphyted plants.

epiphyted area (A). Three types of epiphytic structures on eelgrass canopies were used to model three levels of epiphytic areas and compared to the non-epiphyted case.

The sediment trapped by the plant leaves was found to follow $TM_p = A^{0.27}h_v^{2.46}$. Therefore, the total mass of sediment attached to plant leaves increased with both the total epiphytic area and plant height. Increasing the effective plant height by 3.2% (when comparing E2 and E3) and 10.4% (when comparing E1 and E3) resulted in an increase in the total

mass of sediment captured on the plant leaves of 7.9%–27.7%, respectively. Similarly, increasing the total epiphytic area by 2.5 and 3 (comparing E2 and E3, and E1 and E3, respectively) led to an increase in the total mass of sediment attached to the leaves of 27.7% and 34.5%, respectively. As the accumulation of sediment on plant leaves increases with the epiphytic area, it might produce a negative feedback on seagrasses, reducing their gas exchange capabilities (Pujol et al., 2019) and their ability to meet light requirements (Brodersen and Kühl, 2022), due to the presence of epiphytes leading to a build-up on the diffusive boundary layer which may impeded oxygen transfer between the seagrass leaf and the surrounding water (Noisette et al., 2020). However, this negative effect might be counteracted in dense canopies, which capture less sediment per plant leaf but a higher overall amount when considering the sediment captured by the entire canopy (Barcelona et al., 2021b). Furthermore, the mass of sediment in suspension slightly decreases with the epiphytic area following $TM_s = A^{-0.33}h_v^{3.43}$. That is, the presence of epiphytes on the surface of the plant leaves reduces the mass of suspended sediment, resulting in a clearer water column. This result partially counteracts the negative effects of epiphyte presence, which otherwise would reduce the light availability and compromise the light requirements for plant leaves (Brodersen and Kühl, 2022).

The mass of sediment deposited at the bottom was found to depend on A and h_v following the relationship $TM_b = A^{-0.34}h_v^{3.68}$. This indicates that larger epiphytic areas increase the capture of sediment by plant leaves, resulting in a reduction of the sediment reaching the bottom. Additionally, the mass of sediment settling at the bottom increased with the effective plant height, indicating that higher plant leaves provide a greater surface area for particle capture (Borum, 1987; Ruesink, 2016). Stiffer plants, associated with higher effective plant heights, are expected to enhance the chances of particles settling to the bottom, increasing the overall sediment mass deposited in the bed.

In the absence of epiphytes, the majority of sediment particles, particularly those in the silt and clay ranges, reached the seagrass bottom (93.5%), while only a small portion was trapped by the plant leaves (0.6%). When the entire canopy was epiphyted (100% of plants in the canopy were epiphyted), the sedimentation at the seagrass bottom diminished to 90.0%, while the particles captured by the epiphyted leaves increased to 6.0%. Notably, the epiphyte with the greater surface area (E3), captured 10 times more sediment on the leaves when compared to the non-epiphyted canopy. In all cases with epiphytes, the volume of suspended sediment was lower than in cases without epiphytes. Therefore, colonization of epiphytes on eelgrass leaves may regulate the sedimentation stocks in each canopy compartment and reduce the amount of suspended sediment within the canopy, enhancing the role of the seagrass in clearing the water column.

However, in cases with a high epiphytic area, the presence of epiphytes on seagrass leaves, along with an increase in the sediment captured by leaves might lead to a reduction in available light, which is essential for plant requirements (Brodersen and Kühl, 2022). While moderate epiphytic cases may modulate light harvesting, high percentages of epiphytes can have a negative effect on seagrasses, compromising the survival of the canopy (Brodersen and Kühl, 2022). Generally, there is higher leaf growth and productivity at the centre of a seagrass meadow than at the edges (Turner, 2007). However, in dense seagrass beds, light competition can result in greater productivity at the edges compared to the centre (Nakaoka and Aioi, 1999). Also, a high epiphytic community growing on long seagrass leaves in the centre of a meadow might also compromise the seagrass, which experiences less light stress at the edges compared to the centre.

The percentage of epiphytic area was found to have no effect on eelgrass growth up to 60% (Ruesink, 2016). However, other studies have found a reduction in seagrass productivity with an increase in epiphyte mass (Reynolds et al., 2014; Whalen et al., 2013). Therefore, differences in seagrass responses to epiphytic areas might arise when resources are below saturating levels (Sand-Jensen, 1977), which could explain variations found between studies.

The variation in canopy epiphytic area may also impact the flexural capacity of plants, resulting in more rigid or more flexible structures which can modify plant behaviour under different hydrodynamic conditions. Rigid plants can produce more turbulent kinetic energy than flexible plants can (Barcelona et al., 2023b), which subsequently reduces the thickness of the diffuse boundary layer through increased flow velocity (Pujol et al., 2019) and potentially alters nutrient uptake (Cornelisen and Thomas, 2004).

Eelgrass, being an annual species, undergoes variations in leaf length during the year (Olesen and Sand-Jensen, 1994), resulting in seasonal changes in the available leaf area for epiphytes (Brodersen and Kühl, 2022). The non-dimensional model proposed indicates that the ecological function of the seagrass leaves in capturing sediment is going to vary following an annual cycle. Therefore, these seasonal variations in epiphytes may play a significant role in the sediment retention in coastal areas. This ecological service provided by eelgrass is of relevance considering the observed increase in heavy rainfall events that produce particle sediment-laden plumes in Europe in recent years (Vautard et al., 2014). Epiphytes also contribute to reducing the impact of the sediment output from the dredging activities related to coastal development (Wu et al., 2018).

Therefore, the structural characteristics of plant and canopies, in addition to hydrodynamic conditions, time of the year, and imposed natural or anthropogenic disturbances, are crucial factors for the development of seagrass habitats (Barcelona et al., 2021a, 2021b, 2021c, 2023a, 2023b; Duarte et al., 2005, 2013; Eckardt et al., 2023; Granata et al., 2001; Hendriks et al., 2008). As shown in this study, epiphyte presence on plant leaves is also a key component to consider when determining the overall behavior of the canopy and its role in the capture of sediment from sediment output sources.

The hypothesis raised in the introduction has been confirmed. That is, the morphology and quantity of the epiphytes colonizing a *Z. marina* meadow have been found to be enhance the capture of particles by seagrass leaves, with epiphytes possessing larger effective areas capable of trapping more particles compared to those with smaller epiphytic areas. This behavior impacts on the other compartments. Then, the epiphytic community has been also found to modify both the deposition of sediment on the bed and the suspended sediment, with a decrease of the sediment deposited and the sediment suspended as the epiphytic area increased. These laboratory results a first step to understand the role of real epiphytic communities in the field in trapping suspended particles.

5. Conclusions

The current study demonstrates the significant role epiphytes play in the capture of sediment by an eelgrass canopy under an oscillatory flow regime. Three epiphyte models were used to quantify the impact their morphology has on sediment capture. Sediment particles originating from an external source interacted with the canopy, either becoming trapped on the epiphytic surfaces of plant leaves, remaining suspended within the canopy, or settling to the bottom bed. The mass of sediment trapped by the epiphytic leaves, accumulated within the canopy bed, and remaining in suspension, was found to be a function of the effective plant height (h_v) and the total epiphytic area (A).

This study demonstrates that eelgrass canopies with higher epiphytic leaf areas and longer effective leaf lengths (h_v) are prone to increase the mass sediment captured by the epiphyted plants. Longer plant leaves are expected to provide a greater surface area for epiphyte attachment compared to shorter leaves. Therefore, canopies with higher epiphyted cover would promote an increase in the sediment capture by plants, thereby reducing the amount of sediment that reaches the seabed. The magnitude of sediment mass trapped by the epiphyted canopy is particularly pronounced for canopies with the largest epiphytic areas, with a 34.5% increase compared to canopies with smaller epiphytic areas. For the epiphyte with the greatest surface area, the sediment mass

trapped within the leaves can be 10 times greater than that captured by leaves without epiphytes.

This study also demonstrates eelgrass meadow vulnerability when subjected to extensive epiphytic growth, as it leads to a substantial accumulation of sediment on seagrass leaves, which can pose challenges to plant survival by reducing gas exchange and light availability. Therefore, the fate of a meadow might be dependent on the balance between the different structural parameters including the canopy density and extension, and effective leaf length, and epiphytic area. This manuscript has shown the effect of the effective leaf length and the epiphytic area that, collectively, may modify the overall functioning of an eelgrass meadow.

CRediT authorship contribution statement

Aina Barcelona: Conceptualization, Data curation, Formal analysis, Methodology, Writing-original draft, Writing-review & editing. Jordi Colomer: Data curation, Writing-review & editing. Teresa Serra: Writing-review & editing, Funding acquisition. Damboia Cossa: Writing-review & editing. Eduardo Infantes: Conceptualization, Writing-review & editing, Funding acquisition, Supervision.

Declaration of competing interest

The authors declare that they have no known competing financial interests or personal relationships that could have appeared to influence the work reported in this paper.

Data availability

Data will be made available on request.

Acknowledgements

We would like to thank FORMAS grant Dnr. 2019-01192. We would also like to thank Michael Gitzen, Tristan Dickinson, and Kirsten Wohak for the field and laboratory assistance. This work was supported by the Ministerio de Economía y Competitividad of the Spanish Government through Grant PID2021-123860OB-100. Aina Barcelona was funded by the pre-doctoral grant 2020 FI SDUR 00043 from the “Generalitat de Catalunya”.

References

Agawin, N.S.R., Duarte, C.M., 2002. Evidence of direct particle trapping by a tropical seagrass meadow. Estuaries 25, 1205–1209. https://doi.org/10.1007/BF02692217.

Baggett, L.P., Heck, K.L.J., Frankovich, T.A., Armitage, A.R., Fourqurean, J.W., 2010. Nutrient enrichment, grazer identity, and their effects on epiphytic algal assemblages: field experiments in subtropical turtlegrass Thalassia testudinum meadows. Mar. Ecol. Prog. Ser. 406, 33–45. https://doi.org/10.3354/meps08533.

Balata, D., Bertocci, I., Piazzi, L., Nesti, U., 2008. Comparison between epiphyte assemblages of leaves and rhizomes of the seagrass Posidonia oceanica subjected to different levels of anthropogenic eutrophication. Estuar. Coast Shelf Sci. 79, 533–540. https://doi.org/10.1016/j.ecss.2008.05.009.

Barcelona, A., Colomer, J., Serra, T., 2023a. Spatial sedimentation and plant captured sediment within seagrass patches. Mar. Environ. Res. 188, 105997 https://doi.org/10.1016/j.marenvres.2023.105997.

Barcelona, A., Colomer, J., Serra, T., 2023b. Stem stiffness functionality in a submerged canopy patch under oscillatory flow. Sci. Rep. 13, 1904. https://doi.org/10.1038/s41598-023-28077-2.

Barcelona, A., Colomer, J., Soler, M., Gracias, N., Serra, T., 2021a. Meadow fragmentation influences Posidonia oceanica density at the edge of nearby gaps. Estuar. Coast Shelf Sci. 249, 107106 https://doi.org/10.1016/j.ecss.2020.107106.

Barcelona, A., Oldham, C., Colomer, J., Garcia-Orellana, J., Serra, T., 2021b. Particle capture by seagrass canopies under an oscillatory flow. Coast. Eng. 169, 103972 https://doi.org/10.1016/j.coastaleng.2021.103972.

Barcelona, A., Oldham, C., Colomer, J., Serra, T., 2021c. Functional dynamics of vegetated model patches: the minimum patch size effect for canopy restoration. Sci. Total Environ. 795, 148854 https://doi.org/10.1016/j.scitotenv.2021.148854.

Ben Brahim, M., Hamza, A., Hannachi, I., Rebai, A., Jarboui, O., Bouain, A., Aleya, L., 2010. Variability in the structure of epiphytic assemblages of Posidonia oceanica in relation to human interferences in the Gulf of Gabes, Tunisia. Mar. Environ. Res. 70, 411–421. https://doi.org/10.1016/j.marenvres.2010.08.005.

Ben Brahim, M., Mabrouk, L., Hamza, A., Jribi, I., 2020. Comparison of spatial scale variability of shoot density and epiphytic leaf assemblages of Halophila stipulacea and Cymodocea nodosa on the Eastern Coast of Tunisia. Plant Biosystems - An International Journal Dealing with all Aspects of Plant Biology 154, 413–426. https://doi.org/10.1080/11263504.2019.1674399.

Borowitzka, M.A., Lavery, P.S., van Keulen, M., 2005. Epiphytes of seagrasses. In: Seagrass:Biology, Ecologyl and Conservation. Springer Netherlands, Dordrecht, pp. 441–461. https://doi.org/10.1007/978-1-4020-2983-7_19.

Borum, J., 1987. Dynamics of epiphyton on eelgrass (Zostera marina L.) leaves: relative roles of algal growth, herbivory, and substratum turnover. Limnol. Oceanogr. 32, 986–992. https://doi.org/10.4319/lo.1987.32.4.0986.

Boström, C., Baden, S., Bockelmann, A., Dromph, K., Fredriksen, S., Gustafsson, C., Krause-Jensen, D., Möller, T., Nielsen, S.L., Olesen, B., Olsen, J., Pihl, L., Rinde, E., 2014. Distribution, structure and function of Nordic eelgrass *(Zostera marina)* ecosystems: implications for coastal management and conservation. Aquat. Conserv. 24, 410–434. https://doi.org/10.1002/aqc.2424.

Brodersen, K.E., Kühl, M., 2022. Effects of epiphytes on the seagrass phyllosphere. Front. Mar. Sci. 9 https://doi.org/10.3389/fmars.2022.821614.

Brouwer, S., Humphries, P., Holland, A., McCasker, N., 2023. Effect of suspended sediment concentration on the clearance and biodeposition rates of an Australian freshwater mussel (Hyriidae: Alathyria jacksoni). Freshw. Biol. https://doi.org/10.1111/fwb.14137.

Cambridge, M., How, J., Lavery, P., Vanderklift, M., 2007. Retrospective analysis of epiphyte assemblages in relation to seagrass loss in a eutrophic coastal embayment. Mar. Ecol. Prog. Ser. 346, 97–107. https://doi.org/10.3354/meps06993.

Colomer, J., Ross, J.A., Casamitjana, X., 1998. Sediment entrainment in karst basins. Aquat. Sci. 60, 338. https://doi.org/10.1007/s000270050045.

Cornelisen, C.D., Thomas, F.I.M., 2004. Ammonium and nitrate uptake by leaves of the seagrass Thalassia testudinum: impact of hydrodynamic regime and epiphyte cover on uptake rates. J. Mar. Syst. 49, 177–194. https://doi.org/10.1016/j.jmarsys.2003.05.008.

de los Santos, C.B., Krång, A.-S., Infantes, E., 2021. Microplastic retention by marine vegetated canopies: simulations with seagrass meadows in a hydraulic flume. Environ. Pollut. 269, 116050 https://doi.org/10.1016/j.envpol.2020.116050.

Duarte, C.M., Losada, I.J., Hendriks, I.E., Mazarrasa, I., Marbà, N., 2013. The role of coastal plant communities for climate change mitigation and adaptation. Nat. Clim. Change 3, 961–968. https://doi.org/10.1038/nclimate1970.

Duarte, C.M., Middelburg, J.J., Caraco, N., 2005. Major role of marine vegetation on the oceanic carbon cycle. Biogeosciences 2, 1–8. https://doi.org/10.5194/bg-2-1-2005.

Eckardt, N.A., Ainsworth, E.A., Bahuguna, R.N., Broadley, M.R., Busch, W., Carpita, N.C., Castrillo, G., Chory, J., DeHaan, L.R., Duarte, C.M., Henry, A., Jagadish, S.V.K., Langdale, J.A., Leakey, A.D.B., Liao, J.C., Lu, K.-J., McCann, M.C., McKay, J.K., Odeny, D.A., Jorge de Oliveira, E., Platten, J.D., Rabbi, I., Rim, E.Y., Ronald, P.C., Salt, D.E., Shigenaga, A.M., Wang, E., Wolfe, M., Zhang, X., 2023. Climate change challenges, plant science solutions. Plant Cell 35, 24–66. https://doi.org/10.1093/plcell/koac303.

Fonseca, M.S., Koehl, M.A.R., 2006. Flow in seagrass canopies: the influence of patch width. Estuar. Coast Shelf Sci. 67, 1–9. https://doi.org/10.1016/j.ecss.2005.09.018.

Gacia, E., Granata, T.C., Duarte, C.M., 1999. An approach to measurement of particle flux and sediment retention within seagrass (Posidonia oceanica) meadows. Aquat. Bot. https://doi.org/10.1016/S0304-3770(99)00044-3.

García-Redondo, V., Bárbara, I., Díaz-Tapia, P., 2019. Biodiversity of epiphytic macroalgae (Chlorophyta, Ochrophyta and Rhodophyta) on leaves of Zostera marina in the northwestern Iberian Peninsula. An. del Jardín Botánico Madr. 76, 78. https://doi.org/10.3989/ajbm.2502.

Goring, D.G., Nikora, V.I., 2002. Despiking Acoustic Doppler velocimeter Data. J. Hydraul. Eng. 128, 117–126. https://doi.org/10.1061/(ASCE)0733-9429(2002)128:1(117).

Granata, T.C., Serra, T., Colomer, J., Casamitjana, X., Duarte, C., Gacia, E., 2001. Flow and particle distributions in a nearshore seagrass meadow before and after a storm. Mar. Ecol. Prog. Ser. 218, 95–106. https://doi.org/10.3354/meps218095.

Grifoll, M., Gracia, V., Aretxabaleta, A., Guillén, J., Espino, M., Warner, J., 2014. Formation of fine sediment deposition from a flash flood river in the Mediterranean Sea. J. Geophys. Res-Oceans. 119 (9), 5837–5853. https://doi.org/10.1002/2014JC010187.

Hendriks, I.E., Sintes, T., Bouma, T.J., Duarte, C.M., 2008. Experimental assessment and modeling evaluation of the effects of the seagrass Posidonia oceanica on flow and particle trapping. Mar. Ecol. Prog. Ser. 356, 163–173. https://doi.org/10.3354/meps07316.

Infantes, E., Hoeks, S., Adams, M., van der Heide, T., van Katwijk, M., Bouma, T., 2022. Seagrass roots strongly reduce cliff erosion rates in sandy sediments. Mar. Ecol. Prog. Ser. 700, 1–12. https://doi.org/10.3354/meps14196.

Infantes, E., Orfila, A., Simarro, G., Terrados, J., Luhar, M., Nepf, H., 2012. Effect of a seagrass (Posidonia oceanica) meadow on wave propagation. Mar. Ecol. Prog. Ser. 456, 63–72. https://doi.org/10.3354/meps09754.

Jankowska, E., Michel, L.N., Zaborska, A., Włodarska-Kowalczuk, M., 2016. Sediment carbon sink in low-density temperate eelgrass meadows (Baltic Sea). J Geophys Res Biogeosci 121, 2918–2934. https://doi.org/10.1002/2016JG003424.

Lowe, R.J., Koseff, J.R., Monismith, S.G., Falter, J.L., 2005. Oscillatory flow through submerged canopies: 2. Canopy mass transfer. J. Geophys. Res. 110, C10017 https://doi.org/10.1029/2004JC002789.

Luhar, M., Coutu, S., Infantes, E., Fox, S., Nepf, H., 2010. Wave-induced velocities inside a model seagrass bed. J Geophys Res Oceans 115. https://doi.org/10.1029/2010JC006345.

Mancini, M., Serra, T., Colomer, J., Solari, L., 2023. Suspended sediments mediate microplastic sedimentation in unidirectional flows. Sci. Total Environ. 890 https://doi.org/10.1016/j.scitotenv.2023.164363.

Marin-Diaz, B., Bouma, T.J., Infantes, E., 2020. Role of eelgrass on bed-load transport and sediment resuspension under oscillatory flow. Limnol. Oceanogr. 65, 426–436. https://doi.org/10.1002/lno.11312.

Mutlu, E., Karaca, D., Duman, G.S., Şahin, A., Özvarol, Y., Olguner, C., 2022. Seasonality and phenology of an epiphytic calcareous red alga, Hydrolithon boreale, on the leaves of Posidonia oceanica (L) Delile in the Turkish water. Environ. Sci. Pollut. Control Ser. 30, 17193–17213. https://doi.org/10.1007/s11356-022-23333-w.

Nakaoka, M., Aioi, K., 1999. Growth of seagrass Halophila ovalis at dugong trails compared to existing within-patch variation in a Thailand intertidal flat. Mar. Ecol. Prog. Ser. 184, 97–103. https://doi.org/10.3354/meps184097.

Noisette, F., Depetris, A., Kühl, M., Brodersen, K.E., 2020. Flow and epiphyte growth effects on the thermal, optical and chemical microenvironment in the leaf phyllosphere of seagrass (Zostera marina). J. R. Soc. Interface 17, 20200485. https://doi.org/10.1098/rsif.2020.0485.

Olesen, B., Sand-Jensen, K., 1994. Demography of shallow eelgrass (Zostera marina) Populations–shoot dynamics and biomass development. J. Ecol. 82, 379. https://doi.org/10.2307/2261305.

Pineda, M.-C., Strehlow, B., Kamp, J., Duckworth, A., Jones, R., Webster, N.S., 2017. Effects of combined dredging-related stressors on sponges: a laboratory approach using realistic scenarios. Sci. Rep. 7, 5155. https://doi.org/10.1038/s41598-017-05251-x.

Pujol, D., Abdolahpour, M., Lavery, P.S., McMahon, K., Oldham, C., 2019. Flow velocity and nutrient uptake in marine canopies. Mar. Ecol. Prog. Ser. 622, 17–30. https://doi.org/10.3354/meps12987.

Pujol, D., Serra, T., Colomer, J., Casamitjana, X., 2013. Flow structure in canopy models dominated by progressive waves. J. Hydrol. (Amst.) 486, 281–292. https://doi.org/10.1016/j.jhydrol.2013.01.024.

Reyes, J., Sanson, M., Afonso-Carrillo, J., 1998. Distribution of the Epiphytes along the Leaves of Cymodocea Nodosa in the Canary Islands. Botanica Marina.

Reynolds, P.L., Richardson, J.P., Duffy, J.E., 2014. Field experimental evidence that grazers mediate transition between microalgal and seagrass dominance. Limnol. Oceanogr. 59, 1053–1064. https://doi.org/10.4319/lo.2014.59.3.1053.

Röhr, M.E., Holmer, M., Baum, J.K., Björk, M., Boyer, K., Chin, D., Chalifour, L., Cimon, S., Cusson, M., Dahl, M., Deyanova, D., Duffy, J.E., Eklöf, J.S., Geyer, J.K., Griffin, J.N., Gullström, M., Hereu, C.M., Hori, M., Hovel, K.A., Hughes, A.R., Jorgensen, P., Kiriakopolos, S., Moksnes, P.-O., Nakaoka, M., O'Connor, M.I., Peterson, B., Reiss, K., Reynolds, P.L., Rossi, F., Ruesink, J., Santos, R., Stachowicz, J. J., Tomas, F., Lee, K.-S., Unsworth, R.K.F., Boström, C., 2018. Blue carbon storage capacity of temperate eelgrass (Zostera marina) meadows. Global Biogeochem. Cycles 32, 1457–1475. https://doi.org/10.1029/2018GB005941.

Ros, À., Colomer, J., Serra, T., Pujol, D., Soler, M., Casamitjana, X., 2014. Experimental observations on sediment resuspension within submerged model canopies under oscillatory flow. Continent. Shelf Res. 91, 220–231. https://doi.org/10.1016/j.csr.2014.10.004.

Ruesink, J.L., 2016. Epiphyte load and seagrass performance are decoupled in an estuary with low eutrophication risk. J. Exp. Mar. Biol. Ecol. 481, 1–8. https://doi.org/10.1016/j.jembe.2016.03.022.

Sand-Jensen, K., 1977. Effect of epiphytes on eelgrass photosynthesis. Aquat. Bot. 3, 55–63. https://doi.org/10.1016/0304-3770(77)90004-3.

Serra, T., Oldham, C., Colomer, J., 2018. Local hydrodynamics at edges of marine canopies under oscillatory flows. PLoS One 13. https://doi.org/10.1371/journal.pone.0201737.

Somma, E., Terlizzi, A., Costantini, M., Madeira, M., Zupo, V., 2023. Global changes alter the successions of early Colonizers of benthic surfaces. J. Mar. Sci. Eng. 11, 1232. https://doi.org/10.3390/jmse11061232.

Trautman, D., Borowitzka, M., 1999. Distribution of the epiphytic organisms on Posidonia australis and P. sinuosa, two seagrasses with differing leaf morphology. Mar. Ecol. Prog. Ser. 179, 215–229. https://doi.org/10.3354/meps179215.

Turner, S.J., 2007. Growth and productivity of intertidal Zostera capricorni in New Zealand estuaries. N. Z. J. Mar. Freshw. Res. 41, 77–90. https://doi.org/10.1080/00288330709509897.

Unsworth, R.K.F., Williams, B., Jones, B.L., Cullen-Unsworth, L.C., 2017. Rocking the boat: damage to eelgrass by swinging boat moorings. Front. Plant Sci. 8 https://doi.org/10.3389/fpls.2017.01309.

Vautard, R., Gobiet, A., Sobolowski, S., Kjellström, E., Stegehuis, A., Watkiss, P., Mendlik, T., Landgren, O., Nikulin, G., Teichmann, C., Jacob, D., 2014. The European climate under a 2 °C global warming. Environ. Res. Lett. 9, 034006 https://doi.org/10.1088/1748-9326/9/3/034006.

Ward, E.A., Aldis, C., Wade, T., Miliou, A., Tsimpidis, T., Cameron, T.C., 2022. Is all seagrass habitat equal? Seasonal, spatial, and Interspecific variation in productivity dynamics within mediterranean seagrass habitat. Front. Mar. Sci. 9 https://doi.org/10.3389/fmars.2022.891467.

Whalen, M.A., Duffy, J.E., Grace, J.B., 2013. Temporal shifts in top-down vs. bottom-up control of epiphytic algae in a seagrass ecosystem. Ecology 94, 510–520. https://doi.org/10.1890/12-0156.1.

Wu, P.P.-Y., McMahon, K., Rasheed, M.A., Kendrick, G.A., York, P.H., Chartrand, K., Caley, M.J., Mengersen, K., 2018. Managing seagrass resilience under cumulative dredging affecting light: Predicting risk using dynamic Bayesian networks. J. Appl. Ecol. 55, 1339–1350. https://doi.org/10.1111/1365-2664.13037.

Zhang, Y., Tang, C., Nepf, H., 2018. Turbulent kinetic energy in submerged model canopies under oscillatory flow. Water Resour. Res. 54, 1734–1750. https://doi.org/10.1002/2017WR021732.

Zhao, L., Ru, S., He, J., Zhang, Z., Song, X., Wang, D., Li, X., Wang, J., 2022. Eelgrass (Zostera marina) and its epiphytic bacteria facilitate the sinking of microplastics in the seawater. Environ. Pollut. 292, 118337 https://doi.org/10.1016/j.envpol.2021.118337.